MARTIN MARIETTA ENERGY SYSTEMS LIBRARIES

3 4456 0250861 3

cy. 2

ORNL-4572
UC-10 — Chemical Separations Processes
for Plutonium and Uranium

CHEMICAL TECHNOLOGY DIVISION

ANNUAL PROGRESS REPORT

FOR PERIOD ENDING MAY 31, 1970

OAK RIDGE NATIONAL LABORATORY
CENTRAL RESEARCH LIBRARY
DOCUMENT COLLECTION
LIBRARY LOAN COPY
DO NOT TRANSFER TO ANOTHER PERSON
If you wish someone else to see this document, send in name with document and the library will arrange a loan.

OAK RIDGE NATIONAL LABORATORY
operated by
UNION CARBIDE CORPORATION
for the
U.S. ATOMIC ENERGY COMMISSION

Printed in the United States of America. Available from Clearinghouse for Federal
Scientific and Technical Information, National Bureau of Standards,
U.S. Department of Commerce, Springfield, Virginia 22151
Price: Printed Copy $3.00; Microfiche $0.65

LEGAL NOTICE

This report was prepared as an account of Government sponsored work. Neither the United States, nor the Commission, nor any person acting on behalf of the Commission:

A. Makes any warranty or representation, expressed or implied, with respect to the accuracy, completeness, or usefulness of the information contained in this report, or that the use of any information, apparatus, method, or process disclosed in this report may not infringe privately owned rights; or

B. Assumes any liabilities with respect to the use of, or for damages resulting from the use of any information, apparatus, method, or process disclosed in this report.

As used in the above, "person acting on behalf of the Commission" includes any employee or contractor of the Commission, or employee of such contractor, to the extent that such employee or contractor of the Commission, or employee of such contractor prepares, disseminates, or provides access to, any information pursuant to his employment or contract with the Commission, or his employment with such contractor.

ORNL-4572

Contract No. W-7405-eng-26

CHEMICAL TECHNOLOGY DIVISION

ANNUAL PROGRESS REPORT

for Period Ending May 31, 1970

D. E. Ferguson — Division Director
K. B. Brown — Assistant Division Director
R. G. Wymer — Chemical Development Section A Chief
R. E. Blanco — Chemical Development Section B Chief
M. E. Whatley — Unit Operations Section Chief
H. E. Goeller — Process Design Section Chief
R. E. Brooksbank — Pilot Plant Section Chief

OCTOBER 1970

OAK RIDGE NATIONAL LABORATORY
Oak Ridge, Tennessee
operated by
UNION CARBIDE CORPORATION
for the
U. S. ATOMIC ENERGY COMMISSION

MARTIN MARIETTA ENERGY SYSTEMS LIBRARIES

3 4456 0250861 3

Reports previously issued in this series are as follows:

ORNL-2392	Period Ending August 31, 1957
ORNL-2576	Period Ending August 31, 1958
ORNL-2788	Period Ending August 31, 1959
ORNL-2993	Period Ending August 31, 1960
ORNL-3153	Period Ending May 31, 1961
ORNL-3314	Period Ending May 31, 1962
ORNL-3452	Period Ending May 31, 1963
ORNL-3627	Period Ending May 31, 1964
ORNL-3830	Period Ending May 31, 1965
ORNL-3945	Period Ending May 31, 1966
ORNL-4145	Period Ending May 31, 1967
ORNL-4272	Period Ending May 31, 1968
ORNL-4422	Period Ending May 31, 1969

Contents

SUMMARY vii

1. MOLTEN-SALT REACTOR PROCESSING 1
   - 1.1 Molten-Salt Breeder Reactor Flowsheet Analysis 1
   - 1.2 Measurement of Distribution Coefficients in Molten-Salt–Metal Systems 11
   - 1.3 Other Chemical Development Studies 16
   - 1.4 Reductive Extraction Engineering Studies 18
   - 1.5 Demonstration of the Metal-Transfer Process for Removing Rare Earths 20
   - 1.6 Contactor Studies of a Simulated Molten-Salt–Liquid Bismuth System 21
   - 1.7 Electrolytic Cell Development 22
   - 1.8 Axial Mixing in Open Columns 27
   - 1.9 Development of a Frozen-Wall Fluorinator 28
   - 1.10 Design and Preparation of $^{239}PuF_3$ Capsules for Small Refueling Additions to the MSRE 30
   - 1.11 Distillation of MSRE Fuel Carrier Salt 32
   - 1.12 Design of a Processing Materials Test Stand and the First Molybdenum Reductive Extraction Equipment 35

2. DEVELOPMENT OF AQUEOUS PROCESSES FOR FAST REACTOR FUELS 37
   - 2.1 Shipping and Receiving 38
   - 2.2 Head-End Processing 44
   - 2.3 Removal of Volatile Fission Products 54
   - 2.4 Dissolution and Feed Preparation 55
   - 2.5 Solvent Extraction with TBP 60
   - 2.6 Removal of Iodine from Off-Gas 67
   - 2.7 Radiation, Shielding, and Criticality Studies 75
   - 2.8 Engineering Studies 82

3. DEVELOPMENT OF METHODS FOR REPROCESSING HTGR FUELS 85
   - 3.1 Head-End Reprocessing Studies with Unirradiated HTGR Fuels 85
   - 3.2 Head-End Reprocessing Studies with Irradiated HTGR Fuels 90
   - 3.3 Procurement of Irradiated HTGR Fuels for Head-End Studies 93

4. WASTE TREATMENT AND DISPOSAL 98
4.1 Engineering, Economic, and Safety Evaluations 98
4.2 High-Level Radioactive Waste 102
4.3 Separation of Radioactive Xenon and Krypton from Other Gases by Using Permselective Membranes 106
4.4 Radioactive Waste Repository in Salt 107

5. TRANSURANIUM-ELEMENT PROCESSING 109
5.1 TRU Operations 109
5.2 Isolation and Purification of TRU Products 114
5.3 Special Projects 115
5.4 Development of Chemical Processes 117
5.5 Recovery of ^{252}Cf for the USAEC Market Evaluation Program 123
5.6 Californium Facility at TURF 123
5.7 Transplutonium-Element Research 124
5.8 Collaborative Research with the Transuranium Research Laboratory 134

6. DEVELOPMENT OF THE THORIUM FUEL CYCLE 135
6.1 Recycle of the Alcohol Used in the Microsphere-Forming Column 135
6.2 Development of Techniques for Drying and Firing Gel Microspheres 137
6.3 Development of Fluidized-Bed Column Equipment 140
6.4 Preparation of Microspheres in Nonfluidized-Bed Columns 140
6.5 Preparation of Test Material for Recycle Test Elements 142
6.6 ^{233}U Storage, Purification, and Distribution 144

7. SOL-GEL PROCESSES FOR THE URANIUM FUEL CYCLE 149
7.1 Preparation of UO_2 Sol by the CUSP Process 149
7.2 Development of the UO_2-PuO_2 Sol-Gel Process 155
7.3 Microsphere Forming Studies 166
7.4 Preparation of UO_2-PuO_2 Materials 168

8. CONVERSION STUDIES IN THE LMFBR FUEL CYCLE 170
8.1 Cost Studies 170
8.2 Preparation of Sinterable UO_2 Fines 173

9. PREPARATION OF $^{233}UO_2$ FOR LIGHT WATER BREEDER REACTORS 174
9.1 Process Development and Flowsheets 174
9.2 Plant Modifications 177
9.3 Design of Equipment for the UO_2 Conversion Line 177
9.4 Storage Systems 177
9.5 Site Preparation 178

10. SEPARATIONS CHEMISTRY RESEARCH 181
10.1 Extraction of Metal Sulfates and Nitrates by Amines 181
10.2 New Separations Agents 181
10.3 Beryllium Purification by Solvent Extraction 184
10.4 Recovery of Uranium from Commercial Phosphoric Acid 184
10.5 Displacement Elution of Transplutonium Actinides from Ion Exchange Resins 186
10.6 Distribution Equilibria and Mechanisms 187
10.7 Relative Potentials of the Bk(IV)-Bk(III) and Ce(IV)-Ce(III) Couples 191
10.8 Relative Basicities of Lanthanides and Actinides 192
10.9 Kinetics of Metal Ion Extractions by Organophosphorus Acids 194
10.10 Aggregation and Activity Coefficients in Solvent Phases 195

11. CHEMICAL APPLICATIONS OF NUCLEAR EXPLOSIONS 196
11.1 Copper Ores 196
11.2 Recovery of Oil from Shale 197

12. BIOCHEMICAL TECHNOLOGY 199
MACROMOLECULAR SEPARATIONS 199
12.1 Effect of Divalent Metal Ions on Reversed-Phase Chromatographic (RPC) Separation of Transfer Ribonucleic Acids 199
12.2 Separation of Isoaccepting Transfer Ribonucleic Acids Following Chemical Derivatization 202
12.3 Preparation of Transfer Ribonucleic Acids from Beef Liver 206
12.4 Separation of Ribosomal Ribonucleic Acids 207
12.5 Engineering Scaleup and Preparation of Purified *E. coli* Transfer Ribonucleic Acids 210
12.6 Distribution of Purified Transfer Ribonucleic Acids 213
BODY FLUIDS ANALYSES 213
12.7 Prototype Analyzers 214
12.8 Separation Systems 215
12.9 System Components 217
12.10 Identification of Body Fluid Constituents 217
12.11 Applications and Experimental Results 220
12.12 Data Acquisition and Analysis 222
WATER POLLUTION STUDIES 223
12.13 Preparation of Samples 223
12.14 Analytical Systems 223

13. IRRADIATION EFFECTS ON HETEROGENEOUS SYSTEMS 225
13.1 Isotope Enrichment by (n,γ) Reactions in Molecular Sieves: The Campbell Reaction 225
13.2 Campbell Reaction by Alpha Bombardment in a Molecular Sieve 229

14. SPECTROPHOTOMETRIC STUDIES OF SOLUTIONS OF LANTHANIDES AND ACTINIDES 231
14.1 High-Energy Absorption Bands vs Concentrations of H_2O and D_2O to 380°C 231
14.2 Effects of Temperature on Aqueous Am^{3+} Complexes 231
14.3 Emission Spectra of the Transuranium Elements 233
14.4 Densities of Aqueous Rare-Earth Solutions to 374°C 233
14.5 Protonic Wave Functions and Spectra 233

15. REACTOR EVALUATION STUDIES 236
15.1 The Oak Ridge Systems Analysis Code 236
15.2 Optimal Dispatching of Electric Power Generation Plants 236
15.3 Dynamic Programming for Expansion Planning of the Nuclear Power Industry 239

16. PREPARATION AND PROPERTIES OF ACTINIDE OXIDES 242
16.1 Mathematical Models of Colloidal Systems 242
16.2 Oxidation of UO_2 Sols 243
16.3 Adsorption of CO_2 by Sols 244
16.4 Electrokinetic Studies of Lanthanide Sols 245
16.5 Preparation of Carbides and Carbonitrides 246

17. CHEMICAL ENGINEERING RESEARCH 251
17.1 Mass Transfer of Water from Sol Droplets 251
17.2 Production of Sol-Gel Microspheres of Small Uniform Size 253
17.3 Axial Dispersion in Packed Columns for Contacting Liquids with a High Density Difference 253
17.4 Development of the Stacked-Clone Contactor 256

18. MISCELLANEOUS PROGRAMS 258
18.1 Quality Assurance Program 258
18.2 Evaluation of the Radiation Resistance of Selected Protective Coatings (Paints) 258

19. NUCLEAR-POWERED AGRO-INDUSTRIAL COMPLEXES: SPECIAL STUDIES 262

PUBLICATIONS, SPEECHES, AND SEMINARS 263

ORGANIZATION CHART 277

Summary

1. MOLTEN-SALT REACTOR PROCESSING

1.1 Molten-Salt Breeder Reactor Flowsheet Analysis

A flowsheet is given for processing a single-fluid molten-salt breeder reactor (MSBR). This flowsheet is based on the use of a fluorination–reductive extraction process for protactinium isolation and a metal-transfer process for rare-earth removal. These processes are described, and operating conditions of interest are discussed.

The effects of a number of processing plant variables on the performance of an MSBR were determined by using the MATADOR computer code.

1.2 Measurement of Distribution Coefficients in Molten-Salt–Metal Systems

The distribution of thorium, rare earths, and other elements between molten lithium halide-containing salts and liquid bismuth solutions is being studied as part of the development of a metal-transfer process for removing rare-earth and other fission products from single-fluid MSBR fuels. The distribution coefficient data show that, from a chemical viewpoint, LiCl and LiBr will be equally good as acceptor salts in the process. Rare-earth–thorium separation factors of at least 10^4 are attainable, using either salt. The distribution coefficients were not markedly affected by changes in temperature. Contamination of the acceptor salt with fluoride fuel salt was found to reduce the rare-earth–thorium separation factor. The distribution of barium between $LiF\text{-}BeF_2\text{-}ThF_4$ (72-16-12 mole %) and liquid bismuth was found to be nearly identical to that of europium. Distribution coefficients for several lanthanide and actinide elements were obtained at 600°C, using $LiF\text{-}BeF_2$ (66.7-33.3 mole %) as the salt phase. Plutonium, americium, and californium behaved similarly; their distribution coefficients, however, were about a factor of 10 higher than those for curium. The data indicated that both Am(III) and Am(II) were present in the salt phase, whereas the other transuranium elements were trivalent in the salt. Estimates of the free energies of formation of LaF_3, ThF_4, UF_3, and PuF_3 at 600°C were made, using distribution coefficient data.

1.3 Other Chemical Development Studies

Preliminary studies showed that the solubility of metallic bismuth in $LiF\text{-}BeF_2\text{-}ThF_4$ (72-16-12 mole %) was less than 5 ppm at 700°C. The solubility of BiF_3 was found to be at least 4 mole % in both $LiF\text{-}BeF_2$ (66.7-33.3 mole %) and $LiF\text{-}BeF_2\text{-}ThF_4$ (72-16-12 mole %) at 600°C. Graphite was the only material tested that was not rapidly attacked by BiF_3 dissolved in fluoride melts.

1.4 Reductive Extraction Engineering Studies

Equipment for semicontinuous engineering experiments on reductive extraction was put into operation. Eight hydrodynamic runs were made during which molten salt (72-16-12 mole % $LiF\text{-}BeF_2\text{-}ThF_4$) and bismuth were countercurrently contacted in an 0.82-in.-ID column packed with ¼-in.-diam right circular molybdenum cylinders. Some modifications to the original equipment were necessary in order to solve problems of flow control.

The original column was replaced with a similar column packed with ¼-in.-diam molybdenum raschig rings. Three hydrodynamic runs with the new column provided an excellent confirmation of a flooding correlation developed in work with a mercury-water system. The system is ready for study of mass transfer between the two phases.

1.5 Demonstration of the Metal-Transfer Process for Removing Rare Earths

Equipment has been installed for the study and demonstration of the metal-transfer process for removing rare earths from the fuel salt of single-fluid MSBR's. A quartz pump for circulating LiCl has operated

satisfactorily at pumping rates of 30 to 125 ml/min; however, testing has shown a need for improved methods for initially purifying the LiCl in order to prevent attack of the quartz.

1.6 Contactor Studies of a Simulated Molten-Salt–Liquid Bismuth System

The study of the hydrodynamics of packed columns has been continued using mercury and water to simulate bismuth and molten salt. The dispersed phase (metal) holdup can be approximated over a wide range of flow conditions by use of a characteristic slip velocity that is dependent on the packing size. A flooding correlation developed through study of the mercury-water system predicted flooding rates that are in excellent agreement with values measured for a molten-salt–bismuth system.

Coefficients for axial dispersion in the continuous (water) phase were measured in columns packed with $^3/_8$-in.-diam raschig rings; the average value of the dispersion coefficient was found to be approximately 3.5 cm^2/sec. Several devices for reducing axial mixing were tested.

1.7 Electrolytic Cell Development

Several of the proposed flowsheets for processing molten-salt breeder reactors require the use of electrolytic cells; thus the study and development of electrolytic cells are under way. Results of experiments made with static cells indicate that heat generation and heat transfer in cells can be studied using ac power, which does not produce the electrolytic products obtained by using dc power, and that a graphite anode cannot be used unless some means for removing CF_4 gas from the anode surface is found.

Several experiments were made to study the use of frozen salt as an electrical insulator as well as a means for providing corrosion protection. It was found that a frozen salt layer can be maintained in the presence of high current densities if sufficient cooling is provided. Experiments with static cells were also carried out to identify the source of the black material that has formed in the salt during all of the runs made thus far. It was concluded that an ac component in the nominal dc power supply was not responsible for the presence of this dark material and that the material is not formed at cell temperatures of 675 to 680°C. Apparently, the presence of the dark material is not associated with the use of bismuth electrodes in these cells; however, it may be related to the use of quartz as the cell containment vessel.

A facility for testing electrolytic cells under flow conditions is being installed. Salt and bismuth will be circulated by gas-lift pumps, and measurement of the salt and bismuth flow rates will be accomplished by gravity-head-type orifice flowmeters. Experiments for determining orifice coefficients with bismuth indicate that the precise determination of bismuth flow rates will be difficult.

1.8 Axial Mixing in Open Columns

Studies of axial mixing in open bubble columns during the countercurrent flow of air and water were completed. Data are presented to show the effects of the viscosity and surface tension of the liquid phase, the column diameter, and the air inlet diameter.

1.9 Development of a Frozen-Wall Fluorinator

Radio-frequency heating was used as a method for generating heat in molten salt in studies of frozen-wall fluorinators with nonradioactive salt. Approximate expressions for the rate of heat generation in molten salt and in an adjacent metal wall were derived; the general validity of these expressions was substantiated by tests with a system in which sulfuric acid was used as a substitute for molten salt. Results of these tests indicate that rf heating is practical for nonradioactive experiments, although a number of problems with this approach must still be solved.

1.10 Design and Preparation of $^{239}PuF_3$ Capsules for Small Refueling Additions to the MSRE

Eight specially designed capsules were filled with $^{239}PuF_3$ powder for refueling additions to the MSRE. The capsule design was based on the standard 50-g MSRE sample capsule. Each capsule contained approximately 40 g of PuF_3.

1.11 Distillation of MSRE Fuel Carrier Salt

The molten-salt still was installed at the MSRE in order to demonstrate the distillation of irradiated fuel carrier salt. Although the quantity of salt processed was less than that anticipated (12 liters vs 48 liters), the objectives of the experiment were realized. Final analyses were obtained for the 11 condensate samples taken during the experiment. The effective relative volatilities (with respect to LiF) of the major components and $^{95}ZrF_4$ were essentially constant during the run and agreed with earlier measurements from equilibrium stills. The effective relative volatilities of most

of the alkaline-earth and rare-earth fission products were substantially higher than values measured in equilibrium stills; however, the effective relative volatilities of ^{137}Cs and ^{155}Eu were lower. Possible causes for these discrepancies include: (1) entrainment of droplets of still-pot liquid in the vapor, (2) concentration gradients in the still pot, and (3) contamination of samples during their preparation for radiochemical analysis.

1.12 Design of a Processing Materials Test Stand and the First Molybdenum Reductive Extraction Equipment

Carbon steel has not been entirely satisfactory as the material of construction for reductive extraction systems handling bismuth. Significant progress in molybdenum fabrication techniques has led to the decision to build a small molybdenum reductive extraction system consisting of a packed extraction column with gas-lift recirculation systems for pumping bismuth and salt through the column. Preliminary design of the system is under way, and metallurgical and fabrication problems are being investigated.

2. DEVELOPMENT OF AQUEOUS PROCESSES FOR FAST REACTOR FUELS

2.1 Shipping and Receiving

Economic considerations will require that spent nuclear fuel be transported from diversely located reactors to central reprocessing facilities. For shipment of LMFBR spent fuel, recent findings confirm the desirability of the features of the cask concept that employs steel for shielding as well as structural material, and that uses liquid sodium to transport heat from multiple fuel subassemblies to the inner wall of the cask. A heat-transport test in a simulated cask has provided additional assurance that temperature differences in a sodium-filled cask will be small if thermal convection is not seriously impeded. Small-scale models of steel casks have shown excellent resistance to damage by impact. The practical capability for reducing impact damage to negligible levels was demonstrated with an ORNL-originated energy absorber.

2.2 Head-End Processing

A computer code was developed to calculate the non-steady-state temperatures of fuel rods in a hexagonal LMFBR fuel subassembly in which the temperature is increasing as a result of heat produced by radioactive decay. Heat transfer between fuel rods within an assembly was assumed to be solely by radiation, while heat from the shroud encapsulating the array was assumed to be dissipated both by radiation and by natural convection to the surroundings. Typical results for an Atomics International (AI) reference fuel subassembly for various heat generation rates are presented.

The ORIGEN code was employed to determine the heat generation rates for: the AI Reference Oxide core (specific power, 148 Mw/metric ton; burnup, 80,000 Mwd/metric ton); the Fast Test Reactor (or the Fast Fuel Test Facility Reactor) core (specific power, 100 Mw/metric ton; burnup, 45,000 Mwd/metric ton); the AI Follow-On inner core (specific power, 105 Mw/metric ton; burnup, 77,000 Mwd/metric ton); and the General Electric Follow-On inner core (specific power, 138 Mw/metric ton; burnup, 101,000 Mwd/metric ton). The results are presented in terms of the heat flux at the surface of the fuel rod.

In subassembly dismantling studies with a plasma-arc torch, preliminary trial results of the slitting of a section of a prototype shroud were very promising.

An analysis of the shearing of LMFBR fuel in a bundle shear showed that terminal piece restraint, shearing in the presence of sodium, and the production of discrete pieces of sheared shroud sufficiently small to pass through the shear discharge port and process lines without jamming are three important problems needing extensive investigation.

Several melt-declad experiments of an exploratory nature have been made to determine the feasibility of an alternative reprocessing method to replace the mechanical head-end step. By heating urania pellet–stainless steel specimens to 1500 to 1600°C, it was possible to expose the urania fuel surfaces and to separate, by gravity, 47 to 90 wt % of the steel from the fuel. The urania loss to the steel was on the order of 0.001 to 0.002 wt %. At present, no further melt-declad experiments are planned at ORNL.

2.3 Removal of Volatile Fission Products

A head-end treatment for removing iodine, krypton, xenon, and tritium was evaluated with 15% PuO_2–85% UO_2 fuel specimens that had been irradiated to about 20,000 Mwd/ton and cooled 32 to 65 days. Shearing the fuel rods released about 50% of the ^{85}Kr and ^{133}Xe but none of the other radionuclides. From 8 to 67% of the ^{131}I had migrated from the fuel and was found in the gas plenum and end plugs. Heating the sheared fuel rods in oxygen at 450, 650, or 750°C

removed from 32 to 74% of the remaining iodine. A total of about 75% of the ^{85}Kr and ^{133}Xe and 63 to 81% of the ^{131}I were separated from the sheared fuel rods prior to dissolution. Only about 4% of the calculated yield of tritium was found, and essentially all of this was released from the fuel during the oxidation treatment. Apparently, most of the tritium had escaped from the fuel rods during irradiation.

2.4 Dissolution and Feed Preparation

In small-scale dissolution tests with stainless-steel-clad, coprecipitated 20% PuO_2–80% UO_2 pellet fuel (irradiated to 1800 Mwd/ton), the times required to dissolve 99.9% of the U + Pu were about 40 and 400 min, respectively, with boiling 12 *M* HNO_3 and 8 *M* HNO_3. Three 4-hr leaches of 15% PuO_2–85% UO_2 sol-gel fuel that had been irradiated to a burnup of 20,000 Mwd/ton resulted in the recovery of more than 99.9% of the plutonium. When a sample of this fuel was heated in oxygen at 750°C prior to dissolution, only about 85% of the plutonium dissolved in 12 hr owing to interference from thoria (present as an insulator pellet), which had diffused into the fuel column during irradiation.

Results of studies of the solubilities of fission products in nitric acid indicate that less than 20% of the ^{95}Nb will be dissolved when 30-day-cooled LMFBR fuels are leached.

No significant evolution of gas or dissolution of uranium and plutonium occurred when irradiated 20% PuC–80% UC was heated with water. When the "ash" obtained by oxidizing this fuel with oxygen at 450°C was leached with boiling 8 *M* HNO_3, 99.0 to 99.76% of the plutonium was dissolved. Recoveries of plutonium were higher (about 99.9%) when the carbide fuel was leached directly with 8 *M* HNO_3.

Results of a study in which iodine was sparged from nitric acid solutions showed that removal of the last few percent of ^{131}I (present as tracer along with carrier iodine) is difficult. Addition of carrier iodine near the end of the sparging treatment was ineffective in promoting the removal of the residual ^{131}I, owing to a lack of reaction (or exchange) of the iodine species.

2.5 Solvent Extraction with TBP

A computer program, SEPHIS, that predicts stage distribution data for plutonium, uranium, and nitric acid in the extraction and stripping systems has been written.

In laboratory experiments, the maximum concentration to which 15% TBP solvent could be loaded with plutonium at 23°C without the formation of a third phase increased from 20 g/liter to 40 g/liter as the ionic strength of the solution was increased from 2 *M* to 10 *M*; no third-phase formation occurred at 40°C under any conditions used.

Two cyclic batch solvent extraction experiments were performed with solutions of short-cooled LMFBR fuel specimens. Although the results were erratic, there was no indication that a radiation dose as high as 0.45 whr $liter^{-1}$ $cycle^{-1}$ adversely affected the performance of the solvent. The solvent radiation doses that will result when 30-day-cooled mixed core and blanket material is processed in pulsed columns are estimated to be about 0.12 and 0.26 whr $liter^{-1}$ $cycle^{-1}$, respectively, for 15% and 30% TBP; in processing core material alone, the estimated doses are 0.19 and 0.41 whr $liter^{-1}$ $cycle^{-1}$.

Rate constants were determined for the decomposition of TBP in nitric acid. The solubility of zirconium dibutyl phosphate, expressed in milligrams of zirconium per liter, was determined to be 0.80 in 3 *M* HNO_3 and 1.74 in 5 *M* HNO_3.

Exposure of uranium-bearing solvent to light caused a significant increase in the amount of uranium that was retained by the solvent through the stripping and solvent wash cycles.

The evaluation of trihexyl phosphate as a potential alternative extractant (to TBP) was begun. This compound has a distribution to dilute nitric acid solutions that is less than 0.001 g/liter – a factor of at least 200 lower than that of TBP.

An engineering review of the stacked-clone contactor indicates that this machine is not particularly adaptable to the processing of LMFBR fuels, at least in large processing plants.

2.6 Removal of Iodine from Off-Gas

In laboratory studies, decontamination factors (DF's) higher than 10^5 were obtained in scrubbing methyl iodide from air with 0.1 *M* $Hg(NO_3)_2$–0.1 *M* HNO_3 solution in bubble columns. Owing to slow reaction kinetics, much lower efficiencies are obtained in packed columns operated with the gas phase continuous; the use of porous packings to increase the solution volume holdup improves the efficiencies of the packed columns.

Effective trapping of methyl iodide from air at 200°C was demonstrated with silver, cadmium, and potassium zeolites, and with silver-containing alumina. The silver zeolite was the most efficient and showed the highest capacity for iodine. For example, trapping efficiencies of 99.99% and higher were obtained for methyl iodide

injection levels up to about 80 mg per cm^3 of silver zeolite.

The catalytic oxidation of organic vapors in process off-gases is being studied as a means of improving the efficiency and preventing the poisoning of iodine sorbent beds. Using Hopcalite (CuO-MnO_2) catalyst and a gas residence time in the catalyst bed of about 0.25 sec, 2 ppm of methane in air was completely decomposed at about 300°C; the complete destruction of 137 ppm and 256 ppm of butane in air was obtained at about 150 and 225°C respectively.

About 20% of the iodine was volatilized readily from a 0.1 *M* NaOH solution prepared by mixing a water solution of I_2 with caustic solution. The volatile species reacts rapidly with CCl_4 and other solvents.

In engineering-scale experiments with the TRU dissolver off-gas system, overall iodine DF's in excess of 10^6 were demonstrated across a system consisting of two liquid scrubbers and a Hopcalite bed–charcoal bed system. The effectiveness of the charcoal bed (DF > 10^4) was not reduced when preceded by a scrubber with an iodine removal efficiency in excess of 99%. A serious reduction in charcoal bed effectiveness over a seven-month period points up the need for a better understanding of factors affecting the life of solid sorbent beds.

2.7 Radiation, Shielding, and Criticality Studies

The objective of this series of studies is to provide basic nuclear data to support the design and development of the LMFBR fuel cycle. Accomplishments in the past year have included the development of a capability in the ORIGEN program for computing the photon and neutron spectra of radioactive fuels, the calculation of the transient concentrations of radionuclides in a variety of fuels of interest in the LMFBR program, and the development of parametric data for use in the design of shields for spent-fuel shipping casks. Criticality calculations were made to aid in the preliminary design and development of spent-fuel shipping casks, fuel element storage arrays, fuel element dissolvers, and plutonium product storage tanks.

2.8 Engineering Studies

A study was made to determine the capability of an existing commercial reprocessing facility for treating early LMFBR fuels. Currently, this is prohibited by the possible presence of metallic sodium in defective fuel rods and the lack of a method that will ensure its safe reaction and be compatible with existing facilities. If this restriction were removed by the development of a suitable sodium deactivation technique, the maximum permissible radioiodine emission rate would limit the minimum decay time for such fuels to about 200 days.

3. DEVELOPMENT OF METHODS FOR REPROCESSING HTGR FUELS

Head-end methods are being developed for HTGR fuels. Both the Ft. St. Vrain and 1100-Mw (electrical) reference reactor fuels are included in the development program. An important programmatic change that occurred in the past year is the firm decision by Gulf General Atomic to use bonded graphite fuel sticks rather than loose fuel particles in the graphite elements. Ft. St. Vrain fuel sticks contain TRISO-coated (i.e., an SiC layer sandwiched between two isotropic carbon layers) $(U,Th)C_2$ and ThC_2 particles. The SiC coating remains intact during the burning step, and methods are being developed to physically separate the particles. The 1100-Mw (electrical) reference fuel consists of TRISO-coated fissile particles ($^{235}UC_2$) and BISO-coated (i.e., two pyrocarbon layers) fertile ($^{233}U,Th)O_2$ particles. The basic concept remains the same; that is, for minimum power cost, the driver ^{235}U fuel should be maintained separate from the bred ^{233}U and thorium in the fuel cycle. Burning the BISO-coated $(U,Th)C_2$ particles in a fluidized bed converts them into a finely divided oxide powder; the ($^{233}U,Th)O_2$ particles may retain their shape. Methods are being developed to separate the fissile particles, the alumina used in the fluidized-bed burner, and the fertile particles (or residue). Tentatively, our aim is to limit the loss of ^{233}U to the ^{235}U stream to about 5% and the inclusion of ^{235}U in the ^{233}U stream to about 10%.

3.1 Head-End Reprocessing Studies with Unirradiated HTGR Fuels

In small-scale tests, a resin-bonded fuel stick containing fissile and fertile SiC-coated fuel particles was crushed in a jaw crusher with a $^5/_8$-in. opening. The resulting product was tumbled, burned in a fluidized bed, and then sieved. Separation of the fissile and the fertile SiC-coated particles by this method was not successful. This fuel stick was an early model made with a thermosetting resin and a graphite-filler bonding agent. During the above operations, a component of the bonded matrix apparently reacted with the SiC layer to form a glassy surface. As a result, the glassy SiC particles formed small agglomerates and were only partially separable even after being leached twice with

11 M HNO_3–0.1 M Al^{3+}–0.05 M HF, tumbled in a 1¼ × 12 in. Teflon pipe, and screened repeatedly. The crossover of ^{235}U to ^{232}Th was estimated at 28 to 42% in the original fluidized-bed product and 4 to 18% after all treatments.

Unirradiated fuel samples containing TRISO-coated ThO_2 and UO_2 particles were obtained as stand-ins for the TRISO-coated particle fuels described above and were crushed in a hammer mill using ¾-in. and ⅜-in. grate spacings. About 45% of the graphite in the product (i.e., pieces larger than 4 to 12 mesh) did not contain any fuel particles and could be separated from the fuel. In two separate tests, the SiC and pyrocarbon coatings on 2.17% and 0.1% of the UO_2 particles and on 1.07% and 1.52% of the ThO_2 particles were broken in the tests with the ¾-in. grating.

The fraction of particles broken on burning the crushed fuel in a 2-in.-diam fluidized bed containing alumina as the fluidized heat-transfer medium was determined as a function of oxygen concentration in the reagent gas. When an oxygen concentration of 70% was used, the total breakage of coatings for both the crushing and burning operations was 5.7% for the UO_2 particles and 4.67% for the ThO_2 particles.

3.2 Head-End Reprocessing Studies with Irradiated HTGR Fuels

Dragon Reactor fuel compact 8375, which had been irradiated to a burnup of 15,000 Mwd/ton, was subdivided by sawing and crushing; then the resulting product was burned in a bed with fluidized alumina and sieved to separate the SiC-coated fuel particles from the alumina. The fuel particles were ground to shatter the SiC shells, burned in a static bed, and leached to recover the heavy metals and fission products. Analyses of controls showed that the original fuel apparently contained 2 to 3% broken particles. Bead breakage was 1.0 and 11.3% in crushing at ⅝-in. and ⅛-in. jaw openings respectively. These results show that crushing is preferable to sawing, since fewer particles are fractured during crushing if the fuel is reduced to a similar-sized product by each method. Crushing at a ⅝-in. jaw opening appears attractive for the first size reduction.

Fission gas (^{3}H and ^{85}Kr) releases were measured for each head-end reprocessing step. Essentially all of the ^{85}Kr (~98%) was released on grinding and burning the SiC-coated particles. About 30 to 40% of the total ^{3}H was released in the first burning step, which removes the matrix graphite and outer pyrocarbon coats. This ^{3}H was probably formed by neutron reactions with light atoms in the matrix graphite and/or ^{3}He in the coolant gas. Most of the ^{3}H produced by ternary fission was released when the SiC-coated particles were ruptured and burned. About 3 to 7% of the total tritium remained with the burned fuel and was released on dissolution. Burner conditions were probably not optimum for the complete release of ^{85}Kr and ^{3}H.

3.3 Procurement of Irradiated HTGR Fuels for Head-End Studies

We have requested additional samples of irradiated Dragon compacts. These compacts were selected because of the similarity of their fuel particles to coated-particle HTGR fuels that are presently being considered in the United States. Another source of irradiated samples is ORNL sol-gel recycle fuel particles that have been irradiated as compacts in the Dragon reactor. Samples of both of these materials should be available by late 1970.

In addition, the following two irradiation programs are under way to provide irradiated materials for head-end studies and for evaluating coated-particle fuel: (1) Two capsules will be irradiated in the ETR. Small samples of the principal recycle and makeup (^{235}U) fuel will be tested at 750, 950, 1050, and 1300°C to burnups of approximately 4×10^{21} to 6×10^{21} fast fluence (i.e., *nvt*). (2) Eight recycle test elements have been designed; six of these have been fabricated for insertion into the Peach Bottom reactor in the summer of 1970 for an exposure period of one, two, or three years at 1.4×10^{21}, 2.8×10^{21}, and 4.2×10^{21} fast fluence. The other two will be completed and inserted in February 1971.

4. WASTE TREATMENT AND DISPOSAL

4.1 Engineering, Economic, and Safety Evaluations

An economic analysis of the wastes expected from the aqueous processing of fuels from three types of reactors – light water (LWR), liquid-metal-cooled fast breeder (LMFBR), and high-temperature gas-cooled (HTGR) – was completed. Optimal trajectories of the waste management operations and costs ranging from 0.03 to 0.04 mill/kwhr were obtained. It was found that only a slight economic penalty is incurred by combining various low-level process waste streams with the first-cycle raffinate (fission product) wastes. Immediate solidification of combined waste streams from processing 150-day-decayed LWR fuels to form dispersions of waste oxides in a sodium tetraborate matrix does not increase the total cost of management

over that estimated for managing only the fission product waste. However, in the case of wastes generated by processing 30-day-decayed LMFBR fuels, the fission product waste requires interim storage as a liquid before it can be solidified, and the cost of managing combined wastes can range up to 10% more than that for the fission product waste alone. In general, the management of LMFBR wastes appears to cost about 10% more than that of LWR wastes.

A study was made to assess the implications of managing ^{85}Kr, after its separation from the off-gas of spent-fuel processing plants, by encapsulation in standard pressure cylinders and shipment to a salt-mine repository for long-term storage. From the standpoints of the projected scale of operation, the estimated costs, and considerations of safety, the proposed method appears to be reasonable over the next several decades.

4.2 High-Level Radioactive Waste

An improved version of the pot calcination process was developed for solidifying the high-level radioactive waste that is generated by the aqueous processing of LWR and LMFBR fuels. Boron-, sodium-, and silicon-bearing compounds are added to the waste; then the solution is evaporated, calcined, and melted in the previously developed calcination equipment, using a rising-level operating technique. A superior product, which consists of a dispersion of calcine in glass, is formed. About 50 wt % (33 vol %) is the highest loading of solids that borosilicate glasses can accommodate and still yield a product that is free of voids. This is about twice the volume of solids that can be dissolved in glass or ceramic products, using the conventional glass-forming processes, and is about equal to that obtained in a calcined product. The thermal conductivity of the borosilicate glass product, namely, 1.25 Btu hr^{-1} ft^{-1} $°F^{-1}$ at 400°F, is about four times that of the calcined product, twice that of the glass product, and roughly equal to that of the ceramic product. Leach rates, expressed as the fraction leached $(cm^2/g)^{-1}$ day^{-1}, of these dispersions range from 10^{-4} to 10^{-5}. Thus these dispersions are about a thousand times more insoluble than a calcined product, roughly equal in solubility to the ceramic product, and about ten times more soluble than a glass product. Tests, using the rising-level technique in 6-in.-diam pots at 900°C, were successful with feed rates as high as 5.5 liters/hr. Foaming problems usually encountered in borate and borosilicate mixes did not occur. Corrosion of the stainless steel was negligible.

The encapsulation of fission product gases in various solid media was studied as a possible method for immobilizing these gases during interim storage, transportation, and ultimate storage. Three media – glass, plastics, and metals – were investigated for use in encapsulation. The combination of known techniques and extrapolated test results showed that gas loadings of up to 50% of those currently obtained in cylinder storage are obtainable by using either pressurized steel bulbs or molecular sieves in a matrix of epoxy resin. Loadings up to at least 7.5% should be obtainable by direct dispersion of the gases in glass. Other possible encapsulation methods were also considered.

4.3 Separation of Radioactive Xenon and Krypton from Other Gases by Using Permselective Membranes

The permeability and separation factors for krypton, xenon, and several other gases were measured using sheets of thin silicone-rubber membrane. Applications of this process to the nuclear industry include the removal of the radioactive noble gases from: (1) the off-gas from a plant for recovering spent nuclear fuels, (2) a reactor containment building following a nuclear accident, or (3) the cover gas of a liquid-metal-cooled fast breeder reactor (LMFBR). Exposure of the membrane to irradiation would not limit the first two applications, but the LMFBR cover gas would have to be stored to allow decay of the short-lived gases prior to processing in a membrane plant. The cost of removing the noble gases from a 5-metric ton/day reprocessing plant would be about $280,000 to $420,000.

4.4 Radioactive Waste Repository in Salt

A conceptual design of a demonstrational salt-mine repository for the permanent storage of high-level and alpha-contaminated solid wastes is under way, in cooperation with the Health Physics and General Engineering Divisions. This repository can be expanded to handle all of the wastes projected for the civilian nuclear power industry over the remainder of this century. It is presently scheduled to become operational for alpha-contaminated wastes in 1973 and for high-level solidified wastes in 1975.

5. TRANSURANIUM-ELEMENT PROCESSING

Work on the USAEC Heavy Element Production Program is centered in two facilities at ORNL – the High Flux Isotope Reactor (HFIR) and the Transuranium Processing Plant (TRU). During this, the fourth year of operation of these facilities, more than 50 mg of californium was recovered; this is nearly three times the total produced in the three previous years. A

highlight of this year was the construction and startup of a new facility for all californium handling and source preparation work. An unused cell in the TURF facility was equipped for the operations involved.

The phases of the program that are under the direction of the Chemical Technology Division, including the operation of TRU, isolation and purification of products, development of chemical processes, and some chemical studies of the actinide elements, are reported here. Target fabrication work, which is directed by the Metals and Ceramics Division, is described in detail in reports issued by that Division.

5.1 TRU Operations

Since 1966, TRU has been the only source of significant quantities of berkelium, californium, einsteinium, and fermium in the United States. The role of TRU as a production facility is somewhat unusual in that many of the processes used routinely are new and are continually being improved at the same time that they are employed in production runs.

During the first three years of operation of TRU, we demonstrated all of the processing and recovery steps required to recover transuranium elements from irradiated HFIR targets and to purify the transcurium elements. With the remote target fabrication line, we fabricated curium oxide recycle targets, using oxide that had been produced in the sol-gel development program.

This year we put into operation the equipment for making americium-curium oxide microspheres for use in fabricating recycle targets. We have now demonstrated all of the process steps that are required in TRU.

Three campaigns were made this year to process irradiated HFIR targets, and four campaigns were made to produce americium and curium oxide for use in fabricating targets. About 7 mg of ^{249}Bk, 54 mg of ^{252}Cf, 380 μg of ^{253}Es, and 5×10^8 atoms of ^{257}Fm were recovered from the irradiated targets. These amounts are about three times the totals produced in all previous years. One hundred two shipments of transuranium elements were made to experimenters.

The sol-gel process and equipment that were developed last year to produce americium-curium oxide microspheres did not perform satisfactorily in-cell and, therefore, had to be modified extensively. We produced 294 g of americium-curium oxide that was suitable for incorporation into targets while we were studying and modifying the process and equipment. There are still three major difficulties: (1) up to 20% of the product is lost (to rework) during the washing of the americium-curium hydroxide during sol formation, (2) we have to grind the oxide to obtain the required particle size distribution, and (3) product yields have been low (i.e., in the range of 50 to 70%), based on the amount of sol fed to the gel-forming step.

Twelve targets containing americium and curium, one target containing plutonium, one special target, and numerous rabbits were fabricated this year.

A Hopcalite-bed–charcoal-bed system to remove radioiodine from the entire vessel and cubicle off-gas (450 cfm) is being designed. The experimental system (3 cfm), which was used last year to demonstrate the process, has been dismantled. During the three target-processing campaigns this year, we performed some iodine experiments in conjunction with Liquid Metal Fast Breeder (LMFBR) programs (see Sects. 2.3 and 2.6) and used their experimental equipment to prevent iodine release. During the three- or four-week-long period required to complete each of the three campaigns, only 325, 52, and 40 mc, respectively, of ^{131}I were released from the HFIR stack.

The problem with target failures during irradiation in the HFIR has apparently been resolved. In the third campaign to process targets, we dissolved and processed six special test targets that had been irradiated for about two full-power years in the HFIR (about 0.82 fission per original plutonium atom). Since a typical target would normally be dissolved and processed after having been irradiated to a burnup of no more than 0.6 fission per original actinide atom, we believe that no more target failures will be experienced. Our solution to this problem was to press the target pellets to only 80% of theoretical density (instead of the previous 90%), which leaves more space for fission products to accumulate and thereby reduces the internal stresses that are generated in the target.

We are developing a nondestructive neutron activation technique for assaying the ^{252}Cf contents of neutron sources and californium shipping containers. This technique involves counting the ^{24}Na that is produced in aluminum disks activated by the fast neutrons emitted by the ^{252}Cf sources. The precision is quite good for sources containing at least 200 μg of ^{252}Cf; however, we need to improve the calibration since we are obtaining consistently low results.

5.2 Isolation and Purification of TRU Products

The final purification of the transplutonium products and the isolation of second-growth isotopes are performed in cell 5 and the shielded cave complex. Products from these operations during this report

period included 40 g of highly purified ^{243}Am. Special separations included the isolation of 60 μg of ^{253}Es and about 1 mg of ^{248}Cm, which had grown into highly purified californium. Sixty micrograms of ^{249}Cf was separated from purified ^{249}Bk.

5.3 Special Projects

A number of special projects were undertaken in cooperation with other groups, both at ORNL and elsewhere. These projects included: (1) fabrication of seven ^{252}Cf neutron sources, which contained from about 100 μg to about 2 mg of ^{252}Cf, (2) fabrication of a high-energy gamma-ray source, containing 1 mg of ^{244}Cm and 200 mg of ^{13}C, which is useful for calibrating high-energy gamma-ray detectors because it emits a sharply defined 6130-kev gamma ray, (3) production of 19.4 μg of isotopically pure ^{253}Es, by irradiation and processing of four ^{252}Cf rabbits, to meet specific scheduling requirements of a customer's experiments, and (4) production of about 155 μg of ^{250}Cf (87% isotopic purity) for use as a target for transactinide element production in the Berkeley HILAC and about 6 μg of ^{250}Cf (98% isotopic purity), part of which was sent to the Los Alamos Scientific Laboratory for use in fission cross-section studies.

5.4 Development of Chemical Processes

An alternative process for the preparation of $(Am\text{-}Cm)O_2$ for HFIR targets was investigated. In this process, the actinides in nitrate solution are sorbed on cation exchange resin, which is then thermally decomposed to produce the oxide particles. Spherical particles of adequate strength have been produced in initial experiments, and studies are in progress to consistently prepare material that is sufficiently dense to provide satisfactory HFIR target loadings.

A resin loading technique was also used as the primary method for preparing ^{252}Cf neutron sources. The technique was modified to prepare ^{252}Cf targets for irradiation in HFIR.

Laboratory studies of displacement elution systems for actinide-lanthanide separations were continued (see Sect. 10.5), and a method to provide interactinide separations by extraction chromatography was developed. In this system, di(2-ethylhexyl)phosphoric acid is held immobile on a porous glass matrix (Bio-Glass 500) and used in an ion exchange mode. A separation factor of 10^6 was demonstrated in separations of ^{248}Cm from ^{252}Cf, using this method.

In our continued efforts to improve analytical procedures, a gamma counting method for berkelium analysis was developed. This method involves isolating and counting ^{245}Am from the alpha branching decay of ^{249}Bk. A second technique, in which the analysis of berkelium is based on the direct measurement of the 327.3-kev gamma radiation associated with the alpha branching, was also developed. The gamma incidence per berkelium decay is 1.426×10^{-7}.

A method of producing selected rare isotopes at greatly enriched concentrations was discovered and tested with several lanthanide and actinide elements (see Sect. 13). Typically, about 50% of the product isotope, along with approximately 1% of the unreacted target isotope, is recovered. Products are enriched by a factor of about 50, as compared with products obtained from conventional irradiations. Work is in progress to develop this into a practical process for the production of ^{247}Cm from ^{246}Cm.

5.5 Recovery of ^{252}Cf for the USAEC Market Evaluation Program

The AEC Division of Production has undertaken a market evaluation program to estimate the long-term demand for ^{252}Cf. Californium is now being produced at the Savannah River Plant (SRP) by irradiation of materials in two forms: (1) ^{242}Pu contained in 86 tubes that are 4 in. in diameter and have active lengths of about 4 ft, and (2) a mixture of americium and curium contained in 163 slugs that are 1 in. in diameter and 6 in. long.

Because of the unique services available at TRU and the present lack of similar facilities for processing these materials at the SRP, arrangements have been made for the irradiated americium-curium slugs to be processed in TRU during the coming year. About 400 mg of ^{252}Cf is expected to be recovered. The berkelium and einsteinium that are associated with the californium will be made available to researchers through the Transplutonium Committee. The TRU operations group will be expanded by about 15% during fiscal year 1971 in order to handle the increased processing load.

5.6 Californium Facility at TURF

An unused cell in the TURF facility has been equipped to provide space for purification and encapsulation of californium. It was placed in operation in March 1970. A primary objective of the preparation of this facility was to provide a ^{244}Cm-clean environment so that extremely pure ^{248}Cm, the alpha decay product of ^{252}Cf, may be recovered from aged sources or stored solutions. The facility has three work stations, situated opposite viewing windows, for: (1) final purification of californium; (2) recovery of ^{248}Cm; and (3) source fabrication and packaging operations. Weak spots in the

neutron shielding, primarily in the zinc bromide viewing windows, will limit the amount of californium that can be handled to the range of 100 mg. To date, 35 mg has been handled in the facility; no shielding problems have been encountered.

5.7 Transplutonium-Element Research

A systematic study of actinide element chemistry and of comparative lanthanide element chemistry is being made to increase our basic understanding of actinide systems. This program includes the investigation of problems involving solution chemistry, with particular emphasis on the formation of complexes and on the preparation of solid actinide compounds that will be characterized by x-ray diffraction, electron microscopy, thermogravimetry, differential thermal analysis, and metallographic examination.

The investigation of lanthanide and actinide sulfate complexes by amine extraction was completed for americium, curium, berkelium, californium, and einsteinium. As expected, the complex systems and the formation constants for each were similar. Also, as expected, these values were close to those for europium (representing the lanthanides). The thermodynamic formation constants at zero ionic strength for the mono-, di-, and trisulfate complexes of all six elements fall within the following ranges: $K_{01} = (4.2–7.3) \times 10^3$, $K_{02} = (3.7–6.4) \times 10^5$, and $K_{03} = (0.9–2.2) \times 10^5$.

A comparative study of methods for preparing anhydrous chlorides of the lanthanides has been concluded, and the results will be applied to actinides in the Transuranium Research Laboratory (TRL). Ytterbium was the only lanthanide that failed to form an anhydrous chloride completely free of oxychloride. The best results were obtained by passing hot HCl gas over mixtures of oxide and NH_4Cl; however, the more convenient method of using hot phosgene should give satisfactory results for most applications at TRL.

A study of the preparation and properties of actinide hydrides and their use in preparing other actinide compounds has been initiated. The design of the preparation and measuring system is conventional, except for modifications to permit work with small quantities of material in complete alpha containment. All of the necessary special equipment has been procured, and the system is nearly ready for testing by preparation and measurements of a known lanthanide hydride.

The thermal stability of various lanthanide and actinide compounds is of interest to several programs in the Chemical Technology Division. Some recent work on the hydroxides of the lanthanides and the carbides of plutonium and uranium-plutonium is reported. Thermogravimetric and differential thermal analysis equipment was used in these studies. Hydroxide preparations of all the lanthanides and yttrium were examined. It was found that the thermal decomposition of the amorphous and crystalline preparations was different for each element but that the decomposition of each form was very similar for all the lanthanides. The work on uranium-plutonium and plutonium carbides involved examination of the high-temperature carbothermic reduction of the dioxides with carbon. The PuO_2 mixtures were prepared by a sol-gel process, and the study was designed to provide information for optimizing process reaction conditions. These mixtures differed from the usual mechanically blended oxide-carbon mixtures as a result of the intimate contact of the very small primary particles (<400 A, as determined by electron microscopic studies). The reactions were studied in argon and in vacuum by thermogravimetry.

The study of the hydrous oxides and hydroxides of the lanthanide and actinide elements was continued in this report period. These compounds are of interest because of their use in sol-gel processes, as well as in comparative studies of the two series of elements. The materials have been studied mainly by electron microscopy, x-ray diffraction, and electron diffraction. The elements investigated include all of the lanthanides and the actinides from plutonium to einsteinium. Work to date has shown that the initial hydroxide precipitates of these elements consist of very small (<50-A-diam) particles that give amorphous-like diffraction patterns. However, with sufficient aging in aqueous media, these materials became crystalline. With several of the elements, the microstructure of the particles also changed after crystallization. The rate of conversion to the crystalline state, the crystal structure, and the microstructure obtained were found to be functions of a particular element, its valency, and its position in the periodic chart. The microstructures of the crystalline materials were of special interest since they were used to aid in the identification of the transplutonium products. The effects of variables in the preparation procedure were also studied to ascertain what changes in microstructure might be brought about by the microtechniques used for the transplutonium elements.

5.8 Collaborative Research with the Transuranium Research Laboratory

Several research projects were conducted in collaboration with the Transuranium Research Laboratory

(TRL). The neutron cross-section values for ^{251}Cf and ^{257}Fm depletion in the HFIR were determined to be 5900 and 6100 barns respectively. The method previously used for determining the II-III oxidation potentials of transplutonium elements by correlation of the electron transfer bands to known redox potentials has been extended to the prediction of III-IV oxidation potentials. The III-IV oxidation potentials for americium, curium, berkelium, californium, and einsteinium are calculated to be −2.0, −3.1, −1.6, −3.3, and −4.6 v respectively. Formal potentials for Bk(III-IV) oxidation in 7 *M* H_3PO_4, 1 *M* $HClO_4$, 1 *M* HNO_3, 1 *M* H_2SO_4, and 3 *M* K_2CO_3 were determined by direct potentiometry to be −1.10, −1.61, −1.51, −1.36, and −0.10 v respectively. Two forms of berkelium metal have been identified: the high-temperature form, which is a face-centered cubic structure, and the low-temperature form, which is a double hexagonal close-packed structure.

6. DEVELOPMENT OF THE THORIUM FUEL CYCLE

6.1 Recycle of the Alcohol Used in the Microsphere-Forming Column

Studies of methods for recycle of the 2-ethyl-1-hexanol (2EH) included methods for preventing chemical degradation of the alcohol by the water removal distillation system as well as a method for recovering totally purified 2EH. Laboratory studies showed that reactions of nitric acid with 2EH and surfactants during distillation could essentially be eliminated by removal of the acid prior to the distillation step by contacting the 2EH with alkaline solutions or ion exchange resins.

We tested an alkaline solution scrubbing method during continuous operations of the sphere-forming column used in engineering development studies but did not achieve satisfactory results because of emulsification and entrainment. Emulsification was ameliorated, but not eliminated, by carrying out the scrubbing in a packed column with the organic phase continuous. A membrane-type liquid-liquid separator (Selas Corporation) used in conjunction with the packed column for phase separation proved to be unsatisfactory due to plugging. We have substituted a resin-bed column in the solvent recycle circuit of the forming column for the alkaline scrubber. No phase separations are required in the ion exchange method, and emulsion and entrainment problems are avoided. The performance of the ion exchange column is presently being evaluated.

Distillation appears feasible if total 2EH purification is required. Pure 2EH was obtained at the relatively low distillation temperature of 100°C as well as at 150 and 180°C. At 100°C, both an alcohol phase and a water phase were present in the still pot; at the higher temperatures, only a single phase was present.

6.2 Development of Techniques for Drying and Firing Gel Microspheres

Fixed-bed dryers (capacity, 20 kg) suitable for drying ThO_2-UO_3 gel spheres were designed, built, and tested. Operations with 20-kg batches were satisfactory.

Gel drying studies showed that the nitric acid present in gel spheres reacts with the sorbed alcohol during drying in steam. The rate at which the drying temperature is increased must be both slow and uniform in fixed beds so that the chemical reaction rate can be controlled and the rate at which heat is liberated by the reaction is not excessive. A purge of steam through the bed of spheres enhances the desorption and vaporization of the organic reactants and thus serves to reduce the quantity of organic materials that are available for reaction with nitric acid. Firing studies show that carbonaceous materials and other volatiles remaining after drying are removed before any appreciable shrinkage or densification of ThO_2-UO_3 gel spheres occurs; thus no problems are encountered in attaining the density and chemical composition specified for calcined products.

Dried ThO_2-UO_3 gel spheres were successfully fired in a 10-kg fixed-bed calciner to 1150°C, and product specifications were met.

6.3 Development of Fluidized-Bed Column Equipment

A report that presents information concerning the design and operation of fluidized-bed columns for gel sphere preparation has been published. Major topics are fluidization requirements, control of alcohol compositions, and capacity limitations.

6.4 Preparation of Microspheres in Nonfluidized-Bed Columns

Preparation of gel spheres without fluidization is simpler than preparation in fluidized-bed columns; however, the sol droplets that are introduced into a nonfluidized column must be small enough to gel before they settle to the bottom. The requirements for the nonfluidized procedure were calculated by combining mass-transfer and settling correlations via a computer program. The calculations and experimental results show that sol droplets initially smaller than 300 μ are easily gelled, while droplets initially larger than

300 μ require long free-fall distances (column heights) when 2EH is used as the drying alcohol and undergo shape distortion when isoamyl alcohol is used.

6.5 Preparation of Test Material for Recycle Test Elements

During the past year, microspheres of ThO_2, ThO_2-$^{235}UO_2$ (Th/U atom ratio, 4.2), ThO_2-$^{235}UO_2$ (Th/U atom ratio, 2), and $^{235}UO_2$ were produced for use in the preparation of eight Recycle Test Elements (RTE's). The RTE's will be used in hot-cell studies of head-end reprocessing operations and of the products of fuel fabrication operations.

The ThO_2 microspheres (1300 g) were not specially prepared, but were taken from material on hand. Batches of ThO_2-$^{235}UO_2$ microspheres with Th/U atom ratios of both 4.2 (1000 g) and 2 (2700 g) were prepared in engineering-scale sol-gel equipment that had been used previously to prepare 32 kg of ThO_2-$^{233}UO_2$ (Th/U ratio, 3). The sol was prepared by a solvent extraction process.

The $^{235}UO_2$ microspheres (300 g) were made using sol prepared by the ORNL precipitation-peptization method.

Six of the eight RTE's have been fabricated using the above material. The remaining two will be fabricated late in 1970.

6.6 ^{233}U Storage, Purification, and Distribution

The Oak Ridge National Laboratory facility for storing and handling ^{233}U is being augmented by the addition of nine wells for storing solids and five tanks for storing solutions. This change increases the solids storage space by 80% and the solution storage capacity by 100%. A nitrate-to-oxide conversion line with a capacity of 22 kg of ^{233}U per week is being installed.

During the past year, 44 kg of ^{233}U was received by the facility, and 7 kg of ^{233}U was shipped out.

Experience with the TRUST (Thorium Reactor Uranium Storage Tank) facility during the past year has shown the practicability of using borosilicate-glass raschig rings for criticality control in large tanks of solutions of fissile isotopes.

7. SOL-GEL PROCESSES FOR THE URANIUM FUEL CYCLE

Sol-gel processes are ideally suited for the preparation of LMFBR fuel since they can be readily adapted to continuous and remote operations for processing materials behind shielding. In the processes under development, sols are prepared by the controlled extraction of nitrate from uranium nitrate and plutonium nitrate solutions, which are the products from fuel reprocessing plants. The sols are then converted into the desired forms required for subsequent fabrication into recycle fuel elements; this form usually consists of high-density oxide microspheres for use in Sphere-Pac operations.

7.1 Preparation of UO_2 Sol by the CUSP Process

The CUSP (*C*oncentrated *U*rania *S*ol *P*reparation) process was used in engineering-scale equipment throughout this report period to prepare urania sols containing more than 230 kg of UO_2. High-quality products were consistently obtained. A new set of equipment for preparing urania sols at a 1-kg-per-batch level by the CUSP process was assembled to test variations in chemical and operating process conditions. This equipment will allow us to reduce the amount of material and manpower usually necessary for engineering-scale operations. For example, one individual can prepare 1 kg of UO_2 as sol in this equipment in three 8-hr days.

During the engineering-scale operations of the CUSP process, solvent regeneration was complicated by the presence of small quantities of colloidal uranium in the solvent. These particles are not effectively removed by standard solvent treatments such as nitric acid, water, and caustic scrubbing. However, a treatment that consists in scrubbing the solvent with 1 *M* HNO_3–0.4 *M* $HC_2H_3O_2$ has been found to remove about 96% of the uranium.

A column with a spray header to disperse the aqueous phase into the extractant, Amberlite LA-2, is an effective contactor for the extraction of nitrate to form urania sol by the CUSP process. This type of contactor is being considered for use with the large engineering-scale equipment.

7.2 Development of the UO_2-PuO_2 Sol-Gel Process

In continued laboratory work to develop a solvent extraction process for the preparation of mixed UO_2-PuO_2 sol, we are studying a process in which CUSP-prepared urania sol is pretreated to remove excess formate and is then mixed with a high-nitrate plutonia sol produced by an alcohol extraction process (APEX). Development efforts have been concentrated on evaluation and optimization of the APEX process, mixed-sol compatibility studies, and formation of microspheres from mixed sols prepared by the CUSP and APEX processes.

Plutonia sols with a NO_3^-/Pu mole ratio of 0.6 to 0.8 can be prepared by the APEX process. The procedure requires extraction of nitric acid into *n*-hexanol from a dilute nitric acid solution of $Pu(NO_3)_4$ to decrease the NO_3^-/Pu mole ratio to about 2.5, digestion at 100°C, and reextraction to produce a sol with a NO_3^-/Pu mole ratio of 1.0. The sol can then be concentrated to greater than 1 *M* in plutonium by evaporation, and additional nitrate can be extracted to provide a final NO_3^-/Pu mole ratio of 0.6 to 0.8. Solvent extraction equipment with a capacity of 10 g of plutonium was fabricated and used in laboratory studies to consistently prepare stable, highly crystalline sols containing very little ionic plutonium (<1%).

Since thickening or gelling limits the useful shelf life of mixed UO_2-PuO_2 sols, mixed-sol compatibility studies were continued. We have demonstrated that mixed-sol stability is a function of the formic acid, nitric acid, and sol concentrations, as well as of temperature. We have also found that a significant change occurs in the absorption spectrum of a PuO_2 sol when small amounts of formic acid are added. Results of spectrophotometric studies show that the hydrolytic behavior of plutonium(IV) formate is strikingly different from the behavior of plutonium(IV) nitrate solutions. The data from these tests indicate that the instability of mixed sols is related to a redistribution of anions when the sols are mixed. The initiating step appears to involve a preferential association of $HCOO^-$ (or HCOOH) with PuO_2 crystallites and a release of NO_3^-. Following this reaction, colloid instability and gelation could result from several mechanisms. Although the exact mechanisms are still not known, adequate mixed-sol stability for process needs can be obtained by close adherence to practices suggested by the results of this study.

In microsphere forming experiments, mixed CUSP-APEX sols were formed into microspheres by virtue of two expedients that prolong the time prior to gelation after mixing and prevent extensive cracking of gelled microspheres during drying and calcining. The first expedient is partial removal of formic acid from the CUSP-prepared sol prior to mixing the sols. The second is cooling the mixed sol to about 5°C. Sparging the sphere-forming alcohol with argon and limiting the contact time between the microspheres and the drying alcohol were also found to be effective in decreasing or eliminating sphere cracking. The results obtained in two series of microsphere-forming experiments were quite encouraging in that good yields of product microspheres were obtained in consecutive runs in each series. However, variations in product yields and microsphere characteristics indicate the presence of subtle variations in sol properties and sphere-forming variables that are not, as yet, adequately understood.

7.3 Microsphere Forming Studies

Optimum conditions for forming a sol into gel microspheres change in a complex manner as the properties of the sol vary. A complete understanding of these relationships, especially for urania sols, has not yet been attained. Since the CUSP process now makes it possible for us to prepare sols reproducibly, the formation of microspheres from CUSP-prepared sols is being studied in detail. Although further work remains to be done, qualitative conclusions about the effects of some of the variables can be made on the basis of the work performed thus far. Good yields of 700-μ-diam gel spheres were obtained from 1 *M* sols formed, at a pH of 4.5, in 2-ethyl-1-hexanol containing 0.2 vol % Span 80, 0.05 or 0.20 vol % Ethomeen S/15, and approximately 1.0 vol % H_2O.

7.4 Preparation of UO_2-PuO_2 Materials

We still must rely on the precipitation-peptization process and the precipitation-peptization-baking process for preparing enriched urania sols and plutonia sols respectively. Facilities are not yet available for preparing enriched urania sols by the CUSP process or for preparing high-nitrate plutonia sols by the APEX process. During the past year, about 3 kg of plutonia was converted into high-quality PuO_2 sols and about 14 kg of enriched uranium was converted into urania sols. These materials were used to prepare mixed urania-plutonia microspheres and shards for use in irradiation tests. About 1.4 kg of 425- to 595-μ-diam microspheres and 364 g of <44-μ-diam microspheres of 80% $^{235}UO_2$–20% PuO_2 were prepared for use in the EBR II, series 2 irradiation tests.

8. CONVERSION STUDIES IN THE LMFBR FUEL CYCLE

8.1 Cost Studies

In the conversion of depleted UF_6 and $Pu(NO_3)_4$ solution to LMFBR core fuel assemblies, the estimated costs for the Sol-Gel Sphere-Pac process were about \$20/kg less than those for three competing pellet processes. A large fraction of this cost differential was associated with loss of material and scrap recovery.

Many of the radiation problems associated with shipping and storing plutonium can be circumvented by

converting plutonium to the form of oxide particles rather than keeping it in solution as is the current practice. It is anticipated that these problems will increase as the expected changes in isotopic composition take place in the plutonium produced in the future.

Preliminary studies of the costs of shipping four types of plutonium products indicate that substantial savings may be realized by shipping plutonium or plutonium-uranium mixtures in the form of oxide microspheres or other dense oxide forms instead of as nitrate solutions.

8.2 Preparation of Sinterable UO_2 Fines

Small $(U,Pu)O_2$ gel spheres should have important advantages as feed for preparing nuclear fuel pellets. Preliminary studies are in progress with sol-gel UO_2 spheroids prepared in nonfluidized columns.

9. PREPARATION OF $^{233}UO_2$ FOR LIGHT WATER BREEDER REACTORS

ORNL participation in the Light Water Breeder Reactor Program, under contract with Bettis Atomic Power Laboratory, involves: (1) the receipt and storage of approximately 640 kg of ^{233}U (400 kg as UNH and 240 kg as UO_3), (2) the purification of this material in small batches (~20 kg of ^{233}U per week) to remove ^{232}U daughters, (3) the conversion of this UNH to ceramic-grade UO_2 powder at the rate of about 20 kg of ^{233}U per week, (4) the packaging and shipping of the UO_2 to BAPL for blending with thoria and pressing into pellets, and (5) the recovery of 175 to 225 kg of ^{233}U from an estimated six to seven tons of urania-thoria scrap from the Bettis operation.

This program will require additional storage facilities for both oxide and solution, a new dissolver for recovering ^{233}U from the thoria-urania scrap, modifications to the present purification system, and a complete oxide conversion line. The facility is presently scheduled to begin production in October 1971.

The installation of the solids storage facility, consisting of nine 4-in.-diam, 15-ft-deep vertical holes in the shielding walls between cells 1 and 2, Bldg. 3019, is complete and ready to receive $^{233}UO_3$ from Savannah River. This material will begin arriving on June 15, 1970, and will be received at the rate of 25 kg per week thereafter. The five additional nitrate solution storage tanks are installed in the pipe tunnel. The piping is 50% complete.

The design of the scrap dissolver, the modifications to the solvent extraction system, the solvent wash system, and the thorium removal system (ion exchange columns) are proceeding on schedule and are expected to be completed by July 15, 1970.

The detailed design of the nitrate-to-oxide conversion line is well under way; the first of six enclosures is completed and ready for construction.

The oxide conversion line will be located in Bldg. 3019 in an area that presently houses plutonium fabrication equipment. A laboratory to house this equipment is presently under construction in Bldg. 4508 by the CPFF contractor.

10. SEPARATIONS CHEMISTRY RESEARCH

New separations methods and reagents are being developed, principally for uses in radiochemical processing but also for other purposes extending from extractive metallurgy to biochemical separations. The program in separations chemistry can be divided into three parallel and interdependent types of research activity: (1) descriptive chemical studies (Sects. 10.1 and 10.2) of the reactions of substances to be separated and of separations reagents, of the controlling variables in particular separations, and of potential new reagents and methods; (2) development (Sects. 10.3–10.5) of selected separations and methods into specific complete processes, both where no workable process exists and where existing processes can be improved, carried where warranted to the point that large-scale performance can be predicted; and (3) fundamental chemical studies (Sects. 10.6–10.10) of the species, equilibria, and reaction mechanisms involved in separations systems, both to increase knowledge and to help define potential applications.

10.1 Extraction of Metal Sulfates and Nitrates by Amines

As part of the program that is concerned with surveying the extraction characteristics of many metals from various systems, data were obtained for the extraction of 19 metals from Li_2SO_4–0.2 N H_2SO_4 (ranging from 0.3 to 5 N sulfate) and $LiNO_3$–0.2 N HNO_3 (0.5 to 10 N nitrate) solutions with representative primary, secondary, tertiary, and quaternary amines. Extraction coefficients higher than 1 were obtained for Ru(III), In(III), Sn(II), Ta(V), W(VI), Re(VII), Os(IV), Pt(IV), Au(III), Bi(III), and Th(IV) in the sulfate system and for Ru(III), Re(VII), Os(IV), Pt(IV), Au(III), Bi(III), and Th(IV) in the nitrate system.

10.2 New Separations Agents

We are continuing to investigate, for potential utility in solvent extraction or other separations methods,

compounds that are (1) newly available commercially, (2) submitted by manufacturers for testing, or (3) specially procured for testing of class or structure.

Extractions of uranium(VI) chloride, nitrate, and sulfate and of plutonium(IV) nitrate by the corresponding methyltrioctylphosphonium (MTOP) salts were qualitatively similar to extractions by the analogous Adogen 464 (methyltrialkylammonium) compound. Coefficients were higher for extractions with the MTOP salts from slightly acidic chloride and nitrate solutions, but were higher for extractions with the Adogen 464 compound from nitric acid and slightly acidic sulfate solutions.

We are encouraged by results of scouting tests to prepare plastic microbeads with an adhering surface layer of quaternary ammonium chloride, for use as a nonporous ion-exchange chromatography medium.

Infrared spectra were obtained for three unsymmetrical methyl alkyl sulfoxide extractants previously synthesized (cf. Sect. 10.6).

10.3 Beryllium Purification by Solvent Extraction

Additional evaluation tests of the solvent extraction process (using a quaternary ammonium carbonate extractant) for preparing very pure beryllium hydroxide showed that the purity of the product, with respect to boron content, is significantly improved by adding a small amount of mannitol to the aqueous feed and scrub solutions to complex the boron and prevent its extraction.

10.4 Recovery of Uranium from Commercial Phosphoric Acid

A process for recovering uranium from wet-process phosphoric acid by extraction with di(2-ethylhexyl)phosphoric acid (D2EHPA) plus trioctylphosphine oxide (TOPO) in a kerosene diluent was demonstrated successfully in bench-scale mixer-settler tests. The uranium was stripped from the solvent with ammonium carbonate solution and precipitated by heating the solution. Because of the difficulty of certain steps in the product recovery portion of the flowsheet, uranium recoveries in the precipitation step have been limited to 90 to 95%. An improved process, using reductive stripping, was developed and demonstrated in continuous equipment. In the new process, the uranium is reduced and stripped from the D2EHPA-TOPO solvent to give a relatively concentrated uranium solution that is highly amenable to processing in a second extraction cycle. Chemical reagent costs for this process are much lower, and uranium recoveries are higher, than corresponding values for the carbonate stripping process.

10.5 Displacement Elution of Transplutonium Actinides from Ion Exchange Resins

In the continuing development of displacement elution of the transplutonium elements with aminopolyacetic acids, californium was eluted slightly ahead of curium and was decontaminated from curium and americium by a factor of about 10^3 (adequate for an initial separation). The last trivalent actinide to be eluted (americium) was slightly overlapped by the first lanthanide (europium) eluted. Equipment is being built for a rack in cell 5 of TRU for further evaluation of displacement elution.

10.6 Distribution Equilibria and Mechanisms

The survey of extractions by dialkyl sulfoxides and the detailed study of iron(III) chloride extraction by methyl 4,8-dimethylnonyl sulfoxide were completed, and a paper describing the results of the work has been submitted for publication.

In a study of the aqueous thiocyanate complexes of trivalent actinides (and lanthanides), contradictory qualitative results were obtained at high ligand concentration and ionic strength from distribution equilibria vs electromigration and spectrophotometry. The last two methods indicated the existence of both neutral and anionic species, while the first (via the usual assumptions and interpretations) indicated only cationic species. Such results may raise a question as to the general validity of accepted methods of investigating complexes by distribution equilibria.

A liquid-scintillation alpha counting method was developed to provide rapid, accurate, and highly sensitive analyses of the transplutonium elements. It includes the development of an extractive scintillator that eliminates the need for solubilizers for aqueous samples, and gives highly reproducible results. The speed, sensitivity, and precision of this system are all much better than those attainable with dried plates in a 2π proportional counter. In addition, although the energy resolution of this system cannot approach that of a surface barrier detector, energy degradation by variable self-shielding is eliminated; thus the peaks are well defined, and useful quantitative discrimination between nuclides is possible in a number of cases. The alpha spectra of several actinide nuclides were compiled.

In support of development of the Campbell reaction (Sect. 13), the ion exchange loading of a molecular sieve zeolite with each of the natural lanthanides and

yttrium was examined. The reversible capacity was nearly the same for yttrium and all the lanthanides (except cerium), that is, approximately 1 milligram-atom (3 meq) per gram of Linde X (faujasite type) molecular sieve.

10.7 Relative Potentials of the Bk(IV)-Bk(III) and Ce(IV)-Ce(III) Couples

In the continuing study of the difference between the formal potentials of the Bk(IV)/(III) and Ce(IV)/(III) couples by means of a selective extraction system, measurements were completed for nitric and perchloric acid solutions over the range of 1 to 8 *M* acid; preliminary values were obtained for sulfuric acid solutions. The ΔE, that is, $E_{Ce} - E_{Bk} = 0.059 \log ([Bk(IV)][Ce(III)]/[Ce(IV)][Bk(III)])$, reached maxima near 0.11 v in 4 *N* $HClO_4$ and near 0.08 v in 2 *N* HNO_3. They appeared to be nearly constant, that is, about 0.05 v, in H_2SO_4.

10.8 Relative Basicities of Lanthanides and Actinides

The relative basicities of most of the lanthanides (remeasured with improved accuracy and precision over previous measurements) and of americium and curium were determined by titration with 0.05 *M* NaOH. The basicities of the lanthanides decreased with increasing atomic number, in accord with their decreasing atomic radii. The basicity of americium falls between the basicities of neodymium and samarium, while curium proved to be much less basic than americium and even somewhat less basic than any of the lanthanides tested.

As previously reported in the literature for the lanthanides (and for plutonium), titration with alkali is not stoichiometric, indicating some precipitation of basic salt. The deviation from the nominal stoichiometry was greatest for curium, and is nearly consistent with a composition of $CmNO_3(OH)_2$.

10.9 Kinetics of Metal Ion Extractions by Organophosphorus Acids

The previously reported puzzling "induction" period in the first 10 to 20 hr of each beryllium extraction by di(2-ethylhexyl)phosphoric acid (HA) was found to be due to plasticizer slowly leached from plastic (now eliminated) in the measuring system. When this effect is eliminated, the beryllium first-order rate constant shows a power dependence on the HA concentration of nearly $\frac{3}{4}$ below and $\frac{5}{4}$ above about 0.2 *M* HA, and a power dependence on the aqueous perchloric acid concentration varying between 1 and $\frac{3}{2}$. If the beryllium extraction mechanism resembles that of iron, the $\frac{3}{4}$ power dependence would reflect simultaneous parallel reaction paths involving the extractant anions A^- and HA_2^-.

10.10 Aggregation and Activity Coefficients in Solvent Phases

In the continuing "calibration" of reference solutes for isopiestic and dynamic vapor-pressure osmometry, the osmotic coefficients of dry carbon tetrachloride solutions of benzophenone up to 6 *m* were determined by direct vapor-pressure measurements. The results are fitted by:

$$\phi = 0.5637 - 0.0165m + 0.2003/(0.4591 + m) .$$

The benzophenone in carbon tetrachloride deviates from ideality by 8% at 0.1 *m* and 26% at 1 *m*.

The mean aggregation number, $\bar{n}$, of methyltrioctylphosphonium dimethylphosphate in benzene is 1.8 at 0.5 *m*. It changes only slightly on dilution of the solution to 0.1 *m*, and is not affected by the presence of water.

The values of the mean aggregation numbers for mixtures of di(2-ethylhexyl)phosphoric acid (HA) and its lithium salt (LiA) at 0.125 *M* ΣA are 2.7, 4.0, and 7.8 at $LiA/\Sigma A = 0.125$, 0.25, and 0.5 respectively. This supports identification of the species LiA·3HA in the extraction of lithium by HA.

11. CHEMICAL APPLICATIONS OF NUCLEAR EXPLOSIONS

11.1 Copper Ores

In the purification of cement copper by an electrowinning process, a good separation of copper was obtained from ^{106}Ru; most of the ^{106}Ru accumulated in the cell electrolyte. The ^{106}Ru contamination of the copper was directly proportional to the concentration of ^{106}Ru in the cell electrolyte. About 28% of the ^{185}W was cemented with copper from simulated leach liquors; however, since the concentration of ^{185}W in the leach liquor is expected to be extremely low, this radionuclide appears to be much less important than ^{106}Ru as a contaminant. Solvent extraction studies indicated that a new copper extractant, Kelex 100-25, should provide about the same efficient separation of copper from radionuclides as was obtained previously with LIX-64 extractant.

11.2 Recovery of Oil from Shale

The contamination of shale oil with tritium was much greater when the shale, prior to retorting, was exposed to tritiated water or tritiated hydrogen than when it was exposed to tritiated hydrocarbons. Treating tritium-contaminated shale with a humid gas stream removed more than 87% of the tritium in 14 days at 200°C and about 60% in 6 days at 95°C.

12. BIOCHEMICAL TECHNOLOGY

MACROMOLECULAR SEPARATIONS

12.1 Effect of Divalent Metal Ions on Reversed-Phase Chromatographic (RPC) Separation of Transfer Ribonucleic Acids

The presence of divalent metal ions from group IIA or the transition elements alters the elution sequence, position, multiplicity, and stability of *E. coli* K-12 MO transfer ribonucleic acids (tRNAs) during reversed-phase chromatography. The group IIA ions Mg^{2+}, Ca^{2+}, Sr^{2+}, and Ba^{2+} were all equivalent in effect, in comparison with reversed-phase chromatography runs with no divalent metal or with EDTA. They shifted the elution positions of the tRNAs to lower sodium chloride concentrations, sharpened some tRNA peaks while broadening others, and stabilized certain tRNAs. In general, the transition elements Mn^{2+}, Co^{2+}, and Ni^{2+} resulted in poorer chromatographic resolution and decreased tRNA stability. Practical application can be made of these divalent metal ion effects for the purification of individual tRNAs.

12.2 Separation of Isoaccepting Transfer Ribonucleic Acids Following Chemical Derivatization

A general procedure for the isolation and purification of isoaccepting tRNAs has been developed. It involves aminoacylation and chemical derivatization of the acylated tRNAs, followed by isolation of that group of isoaccepting tRNAs by benzoylated DEAE-cellulose column chromatography. Individual tRNAs are subsequently resolved by reversed-phase chromatography. Methods are being developed for the isolation of the five arginine tRNAs and the five leucine tRNAs from *E. coli* K-12 MO, and purified samples are being prepared.

12.3 Preparation of Transfer Ribonucleic Acids from Beef Liver

Experimental work has been initiated to prepare crude tRNAs from mammalian sources and to subsequently purify individual tRNAs by reversed-phase chromatography. Samples of crude tRNA, which are being prepared by several procedures, are compared with regard to purity and biological activity.

12.4 Separation of Ribosomal Ribonucleic Acids

Reversed-phase chromatography was applied to the separation and purification of 16S and 23S ribosomal RNAs from *E. coli* on a 50-mg scale. A column consisting of tricaprylylmethylammonium chloride extractant dissolved in tetrachlorotetrafluoropropane and supported on Chromosorb W was used. Sodium chloride gradient elution at 5°C in the presence of 3 *M* urea, 0.01 *M* $MgCl_2$, and 0.05 *M* Tris-HCl developed the chromatographic peaks. After rechromatography, the purities of the products were verified by ultracentrifugation, gradient polyacrylamide gel electrophoresis, and end-group analysis. The 16S RNA contained adenosine at the 3′-terminus and had a molecular weight of about 532,000. Other RNAs from mammalian sources were resolved into several component peaks.

12.5 Engineering Scaleup and Preparation of Purified *E. coli* Transfer Ribonucleic Acids

We completed the processing of mixed tRNAs from 52 kg of *E. coli* K-12 MO7 after making adjustments in the flowsheet that had been used previously for *E. coli* B. More than 3 g of purified formylmethionine tRNA and about 1 g each of valine, arginine, and glutamic acid tRNAs were recovered by reversed-phase chromatography. The reliability and reproducibility of large-scale processing methods for recovery and purification of formylmethionine, arginine, and phenylalanine tRNAs were demonstrated with three batches of *E. coli* K-12 MO cells. In the runs that were made to demonstrate reliability and reproducibility, the direct operating cost, which was predominantly manpower, was equivalent to $13.20 per milligram of purified tRNA.

12.6 Distribution of Purified Transfer Ribonucleic Acids

Samples from our stock of almost 10 g of five different purified tRNAs have been distributed to 103 investigators in 10 countries.

BODY FLUIDS ANALYSES

12.7 Prototype Analyzers

Operating results for the prototype analyzers (i.e., one carbohydrate analyzer and three UV-analyzers)

located in other laboratories have, in general, been good. Two of the prototypes have been upgraded by the installation of recently developed equipment. Preliminary testing of a miniaturized version of the UV-analyzer, designated as Mark III, has been satisfactory; the chromatographic resolution of this new model is about the same as that of the earlier, larger prototypes.

12.8 Separation Systems

A reduction in the size of the UV-analyzer was made possible by the development of a folded high-pressure ion exchange column having a chromatographic resolution equivalent to that of a straight column of the same overall length. Improved resolution of constituents eluting at the front of a urine chromatogram was observed when a cation exchange column was coupled to an anion exchange column. The mathematical model of gradient elution chromatography has shown that gradient elution has no effect on the shape of a particular peak, but does shift the elution position of the peak.

12.9 System Components

An improved, modular version of the miniaturized, UV flow photometer has been developed. A miniaturized flow colorimeter, based on the same general design as the photometer, is being evaluated for use with the carbohydrate analyzer.

12.10 Identification of Body Fluid Constituents

Thirty-five UV-absorbing constituents and ten carbohydrates in physiologic body fluids have been positively identified. In addition, the elution positions of an additional 70 UV-absorbing compounds and 8 carbohydrates have been determined. Gas chromatographic data for aromatic carboxylic acids (and their glycine conjugates) isolated from urine indicated a fairly constant increase in relative retention times (methylene units, MU) for the addition of the glycine moiety to the parent acid. Retention times for the various classes of carbohydrates (pentoses, hexoses, disaccharides, and trisaccharides) fell within relatively narrow ranges. Differences between classes were predictably dependent on molecular weight.

12.11 Applications and Experimental Results

Analysis of many different pathologic urine samples by using the UV-analyzer has shown similarities for patients afflicted with similar disorders. Other physiologic fluids that have been studied include blood, cerebrospinal fluid, amniotic fluids, perspiration, and kidney tubal fluid. The determination of peak areas for 12 reference urinary compounds gave analytical results that agreed within ±10% of the quantities placed on the ion exchange column.

12.12 Data Acquisition and Analysis

A modified nonlinear least-squares computer program has been developed for stripping overlapping peaks from chromatographic envelopes and determining peak positions and areas. The program has been devised for use with a small on-line computer with a core memory of 8000 words. Results obtained by using synthetic data indicate that the program is capable of analyzing envelopes containing up to three Gaussian peaks, with errors of less than 5% (based on peak area).

WATER POLLUTION STUDIES

12.13 Preparation of Samples

A concentration step must be used in order to detect refractory organic pollutants on a molecular basis in sewage plant effluents. Vacuum evaporation, followed by freeze drying, has proved to be the most successful method for concentration; a concentration factor of at least 500 was found to be desirable.

12.14 Analytical Systems

More than 100 chromatographic peaks were detected from a sample of the effluent of the primary stage of a sewage plant by using an ion exchange chromatographic system previously developed for analyzing the UV-absorbing constituents of body fluids. More than 70 peaks were resolved from the effluent of the secondary stage of the sewage plant.

13. IRRADIATION EFFECTS ON HETEROGENEOUS SYSTEMS

A new reaction, the Campbell reaction, has been developed for isotopic enrichment of an (n,γ) product. It is analogous to the Szilard-Chalmers reaction in that the recoil energy places the product in a more accessible situation, but differs from it in that synthesis of a stable target compound is not required and the recoil does not need to break a covalent chemical bond. Target ions are sorbed in nonleachable positions in an inorganic ion exchanger, and product ions recoil to leachable posi-

tions. Lanthanide (and yttrium) and actinide target ions have been sorbed in Linde X molecular sieve, a faujasite zeolite with two sizes of interconnected pores. Heat treatment induces the transfer of absorbed ions from the large pores to the small pores; then recoil presumably returns these ions to the large pores. Typical enrichment factors have been 50 to 100 for $^{141}Pr(n,\gamma)^{142}Pr$, 10 to 15 for $^{241}Am(n,\gamma)^{242}Am$, and (in cyclotron irradiation in attempts to produce "weightless" product for physics experiments) 5 to 10 for $^{158}Gd(\alpha,3n)^{159}Dy$.

14. SPECTROPHOTOMETRIC STUDIES OF SOLUTIONS OF LANTHANIDES AND ACTINIDES

Spectrophotometric techniques for studying aqueous solutions, especially of the lanthanides, actinides, and transition elements, are being developed and exploited. Studies of non- or low-alpha-active solutions at temperatures less than 100°C are accomplished by regular techniques, while a special spectrophotometer system that is capable of operating at temperatures up to 380°C and pressures up to 10,000 psi has been built to provide containment for alpha-active materials. The latter system has been used in a standard laboratory for studying temperature effects (25 to 380°C) on aqueous $Pr(NO_3)_3$, $Nd(NO_3)_3$, and UO_2SO_4, and on the near-infrared absorption bands of H_2O and of D_2O which interfere with the spectral studies of the metal ions. Further studies will include other lanthanides and low-alpha-active materials. In conjunction with the spectrophotometric studies, the densities of aqueous solutions of lanthanides and actinides are being measured over the temperature range 25 to 400°C. The emission spectra of some transuranium elements in solid matrices and in nonaqueous solution are being examined for the production of transuranium element lasers.

A new concept for hydrogen-containing molecules, namely, that they have protonic wave functions and protonic spectra analogous to their electronic wave functions and spectra, was recognized and developed. The molecular structures of water, ammonia, methane, and some other hydrides were examined by using the variational method to solve the Schrödinger equation with the correct nonrelativistic and spin-free Hamiltonian to find the wave function that gives the lowest ground-state energy. The protonic spectra are listed for H_2O, NH_3, and CH_4.

15. REACTOR EVALUATION STUDIES

This program, which is a joint effort with other ORNL Divisions, especially the Reactor Division and the Metals and Ceramics Division, has the primary purpose of assisting the USAEC in evaluating the technical feasibility and economics of various nuclear power concepts being developed, or being considered for development, under the U.S. civilian power program. Work in this Division during the past year was devoted primarily to the development of computational models for use in the planning of optimal electrical power systems in the United States. Accomplishments included the completion of the Oak Ridge Systems Analysis Code, the development of a dynamic programming algorithm for the dispatching of power generating plants, and the completion of a study of the feasibility of applying advanced dynamic programming procedures to the expansion planning of nuclear power generation systems and the fuel reprocessing industry.

16. PREPARATION AND PROPERTIES OF ACTINIDE OXIDES

Studies of a wide range of actinide and lanthanide sols were continued. A mathematical model of sols such as nitrate-stabilized thoria successfully accounts for their stability and slow agglomeration or rapid flocculation as a function of zeta potential and electrolyte concentration. It also provides an explanation for the observation that slow agglomeration produces linear strings of the sol particles. Continued measurements of the kinetics of air and oxygen oxidation of urania sols indicate that the oxidation is primarily limited to the surface, penetrating the particles relatively slowly. The study of the adsorption of carbon dioxide by thoria sols was directed principally toward the possibility of measuring in situ the (wet) surface area of sols. The results were partially encouraging, but showed that significant unrecognized variables still exist.

The titration of positively charged nitrate-stabilized lanthanide hydroxide sols to zero zeta potential with sodium hydroxide showed a surprising direct correlation of the amount of hydroxide required with the amount of nitrate in the sol. When lanthanide sols were aged at pH levels higher than 7, the positive zeta potential decreased; when the pH was near 11, the zeta potential became negative. These results account for previous seemingly erratic charge reversals.

Conditions were identified for the successful production of dense microspheres and shards of uranium-plutonium (80%-20%) monocarbide and carbonitride. Single-phase, low-oxygen monocarbide is difficult to prepare, and strict adherence to stipulated conditions is mandatory. More tolerance is permissible in the preparation of the carbonitrides. Kinetic studies showed

that carbon is the dominant component of the solid reactants, and provided a basis for optimizing the preparation of advanced fuels.

17. CHEMICAL ENGINEERING RESEARCH

17.1 Mass Transfer of Water from Sol Droplets

The microsphere forming operation in the ORNL sol-gel process for the fabrication of nuclear reactor fuels has provided a system that is amenable to unusually precise mass-transfer measurements. In earlier experiments involving such measurements, a single droplet of either water or thoria sol was fluidized with a relatively dry immiscible alcohol in a Plexiglas chamber, where the decrease in droplet diameter with time was measured optically. Classical correlations of the Sherwood number with the Reynolds number and Schmidt number were found to fit the data well. In recent experiments, the range of Schmidt numbers has been extended by varying the type of alcohol used and the temperature. Analysis of the operation by fundamental equations involving the sphere drag coefficients is being attempted.

17.2 Production of Sol-Gel Microspheres of Small Uniform Size

Ultrasonic techniques are being applied to the production of uniform sol spheres having diameters smaller than the present practical limit of 100 μ. Both nonresonant and resonant devices are being tested. These techniques are variations of the original technique for dispersing the sol in a dry immiscible alcohol phase.

17.3 Axial Dispersion in Packed Columns for Contacting Liquids with a High Density Difference

We are studying axial dispersion in countercurrent packed columns operating with mercury and water. This system is similar to reductive extraction columns, such as those proposed for use in processing molten salt breeder reactors, which employ high-density fluids that frequently do not wet the packing. This is contrary to the usual experience with conventional aqueous-organic systems in which the packing is wet by one or both of the phases. Measurements of axial diffusion coefficients with $^3/_8$-in.-diam raschig rings over a wide range of mercury and water rates show no significant dependence of the dispersion coefficient on the flow rate of either phase. The average value of the dispersion coefficient is 3.5 cm^2/sec.

Several devices to reduce axial dispersion in columns have been tested. These devices force the continuous (salt or water) phase through relatively small openings, where high local velocities can be achieved even though the overall flow rate of that phase is low. The amount of backflow through the devices was found to be a function of both the size of the opening through which the continuous phase flows and the velocity of the phase through the opening. We have demonstrated that, when the water flow rate is sufficiently high, the fraction of backflow can be reduced to less than 15% for sieve openings as large as $^3/_8$ in. Although the present backflow preventers significantly reduce column capacity, future designs are expected to have higher throughputs.

A simplified method to estimate the effect of axial dispersion on countercurrent column performance has been developed. Column efficiency (height of a plug flow column divided by the height of a back-mixed column) is given as a simple function of common design parameters. The equation is in reasonable agreement with the far more complex exact solution over a wide range of operating conditions.

17.4 Development of the Stacked-Clone Contactor

Developmental work on the stacked-clone contactor included tests with the multiclone stacked-clone contactor – a unit with 12 stages, each of which contains nine parallel hydroclones scaled to three-eighths of the original, standard size. Modifications of the pump increased the capacity to 20% over that reported last year. In its present form, this contactor has a shorter residence time per theoretical stage than any other existing solvent extraction device.

After four years of continuous operation, a prototype of the centrifugal pump used in the standard stacked-clone contactor finally failed due to a fracture of a peripheral plastic line. This failure was not related to the functioning parts of the pump, which showed less than 5 mils of wear during the test. Extrapolated life is estimated at 8 to 12 years of continuous operation.

18. MISCELLANEOUS PROGRAMS

18.1 Quality Assurance Program

Formalized quality assurance procedures are being applied to significant projects that are in progress in the Chemical Technology Division. Previous projects have had similar procedures applied to them; however, present practice calls, in addition, for the retention of plans and records so that each project can be audited.

The Division's initial efforts involve several programs already under way.

18.2 Evaluation of the Radiation Resistance of Selected Protective Coatings (Paints)

Results of tests in which selected commercial protective coatings were exposed to a ^{60}Co source with an intensity of 6×10^5 r/hr at a temperature of 40 to 50°C indicate that most of these coatings have improved formulations which are more resistant to radiation in air than those in earlier tests. The epoxies, modified phenolics, and phenolics exhibited the best resistance in deionized water; the average failure level was 1.6×10^9 rads, with maxima above 3×10^9 rads.

19. NUCLEAR-POWERED AGRO-INDUSTRIAL COMPLEXES: SPECIAL STUDIES

Several members of the Chemical Technology Division continued their participation in the agro-industrial studies which were begun during the summer of 1967. Work this year included the following topics: (1) aquaculture – the intensive cultivation of aquatic species, and (2) nutrition economics – the cost of furnishing an adequate diet to a representative population.

19.1 Aquaculture

The potential of utilizing waste heat from energy centers (power stations and desalination plants) for intensive aquaculture was considered. For example, in dual-purpose nuclear desalination plants, heat energy that remains after electricity and fresh water are produced must be carried away by a stream of ambient-temperature seawater. This evaporator coolant water, ordinarily larger in volume than the fresh water produced, could be utilized for the culture of aquatic species instead of merely being discharged to the sea.

In principle, flowing streams (either seawater or fresh water) are media that can be engineered for intensive aquaculture, because dissolved oxygen can be uniformly distributed and fish waste metabolites can be flushed away. With a source of electricity nearby, power is conveniently available to operate mixing devices that can blend ambient-temperature seawater with the coolant water and thus suitably adjust the temperature of the culture stream to maximize fish growth. One other key requirement is the availability of a low-cost nutritionally balanced artificial food for feeding the fish, so that the population of aquatic species being cultured is not limited by the natural food supply of the water stream. This concept could also be applicable to work in the area of thermal pollution (e.g., in the study of potential productive uses of waste heat), a subject of increasing concern nowadays.

A year-round source of constant-temperature water also implies that a culture facility could operate on a continuous basis and could supply a product of uniformly sized cultured fish – a very important marketing asset. In batch culture on a seasonal basis, a whole spectrum of fish sizes is normally the result; thus only a small fraction of the total yield is of significant commercial value.

A conceptual design for a continuous culture facility was proposed using shrimp and seawater as a model and taking into account published biological and technological data on shrimp. A cost estimate and a cost sensitivity analysis, together with some marketing analyses, were made for the design to put the potential shrimp production capacity in its proper perspective.

For each billion gallons of blended seawater available at 80°F, an annual capacity of 10,000,000 lb of cultured shrimp was projected, assuming a unit yield of 20,000 lb/acre-year. The return on investment was estimated to be over 20%, assuming that the cultured product was worth $1.00 per pound of whole shrimp, the site improvement capital cost was $27,000/acre, the food conversion ratio was 3 lb of *dry* food fed per pound of *wet* fish produced at a food cost of $0.10/lb, the labor wage rate was $2.00/man-hour, and the labor productivity was 100,000 lb of fish handled per man-year. Production costs for culturing shrimp were most sensitive to the food conversion ratio and least sensitive to the labor factors; the capital cost for site improvement was found to be intermediate in cost sensitivity. Published data on shrimp consumption in this country show that 10,000,000 lb annually represents only a small fraction of the total supply (i.e., 5% of the 1968 domestic catch and 2% of the 1968 total U.S. supply, including imports). Marketing data indicate that within 10 years the world-wide shrimp demand will outstrip the estimated world-wide annual shrimp supply and that other sources of shrimp supply, like shrimp culture, will be needed to supplement harvested supplies in order to continue to meet the expected growth in world demand.

19.2 Nutrition Economics

One application of nuclear-powered agro-industrial complexes is to make arid coastal areas productive, particularly in developing countries of the world. Intensive farming of desert soils might provide grains

and legumes to furnish a nutritionally improved diet to a regional population. Nutrition economics as applied to desalination agriculture examines the cost of providing such diets as a function of the cost of water.

The diet of a given population may be measured in terms of quantity and quality of the food consumed. Aside from the obvious need for a minimum food energy requirement to prevent starvation, nutritionists also specify that this energy intake must be properly apportioned between calories of carbohydrates, protein, and fats in order to preserve good health in the population at large and, more importantly, to allow children to reach their full genetic potential by maintaining normal physical and mental growth.

For this study, population was divided into six age groups, each with its own daily total food energy intake requirements. Two diets were compared: the minimum diet, in which 73% of an individual's calories came from carbohydrates, 7% from protein, and 20% from fat; and the better-quality, U.S. recommended diet, in which the calorie percentages were 53% for carbohydrates, 12% for protein, and 35% for fat. The grains corn, wheat, and rice were the sources of the carbohydrate calories. Each of these was supplemented with peanut to upgrade protein quality and to provide needed fat in the diet in concentrated form.

With the minimum diet, the daily cost (excluding water costs) per thousand inhabitants was calculated to be $23 for corn and peanuts, $33 for wheat and peanuts, and $44 for rice and peanuts. For costs ranging from 10 to 50¢ per thousand gallons, water added $15 to $74, $19 to $93, and $23 to $113, respectively, to each of the above combinations. With the U.S. recommended diet, daily costs (excluding water costs) were $26, $31, and $40; water costs added $16 to $78, $18 to $89, and $21 to $106 respectively. Thus, the daily cost (including water costs) might range from about 4¢ to about 15–16¢ per person, depending on the type of diet furnished.

The corn-peanut combination was calculated to be the diet of lowest cost, but it was also the poorest in protein quality. Wheat-peanut and rice-peanut combinations were successively more expensive. Unexpectedly, however, the cost of providing the better-quality recommended diet in both of these cases was found to be less than the cost of the minimum diet and was less sensitive to the cost of water. The reason for this is that peanuts have more total energy calories, particularly with regard to fat and protein, than wheat and rice. The savings in the reduction of grain for the carbohydrate requirement in stepping up from the minimum to the U.S. recommended diet was more than the additional cost of providing more peanut for protein and fat.

1. Molten-Salt Reactor Processing

The Oak Ridge National Laboratory is developing a molten-salt breeder reactor (MSBR) which would operate on the ^{232}Th-^{233}U fuel cycle to produce low-cost power while producing more fissile material than is consumed. The reactor would use a molten fluoride salt (72-16-12 mole % LiF-BeF_2-ThF_4) as the fuel and graphite as the moderator. If the reactor is to operate as a breeder, ^{233}Pa must be isolated from the region of high neutron flux during its decay to ^{233}U. Also, the rare-earth fission products must be removed on a 25- to 100-day cycle. The Chemical Technology Division is responsible for developing an on-site processing plant to economically effect these operations. Processes that employ liquid-liquid extraction of the reactor salt with a bismuth phase containing reductants appear to offer the best means to this end and have been the major subjects of our studies.

During this reporting period, significant revisions were made in the conceptual flowsheets that form the basis for our developmental effort. The discovery that the thorium distribution coefficient in an LiCl-bismuth system is high and that the rare-earth distribution coefficient in this system is low (a separation factor of 10^4 or greater) has allowed us to turn to a metal-transfer process that is much more attractive than the previous rare-earth removal system, which exploited separation factors in the range of 1.2 to 3.5. The new process does not require an electrolyzer. The major part of our effort with regard to chemical development has been devoted to the definition of the distribution of important materials between a reducing bismuth phase and possible acceptor salts such as LiCl or LiBr.

The analysis of flowsheets using this new concept has led us to consider alternative protactinium isolation methods that do not require an electrolyzer. The obvious and most desirable alternative is fluorination for removing the uranium before the reductive extraction step. Calculations made for a combination of the fluorination–reductive extraction and the metal-transfer flowsheets indicate good system performance.

In spite of the revisions made in our previous flowsheets and the consideration of alternative protactinium isolation methods, our developmental program has not required drastic modification. In fact, many of the operations required for the new processes are the same as those required for the earlier ones. Our work on contactor development has continued both with the flow-through system, using bismuth and salt, and with the mercury-water simulation of the salt-bismuth system. Our axial mixing studies with the simulated system have led to the design of a backmixing preventer that seems to be quite effective at flow ratios (dispersed phase/continuous phase) of 50 or higher. We have increased our efforts to develop a continuous fluorinator that will be protected from corrosion by a layer of frozen salt deposited on its metal surfaces. The work on electrolytic cells has been given lower priority, but has not been terminated since a reliable method for producing reductant from process salt streams would be useful.

We have initiated work toward the development of a continuous process for preparing molten salt. We have also assisted the MSRE operation by preparing capsules loaded with $^{239}PuF_3$ for use in adding ^{239}Pu to the fuel.

1.1 MOLTEN-SALT BREEDER REACTOR FLOWSHEET ANALYSIS

MSBR Processing by Fluorination–Reductive Extraction and a Metal-Transfer Process

We have now adopted a flowsheet that uses fluorination–reductive extraction for protactinium isolation and a metal-transfer process for rare-earth removal. These processes are described in detail in later sections of this report; this section will be limited to a description and an analysis of the flowsheet shown in Fig. 1.1.

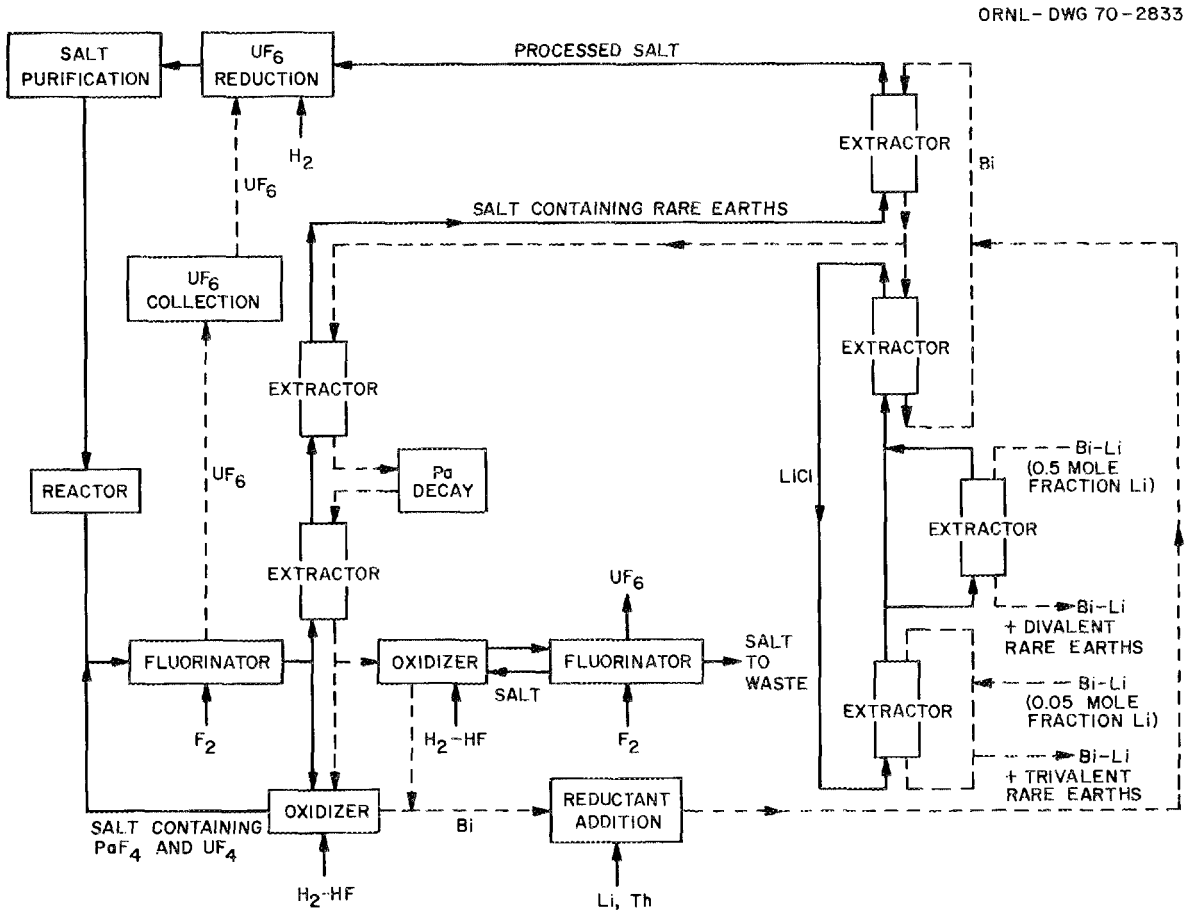

Fig. 1.1. Flowsheet for Processing a Single-Fluid MSBR by Fluorination–Reductive Extraction and the Metal-Transfer Process.

Salt withdrawn from the reactor is fed to a fluorinator, where most of the uranium is removed as UF_6. Most of the salt leaving the fluorinator is fed to a reductive extraction column, where the remaining uranium is removed and the protactinium is extracted into a bismuth stream. The bismuth stream containing the extracted protactinium flows through a tank of sufficient volume to contain most of the protactinium in the reactor system. Most of the bismuth stream exiting from the extraction column is contacted with an H_2-HF mixture in the presence of about 10% of the salt leaving the fluorinator in order to transfer materials such as uranium and protactinium to the salt stream. This salt stream is then recycled to the fluorinator.

The bismuth stream leaving the lower column also contains several materials that must be removed for satisfactory operation of an MSBR. The most important of these are fission product zirconium, which can be an important neutron absorber, and corrosion-product nickel, which forms an intermetallic Ni-Th compound having a low solubility in bismuth. These materials and others that do not form volatile fluorides during fluorination are removed by hydrofluorination, in the presence of a salt stream, of a small fraction of the bismuth stream exiting from the lower column. The salt is then fluorinated for the removal of uranium. Sufficient time is allowed for the decay of ^{233}Pa so that the rate at which this material is lost is acceptably low. The remaining materials, including Zr, Ni, ^{231}Pa, and Pu, are withdrawn in the salt stream from the fluorinator. Oxidation of part of the metal stream leaving the lower contactor was selected as a means for removing these materials since this method results in the discard of very little Li or Th and no Be; the discard of salt from other points in the system would result in much higher removal rates for the major components LiF, BeF_2, and ThF_4.

The bismuth streams leaving the hydrofluorinators are combined, and sufficient reductant (lithium and thorium) is added for operation of the protactinium isolation system. Effectively, the resulting stream is fed to the upper column of the protactinium isolation system; actually, it first passes through a captive bismuth phase in the rare-earth removal system in order to purge uranium and protactinium from this volume.

The salt stream leaving the upper column of the protactinium isolation system contains negligible amounts of uranium and protactinium but contains the rare earths at essentially the reactor concentration. This stream is fed to the rare-earth removal system, where fractions of the rare earths are removed from the fuel carrier salt by countercurrent contact with bismuth containing lithium and thorium. The bismuth stream is then contacted with LiCl to which the rare earths, along with a negligible amount of thorium, have been transferred. The rare earths are subsequently removed from the LiCl by contact with bismuth containing a high concentration of ^{7}Li. To minimize the quantity of ^{7}Li required, separate contactors are used for removing the divalent and trivalent rare earths. Only about 2% of the LiCl is fed to the contactor in which the divalent materials are removed.

Calculations have been made for a range of operating conditions in order to evaluate the flowsheet just described. In making these calculations, the MATADOR code[1] was used to determine the reactor breeding ratio for each set of processing plant operating conditions examined. Processing cost data are not available for this flowsheet or for the reference flowsheet that uses electrolyzers in both the protactinium and rare-earth removal systems. In the absence of these data, we examined processing conditions which would result in the same reactor performance (i.e., the same breeding ratio) as that obtained with the previous reference flowsheet.

Although the optimum operating conditions which will result in a breeding ratio equal to that of the reference reactor and processing system (i.e., 1.063) have not been determined, the following conditions are believed to be representative. The reactor was processed on a 10-day cycle, with the complete fuel salt stream (0.88 gpm) passing through both the protactinium isolation and the rare-earth removal systems. The resulting protactinium removal time was 10 days, and 340 to 430 equivalents of reductant were required per day, costing 0.012 to 0.015 mill/kwhr. The protactinium isolation columns were less than 8 in. in diameter; the total number of required stages was less than 10. The protactinium isolation system also resulted in a 10-day removal time for materials that are more noble than thorium but do not have volatile fluorides. These include Zr, ^{231}Pa, Pu, the seminoble metals, and corrosion products.

The rare-earth removal system consisted of three primary contactors: (1) a 7.1-in.-diam, six-stage column in which the rare earths are transferred from the fuel salt to a 12.5-gpm bismuth stream, (2) a 13-in.-diam, six-stage column in which the rare earths are transferred from the bismuth to a 33.4-gpm LiCl stream, and (3) a 12.3-in.-diam column in which the trivalent rare earths are transferred from the LiCl to an 8.1-gpm bismuth stream having a lithium concentration of 0.05 mole fraction. Two percent of the LiCl (0.69 gpm) was contacted with a Bi stream (1.5 cm^3/min) having an Li concentration of 0.5 mole fraction for removal of the divalent fission products such as Sm, Eu, Ba, and Sr. The total lithium consumption rate for the rare-earth system was 119 moles/day, which is equivalent to a cost of 0.0042 mill/kwhr.

The rare-earth removal times ranged from 15.5 days for cerium to 50.4 days for europium. The distribution data for Nd were considered to be representative of Y and rare earths (i.e., Pr and Pm) for which distribution data are not available. It is believed that this results in conservative estimates of removal times for these materials.

The costs for the reductant that is required in both the protactinium isolation system and the rare-earth removal system constitute only a small fraction of the total processing costs and indicate that one can purchase reductant rather than use an electrolytic cell for producing this material.

Isolation of Protactinium Using Fluorination–Reductive Extraction

The fact that the new process for removing rare earths from a single-fluid MSBR does not require an electrolytic cell has led us to consider protactinium isolation systems that do not require electrolyzers. One protactinium isolation method by which an electrolyzer can be avoided is fluorination–reductive extraction. In this method, most of the uranium would be removed from the fuel salt by fluorination prior to isolation of the protactinium by reductive extraction.

The fluorination–reductive extraction system for isolating protactinium is shown in its simplest form in

[1] *Chem. Technol. Div. Ann. Progr. Rept. May 31, 1969,* ORNL-4422, p. 10.

Fig. 1.2. The salt stream from the reactor first passes through a fluorinator, where most of the uranium is removed by fluorination. Then, approximately 90% of the salt leaving the fluorinator is fed to an extraction column, where it is countercurrently contacted with a bismuth stream containing lithium and thorium. The uranium is preferentially removed from the salt in the lower extractor, and the protactinium is removed by the upper contactor. A tank through which the bismuth flows is provided for retaining most of the protactinium in the system.

The bismuth stream exiting from the lower contactor contains some protactinium, as well as the uranium that was not removed in the fluorinator and the uranium that was produced from the decay of protactinium. This stream is contacted with an H_2-HF mixture in the presence of approximately 10% of the salt flowing from the fluorinator in order to transfer the uranium and the protactinium to the salt. The salt stream, containing UF_4 and PaF_4, is then returned to a point upstream of the fluorinator, where most of the uranium is removed. The protactinium passes through the fluorinator and is subsequently extracted into the bismuth. Reductant (Li and Th) is added to the Bi stream leaving the oxidizer, and the resulting stream is returned to the upper contactor. The salt stream leaving the upper contactor is essentially free of uranium and protactinium and would be processed for the removal of rare earths before being returned to the reactor.

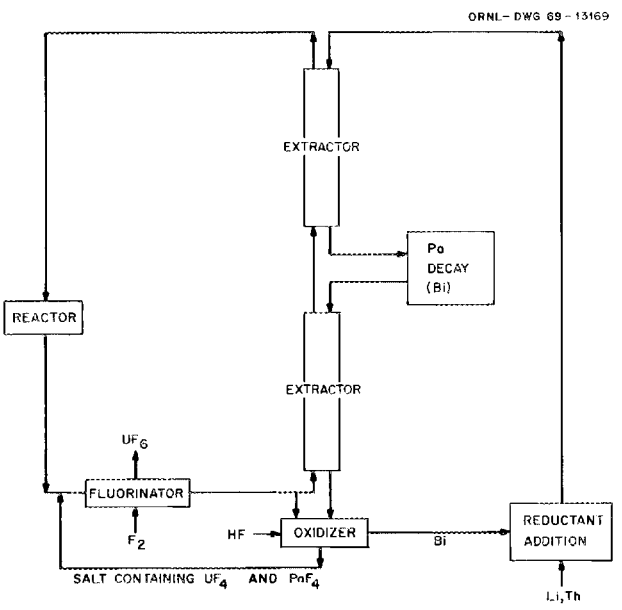

Fig. 1.2. Protactinium Isolation by Fluorination–Reductive Extraction.

Calculations have shown that the system is quite stable with respect to variations as large as 20% for most of the important parameters: flow rates, reductant concentrations, a number of extraction stages. The required uranium removal efficiency in the fluorinator is less than 90%. The number of stages required in the extractors is relatively low, and the metal-to-salt flow ratio (about 0.26) is in a range where the effects of axial mixing in packed column extractors will be negligible. Since the protactinium removal efficiency is very high and the system is quite stable, materials such as ^{231}Pa, Zr, and Pu should accumulate with the ^{233}Pa. These materials can be removed by hydrofluorination, in the presence of salt, of a small fraction of the bismuth stream leaving the lower extractor; the salt is then fluorinated for uranium recovery. Because sufficient decay time would be allowed for most of the ^{233}Pa to decay to ^{233}U, the ^{233}Pa and ^{233}U losses would be acceptably low.

Operating conditions that will yield a 10-day protactinium removal time include a fuel salt flow rate of 0.88 gpm (10-day processing cycle), a bismuth flow rate of 0.23 gpm, two stages in the lower contactor and six to eight stages in the upper contactor, and a decay tank volume of 200 to 300 ft^3. The required quantity of reductant is 340 to 430 equivalents per day, which will cost 0.012 to 0.015 mill/kwhr if ^7Li is purchased.

Rare-Earth Removal Using the Metal-Transfer Process

We have devised a new method, called the metal-transfer process, for removing rare-earth and alkaline-earth fission products from the fuel salt of a single-fluid MSBR. In this process, bismuth containing thorium and lithium is used to transport the rare-earth fission products from the reactor fuel salt to an acceptor salt. Although LiCl is the preferred acceptor salt, LiBr or LiCl-LiBr mixtures could also be used.

Both thorium and rare earths transfer to the bismuth; however, because of favorable distribution coefficients, only a small fraction of the thorium transfers with the rare earths from the bismuth to the LiCl. The effective thorium–rare-earth separation factors for the various rare earths range from about 10^4 to about 10^8. The final step of the process is removal of the rare earths from the LiCl by extraction with bismuth containing 0.05 to 0.50 mole fraction lithium. The new process does not require an electrolytic cell. This is an important advantage over the earlier reductive extraction process, which also had the disadvantage of rare-earth–thorium separation factors near 1.

The conceptual process flowsheet (Fig. 1.3) includes four contactors (or extractors) that operate at about 640°C. Fuel salt from the Pa isolation system, which is free of U and Pa but contains the rare earths at the reactor concentration, is countercurrently contacted with Bi containing approximately 0.002 mole fraction Li and 0.0025 mole fraction Th (90% of Th solubility) in contactor 1. Fractions of the rare earths transfer to the downflowing metal stream and are carried into contactor 2. Here, the Bi stream is contacted countercurrently with LiCl, and fractions of the rare earths and a trace of the Th transfer to the LiCl. The resulting LiCl stream is routed to contactor 4, where it is contacted with a Bi solution having an Li concentration of 0.05 mole fraction for removal of trivalent rare earths. About 2% of the LiCl is routed to contactor 3, where it is contacted with a Bi solution having an Li concentration of 0.5 mole fraction for removal of divalent rare earths (Sm and Eu) and the alkaline earths (Ba and Sr).

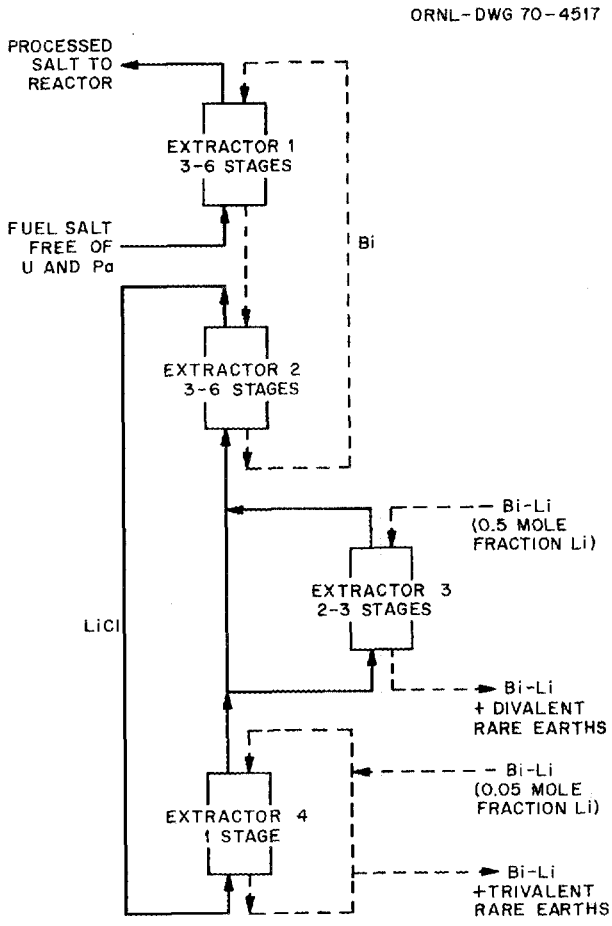

Fig. 1.3. Metal-Transfer Process for Removal of Rare Earths from a Single-Fluid MSBR.

The LiCl from contactors 3 and 4 (still containing some rare earths) is then returned to contactor 2.

Calculations were made to identify the important system parameters. It was found that there is considerable latitude in choosing operating conditions which will yield a stated removal time. The number of stages required in the contactors is low: less than 6 in contactors 1 and 2, 3 or less in contactor 3, and 1 in contactor 4. The process appears to be essentially insensitive to minor variations in operating conditions such as flow ratios, reductant concentrations, and temperature. The required salt and bismuth flow rates depend on the desired rare-earth removal times. Earlier in this section, we discussed a flowsheet and operating conditions that result in an effective rare-earth removal time of about 25 days, although the actual removal times for the various rare earths range from 15 to 50 days.

Material Balance Calculations for the Reactor System

MATADOR,[1] a computer code for calculating material balances at steady state, has been used to determine the effects of a number of processing plant variables on the nuclear performance of a molten-salt breeder reactor (MSBR). Calculations were made for a processing plant with a 50-day removal time for rare earths and halogens, a 3-day protactinium cycle time, and a 50-sec noble gas and noble metal stripping time. The investigated variables include the fuel salt discard cycle time, the zirconium and seminoble metal removal time, and the protactinium removal efficiency. The reactor under consideration was a single-fluid 2250-Mw (thermal) MSBR containing 1680 ft^3 of salt of nominal composition 71.7-16.0-12.0-0.3 mole % LiF-BeF_2-ThF_4-UF_4. Calculations were also made to show the effect of removing individual fission products; in this case, the calculations assumed a 2250-Mw(thermal) MSBR fueled with 1220 ft^3 of salt of nominal composition 67.7-20.0-12.0-0.3 mole % LiF-BeF_2-ThF_4-UF_4.

Fuel Salt Discard Cycle. – In the previous reference flowsheet for MSBR processing, discard of salt was the only mechanism designated for removal of the elements Rb, Cs, Zr, and Ba from the fuel salt. An investigation was made of the effect of the fuel salt discard cycle on the neutron poisoning by these materials. Over the range of discard times from 800 to 3000 days, the "lumped" fission product poisoning increased from 1.65 to 1.71 absorptions per fissile absorption, an

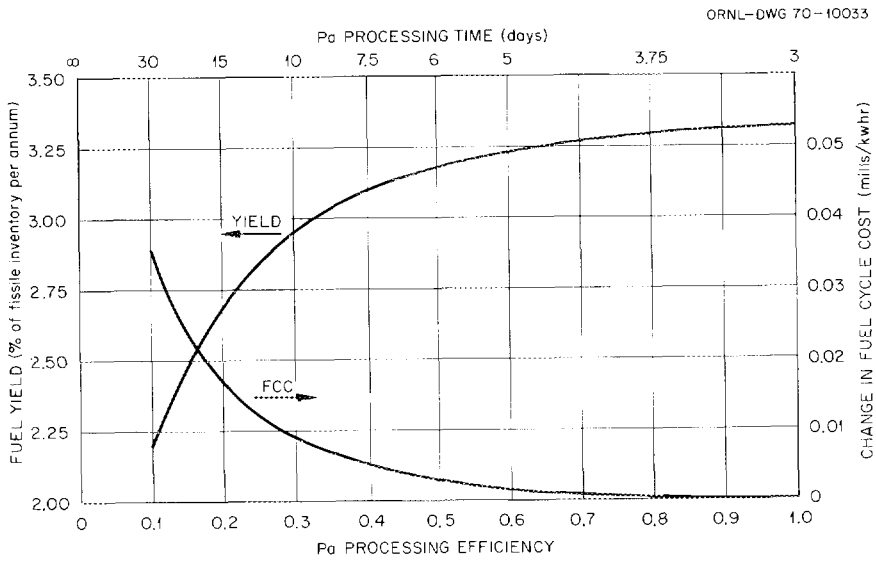

Fig. 1.4. MSBR Performance as a Function of Protactinium Processing Efficiency.

increase of less than 4%.[2] The increase in fuel cycle cost due to this loss in breeding gain is small as compared with the cost of the fuel salt itself, which indicates that a 3000-day discard cycle is economical. Longer cycle times are not possible since the solubility limit of the rare earths in the waste salt leaving the processing plant would be exceeded. A 3000-day discard cycle, corresponding to a salt discard rate of 0.4 ft^3/day, costs approximately $250,000 annually; further processing of this stream to recover the carrier salt may be economical.

Zirconium and Seminoble Metal Removal. – Because fission product zirconium is very similar in chemical behavior to uranium, an additional processing step is required for its removal from the fuel salt. An investigation was made to determine the removal time required to maintain neutron absorptions by zirconium at an acceptably low level. Zirconium poison fractions of 0.0095, 0.0388, and 0.52 absorption per fissile absorption were calculated from removal times of 50, 200, and 800 days respectively. A removal time of 200 days, which appears to be satisfactory, would require the continuous processing of 1.5% of the circulating bismuth in the protactinium isolation system, or about 6.7 ft^3 of bismuth per day.

The Zr removal process will also remove corrosion products, such as Fe and Ni, and the fission products Zn, Ge, Cd, In, and Sn from the fuel salt. The fission products will be removed at the rate of 3.2 moles/day for a 200-day Zr removal time. The process stream, which will be composed primarily of isotopes of Zr (0.991 mole fraction) and Sn (0.008 mole fraction), will have a heat generation rate of 0.42 Mw.

Protactinium Removal Efficiency. – The protactinium isolation system proposed for the MSBR will not operate at 100% efficiency. Therefore, the effective protactinium removal time will be greater than the three-day process cycle time. The effects of the protactinium removal efficiency on the fuel yield and the fuel cycle cost are shown in Fig. 1.4 for removal times of 3 to 30 days. The reactor performance is seen to vary only slightly for removal times of 3 to 5 days – the expected operating range.

MSBR Off-Gas System

A series of calculations has been made to determine the production and heat generation rates of fission products expected to be present in the MSBR off-gas system. Although the majority of the volatile fission products will be carried by the helium purge stream leaving the reactor, the noble-metal fission products and the salt inventory in the rare-earth processing plant will constitute constant sources of volatile radionuclides. Table 1.1 summarizes the important sources of volatile radionuclides in an MSBR processing plant.

[2] The lumped fission product poisoning does not include a fixed poisoning of 0.005 due to ^{135}Xe.

Table 1.1. Production of Volatile Radioactive Isotopes in an MSBR Continuous Processing Plant

Isotope	Half-Life	Rate (gram-atoms/Mwd) at Which Volatile Radioactive Isotopes Are: Removed by Sparging with Helium	Evolved from Separated Noble Metals	Recovered from Fluorinator in Pa Isolation System	Evolved from Salt in Rare-Earth Processing Plant	Recovered from Fluorinator in Rare-Earth Processing Plant	Produced (Total)	Total Activity Production Rate (curies/Mwd)
^{3}H	12.26 y	4.48×10^{-7}					4.98×10^{-7}	1.41×10^{-2}
^{83m}Kr	1.86 h	1.48×10^{-5}	2.90×10^{-5}	3.82×10^{-8}	7.72×10^{-8}		4.39×10^{-5}	7.23×10^{4}
^{85m}Kr	4.4 h	8.35×10^{-5}	1.66×10^{-5}	3.80×10^{-9}	1.03×10^{-8}		1.00×10^{-4}	6.74×10^{4}
^{85}Kr	10.76 y	5.64×10^{-6}	3.81×10^{-6}	8.75×10^{-10}	2.36×10^{-9}		9.45×10^{-6}	3.06×10^{-1}
^{87}Kr	76 m	1.83×10^{-4}		3.02×10^{-9}	9.60×10^{-7}		1.83×10^{-4}	4.41×10^{5}
^{88}Kr	2.80 h	2.21×10^{-4}		1.04×10^{-9}	6.93×10^{-9}		2.21×10^{-4}	2.41×10^{5}
Total Kr[a]		8.84×10^{-4}	1.09×10^{-4}	4.70×10^{-8}	1.24×10^{-7}		9.93×10^{-4}	2.70×10^{7}
^{129}I	1.7×10^{7} y		8.35×10^{-5}	1.18×10^{-6}		2.40×10^{-7}	8.49×10^{-5}	1.74×10^{-6}
^{131}I	8.05 d		1.20×10^{-4}	1.19×10^{-6}		2.13×10^{-9}	1.21×10^{-4}	1.91×10^{3}
^{132}I	2.26 h		1.94×10^{-4}	1.43×10^{-8}			1.94×10^{-4}	2.57×10^{5}
^{133}I	20.3 h		2.30×10^{-4}	6.44×10^{-7}			2.31×10^{-4}	3.36×10^{4}
^{134}I	5.20 m		2.20×10^{-4}	3.47×10^{-8}			2.20×10^{-4}	7.63×10^{5}
^{135}I	6.68 h		2.84×10^{-5}	1.32×10^{-6}			2.97×10^{-5}	1.35×10^{4}
Total I[a]			8.74×10^{-4}	4.45×10^{-6}		8.90×10^{-7}	8.54×10^{-4}	1.07×10^{6}
^{131}Xe	11.8 d	4.89×10^{-8}	9.60×10^{-7}	9.60×10^{-9}	1.93×10^{-8}	1.70×10^{-11}	1.12×10^{-6}	1.21×10^{1}
^{133m}Xe	2.26 d	7.34×10^{-7}	5.51×10^{-6}	1.54×10^{-8}	3.14×10^{-8}		6.29×10^{-6}	3.54×10^{2}
^{133}Xe	5.27 d	2.90×10^{-5}	2.30×10^{-4}	6.44×10^{-7}	1.30×10^{-6}		2.60×10^{-4}	6.26×10^{3}
^{135m}Xe	15.6 m	4.66×10^{-5}	8.51×10^{-6}	3.96×10^{-7}	6.03×10^{-7}		5.61×10^{-5}	6.59×10^{5}
^{135}Xe	9.14 h	1.64×10^{-4}	2.84×10^{-5}	1.32×10^{-6}	2.01×10^{-6}		1.96×10^{-4}	6.49×10^{4}
Total Xe[a]		1.07×10^{-3}	7.18×10^{-4}	3.21×10^{-6}	2.52×10^{-6}	1.70×10^{-11}	1.79×10^{-3}	2.84×10^{7}

[a]Total production rates include stable isotopes not shown. Total activity includes very short-lived isotopes not shown.

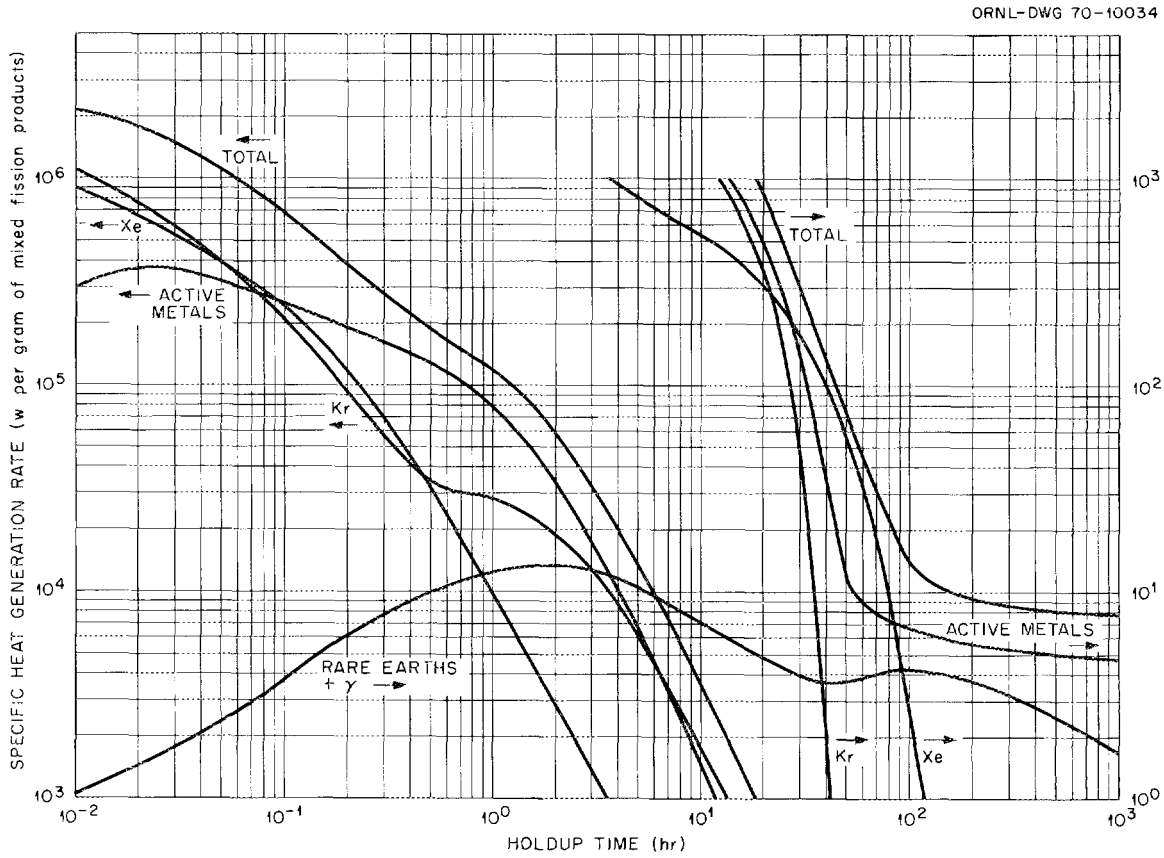

Fig. 1.5. Specific Heat Generation Rates of Noble Gases and Their Daughters as a Function of Holdup Time in a 2250-Mw (Thermal) MSBR Off-Gas System.

Calculations have also been made to study the behavior of the noble-gas and noble-metal fission product groups as a function of holdup time in the off-gas system. In these calculations, it was assumed that the two fission product groups migrated to the circulating helium bubbles with a 50-sec residence time in the fuel salt and that the helium bubbles were stripped on a 110-sec cycle. For these conditions, 500 g of noble gases and 683 g of noble metals are removed daily from the fuel salt of a 2250-Mw (thermal) MSBR. Figure 1.5 shows the specific heat generation rates of the separated noble gases and their daughters as a function of holdup time. The heat generation rate decreases rapidly from an initial value of 3.3×10^6 w per gram of mixed fission products to less than 10 w/g after one week. After the first 5 min, the active metals constitute the principal source of heat. Figure 1.6 depicts the specific heat generation rates of the noble-metal fission products (Se, Nb, Mo, Tc, Ru, Rh, Pd, Ag, and Te) and their daughters as a function of holdup time. The noble metals are removed from the reactor with an initial heat generation rate of 3.07×10^6 w/g and continue to be the single largest source of heat up to a holdup time of 3 hr, when iodine and bromine became equally important. Figure 1.6 illustrates the dependence of the design of the off-gas system on the behavior of the noble-metal smoke in the reactor. If the elements contained in this smoke plate out on metal and graphite surfaces in large quantities, thereby increasing their decay time prior to entering the off-gas system, the heat load on the off-gas system will be greatly reduced and the chemical composition of the off-gas stream will be significantly altered.

Effects of Removing Individual Fission Products. – A significant improvement in reactor performance results from the removal of certain elements, including the rare earths, Zr, Ba, and Sr. Figures 1.7–1.10 illustrate the effects of removing the four most important fission product elements – Nd, Sm, Pm, and Zr – on the performance of the reference 2250-Mw (thermal)

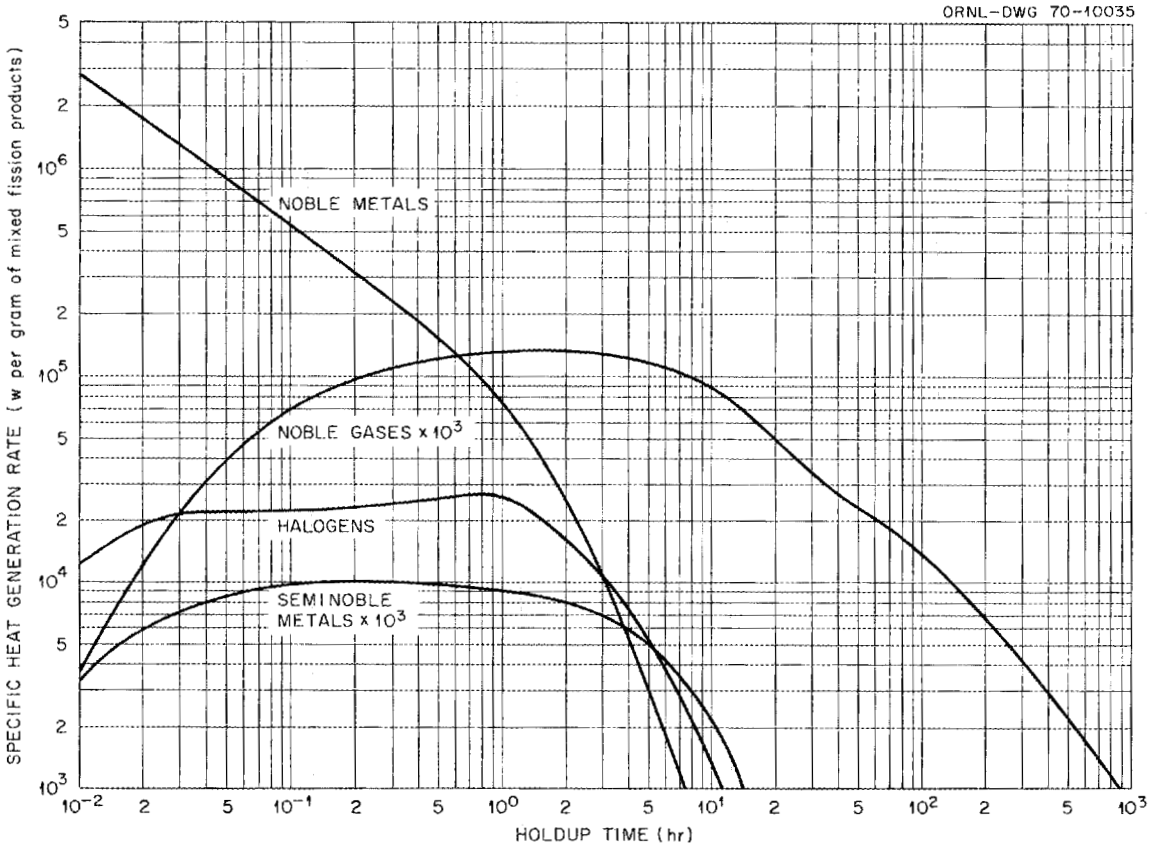

Fig. 1.6. Specific Heat Generation Rates of Noble Metals and Their Daughters Produced in a 2250-Mw (Thermal) MSBR as a Function of Decay Time.

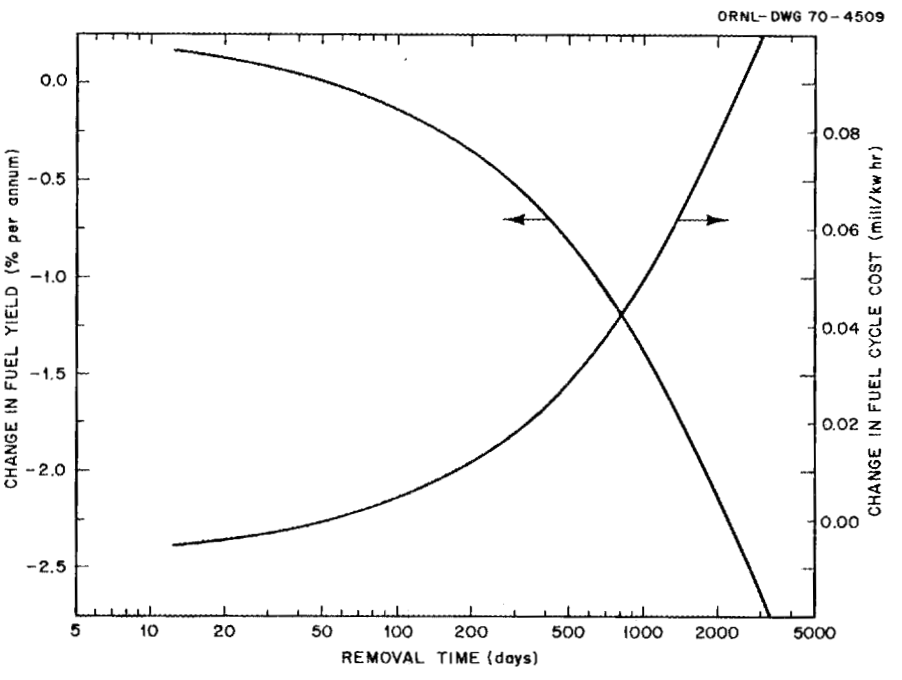

Fig. 1.7. Effect of Neodymium Removal Time on MSBR Performance.

MSBR. The changes in fuel yield and fuel cycle cost from those determined for the base case are shown as functions of element removal time. The changes in fuel cycle cost result only from changes in the inventory charges to excess fissile material that would be required if an element were removed less efficiently than in the base case. For a number of materials, primarily the noble metals, no significant variation in reactor performance was observed over the range of removal times investigated. The lack of influence of the noble metals

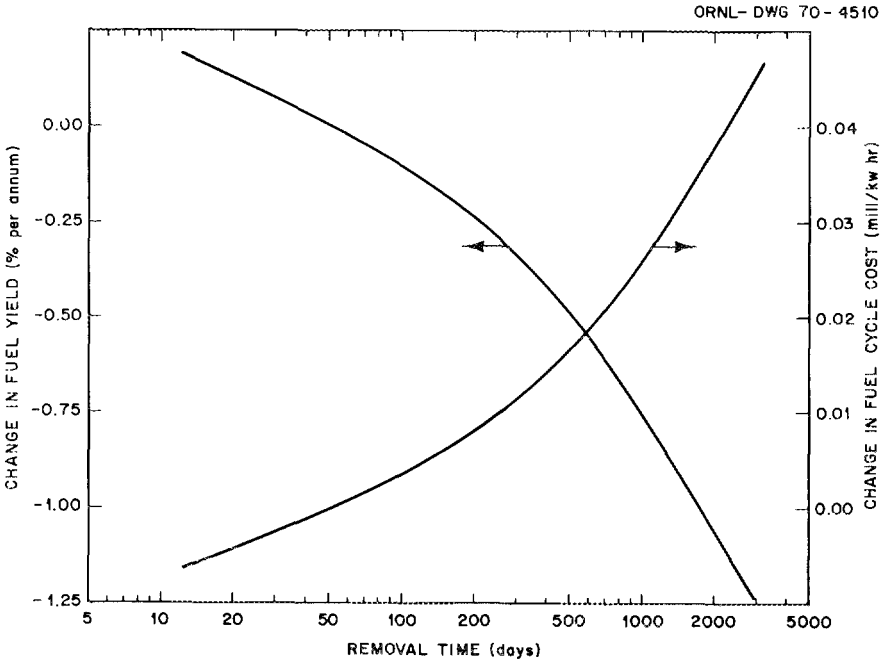

Fig. 1.8. Effect of Samarium Removal Time on MSBR Performance.

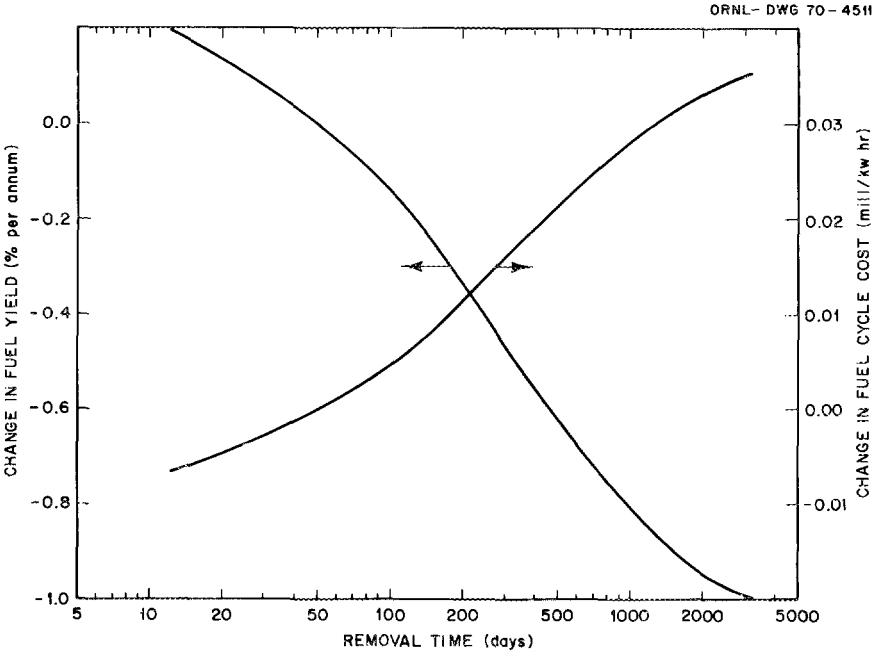

Fig. 1.9. Effect of Promethium Removal Time on MSBR Performance.

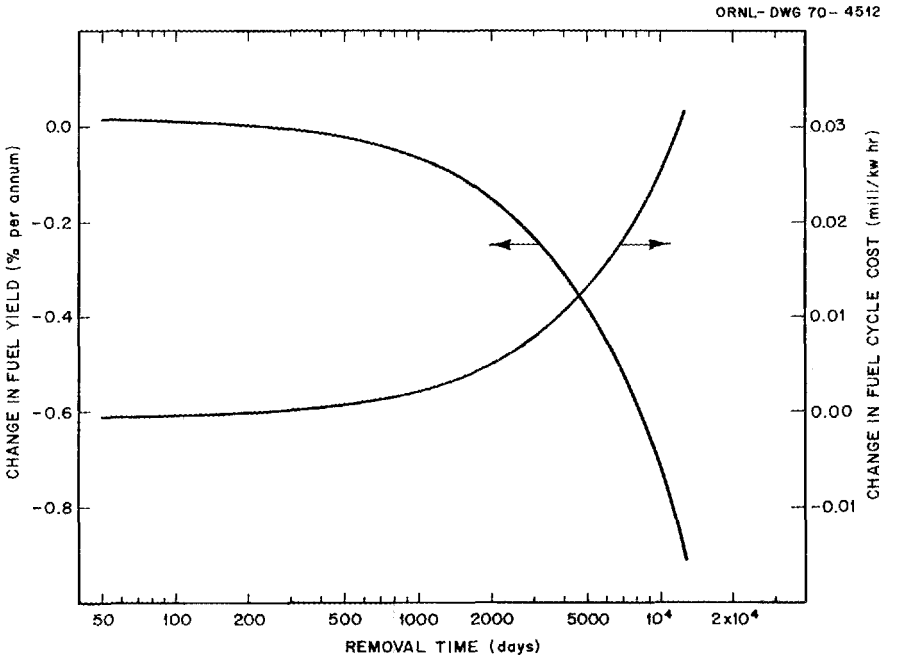

Fig. 1.10. Effect of Zirconium Removal Time on MSBR Performance.

results from the assumption that these materials are removed on a short (50-sec) cycle in the base case. However, if longer removal times were established, removal of these elements by chemical processing would become important.

1.2 MEASUREMENT OF DISTRIBUTION COEFFICIENTS IN MOLTEN SALT–METAL SYSTEMS

Laboratory development of both a metal-transfer process (Sect. 1.1) and a reductive extraction[3] technique for the processing of MSBR fuels was continued during the past year. The metal-transfer process involves the reductive extraction of rare earths and thorium from the $LiF\text{-}BeF_2\text{-}ThF_4$ fuel salt into liquid bismuth and the subsequent selective oxidative extraction of the rare earths into an acceptor salt such as LiCl or LiBr. The rare earths, and the trace of thorium present with them, are stripped from the acceptor salt by a lithium-bismuth solution in which the lithium concentration is at least 5 at. %. A rare-earth–thorium separation factor of at least 10^4 is possible by this technique. Laboratory work has consisted mainly of the measurement of the equilibrium distribution of actinide, lanthanide, and other elements between the respective molten salts and liquid bismuth solutions.

The distribution of an element M between a liquid bismuth phase and a salt containing a lithium halide (LiX) can be expressed by the general reaction

$$MX_{n(salt)} + nLi_{(Bi)} = M_{(Bi)} + nLiX_{(salt)} \,. \qquad (1)$$

At a given temperature, an equilibrium constant for reaction (1) can be written as

$$K = \frac{a_M a^n_{LiX}}{a_{MX_n} a^n_{Li}} = \frac{N_M \gamma_M N^n_{LiX} \gamma^n_{LiX}}{N_{MX_n} \gamma_{MX_n} N^n_{Li} \gamma^n_{Li}} \,, \qquad (2)$$

in which a is the activity, N denotes mole fraction, and γ is an activity coefficient referred to the pure solid or liquid. In the systems investigated, each component in the bismuth phase was present at low concentration; therefore, values of γ_M and γ_{Li} should be practically constant. In the salt phase, MX_n was either a solute present at low concentration or a major component (e.g., LiF, ThF_4, or LiCl) whose concentration was not significantly affected by the equilibria involved. Therefore, activity coefficients for the components of the salt phase would also be essentially constant. When the respective activity coefficients and N_{LiX} are constant,

[3] M. E. Whatley *et al.*, *Nucl. Appl. Technol.* 8, 170 (1970).

Eq. (2) reduces to:

$$K^* = \frac{K'}{N^n_{LiX}} = \frac{N_M}{N_{MX_n} N^n_{Li}} . \quad (3)$$

By defining the distribution coefficient as

$$D_M = \frac{N_M}{N_{MX_n}} , \quad (4)$$

Eq. (3) can be written as

$$D_M = (N^n_{Li})K^* , \quad (5)$$

or, in logarithmic form,

$$\log D_M = n \log N_{Li} + \log K^* . \quad (6)$$

Thus, if the assumptions made regarding the activity coefficients are valid, a plot of log D_M vs log N_{Li} should give a line having a slope equal to the valence of component M^{n+} in the salt phase.

Distribution Coefficients Obtained with LiCl and LiBr

The equilibrium distribution of several lanthanide and actinide elements and of barium between liquid bismuth solutions and the potential acceptor salts LiCl and LiBr has been determined. Some experiments were also conducted with an LiCl-LiF or LiBr-LiF salt phase to determine the effect of fluoride on the metal-transfer process in the event that the acceptor salt became contaminated with fuel salt.

The apparatus and general technique have been described elsewhere.[4,5] The two-phase salt-bismuth systems were contained in either molybdenum or mild-steel crucibles. In experiments with lanthanum and neodymium, dried salt and bismuth were heated together to the desired temperature under an atmosphere of pure argon; then, a small amount of thorium was added to remove residual oxide from the salt. Finally, a piece of the rare-earth metal was added to the system in an amount such that about half of the rare earth was converted to the halide and dissolved in the salt, while the other half remained in the bismuth. The rare earth in the salt was extracted into the bismuth phase in increments by the periodic addition of lithium-bismuth alloy to the system. In some experiments, barium metal was added to the system when extraction of the rare earth was practically complete, and addition of the lithium-bismuth alloy was continued. At least 4 hr was allowed for equilibration after each addition of alloy; then, a filtered sample of each phase was taken. Analyses of these samples provided the basis for the calculation of the distribution coefficients. In other experiments, bismuth and dry salt, along with the appropriate amounts of thorium and uranium metals (or samarium or europium oxide) were loaded into a molybdenum crucible. After the two-phase system had been heated to the desired temperature, the system was treated with either an HCl-H_2 or an HBr-H_2 mixture to convert the metals or oxide to their respective halides (which dissolved in the salt) and to remove residual oxygen from the system. After treatment with pure hydrogen for several hours, the system was sparged with pure argon. Extraction of the thorium, uranium, and rare earth from the salt was effected by the incremental addition of lithium-bismuth alloy to the system, using the procedure outlined above. The thorium that was used in some of the experiments had been irradiated to provide about 1 mc of ^{233}Pa. Gamma-counting of samples from these experiments produced the protactinium data presented below.

In all cases, plots of log D_M vs log N_{Li} were linear and gave the slopes expected for the respective elements. This result supports the assumptions made in the derivation of Eq. (6). Some of the distribution coefficient data obtained in these studies are shown in Figs. 1.11 and 1.12. Data obtained at 640°C for thorium, lanthanum, and samarium, using LiCl as the salt phase, are presented in Fig. 1.11 as plots of log D vs log N_{Li}. The slopes of the lines indicate that the values of n are 4, 3, and 2 for thorium, lanthanum, and samarium respectively. Plots of log D_{Pa} vs log D_{Th} and of log D_U vs log D_{Th}, using data obtained with LiCl at 640°C, are shown in Fig. 1.12. The slopes of the respective lines show that protactinium was tetravalent and that uranium was trivalent in the salt under the experimental conditions employed. Values of log K^* obtained thus far in our studies, using a variety of salts, are compiled in Table 1.2. These results show that, from a chemical standpoint, LiCl and LiBr will be equally good as acceptor salts, and that the distribution behavior of most of the elements will be rather insensitive to temperature changes.

[4] L. M. Ferris *et al.*, "Isolation of Protactinium from Single-Fluid Molten-Salt Breeder Reactor Fuels By Selecting Extraction into Li-Th-Bi Solutions," to be published in the *Proceedings of the Third International Protactinium Conference, Mittenwald, Germany, Apr. 14–19, 1969.*

[5] L. M. Ferris *et al.*, "Equilibrium Distribution of Actinide and Lanthanide Elements Between Molten Fluoride Salts and Liquid Bismuth Solutions," *J. Inorg. Nucl. Chem.* (in press).

Table 1.2. Values of log K^* Derived from Distribution Coefficient Data

$\log D = n \log N_{Li} + \log K^*$

Temperature (°C)	Salt	Element	log K^*
630	LiCl	Eu^{2+}	2.301
640	LiCl	Ba^{2+}	1.702
		La^{3+}	7.973
		Nd^{3+}	8.633
		Sm^{2+}	2.886
		Th^{4+}	15.358
		Pa^{4+}	17.838
		U^{3+}	11.278
640	LiCl-LiF (98.1-1.9 mole %)	Th^{4+}	13.974
640	LiCl-LiF (96-4 mole %)	Th^{4+}	12.90
		Pa^{4+}	14.7
		U^{3+}	10.80
640	LiCl-LiF (90-10 mole %)	La^{3+}	7.288
		Th^{4+}	11.309
600	LiCl-LiF (80-20 mole %)	La^{3+}	7.235
		Nd^{3+}	7.644
		Th^{4+}	10.964
640	LiCl-LiF (80-20 mole %)	La^{3+}	7.124
		Th^{4+}	10.629
700	LiCl-LiF (80-20 mole %)	Nd^{3+}	6.732
		Th^{4+}	9.602
575	LiBr	Ba^{2+}	1.497
600	LiBr	Ba^{2+}	1.443
		La^{3+}	9.079
		Nd^{3+}	8.919
		Th^{4+}	16.16
640	LiBr	La^{3+}	8.266
		Nd^{3+}	8.834
650	LiBr	Ba^{2+}	1.358
700	LiBr	Ba^{2+}	1.316
		Nd^{3+}	8.430
600	LiBr-LiF (90-10 mole %)	La^{3+}	8.158
		Th^{4+}	12.380
600	LiBr-LiF (80-20 mole %)	La^{3+}	7.840
		Th^{4+}	11.373

Inspection of the data in Table 1.2 reveals that the presence of fluoride in either LiCl or LiBr causes a change in distribution behavior, particularly that of thorium. This is illustrated by the data obtained for thorium and lanthanum in LiCl-LiF and LiBr-LiF solutions at 640 and 600°C respectively (Fig. 1.13). These data show that the thorium-lanthanum separation factor would be decreased if the acceptor salt became contaminated with LiF-BeF_2-ThF_4 fuel salt.

Distribution Coefficients Obtained with Fluoride Salts

Measurement of the distribution of various elements between fluoride salts and liquid bismuth solutions has

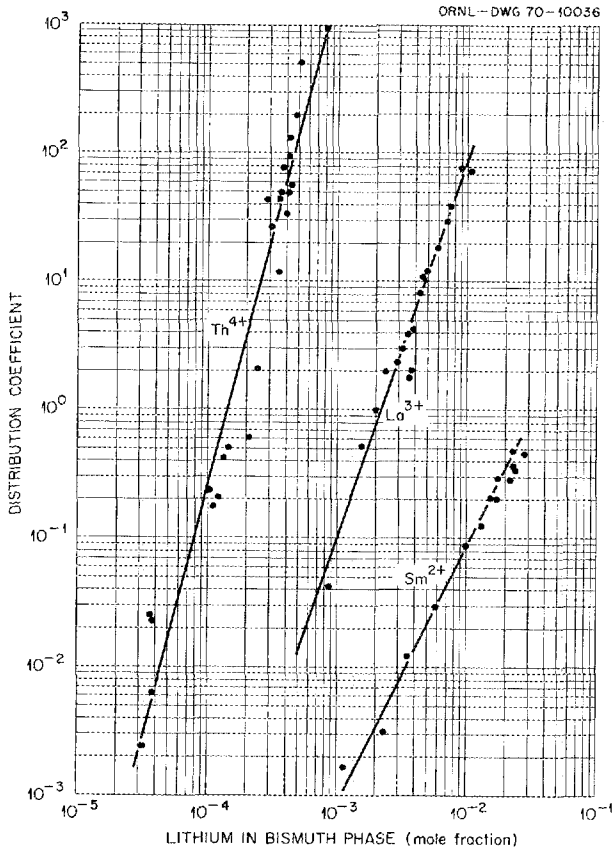

Fig. 1.11. Equilibrium Distribution of Thorium, Lanthanum, and Samarium Between Molten LiCl and Liquid Bismuth Solutions at 640°C.

been continued in support of both the reductive extraction process[3] and the metal-transfer process (Sect. 1.1). The apparatus and experimental technique have been described elsewhere.[4,5] Distribution coefficients for barium were determined at 600 to 690°C, using LiF-BeF_2-ThF_4 (72-16-12 mole %) as the salt phase. The data at each temperature could be expressed as $\log D_{Ba} = 2 \log N_{Li} + \log K^*$. The values obtained for $\log K^*$ are as follows:

Temperature (°C)	log K^*
600	4.049
645	3.678
690	3.530

The distribution coefficients measured for barium were very nearly the same as those obtained previously[5] for europium with LiF-BeF_2-ThF_4 (72-16-12 mole %). Since the distribution coefficients for barium and europium were also about the same when LiCl was used

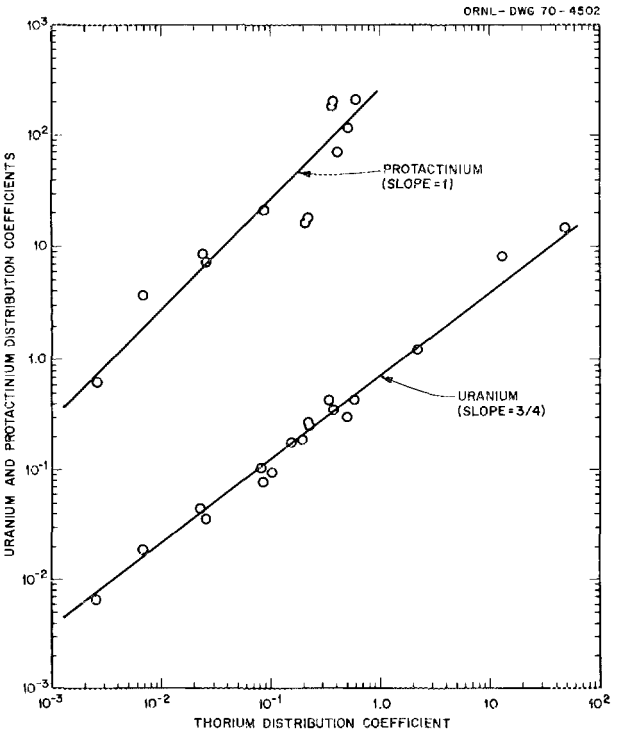

Fig. 1.12. Distribution Coefficients for Thorium, Uranium, and Protactinium Obtained with Molten LiCl and Liquid Bismuth Solutions at 640°C.

Table 1.3. Values of log K^* Obtained for Several Elements, Using LiF-BeF_2 (66.7-33.3 Mole %) as the Salt Phase

Temperature (°C)	Element	n	log K^*
600	Ba	2	4.021
600	La	3	7.452
600	Nd	3	8.347
600	Sm	2	5.101
600	Th	4	10.453
600	U	3	12.733
600	Pu	3	11.793
600	Am	2.6[a]	10.29[a]
600	Cm	3	11.00
600	Cf	3	12.00
640	Ba	2	3.728
700	La	3	6.890

[a] N_{Li} between 10^{-4} and 10^{-3}.

as the salt phase (Table 1.2), the behavior of these two elements in the reductive extraction and metal-transfer processes is expected to be nearly identical.

Additional distribution coefficient data were obtained with LiF-BeF_2 (66.7-33.3 mole %) since this salt was once considered as an acceptor in a metal-transfer

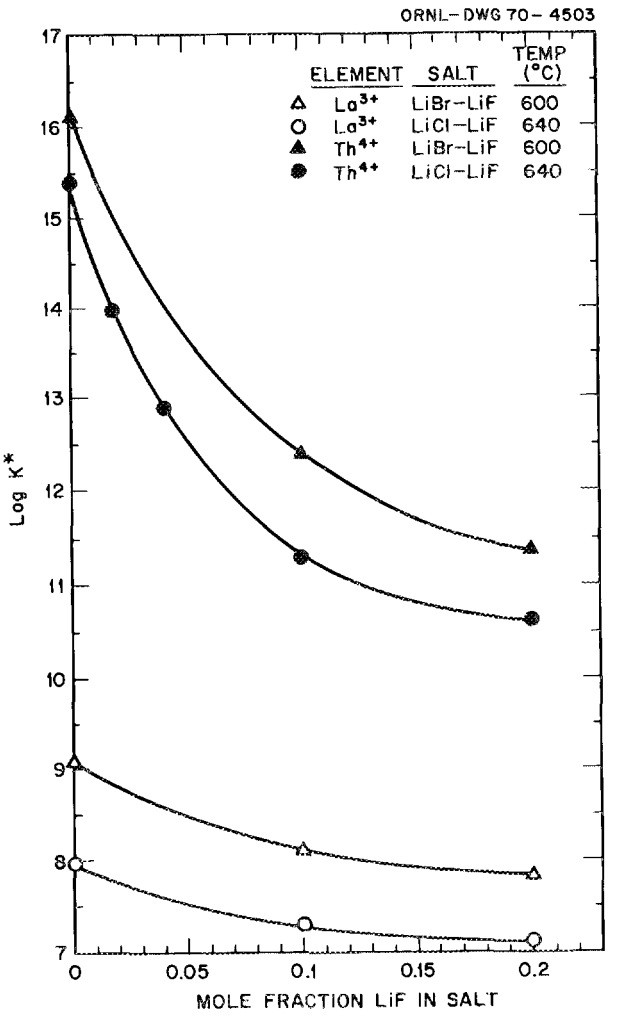

Fig. 1.13., Values of log K^* for Lanthanum and Thorium Obtained with LiBr-LiF and LiCl-LiF Solutions.

system.[6] Data for uranium, thorium, protactinium, and europium at 600°C have been reported elsewhere.[4-6] Values of log K^* determined for other elements are given in Table 1.3. In the experiments involving the transuranium elements, each element except americium was found to exist in the salt phase primarily as a trivalent species. Apparently, both Am(II) and Am(III) were present under the experimental conditions employed. This is best illustrated by comparing the behavior of americium with that of curium. A plot of log D_{Cm} vs log N_{Li} yielded a line having a slope very close to 3 (Fig. 1.14), whereas a similar plot indicated that the apparent valence of the americium species in

[6] *Chem. Technol. Div. Ann. Progr. Rept. May 31, 1969,* ORNL-4422, p. 25.

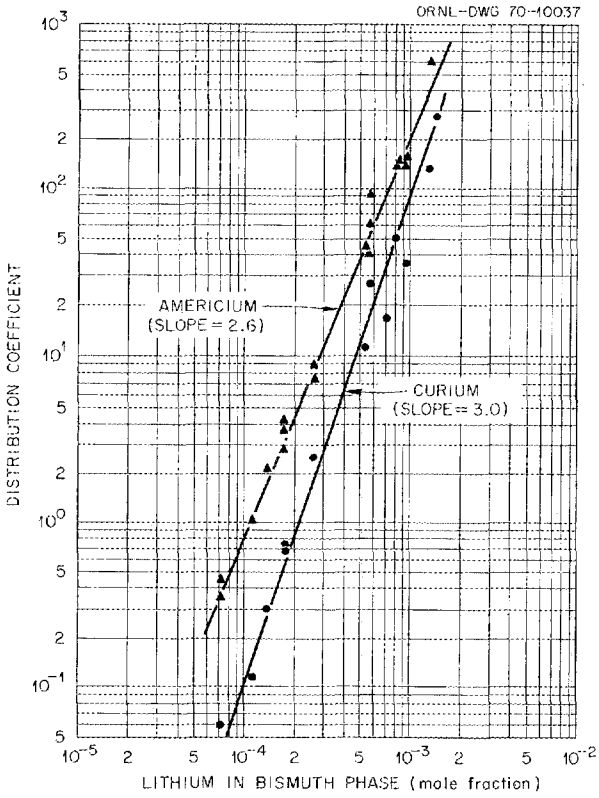

Fig. 1.14. Equilibrium Distribution of Americium and Curium Between Liquid Bismuth Solutions and LiF-BeF$_2$ (66.7-33.3 Mole %) at 600°C.

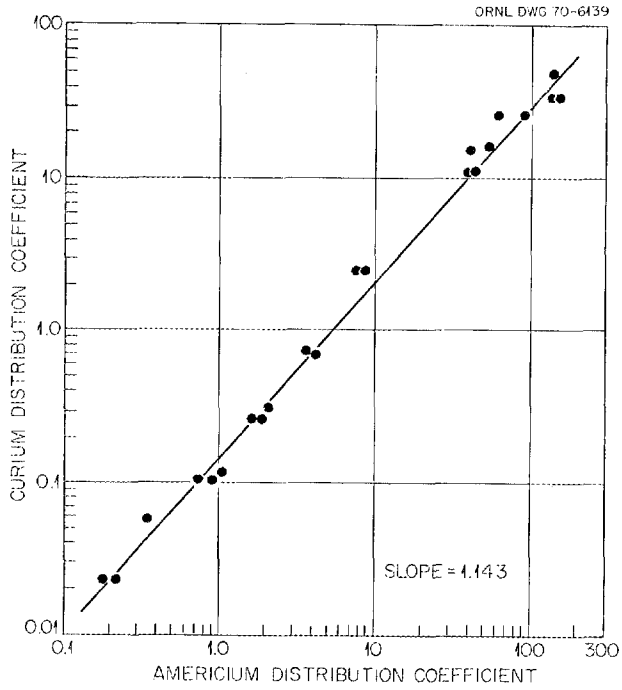

Fig. 1.15. Distribution Coefficients for Curium and Americium, Using LiF-BeF$_2$ (66.7-33.3 Mole %) as the Salt Phase at 600°C.

the salt was about 2.6 (Fig. 1.14). The existence of Am(II) in the salt phase was also indicated by a plot of $\log D_{Cm}$ vs $\log D_{Am}$; this plot (Fig. 1.15) gave a line of slope 1.143, which also corresponds to an apparent americium valence of 2.6, assuming that curium is trivalent. The distribution coefficients for plutonium, americium, and californium were all about equal, and were about a factor of 10 higher than those for curium, other conditions being the same.

The general behavior of these transuranium elements is very similar to that observed when LiF-BeF$_2$-ThF$_4$ (72-16-12 mole %) was used as the salt phase.[5]

Estimated Free Energies of Formation of Some Lanthanide and Actinide Fluorides, Using Distribution Coefficient Data

Reaction (1) for the distribution of an element between a liquid bismuth phase and an LiF-containing salt phase can be written as

$$MF_{n(salt)} + nLi_{(Bi)} = M_{(Bi)} + nLiF_{(salt)} \,. \qquad (7)$$

The Gibbs standard free energy change for reaction (7) is

$$\Delta G^\circ = n\,\Delta G^f_{LiF} - \Delta G^f_{MF_n} = -(2.3RT)\log K \,. \qquad (8)$$

From Eqs. (2) and (3), we obtain:

$$\log K = \log K^* + \log \gamma_M + n \log N_{LiF} + n \log \gamma_{LiF} - \log \gamma_{MF_n} - n \log \gamma_{Li} \,. \qquad (9)$$

Substituting Eq. (9) into Eq. (8) and rearranging gives

$$\Delta G^f_{MF_n} = n\,\Delta G^f_{LiF} + (2.3RT)(\log K^* + \log \gamma_M + n \log N_{LiF} + n \log \gamma_{LiF} - \log \gamma_{MF_n} - n \log \gamma_{Li}) \,. \qquad (10)$$

Values of $\log K^*$ have been obtained for several elements using LiF-BeF$_2$ (66.7-33.3 mole %) as the salt phase (Table 1.3). Other data necessary for the estimation of ΔG^f for LaF$_3$, ThF$_4$, UF$_3$, and PuF$_3$ are available in the literature. Values of ΔG^f_{LiF} are given in

Table 1.4. Estimated Free Energies of Formation, Using Values of log K^* Obtained with $LiF-BeF_2$ (66.7-33.3 Mole %)

Compound	Temperature (°C)	$-\Delta G^f$ (kcal/mole)	
		This work	Literature
LaF_3	600	362	366 (ref. 18)
LaF_3	700	355	360 (ref. 18)
ThF_4	600	436	441 (ref. 19)
UF_3	600	310	313 (ref. 18)
PuF_3	600	328	337 (ref. 20)

the JANAF tables.[7] Values for γ_M were taken from the following sources: (1) γ_{Li} from Foster *et al.*,[8] (2) γ_{La} from Kober *et al.*;[9] (3) γ_U from Lebedev *et al.*;[10] (4) γ_{Pu} from Lebedev *et al.*;[11] and (5) γ_{Th} from Brookhaven National Laboratory data as correlated by Ferris.[12] Activity coefficients for components in the salt phase can be estimated from the following sources: (1) γ_{LiF} from Hitch and Baes;[13] (2) γ_{LaF_3} from solubility data reported by Strehlow *et al.*;[14] (3) γ_{UF_3} from solubility data reported by Shaffer *et al.*;[15] (4) γ_{PuF_3} from solubility data obtained by Mailen *et al.*;[16] and (5) γ_{ThF_4} by assuming it to be the same as γ_{UF_4} as given by Long and Blankenship.[17] The estimated values of ΔG^f, along with recently reported values from other sources,[18-20] are given in Table 1.4.

1.3 OTHER CHEMICAL DEVELOPMENT STUDIES

In the chemical processing of MSBR fuel by either the reductive extraction or the metal-transfer process, the fuel salt will be contacted with liquid bismuth. Nickel-base alloys are corroded by bismuth; therefore, the presence of bismuth in the fuel salt could cause serious damage to a reactor vessel constructed of Hastelloy N. It follows, then, that a means for returning bismuth-free fuel salt to the reactor must be devised in order to prevent possible corrosion of the reactor vessel. The potential problems involved in a bismuth-removal method would be easier to define if we could determine the solubility of bismuth in MSBR fuel salt. Toward this end, we conducted an experiment in which we attempted to measure the solubility of bismuth in $LiF-BeF_2-ThF_4$ (72-16-12 mole %). About 125 g of salt and 5 g of bismuth were heated to 700°C in a mild-steel container, with the system under an atmosphere of purified argon. Filtered samples of the salt were taken periodically. These samples were analyzed for bismuth by both a polarographic method and a spectroscopic method. After 75 days at 700°C the system was cooled to 600°C and held for an additional 35 days. Although the analytical data obtained[21] were erratic and inconsistent, it is obvious that the solubility of bismuth in the salt was low (<5 ppm) under the conditions of the experiment. The cause of the disparity between the two analytical methods is not known and must be found before meaningful data can be obtained.

Bismuth trifluoride is expected to be produced at the anode in the electrolytic cells required for the reductive extraction process.[3] Therefore, information on the solubility of BiF_3 in molten fluoride salts and on the corrosiveness of salts containing BiF_3 is desirable. In preliminary experiments,[21] we have found BiF_3 to have a solubility of at least 4 mole % in both $LiF-BeF_2$ (66.7-33.3 mole %) and in $LiF-BeF_2-ThF_4$ (72-16-12 mole %) at 600°C. Graphite was the only material we

[7] *JANAF (Joint Army-Navy-Air Force) Interim Thermochemical Tables,* Thermal Research Laboratory, Dow Chemical Co., Midland, Mich., 1965.

[8] M. S. Foster, S. E. Wood, and C. E. Crouthamel, *Inorg. Chem.* 3, 1428 (1964).

[9] V. I. Kober, V. A. Lebedev, I. F. Nichkov, and S. P. Raspopin, *Zh. Fiz. Khim.* 42, 686 (1968).

[10] V. A. Lebedev, I. F. Nichkov, and S. P. Raspopin, *Zh. Fiz. Khim.* 42, 690 (1968).

[11] V. A. Lebedev, L. G. Babikov, S. K. Vavilov, I. F. Nichkov, S. P. Raspopin, and O. V. Skiba, *Soviet J. At. Energy (English Transl.)* 27, 59 (1969).

[12] L. M. Ferris, *Some Aspects of the Thermodynamics of the Extraction of Uranium, Thorium, and Rare Earths from Molten LiF-BeF₂ into Liquid Li-Bi Solutions,* ORNL-TM-2486 (March 1969).

[13] B. F. Hitch and C. F. Baes, Jr., *Inorg. Chem.* 8, 201 (1969).

[14] R. A. Strehlow, W. T. Ward, G. M. Watson, and W. R. Grimes, *Reactor Chem. Div. Ann. Progr. Rept. Jan. 31, 1960,* ORNL-2931, p. 78.

[15] J. H. Shaffer *et al., Reactor Chem. Div. Ann. Progr. Rept. Jan. 31, 1964,* ORNL-3591, p. 50.

[16] J. C. Mailen, F. J. Smith, and L. M. Ferris, *MSR Program Semiann. Progr. Rept. Aug. 31, 1969,* ORNL-4449, p. 219.

[17] G. Long and F. F. Blankenship, *The Stability of Uranium Trifluoride. Part II. Stability in Molten Fluoride Solution,* ORNL-TM-2065 (November 1969).

[18] C. F. Baes, Jr., "The Chemistry and Thermodynamics of Molten Salt Reactor Fuels," p. 617 in *Nuclear Metallurgy,* vol. 15, ed. by P. Chiotti, CONF-690801 (1969).

[19] D. Brown, *Halides of the Lanthanides and Actinides,* p. 244, Wiley, New York, 1968.

[20] C. F. Baes, Jr., C. E. Bamberger, and R. G. Ross, private communication, March 1970.

[21] *MSR Program Semiann. Progr. Rept. Feb. 28, 1970,* ORNL-4548.

Table 1.5. Results of Experiment Made to Test the Solubility of BiF_3 in $LiF-BeF_2$ (66.7-33.3 Mole %)

Sample No.[a]	Temp (°C)	Cumulative Time of Expt (hr)	Time at Indicated Temp (hr)	Analyses of Samples (wt %)		Cumulative Time of Exposure to Molybdenum (min)
				Bismuth	Molybdenum	
1	605	28.5	28.5	29.6		10
2	550	41.25	12.75	20.2		170
3	497	124.75	83.5	20.3		195
4	524	145.75	21.0	20.8		491
5	578	163.75	18.0	19.5		541
6	600	187.75	24.0	13.3	2.22	613
	600	196.0[b]	8.25[b]			1108[b]

[a]In chronological sequence.
[b]Thermowell penetrated at this time, and experiment was terminated.

tested that was not rapidly attacked by BiF_3 dissolved in the salt solution.

The BiF_3 used in these experiments was prepared from commercial BiF_3, which had the approximate composition BiF_3-BiOF (62-38 mole %). Treatment of this material with gaseous HF, first, for about 18 hr at 150°C and, then, for 5 to 6 hr at 500°C, resulted in a product that contained less than 3 mole % BiOF. The weight increase during the HF treatment agreed well with that calculated from the initial and final oxygen analyses of the material. Other chemical analyses showed that the F/Bi atom ratio increased from about 2.3 to 3.0 during hydrofluorination. The product had a melting point higher than 700°C and did not attack graphite. When the HF treatment was conducted in a platinum vessel, a small amount of metallic bismuth was formed and the platinum became very brittle. Embrittlement of platinum by BiF_3 has been observed previously.[22]

Two experiments were conducted to obtain information on the solubility of BiF_3 in molten fluoride salts and to assess the corrosiveness of melts containing dissolved BiF_3. In the first experiment, BiF_3 and $LiF-BeF_2-ThF_4$ (72-16-12 mole %) were heated under argon in a graphite container to 600°C. A solution that was 20 mole % BiF_3 would have been produced if all the trifluoride had dissolved. Attempts to get filtered samples of the liquid at 600°C were futile; the stainless steel samplers were so badly corroded in only 1- to 5-min exposures that they would not function. Metallic bismuth was one of the corrosion products. When a nickel thermowell was immersed into the system, the bottom was corroded away, by reaction with BiF_3 and/or by dissolution in liquid bismuth, and salt was ejected from the tube. The frozen salt did not appear to contain metallic bismuth and had the apparent composition $LiF-BeF_2-ThF_4-BiF_3$ (68.1-14.7-11.5-5.7 mole %). The LiF/ThF_4 and LiF/BeF_2 mole ratios were 5.9 and 4.6, which are about the same as those in $LiF-BeF_2-ThF_4$ (72-16-12 mole %). The graphite container showed no visible signs of attack and underwent no significant weight change.

In the second experiment, $LiF-BeF_2$ (66.7-33.3 mole %) and enough BiF_3 to produce a solution 5.2 mole % (24 wt %) in BiF_3 were loaded into a graphite vessel and heated to 605°C under argon. After about 28 hr, a filtered sample of the liquid was taken; then, the temperature of the system was varied between 497 and 600°C, with filtered samples being withdrawn at each temperature. Molybdenum samplers were used throughout this experiment. The system was exposed to molybdenum only during sampling (less than 10 min for each sample) and during measurement of the temperature (when a molybdenum thermowell was introduced). After a slight initial decrease, the bismuth content of the solution remained constant at about 20 wt % (equivalent to about 4.1 mole % BiF_3) throughout the first part of the experiment, even when the temperature was decreased to 497°C (Table 1.5). In this part of the experiment, it was noted that the amount of metallic bismuth in the samples, although small, was increasing with the number of samples taken, that is, as the exposure to molybdenum increased. After the fifth sample had been taken, the temperature of the system was returned to 600°C and held there for 24 hr (Table 1.5). During this time, the bismuth concentration in the

[22]D. Cubicciotti, *J. Electrochem. Soc.* **115**, 1138 (1968).

salt decreased to about 13%; the amount of molybdenum found in the salt (2.2%) was only about two-thirds of that expected from the reaction $BiF_3 + Mo \rightarrow MoF_3 + Bi$. After the sixth sample had been taken, the molybdenum thermowell was immersed in the liquid. The system was maintained at 600°C for about 8 hr before the thermowell was penetrated, apparently by reaction with BiF_3.

The results of these preliminary studies lead to the following conclusions: (1) Oxygen that is present in BiF_3 as BiOF or similar compounds can be essentially removed by hydrofluorination. (2) The solubility of BiF_3 in fluoride salts, particularly $LiF\text{-}BeF_2\text{-}ThF_4$ (72-16-12 mole %), appears to be sufficiently high to permit efficient operation of the electrolytic cell required in the protactinium isolation portion of the reductive extraction process.[3] (3) Of the materials tested, graphite is the only one that was not readily attacked by fluoride melts containing BiF_3.

1.4 REDUCTIVE EXTRACTION ENGINEERING STUDIES

In spite of difficulties encountered in handling molten salt and bismuth in a carbon-steel system, eight hydrodynamic runs were made in which the two phases were contacted in an 0.82-in.-ID packed column. In the course of these experiments, some modifications were made to the original equipment[23] in order to solve problems of flow control. The original column was then replaced with a column packed with ¼-in.-diam raschig rings. Three hydrodynamic runs in the new column provided an excellent confirmation of the flooding correlation developed in work with the mercury-water system. The system is now ready to be used in mass-transfer experiments.

After completion of equipment installation, about 200 kg of bismuth was charged to the graphite crucible in the treatment vessel. The oxides present were reduced by hydrogen sparging at 650°C, and about 300 g of thorium metal was then added to convert any remaining oxide to ThO_2. Iron oxide in the system was reduced by treatment with hydrogen at 600°C, followed by transfer of the thorium-bismuth solution through the system. About 53 kg of $LiF\text{-}BeF_2\text{-}ThF_4$ (72-16-12 mole %) was charged to the treatment vessel, and the bismuth and salt were sparged at 600°C with 30% HF in hydrogen for 30 hr to remove oxides. The dissolved HF was then removed by hydrogen sparging.

As the result of flow control problems with the salt phase, plugs produced in bismuth transfer lines by the mass transfer of iron, and, in one instance, a salt leak in a transfer line, countercurrent flow of bismuth and salt through the packed column was achieved for only brief periods of time during the first few hydrodynamic experiments. The addition of a bismuth-salt separator at the low point of the salt overflow seal was effective in preventing the accumulation of bismuth, which had contributed to cyclic variations in the salt flow rate. In addition to this modification, the jackleg column used for measuring the pressure at the base of the column was provided with automatic level control. Manual control of the level had been unsatisfactory, particularly for coping with rapid changes in the salt flow caused by the cyclic accumulation of bismuth in the salt overflow loop. Flow rates in initial experiments were in the range 50 to 90 ml/min.

The formation of porous iron plugs was first detected in the transfer line carrying bismuth from the column to the bismuth catch tank. After the plugged line had been replaced, the operating temperature of the bismuth feed and catch tanks was reduced from 625°C to about 540°C in order to reduce the solubility of iron in bismuth from about 70 ppm to about 25 ppm. Resistance heaters on the bismuth feed line were capable of increasing the bismuth temperature to 600°C before it entered the column.

Mass transfer of iron by the bismuth continued to be a problem during experimental work with the original column, despite the change in the operating temperature of the bismuth feed tank. The transfer line most susceptible to iron precipitation was the bismuth drain line between the column and the bismuth sampler – a line that was normally filled with bismuth. However, iron deposits also blocked the salt line between the jackleg and the column; this line contained bismuth only during periods of cyclic salt and bismuth flow. As plugged lines were removed, they were replaced with larger-diameter tubing. In addition, following run 7, Zircaloy-2 equivalent to about 100 wt ppm zirconium in bismuth was added to the bismuth feed tank in an attempt to inhibit the mass transfer of the iron. The effectiveness of this measure has not been established because samples of the phases taken after run 8 showed that the zirconium had been oxidized from the bismuth to the salt phase.

Run 5 was the most successful run with the original column. It began with a bismuth flow of 90 ml/min, and salt flow was started about 30 min later. The pressure at the bottom of the column, as measured by the bubbler in the salt jackleg, became steady about 5

[23] *Chem. Technol. Div. Ann. Progr. Rept. May 31, 1969,* ORNL-4422, p. 32.

min after the salt jackleg filled, and remained steady for about 12 min. Then, a gradual increase in pressure, another 12-min steady period, and a second pressure increase occurred in succession. The next, and last, steady period lasted 41 min. By assuming that the pressure was predominantly due to the static pressure of both phases, a value for bismuth holdup was calculated for each of these steady periods, as shown in the table below.

Bi Flow (ml/min)	Salt Flow (ml/min)	Bi Holdup (vol %)
75	75	16
81	75	21
87	75–150	28

During the last steady period, the salt flow was doubled; however, there was apparently no change in column pressure. When the salt flow rate reached 150 ml/min (a bismuth flow rate of 87 ml/min), flooding of the column caused oscillation in the salt flow rate. A short time later, a metal chip caught in the valve that controls the level of the salt jackleg and caused even greater oscillation.

Run 6 was successful in that countercurrent flow was obtained in the column. The bismuth flow rate in the period of steady flow gradually increased from 155 ml/min to 175 ml/min and then decreased steadily to about 120 ml/min over a 30-min period. During the same period, the salt flow rate slowly oscillated from 65 to 80 ml/min. Also, during this time, the bismuth holdup, as indicated by column pressure, varied from 70 to 82% and finally decreased to 70%.

An iron plug in the bismuth exit line during run 7 caused bismuth to overflow into the salt exit line. Even after the bismuth exit line had been replaced, the flow rates for bismuth and salt continued to be intermittent (run 8), probably as a result of iron deposits in the column.

The decision to replace the column stemmed from the observed decrease in flooding rate and from the high values obtained in argon pressure drop measurements for the drained column (i.e., they were about 2.5 times those for a reference column packed with polyethylene cylinders). Radiographs of the column made before and after run 8 showed an unusually close packing arrangement of the ¼-in.-diam molybdenum cylinders, but did not clearly show the presence of dendritic iron deposits. Later, when the column was sectioned for direct examination, we found deposits in the lower half of the column. Air oxidation of the carbon-steel column was severe, amounting to a loss of about 0.050 in. of the wall thickness. High-temperature aluminum paint applied to the exterior of the column appeared to provide little protection against oxidation. Components and transfer lines that have been replaced since removal of the column have been painted with Markal CR,[24] which has been observed to be superior during cyclic tests by the Metals and Ceramics Division.

A new column, similar to the original column but packed with ¼-in.-diam molybdenum raschig rings, was installed in the system. The void fraction of the new column (84%) is much higher than that for the original column (~40%) and should permit higher flow rates and minimize the effect of a moderate amount of iron precipitation. The bismuth-salt disengaging section at each end of the column was modified to improve separation of the phases; minor improvements were made in the design of the entrainment detector located in the salt overflow loop. To serve as a base line for future diagnostic tests of the column, x rays were made of the packed section, and pressure drop measurements, using flowing argon, were made across the column.

Three successful runs have been made with the new column packed with ¼-in.-diam raschig rings. Run 9 was made to demonstrate flooding at equal flow rates of each phase. In addition, however, points were

[24] Markal CR is a product of the Markal Co., Chicago, Ill.

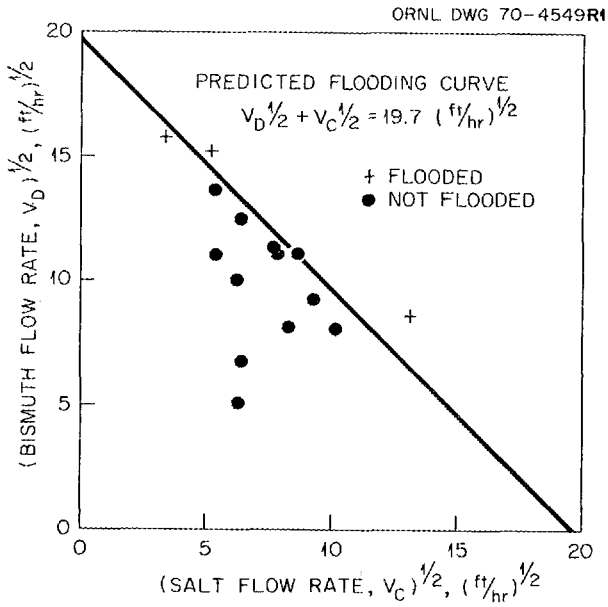

Fig. 1.16. Flooding Data for the Bismuth-Salt System, as Compared with the Flooding Curve Predicted from Data for a Mercury-Water System. Conditions: 0.824-in.-ID column packed with ¼-in.-diam raschig rings, ϵ = 0.84; temperature, 600°C; molten salt, $LiF-BeF_2-ThF_4$ (72-16-12 mole %).

obtained at both higher and lower bismuth-to-salt flow ratios. In runs 10 and 11, the salt flow was kept at a minimum (50 to 60 ml/min), while the bismuth rate was increased stepwise until a flooding point was obtained. These data provide an excellent test of a flooding correlation developed from studies with a mercury-water system (Sect. 1.6). A comparison of predicted and measured flooding data for the bismuth-salt system is shown in Fig. 1.16, where the square root of the flow rate of the dispersed phase (bismuth) is plotted against the square root of the flow rate of the continuous phase (salt). All flow conditions represented by points that lie on or above the predicted flooding line should result in a flooded system, and all points below the predicted line should represent nonflooded conditions. As may be seen, the agreement between predicted and measured values is excellent.

1.5 DEMONSTRATION OF THE METAL-TRANSFER PROCESS FOR REMOVING RARE EARTHS

Equipment has been fabricated for the demonstration and study of the metal-transfer process for removing rare earths from single-fluid MSBR fuel salt. The first series of experiments will be made in a carbon-steel vessel 24 in. high and 6 in. in diameter, as shown in Fig. 1.17. An internal partition divides the vessel into two equal-volume compartments but terminates ½ in. above the bottom to allow communication at this level. A bismuth phase saturated with thorium will fill the first

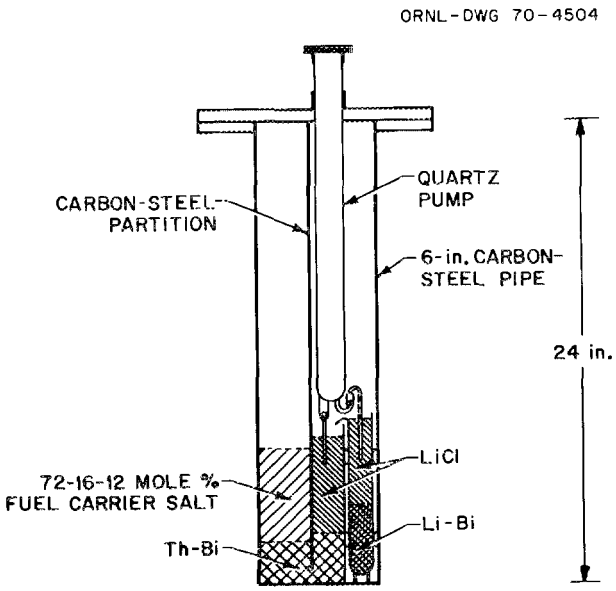

Fig. 1.17. Carbon-Steel Vessel for Use in the Metal-Transfer Experiment.

2 in. of the vessel; a fluoride salt phase (72-16-12 mole % LiF-BeF_2-ThF_4) and an LiCl phase in separate compartments, each having a depth of about 3 to 4 in., are located above the bismuth-thorium phase. The fluoride salt will initially contain about 0.3 mole % LaF_3. The compartment that holds the LiCl accommodates a double-walled carbon-steel cup, approximately 1.5 in. in diameter and 9 in. high. The inner wall of the cup is electrically insulated from the remainder of the vessel by quartz spacers. During the experiment, the cup will hold about 200 cc of bismuth containing 0.4 mole fraction lithium metal. Molten LiCl will be circulated through the cup containing the Li-Bi alloy by a pump operated with argon. Provision has been made for sampling all phases and for mixing the metal phases.

At the beginning of the experiment, the three phases in contact (fuel salt, bismuth, and LiCl) will be allowed to come to equilibrium, and samples will be taken. The LiCl will then be pumped through the reservoir containing the Li-Bi solution at the rate of about 25 cm^3/min in order to remove $LaCl_3$ from the LiCl. The stripped LiCl will overflow the reservoir cup and return to the initial LiCl volume. After a period of about 3 hr, the circulation of LiCl will be stopped, and the system will be allowed to come to equilibrium. Then, samples will again be taken. At this point, it is estimated that about 20% of the lanthanum initially present will have been transferred to the Li-Bi strip solution. The experiment will be continued until the desired fraction of the lanthanum (i.e., 50 to 90%) has been transferred to the strip solution.

Two quartz pumps with sapphire check valves have been tested for circulating molten LiCl at 650°C. The first pump was tested in LiCl that had been dried at 225°C. The pump operated successfully for a few hours, but we had difficulties with short circuits in the electrical probes and observed a gradual deterioration of the quartz that was in contact with the LiCl. After exposure to molten LiCl for about seven days, the sapphire balls used as check valves were found to be in good condition. The tungsten electrical probes were also in good condition. The electrical leakage between the probes was apparently the result of a film of LiCl that had formed over the insulators. The quartz components of the system were badly etched and, in some areas, were about ready to disintegrate. The rapid corrosion of the quartz was probably caused by the presence of moisture or other impurities (that had not been removed by heating) in the LiCl.

The second quartz pump was tested in LiCl that had been previously purified by contacting with Th-Bi at 650°C. A molybdenum cup containing Th-Bi was

placed in the bottom of the pump test vessel to further purify the LiCl. This pump has operated satisfactorily at pumping rates of 30 to 125 ml/min for seven days; at present, the test is continuing. The attack on the quartz by the LiCl has been much less severe in this test than in the previous one in which impure LiCl was used. The results obtained thus far indicate that this type of pump will be satisfactory for the metal-transfer experiment.

1.6 CONTACTOR STUDIES OF A SIMULATED MOLTEN-SALT–LIQUID BISMUTH SYSTEM

Pressure Drop, Holdup, and Flooding in Packed Columns

We are continuing to study the hydrodynamics of packed columns, using mercury and water to simulate bismuth and molten salt. Previous studies showed the desirability of using fairly large packing materials (¼ in. in diameter or greater). Packing material of this size disperses the metal phase into small droplets with high interfacial area, while smaller-size packing coalesces the metal and produces relatively low interfacial areas. The previous studies were made in a 1-in.-diam column, where ¼-in.-diam packing was the largest size that could be tested (even then, the column-to-packing-diameter ratio of 4 was not large enough to permit wall effects to be neglected).

To allow investigation of larger-size packing materials, a 2-in.-ID column was constructed, and a larger mercury pump was procured. Three packing materials have been studied in this system: ¼-in. solid cylinders, and ⅜- and ½-in.-diam raschig rings. The first two materials were tested by students from the MIT Practice School. Solid ¼-in.-diam cylinders were also tested in the 1-in.-diam column; results from the two columns are in very good agreement.

In the case of each of the three packing materials, the dispersed-phase (metal) holdup can be approximated over the wide range of flow conditions tested by use of a characteristic slip velocity, V_s, which is defined as:

$$V_s = \frac{V_d}{X} + \frac{V_c}{1-X}, \qquad (1)$$

where

V_d = superficial velocity of the dispersed phase,

V_c = superficial velocity of the continuous phase,

X = fraction of column void volume occupied by the dispersed phase.

For ¼- and ⅜-in.-diam packing, the slip velocity is related to the flooding rate as follows:

$$V_d^{1/2} + V_c^{1/2} = V_s^{1/2} . \qquad (2)$$

It appears that the flooding data for ¼-in. solid packing and for ⅜-in. raschig rings can be represented by a single curve if the superficial velocities are divided by the void fraction, as shown in Fig. 1.18. The resulting curve is linear and has a negative slope of approximately 1 when the square roots of the phase velocities are plotted against each other. These conditions correspond to a constant slip velocity at flooding. Thus far, flooding data have not been measured with ½-in. rings; however, the results are expected to correspond to a slip velocity of approximately 1600 ft/hr.

Flooding, pressure drop, and holdup in salt-bismuth systems have been estimated from the mercury-water data. The slip velocity observed for a given packing size is assumed to be proportional both to the density difference between the two phases and to the packing void fraction. The viscosity of the continuous phase has been assumed to be of little importance since the interaction between phases is believed to be largely inertial rather than viscous. The resulting flooding correlation is given by:

$$V_d^{1/2} + V_c^{1/2} = \sqrt{77\epsilon\,\Delta\rho} ,$$

where

V_d = superficial velocity of discontinuous phase, ft/hr,

V_c = superficial velocity of continuous phase, ft/hr,

ϵ = column void fraction,

$\Delta\rho$ = difference in densities of phases, g/cm^3.

A comparison of the flooding rates predicted by this relation and the values determined experimentally with a salt-bismuth system is given in Sect. 1.4. The agreement is excellent.

Axial Mixing in Packed Columns

Axial mixing can be important in evaluating the performance of reductive extraction columns, particularly with the high metal-to-salt flow ratios required in some of the proposed flowsheets. We are studying axial mixing in packed columns, using mercury and water to simulate bismuth and salt. The results obtained have been used to estimate the effect of backmixing on proposed contactors; also, tests have been made of

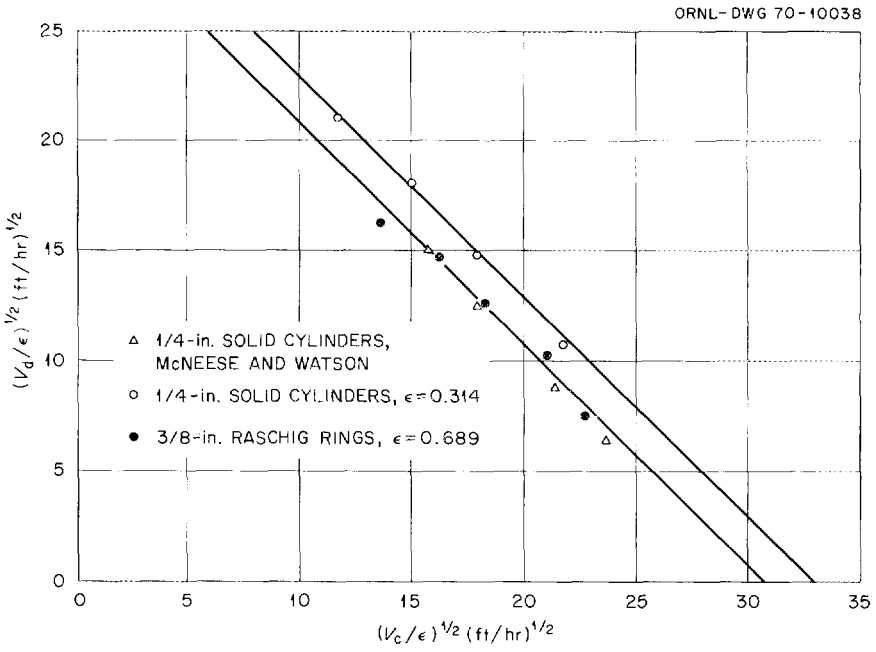

Fig. 1.18. Flooding Lines for $^1/_4$-in. Solid Cylinders and $^3/_8$-in. Raschig Rings.

ordinary packed columns modified to reduce the effect of axial mixing to an acceptable level. These studies are summarized below; details of the work are given in Sect. 17.

Axial dispersion coefficients in the continuous (water) phase were measured over a wide range of mercury and water flow rates during countercurrent flow of the two phases through columns packed with $^3/_8$-in.-diam raschig rings. No significant dependence of the dispersion coefficient on the flow rate of either phase has been found; the average value of the dispersion coefficient is approximately 3.5 cm^2/sec. This is contrary to the usual experience with conventional aqueous-organic systems in which the packing is wet by one or both phases.

A simplified method was developed to estimate the effect of axial mixing on countercurrent column performance. Column efficiency (i.e., the height of a plug flow column divided by the height of a backmixed column) is given as a simple function of common design parameters. The equation is in reasonable agreement with the complex exact solution over a wide range of operating conditions. Application of this method to the proposed flowsheets showed that axial mixing would be severe in only one proposed rare-earth removal system. Even here, however, the use of moderately effective devices to reduce axial mixing would result in reasonable column heights.

Several devices to reduce axial mixing were tested. These devices, called preventers, force the continuous (salt or water) phase through relatively small openings, where high local velocities can be achieved even when the overall flow rate of that phase is low. The amount of backflow through the devices was found to be a function of both the size of the opening through which the continuous phase flows and the velocity of this phase through the opening. Less than 15% backflow is obtained with openings up to $^3/_8$ in. in diameter. The present backflow preventers significantly reduce column capacity; however, future designs are expected to have less effect on capacity.

1.7 ELECTROLYTIC CELL DEVELOPMENT

Several of the proposed flowsheets for processing MSBR's require the use of electrolytic cells for reducing thorium and lithium into a bismuth cathode from fluoride salt mixtures bearing these materials, and for producing an oxidant (BiF_3 in molten salt) at a bismuth anode. The bismuth anode would be used to oxidize materials such as uranium, protactinium, thorium, and rare earths from a bismuth stream. An experimental program for the study and development of electrolytic cells is under way. To date, the experimental work has been carried out in static cells of various designs;

however, a facility that will allow operation of electrolytic cells under flow conditions at steady state is nearing completion.

Static-Cell Experiments

The experiments with static cells have been directed toward solving three problems concerning the electrolyzer in the reductive extraction process: (1) finding an electrically insulating material that is capable of withstanding the highly corrosive cell environment, (2) devising a method for removing the heat that is generated by the resistance losses in the salt, and (3) identifying a black material that has formed in the salt during each of the electrolysis experiments.

Because frozen salt has the required insulating properties and is also inert, experiments are being carried out to explore the potential of forming protective frozen salt films in electrolytic cells. Runs were made in which frozen films were formed along the tops of quartz and beryllium oxide electrode dividers. One experiment involved the use of an all-metal cell that required a frozen film to completely cover a cup containing the bismuth anode.

Pursuant to the heat generation problem, cell performance was evaluated with both ac and dc sources to determine whether heat-transfer studies could be carried out using an ac source; if feasible, this arrangement would eliminate the complication of electrochemical reactions encountered when dc sources are used. A graphite anode was tested to explore the possibility of using a solid anode in close proximity to the cathode. A small anode-to-cathode distance is important since this reduces the cell resistance and, in turn, the amount of heat generated.

Three experiments were made in an effort to identify the black material that forms in the salt during electrolysis. In one experiment, batteries were used to provide a constant applied voltage; the second experiment contained no bismuth in the cell; and the third experiment was carried out with no quartz present. These experiments are summarized below.

Alternating Current Experiment. – Heat generation and heat transfer are important aspects of electrolytic cell operation. The use of ac power with electrolytic cells should provide the same distribution of heat generation that will be present in cells operating with dc power and should permit the heat-transfer aspects of cell operation to be studied without the associated mass-transfer effects produced by dc power. An experiment using ac power was made in a 4-in.-diam quartz cell having semicircular bismuth electrodes, each of which had an area of 33.7 cm^2. The cell contained about 400 cm^3 each of bismuth and molten salt (66-34 mole % $LiF\text{-}BeF_2$) and was operated at temperatures from 500 to 750°C with current densities as high as 5 amp/cm^2. The measured cell resistance was the same, regardless of whether alternating or direct current was used. Although the salt was somewhat less transparent after operation with ac power, it was concluded that ac power can be used without undesirable reactions or side effects.

Graphite Anode Experiment. – The use of a solid anode, such as graphite, has potential advantages. For example, considerably more freedom in relative placement of the anode-cathode surfaces is possible; this may allow reduction of the distances separating the electrode surfaces and, hence, the heat generation.

A test was made of the feasibility of using a graphite anode in an electrolytic cell operating at a high current density. The cell consisted of a flat-bottomed 4-in.-diam quartz tube containing 6.7 kg of bismuth and 1.5 kg of molten salt (66-34 mole % $LiF\text{-}BeF_2$). The bismuth pool served as the cathode. The anode was a 1-in.-diam graphite rod located in the salt about ¼ in. from the bismuth surface. The bottom of the rod was cut at a 10° angle to facilitate disengagement of the CF_4 that formed on the graphite surface. The cathode area was 71 cm^2, and the anode area was 5 cm^2 (considering the bottom of the rod only). The operating temperature was 500°C. The cell polarized rapidly when dc voltage (15 v) was applied to the electrodes. The initial current was 45 amp (9 amp/cm^2 at the anode); however, the current rapidly decreased to 22.5 amp after 5 sec, to 4.5 amp after 17 sec, and reached a nearly constant value between 0.2 and 0.4 amp with intermittent increases in current. The cell was also operated with ac voltage to demonstrate that polarization of the anode had limited the current. The alternating current varied linearly from 12 to 260 amp for applied voltages of 1 to 20 v. It appears that a graphite anode cannot be operated at desired current densities unless a means can be found for stripping CF_4 gas from the anode surface.

All-Metal Static Cell Experiment. – The equipment for the all-metal static cell experiment has been described in detail elsewhere.[25] Briefly, the all-metal cell consisted of a cooled anode cup, which was surrounded by a 6-in.-diam annular bismuth cathode. The cup had an inside diameter of 1¾ in., an outside diameter of 2¾ in., and a total height of 2¼ in. In

[25] M. S. Lin and L. E. McNeese, *MSR Program Semiann. Progr. Rept. Feb. 28, 1969*, ORNL-4396, p. 291.

operation, a layer of frozen salt was formed on the anode container to prevent its oxidation. The cell was charged with sufficient molten salt and bismuth to produce salt and metal depths of about 4.8 and 3.5 in. respectively.

It was found that a layer of frozen salt could be formed on the anode cup and could be maintained after the cup was lowered into the bismuth cathode pool. However, the thickness of the frozen salt could not be controlled by adjusting the coolant (nitrogen and water) flow rate to the cup. Direct current was applied to the cell three times during the experiment. In the first instance, 2.6 v was applied; the cell potential was 1.5 v (as compared with 2.2 v observed in quartz cells), and the cell resistance was 0.1 ohm. The cell shorted when part of the frozen salt was melted.

In the two subsequent runs, the measured cell resistances were 1.35 and 6 ohms respectively. This variation in resistance was due mainly to the change in effective anode area. The cell potential remained at about 1.5 v for the second run but was only about 0.2 v for the last run. The high resistance and the low cell potential of the last run suggested that the anode was fully covered with frozen salt and that a small portion of the mild-steel cooling tube was unprotected. Inspection of the cell after cooling revealed that the top section of the coolant exit line had not been covered by frozen salt and had corroded through, allowing cooling water to enter the cell.

Experiment with Frozen Salt on Quartz Electrode Divider. — A test was made with a static quartz cell to assess the difficulty of maintaining a protective film of frozen salt in a region of high heat generation while part of the frozen salt was in contact with molten bismuth. A U-shaped cooling tube fabricated from $\frac{1}{4}$-in. tubing was placed about $\frac{1}{4}$ in. above the quartz divider in a 4-in.-diam quartz cell. The area of each semicircular electrode was about 30 cm^2.

With no current passing through the cell and with a purge of argon (0.1 to 0.2 scfh) in each electrode, a salt film was easily formed on the tube by using a mixture of nitrogen and water as coolant. The temperature of the salt (66-34 mole % $LiF\text{-}BeF_2$) in the cell was approximately 510°C. The frozen film was thicker at the two 90° bends than along the straight section of the tube. The thickness of frozen material decreased from about $\frac{5}{16}$ in. at the colder end of the divider to about $\frac{3}{16}$ in. at the warmer end.

With the initiation of current flow (alternating current was used to avoid the formation of BiF_3, which would react with the quartz), the molten salt turned a brownish color. With a heat generation rate of 37.5 w, the salt film was visible and appeared to be as thick ($\sim\frac{1}{4}$ in.) as with no current flow. At higher currents, the salt in the cell became opaque, and observation of the salt film was not possible. The cell was operated with heat generation rates as high as 85 w, after which the current and the coolant flow were turned off. This apparently induced thermal stresses in the quartz, and caused it to crack, allowing molten salt to flow out of the cell.

Examination of the cell after the salt had drained from it showed that a salt layer approximately $\frac{1}{2}$ in. thick remained on the coolant tube. This salt layer is believed to represent the layer present at the end of the experiment since the salt drained from the cell in less than 30 sec.

Experiment with Frozen Salt on Beryllium Oxide Electrode Divider. — The operation of an electrolytic cell should be simplified somewhat if frozen salt is not the sole source of electrical insulation and corrosion protection. For example, the two bismuth electrodes could be separated by a BeO insulator, while the small area of the BeO that might be exposed to molten salt (containing corrosive BiF_3) would be protected by a layer of frozen salt. Beryllium oxide is only slightly soluble in molten salt.

We tested a cell that used a $2\frac{1}{2}$-in.-OD beryllium oxide cup to contain bismuth for the anode and to electrically insulate the anode from the cathode. A cooling ring, made of low-carbon steel and located just above the rim of the BeO cup, was used to support the cup and to cover the rim of the cup with a protective frozen salt film. Coolant was introduced to the ring and removed from it through tubes that also served as the anode electrical lead. The anode cup, which had a cross-sectional area of about 13 cm^2, was placed in a 6-in.-diam quartz vessel containing the bismuth cathode pool. An earlier experiment with a 4-in.-diam quartz cell vessel was unsuccessful because frozen salt bridged the gap between the cooling ring and the quartz wall of the vessel. The assembled cell is shown in Fig. 1.19.

The cell was charged with 16 kg of purified bismuth and 2.4 kg of salt (66-34 mole % $LiF\text{-}BeF_2$). Two successful runs were made in which a frozen salt film was maintained on the portion of the BeO cup that was in contact with the salt. The cell was operated in such a way that an unmistakable means for detecting melting of the frozen salt film was provided; if the film melted, the cooling ring (which was in electrical contact with the anode) would contact the bismuth in the cathode pool, causing a short circuit and a very high current.

In the first run, the cell was operated with current densities of 1.5 to 1.9 amp/cm^2 (based on the initial

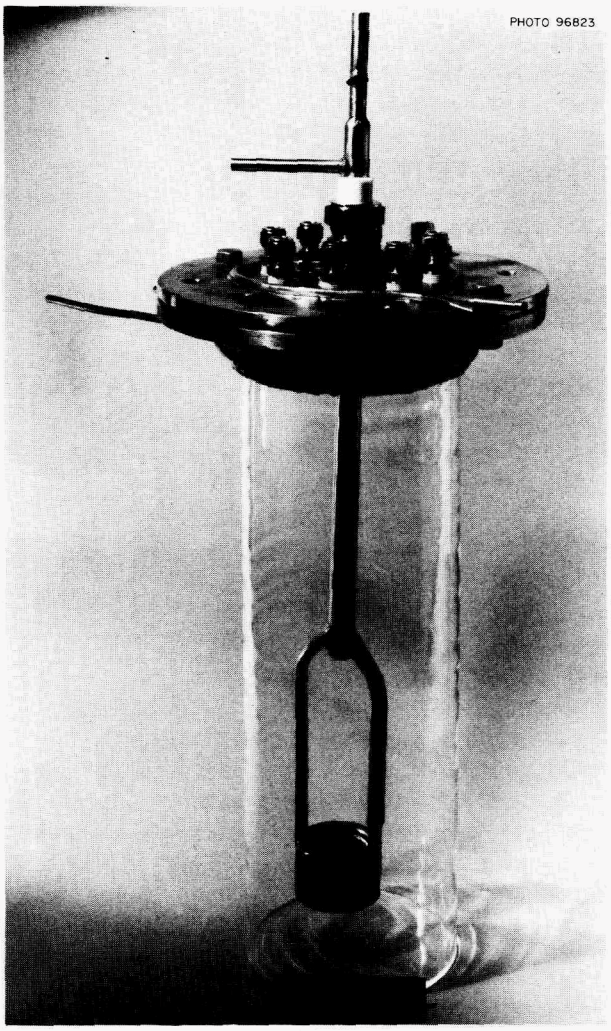

Fig. 1.19. Assembled Cell.

area of the anode) for about 1 hr. The coolant was nitrogen, and the bulk salt and bismuth temperatures were between 465 and 470°C. In the second run, the cell was operated with current densities of 1.5 to 2.8 amp/cm^2 for about 80 min. The coolant was a nitrogen-water mixture. The salt and bismuth temperatures were also 465 to 470°C in this run.

These experiments indicate that a frozen salt layer can be maintained in the presence of high current densities if sufficient cooling is provided. Also, it was found that the initial salt and bismuth temperatures must be within about 10°C of the salt liquidus temperature.

Experiment Without AC Ripple in Power Supply. – The rectifier that has supplied dc power for all the electrolysis experiments made thus far produces a direct current with appreciable ac ripple due to incomplete filtering. The ac component has been suspected to be the cause of the formation of a dark material observed in the salt since it has been reported[26] that sols of electrode metals in molten salts can be produced by the use of alternating current. A test was made to determine whether this dark material would be formed when direct current having no ac component was used. The cell used for this test was made from a 4-in.-diam quartz tube and contained a 3-in.-high quartz divider, which separated two semicylindrical bismuth electrodes having a surface area of about 30 cm^2 each. The cell contained bismuth that had been purified by H_2 sparging and molten salt (66-34 mole % LiF-BeF_2) that had been sparged with H_2 to remove residual HF. The power supply consisted of five 6-v lead-acid storage batteries, each of which was rated at 200 amp-hr.

The cell was operated initially at 500°C with a current of 3 amp. Dark-colored material could be seen rising from the anode surface, accompanied by some gas evolution; within 9 min, the salt became opaque. After standing overnight, the salt cleared up. Another run at 600°C with a current of 2 amp caused the cell to become opaque within 6 min as the result of material emanating from the anode. The salt again became clear after standing overnight.

Two additional runs were made: one at a cell temperature of 675°C and a current of 2.8 amp, and the other at a cell temperature of 680°C and a current as high as 45 amp. No dark material was formed during these runs.

The conclusions to be drawn from this experiment are: (1) that the ac ripple in the power supply is not responsible for the production of dark-colored material, and (2) the dark material may not be formed at high temperatures. This material could be a product (such as BiF_3) of the reaction of the anode with quartz in the cell. At higher temperatures, the anodic reaction product is not seen.

Experiment with Non-Bismuth Electrodes. – An experiment was made, using a 4-in.-diam quartz cell with no electrode divider, to determine whether the dark material would form in molten salt when an electrode material other than bismuth was used. In this test, two molybdenum electrodes were inserted into the molten salt (66-34 mole % LiF-BeF_2); one of the electrodes was a ¼-in.-diam molybdenum rod located in the center of the cell; the other was a ¼-in.-diam

[26] H. W. Kohn and F. F. Blankenship, *MSR Program Semiann. Progr. Rept. Aug. 31, 1968,* ORNL-4344, p. 150.

molybdenum tube, with a quartz sheath over most of its length, which was located near the side of the cell. When a direct current of 5 amp was used, the salt in the cell darkened completely within about 1 min. Although it cleared substantially overnight, we observed a few large particles of black material suspended in the salt and a scum of black material present at the salt-gas interface. When a 5-amp dc current was again passed through the salt, the salt became completely opaque within 1 min. A small amount of gas evolution was observed at the anode. We conclude that the formation of black material during electrolysis is not peculiar to the use of bismuth electrodes.

All-Metal Electrolytic Cell Experiment. – The third experiment in this series was made to determine whether dark material is formed when no quartz is present. The cell vessel in this experiment was an 18-in. section of mild-steel sched 40 pipe. One electrode consisted of a $3\frac{1}{8}$-in.-deep bismuth pool, and the other was a $\frac{1}{4}$-in.-diam mild-steel rod placed at the center of the vessel, $\frac{1}{2}$ to 1 in. above the bismuth pool. Observations in the salt phase were made using the bismuth surface as a mirror to reflect light to a sight glass in the top flange of the vessel. A $3\frac{1}{4}$-in.-deep layer of molten salt (66-34 mole % $LiF\text{-}BeF_2$) was present above the bismuth. The bismuth had been sparged at 700°C with H_2 to reduce oxides, and the salt had been sparged with H_2 to remove dissolved HF.

With the iron rod cathodic, a current of 19 to 22 amp was passed between the electrodes (a current density of 1.8 to 2.0 amp/cm^2, based on the total immersed area of the rod) for a period of 7.5 min. The cell temperature was 550°C. During the passage of electric current, no black material was seen in the salt. About 16.5 g of material, which analyzed 9 wt % Be, 17 wt % Li, and 71.8 wt % F, was deposited on the iron cathode.

The fact that the salt remained transparent in this test indicates that the presence of quartz in other cells may have played some role in the formation of black material in the salt. However, the lack of a bismuth cathode into which lithium could be reduced may have resulted in a system, in this test, that is too different from previous cells to permit firm conclusions to be drawn.

Flow Electrolytic Cell Facility

Not all of the information necessary for the design of an electrolyzer can be obtained from experiments with static cells. A measurement of current efficiency can be made most conveniently in a system in which molten salt flows through the electrolyte compartment and bismuth flows through the cathode compartment. A system for performing such an experiment, described earlier,[27] is being installed in Building 3541. The cell containment vessel, gas-lift pumps, flow measuring devices, transfer lines, and a mixer-settler tank for equilibrating the salt and bismuth streams have been fabricated, assembled, and installed in a walk-in hood. This equipment is shown in Fig. 1.20. All of the heaters and thermocouples have been attached, and the equipment has been insulated. Gas supplies, electrical power, and instrumentation for the experiment are now being installed.

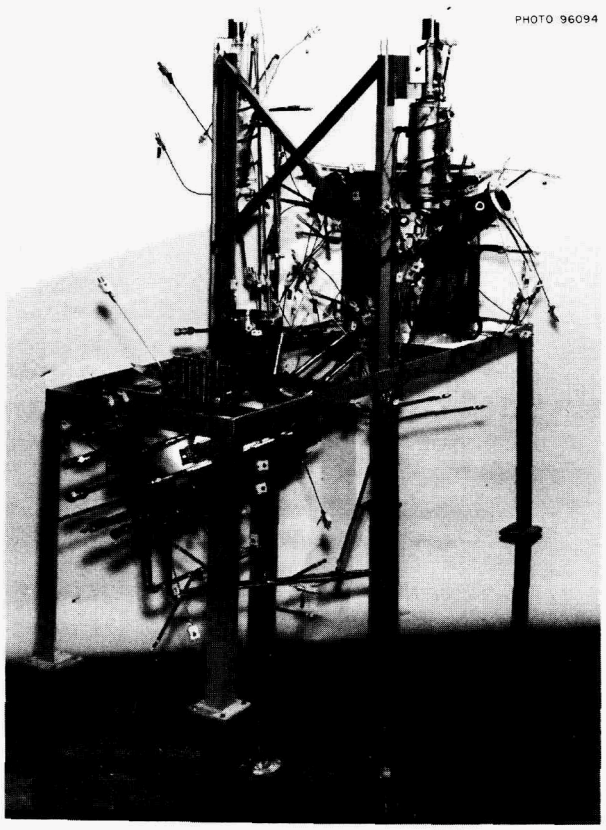

Fig. 1.20. Equipment for Experiments to Determine Current Efficiency.

A salt treatment vessel, 16 in. OD with a type 304 stainless steel outer shell and a graphite liner, is also provided.

Porous molybdenum filters are included to remove reduced iron from the purified salt and bismuth.

Salt and bismuth will be recirculated by gas-lift pumps; the flow rates will be controlled by varying the

[27] E. L. Nicholson *et al.*, *MSR Program Semiann. Progr. Rept. Feb. 28, 1969*, ORNL-4396, p. 296.

gas flow to the lift pumps. Disengagement of the gas from the liquid and damping of the flow from the lift pumps are accomplished in disengagement vessels that also act as gravity-head-type orifice flowmeters. Since these orifice flowmeters are not of standard design, experimental determination of the orifice discharge coefficient is required.

Several orifice coefficient measurements have been made with mercury and water, and three measurements have been made with bismuth for an orifice 0.3 cm in diameter. To date, the results for bismuth have shown considerable scatter.

1.8 AXIAL MIXING IN OPEN COLUMNS

Two studies of axial mixing in open bubble columns during countercurrent flow were completed by students from the MIT Practice School.[28,29] These data are important in the design of continuous fluorinators. Bautista and McNeese[30] previously reported studies of axial mixing in the same 2-in.-diam column, using air and water. The experimental technique involved photometric measurement of the steady-state concentration profile in the column of a tracer (cupric nitrate), which is fed continuously to the bottom of the column. The present study was undertaken to obtain data on the dependence of the axial dispersion coefficient on two physical properties: continuous-phase viscosity and interfacial tension.

In the first study, axial mixing was studied in a 2-in.-diam column during the countercurrent flow of air and glycerol or butanol solutions.[28] Molten salts of interest have a viscosity of about 30 centipoises; water (used in previous studies) has a viscosity of approximately 1 centipoise, and the viscosity of the glycerol solution used in this study is 15 centipoises. The surface tension of molten salts of interest is 100 to 200 dynes/cm, while the butanol solutions had surface tensions between 37.8 and that of water (72 dynes/cm).

The results of the study are summarized in Fig. 1.21, where the dispersion coefficient is shown as a function of the air flow rate. The dashed line represents the earlier results of Bautista and McNeese, who found that the data from their experiments (in which water and air were used) fall into two regions. The first region, which covers low gas rates, corresponds to conditions that

[28] A. M. Sheikh and J. D. Dearth, *Axial Mixing in an Open Bubble Column*, CEPS-X-91 (in press).

[29] A. Jeje and C. Buzzato, *Axial Mixing in an Open Bubble Column, Part II*, CEPS-X-102 (in preparation).

[30] M. S. Bautista and L. E. McNeese, *MSR Program Semiann. Progr. Rept. Aug. 31, 1969*, ORNL-4449, p. 240.

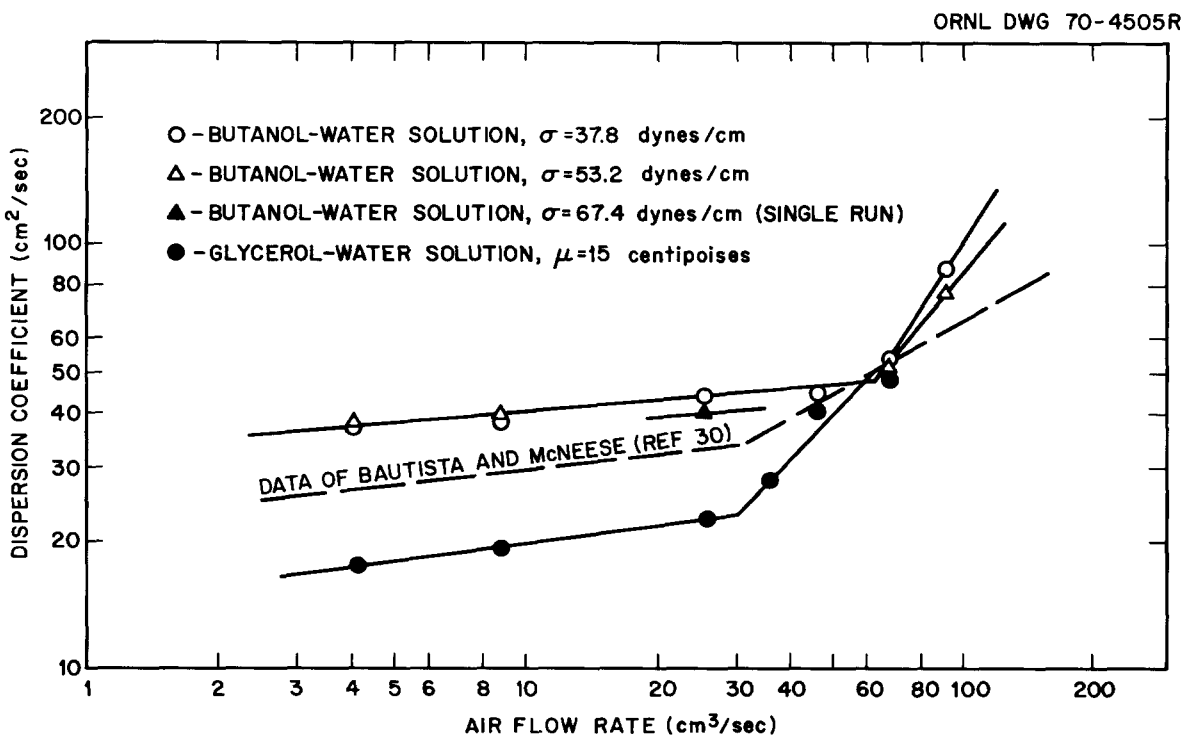

Fig. 1.21. Effects of Gas Flow Rate, Liquid-Phase Viscosity, and Surface Tension on Axial Dispersion Coefficient.

prevail when individual bubbles formed at the orifice travel up the column without coalescence. The second region, which occurs at gas flow rates above 30 cm^3/sec, corresponds to "slugging" flow.

Increasing the viscosity of the liquid phase to 15 centipoises (by adding glycerol) decreased the dispersion coefficient in the "bubble" (lower) region; however, the transition point between the regions was not changed. The coefficient increased more rapidly with air flow rate in the slugging region, at least in the area up to the Bautista-McNeese curve. Decreasing the surface tension (by adding butanol) increased the dispersion coefficient in the bubble region, although there is little difference between the data from solutions having surface tensions of 37.8 and 53.2 dynes/cm. The transition point occurred at a higher air flow rate, and the bubble-region portion of this curve intersected the slugging-region portion of the curve of Bautista and McNeese. The dependence of the dispersion coefficient on air flow rate appears to be somewhat greater in this case than when water alone was used, but more data are needed to establish such a conclusion.

This study was especially useful since it represented the first systematic attempt to vary physical properties in a bubble column. Additional studies in the future may include changes in the column and orifice diameters as well as in physical properties.

In a second study, the effects of column diameter and air inlet diameter on axial dispersion coefficient were investigated using air and water. Column diameters of 1½, 2, and 3 in., and air inlet diameters of 0.02, 0.04, and 0.085 in., were used. No effect of air inlet diameter was detected.

The Bautista-McNeese curve, shown in Fig. 1.21, was reproduced using all three air inlet diameters. The air holdup in the column was found to be independent of inlet diameter, indicating the same bubble size distribution in each case. Such behavior is expected when "chain bubbling" occurs, that is, when new bubbles are formed before old bubbles are released from the inlet tube.

Results of this study showed that the dispersion coefficient is not a strong function of column diameter. As shown in Fig. 1.22, most of the data points fell close to those of Bautista and McNeese. In the slugging region, data from the different column diameters have different slopes, which implies that the curves will diverge at higher flow rates; however, for the flow rates studied, they remain near the reference curve (for a 2-in.-diam column). At low flow rates, only the data from the 1½-in. column deviate significantly from the

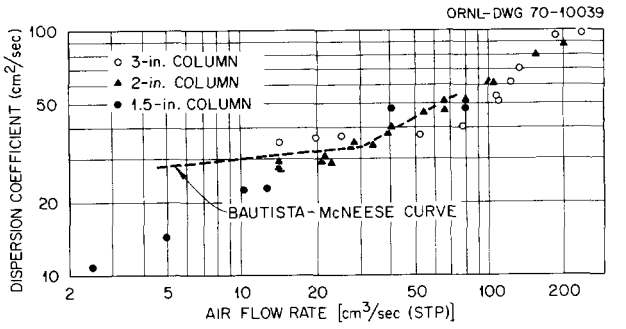

Fig. 1.22. Effect of Column Diameter on Dispersion Coefficient in an Open Column.

data for the 2-in. column. This deviation has been confirmed by runs made subsequent to the MIT study.

1.9 DEVELOPMENT OF A FROZEN-WALL FLUORINATOR

The fluorination of molten salt for removal of uranium is required at several points in processes being considered for the isolation of protactinium and the removal of rare earths. The fluorinators will be protected from corrosion by freezing a layer of salt on the metal surfaces that potentially contact both F_2 and molten salt. Although the separate aspects of such operations (continuous or batch fluorination, and frozen film formation) have been shown experimentally to be feasible, the testing of a fluorinator protected against corrosion by means of a frozen wall has been hampered by the lack of a heat generation source that is corrosion resistant. A heat source of this type will be provided in a reactor processing plant by the decay of fission products in the salt.

Radio-frequency induction heating appears to provide a suitable heat source for experimental work on fluorinator development; therefore, its use is being studied. The heat would be generated in the molten salt (a conductor) via eddy currents (induced by an alternating magnetic field) which would be generated by a coil not in contact with the molten salt. This method of generating heat in the salt has the disadvantage that heat would also be generated in the metal walls of the fluorinator, although this can be minimized by choosing a favorable geometry.

Two promising coil configurations that have been considered are illustrated in Fig. 1.23. In the first configuration (configuration I), the induction coil is located just inside the metal wall of the cylindrical fluorinator vessel and is embedded in a frozen salt film on the vessel wall. Heat would be generated by the

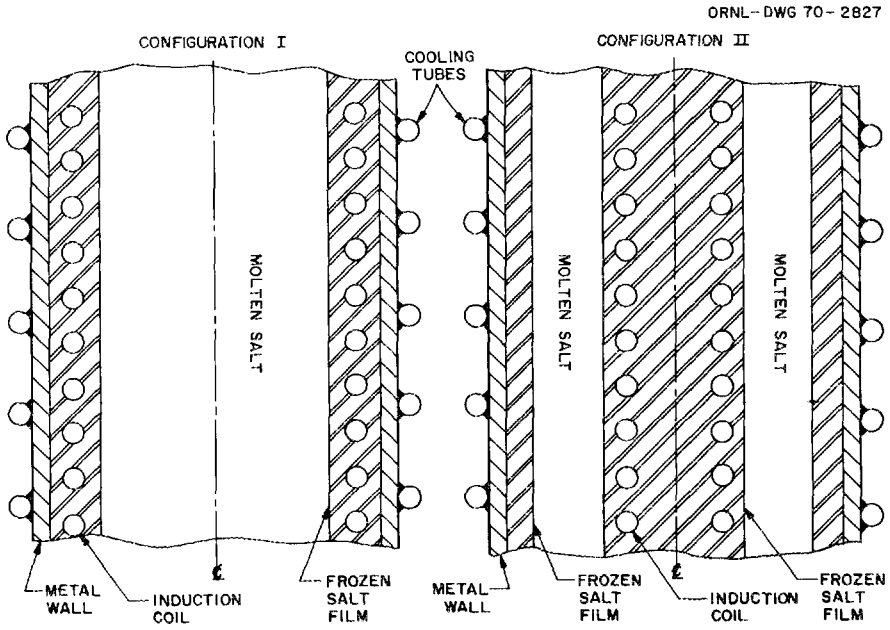

Fig. 1.23. Induction Coil Configurations for Frozen-Wall Fluorinator Tests.

magnetic field inside the coil, and neither the coil nor the vessel wall would contact the molten salt and fluorine. In the second configuration (configuration II), the induction coil would be much smaller in diameter than the fluorinator vessel and would be located at the center of the fluorinator. A coolant would be passed through the induction coil in order to cover the coil with a layer of frozen salt and thereby isolate it from contact with molten salt and fluorine. Heat would be generated in the molten salt (and in the vessel wall) by the magnetic field outside the coil. The second configuration would require a greater total heat generation rate than the first configuration since a larger area would be covered with frozen salt.

Mathematical Analysis

Initial work was directed toward a mathematical analysis of several coil configurations in order to assess the feasibility of rf heating and to identify important system parameters. Several configurations, including the two shown in Fig. 1.23, were considered.

In one configuration, the induction coil was located outside the fluorinator vessel wall, which would be relatively thin to allow power to be transmitted through it. However, it appeared that, for systems having dimensions of interest, most of the heat generation would occur in the metal wall; thus this configuration was not considered further. Since configuration I is more amenable to mathematical analysis than configuration II, it was used to derive expressions for predicting coil performance. These expressions were then used to predict the performance of the following two systems:

1. a salt system having the approximate dimensions of an experimental frozen-wall fluorinator, which will be built later, and
2. a sulfuric acid system (having properties similar to the molten salt system), which is being used to verify the derived expression and to evaluate configuration II.

The fluorinator system that was examined can be described as follows: the salt was $LiF\text{-}BeF_2\text{-}ThF_4$ (68-20-12 mole %); the inside diameter of the ¼-in.-thick vessel was 4.9 in.; the mean diameter of the induction coil was 3.9 in.; and the frozen salt extended 1.5 in. inward from the wall, covering the coil and leaving a 1.9-in.-diam molten core. The metal was assumed to have the same electrical properties as Monel. The heat generation rate (in the molten salt) required to maintain this frozen salt layer is 63 w per centimeter of fluorinator length. The calculated induction current in the coil (at an assumed frequency of 500 kHz) necessary to produce this power in the salt was 24.7 amp. The calculated I^2R loss in the induction coil was 55 w per centimeter of fluorinator length. The heat

generation rate in the pipe outside the coil was estimated by assuming that the magnetic field strength just outside the coil was equal to the magnetic field strength just inside the coil. This assumption is equivalent to assuming that the length of the coil is very small as compared with its diameter. Using this assumption, the heat generation rate in the vessel wall was calculated to be 65 w/cm (about 1.05 times the heat generated in the salt). Removal of the heat generated in the vessel wall, as well as that generated in the salt, would be practical. These calculations indicate that, for a 5-ft-long fluorinator vessel, a 28-kw rf generator would be required. Similar calculations could not be conveniently made for configuration II.

Experimental Work

In order to verify the values predicted for configuration I and to evaluate the performance of configuration II, experiments were performed in which a 29 wt % H_2SO_4 solution was used as a substitute for molten salt. Heat generation rates were measured in the acid solution and in a Monel pipe surrounding this solution. The acid solution was contained in a two-liter graduated cylinder having an inside diameter of 3¼ in. The pipe was a 6-in.-long section of 6-in. sched 40 Monel pipe. The coil for the test with configuration I was 4 in. ID by 6 in. long, and consisted of 20 turns of ¼-in.-diam copper tubing; this coil was placed around the acid container, and the 6-in. pipe was placed around the coil. The coil for configuration II was 1¼ in. OD by 6 in. long, and consisted of 20 turns of ¼-in.-diam copper tubing. It was placed in a 1⅜-in.-OD glass tube, which was immersed in the center of the acid. The heat generation rates were obtained by measuring the rate of temperature increase in the acid and in the pipe.

In three runs with configuration I, the ratio of heat generated in the pipe to that generated in the acid averaged 1.3. The frequency in the test was 350 kHz, and the conductivity of the acid was about 0.75 millimho/cm. The heat generation rate in the acid was about 19 w per centimeter of coil length; this was kept low to prevent the acid from boiling. The predicted value for the ratio of heat generated in the pipe to that generated in the acid was 0.58 (this value was calculated using the properties, conditions, and dimensions of the experimental system, and making the same assumptions that were outlined in the previous section), which is approximately one-half the measured value. Deviations of this magnitude between the predicted and measured values for the heat generation rate are not surprising since the method used for calculating heat generation in the pipe was an approximate one.

In five runs with configuration II, the ratio of heat generated in the pipe to that generated in the acid averaged 0.069. The frequency in this test was 440 kHz. The heat generation rate in the acid, using configuration II, was about 16 w per centimeter of coil length, although a higher plate voltage was used than in the experiments with configuration I. This indicates that the coupling of the magnetic field with the acid solution was poorer with configuration II than with configuration I; this is to be expected since the magnetic field strength outside a coil is smaller than that inside a coil. However, the indications are that, even though little heat was generated in the pipe walls with configuration II, the efficiency of heating the salt could still be much less than if configuration I were used, because the heat generation in the coil itself might be large as compared with heat generation in the salt. This aspect will be explored in future experiments when means to measure the coil current have been obtained.

In general, results of these preliminary experiments and calculations encourage us to believe that inductive heating is a reasonable method for supplying heat to a frozen-wall-fluorinator experiment in which there is no internal heat source resulting from fission product decay. Disagreement between the measured and the calculated values of relative heat generation rates indicates that the design of an experimental fluorinator system must rely heavily on empirically obtained relationships. An experimental program is under way to obtain this information.

1.10 DESIGN AND PREPARATION OF $^{239}PuF_3$ CAPSULES FOR SMALL REFUELING ADDITIONS TO THE MSRE

In order to provide operating experience with a molten salt reactor that had been fueled with ^{239}Pu, PuF_3 was added to the MSRE to compensate for fuel burnup. A total of 229 g of $^{239}PuF_3$ powder was charged (at the approximate rate of 5 g of plutonium per full-power day) during September and October 1969. The powder was added to the reactor in special capsules that had been loaded in Building 3019.

After considering the problems of preparing various Pu-Li-Be fluoride salt mixtures, we concluded that the direct addition of $^{239}PuF_3$ powder to the fuel salt was the preferred method. Therefore, we obtained about 1 kg of plutonium (in the form of 5-μ PuF_3 powder) from the Los Alamos Scientific Laboratory. The plutonium in this powder was 94% ^{239}Pu, 5.5% ^{240}Pu,

and 0.5% ^{241}Pu; the ^{241}Am content of the powder was 50 ppm.

The design of the capsule used in adding the powder to the reactor was based on the standard MSRE sample capsule, which has a capacity of 50 g of salt. The overall dimensions of the capsule were retained, but the capsule itself was modified by drilling twelve ¼-in.-diam holes and one ⅜-in.-diam hole on the side and the bottom respectively. (A capsule with its handling attachment is shown in Fig. 1.24.) Each hole was covered with a mechanically retained 4-mil-thick zirconium foil disk that would react with the UF_4 and dissolve in the circulating salt in the pump bowl. This would, in turn, permit the PuF_3 powder to dissolve in the fuel salt. Laboratory tests verified that dissolution would be rapid and that the solubility of PuF_3 in fuel salt was adequate even for a reactor fueled entirely with plutonium. Pressure tests of the capsule at 5 psi showed no leakage of the joint between the foil disks and the capsule wall. The capsule is vented through a sintered nickel filter positioned in a small hole in the top of the capsule to prevent a heat-induced buildup of internal pressure and premature rupturing of the foil disks prior to immersion in the salt. The capsule was designed to provide effective containment of the PuF_3 powder during shipment to the MSRE and charging into the reactor pump bowl via the sampler-enricher system.

Both a 6-ft glove box and a 3-ft glove box in Building 3019 were used for the capsule filling operation. The 6-ft glove box was divided into two sections by a plastic sheet (with a slit for passage) to provide a contamination barrier between the sections. The capsules were filled by scooping PuF_3 powder (about 1 g at a time) into them and tamping; when the filling operation was complete, the top plugs were inserted and pinned in place on the contaminated side of the box. The capsules were then wiped off and passed through to the clean side, where they were weighed and the crevices at the junction of the cap and capsule were sealed with lacquer. The sealed capsules were inserted in metal sampler-enricher transport tubes as they were bagged from the glove box. The sealed transport tubes were, in turn, bagged into the small glove box, where they were checked for exterior contamination before being individually sealed in plastic and taken to the MSRE. The capsule filling procedures were thoroughly tested, using talcum powder as a stand-in for PuF_3, before any plutonium was introduced into the glove box.

Eight capsules were filled with a total of 311 g of $^{239}PuF_3$ powder in September 1969. The first of these capsules contained 31.6 g of PuF_3. As the loading technique improved, more PuF_3 was compacted into each capsule; the last six capsules contained from 39.2 to 42.2 g of PuF_3. No problems were encountered in

PHOTO 97117

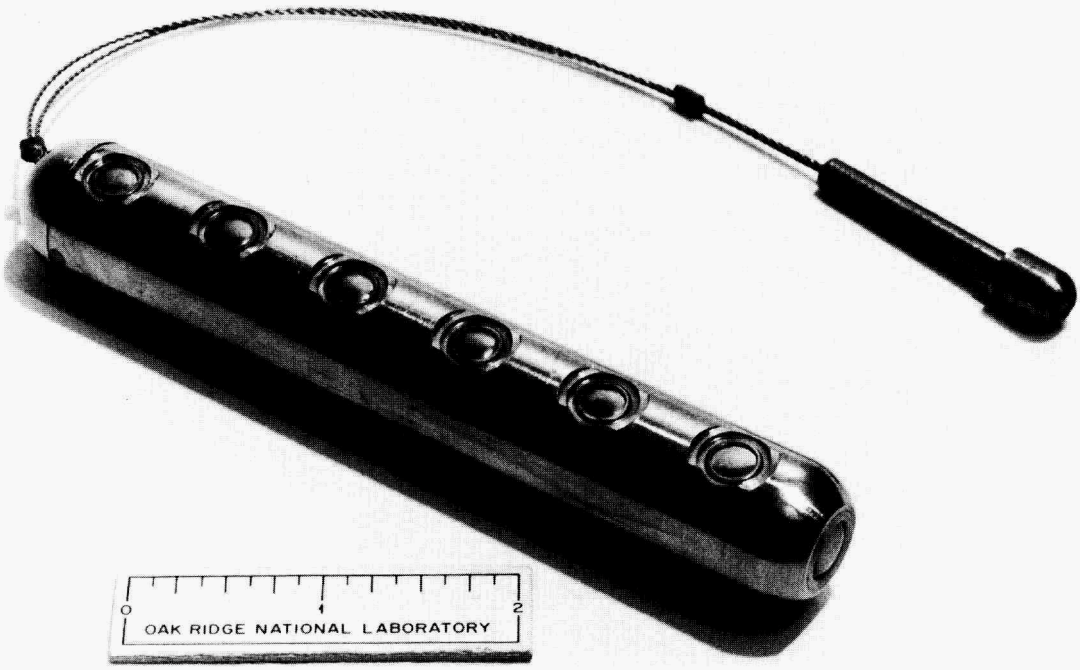

Fig. 1.24. $^{239}PuF_3$ Capsule for MSRE Refueling.

the filling operation or in packaging the capsules in the MSRE fuel sampler-enricher transport tubes. Transferable activity was removed from the exteriors of the loaded containers before they were sealed in plastic bags, and no detectable contamination escaped from the glove-box operation.

To date, six of the capsules have been added to the MSRE fuel salt. As expected, the zirconium foil "windows" of each capsule dissolved in 15 to 30 min. The time required (2 to 4 hr) for dissolving the powder was found to be dependent on the pump circulation rate, but was satisfactory in each case. The progress of the dissolution was followed via reactivity changes. Similar techniques could probably be used with much larger powder containers to add plutonium to a barren salt for use as fuel salt for the MSRE.

1.11 DISTILLATION OF MSRE FUEL CARRIER SALT

Following the nonradioactive experiments,[31] the molten-salt still was installed in the spare cell at the MSRE for demonstrating low-pressure, high-temperature distillation of the MSRE fuel carrier salt. Results of the nonradioactive tests had suggested that minor equipment changes would be advantageous for the operation at the MSRE. Accordingly, the following modifications were made: Additional thermocouples were installed on the feed line to the still pot, on argon feed lines, and on off-gas lines to give better coverage of temperatures. Lines heated with Calrods were electrically insulated from the heater sheath to prevent the heated line from being accidentally placed in the electrical circuit in the event of a Calrod failure. The configuration of the feed line to the still pot was changed to make plugging by metal deposition less likely. Improved electrical insulation and shielding were added to the still-pot level instrumentation to improve the performance of these instruments.

A new condensate sampler was designed and built.[32] It was similar to equipment used to add ^{233}U to the fuel drain tanks, but had modifications to allow samples to be taken without disturbing the operation of the still.

Fuel carrier salt (containing no uranium) was transferred from the fuel storage tank (FST) to the still feed tank by evacuating the still feed tank, which contained about 2 liters of unirradiated salt, to 1.5 psia. After about 12 liters of salt had been transferred from the FST, the feed tank pressure increased from 4 psia to atmospheric pressure over a period of about 2 min, indicating that gas was being drawn through the transfer line. Repeated attempts to transfer more salt by evacuating the still feed tank failed, although the bubbler in the FST indicated that additional salt was present. After establishing that the freeze valve in the transfer line could be sealed, we decided to proceed with the experiment.

To start the experiment, 7 liters of salt was transferred from the feed tank to the still pot. The still pot was heated to 900°C, and distillation was initiated by decreasing the condenser pressure to 0.2 mm Hg. The salt remaining in the feed tank was fed with the automatic control system, which maintained an approximately constant level in the still pot. When the remainder of the salt in the feed tank (7 liters) had been fed to the still pot, a salt plug was frozen in the still-pot feed line, and 4 of the 7 liters of salt in the still pot was subsequently evaporated. The still-pot temperature during this part of the run was 980°C, and the condenser pressure was about 0.1 mm Hg.

During the first part of the run (semicontinuous), the average distillation rate was 0.57 liter/hr; during the second part (batch), the average rate was about 0.36 liter/hr. These rates were lower than rates achieved in the nonradioactive operation (0.7 to 1.2 liters/hr) because of differences in operating conditions.

Eleven condensate samples were taken during the run at approximately 90-min intervals. Radiation readings (at contact) ranged from 4 r/hr for the first sample to 500 mr/hr for the last sample. The predominant activity was ^{137}Cs.

Final analyses were obtained for the 11 condensate samples taken during the MSRE distillation experiment; these samples were analyzed for LiF, BeF_2, ZrF_4, and the fission products ^{95}Zr, ^{144}Ce, ^{147}Pm, ^{155}Eu, ^{91}Y, ^{90}Sr, ^{89}Sr, and ^{137}Cs. The results of these analyses were presented in terms of an effective relative volatility, with respect to LiF, which is defined by the relationship:

$$\alpha_{i-\mathrm{LiF}} \equiv \frac{Y_i/X_i}{Y_{\mathrm{LiF}}/X_{\mathrm{LiF}}}, \qquad (1)$$

where Y_{LiF} and Y_i are mole fractions in the condensate and X_{LiF} and X_i are mole fractions in the still pot. Concentrations in the still pot were not measured directly; however, data taken during the experiment allowed these concentrations to be estimated from material balances for each component.

[31] *Chem. Technol. Div. Ann. Progr. Rept. May 31, 1969,* ORNL-4422, p. 44.

[32] J. R. Hightower *et al., MSR Program Semiann. Progr. Rept. Feb. 28, 1969,* ORNL-4396, p. 298.

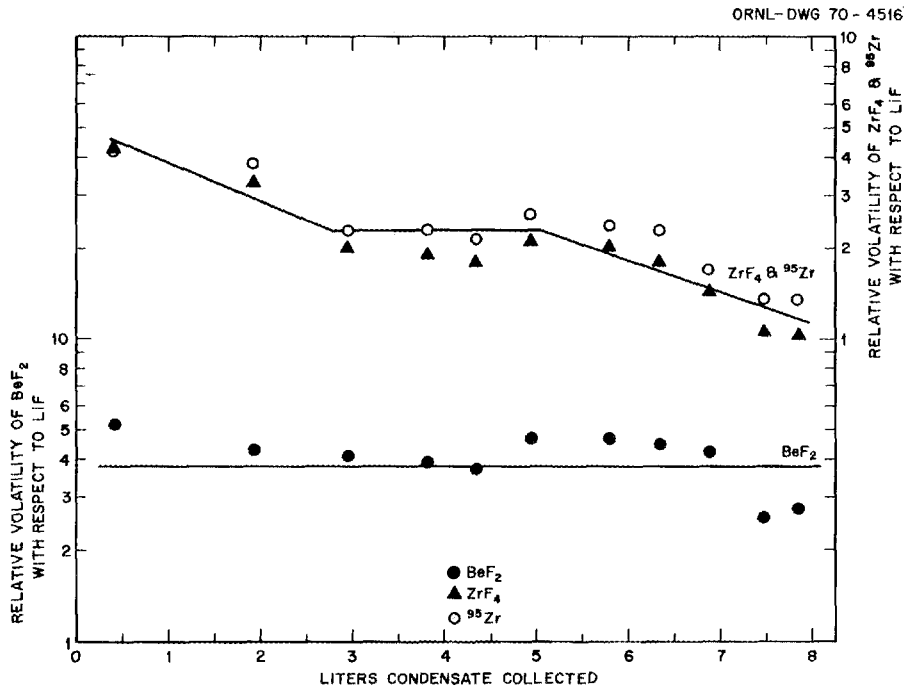

Fig. 1.25. Effective Relative Volatilities of ZrF_4, ^{95}Zr, and BeF_2 for the MSRE Distillation Experiment.

The effective relative volatilities of the major salt constituents (BeF_2 and ZrF_4) and of fission product ^{95}Zr are shown in Fig. 1.25. The effective relative volatility of BeF_2 remained essentially constant during the run, averaging 3.8. This value agrees favorably with the value (3.9) measured by Smith, Ferris, and Thompson,[33] but is slightly lower than the value (4.7) measured by Hightower and McNeese.[34] Slight inaccuracies in calculations and analyses would account for this difference. The effective relative volatilities of fission product ^{95}Zr and of the natural ZrF_4 present in the carrier salt are in agreement.

Figure 1.25 shows that α_{ZrF_4-LiF} decreased from an initial value near 4 at the start of the run to about 1 at the end of the run. These values bracket the value of 2.2 measured by Smith *et al.*[33] for a salt mixture having a ZrF_4 concentration of 0.0008 mole fraction (which is about 2% of that present during the distillation experiment).

[33]F. J. Smith, L. M. Ferris, and C. T. Thompson, *Liquid-Vapor Equilibria in LiF-BeF$_2$ and LiF-BeF$_2$-ThF$_4$ Systems*, ORNL-4415 (June 1969).

[34]J. R. Hightower, Jr., and L. E. McNeese, *Measurement of the Relative Volatilities of Fluorides of Ce, La, Pr, Nd, Sm, Eu, Ba, Sr, Y, and Zr in Mixtures of LiF and BeF$_2$*, ORNL-TM-2058 (January 1968).

The effective relative volatilities for the lanthanide fission products ^{144}Ce, ^{147}Pm, and ^{155}Eu are shown in Fig. 1.26. The effective relative volatility of ^{144}Ce increased sharply from 6.1×10^{-4} at the time the first sample was withdrawn to about 1.0×10^{-2}, where it remained during the remainder of the run (except for the fifth sample, which was lower than 1.0×10^{-2} by a factor of 3). The initial value was only 1.5 to 3.4 times the value measured in an equilibrium still,[34] whereas the values during most of the run were 24 to 56 times the value measured in the equilibrium still.

The effective relative volatility for ^{147}Pm was based on a computed feed concentration and took into account the MSRE power history. The computed feed concentration of ^{147}Pm was thought to be a more accurate value than the measured feed concentration since measured concentrations of other lanthanide fission products had been in good agreement with computed concentrations. As in the case of ^{144}Ce, the relative volatility of ^{147}Pm at the time the first sample was taken was low, that is, less than 7.8×10^{-4}; it then increased sharply to about 3.4×10^{-3} for the other samples. Again, as in the case of ^{144}Ce, the relative volatility at the time the fifth sample was taken was low. The relative volatility of promethium had not been measured previously.

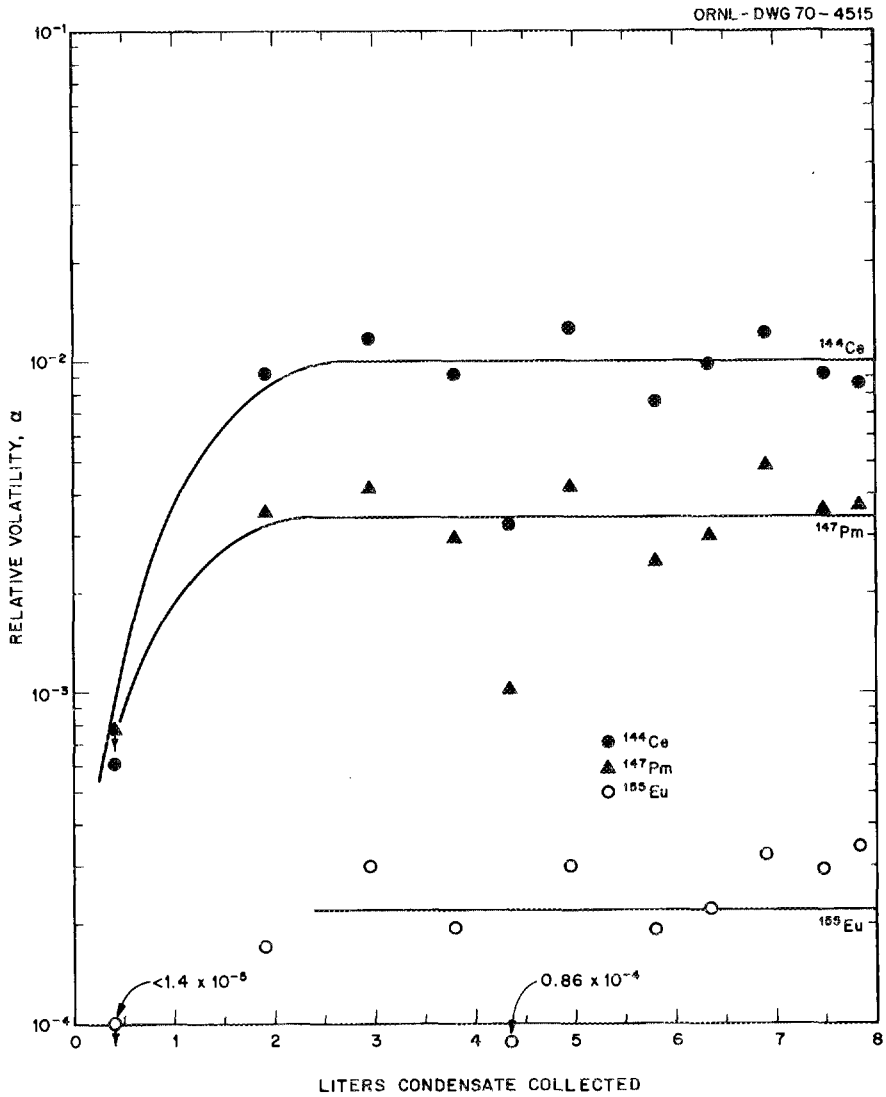

Fig. 1.26. Effective Relative Volatilities of ^{144}Ce, ^{147}Pm, and ^{155}Eu in the MSRE Distillation Experiment.

The variation of the relative volatility of ^{155}Eu during the run closely paralleled the variations for ^{144}Ce and ^{147}Pm. The value for the first sample was less than 1.4×10^{-5}; however, the values for all other samples except the fifth sample were higher (i.e., about 2.2×10^{-4}). The value for the fifth sample was lower than this by a factor of 2.6. The effective relative volatilities measured during the MSRE distillation experiment (based on a computed feed concentration of ^{155}Eu) were lower than the value (1.1×10^{-3}) measured in recirculating equilibrium stills. However, the analyses of ^{155}Eu in the condensate are suspect since there was some difficulty in the analysis; therefore, results of the analyses of the condensate samples for ^{155}Eu were reported as approximate values only. On the other hand, it is significant that the variation of $\alpha_{^{155}Eu\text{-}LiF}$ during the run closely paralleled the variations of the relative volatilities of ^{144}Ce and ^{147}Pm.

During the run, the effective relative volatility of ^{91}Y averaged 1.4×10^{-2}, about 410 times the value measured in recirculating equilibrium stills. The variation of $\alpha_{^{91}Y\text{-}LiF}$ during the run was similar to variations of relative volatilities of the lanthanides. Most noticeable was the low value for the fifth sample. During the run, the effective relative volatility of ^{90}Sr (based on the measured concentration in the feed)

averaged 4.1×10^{-3}, about 84 times the value measured in recirculating equilibrium stills. The average value of the relative volatility of ^{89}Sr (based on a computed concentration in the feed) was 0.193, about 3900 times the value measured in equilibrium stills. The ratio of the ^{89}Sr to ^{90}Sr activities in the condensate samples should have been about 0.002 in each case (or, at least, should have remained constant); however, it varied from 0.22 to greater than 10. The highest effective relative volatility of ^{137}Cs was only about 20% of the value measured by Smith *et al.* for $LiF\text{-}BeF_2$ systems.

As seen from the previous results, all of the components except beryllium and zirconium had effective relative volatilities that differed (in some cases, drastically) from values predicted from work with equilibrium systems. Possible causes for these discrepancies include: (1) entrainment of droplets of still-pot liquid in the vapor, (2) concentration gradients in the still pot, and (3) contamination of samples during their preparation for radiochemical analysis.

1.12 DESIGN OF A PROCESSING MATERIALS TEST STAND AND THE FIRST MOLYBDENUM REDUCTIVE EXTRACTION EQUIPMENT

Carbon steel has been used as a readily available material of construction for reductive extraction engineering development equipment because it has relatively good resistance to both molten salt and bismuth. However, plugging by mass-transfer deposits of iron precipitated from the bismuth phase in cooler parts of the equipment has been a problem.[35] It has always been apparent that carbon steel is not a satisfactory material for extended use.[36]

The refractory metals molybdenum, tungsten, and tantalum have demonstrated good resistance to salt and bismuth; however, the costs, fabrication problems, and protective atmosphere requirements associated with these metals raise questions about their use in processing plants. Of the three metals, molybdenum appears to be the best for processing applications; tubing, plate, and billets are commercially available in a limited range of sizes. Recent development work[37] by the Metals and Ceramics Division indicates that it may be feasible to fabricate small-scale equipment from molybdenum; therefore, a cooperative project between the Chemical Technology and the Metals and Ceramics Divisions is in progress to develop the necessary fabrication techniques for building molybdenum process equipment.

A preliminary design has been made for a materials test stand and for the first molybdenum equipment to be operated in the test stand. The first equipment will demonstrate the fabrication of a complex refractory metal system, will test the suitability of molybdenum as a material of construction for processing, and will provide engineering data on packed column performance with a salt-bismuth system.

The test stand assembly will be installed in a beryllium containment area in Building 4505 and will include the instrumentation, the high-purity gas supply systems, and the fill-and-dump vessel for the salt and bismuth used in the test equipment, as well as the containment vessel for the test stand. This containment vessel, about 20 in. in diameter by 14 ft high, will be heated and filled with an inert gas for high-temperature operation of the molybdenum equipment.

The molybdenum equipment will consist of a simple, very small-scale reductive extraction system containing a 1-in.-diam by 5-ft-high packed column with 3½-in.-diam upper and lower disengaging sections. Salt and bismuth will be circulated countercurrently through the column by gas-lift pumps, which will pump the streams to elevated 3½-in.-diam head pots for sampling, gas separation, flow measurement, and gravity flow back through the column. Instrumentation will also include a system for detecting the interface in the lower disengagement section of the column and a system for measuring the pressure drop through the packed column. The molybdenum equipment will be suspended by molybdenum hangers from the top flange of the test-stand containment vessel so that the equipment can be lifted out for inspection, repair, or alterations to permit other materials, instrumentation, or flow systems to be tested.

A preliminary full-size layout of the test stand and the molybdenum equipment has been detailed to pinpoint the problems of clearances and orientation of vessel nozzles and lines. Evaluations of mechanical fittings and developmental work by the Metals and

[35] *MSR Program Semiann. Progr. Rept. Aug. 31, 1969*, ORNL-4449, pp. 229–30.

[36] H. Suskind *et al.*, *Corrosion Studies for a Fused Salt–Liquid Metal Extraction Process for the Liquid Metal Fuel Reactor*, BNL-585 (T-146) (June 30, 1960).

[37] *MSR Program Semiann. Progr. Rept. Aug. 31, 1969*, ORNL-4449, pp. 210–13.

Ceramics Division on extrusion, welding, and brazing are needed before the assembly method for the required joints can be specified.

An indication of the relative size of this molybdenum equipment can be gained by noting that the column cross-sectional area is about $1/80$, and the packed height is about $1/5$, of the corresponding dimensions which might be required for a plant-size protactinium extraction column. Successful fabrication and operation of the very small-scale experimental system will represent a significant advance in molybdenum fabrication techniques.

2. Development of Aqueous Processes for Fast Reactor Fuels

Beginning in the 1980's, reprocessing of large quantities of fissile material from LMFBR reactors will be required. The problems that will be encountered during the reprocessing of this material will be different from those that have been encountered with light-water reactor (LWR) fuels for the following reasons: (1) The major fissile material in LMFBR reactors is plutonium rather than ^{235}U. (2) The fissile content of the LMFBR fuel is higher, by a factor of about 7 in the core section and by a factor of about 3 when all the material to be processed is considered, than that of the LWR fuel. (3) The average fission product content will be somewhat higher (the localized fission product content may be three times higher) than that encountered in LWR fuel. (4) The specific power of the LMFBR is higher, by a factor of about 5, than that of the LWR. (5) Processing of the LMFBR fuel after short decay periods will be advantageous, owing to the high fissile content (and high inventory costs) of the core material.

The Purex solvent extraction process, which is employed by nearly every major fuel processing facility in existence today, will be applicable in the processing of LMFBR fuels. The process versatility, the ease of adaptation of the process to continuous high-capacity throughput, and the vast operating experience that has been attained in the major processing facilities make this aqueous solvent extraction process an obvious and reliable choice. It appears feasible, with plant modifications, to process fuel from early LMFBR reactors, where preprocessing decay is acceptable, in existing fuel reprocessing facilities.

Aqueous reprocessing is most economically accomplished in large central facilities to which fuel is shipped from various reactor sites. The problem of fuel shipment, which is difficult even with LWR fuels, is aggravated in the case of LMFBR fuels by the high specific power of the fuel and the need to ship after only short decay times. We are working toward development of equipment and techniques for shipment that will ensure safety and containment under accident conditions.

The preparation of LMFBR fuel for solvent extraction is more difficult than that of LWR fuel because of increased heat generation, vastly increased amounts of radioiodine (if the fuel is processed after short decay periods), and the presence of substantial quantities of relatively difficult-to-dissolve plutonium and fission products. We are making studies of the dissolution rates for irradiated fuel and of equipment that will be suitable for the accomplishment of certain of the mechanical operations (e.g., shearing). Improved containment of each equipment item and reduction of the quantity of contaminated off-gas are among the primary goals.

Disposal of the tritium that is produced during the fissioning of uranium and plutonium is not currently a problem because of the relatively small amount being produced. However, when the nuclear capacity expands by several orders of magnitude and the size and number of processing facilities increase, there will be a definite need to minimize the discharge of tritium to the environment. A process that, hopefully, will isolate the tritium prior to its dilution with dissolver solution is under development. (If the tritium becomes mixed with the dissolver solution, its isolation and recovery will be impractical.) This process involves an oxidative heat treatment, which will also liberate other volatile fission products such as iodine, xenon, and krypton.

The treatment of off-gas is a major consideration in the processing of fuels that have been cooled less than 120 days. Removal efficiencies for radioiodine of 10^8 will be required for large-scale plants which process fuel that has been cooled for about 30 days. While no processing facility in existence today has the capacity (or the need) for this degree of removal, the recent development of several efficient iodine trapping systems, for example, silver zeolite sorber, gives us confidence that such a plant is not beyond reasonable

attainment. In the processing of short-decayed fuels, substantial quantities of radioactive xenon will also be present in the off-gas streams; it, along with ^{85}Kr, can be removed by various proven means and by other rare gas removal methods that are being developed.

The solvent extraction processing of LMFBR fuels must take into consideration (1) higher plutonium contents and (2) increased fission product activity in the feed. The second problem will cause difficulty in both plutonium valence control (necessary for good plutonium recovery) and solvent stability. The first will affect process and/or equipment design (to avoid criticality), as well as the choice of reductant to be used in the partitioning step. Neither of these problems appears to be serious in view of currently available information and of existing means for operating within the limitations.

Our work has been directed, in a considerable measure, toward clear definitions of the problems and a delineation of the most profitable areas of investigation. In the future we expect to develop the equipment and the process flowsheet conditions that are required to demonstrate safe and economic shipment and the processing of short-cooled LMFBR fuel. While this is a challenging problem, we are confident that the solution lies in the extension of current practice and/or technology.

2.1 SHIPPING AND RECEIVING

The processing of spent fuels from LMFBR facilities is economically similar to other manufacturing operations in which a large capital investment is required for satisfactory accomplishment of the task. Small-capacity plants cannot be competitive with large-capacity plants; hence, an economic need exists for transporting spent fuel from many reactors located over a widespread area to a central reprocessing facility.

The shipment of fuels from LMFBR's will be more difficult than the shipment of fuel from light-water reactors (LWR's) because of the higher specific power at which LMFBR's operate, the configuration of their fuel, and an economic need to reprocess LMFBR fuel after very short decay times. The LMFBR fuel subassemblies are generally expected to contain a greater number of closely spaced fuel rods than an LWR fuel subassembly, and to be encased within a wrapper. Both of these characteristics will impede the dissipation of heat from the fuel subassembly. In addition, the fueled portion of the LMFBR subassembly comprises only a small percentage (less than 25% in some instances) of the total subassembly length, whereas nearly all of the length of an LWR subassembly is fueled.

Cask Concept

Although additional information has been developed during the past year and the comparative merits of the concept proposed over a year ago have been under constant, critical evaluation, the preferred concept of LMFBR fuel shipment has not changed materially. This concept involves the containment of multiple spent-fuel subassemblies in a mobile liquid having good heat-transport characteristics and low vapor pressure (sodium) inside a shielded, leak-tight container of superior resistance to damage by impact and heat. The fuel subassemblies are maintained in a predetermined orderly array in the liquid by means of a movable support structure. Relatively small (~8-in.-diam) ports, which are well protected against damage due to impact, are used for access to the shielded container. This concept does not require, although it does not preclude, the use of individual containers for each fuel subassembly.

Unique to this concept is the premise that a liquid coolant can be totally contained within the fuel cavity of the cask under all the conditions specified by federal regulations. A liquid coolant of appreciable thermal conductivity, specific heat, and thermal expansion is necessary in order to provide a highly effective means for transporting heat from the fuel rods to the container walls. However, the safety of this system is dependent upon the capacity to retain the coolant and any gases that may also be present in the fuel cavity. Therefore, our prime objectives are to establish that the contents of a properly designed and constructed shipping cask can be totally retained under both normal and accident conditions and to gain acceptance, by regulatory authorities, of the concept of a leakproof fuel container. Other objectives are incidental to these and are generally related to the optimization of design features and/or to other aspects of protecting the public from damaging radiation.

Engineering Evaluation

A recent engineering evaluation of spent LMFBR fuel shipment[1] essentially expanded upon a similar evaluation made during the previous year.[2] In addition to the general objectives of the previous study, the objectives of the more recent evaluation included the following: (1) a comparison of the characteristics of LMFBR fuel

[1] J. D. Rollins, *An Engineering Evaluation of LMFBR Spent Fuel Shipment*, ORNL-TM-2723 (in preparation).

[2] *Chem. Technol. Div. Ann. Progr. Rept. May 31, 1969*, ORNL-4422, p. 50.

with those of LWR fuel, with the aim of supporting the need for liquid coolants inside LMFBR shipping casks, (2) an investigation of the neutron shielding problem and its effect on LMFBR shipping casks as a function of fuel element capacity, (3) a determination of the consequences of canning fuel subassemblies, (4) a comparison of alternative cask designs on the basis of economics, and (5) an evaluation of the safety of a typical LMFBR shipping cask in terms of compliance with applicable regulatory criteria. The major efforts are discussed below.

Heat-Transfer Studies. – The thermal characteristics of LMFBR fuel were compared with those of LWR fuel under conditions of radiative heat transfer only to illustrate the necessity for improved cooling in the case of LMFBR fuel shipment. Table 2.1 lists the results of the calculations, which indicate that the maximum temperature attained by the fuel cladding in an LMFBR fuel subassembly [either Fast Test Reactor (FTR) or Atomics International (AI) Follow-On types] cooled for 30 days is several hundred degrees higher than that reached in an LWR fuel subassembly cooled for the same length of time. The temperature difference is even more pronounced if the comparison is made on the basis that the LWR fuel has cooled for 180 days (typical cooling periods for LWR fuels prior to reprocessing range from 120 to 180 days). The reasons for the higher fuel cladding temperatures in the LMFBR subassemblies include a more compact fuel rod array (triangular as opposed to square), a greater number of rows of fuel rods, higher linear heat generation rates, and a smaller pitch-to-rod-diameter ratio. Results such as the above tend to support the need for an effective heat-transport medium (e.g., liquid sodium) inside the fuel cavity of LMFBR shipping casks in order to transport fuel subassemblies safely after short cooling periods. Additional calculations were made to determine the cladding temperature for LMFBR fuel in casks that incorporated various types of coolants and coolant combinations. These calculations were accomplished through use of the LMYRA code, which is discussed below.

Radiation Shielding Studies. – We have assessed the neutron shielding problem as it relates to LMFBR, LWR, and LWR recycle fuel shipments. Our findings show that LMFBR fuel shipments will present a somewhat greater neutron shielding problem than fuel shipments from LWR's fueled with ^{235}U, but less than shipments from LWR's fueled with plutonium (see Sect. 2.7). For the case of typical LMFBR fuel (i.e., AI Follow-On fuel) shipments in 7-, 18-, and 36-element casks, it was determined that augmentation of the gamma shielding component of the cask (~20 in. of steel) with 2.7, 3.5, and 4.2 in., respectively, of water (or equivalent neutron shielding) would be required to limit the total (neutron plus gamma) external dose rates to acceptable levels (see Sect. 2.7). Parametric studies of the attenuation of transuranium-element neutrons (produced in spent fuels) by iron, lead, and uranium indicated that the above neutron shielding thicknesses would need to be slightly increased in the case of lead- and uranium-shielded casks. If water is utilized as the neutron shielding material, boron will have to be added to minimize the radiation resulting from neutron capture by hydrogen. The overall effect of the neutron shielding problem is to increase both the cask weight and the cost to some extent. Preliminary investigations indicate that a variety of methods are available to the

Table 2.1. Maximum Fuel Cladding Temperatures in Typical LWR and LMFBR Fuel Subassemblies in Air as a Function of Decay Time and Shroud Temperature

Subassembly Shroud Temperature (°F)	Decay Time (days)	Temperature of Cladding for Center Rod[a] (°F)		
		PWR[b]	FTR-LMFBR[c]	AI Follow-On LMFBR[d]
400	30	1410	1830	2120
400	180	1030	1280	1530
400	385		1030	1240
400	700			1030
800	30	1480	1870	2150
800	180	1160	1370	1590
800	390		1160	1330
800	705			1160

[a]Excluding axial peaking factors.
[b]Burnup, 33,000 Mwd/metric ton; specific power, 30 kw/kg; 225-pin square array.
[c]Burnup, 45,000 Mwd/metric ton; specific power, 100 kw/kg; 217-pin hexagonal array.
[d]Burnup, 77,000 Mwd/metric ton; specific power, 105 kw/kg; 217-pin hexagonal array.

cask designer for retaining the additional neutron shield while providing for the movement of decay heat across the shield. However, the relative merits of alternative design approaches are yet to be evaluated on the basis of cask weight, cost, and, in some cases, feasibility.

Criticality Studies. – Parametric criticality studies were conducted for typical LMFBR fuel subassembly arrays in steel-shielded casks in which the number of fuel subassemblies, the intersubassembly spacing, and the cask coolant were varied. Results indicated that criticality is not a major design problem in LMFBR shipping casks. Although LMFBR fuel is highly enriched with plutonium, it is undermoderated in the LMFBR subassembly configuration and is thus required in relatively large amounts to achieve criticality. A k_{eff} value of 1.0 will be approached only in close-packed arrays of 36 or more subassemblies, and even then only in the case of the AI Reference Oxide fuel, which has greater rod spacings and a higher fissile content than the other fuels that we have considered.

Calculations were made to determine the effect of replacing sodium (the coolant fluid) with air or water on the reactivity of the fuel mass. (If the cask seals maintain their integrity under the hypothetical accident conditions, as appears likely based on current data, there will be no replacement of sodium.) These calculations indicated that such a replacement would result in reduced k_{eff} values for large arrays of typical fuel subassemblies, which are separated by small amounts (i.e., $\frac{1}{8}$ to $\frac{1}{4}$ in.) of stainless steel. Additional calculations showed that fuel compaction (within each subassembly, but not the complement of fuel as a whole) would result in a reactivity increase of about 3%.

LMYRA Code. – A computer code was developed to compare rapidly a multiplicity of systems for shipping spent LMFBR fuel. Subject to imposed technical restrictions (on temperatures, weight, radiation levels, structural integrity, etc.), the code generates a design and optimal postirradiation shipping time that will result in a minimum shipping cost for each of several hundred possible concepts. The concepts are selected by permuting basic parameters that include the material used for fabricating the gamma shield, the type of coolant, the number of elements per shipment, and the method used for encapsulating the fuel elements (i.e., whether or not the fuel elements are individually encapsulated within high-integrity canisters). Based on the given input data, the calculations indicate clearly that the concept we have been developing (i.e., a steel-shielded, sodium-filled pot with uncanistered fuel) is the most economical. Gross changes in basic input data concerning construction cost or heat transport would be required to modify the conclusion with regard to optimum concept.

Table 2.2 shows the effects of varying some of the parameters. The information in this table is based on a plutonium fissile material value of \$10/g and annual fixed charges of 17% on the fuel value. Reducing the value of the fissile material to \$1/g did not change the choice of optimum concept, although the optimum shipment size was increased to 36 subassemblies and the optimum decay time was increased to 15 days. Also, the same cask concept was optimum when the minimum decay time prior to shipment was limited to 70 days.

Heat-Transfer Experiments

A reduced-scale simulated shipping cask was operated both with water and with mercury as the heat-transport fluid. The operation allowed measurement of the temperature of the heat-transport fluid at points remote from the heat source. The system was such that the observed temperature variations can be related to the temperature variations that would occur in the heat-transport fluid located outside the fuel subassemblies in the fuel cavity of a shipping cask. Except for the large temperature variations observed near the heated end of the mockup, the data that were obtained with this unit were in general agreement with the data previously reported.[3] The temperature variations were found to be due, in some measure, to the presence of horizontal partial baffles, which largely precluded thermal convection across the baffled length. Rotation of the system in such a manner that the baffles were in a vertical attitude materially reduced the temperature drop across the baffled zone, although it still remained significant.

In summary, the data collected using this equipment exhibited a great deal of scatter; however, they indicated that bulk liquid temperatures of heat-transport fluids of widely differing thermal characteristics (e.g., water and mercury) in a vessel in which heat is being transported predominantly by thermal convection over relatively long distances are not widely different. They also indicate that the temperature differences which will be present in a liquid-filled shipping cask will be relatively small if thermal convection is not seriously impeded. These data are insufficient to establish a relationship for temperature variation with changes in fluid properties or cask design.

---

[3] *Chem. Technol. Div. Ann. Progr. Rept. May 31, 1969*, ORNL-4422, p. 52.

Table 2.2. Effects of Selected Parameters on Optimum Cask Characteristics and Shipping Cost

Parameter	Basis for Comparison	Variation			No. Subassemblies per Shipment	Decay Time (days)	Shipping Cost[a] ($/kg core)
Shield material	Uncanistered, sodium-cooled fuel	Steel			27	11	16
		Uranium			18	10	23
		Lead			6	10	27
Fuel coolant	Steel cask, uncanistered fuel	Sodium			27	11	16
		Helium + copper insert			12	211	137
		Helium			3	229	158
Canistering	Steel cask, sodium-cooled	Uncanistered			27	11	16
		Canistered			27	10	27
		Inside	**Outside**	**Insert**			
Coolant systems	Steel cask, canistered fuel	Na	Na		27	10	27
		Li	Li		27	12	29
		Na	HiTec[b]		18	10	29
		Na	Ni shot	Cu	18	10	30
		AlSi[c]	HiTec[b]		12	10	35
		Na	He	Cu	12	15	36
		AlSi	Ni shot	Cu	12	10	37
		Na	He		6	26	45
		Na	Air		6	33	48
		Na	Dow A[d]		6	37	51
		PbL[e]	Dow A[d]		3	25	56
		PbL[e]	He	Cu	18	61	63
		Na	Air	Cu	12	79	72
		PbS[f]	Ni shot	Cu	12	85	80
		He	Dow A[d]		27	220	148
		He	He	Cu	18	222	152
		Air	Dow A[d]		36	252	166
		He	He		6	261	180
		He	Air	Cu	12	267	182
		Air	Air	Cu	12	299	200

[a]Includes inventory cost on fuel prior to shipment.
[b]A low-melting inorganic salt used as a heat-transport medium. Product of E. I. du Pont de Nemours and Co., Inc.
[c]An alloy of aluminum and silicon.
[d]Diphenyl–diphenyl oxide.
[e]Liquid lead.
[f]Solid lead.

Two other test systems are to be used to gain additional information pertaining to heat transport during the shipping step. The first of these, a simulation of a single 217-rod fuel subassembly mounted inside a 10-in.-diam pipe, has been described previously.[3] Failure of electrical heaters and delays in obtaining replacements have prevented operation of this unit. The second unit, a simulation of half the length of a 37-subassembly cask, has been constructed and is now being installed. This unit has also been described previously.[3] We plan to operate the first unit initially with sodium as the heat-transport medium and, later, with other materials in order to gain additional insight into the significant parameters that relate to heat transport by thermal convection. The first of these two test systems will provide information pertaining to intrasubassembly heat transport, while information gained through the use of the second system will relate to extrasubassembly heat transport.

Experiments to Evaluate Cask Integrity

The retention of the medium that is used to transport heat from the fuel rods to the cask interior surface is vital to the safe, economic transport of short-decay LMFBR fuel. It follows that the primary concern is the capacity of the cask system to retain the coolant. The steps being taken to resolve this problem are to employ a cask structure with exceptional inherent strength, to provide seals (for all openings) that are mounted and

protected in such a manner that the risk of damage due to impact forces is minimal, and to minimize the impact forces to which the cask might be exposed (through the use of energy-absorbing structures mounted around the cask). Experimental activities in the area of cask integrity have included: (1) tests of scale-model casks, (2) seal integrity tests, and (3) tests with various types of energy-absorbing devices. Highlights of the work completed under each of these efforts are given in the subsequent paragraphs.

Tests of Scale-Model Casks. – In order to determine the relationship between the damage that is suffered by a small-scale cask and the damage that will be sustained by a large-scale cask when both units are subjected to the same accident conditions (viz., a 30-ft drop onto an unyielding surface), cask models of 1/9.38, 1/18.7, and 1/37.5 scale (based on an 18-subassembly cask) were constructed and tested at the ORNL Drop Tower Facility.[4] Results of these tests indicated that the damage (i.e., the material deformation) to a large-scale cask is slightly less, proportionately, than damage to a small cask. For example, in one series of tests in which the scale of the cask was increased by a factor of 6.25, the vertical deformation of the cask increased by a factor of only 3.7. Supplementary data obtained during this period on $\frac{1}{8}$- and $\frac{1}{6}$-scale models, which had been constructed for other tests (see discussion below), substantiated the foregoing results. All drop tests were performed with the specimen inclined at 15° relative to the vertical axis in order to align the point of impact with the center of gravity. This orientation is the most severe from the standpoint of cask deformation in the area of the sealing surface; however, it does not result in the maximum deceleration. Additional tests are planned whereby the cask models will be dropped in the vertical orientation, thus providing maximum deceleration forces at the seal interface.

Seal Integrity Tests. – In order to obtain in situ seal integrity test data, a $\frac{1}{6}$-scale model cask, which incorporated a Grayloc-type seal (specially mounted and positioned within the cask; see Fig. 2.1) was dropped (on a corner) from a height of 30 ft onto an essentially unyielding surface. A subsequent helium leak check indicated that the helium leakage rate increased from less than 4×10^{-10} cc/sec (the limit of detection) to 2.3×10^{-9} cc/sec as a result of the drop test. The drop test was repeated with the cask at the same attitude (i.e., to permit successive impact on the deformed region). A subsequent leak check indicated that the rate at which helium was leaking through the seal did not increase as a result of the second drop test. This test unit suffered relatively little external deformation and no readily detectable deformation of the internal surface. (Only visual observations of the interior were made.) A seal that was mounted near the cask interior surface might not have been affected by metal deformation; in such a case, it probably would have survived the impact test, but sufficient evidence is not available to confirm this. Additional units with the same design as the one that was tested will be destructively tested for confirmation of the above results.

Another cask port sealing system, which was constructed by the Gamah Corporation (Denver, Colorado), was partially tested by the manufacturer and by ORNL. Although the tests are incomplete, the

PHOTO 981004

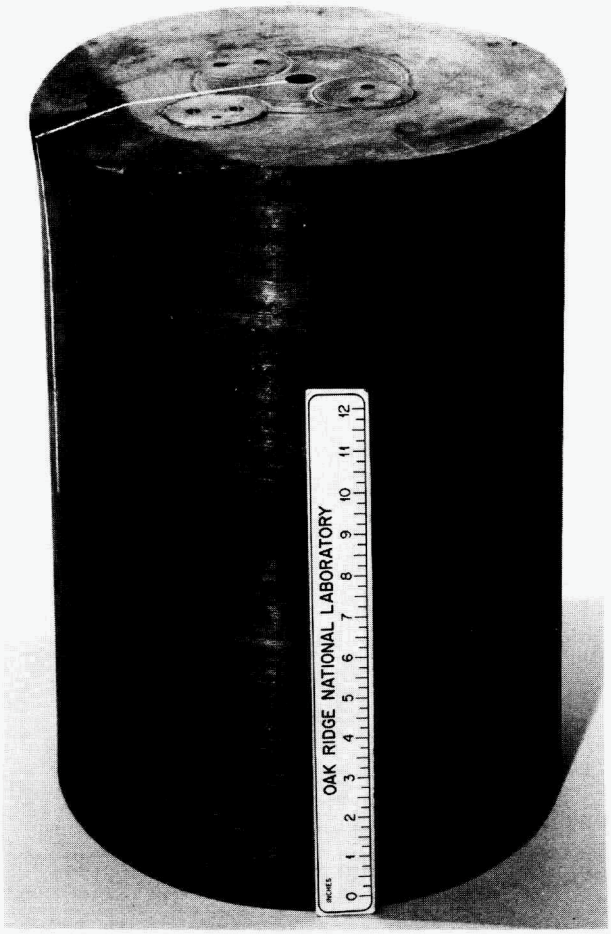

Fig. 2.1. Damaged Portion of One-Sixth-Scale Model Steel Cask After Test by 30-ft Free Fall onto Unyielding Surface.

[4] *LMFBR Fuel Cycle Studies Progress Report for September, No. 7,* ORNL-TM-2748 (November 1969), p. 9.

PHOTO 97260

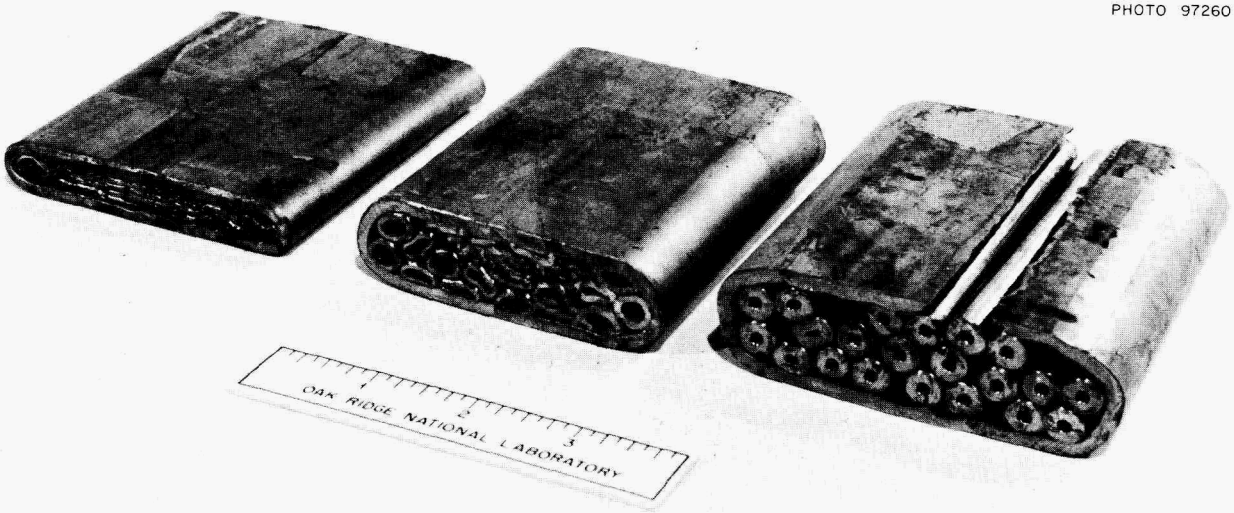

Fig. 2.2. Tube-in-Tube-Type Energy Absorbers Made from Sections of $^3/_8$-in.-OD Tubing with Wall Thicknesses of 0.032, 0.065, and 0.125 in. Each section of tubing has been tested for maximum capability.

results indicate that this system offers promise as a rugged seal. In one test, the 6-in.-diam port exhibited a leak rate of less than 1×10^{-5} cc/sec. We believe that a leak rate of 1×10^{-6} cc/sec would be acceptable.

Energy Absorbers. – An additional margin of safety against damage due to impact can be obtained by providing energy absorbers ("cushions") around the cask to minimize the impact force. The concept of using a number of straight tubes contained in a larger tube (or pipe) for energy absorption evolved from earlier work done on steel rings.[5] The new system is called a tube-in-tube energy absorber. This type of system, although not competitive with commercial energy absorbers in terms of specific energy absorption, represents a good compromise on the basis of cost and overall volume requirements. During the year, parametric tests were conducted in which the number of tubes, tube material, tube size and wall thickness, pipe size, and impact energy were varied. A typical series of tests involved a determination of optimum tube-thickness-to-diameter ratio. In the above case, the tube (type 304 stainless steel) size was held constant at $^3/_8$ in. OD and the tube wall thickness was varied from 0.032 in. to 0.125 in. The results are shown in Fig. 2.2. The 0.032-in.-wall tubing was relatively weak and thus collapsed with minimal energy absorption, whereas the 0.125-in.-wall tubing was so strong that the pipe (2 in. OD, sched 40) could not exert sufficient retaining force to hold the tubes within its perimeter upon imposition of a heavy external force. Most of the impact energy was thus transmitted to the pipe wall, which failed under tension.

Additional tests were made to demonstrate the efficacy of the tube-in-tube type of energy-absorption design. In these tests, a $^1/_8$-scale cask with different-sized absorbers was dropped (on a corner) from a height of 30 ft onto an unyielding surface. Damage to the cask was negligible following a total of nine drop tests in which two 9-in.-long sections of $1^1/_4$-, 2-, or 3-in.-diam pipe (sched 40) containing 9, 22, or 52 type 304 stainless steel tubes ($^3/_8$ in. OD and 0.065 in. wall) were attached to the bottom of the cask (see Fig. 2.3).

Work on a birdcage type of energy absorber[6] was deemphasized, after successful early testing of the tube-in-tube energy absorber, because of its greater cost and complexity. However, before abandoning the birdcage approach, we found that round cross-section tensile members are to be preferred over rectangular ones because the larger cross-section "hinge" portions of round members can be bent in any direction and maintain equal strength. Tensile members of various lengths were elongated at relatively high speed. The length of the portion of the tensile member to be elongated (i.e., that portion having a reduced and

[5] A. Estep, L. R. Shobe, and B. R. Dewey, *Energy Absorption Parameters in Steel Rings*, EM-69-1 (March 1969).

[6] *Chem. Technol. Div. Ann. Progr. Rept. May 31, 1969*, ORNL-4422, p. 55.

PHOTO 97285A

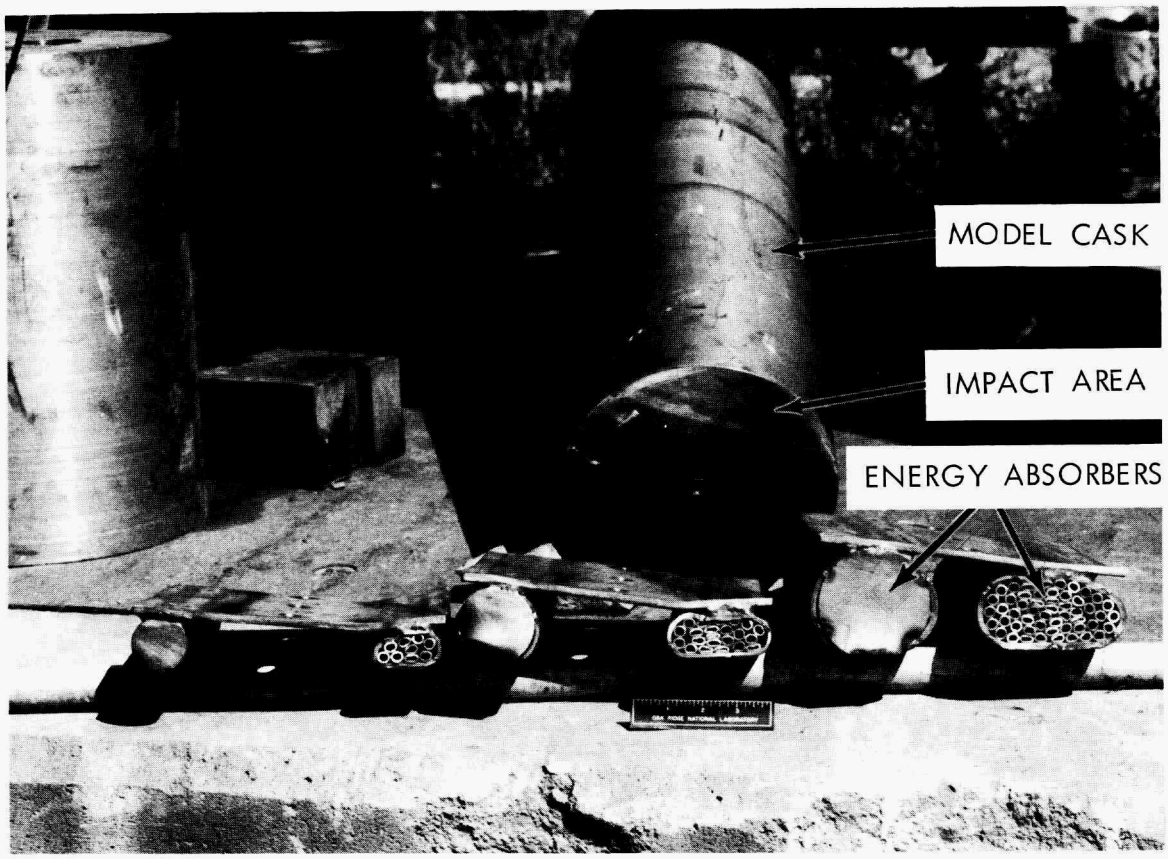

Fig. 2.3. Model Cask with Energy Absorbers. Cask had been dropped 30 ft onto an unyielding surface a total of nine times. Metal at upper portion of cask end has been descaled by impact forces but is not appreciably deformed.

uniform cross section) ranged from 1 to 8 in. Elongations obtained for various specimens were as follows: 1 in., about 60%; 2 in., about 25%; and 8 in., about 13%.

Receiving Facilities

Facilities required for the receipt of LMFBR fuel that is shipped by advanced methods to accommodate the increased heat generation rates existing in short-decayed fuel will be markedly different from the underwater facilities commonly used for receiving LWR fuel shipments. Figure 2.4 presents a concept of a facility for receiving shipments of fuel transported in a sodium-filled shipping cask. The major features of this facility are: (1) a sealed bagging system for avoiding radioactive contamination of all but a minor portion of the cask external surface; (2) a gas-tight, inert-atmosphere cell for handling fuel subassemblies contaminated with metallic sodium; (3) a number of reaction chambers for the nonviolent reaction of sodium with water vapor, followed by subsequent removal of reaction products by liquid water; and (4) a gas-lock system for removal of the deactivated subassemblies prior to storage (under water, if possible).

The concept of the above facility is based on the shipment of fuel subassemblies without benefit of individual containers around each subassembly. It is assumed that the cask can provide adequate containment for coolant and fission products. If either individual or collective containers (in addition to the cask) are required, the complexity of the receiving (and shipping) facilities will be increased materially.

2.2 HEAD-END PROCESSING

The study aimed at developing and evaluating economic head-end processing steps necessary to properly prepare long- and short-decayed LMFBR fuels for aqueous Purex recovery methods is continuing. The principal areas investigated during this report period

ORNL-DWG 70-4559R

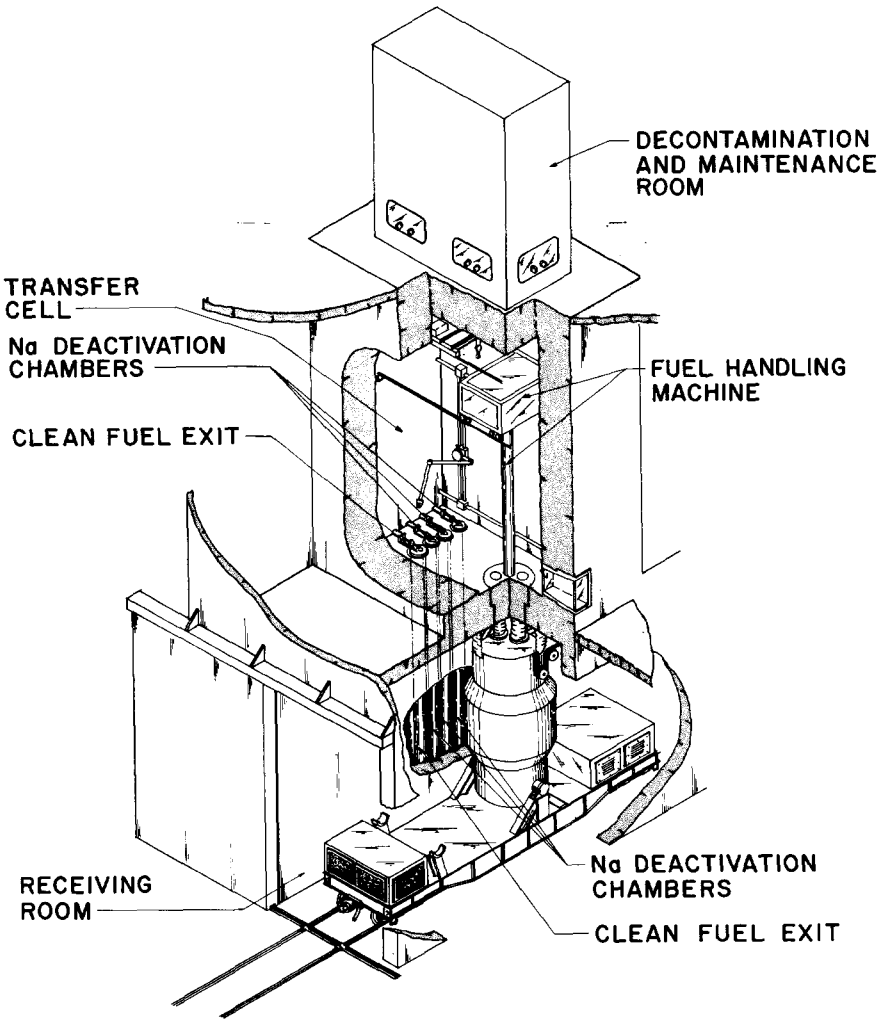

Fig. 2.4. Conceptual Arrangement of Facility for Receiving Sodium-Cooled LMFBR Fuel Shipping Casks.

were: decay heat dissipation, dismantling of multitubular assemblies, shearing, and alternative head-end processes.

Decay Heat Dissipation

A computer code was developed to calculate the non-steady-state temperatures of fuel rods in a hexagonal LMFBR fuel subassembly that has an increasing temperature due to heat produced by radioactive decay. Heat transfer between fuel rods within an assembly was assumed to occur solely by radiation, while heat from the shroud encapsulating the array was assumed to be dissipated both by radiation and by natural convection to the surroundings. The results obtained for an Atomics International (AI) reference fuel subassembly for various heat generation rates are shown in Fig. 2.5. In this case, the emissivity of the radiating surfaces was 0.5. The fuel subassembly was initially at a uniform temperature of 300°F and was suspended vertically in an argon atmosphere of 120°F.

Hottel's crossed-string method[7] was used to derive equations for the blackbody (emissivity = 1.0) view factors or configuration factors for radiation exchange between a rod and each of the rods in the first three rows surrounding it in an array of infinitely long rods on a triangular pitch (Fig. 2.6). In the equations presented below, F_{ij} is the fraction of the radiation

[7]R. Siegel and J. R. Howell, *Thermal Radiation Heat Transfer*, NASA SP-164, vol. II (1969), p. 42.

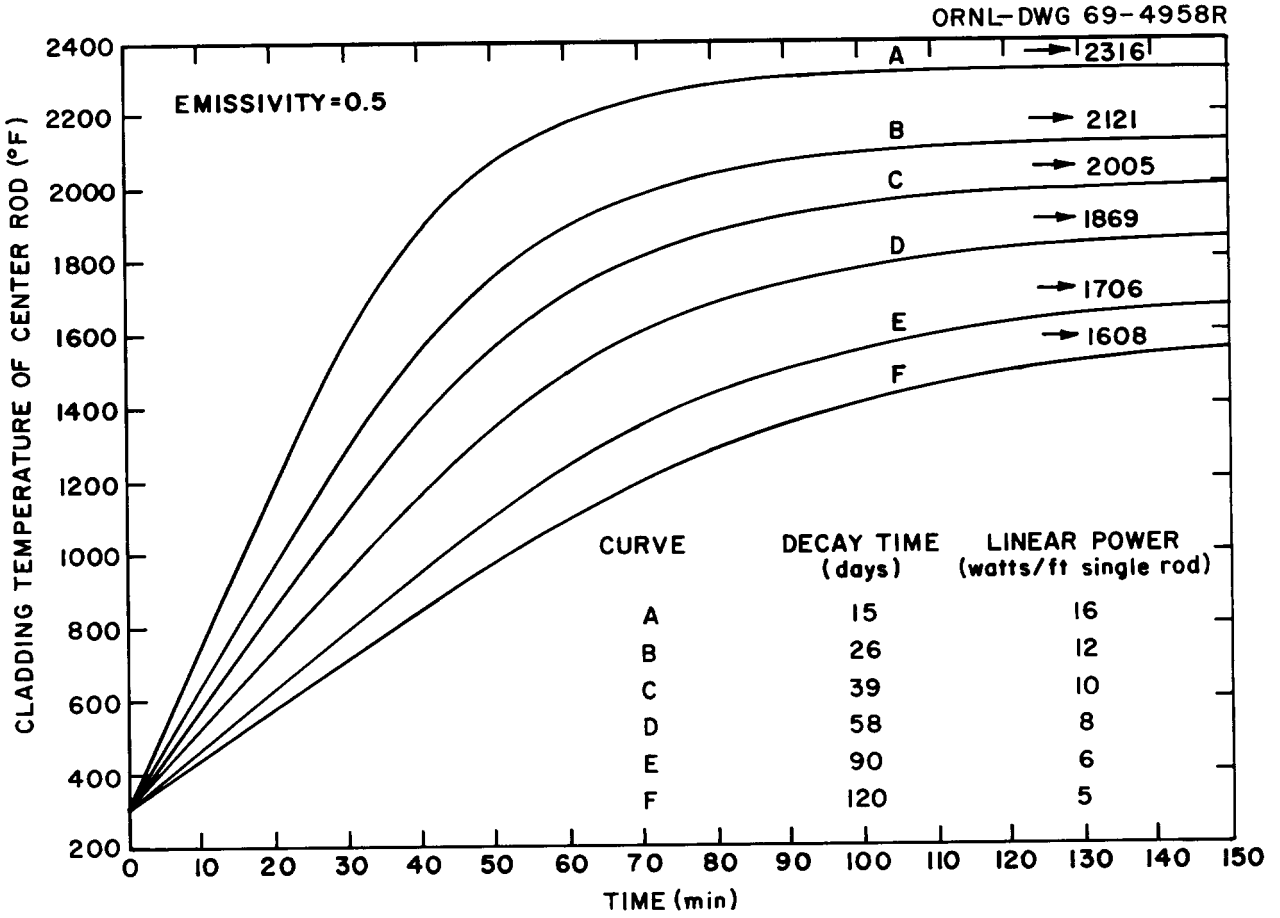

Fig. 2.5. Time-Temperature History of an AI Reference Oxide Fuel Subassembly Without Auxiliary Cooling.

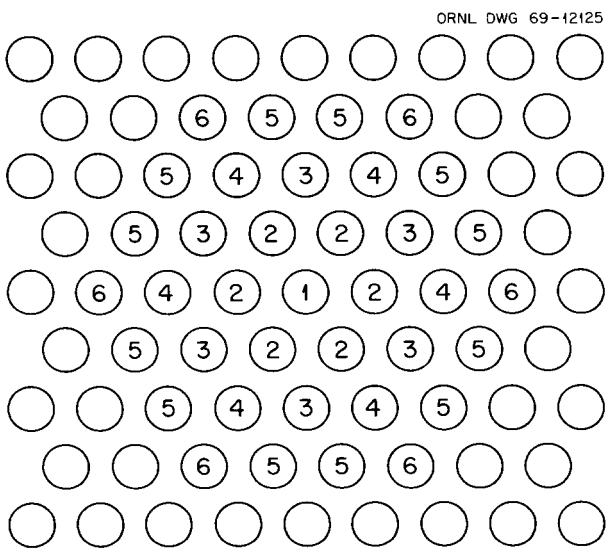

Fig. 2.6. Designation of Rods in Configuration Factor Determinations.

emitted from body i which reaches body j by direct radiation, and PDR is the pitch-to-diameter ratio of the rods.

$$F_{11} = 0, \text{ all PDR}, \tag{1}$$

$$F_{12} = \frac{1}{\pi}\left[\frac{\pi}{6} + \tan^{-1}\sqrt{(\text{PDR})^2 - 1} - \sqrt{(\text{PDR})^2 - 1}\right], \; 1 \leqslant \text{PDR} \leqslant 2/\sqrt{3}, \tag{2}$$

$$F_{12} = \frac{1}{\pi}\left[\frac{\pi}{2} - \text{PDR} - \tan^{-1}\sqrt{(\text{PDR})^2 - 1} + \sqrt{(\text{PDR})^2 - 1}\right], \; \text{PDR} \geqslant 2/\sqrt{3}, \tag{3}$$

$$F_{13} = \frac{1}{\pi}\left[\sqrt{(\text{PDR})^2 - 1} - \tan^{-1}\sqrt{(\text{PDR})^2 - 1}\right], \; 1 \leqslant \text{PDR} \leqslant 2/\sqrt{3}, \tag{4}$$

$$F_{13} = \frac{1}{\pi}\left\{\sqrt{3(\text{PDR})^2 - 1} - \tan^{-1}\sqrt{3(\text{PDR})^2 - 1} - 2\left[\sqrt{(\text{PDR})^2 - 1} - \tan^{-1}\sqrt{(\text{PDR})^2 - 1}\right] - \frac{\pi}{6}\right\},$$

$$2/\sqrt{3} \leqslant \text{PDR} \leqslant 2, \tag{5}$$

$$F_{13} = \frac{1}{\pi}\left[\frac{\pi}{2} - \sqrt{3}\,\text{PDR} - \tan^{-1}\sqrt{3(\text{PDR})^2 - 1} + \sqrt{3(\text{PDR})^2 - 1}\right], \; \text{PDR} \geqslant 2, \tag{6}$$

$$F_{14} = 0, \text{ all PDR}, \tag{7}$$

$$F_{15} = 0, \; 1 \leqslant \text{PDR} \leqslant 2/\sqrt{3}, \tag{8}$$

$$F_{15} = \frac{1}{2\pi}\left\{\sqrt{7(\text{PDR})^2 - 1} - \tan^{-1}\sqrt{7(\text{PDR})^2 - 1} - 2\left[\sqrt{3(\text{PDR})^2 - 1} - \tan^{-1}\sqrt{3(\text{PDR})^2 - 1}\right] + \sqrt{(\text{PDR})^2 - 1} - \tan^{-1}\sqrt{(\text{PDR})^2 - 1} + \tan^{-1}\frac{\sqrt{3}}{9} - \frac{\pi}{6}\right\}, \; 2/\sqrt{3} \leqslant \text{PDR} \leqslant 2, \tag{9}$$

$$F_{15} = \frac{1}{\pi}\left[\sqrt{7(\text{PDR})^2 - 1} - \tan^{-1}\sqrt{7(\text{PDR})^2 - 1} - \sqrt{3(\text{PDR})^2 - 1} + \tan^{-1}\sqrt{3(\text{PDR})^2 - 1} - \sqrt{(\text{PDR})^2 - 1} + \tan^{-1}\sqrt{(\text{PDR})^2 - 1} - \frac{\pi}{3}\right], \; 2 \leqslant \text{PDR} \leqslant 2\sqrt{21}/3, \tag{10}$$

$$F_{15} = \frac{1}{\pi}\left[\frac{\pi}{2} - \sqrt{7}\,\text{PDR} - \tan^{-1}\sqrt{7(\text{PDR})^2 - 1} + \sqrt{7(\text{PDR})^2 - 1}\right], \; \text{PDR} \geqslant 2\sqrt{21}/3, \tag{11}$$

$$F_{16} = 0, \text{ all PDR}. \tag{12}$$

The ORIGEN code[8] was employed to determine the heat generation rates for the AI Reference Oxide core (specific power, 148 Mw/metric ton; burnup, 80,000 Mwd/metric ton), the Fast Test Reactor (FTR) [or Fast Fuel Test Facility Reactor (FFTF)] core (specific power, 100 Mw/metric ton; burnup, 45,000 Mwd/metric ton), the AI Follow-On inner core (specific power, 105 Mw/metric ton; burnup, 77,000 Mwd/metric ton), and the General Electric Follow-On inner core (specific power, 138 Mw/metric ton; burnup, 101,000 Mwd/metric ton). The results in terms of heat flux at the surface of the fuel rods are presented in Fig. 2.7.

[8] *Chem. Technol. Div. Ann. Progr. Rept. May 31, 1969*, ORNL-4422, p. 89.

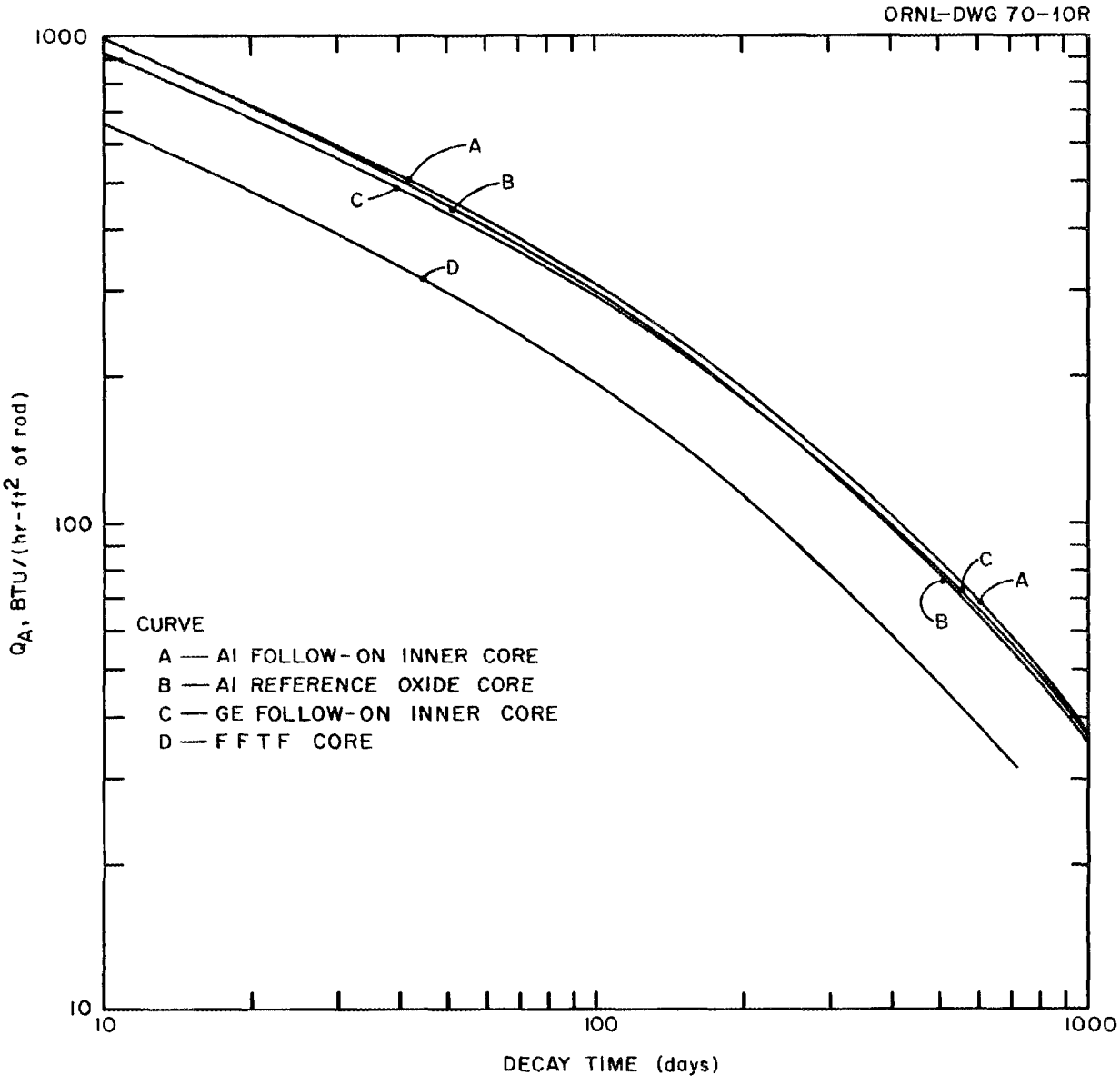

Fig. 2.7. Decay Heat Generation of LMFBR Fuel Rods.

Dismantling of Multitubular LMFBR Fuel Assemblies

In a continuation of dismantling studies, a series of scoping-type tests were made to ascertain the feasibility of deshrouding LMFBR fuel by the plasma-arc cutting method. Other dismantling methods that were reviewed but eliminated included carbon arc–air and laser machining, which were found to be cumbersome and expensive. Laser machining, a slow metal cutting process, is used principally for micromachining and microwelding and, at present, is not feasible for use in gross metal removal as would be required for shroud slitting. In the carbon arc–air process, an electric arc accompanied by a blast of high-pressure (~100-psig) air produces a ragged cut, and the metal melt is blown for a distance of several feet from the work.

The plasma-arc cutting process uses a dc arc in a suitable gas such as argon, a tungsten electrode, and a constricting orifice. The arc and substantially ionized gas (plasma) pass through the orifice and are formed into a small-diameter, high-temperature, high-velocity

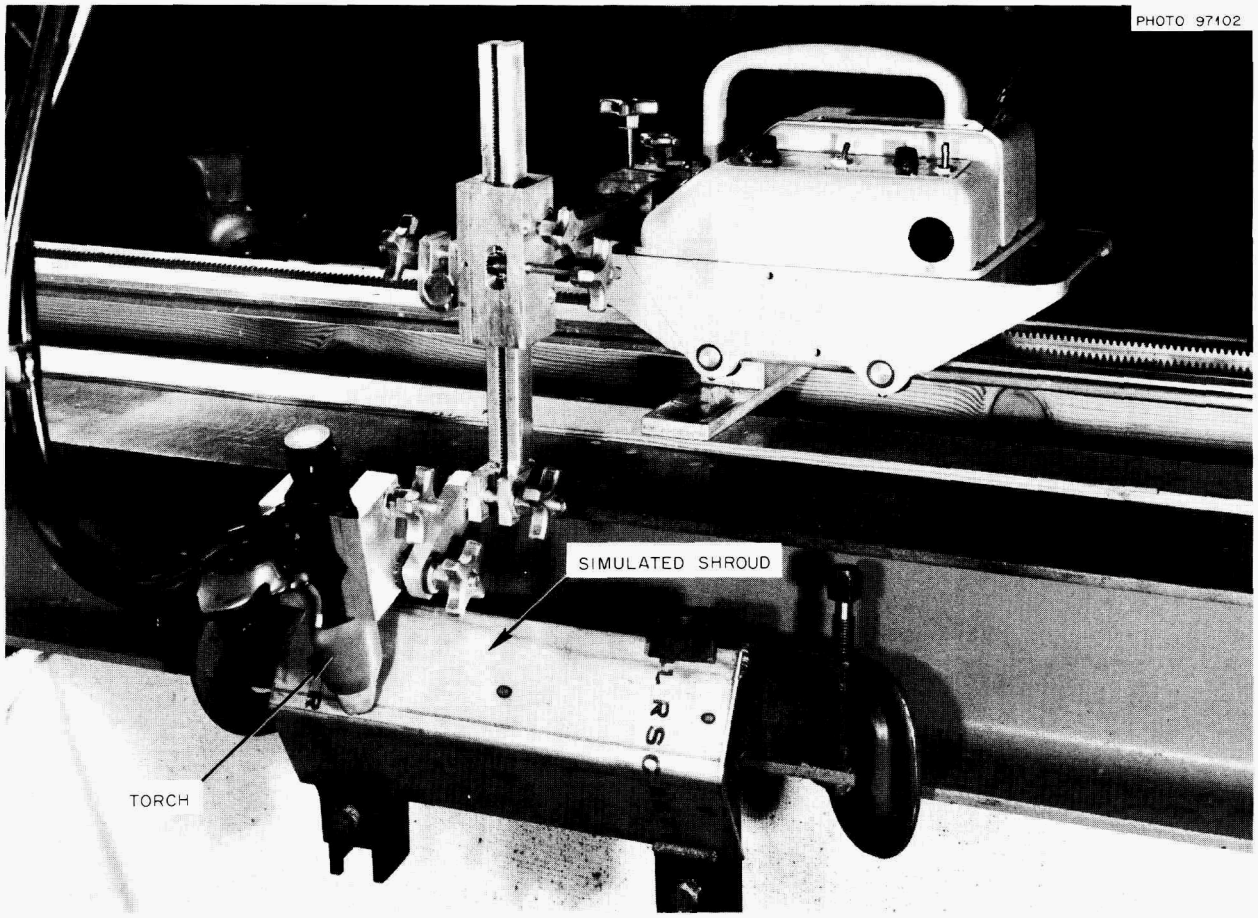

Fig. 2.8. Plasma-Arc Test Unit.

jet. The highly concentrated energy in the plasma jet melts the metal and produces an acceptable cut. Several scoping-type tests were made with the torch attached to a traveling carriage and aligned to cut off the corners of test pieces representing the hexagonal shroud (Fig. 2.8). Prototype fuel rods, $\frac{1}{4}$ in. OD with a 0.091-in.-diam spacer wire wrapping, were positioned in the corner of the hexagonal test workpiece (a $\frac{1}{8}$-in.-thick, 12-in.-long section made of type 304L stainless steel) to ascertain if the plasma arc would cut without damaging the fuel rods. With the torch carriage traveling at the rate of 25 in./min, four different test pieces were cut without causing damage to the fuel tube or spacer wire. The major part of the metal melted and solidified on the side of the workpiece (Fig. 2.9). The success of these tests establishes the plasma arc as a definite contender for slitting the hexagonal shrouds. Additional development will be required, especially the conceptual design and evaluation of a torch shroud tracking device. Operating parameters, such as feasible cutting rates, discharge of melt, etc., will also need investigation to define the limits of this type of cutting.

Shearing

Emphasis on shearing was shifted from the longer-range development of multi- and single-rod shearing parameters to the near-term use of a bundle shear for FTR and Demonstration fuels in existing processing facilities. In addition, some scoping hot-cell studies were made with a single-rod shear. Shearing of some types of light-water reactor (LWR) fuel has been successfully demonstrated by Nuclear Fuel Services, Inc.; however, the shearing of LWR fuels is simpler than the shearing of high-burnup, short-cooled LMFBR fuels because the latter fuels present special problems such as (1) the presence of a liquid-metal coolant, such as sodium, during shearing, (2) the release of gross amounts of fission gases, and (3) the presence of sufficient decay heat to produce maximum cladding temperatures of up to 2120°F.

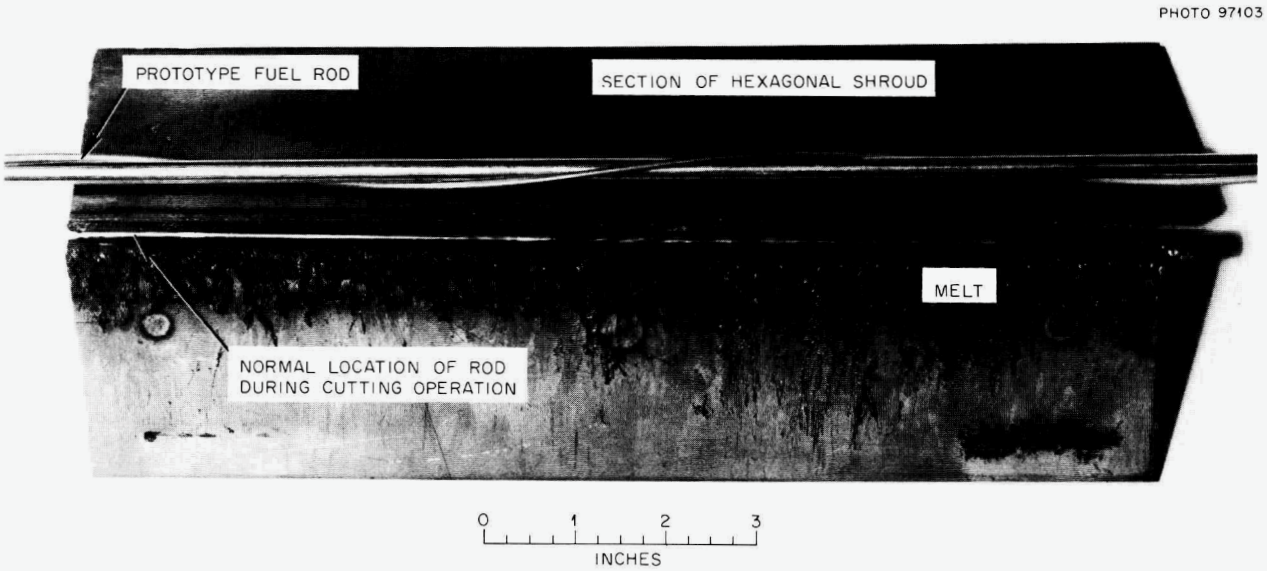

Fig. 2.9. Plasma-Arc Test Piece.

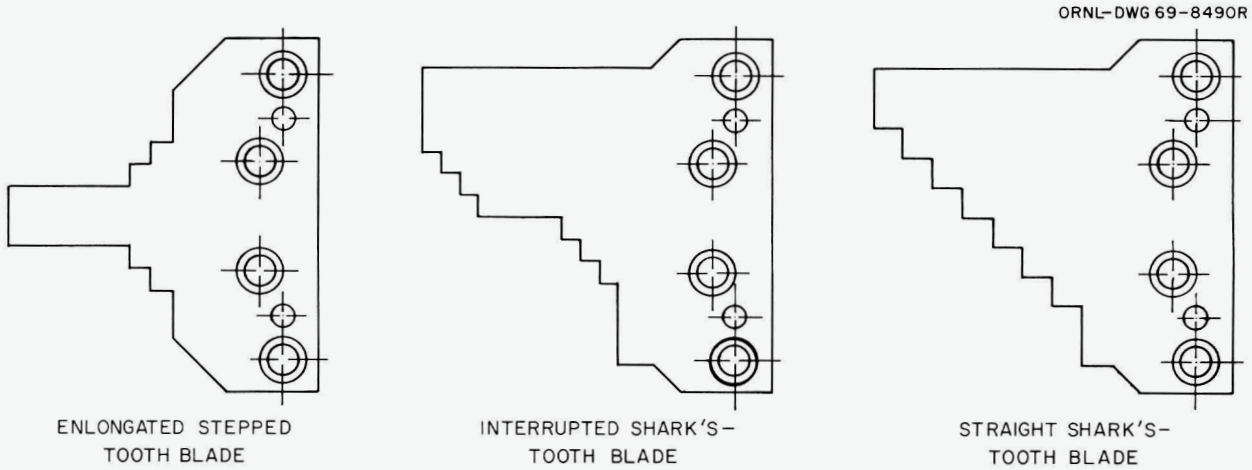

Fig. 2.10. Experimental Deshrouding Shear Blades.

At a burnup of 80,000 Mwd/metric ton, LMFBR fuel may be warped 8 to 12 in., and the stainless steel cladding and the shroud may be swollen 1 to 5%, thus complicating all mechanical operations prior to shearing. Studies on bundle (intact) shearing of fuel assemblies show that data are needed for: (1) the restraining or gagging force that will be necessary to clamp and squeeze out the voids between fuel rods, in order to prevent long pieces from being produced by the pull of the shear blade on the fuel rods, and (2) the shear blade design that will be required for breaking up the shroud into pieces sufficiently small to pass through the shear discharge port and other process lines without jamming. Conceptional designs of three moving and fixed shear blade configurations were completed for the possible investigation and demonstration of breaking of the shroud during bundle shearing (Fig. 2.10). The stroke of the ORNL 250-ton shear was increased from $10\frac{3}{16}$ in. to $12\frac{1}{2}$ in. to accommodate the new elongated and shark's-tooth-type shear blades.

The efforts on the development of a multirod shear and an experimental shear, and on the modifications on the 250-ton shear, had been concluded earlier in order to complete a head-end engineering evaluation study

this year. However, design concepts and fabrication drawings for each of the two shears, as well as for the gagging mechanism, were completed; also, some data on thermal conductivity (k_{eff}) determinations were obtained from small-scale laboratory experiments and from the shearing of prototype fuel.

In the course of producing material (15 liters/batch) for thermal conductivity (k_{eff}) measurements, the multirod shear was used to cut (1) ¼-in.-diam solid type 304L stainless steel rods, and (2) ¼-in.-diam, 15-mil-wall type 304 stainless steel tubes that were filled with porcelain. Eight of the solid rods and 25 of the porcelain-filled tubes were cut per pass. It is estimated that the shear blade has made more than 10,000 cuts on both solid prototype fuel rod arrays and porcelain-filled tubular arrays without showing any appreciable wear on the cutting edge (Fig. 2.11). The A1 tool steel blade, of Rockwell C-59 hardness, operated against Stellite 6-B wear plates. Measurements made on the 1-in. lengths that had been cut from the solid rods show that the void volume in a 6-in.-diam cylinder is 45% and the packing density is 4.35 g/cc; the void volume and the packing density of the porcelain-filled tubes were approximately 60% and 1.88 g/cc respectively.

We have made packing density measurements of 1-in.-long unirradiated sheared pieces of prototype AI core fuel rods, with and without the 0.091-in.-diam

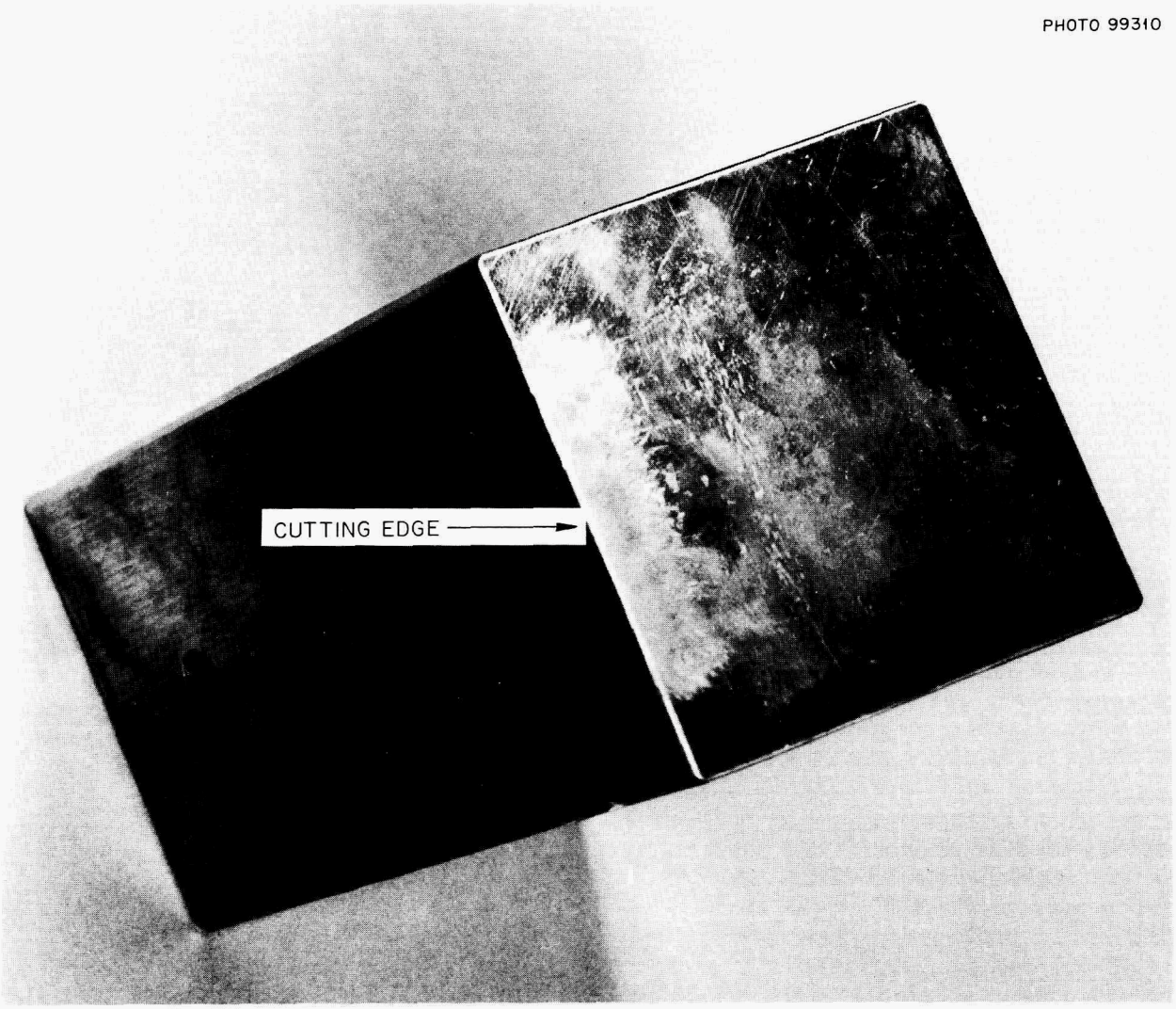

Fig. 2.11. Cutting Edge of ORNL Multirod Shear Blade (A1 Tool Steel, Rockwell C-59) After Approximately 10,000 Shear Cuts (on Both ¼-in.-OD Prototype Solid Stainless Steel Rods and Porcelain-Filled Tubular Arrays).

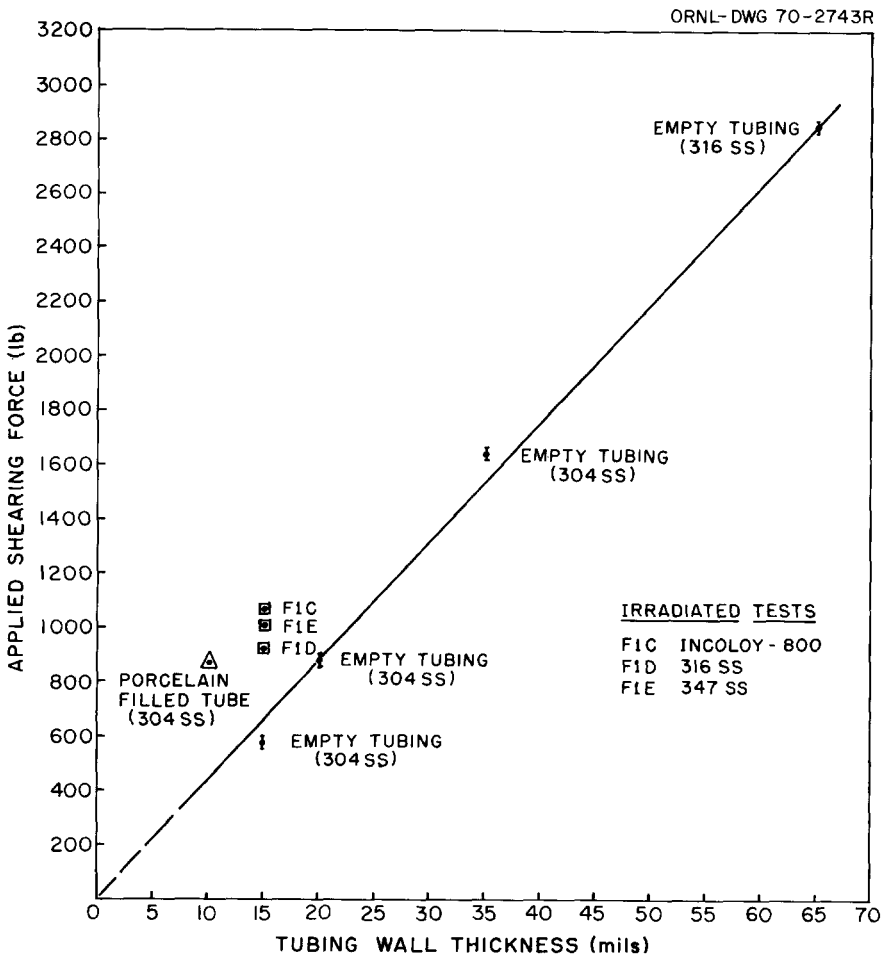

Fig. 2.12. Results of Single-Rod Shearing Tests Conducted in a Hot Cell.

Table 2.3. Packing Densities of 1-in.-long Sheared Sections of Prototype LMFBR Fuel

Cladding: type 304 stainless steel, 0.250 in. OD, 15-mil wall
Wire wrap: 0.091-in.-OD type 304 stainless steel
Rods: type 304 stainless steel, 0.250 in. OD

Condition	Packing Density (g/cc)	Fines (%)
Empty cladding (gas plenum); wire wrapped	1.77	
Clad; porcelain filled; wire wrapped	1.88	7.50
Clad; porcelain filled; gas plenum and cladding included; wire wrapped	1.84	8.00
Solid stainless steel rods	4.35	
Clad; $(U,Pu)O_2$ filled; gas plenum and cladding included; wire wrapped	3.26[a]	
Clad; $(U,Pu)O_2$ filled; wire wrapped	4.20[a]	
Clad; $(U,Pu)O_2$ filled (no wire wrapping)	4.96[a]	

[a]Calculated from data obtained on porcelain.

spacer wire and gas plenum section. These fuel rods, which are made of type 304 stainless steel (ASTM-A-269 grade) were of two types: solid rods, and 0.250-in.-OD by 15-mil-wall tubing. Porcelain was used as a stand-in for $(U,Pu)O_2$ pellets (Table 2.3).

Single-Rod Shearing Tests Conducted in a Hot Cell. – Information was compiled on the force required to shear single irradiated and unirradiated fuel rods, porcelain-filled tubes, and $(U,Pu)O_2$-filled tubes by using a small single-rod shear that was vacuum tight and hydraulic powered. The force required for empty unirradiated 0.25-in.-OD tubing[9] (plenum section) varied linearly with the wall thickness, from 580 lb for 10-mil-wall tubing to approximately 2850 lb for 65-mil-wall material. A force of 880 lb was required to

[9]This tubing met ASTM-A-269 standards.

shear porcelain-filled 0.25-in.-OD tubing with a 10-mil wall thickness (Fig. 2.12).

The force required to shear $(U,Pu)O_2$ rods that had been irradiated in the EBR-II to a burnup of about 1800 Mwd/ton was about the same as that required for the porcelain-filled rods. The 15-mil-wall type 316 stainless tubing required an average force of 1005 lb, while the 15-mil-wall Incoloy 800 tubing required an average force of 1068 lb. All of the cuts, the lengths of which varied from ¾ to ⅞ in., were made with a sharp blade. The blade cut the fuel rods cleanly, with little pillowing or tearing; only 3% of the irradiated, pelletized fuel reported to the fines fraction. In previous tests,[10] shearing 0.25-in.-OD by 10-mil-wall tubing into 0.25-in. lengths dislodged 75% of the sol-gel $(U,Pu)O_2$ (irradiated to a burnup of 20,000 Mwd/ton) from the badly crushed pieces. When the length of the sheared pieces was increased to 0.75 in., only 20% of the $(U,Pu)O_2$ was dislodged. These data illustrate that the quantity of fines produced by shearing is closely related to the amount of cladding deformation produced by the shear blade. No difference in behavior of the irradiated and unirradiated tubing was observed.

Alternative Head-End Process

Melt-decladding is being studied as an alternative for the shear-leach head-end process. By heating fuel assemblies above the melting point of stainless steel (1450°C), it may be possible to separate the molten cladding from the urania-plutonia core material and to volatilize the fission product gases as well.

A summary of some scoping melt-declad experiments is presented in Table 2.4. In each run, 5- to 6-in. lengths of 0.375-in. stainless steel tubing encasing 0.27-in.-diam urania pellets were heated above the melting point of steel in an induction furnace. In all of the runs made after run 4, the specimens were inserted in a 2.5-in.-diam, 18-in.-long cylindrical alumina crucible that had a closed spherical end and was inclined from the horizontal at an angle of 10°. In runs 5–7, at least 90 wt % of the molten stainless steel separated from the urania pellets. Only one stainless steel–urania specimen was present in run 5, whereas four samples were placed side by side in the alumina tube in run 6 and ten specimens were wired together in a stack of conical cross section in run 7. Of 90 urania pellets present in run 7, one intact pellet was carried a distance of about 6 in. by the molten steel flowing to the lower end of the crucible. The amount of urania lost to the separated steel was generally on the order of 0.001 to 0.002 wt %. Loss of urania occurred principally by the floating of oxide fragments on the surface of the molten steel.

Photographs of the urania and stainless steel at the end of runs 5 and 12 are shown in Fig. 2.13. In run 12, two urania pellets were placed at each end of the specimen, and the center 2-in. section of tubing was filled with 10.9 g of urania fragments ranging from 300 to 600 μ in size. The specimen was inserted in a 2.5-in.-diam cylindrical alumina crucible inclined at an angle of 10° from the horizontal. About 75 wt % of the stainless steel (i.e., a total of 38 g) separated from the urania and collected at the lower end of the crucible. The separated steel contained only 10 ppm of uranium. The urania fragments were impregnated with 2.5 g of molten steel during the run and formed a cylindrical mass that remained between the pellets.

The small-scale demonstration experiments show that a considerable quantity of molten steel (47 to 90 wt %) can be separated from the urania pellets; however, the process would require much more study and development before it could be scaled up for use with a reactor fuel element.

[10] *LMFBR Fuel Cycle Studies Progress Report for January 1970, No. 11*, ORNL-TM-2871 (February 1970).

Table 2.4. Summary of Melt-Declad Experiments

Run	Geometry	No. of Specimens	Temperature (°C)	Weight of Stainless Steel (g)	Percent of Stainless Steel Separated
3	5° incline; 0.625-in.-diam Al_2O_3 cylinder	1	1700	32	69
4	6° incline; 0.625-in.-diam Al_2O_3 cylinder	1	1750	32	47
5	10° incline; 2.5-in.-diam Al_2O_3 cylinder	1	1550	32	97
6	10° incline; 2.5-in.-diam Al_2O_3 cylinder	4	1550	132	90
7	10° incline; 2.5-in.-diam Al_2O_3 cylinder	10	1550	286	94
8	10° incline; flat Al_2O_3 boat with 0.25-in.-diam holes	1	1600	27	73
9	10° incline; flat Al_2O_3 boat with 0.25-in.-diam holes	4	1650	107	82
11	10° incline; 2.5-in.-diam Al_2O_3 cylinder	9	1550	243	76
12	10° incline; 2.5-in.-diam Al_2O_3 cylinder	1	1460	38	75

PHOTO 100289

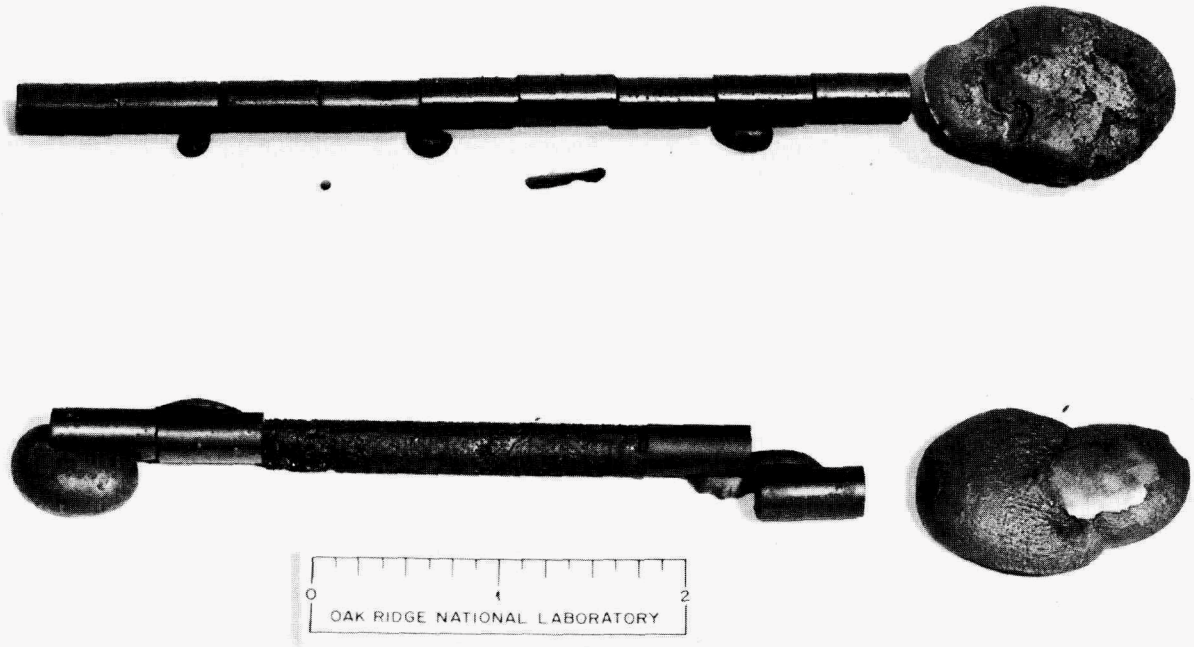

Fig. 2.13. Photographs of the Urania and Stainless Steel from Two Melt-Declad Experiments.

Although no further melt-declad experiments are planned, similar studies at Argonne National Laboratory will be followed.

2.3 REMOVAL OF VOLATILE FISSION PRODUCTS

As the nuclear power industry grows and the number and size of the fuel reprocessing plants increase, the release of radioactive noble gases, tritium, and iodine to the environment will become a much more important consideration than at present. In the future, the removal of essentially all radionuclides from the plant off-gas may be required. Efficient retention of iodine, which requires careful control even in present reprocessing plants, will become much more critical when short-cooled LMFBR fuels are processed.

Exploratory tests were described previously[11,12] of a new head-end processing step (termed voloxidation) designed to release volatile fission product gases from the fuel prior to aqueous processing. The objective of this step is to transfer the iodine, krypton, xenon, and tritium from the fuel into a relatively small volume of gas from which they can be efficiently removed in concentrated form for storage or permanent disposal. Extrapolating from information in the literature and from our preliminary experiments, we are hopeful that this objective can be met by heating the oxide fuel to some reasonable temperature in flowing oxygen or air.

Recent tests were made with short-cooled fuel specimens. This allowed us to study the behavior of ^{131}I in each of the processing operations.

Tests with Short-Cooled Fuel

The behavior of the volatile radionuclides in processing was studied with four irradiated stainless-steel-clad fuel rods containing sol-gel 15% PuO_2–85% UO_2 microspheres. The rods had been irradiated in the ETR to about 20,000 Mwd/ton and cooled 32 to 65 days. About 50% of the ^{85}Kr and ^{133}Xe but essentially none of the other radionuclides were released to the off-gas when the fuel rods were sheared. From 8 to 67%

[11] *Chem. Technol. Div. Ann. Progr. Rept. May 31, 1968,* ORNL-4272, p. 41.

[12] *Chem. Technol. Div. Ann. Progr. Rept. May 31, 1969,* ORNL-4422, p. 67.

Table 2.5. Removal of ^{131}I from Irradiated Fuel by Voloxidation Treatment

Length of Sheared Sections (in.)	Voloxidation Conditions		^{131}I Removed (%)[a]
	Time (hr)	Temperature (°C)	
1/4	8	450	41
1/4	8	650	74
1/4	4	750	32
3/4	8	750	50

[a]Percent of total ^{131}I fed to the voloxidizer.

of the ^{131}I and from 11 to 65% of the $^{134-137}Cs$ had migrated and condensed in the cooler portions of the fuel rods (the gas plenum and end plugs) and were recovered by leaching these sections. The variations within these ranges apparently resulted from differences in the temperature of the fuel in each rod during irradiation.

In the voloxidation tests, the fuel rod segments were heated in a stream of helium and then oxidized at 450, 650, or 750°C for 4 or 8 hr in pure oxygen (0.1 ft^3/hr). In most tests, the weight gain (~12%) upon oxidation was equivalent to the conversion of UO_2 to U_3O_8, although some of the gain may have been due to oxidation of the stainless steel cladding. From 32 to 74% of the ^{131}I in the fuel rods was removed; the best result, 74%, was obtained at 650°C (Table 2.5). About 50% of the ^{85}Kr and ^{133}Xe in the shear fuel rod segments was removed by the voloxidation treatment. Based on the total amounts found in shearing, voloxidation, and dissolution of the fuel following voloxidation, about 75% of the ^{85}Kr and ^{133}Xe and from 63 to 81% of the ^{131}I were separated from the sheared fuel rods prior to dissolution.

Tritium. – Only about 4% of the calculated yield of tritium was found in these experiments. Less than 0.01% of the calculated amount was released during shearing; essentially all of that found was released from the fuel during voloxidation. Apparently, most of the tritium had escaped from the fuel rods during irradiation.

2.4 DISSOLUTION AND FEED PREPARATION

Data on the leaching of irradiated fast reactor fuels are very limited. Information is needed concerning the dissolution rate and the metal recoveries to be expected as a function of the preparation history, the irradiation conditions, and the postirradiation temperature history of the fuel. We are procuring irradiated oxide fuels from as many sources as possible for testing. In addition to metal recovery data, information concerning the composition and physical characteristics of the leach residues is being obtained. Particular attention is also being given, both in laboratory and hot-cell studies, to the behavior of iodine in the dissolver-condenser system and to the use of fumeless dissolving techniques for minimizing the volume and fume content of the off-gas to allow easier separation and containment of the iodine and, possibly, the ^{85}Kr and ^{133}Xe.

Hot-Cell Tests

The effect of nitric acid concentration on the fuel dissolution rate was studied in basket-type leaching tests using stainless-steel-clad, coprecipitated 20% PuO_2–80% UO_2 pellet fuel that had been irradiated in the EBR-II to about 1800 Mwd/ton. Small perforated baskets containing fuel segments were lowered into boiling 8, 10, and 12 *M* HNO_3 of sufficient volume to yield final heavy-metal concentrations of 0.5, 0.75, and 1.0 *M* respectively. The rate of dissolution of most of the fuel was followed by a weighing technique, that is, by determining the weight loss of fuel in the basket. The final solution was filtered to separate undissolved materials; these were washed and analyzed. Finally, the leached cladding was dissolved in 5 *M* HNO_3–2 *M* HCl–0.05 *M* HF and analyzed for uranium, plutonium, and iron. Increasing the nitric acid concentration in the range of 8 to 12 *M* greatly increased the fuel dissolution rate (Fig. 2.14). The times required to dissolve 99.9% of the U + Pu with 12 and 8 *M* HNO_3 were, respectively, about 40 and 400 min. The uranium/plutonium ratio in the final residues was usually in the range of 0.2 to 0.5 (as compared with the ratio of 5 in the original fuel), indicating that some of the plutonium in the irradiated fuel rods was wholly or partially segregated. Based on iron analyses, about 5% of the stainless steel cladding was dissolved in these leaching tests.

As a part of the processing campaign with short-cooled 15% PuO_2–85% UO_2 sol-gel fuel (irradiated to about 20,000 Mwd/ton), fuel segments were given three 4-hr leaches in boiling 8 *M* HNO_3 and one 4-hr leach in boiling 8 *M* HNO_3–0.05 *M* HF after voloxidation (see Sect. 2.3). Leaching data were also obtained for unoxidized fuel and for fuel that had not been irradiated. Plutonium recoveries from the last two samples were 99.9% or higher in the first three leaches (with 8 *M* HNO_3). However, the presence of a thoria

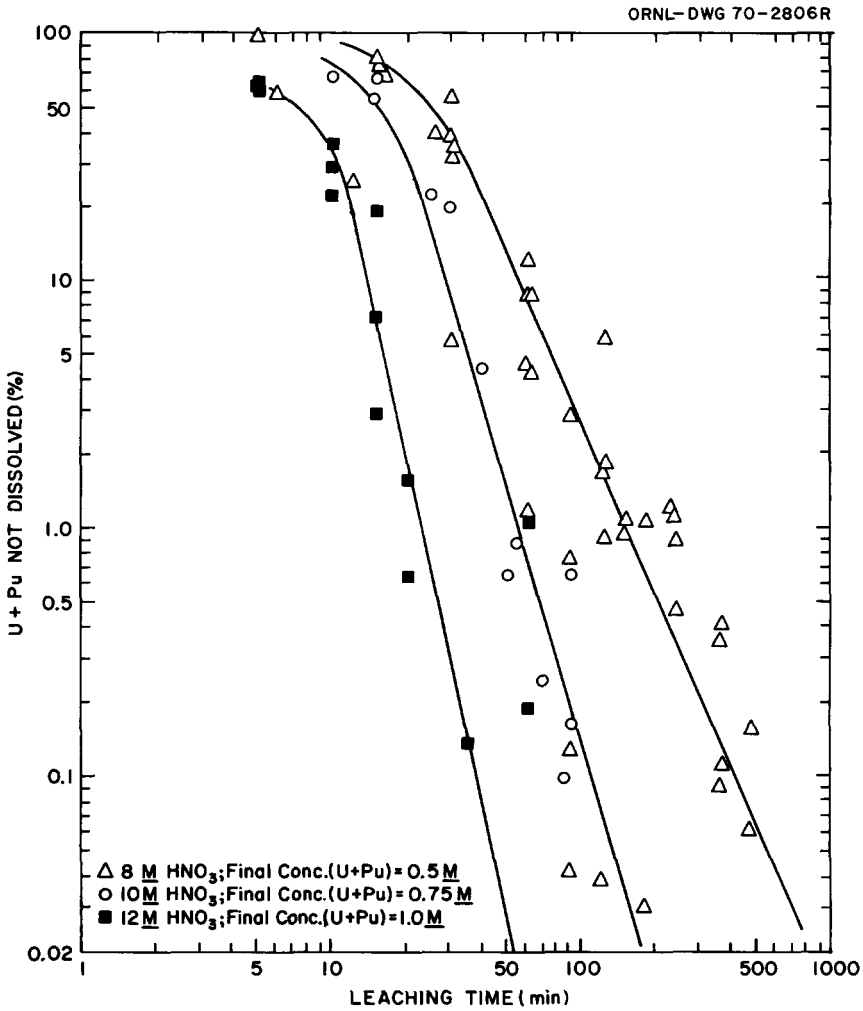

Fig. 2.14. Dissolution Rate of 20% PuO_2–80% UO_2 (1800 Mwd/ton) in Boiling Nitric Acid.

impurity, which diffused from the insulator pellets[13] into the fuel column, had a strong adverse effect on the leachability of the fuel samples that had been voloxidized. The oxidation of the $(U,Pu,Th)O_2$ evidently caused disproportionation of the UO_2 to U_3O_8, leaving a stable fluorite lattice of $(Th,Pu)O_2$ that was not dissolved by prolonged leaching with 8 *M* HNO_3. The effect was much more pronounced for samples that had been oxidized at 750°C than for those oxidized at 450°C; for example, the amounts of undissolved plutonium after 12 hr of leaching were about 15 and 2% respectively. However, the plutonium in these residues was dissolved successfully in the fourth leach with the solution that contained HF.

The undissolved residues remaining after the four leaches contained about 0.05% of the plutonium, less than 0.09% of the uranium, up to 30% of the ^{95}Nb, and up to 65% of the $^{103-106}Ru$. The three nitric acid leaches dissolved about 5% of the type 304 stainless steel cladding; HF in the fourth leach accelerated the corrosion of the cladding as expected, giving as high as 18 to 36% dissolution. The leached cladding, which was finally dissolved for material balance purposes, contained about 0.02 mg of plutonium per gram, that is, about 20 g of plutonium per ton of leached cladding.

[13]The fuel rods for the tests contained thoria rather than urania insulator pellets to aid in the mass spectrometric determination of the burnup by minimizing the introduction of uranium and plutonium isotopes into the fuel. Unfortunately, the flux in the irradiation position at the reactor was much higher than predicted, causing melting and cross-mixing of the thoria into the urania-plutonia fuel column and of the fuel into the plenum sections.

This amount of plutonium is less than 0.01% of the original plutonium in the fuel.

In these tests, we found essentially no tritium in the fuel solutions, off-gas scrub solutions, or off-gas samples when we dissolved fuel specimens that had been oxidized. In the test with the unoxidized sample, all of the tritium was found in the fuel solution (as expected). Up to about 90% of the ^{131}I that was in the unoxidized fuel sample was released from the dissolver solution during dissolution, and was recovered in the scrubber solutions and by leaching the condenser and dissolver. Smaller quantities of ^{131}I were released when oxidized fuel was dissolved.

Solubilities of Fission Products

A synthetic fission product solution was prepared by using nonradioactive chemicals. Each fission product element was present at a concentration equal to its expected value if mixed core and blanket materials from the AI Reference Oxide Reactor were dissolved to a final concentration of 500 g (U + Pu)/liter in 2.8 *M* HNO_3. However, the solution did not contain uranium or plutonium. Each fission product element (a total of 26), except the gaseous elements (Xe, Kr), ^3H, I, Br, Nb, Sn, Sb, Ge, Tc, and Pm, was included if its calculated concentration[14] equaled or exceeded 0.1 mg/kg (U + Pu). Ruthenium dissolved readily, as nitrosyl ruthenium hydroxide [$RuNO(OH)_3 \cdot H_2O$], although up to 60% of this element has been found in undissolved residues in hot-cell dissolution tests with LMFBR fuel specimens.

The solubility of niobium in various concentrations of nitric acid was determined by spectrographic analyses of the material obtained by filtering the reaction mixture produced by adding small volumes of a concentrated aqueous solution of $K_8Nb_6O_{19} \cdot 16H_2O$ to nitric acid solutions. Analytical data for 1, 3, and 5 *M* HNO_3 from duplicate tests were 0.24 and 0.30, 0.42 and 0.72, and 1.2 and 0.16 mg of Nb per liter respectively. The discrepancy between the last two values at 5 *M* HNO_3 is unexplained. These values are much lower than the niobium concentration (i.e., ~5 mg/liter) that would result if all the niobium dissolved on preparation of a short-cooled feed solution with a heavy-metal concentration of about 70 g/liter. Similarly, tin was shown to have a solubility in 1, 3, and 5 *M* HNO_3 of less than 1 mg/liter, as compared with a value of about 5.5 mg/liter that would be obtained if all of the tin dissolved in the fuel solution. These measurements indicate that more than 80% of the tin and niobium will be present in the undissolved residue after feed adjustment.

Silver introduced unexpected complications since it precipitated nearly quantitatively from our stock solution as a chloride as the result of impurities present in the chemicals. This indicates that AgI, which is much less soluble than silver chloride, could precipitate in LMFBR fuel dissolver solutions. Except for losses of iodine by vaporization, silver and iodine would be present in approximately stoichiometric quantities, that is, about 3.5×10^{-3} gram-atom of each per kilogram of U + Pu. Studies were initiated to determine the stability of AgI in boiling nitric acid and nitric acid–fission product–uranium solutions. These tests included, in some cases, the addition of sodium nitrite, which is present in dissolver solutions and which oxidizes soluble I^- to I_2. In initial tests, AgI appeared to be stable in the nitric acid solutions, although some of the iodide was oxidized to iodine when silver and iodide were initially present in equal amounts as AgI. No iodine evolution was observed visually in tests with only 10 and 20% of the expected iodide present (as AgI) but 100% of the expected Ag present (the balance as soluble $AgNO_3$). The results of these latter tests correspond to the separation of 90% or 80% of the iodine from the fuel in head-end processing steps.

Tests with Irradiated Carbide Fuel

Unclad, fractured pellet (20% PuC–80% UC) remnants from a United Nuclear Corporation EBR-II irradiation experiment[15] were divided into several aliquots for hot-cell tests. The fuel had been irradiated to about 26,000 Mwd/ton.

Reaction of the irradiated 20% PuC–80% UC with demineralized water was studied to determine the effect of accidental exposure of the fuel in a ruptured element to the water in a storage canal. Small fragments of the fuel were contacted with water. The temperature of the water was held at 25°C for 4 hr, then at 85°C for 4 hr, and finally at 27°C for 16 hr. No significant volume of gas was evolved, in contrast to earlier experiments in which irradiated (U,Pu)C showed some hydrolysis in water. The leach water contained about 1% of the gross gamma emitters (predominantly ^{137}Cs) but no heavy metals. The (U,Pu)C pieces were then boiled in fresh

[14] *LMFBR Fuel Cycle Studies Progress Report for August, No. 6*, ORNL-TM-2710 (October 1969), pp. 19–22.

[15] D. Stahl and A. Strasser, *Post-Irradiation Examination of High-Density (U,Pu)C Pellet-Fueled EBR-II Rods Irradiated to 30,000 Mwd/ton*, UNC-5198 (January 1968).

Table 2.6. Release of ^{85}Kr from Irradiated (U,Pu)C

Conditions: temperature, 450°C; oxygen flow rate, 0.1 ft^3/hr; duration of test, 1 hr

	Test No.		
	1	2	3
Fuel weight, g	2.57	2.16	1.56
CO_2 formed, cm^3 per g of fuel	103	2.7	<0.1
^{85}Kr released, % of total[a]	94	81	97

[a]Average amount of ^{85}Kr in the fuel was about 1.7 mc/g.

Table 2.7. Results of Dissolving Oxidized (U,Pu)C in Boiling 8 *M* HNO_3

	Test No.		
	1	2	3
Original carbide weight, g	2.57	2.16	1.56
Final oxide weight, g	2.78	2.10	1.61
Dissolution time, hr	19.0	8.2	7.5
Residue, % of initial fuel weight	0.54	0.41	0.13
Undissolved, % of total			
Uranium	0.08	0.15	0.02
Plutonium	1.0	0.50	0.24
Gamma emitters	2.4	4.9	5.1

water for 3 hr. Again, there was no gas evolution or dissolution of uranium and plutonium; however, an additional 2.5% of the ^{137}Cs dissolved.

Oxidation of Carbides with Oxygen. – Portions of unclad fractured pellets were suspended in a platinum bucket in a stainless steel burner at 450°C and reacted with oxygen for 1 hr. After each oxidation test, the burner was leached with nitric acid to determine the extent to which (if at all) fission products had condensed on the walls and the amount of uranium and plutonium that had fallen from the platinum bucket during the oxidation. In three experiments, the amounts of ^{85}Kr released from the fuel ranged from 81 to 97% (Table 2.6). In the first experiment, the carbide carbon was quantitatively converted to CO_2. Little CO_2 was detected in the second experiment and essentially none was detected in the third, apparently because the carbon was converted to methane or CO by reaction with residual water left in the burner from the previous leaching step. The tritium appeared in the off-gas scrubber that contained 0.1 *M* HNO_3. None was detected in the molecular sieve traps or during subsequent dissolution of the oxidized fuel. The amount of tritium found was only 0.25% of the amount calculated from the fast fission yield for ^{239}Pu. Direct dissolution of a sample of the irradiated carbide fuel in nitric acid indicated that only about 0.63% of the calculated yield of tritium was present. Fission product analyses indicated that some of the ^{137}Cs and ^{106}Ru had volatilized and then condensed on the cooler portions of the burner. However, less than 0.01% of the gamma-emitting nuclides were found in the 0.1 *M* HNO_3 off-gas scrubber, as compared with 36% of the ^{137}Cs and 2% of the ^{106}Ru found previously[16] when (U,Pu)C was burned in oxygen at 800°C.

[16]J. R. Flanary *et al.*, *Hot-Cell Studies of Aqueous Dissolution Processes for Irradiated Carbide Reactor Fuels*, ORNL-3660 (September 1964).

The "ash" from the oxidations was leached with boiling 8 *M* HNO_3 under reflux for 19 hr in the first test and about 8 hr in the second and third tests. Uranium losses were less than 0.2% in each case, but plutonium losses ranged from 0.24 to 1.0% (Table 2.7).

Direct Dissolution of Irradiated (U,Pu)C. – Three portions of the irradiated 20% PuC–80% UC were dissolved in nitric acid. The initial vigorous reaction was controlled by the slow addition of HNO_3 to the fuel fragments immersed in cold water. Later, heat, along with additional acid, was applied to bring the acid concentration to about 8 *M*. The leaching times in the three tests ranged from 3 to 7 hr. Losses of plutonium to the residues ranged from 0.04 to 0.13% and averaged 0.09%. The uranium loss was less than 0.1% in each test. The soluble carbon contents of the fuel solutions from two of the tests were 2.9 and 2.1 mg/ml, which are equivalent to about 68% and 59%, respectively, of the carbide carbon in the (U,Pu)C pellets. Presumably, the remaining carbon was evolved as a gaseous product. Earlier experiments indicated that about one-half of the carbide carbon is evolved as CO_2 when UC is dissolved in nitric acid.[16]

Volatilization of Iodine from Feed Solutions

Variables affecting the volatilization of iodine from nitric acid solutions are being studied as guidelines for the development of methods for achieving efficient removal of iodine from the solvent extraction feed solution. Separation of essentially all of the iodine from the uranium and plutonium prior to solvent extraction would greatly facilitate attainment of the very high processing plant retention factors for iodine that will be needed in processing short-cooled fuels.

Volatilization tests with 4 *M* HNO_3 solutions containing carrier iodine and ^{131}I tracer suggest that the

volatilization of I_2 may be affected at low I_2 concentrations ($<5 \times 10^{-5}$ M) by the hydrolytic reaction

$$I_2 + H_2O \rightleftharpoons HOI + I^- + H^+ ,$$

in which the iodide ion (I^-) is rapidly reoxidized back to elemental iodine (I_2) by the nitric acid, particularly when nitrite is present. The tests have also shown that, after most of the iodine has been volatilized, the residual ^{131}I does not readily react or exchange with fresh carrier iodine. The net effect is that, based on present knowledge, achieving essentially complete volatilization of the radioiodine will be a difficult task even if relatively large amounts of carrier iodine are added. In actual feed solutions, the formation of stable complexes of iodine with certain fission product metals may also be expected to retard iodine volatilization.

In a series of sparging (transpiration) tests with 250 ml of 4 M HNO_3 and a gas flow rate of 67.5 ml/min, the rate constants were 0.0037, 0.0066, 0.0090, and 0.0013 min^{-1}, respectively, at 40, 50, 60, and 70°C. The sparge gas was a 2:1 mixture of N_2 and N_2O_3. The use of N_2O_3 (or NO or NO_2) is required to establish the proper redox conditions. Usually, the initial iodine concentration was 5×10^{-4} M I_2 (plus tracer ^{131}I). The concentration change with time was followed by counting samples of the sparged solution.

A typical volatilization curve obtained in these sparging tests is shown in Fig. 2.15. The linear part of the semilogarithmic plot shows that the first-order relationship, $-(dc/dt) = kc$, where the iodine partial pressure is proportional to the iodine concentration (Henry's law), is obeyed initially. The curvature shown after approximately 95% of the iodine has volatilized suggests that part of the iodine is hydrolyzed and that the use of Henry's law is invalidated since c does not represent the true iodine concentration.

In many cases, I_2 or KI, which is rapidly oxidized to I_2, was added to the iodine-depleted solution of a transpiration test to increase the carrier concentration to the initial 5×10^{-4} M I_2. Continuing the transpiration tests with these solutions did not remove a significant fraction of the remaining tracer iodine. The tracer apparently did not exchange appreciably with the new carrier.

Some distillation experiments were made at about 105°C with 4 M HNO_3. In this case, water vapor serves as the effective carrier gas. A small amount of N_2O_3 is also required to maintain the proper redox condition. Since the partial pressure of iodine is very high, only about 2% of the volume must be distilled to obtain greater than 95% iodine removal. Further iodine

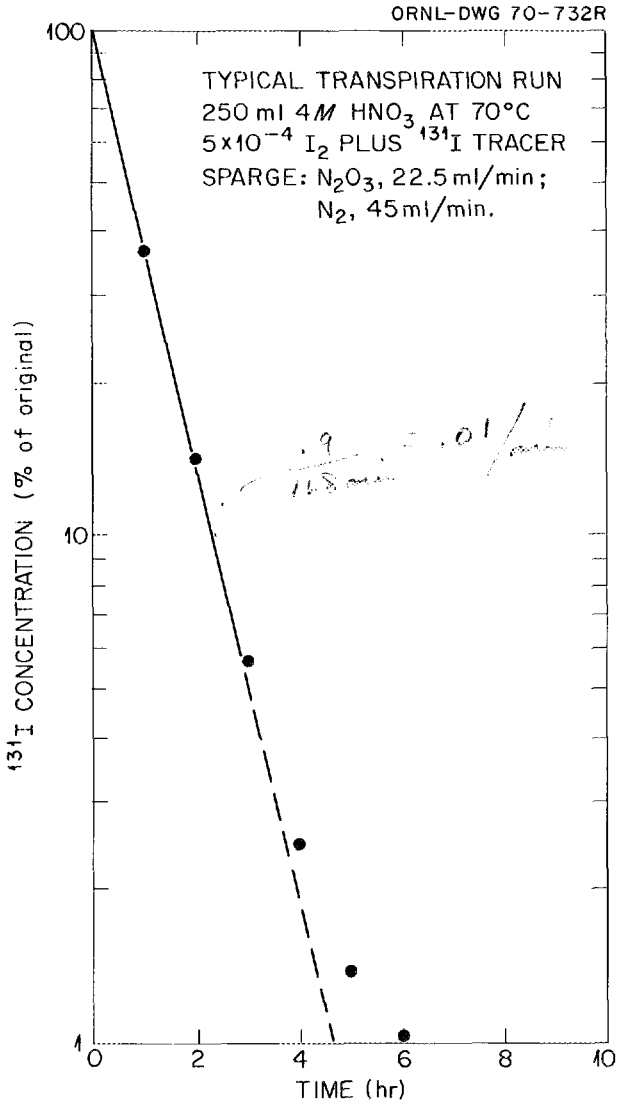

Fig. 2.15. Sparging of Iodine from 4 M HNO_3.

volatilization is slow and the addition of carrier iodine does not markedly increase the rate of removal. After distillation of 10 to 20% of the original volume of solution, the activity of the iodine tracer slowly decreases to about 0.5% of its original value.

Studies of the exchange of ^{131}I tracer with carrier iodine were made with the residual solutions after distillation; these solutions usually contained less than 5% of the original ^{131}I tracer. The original concentration of iodine (5×10^{-4} M) was restored by adding cold iodine carrier, and the solution was then extracted with CCl_4. An ^{131}I extraction coefficient (E_a^o) of 1 was usually obtained. In two tests in which the solution was autoclaved at 250°C for several hours prior to the

solvent extraction step, the extraction coefficients were 45 and 75; the latter value is close to the value (~90) reported in the literature for elemental iodine extraction. These results show that high temperature or, perhaps, high pressure promoted the rate of exchange between the ^{131}I tracer and carrier iodine. A second reaction also promoted the exchange reaction. The residual solution was made alkaline (about 1.5 N OH^-) and then reacidified with HNO_3 (about 2 N H^+). Extraction with CCl_4 after this treatment always gave extraction coefficients of 25 or larger.

These experiments are significant when we consider iodine removal in the dissolution–feed adjustment systems. If 99% removal of iodine (i.e., an iodine DF of 10^2) is achieved by sparging or distilling the dissolver solution, it is apparently not feasible to obtain 99.99% removal (a DF of 10^4) simply by adding cold iodine to restore the original iodine concentrations and repeating the sparging or distillation step.

Dissolution Equipment Concepts

A prototype continuous screw-type dissolver was designed for use in material transport and leaching studies. This unit is expected to have a capacity of 5 kg of (U + Pu) per hour with sheared LMFBR prototype fuel. It features a stainless steel screw to advance material through the dissolver. This screw is enclosed within a perforated sheath to contain fuel pieces and wire spacers. Powdered material that passes through the sheath will be mixed by using a spiral stainless steel wire brush or tape to wipe the external heated stationary housing. This unit has evolved from a study of several dissolver concepts and from studies made with spiral brushes for fuel transport. The use of a brush as the sole means of fuel transport is unsatisfactory since the wire spacers became entangled permanently within the brush. However, the brush will prevent powdered material from caking on the dissolver wall, which is heated, and allow new surfaces to be presented continuously to the dissolvent. A spiral tape should produce the same result but has not yet been tested.

2.5 SOLVENT EXTRACTION WITH TBP

Initial emphasis in the solvent extraction studies has been on establishing flowsheet conditions for the interim processing of LMFBR fuels in an existing plant. The first-cycle solvent extraction flowsheet is based on the use of 15% TBP and feeds of low plutonium concentration in existing geometrically unrestricted equipment. Boron poisoning might also be used for criticality control. The overall process calls for the coextraction and partitioning of plutonium from uranium in the first cycle, followed by two TBP cycles for further purification of the plutonium. Alternatively, amine extraction or anion exchange may be used in place of TBP extraction for the third cycle. In addition, where pertinent, the studies are being expanded to include those of a more general nature in order to define the most suitable flowsheets for use in plants designed specifically for processing LMFBR fuels.

Extensive studies are being made to obtain a better understanding of the factors affecting solvent degradation and to evaluate our tentative conclusion that problems arising from solvent radiation damage during the processing of short-cooled LMFBR fuels will not seriously impair the efficiency of the Purex process.

Flowsheet Development

The use of the digital computer to simulate the Purex process offers a rapid and inexpensive method for exploring the interrelated effects of varying process parameters in flowsheet development. A successful code can be particularly useful in analyzing process disturbances and detecting conditions that could lead to nuclear criticality.

We have written a program called SEPHIS, which is patterned after a model suggested by Lowe.[17] An important difference is that our program handles mass-transfer equilibrium data for plutonium, uranium, and nitric acid in a manner suggested by researchers in Germany and improved by Horner.[18] The program predicts the concentrations of each solute in both liquid phases of every stage as a function of time. It has been used to establish flowsheet conditions for processing various potential LMFBR fuels and to aid in setting up initial concentration profiles for laboratory batch-countercurrent runs. Agreement between the data from laboratory batch-countercurrent runs and data predicted using SEPHIS has been good. The comparison for the first-cycle coextraction of uranium and Pu(IV) at 25°C using 15% TBP–85% n-dodecane is shown in Table 2.8. Good agreement (results not shown) was also obtained for the second-cycle extraction of plutonium.

---

[17] J. T. Lowe, "Calculations of the Transient Behavior of Solvent Extraction Processes," *Ind. Eng. Chem., Process Design Develop.* 7, 362–66 (1968).

[18] D. E. Horner, *A Mathematical Model and a Computer Program for Estimating Distribution Coefficients for Plutonium, Uranium, and Nitric Acid Extractions with Tri-n-butyl Phosphate*, ORNL-TM-2711 (February 1970).

Table 2.8. Comparison of Experimental and Predicted Data for the First-Cycle Coextraction of Uranium and Plutonium

Aqueous feed: 3.2 *M* HNO_3, 67.7 g of U and 4.43 g of Pu(IV) per liter
Extractant: 15% TBP–85% *n*-dodecane
Scrub solution: 2 *M* HNO_3
Relative volumes, feed/organic/scrub: 1.0/1.8/0.3

Stage	Organic Phase						Aqueous Phase					
	U (g/liter)		Pu (g/liter)		HNO_3 (*M*)		U (g/liter)		Pu (g/liter)		HNO_3 (*M*)	
	Found	Predicted	Found	Predicted	Found	Predicted	Found	Predicted	Found	Predicted	Found	Predicted
Scrub-3	38.8	37.6	2.53	2.44	0.21	0.11	18.5	20.6	4.1	5.4	2.07	1.89
Scrub-2	42.1	41.0	2.91	3.35	0.21	0.09	23.0	25.9	5.8	9.1	2.10	1.88
Scrub-1	43.6	41.9	3.05	3.97	0.24	0.09	18.5	26.1	4.2	10.4	2.90	2.04
Feed							67.7		4.43		3.20	
Extraction-1	43.7	41.9	3.21	4.18	0.26	0.12	18.2	21.2	3.75	6.82	3.00	3.15
Extraction-2	13.9	15.3	2.65	4.92	0.29	0.28	2.72	1.74	0.91	1.70	2.90	3.30
Extraction-3	1.28	1.26	0.50	1.22	0.34	0.39	0.11	0.077	0.092	0.224	3.10	3.32
Extraction-4	0.07	0.056	0.074	0.161	0.34	0.40	<0.01	0.003	0.015	0.028	3.10	3.32
Extraction-5	<0.02	0.002	0.009	0.020	0.34	0.40	<0.01	<0.001	0.003	0.003	3.10	3.32
Extraction-6	<0.02	<0.001	0.002	0.002	0.35	0.40	<0.01	<0.001	0.001	<0.001	3.07	3.32
Extraction-7	<0.02	<0.001	<0.001	<0.01	0.39	0.39	<0.01	<0.001	0.001	<0.001	3.01	3.27
Extraction-8	<0.02	<0.001	0.004	<0.001	0.30	0.36	<0.01	<0.001	0.010	<0.001	2.64	2.77

Additional comparisons with laboratory results, especially for stripping operations, are being made to confirm the accuracy of the code over a wide range of experimental conditions.

Effect of Temperature on Plutonium Extraction. — In batch extractions with 15% TBP from a solution with a U/Pu ratio of 8, the plutonium extraction coefficient increased by a factor of about 3.5 as the temperature was increased from 23 to 60°C (Fig. 2.16). This relatively large temperature effect is due primarily to a decrease in competition for the extractant by uranium and nitric acid, which are extracted less efficiently at the higher temperatures. In the absence of uranium and at solvent loadings of about 15 g of plutonium per liter, the plutonium extraction coefficient increased from 3.8 to 4.1 as the temperature was increased from 30°C to 60°C.

Formation of a Third Phase. — In the TBP extraction system, a third liquid phase can form at high plutonium loadings. The maximum plutonium concentration obtainable in the solvent without the formation of a third phase increases as the aqueous-phase acidity, the total nitrate concentration, or the ionic strength is increased. Correlations with the ionic strength are shown in Fig. 2.17. With 15% TBP, the maximum loading obtainable without third-phase formation increased from about 20 g to 40 g of plutonium per liter as the ionic strength was increased from 2 *M* to 10 *M*. At equivalent ionic strengths, the maximum concentrations obtainable with 30% TBP were about 1.7 times those for 15% TBP.

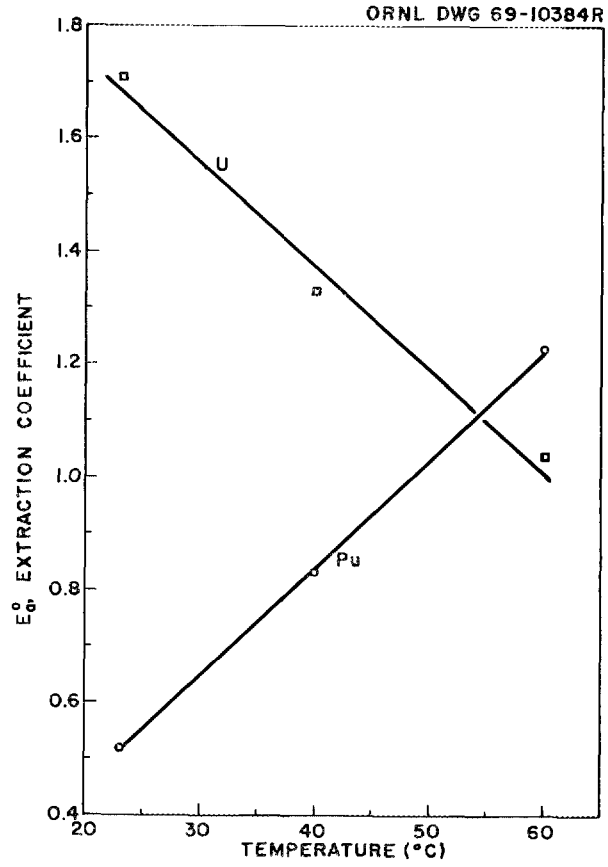

Fig. 2.16. Effect of Temperature on Plutonium and Uranium Extraction with 15% TBP–85% *n*-Dodecane. Aqueous phase: 3 *M* HNO_3, 7 g of Pu and 58 g of U per liter. Phase ratio: 1/1.

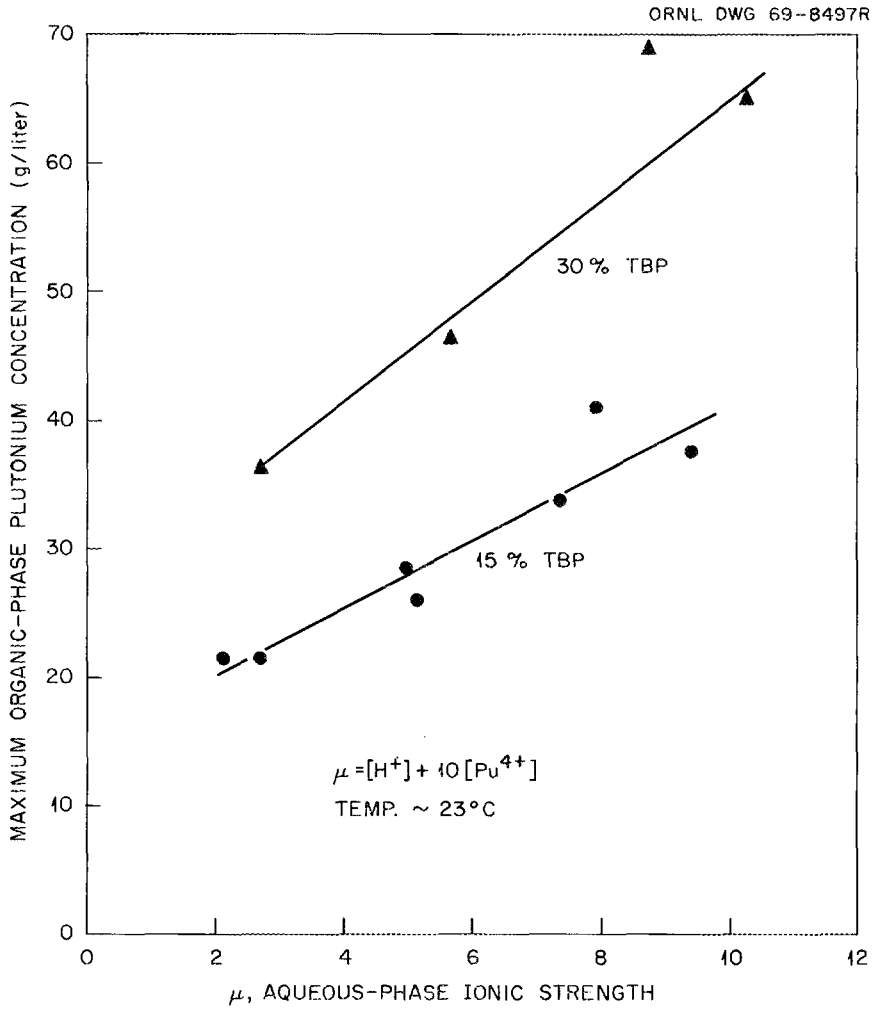

Fig. 2.17. Maximum Plutonium Loading of TBP–*n*-Dodecane Solvent Without Third-Phase Formation. Aqueous phase: $Pu(NO_3)_4$-HNO_3.

These data were obtained at 23°C. Results of subsequent tests have shown that the tendency for third-phase formation is much lower at higher temperatures. For example, at 40°C, we were not able to produce a third phase under any of the conditions tried, even when the plutonium concentration in the 15% TBP solvent was as high as 46 g/liter.

Stability of the Solvent

Two four-cycle batch crosscurrent solvent extraction experiments were performed with a solution of PuO_2-UO_2 fuel that had been irradiated to about 20,000 Mwd/ton and cooled 90 days. In these tests, the 15% TBP–85% *n*-dodecane solvent was contacted with feed under conditions that gave an estimated radiation dose to the solvent of 0.15 whr liter^{-1} cycle^{-1} in run 1 and 0.45 whr liter^{-1} cycle^{-1} in run 2; the difference in solvent exposures resulted from an increase in the extraction contact time (13 min in the first run vs 39 min in the second). The solvent was then scrubbed, stripped, and washed (twice with 0.1 *M* Na_2CO_3 and once with 3 *M* HNO_3) before being subjected to the next extraction cycle (Table 2.9). This was continued for four cycles to give cumulative solvent exposures of 0.60 and 1.84 whr/liter, respectively, in runs 1 and 2. The aqueous phase from the first extraction contact was contacted with six successive volumes of fresh solvent to complete the recovery of plutonium. The fission-product power level of the feed solution was about 2 (beta + gamma) w/liter.

The following tentative conclusions can be drawn from the results of the experiments:

Table 2.9. Conditions[a] Used in the Solvent Extraction Experiments

Stream	Composition
Feed (1.0 volume)	3 *M* HNO_3; 95 g of uranium and 20 g of plutonium per liter; 1.8×10^{11} gross beta counts min^{-1} ml^{-1}; 1.26×10^{11} gross gamma counts min^{-1} ml^{-1}
Scrub (0.3 volume)	2 *M* HNO_3; 21 g of uranium and 5 g of plutonium per liter
Solvent (1.8 volumes)	15% TBP in *n*-dodecane
Strip (0.9 volume)	0.10 *M* HNO_3
Solvent wash (0.45 volume)	0.1 *M* Na_2CO_3 (twice); 3.0 *M* HNO_3 (once)

[a]One complete solvent cycle consisted of one extraction contact, four scrub contacts, seven strip contacts, and the solvent wash.

1. The uranium loss to the raffinate was less than 0.001% in each cycle of each run. The plutonium loss to the raffinate in the first run ranged from 0.02 to 0.03%; in the second run, it increased from about 0.01% in the first cycle to 0.05% in each of the subsequent three cycles.
2. In the first run, losses of uranium and plutonium to the stripped solvent were less than 0.02% in the first cycle; because of insufficient sample volumes, the losses could not be determined for the remaining three cycles. However, the analysis of the washed solvent following the fourth cycle showed no significant retention of plutonium and uranium. In the second run, losses of plutonium to the stripped solvent were low (<0.02%) in the first two cycles. However, in cycles 3 and 4, the losses increased to 0.04% and 0.43% respectively. Uranium losses to the stripped solvent were low (<0.02%) in the first three cycles but increased to 0.35% in the last cycle. The high retention of plutonium and uranium by the solvent in the last cycle is unexplained. The carbonate wash treatments were not effective in removing the retained plutonium and uranium from the solvent, indicating that retention of these metals was caused by solvent degradation products other than dibutylphosphoric acid (a degradation product of TBP). More recent work indicates that solvent degradation from exposure to ultraviolet light (in the hot cell) may have been responsible for the observed effects.
3. Phase separation times for the extraction, scrubbing, and stripping contacts did not change significantly with cycling or with the level of radiation exposure, as shown below:

Operation	Phase Separation Time (sec)
Extraction	44 ± 4
Scrubbing	23 ± 2
Stripping	29 ± 4

4. Fission product decontamination data for these runs were erratic and do not allow positive conclusions concerning the effects, if any, of solvent radiation exposure on decontamination efficiencies.

Solvent Radiation Dose Estimates. – Estimates were made of the radiation dose that would be received by the solvent during the processing of AI Reference Oxide fuel (cooled 30 days) in pulsed columns. A range of feed and TBP concentrations was considered (Fig. 2.18). According to these estimates, the processing of mixed core and blanket material having an average burnup of 33,000 Mwd/metric ton with 15% TBP–*n*-dodecane would result in a solvent dose of about 0.11 whr $liter^{-1}$ $cycle^{-1}$. This value assumes a feed concentration of 70 g (U + Pu)/liter, a feed power density of 5.5 (beta + gamma) w/liter, and operation of an organic-phase-continuous pulsed extraction column at 80% of flooding. The solvent dose is relatively insensitive to changes in U + Pu concentration in the aqueous feed. On the other hand, increasing the TBP concentration from 15% to 30% increases the exposure by a factor of about 2. Also, the estimated exposures for processing core material alone are about 60% higher than for processing mixed core and blanket material. These estimates include an allowance (20% of the beta-gamma dose) for alpha radiation and for radiation from ^{131}I that may have accumulated in the solvent.

Decomposition of TBP and Precipitation of the Decomposition Products. – Studies of the decomposition of TBP when it is dissolved in 1, 3, and 5 *M* HNO_3 at 35, 50, and 75°C were completed. Gas chromatography was used to determine the quantities of methyl dibutyl phosphate, dimethyl monobutyl phosphate, and trimethyl phosphate that were formed by methylating[19] the corresponding TBP decomposition

[19]A. H. Kibbey and W. Davis, Jr., *Methylation and Gas Chromatographic Analysis of the Decomposition Products of Tributyl Phosphate,* ORNL-TM-2289 (Aug. 1, 1968).

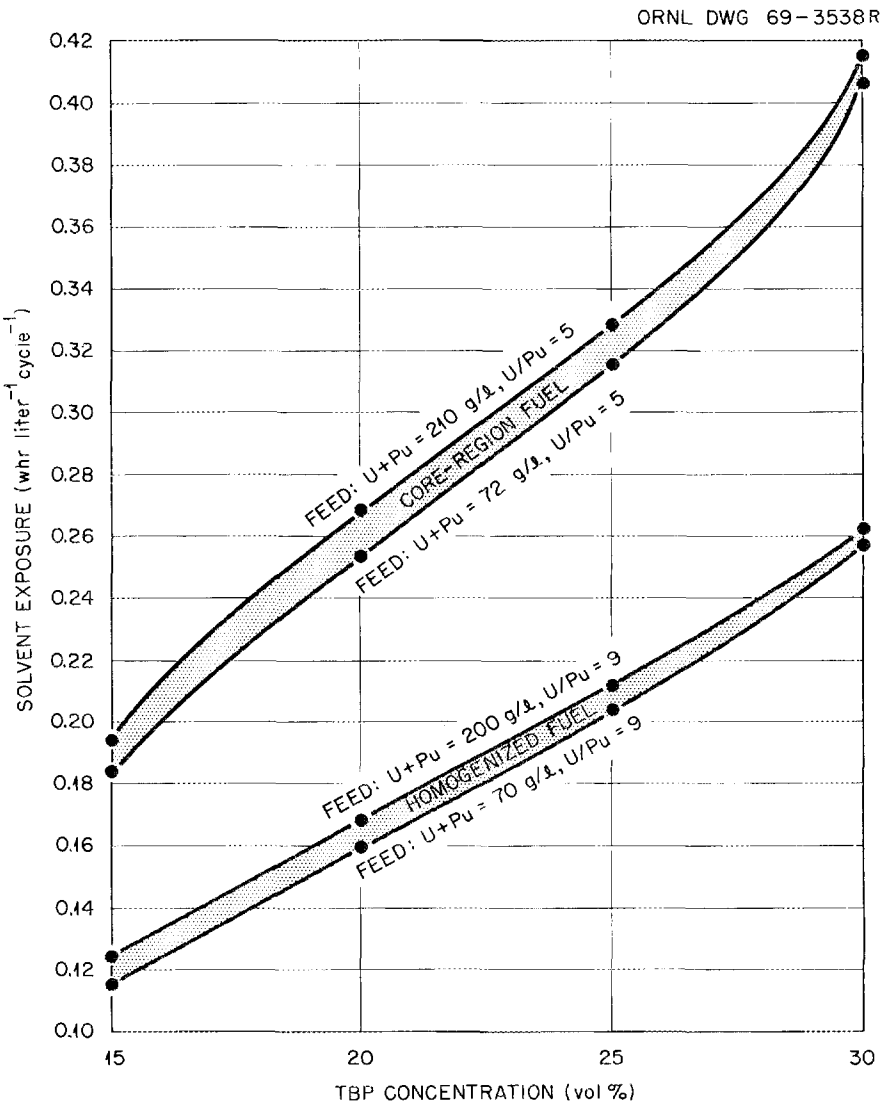

Fig. 2.18. Estimated Solvent Radiation Doses in Processing Al Core-Region Fuel Alone or Mixed Core and Blanket Material in Pulsed Columns.

products: dibutylphosphoric acid (HDBP), monobutylphosphoric acid (H_2MBP), and orthophosphoric acid. Reaction times ranged from 500 to 1500 hr. Only HDBP was formed in significant amounts at 35 and 50°C; at 75°C, significant amounts of H_2MBP were formed at all acidities. The end product, H_3PO_4, was formed in measurable quantities in 3 and 5 M HNO_3 at 75°C, but not in 1 M HNO_3. The data show that there is a dependence of decomposition rate on acidity, but they are not accurate enough to specify this dependence. At 1 to 5 M HNO_3, the measured rates of TBP decomposition (k_1S_0) at 35, 50, and 75°C were (0.6 to 1.2) $\times$ 10^{-4}, (0.3 to 1.0) $\times$ 10^{-3}, and (0.5 to 2.5) $\times$ 10^{-2} millimole liter^{-1} hr^{-1} respectively. These rates correspond to 0.01 to 0.025, 0.06 to 0.2, and 1.0 to 5.3 mg of TBP decomposed per liter of aqueous solution per hour. Here, k_1 is the first-order rate constant for TBP decomposition in the aqueous phase and S_0 is the solubility of TBP in the aqueous phase. Except under unusual conditions, the rates of TBP decomposition given above are probably not significant in terms of the quantities of HDBP required to cause precipitation and emulsion problems in solvent extraction plants.

An unusual but credible situation that could arise in a solvent extraction process is prolonged shutdown dur-

ing which the aqueous and organic phases are separated from each other for a considerable period of time. Experiments on the nature of solid zirconium butyl phosphates that are formed in place by the reaction of zirconium with HDBP or H_2MBP (from the decomposition of TBP dissolved in the aqueous phase) have yielded interesting results. Precipitates that formed at 50°C in solutions containing 0.25 to 1 g of zirconium per liter may be characterized as follows: (1) in 1 *M* HNO_3, the precipitate was predominantly peptized and passed through 0.45-μ Millipore paper; (2) in 3 *M* HNO_3, dispersed, readily filterable particles were formed; (3) in 5 *M* HNO_3, all of the precipitate formed a single sphere of solid plastic. Quantitatively, the precipitates contained 7 to 13 wt % zirconium, instead of 17.4% as would be expected for the simple compound $[(C_4H_9O)_2PO_2]_2ZrO$. Analyses of dried and undried precipitates for phosphorus, hydrogen, and carbon suggest that the precipitate in the aqueous phase contains up to 50 wt % TBP and considerable quantities of water (of hydration). Based on the measured TBP decomposition rates, the actual weights of undried precipitates collected on Millipore paper exceed the weights we would predict for $[(C_4H_9O)_2PO_2]_2ZrO$ by a factor of about 7. This retention of large amounts of TBP and H_2O by zirconium butyl phosphate precipitate may help to explain the bulky precipitates that are collected at the interfaces in operating plants, particularly where mixer-settlers are used.

Solubility data for zirconium dibutyl and monobutyl phosphates that are formed in place in nitric acid solutions were obtained by adding nitric acid solutions containing zirconium (including ^{95}Zr tracer) to nitric acid solutions containing dibutyl- or monobutylphosphoric acids, stirring for 24 hr, and filtering and analyzing the solutions for zirconium by counting techniques. The solubility of the zirconium dibutyl phosphate complex, expressed in milligrams of zirconium per liter, was 0.80 in 3 *M* HNO_3 and 1.74 in 5 *M* HNO_3. A value of 0.42 in 4 *M* HNO_3 was measured previously[20] by a different experimental technique. Based on these solubility data and the expected concentration (~0.21 g/liter) of zirconium in the feed, zirconium dibutyl phosphate should not precipitate at these acid concentrations until the HDBP concentration in the aqueous phase increases to a value in the range of 0.09 to 0.73 mg/liter.

[20]W. Davis, Jr., and H. H. Carmichael, *Solubility of Zirconium Dibutyl Phosphate in Solvent Extraction Solutions*, ORNL-2587 (January 1960).

Studies were initiated to determine the quantities of HDBP needed to cause precipitation and emulsion formation in the two-phase system of the first-cycle extraction system. In these experiments, the organic phase is 15 vol % TBP in *n*-dodecane (1.8 volumes); the aqueous feed solution (1 volume) contains either zirconium in 2 to 3 *M* HNO_3 or nearly the full spectrum of nonradioactive fission products and uranium in 2 to 3 *M* HNO_3; the scrub solution (0.3 volume) is 2 *M* HNO_3. The concentrations of fission products are in proportion to expected values for feeds obtained by dissolving mixed core and blanket material to concentrations ranging from 72 to 300 g of (U + Pu) per liter (the solutions do not contain plutonium or other transuranium elements). The experiments involved adding HDBP, as a component of the scrub solution or, in the larger quantities, as nearly pure $HDBP{\cdot}H_2O$, to vigorously stirred two-phase systems. If the total HDBP concentration is expressed as if it were solely an organic-phase concentration, no precipitation occurred at 50°C in either phase at 170 mg of HDBP per liter when the aqueous feed contained either 91 g of uranium per liter (plus the fission products and nitric acid) or zirconium alone in nitric acid; precipitation did occur in the aqueous phase at 360 mg of HDBP per liter. At an HDBP concentration of 600 to 1000 mg/liter, there was a visible accumulation of solids at the interface after agitation was terminated. At higher HDBP concentrations, precipitation occurred in the organic phase; however, the solid material slowly dissolved. When the HDBP concentration exceeded 4.2 g/liter, the organic-phase suspension still persisted after two days. Thus, precipitation of zirconium at 50°C in the two-phase system requires 200 to 400 mg of HDBP per liter (expressed as though all of the HDBP were in the organic phase) for systems containing fission products at concentrations such as those expected in LMFBR fuel processing operations. This range of HDBP concentration is at least tenfold higher than should result from chemical and radiolytic degradation in normal operation.

Chromatographic Studies of Solvent Degradation Products. – One of the major problems in studying the stability of solvent extraction processing reagents is the difficulty of identifying and separating the small quantities of degradation products that are formed. In view of this, we have begun a program to determine the applicability of liquid and/or gas chromatography to the separation and identification of the degradation products of extractants and diluents that may be used in the solvent extraction processing of LMFBR fuels. A Varian Aerograph micro-adsorption detector and a

Packard 7300 gas chromatographic system have been obtained, and preliminary studies have been initiated with the degradation products of TBP–*n*-dodecane solutions and of long-chain aliphatic amines.

Liquid chromatography experiments using the micro-adsorption detector and pure solutions showed that as little as 1 μg of HDBP or 0.1 μg of TBP was detectable using *n*-heptane containing 0.1 vol % isopropyl alcohol as the carrier liquid. To detect these reagents, the reference chamber was packed with 105- to 115-μ Teflon powder (a nonadsorbing material), and the other chamber was packed with 60- to 74-μ unfired Vycor glass powder (a highly adsorbing material). The solute in the carrier liquid reacted with the porous glass, causing an increase in the temperature that was sensed by a thermistor.

TBP may be separated from HDBP by liquid chromatography using silanized glass beads as the adsorbent and *n*-heptane as the carrier phase. A 5-μl sample of *n*-dodecane solution that was 0.05 *M* in TBP and 0.05 *M* in DBP was injected onto a 10-cm-long, 4.6-mm-diam column packed with 60/80 mesh beads that had been deactivated by silanizing with dimethyldichlorosilane. The effluent was monitored with the micro-adsorption detector. The TBP emerged from the column in 2 min and 6 min, respectively, when *n*-dodecane and HDBP were used as the carrier phases. Both components were identified by their respective retention times as determined by using samples of *n*-dodecane solutions containing the individual components.

Effect of Light on Solvent Degradation. – The effect of light on the chemical degradation of TBP–*n*-dodecane was studied to determine if excessive exposure to light could have been responsible for some anomalous results obtained in a recent cyclic solvent extraction experiment performed in a hot cell. In this experiment, the losses of plutonium and uranium to the stripped solvent increased from a negligible value (<0.02%) in the first cycle to 0.43% and 0.35%, respectively, in the fourth cycle. This did not appear to be a radiation damage effect since it had not been observed in similar tests at comparable radiation exposure levels. It is possible that the observed damage was caused by chemical attack, accelerated by exposure to light, since earlier workers[21] had found that, under certain conditions, the presence of light caused a slow photoreduction of U(VI) to U(IV) accompanied by the decomposition of TBP and the precipitation of uranium(IV) dibutyl phosphate.

Our studies show that, when TBP–*n*-dodecane solutions containing uranium are exposed to light, the amount of uranium retained by the extractant through the stripping and solvent wash cycles increases significantly. A 15% TBP–85% *n*-dodecane solution that had been loaded with uranium by contacting it with 3 *M* HNO_3–0.4 *M* $UO_2(NO_3)_2$ solution was placed about 5 cm from a 100-w mercury vapor (ultraviolet) lamp. Aliquots of the solvent were periodically removed, stripped by consecutive contacts with 0.1 *M* HNO_3, and then washed with 0.3 *M* Na_2CO_3 and 3 *M* HNO_3. After 2 hr of exposure, 0.21% of the uranium was retained through the strip cycle, and 0.01% was retained in the carbonate and acid washes. A control sample that had been kept in the dark retained 0.03% and essentially none of the uranium after the strip and wash cycles respectively. Gas chromatographic studies of the washed samples showed only two peaks, *n*-dodecane and TBP, for the control sample; seven additional minor peaks were found in the sample that had been exposed to light. Increasing the exposure period to 24 hr increased the uranium retention to 1.2% after stripping and 0.04% after washing.

Similar results were obtained on prolonged exposure to a weaker light source. When the uranium-bearing organic was held at a distance of 10 cm from a 15-w fluorescent tube for eight weeks, the uranium that was retained through the stripping cycle leveled off at 3 to 4% after four weeks of exposure (Table 2.10). The amount retained through the wash cycle increased to 1.3% after three weeks, but then decreased on further

Table 2.10. Effect of Light on the Retention of Uranium by TBP

Exposure[a] (weeks)	Uranium Retained by the Organic (%)	
	After Strip[b]	After Solvent Wash[c]
1	1.52	0.12
2	2.41	1.23
3	2.6	1.3
4	3.5	1.0
6	3.4	0.5
6 (control stored in dark)	0.18	<0.01
8	3.8	0.4

[a]Exposure conditions: 15% TBP–85% *n*-dodecane having a uranium concentration of 48 g/liter, held 10 cm from a 15-w fluorescent tube.

[b]Seven consecutive contacts with 0.5 volume of 0.1 *M* HNO_3.

[c]Two consecutive contacts with 0.5 volume of 0.3 *M* Na_2CO_3, followed by contact with 0.5 volume of 3 *M* HNO_3.

[21]R. M. Wagner, *The Hydrolysis Products of Tributyl Phosphate and Their Effect on the Tributyl Phosphate Process for Uranium Recovery*, HW-19959 (April 1951).

exposure. For comparison, in tests with a control solution held in the dark for six weeks, only 0.18% of the uranium was retained after the strip cycle and less than 0.01% remained after washing with carbonate and acid. After two weeks, a black precipitate began to appear on the walls and bottom of the container that had been exposed to light, and this precipitate continued to increase in amount during the term of the experiment. At the end of eight weeks, the concentration of the uranium in the solution had decreased about 15%; presumably, this uranium was present in the precipitate.

Although the observed effects are probably not of importance with respect to plant operation, they could be highly important with respect to laboratory and hot-cell experiments. Therefore, appropriate precautions with regard to light exposure should be taken.

Alternative Extractants

Trialkyl phosphates with longer alkyl chains than TBP are being examined as possible substitutes for the latter. TBP has a relatively high distribution to the aqueous phase (about 0.2 g of TBP per liter of 0 to 3 *M* HNO_3 in contact with 0.5 *M* TBP in *n*-dodecane) during the extraction and stripping contacts. The TBP in the aqueous phase is subject to chemical degradation, particularly at elevated temperatures, to form principally HDBP. Extended holdup of product solutions between process cycles or evaporation of the solutions can lead to the formation of considerable quantities of HDBP, which can cause precipitation or reduced efficiency in the subsequent process cycle. Therefore, the use of longer-chain trialkyl phosphates such as trihexyl phosphate (THP) may be advantageous. Such compounds have extraction properties that are similar to those of TBP but have a lower distribution to the aqueous phase. In addition, it is known that the tendency to form a third phase at high thorium loadings decreases as the length of the alkyl chain is increased.[22] Presumably, this would also apply in the extraction of Pu(IV) and allow higher plutonium loadings (without third-phase formation) than are permissible with TBP.

Preliminary batch shake-outs showed that the coefficients for extraction of uranium from 0.1 to 5 *M* HNO_3 with 0.5 *M* THP or 0.5 *M* tri(2-ethylhexyl) phosphate (T2EHP) were approximately 1.1 to 4 times those obtained with 0.5 *M* TBP (Table 2.11).

The distribution of THP to dilute nitric acid solutions is at least a factor of 200 less than that of TBP. The distribution of the phosphates from 0.5 *M* solutions in *n*-dodecane to 0 to 3 *M* HNO_3 was determined by contacting the phases and measuring the concentration of the phosphate in the resulting aqueous phase by gas chromatographic techniques. The concentration of TBP, in grams per liter, increased from a value of 0.20 in water to a maximum of 0.24 in 1 *M* HNO_3 and then decreased to 0.17 in 3 *M* HNO_3. The concentration of THP was less than 0.001 g/liter in all of these solutions.

Table 2.11. Extraction of Uranium from Nitric Acid with Phosphate Esters[a]

Nitric Acid Conc (*M*)	Uranium Extraction Coefficient (E_a^o)		
	TBP	THP	T2EHP
0.1	0.034	0.11	0.14
0.5	1.09	1.2	1.3
1	2.9	3.6	5.4
3	12	35	24
5	16	25	32

[a]0.5 *M* in *n*-dodecane. Original aqueous phase had a uranium concentration of 0.9 g/liter. Phase ratio was 1/1.

Solvent Extraction Equipment

The current status of the stacked-clone contactor development program was reviewed in order to determine if this unique, high-capacity contactor has advantages that warrant exploitation in the LMFBR program, and, if so, what developmental work would be necessary. In addition, other possible potential applications were considered. Briefly, the study showed that: (1) at the scale of 5 to 10 tons of fuel per day, the stacked-clone contactor is not particularly adaptable to LMFBR processing, and (2) this device might prove useful in a 1-ton/day plant. Further studies of stacked-clone technology will be made only in the event that a specific application for the machine is found.

2.6. REMOVAL OF IODINE FROM OFF-GAS

The retention or control of iodine is one of the major problems to be solved in the development of short-decay processing capability for LMFBR fuels. Overall plant retention factors approaching 10^8 will be required for ^{131}I when 30-day-decay fuel is processed. In order to achieve an iodine retention of this order, new and highly reliable systems for removing iodine from all plant effluent streams must be developed. A significant reduction in the volume of all plant effluents, as compared with past experience, will be necessary to improve the economics of the required treatment systems. We are evaluating numerous potential methods

[22]T. H. Siddall III, *Anal. Chem.* **51**, 41 (1959).

of iodine removal, and, when a system is proved attractive in laboratory tracer-level experiments, small engineering-scale equipment is fabricated and evaluated on actual plant off-gas streams. During the past year, the primary effort in both laboratory-[23] and engineering-scale experiments has dealt with aqueous scrubbing with mercuric nitrate–nitric acid solutions, and with solid sorbents including silver zeolite, activated charcoal, and various plastics. An important feature in the application of solid sorbents is the removal, from the gas stream, of organic contaminants that severely poison charcoal and, to a lesser degree, poison silver zeolites. The use of catalytic oxidation methods to remove all organic materials from the gas stream, and to convert all iodine species to the elemental form, were extensively studied in the laboratory and were tested in engineering-scale experiments.

Scrubbing Iodine from Air with Mercuric Nitrate Solutions

Previous tests[24] showed that mercuric nitrate solutions effectively scrub methyl iodide (and higher alkyl iodides) from air. This, coupled with their known[25] ability for sorbing and fixing elemental iodine, indicates that the mercuric nitrate scrub system potentially represents a high-efficiency system for removing iodine in its more important forms from plant off-gases. Recent tests, however, have shown that, because of slow reaction kinetics, attainment of very high alkyl iodide removal efficiencies is probably limited to operation with relatively low linear gas flow rates through the scrub system.

The reaction rate of methyl iodide in solution with mercuric nitrate was investigated using a technique developed by Hasty[26] for measuring the rate of reaction of methyl iodide with hydrazine solutions. With $Hg(NO_3)_2$–0.005 M HNO_3 solutions, the measured reaction half-life at 30°C decreased by a factor of about 3 as the mercury concentration was increased from 0.005 to 0.02 M:

Mercury Concentration (M)	Reaction Half-Life (min)
0.005	1.36
0.01	0.63
0.015	0.52
0.02	0.44

The reaction with 0.1 M mercury solutions was too rapid to allow measurement of the reaction rate by this technique.

Extremely efficient removal of methyl iodide from air was demonstrated by dispersing air containing ^{131}I-labeled methyl iodide through a glass frit, at the rate of 100 cc/min, into a column of 0.1 M $Hg(NO_3)_2$–0.1 M HNO_3 solution. With a 15-in. depth of solution (225 ml) in the column, the iodine decontamination factor (DF) was 8.6×10^3. With 30 in. of solution, the DF was 8×10^4; with two columns in series, each containing 15 in. of solution, the DF was 7.6×10^5.

The high DF's obtained in bubble columns are not readily obtainable in packed columns operated with the gas phase continuous. Use of the latter is preferred in order to minimize the pressure drop across the scrub column. The efficiency of methyl iodide removal is governed primarily by the relatively slow rate of reaction of methyl iodide with mercuric ion in the aqueous phase to form a mercuric iodide complex, rather than by the rate of transfer of methyl iodide from the gas phase to the aqueous phase. (Under good contacting conditions, the latter rate is rapid.) The methyl iodide absorption coefficient, D_G^L (the ratio of methyl iodide concentration in the aqueous phase to its concentration in the gas phase), is only about 4 at 25°C. At tolerable solution pumping rates, high iodine DF's across the scrub column are obtained only when $V_{LH}/V_G{}^*$ is considerably larger than unity, where V_{LH} is the liquid-volume holdup in the column and $V_G{}^*$ is the gas volume throughput for a time period equivalent to the half-life of the reaction. Results are improved, of course, by increasing the mercury concentration to increase the reaction rate in the aqueous phase. However, since the holdup of solution in a conventional packed column is low, high DF's are obtained only at relatively low linear gas flow rates.

The limitations described for efficient methyl iodide removal apparently do not apply (or are much less severe) to the scrubbing of elemental iodine from the gas stream. Although the rate of reaction of mercuric ion with I_2 in the aqueous phase has not been measured, it is apparently rapid as compared with its reaction with methyl iodide. In addition, the relatively

---

[23] R. E. Adams, R. D. Ackley, Zell Combs, R. L. Bennett, and Ruth Slusher of the ORNL Reactor Chemistry Division are participating in the laboratory studies.

[24] *Chem. Technol. Div. Ann. Progr. Rept. May 31, 1969*, ORNL-4422, pp. 84–87.

[25] R. W. Stromatt, *Removal of Radioiodine from Purex Off-Gas with Nitric Acid and with Nitric Acid–Mercuric Nitrate Solutions*, HW-55735 (1958).

[26] L. C. Schwendiman, R. A. Hasty, and A. K. Postma, *The Washout of Methyl Iodide by Hydrazine Sprays, Final Report*, BNWL-935 (November 1968).

Table 2.12. Results of Scrubbing Methyl Iodide and Elemental Iodine from Air with Mercuric Nitrate–Nitric Acid Solutions in Packed Columns

Procedure: air containing CH_3I or I_2 was passed through a 2-in.-diam column containing 3 ft of packing wet with flowing scrub solution; iodine concentration in the inlet air ranged from 0.01 to 0.3 mg/liter

Iodine Species	Hg^{2+} Conc[a] (*M*)	Packing Material[b]	Flow (liters/min)		Approx Liquid Holdup in Column (liters)	Iodine Decontamination Factor
			Air	Scrub Solution		
CH_3I	0.2	A	2	0.10	0.055	1.8
			2	0.30	0.075	2.7
			0.5	0.10	0.055	18
			0.5	0.30	0.075	44
CH_3I	0.2	B	2	0.10	0.90	300, 330
			2	0.05	0.65	1,120
			2	0.015	0.60	1,130
			5	0.10	0.90	14
CH_3I	0.4	B	2	0.015	0.60	14,000
			5[c]	0.015	0.60	96
CH_3I	0.4	C	0.5	0.10	0.37	640
			2	0.05	0.32	6
I_2	0.4	B	2	0.015	0.60	1,070
			2	0.05	0.65	1,130
			5	0.05	0.65	1,180
I_2	0.4	C	2	0.10	0.37	760
			5	0.10	0.37	900
			15	0.10	0.37	1,080

[a]The HNO_3 concentrations were 0.1 *M* and 0.2 *M* for 0.2 *M* and 0.4 *M* Hg^{2+} solutions respectively.

[b]A – 0.25-in. berl saddles; B – cellulose sponge cut into about 0.25-in. cubes; C – porous ceramic saddles with maximum dimension of about 0.75 in.

[c]Pressure drop across the column was <1 in. of water.

high D_G^L for I_2 of about 80 (vs 4 for methyl iodide) is important in retaining I_2 in the solution long enough for the fixation reaction to occur.

Table 2.12 shows the results of scrubbing tests made with a 2-in.-diam column containing 3 ft of packing. When the column was packed with 0.25-in. berl saddles and the air and scrub solution flow rates were 2 liters/min and 0.1 liter/min, respectively, the DF achieved in scrubbing methyl iodide from air with 0.2 *M* $Hg(NO_3)_2$ solution was only about 2; decreasing the air flow to 0.5 liter/min increased the DF to 18. Use of a porous (sponge) packing, which increased the volume of solution held up in the column by an order of magnitude, greatly improved the results. The DF was as high as 1.1×10^3 with an air flow rate of 2 liters/min; increasing the air flow to 5 liters/min decreased the DF to 14. Increasing the mercury concentration to 0.4 *M* increased the DF's obtained with sponge packing to 1.4×10^4 and 96, respectively, for air flow rates of 2 and 5 liters/min. Much lower efficiencies were obtained with a porous ceramic packing in the form of saddles; however, the size of the packing (~0.75 in.) was much too large for efficient use in a 2-in.-diam column, and the results were probably adversely affected by inefficient transfer of methyl iodide to the aqueous phase.

In tests in which elemental iodine was scrubbed from air with a 0.4 *M* $Hg(NO_3)_2$ solution, DF's of about 10^3 were obtained when either sponge or porous ceramic packing was used. With the latter, increasing the air flow rate from 2 liters/min to 15 liters/min increased the DF from 760 to 1080, presumably because the more turbulent conditions existing in the column at the higher gas flow rate increased the efficiency of I_2 transfer from the gas to the liquid phase.

Trapping of Iodine with Solid Sorbents

We have initiated laboratory studies of solid sorbents for removing iodine in its various forms from gas streams. Our objective is to find systems that have high

efficiencies for removing different iodine species and that will maintain their integrity under all conditions expected to be encountered in treating off-gases from LMFBR fuel processing plants. To date, most of the tests have been made with silver zeolite, which is an efficient sorber and has the advantages of being noncombustible and less subject to poisoning than the treated charcoals. The silver zeolite sorbent, which is prepared by treating Linde molecular sieve (type 13X) with silver nitrate solution, was developed by Maeck[27] and co-workers at Idaho Nuclear Corporation.

Trapping of iodine, originally in the form of methyl iodide, with the silver zeolite was very efficient (>99.99% removal in a 2-in. bed) at 200°C and 400°C but not at 25°C (Table 2.13). Somewhat less efficient removal was obtained with a sample of silver-containing alumina. Other metal zeolites were prepared by treating Linde 13X molecular sieve (originally in the sodium form) with the corresponding metal nitrate or chloride salt. Of these, the potassium and cadmium zeolites showed the most promise; trapping of methyl iodide with a 2-in. bed of these sorbents at 200°C was greater than 99.9% efficient (Table 2.13). Results were only mildly encouraging or poor at 200°C with zeolites in the sodium, lithium, copper, magnesium, strontium, barium, zinc, mercury, lanthanum, cerium, ferrous iron, cobalt, nickel, chromium, lead, or manganese forms (results not shown).

The data of Table 2.13 were obtained in tests in which the iodine loading of the sorbent bed was low, that is, equivalent to about 0.5 mg of methyl iodide per cm^3 of sorbent. However, methyl iodide trapping with silver zeolite at 200°C was highly effective up to injection levels of 100 mg per cm^3 of sorbent (Table 2.14). The efficiency for trapping butyl iodide was also high, although appreciably lower than for methyl iodide. Silver-containing alumina, potassium zeolite, cadmium zeolite, and treated charcoal showed much lower capacities for iodine than did the silver zeolite.

Sorption on Porous Plastics. — It is well known that some plastic materials sorb iodine. One of the more common measurements used in the study of synthetic fibers is the iodine adsorption value of the fiber.[28] Other investigators have found that anion exchange resins sorb molecular iodine from air[29] and from aqueous solutions.[30] More recently we discovered that certain high-porosity plastic materials, available as macroreticular resins, sorb elemental iodine very effectively from nitric acid solution and air streams. An intensive study of these sorbers is now in progress since the preliminary tests indicate that they apparently have potential for use in trapping iodine in the early processing steps, for example, in removing iodine from head-end processing off-gases or from dissolver condensates and dissolver off-gas scrub solutions.

Table 2.13. Results of Trapping Methyl Iodide with Solid Sorbents

Conditions: air containing CH_3I was passed through sorber bed over 2-hr period; total CH_3I injected was about 0.5 mg per cm^3 of sorbent

Sorbent	Temp (°C)	Face Velocity of Air (fpm)	Trapping Efficiency (%)	
			1-in. Depth	2-in. Depth
Untreated zeolite (sodium form)	200	63	45	53
Silver zeolite	25	40		94.6
	200	63		99.99+
	400	90		99.99+
Potassium zeolite	200	63	96.7[a]	99.96[a]
Cadmium zeolite	200	63	98.8[a]	99.95[a]
Ag-alumina[b]	28	40	6.4	12.9
	100	50	99.65	99.99+
	200	63	99.99	99.99+

[a]Average results for two different batches.
[b]GX-100, a commercial silver-containing alumina from North American Carbon Co.

In batch equilibration tests, measured iodine distribution coefficients (i.e., grams of I_2 per gram of sorbent, divided by grams of I_2 per milliliter of aqueous phase) between 20- to 50-mesh Bio Bead SM-2 (nonionic, cross-linked polystyrene beads) and 1×10^{-4} N I_2 ranged from about 200 in water to 1000 to 3000 in 0.5 to 9 M HNO_3. In preliminary column runs with aqueous flow rates of about 2 cm^3 cm^{-2} min^{-1}, 1 g of Bio Bead SM-2 in a 4-mm-diam by 10-cm-long column sorbed 99% of the iodine from 1 M HNO_3–0.0011 N I_2 solution. The bed was loaded with about 24 mg of I_2 per gram of sorbent. About 70% of the iodine was eluted with 25 ml of 0.2 M NaOH. Further sorption-elution cycles showed no deterioration in the capability of the SM-2 to sorb iodine.

[27]W. J. Maeck, D. T. Pence, and J. H. Keller, "A Highly Efficient Inorganic Adsorber for Airborne Iodine Species," pp. 185–203 in *Proceedings of the Tenth Air Cleaning Conference, New York, August 28, 1968,* USAEC Report CONF-680821.

[28]"Study of Polynosic Fibers. V. Crystallinity and Accessibility of Polynosic Fibers," *Bull. Inst. Textile France,* No. 102, pp. 945–62.

[29]A. R. Giona, "Adsorption of Gas-Phase Iodine on Dry Ion-Exchange Resins," *Brit. Chem. Eng.* **10**(2), 82–85 (1965).

[30]B. Sansoni, "Specific Molecular Adsorption of Iodine on Anion Exchangers," *Angew. Chem.* **73**, 493 (1961).

Table 2.14. Results of Trapping Methyl and Butyl Iodides with Solid Sorbents at 200°C

Procedure: Air containing CH_3I or C_4H_9I (1-iodobutane) was passed through bed at face velocity of 63 fpm

Sorbent	Iodine Species	Run Time (hr)	CH_3I or C_4H_9I Injected (mg/cm^3 sorbent)	Trapping Efficiency for 2-in. Bed Depth (%)
Silver zeolite	CH_3I	1	14	99.99+
		2	39	99.99+
		4	82	99.99
		8	164	99.63
		12	235	97.7
Silver zeolite	C_4H_9I	4	17	99.84
		8	35	99.92
		32	140	99.39
		50	218	98.4
Potassium zeolite	CH_3I	0.75	11	77
		2	37	61
Cadmium zeolite	CH_3I	0.75	11	98
		2	37	92
Ag-alumina	CH_3I	1	14	83
		2	39	64
Ag-alumina	C_4H_9I	4	17	94
		8	35	83
		32	140	44
Treated charcoal[a]	CH_3I	1	14	86
		2	39	62

[a]Witco grade 19, 8 × 16 mesh, that was 5% triethylenediamine impregnated. The temperature was 28°C, and the air face velocity was 40 fpm.

Table 2.15. Sorption of Elemental Iodine from Dry Air on Macroreticular Resins

Procedure: dry air containing ~3 mg of ^{131}I-traced I_2 per liter was passed, at the rate of 150 ml/min, through a 5-mm-diam by 10-cm-deep column of sorbent until breakthrough, or for a maximum of 6 hr

Sorbent	Type of Plastic	Bed Loading (mg/cm^3 sorbent)	Iodine Sorbed (%)
Bio Bead SM-1	Polystyrene	51.1	98.8
Bio Bead SM-2	Polystyrene	86.2	99.95[a]
Amberlite series			
XAD-2	Styrene-DVB (20–50 mesh)	172	99.99+
XAD-4	Styrene-DVB	218	99.99+
XAD-7	Acrylic ester	50	99.99+
XAD-8	Acrylic ester (20–50 mesh)	171	99.99+
XAD-9	Acrylic ester containing sulfoxide	184	99.99+
XAD-11	Acrylamide polymer	133	99.99+
XAD-12	Probably acrylic ester with nitrogen-oxygen group	209	99.99+
XAD-284	Styrene-DVB–sulfuric acid	137	99.99+

[a]From observation of the coloring of the sorbent with iodine, there appeared to be some channeling of the gas through the bed. This channeling probably decreased the sorption efficiency.

All of the plastics examined thus far have been effective in removing iodine from dry air streams (Table 2.15). All but one of the resins in the Amberlite series sorbed more than 130 mg of I_2 per gram of sorbent while removing more than 99.99% of the iodine from the air.

Catalytic Oxidation of Organic Vapors

We are studying the destruction of organic impurities in process air streams by catalytic oxidation[31] to form carbon dioxide and water. This is a potentially attractive method for converting the organic iodides to a form (I_2) that can be more readily trapped and thus preventing poisoning of the iodine sorption beds with organic materials. Most of the studies have been made with Hopcalite (CuO-MnO_2) catalyst, which was originally developed for oxidizing CO to CO_2 but is also an effective oxidation catalyst for all organic fumes. Two instrumental methods, gas chromatography and thermal ionization, were used to measure concentrations of organic materials in air that had been passed through the catalyst material.

A study of the oxidation of dodecane, a solvent extraction diluent, revealed that thermal degradation and oxidation proceed in the absence of a catalyst to the extent of possibly 90% at 350°C. However, the different responses obtained in the gas chromatographic and thermal ionization gage methods indicated that thermal oxidation in the absence of a catalyst leads to the production of intermediate organic products rather than complete conversion to CO_2 and H_2O.

The sensitivity limit of the flame ionization gage (Beckman) was approximately 10 ppb; hence this device was used to measure the effectiveness of Hopcalite catalyst with methane-air and butane-air mixtures.

Methane has a symmetric structure, which makes it one of the more difficult compounds to oxidize. It is present in atmospheric air at a concentration of about 2 ppm and might be an important factor in the production of methyl iodide in a processing plant. Figure 2.19 shows the effect of oxidation temperature on the methane oxidation efficiency when air containing 2 ppm of methane was passed through a Hopcalite bed. The residence time of the gas in the bed was about 0.25 sec. About 75% of the methane was oxidized at 250°C, and about 100% was oxidized at 300°C. Butane was oxidized much more readily. With 256 ppm of butane in the air, oxidation was essentially complete at a temperature of about 225°C; with 137 ppm in the air, the required oxidation temperature for complete combustion using the same residence time was about 150°C.

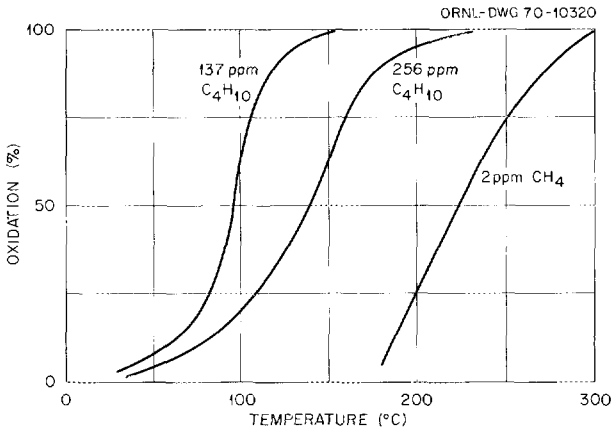

Fig. 2.19. Oxidation of Methane and Butane in Air Using Hopcalite Catalyst. A 1-in. catalyst bed and an air residence time of 0.25 sec were used.

A brief study showed that the catalyst bed can be poisoned by organic phosphates (e.g., TBP used in the solvent extraction process). Passing air containing trimethyl phosphate through the catalyst bed until it contained about 4.5% phosphate almost completely destroyed the catalyst activity. The effect of about one-half this amount of phosphate was roughly equivalent to that which would be observed if the bed was shortened or the gas residence time was decreased by a factor of 2. These studies are continuing; emphasis is on determining the life expectancy of catalyst beds under expected operating conditions.

Chemistry of Uncommon Iodine Species

Certain solid sorbents and the mercuric nitrate scrub system are effective for removing I_2 and organic iodides from gas streams. However, the possibility must be considered that other, possibly more-penetrating, iodine species could be present and limit the decontamination efficiency. We are attempting to generate such species so that their response to treatment can be tested.

It has been postulated that hypoiodous acid, HOI, may occur as an airborne iodine species, at least under conditions that may exist in a Pressurized Water Reactor accident.[32] Our tests have shown that, if a

[31] *Chem. Technol. Div. Ann. Progr. Rept. May 31, 1969,* ORNL-4422, p. 87.

[32] F. O. Cartan *et al.,* "Evidence for Existence of Hypoiodous Acid as a Volatile Iodine Species Produced in Water-Air Mixtures," pp. 342–49 in *Proceedings of the Tenth Air Cleaning Conference, New York, August 1968,* USAEC Report CONF-680821.

water solution of I_2 is added to caustic, surprisingly large amounts of the iodine (possibly as HOI) can be sparged from the solution.

In one test, water 0.00032 *N* in I_2 (traced with ^{131}I) was mixed with an equal volume of 0.2 *M* NaOH to give a 0.1 *M* NaOH–0.00016 *N* I_2 solution. Air was bubbled through 50 ml of this solution for 2 hr at the rate of about 300 ml/min, and the off-gas was passed consecutively through two CCl_4 scrubbers and an iodized charcoal trap. About 20% of the iodine volatilized and was held by the first CCl_4 scrubber, while no iodine was detected in the second CCl_4 scrubber. The amount found in the charcoal was less than 0.003% of the total iodine. Less than 10% of the iodine in the CCl_4 from the first scrubber could be stripped with 0.1 *N* $Na_2S_2O_3$ solution, indicating that the iodine was not in the form of I_2.

Extraction of iodine with CCl_4 (or with other solvents), followed by stripping with $Na_2S_2O_3$ solution, appears to be a useful tool for studying the chemistry of iodine in this system. Table 2.16 shows data on the extractability of iodine with CCl_4 from caustic solutions that had been aged for different periods after preparation. With 0.1 *M* NaOH, the amount of extractable iodine increased from 16.9% at 0.1 hr to about 22% after 1 to 3 hr and then decreased gradually until it was only about 2% after 5 days (although the total iodine content of the solution remained the same). Extraction (or, more probably, iodination of the CCl_4 or of an impurity in the CCl_4) was rapid since approximately the same results were obtained for 1-min and 1-hr contact times. With 0.5 *M* NaOH, the changes in the amount of extractable (reactable) iodine as the solution was aged followed the same pattern as with 0.1 *M* NaOH; however, the extractable amount was higher, reaching a maximum of about 34%.

Table 2.16. Results of the Extraction of Iodine from Caustic Solutions with CCl_4

Procedure: aqueous 0.00032 *N* I_2 solutions were mixed with caustic solutions to give solutions 0.00016 *N* in iodine; samples of the solutions were extracted with CCl_4 (phase ratio of 1/1, 1-min contact) after different aging periods

Aging Period of Aqueous Solution (hr)	Iodine Extracted (%) with:	
	0.1 *M* NaOH	0.5 *M* NaOH
0.1	16.9	24.4
0.4	14.3	27.3
1	21.6	33.7
1.5	21.8	29.2
2	21.8	30.8
2[a]	21.7	25.7
3	22.0	
5	20.8	22.8
24	15.2	9.7
120	2.3	0.8

[a]Extraction contact time of 1 hr.

The amount of iodine that reacts with different solvents varies appreciably. For example, in a comparative test, the fractions of iodine (in %) that were extracted from a 0.1 *M* NaOH solution in 10-min contacts at a 1/1 phase ratio by benzene, dodecane, dichloroethane, carbon tetrachloride, chloroform, and 0.1 *M* 4-*sec*-butyl-2-(α-methylbenzyl)phenol–dodecane were 27, 13, 36, 20, 43, and 28 respectively. We have not yet established whether these differences are due to reaction rate effects. Subsequent contact of the extracts with 0.1 *N* $Na_2S_2O_3$ solution stripped only 1 to 3% of the iodine.

The amount of iodine that can be volatilized from caustic solutions on extended sparging corresponds roughly to the amounts that can be extracted with the more-reactive solvents, thus indicating that the reactive iodine species is volatile. We are trying to substantiate this conclusion. The iodine species that we are preparing is apparently the same as the "active iodine" that was prepared by Cofman[33] by reacting KI-I_2 solution with 0.2 *M* NaOH. Cofman found that the "active iodine" reacted with aqueous-soluble phenols and, therefore, used this reaction in studying the stability of the species, which he concluded was HOI (or IOH). Our tests have shown that adding "cold" KI to the caustic solution up to a concentration ten times that of the original iodine decreases the amount of ^{131}I present as active iodine in proportion to the amount of KI added, indicating that rapid isotopic exchange occurs; the addition of iodate does not change the amount of extractable ^{131}I. If $Na_2S_2O_3$ is present in the caustic solution during the addition of I_2, formation of the active iodine species is completely prevented.

Engineering Demonstration of Iodine Removal from Dissolver Off-Gas

After a particular iodine removal system has been proved attractive in laboratory-scale tests, an engineering-scale demonstration of the system under conditions approximating actual plant conditions is highly desirable. The TRU facility provides an opportunity to test such systems under plant conditions and at ^{131}I

[33]Victor Cofman, "The Active Substance in the Iodination of Phenols," *J. Chem. Soc.* **115**, 1040 (1919).

levels of a few hundred curies per run. An experimental iodine removal system consisting of a catalytic oxidation bed followed by a charcoal bed was installed and operated on the TRU evaporator off-gas system in February 1968. Iodine-131 decontamination factors ranging up to 10^4 and averaging 10^3 were demonstrated over the six-week period of the TRU campaign. Based on these results and further laboratory development of both solid sorbents and liquid scrubbers, the system shown in Fig. 2.20 was installed on the TRU dissolver off-gas in August 1969. Since that time, it has been operated during three target processing campaigns carried out at TRU. Iodine was evolved from the nitric acid dissolver solution to the extent of 97 to 99%, either by air sparging for 8 to 12 hr or by evaporation of approximately 15% of the solution from the dissolver over a 2-hr period. The iodine removal equipment (shown in Fig. 2.20) consists of a condenser and condensate collection pot, a mercuric nitrate scrubber (the first scrubber), a caustic scrubber (the second scrubber), and a Hopcalite bed–charcoal bed system. This iodine removal system is probably not a combination that would be used on an actual plant dissolver off-gas, but was intended to demonstrate the effectiveness of the various components and to verify that the previously demonstrated removal efficiency ($>10^4$) of the Hopcalite bed–charcoal bed system would not be adversely affected by preceding it with other iodine removal systems.

Data from the eight experiments carried out with this equipment are summarized in Table 2.17. Iodine DF's of about 20 to 200 were observed across the mercuric nitrate scrubber during operation with 0.1 *M* mercuric nitrate and about 500 to 1000 when the concentration was increased to 0.4 *M* in the final series (19-DS) of runs. These results are in general agreement with laboratory studies for this type of scrubber. The variations in scrubbing efficiency are normal and are caused by changes in the iodine species fed to the scrubber and a minor change in flow rates. The second scrubber, operating with 0.1 *M* NaOH, demonstrated ^{131}I DF's ranging from 1 to 13. The primary purpose of the second scrubber was to protect downstream equipment from acid vapors. In one instance (run 13-DS-3) in which the first scrubber was operated with 0.1 *M* NaOH, a DF of 160, which is typical of a caustic

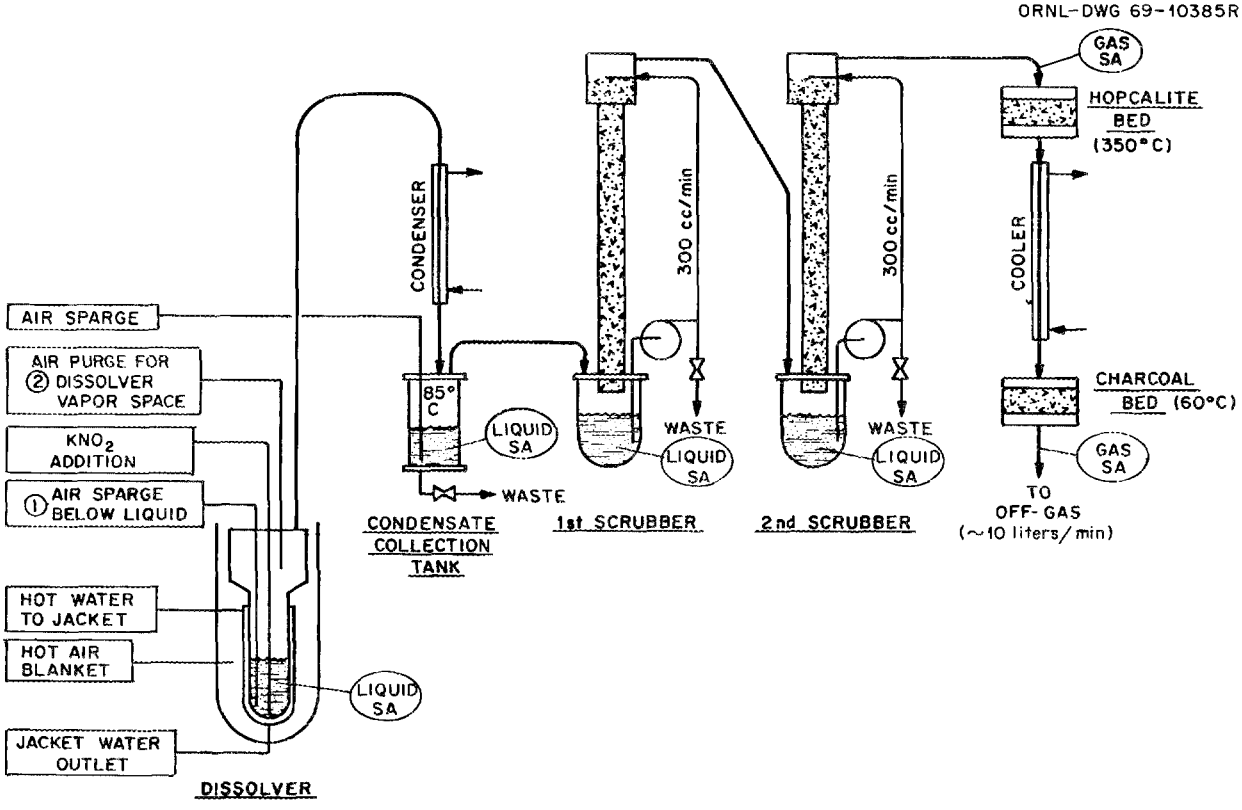

Fig. 2.20. Flowsheet Showing the Off-Gas Iodine Removal System for the TRU Dissolver.

Table 2.17. Summary of Data from Iodine Experiments at TRU

Run	Date	Iodine Passing Through Charcoal Bed (mc)	^{131}I DF			
			First Scrubber	Second Scrubber[a]	Charcoal Bed	Overall
13-DS-1	9/4/69	0.01	18[b]	9	2×10^4	3×10^6
13-DS-2	9/6/69	0.02	29[b]	13	1×10^4	4×10^6
13-DS-3	9/9/69	0.85	160[a]	2	270[c]	1×10^5
16-DS-1	1/27/70	0.01	209[b]	2.5	1.3×10^4	6.6×10^6
16-DS-2	1/30/70	0.48	116[b]	6	186	1.4×10^5
19-DS-1	4/8/70	0.033	1100[d]	1.2	1.7×10^3	3.0×10^6
19-DS-2	4/11/70	5.0	960[d]	3.2	8	2.7×10^4
19-DS-3	4/12/70	3.0	443[d]	4.6	14	3.3×10^4

[a]0.1 *M* NaOH.
[b]0.1 *M* mercuric nitrate plus 0.1 *M* HNO_3.
[c]Charcoal bed saturated with water from high humidity in off-gas.
[d]0.4 *M* mercuric nitrate plus 0.2 *M* HNO_3.

scrubber operating on a primary iodine source, was achieved. In the early runs, the DF's across the catalytic oxidation (Hopcalite) bed and charcoal bed were in excess of 10^4, which is in accord with previous results. However, as indicated by Table 2.17, the effectiveness of the charcoal bed decreased with time to a value of about 10 for the last two runs, indicating some degradation of either the Hopcalite bed or the charcoal bed, or both. The overall system DF in the early runs (i.e., 3×10^6 to 4×10^6) is encouraging and approaches the DF required for an actual plant off-gas system (i.e., 10^7 to 10^8). The loss in effectiveness of the charcoal bed emphasizes the need for an understanding of long-range factors affecting the life of solid sorbent beds. Valuable information in this area will be gained during the coming year, when a Hopcalite bed–charcoal bed system will be installed on the total vessel and cubicle off-gas from the TRU system. Although this system is the primary iodine removal system for the TRU facility and is not experimental in nature, much information can be gained on factors that influence DF and bed life.

2.7 RADIATION, SHIELDING, AND CRITICALITY STUDIES

The objective of this series of studies is to provide basic nuclear data to support the design and development of the LMFBR fuel cycle. The studies of radiation properties and shielding requirements of LMFBR fuels involve correlation of basic nuclear data including decay schemes, neutron cross sections, energy spectra of radiation sources, and thermal power; development of computer programs for the calculation of transient concentrations of radionuclides; calculation of attenuation kerma of shield materials of interest; and application of these data to LMFBR fuel cycle processes. The criticality studies involve compilation and correlation of basic data, liaison with experimental groups, development and verification of computational techniques, and development of criticality parameters and control techniques for specific process applications.

Radiation and Shielding Studies

Accomplishments in the past year have included the development of a capability in the ORIGEN program for computing the photon and neutron spectra of radioactive fuels, the calculation of the transient concentrations of radionuclides in a variety of fuels of interest in the LMFBR program, and the development of parametric data for use in the design of shields for spent-fuel shipping casks.

Development of the ORIGEN Program. – The ORIGEN program was provided with an extensive data library that permits the computation of the energy spectra of photon and neutron sources in mixtures of radionuclides. Within the limitations on available data, the photon sources include those from alpha, beta, and positron decay, internal transition, bremsstrahlung, (α,γ) interactions, and spontaneous fission. The neutron sources include spontaneous fission and (α,n) reactions in oxide fuel. Photon sources in fission products are described by 12 energy groups with energies varying from 0.3 to 5.25 Mev. Photon sources for the actinides are described by 18 energy groups; for these nuclides, the lowest energy group is subdivided into seven smaller

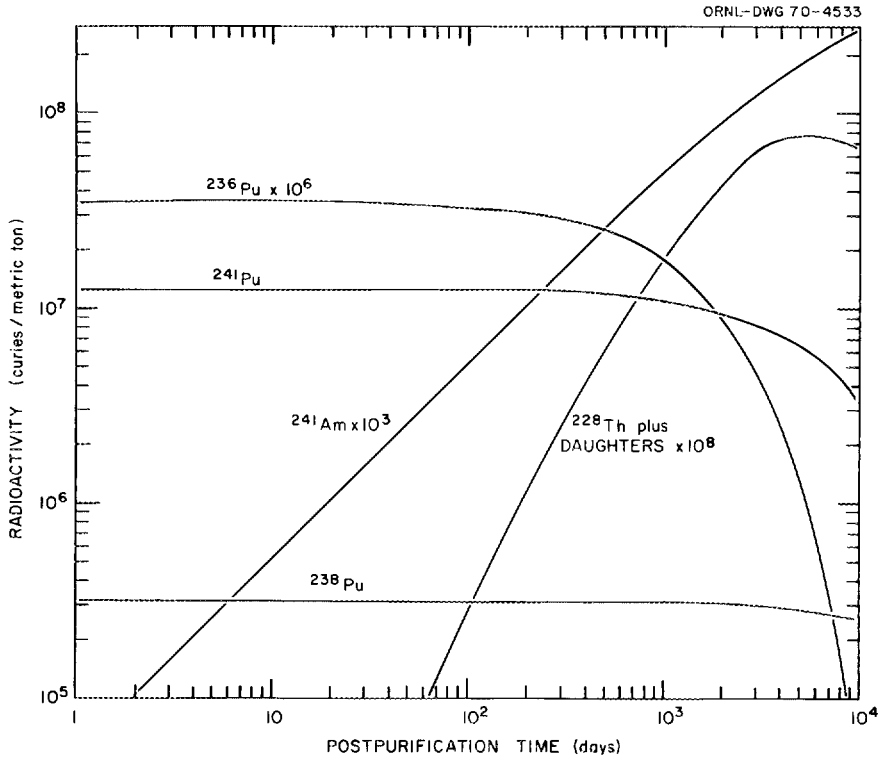

Fig. 2.21. Radioactivity of LWR Plutonium Product as a Function of Postpurification Time.

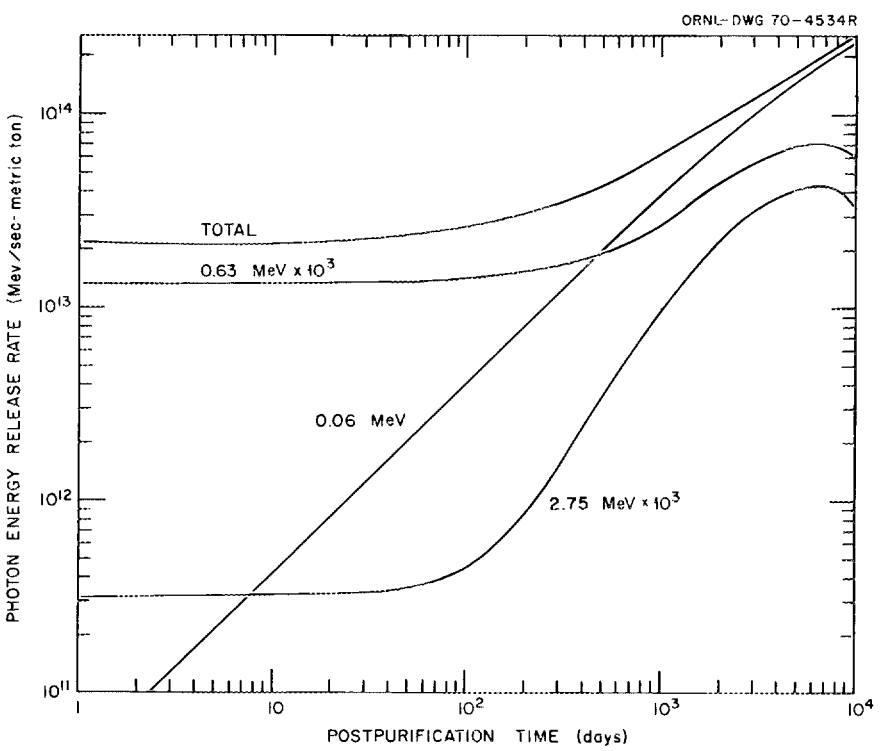

Fig. 2.22. Photon Energy Release Rate of LWR Plutonium Product as a Function of Postpurification Time.

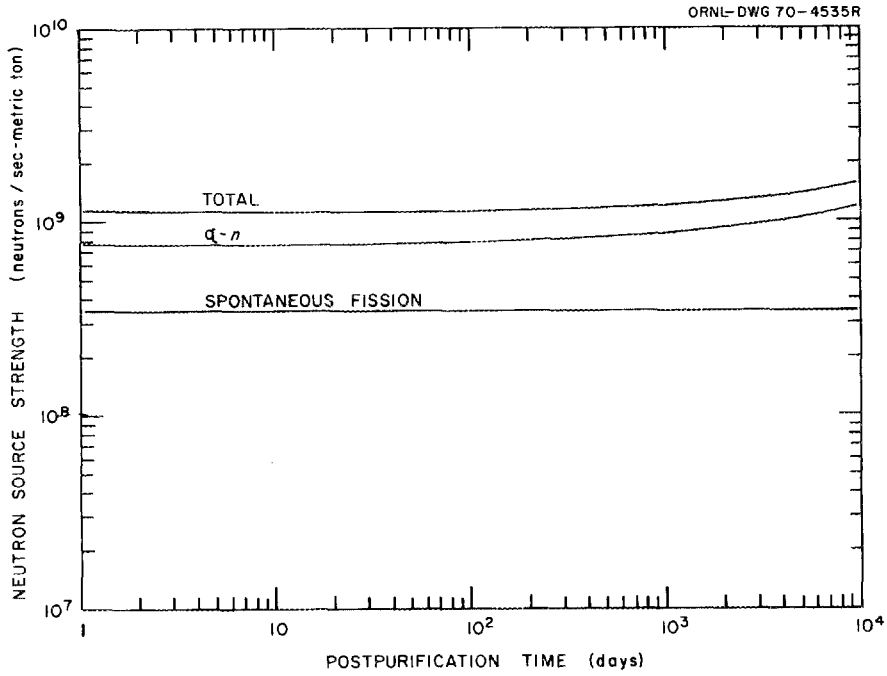

Fig. 2.23. Neutron Source Strength of LWR Plutonium Product as a Function of Postpurification Time.

groups to permit more accurate estimation of x-ray sources.

Figures 2.21–2.23 present the results of computations of the radioactivity, photon energy release rate, and the neutron source strength of plutonium product from a light-water reactor (LWR) as a function of time following the chemical separation from other elements. Initially, this plutonium was assumed to contain 1.9% ^{238}Pu, 59.1% ^{239}Pu, 24.0% ^{240}Pu, 11.1% ^{241}Pu, and 66 ppb of ^{236}Pu.

Actinide Concentrations in Discharged Fuel. – Calculations were made with the ORIGEN program to estimate the isotopic compositions of actinides in fuels discharged from LWR's and LMFBR's[34,35] (Table 2.18). These data are useful for estimating the properties of the plutonium that will be recycled to LMFBR's and for comparing the curium concentrations (and hence the neutron source strength) of LWR fuels with those of LMFBR fuels. The LWR fueled with 3.3% enriched uranium was assumed to have been operated at an average specific power of 30 Mw/metric ton to an exposure of 33,000 Mwd/metric ton. The corresponding values for the LWR fueled with recycled plutonium and natural uranium were assumed to be 27.5 Mw/metric ton and 33,000 Mwd/metric ton. The AI Follow-On LMFBR was assumed to have been charged with a mixture of depleted uranium and plutonium discharged from an LMFBR. The average specific power and exposure were assumed to be 92 Mw/metric ton and 67,000 Mwd/metric ton respectively.

Neutron Shielding Requirements for Spent-Fuel Shipping Casks. – The quantities of plutonium and transplutonium isotopes that are produced in high-burnup LMFBR and LWR fuel necessitate the use of supplementary and/or modified shielding in the design of spent-fuel shipping casks. These isotopes produce neutrons by spontaneous fission and (α,n) reactions with oxygen. Greater than 90% of the neutron source strength is due to ^{242}Cm and ^{244}Cm; in LWR's, 60 to 85% of it results from ^{244}Cm, whereas, in LMFBR's, approximately 70% is generated by ^{242}Cm. The total fixed-neutron sources in LWR's (one cycle), LMFBR's (core), and LWR's (plutonium recycle) were estimated to be 5.5×10^8, 2.2×10^9, and 9.2×10^9 neutrons sec^{-1} (metric ton)$^{-1}$ respectively. The fixed-neutron spectrum is slightly "harder" for fast reactor fuel due to

[34] M. J. Bell, *Heavy Element Composition of Spent Power Reactor Fuels*, ORNL-TM-2897 (May 1970).

[35] M. J. Bell and J. P. Nichols, "Penetrating Radiation Dose Rates and Shield Requirements in Fabrication of Fuels Containing ^{233}U and High Exposure Plutonium," *Proceedings of the Sol-Gel and Fuel Reprocessing Symposium, May 4–7, 1970* (May 1970).

Table 2.18. Composition of Actinides in Fuel Charge and Discharge from LWR's and LMFBR's

Isotope	Composition (g per metric ton of U + Pu charged to reactor)					
	Enriched-Uranium Fuel		Recycle Plutonium plus Natural Uranium		AI Follow-On LMFBR Core	
	Charge	Discharge[a]	Charge	Discharge[a]	Charge	Discharge[a]
^{235}U	33,000	8,090	6,830	1,880	1,670	1,550
^{236}U		4,530		940	0	112
^{238}U	967,000	943,000	967,000	946,000	828,000	760,000
^{237}Np		483		128		199
^{236}Pu		5.9×10^{-4}	1.71×10^{-3}	7.20×10^{-4}	8.4×10^{-3}	4.6×10^{-3}
^{238}Pu		169	488	416	1,670	1,170
^{239}Pu		5,300	15,300	5,690	113,000	109,000
^{240}Pu		2,150	6,220	3,680	43,900	45,100
^{241}Pu		994	2,880	2,420	8,480	6,700
^{242}Pu		345	998	2,160	3,390	3,490
^{241}Am		49.8		177		816
^{243}Am		89.0		1,070		279
^{242}Cm		6.5		43.9		13.8
^{244}Cm		30.1		688		16.6
Total	1,000,000	965,000	1,000,000	965,000	1,000,000	929,000

[a]Concentrations reported after 150 days of postirradiation decay.

a higher (α,n) fraction. An LMFBR source spectrum is approximately 33% (α,n), while LWR fuel spectra are 83 to 93% spontaneous fission.

To determine the effects of these neutron source strengths and spectra on shipping cask dose rate and attendant shielding requirements, neutron and secondary gamma dose calculations were made for 36-, 18-, and 7-element AI Follow-On LMFBR fuel shipping cask designs and for two LWR cask designs that would accommodate either four PWR or ten BWR elements.[36] The LMFBR core, BWR elements, and PWR elements contain 70, 195, and 456 kg of fuel respectively. These calculations were made with the ANISN code,[37] using S_8P_3 and $S_{16}P_3$ approximations and an updated $27n$-20γ coupled cross-section set. Neutron, gamma-ray, and secondary gamma production cross sections were compiled or calculated using GAM-II, MUG, and POPOP4.[38] In addition to fixed-source spectra, neutron multiplication due to fissions in fissile isotopes was accommodated internally in ANISN by use of appropriate fission cross-section data and a ^{239}Pu Cranberg fission spectrum.

The results of these calculations, which are summarized in Table 2.19, indicate that an outer jacket of water containing 1% boron would be required to reduce the neutron-plus-secondary-gamma dose to an acceptable level for all LMFBR fuel casks. The jacket thickness would vary from 6.8 cm for the 7-element cask to 10.7 cm for the 36-element cask. A cask for ten BWR or four PWR plutonium-recycle fuel elements would require a 9-cm borated water jacket, provided the cask cavity is water-filled. It is possible to design a one-cycle BWR and PWR fuel cask without a water jacket, provided the cavity is water-filled and additional shielding is added to reduce the primary gamma dose to less than 5 mrads/hr at 8 ft.

Secondary gamma dose rates have proved to be significant. The fractions of the total non-fission-product dose resulting from secondary gamma radiation were calculated to be 0.76, 0.31, and 0.025 for the 18-element LMFBR cask, the plutonium recycle LWR cask, and the one-cycle LWR cask respectively.

Criticality Studies

During this report period, calculations were made to aid in the preliminary design and development of spent-fuel shipping casks, fuel element storage arrays,

[36]E. D. Arnold and H. F. Soard, "Neutron Shielding Requirements for LMFBR and LWR Fuel Shipping Casks," *Trans. Am. Nucl. Soc.* 13(1), 402 (1970).

[37]W. W. Engle, Jr., *A User's Manual for ANISN, a One-Dimensional Discrete Ordinates Transport Code with Anisotropic Scattering,* Union Carbide Corporation, Nuclear Division, K-1693 (1967).

[38]L. R. Williams and W. E. Ford, Computing Technology Center, Oak Ridge Gaseous Diffusion Plant, unpublished data (November 1969–February 1970).

Table 2.19. Neutron-plus-Secondary-Gamma Dose Rates at the Surface, and at 8 ft from the Surface, of LMFBR and LWR Spent-Fuel Shipping Casks

Type of Reactor Fuel[a,b]	Number of Elements	Neutron Source Strength[c] [n sec^{-1} (metric ton)$^{-1}$]	Fission Product Gamma Shield	Material in Cavity	Outside Shield[d] Thickness (cm)	Neutron-plus-Secondary-Gamma Dose Rate (mrem/hr)	
						Surface	At 8 ft
		$\times 10^6$					
LMFBR	7	670 + 1460	48.6 cm Fe	Na	6.8	5.5	1.0
	18		50.0 cm Fe	Na	8.8	5.5	1.0
	36		51.4 cm Fe	Na	10.7	5.5	1.0
LWR (one-cycle)	4 PWR or 10 BWR	90 + 460	9 in. Pb + 2.5 in. Fe	H_2O	None	29.2	5.9
				None	6.5	25	5
				None	None	316	64
LWR (one-cycle)	4 PWR or 10 BWR	90 + 460	4 in. U[e] + 2 in. Fe	H_2O	None	24.5	5.0
				None	7.9	22.2	4.5
				None	None	343	60.0
LWR (Pu-recycle)	4 PWR or 10 BWR	680 + 8500	9 in. Pb + 2.5 in. Fe	H_2O	8.9	26	5.6
				None	20[f]	26	5.6
				None	None	5260	1070

[a]The LWR fuel (one-cycle and Pu-recycle) had been allowed to cool 150 days; cooling time for the LMFBR fuel was 20 days.
[b]The LMFBR fuel (core) had been irradiated to a burnup of 80,000 Mwd/metric ton; each of the LWR fuels had been irradiated to 33,000 Mwd/metric ton.
[c]The first value shown is for (α,n) reactions; the second value refers to neutrons from spontaneous fissions.
[d]The shield consists of water containing 1% boron unless otherwise specified.
[e]Inside cavity diameter is 2 in. larger than that for the lead shield in order to allow a greater water annulus.
[f]Plus 4 cm Pb.

fuel element dissolvers, and plutonium product storage tanks.

Spent-Fuel Shipping Casks. — A series of calculations was made to investigate the criticality parameters of conceptual LMFBR fuel shipping casks and to compare results obtained by computer programs of varying complexity. It is concluded that relatively simple and inexpensive discrete ordinates calculations (ANISN) with the 16-group Hansen-Roach cross-section set provide adequate results for survey studies of sodium-filled arrays of LMFBR elements that are reflected by steel. It is concluded that an array of 37 core elements in a cask will be subcritical but that the source neutron multiplication factor, $1/(1 - k_{eff})$, may be in the range of 3 to 15, depending on the plutonium concentration of the elements. In general, the neutron multiplication factors are expected to be highest with elements from a small demonstration reactor, or from an LMFBR with a modular core, and lower with elements from a large commercial LMFBR that probably will have a regular geometry and a low plutonium concentration. Techniques that are available for further reduction of the source neutron multiplication include judicious arrangement of core elements of various reactivity within the cask, interspersion of radial blanket elements, and use of lithium instead of sodium as the coolant.

A proposed cask for shipping spent LMFBR fuels will hold 37 elements, will be shielded by 20 in. of iron, and will have 2-in. sodium-filled spaces between elements to permit cooling by convection. Criticality calculations made for a mockup of such a cask containing elements from three conceptual LMFBR's are summarized in Table 2.20. Most of these calculations were made using the ANISN transport code in the S_4 approximation with Hansen-Roach 16-group cross sections. A 123-group XSDRN transport calculation, which used cross sections from the XSDRN library and treated the ^{238}U resonances by the Nordheim Integral Method, resulted in a decrease of 1.4% in k_∞, the neutron multiplication factor for a system with unlimited dimensions. DOT (two-dimensional transport) and KENO (Monte Carlo) calculations, each using 16-group Hansen-Roach cross sections, of k_{eff} for the shipping cask represented by a fueled region, an axial blanket, and an iron reflector in cylindrical geometry agree with the value obtained from two one-dimensional ANISN calculations. In all of the calculations (except for one KENO calculation), the hexagonal geometry of the fuel elements was replaced

Table 2.20. Criticality Calculations for 37-Element Shipping Casks for Various LMFBR Fuel Elements

	Radius[a] (cm)		Axial Dimension (cm)		Calculated k_{eff} or k_∞			
					123-Group XSDRN	16-Group Hansen-Roach		
	Region 1	Region 2	Region 1	Region 2		ANISN	DOT	KENO
AI reference design, outer starter element[b]								
Fuel element, white boundary	7.268		∞			1.6856		
Fuel element + 1 in. sodium; white boundary[c]	7.268	9.935	∞	∞		1.5855		
37 (fuel element + 1 in. sodium); 50-cm Fe reflector	60.432	110.432	∞	∞		1.1177		
∞ (fuel element + 1 in. sodium); axial blanket	∞	∞	60.96	91.44		1.3104		
37-element shipping cask	60.432	110.432	60.96	91.44		(0.924)[d]		
AI Follow-On design, inner element mid-cycle[e]								
Fuel element + 1 in. sodium; white boundary; homogeneous	10.225		∞			1.1031		
37 (fuel element + 1 in. sodium); 50.8-cm Fe reflector	62.196	112.996	∞	∞		0.8308		
∞ (fuel element + 1 in. sodium); axial blanket	∞	∞	54.407	88.697		0.9237		
37-element shipping cask	62.196	112.996	54.407	88.697		(0.696)[d]		
AI Follow-On design, outer element mid-cycle[e]								
Fuel element + 1 in. sodium; white boundary; homogeneous	10.225		∞			1.2528		
37 (fuel element + 1 in. sodium); 50.8-cm Fe reflector	62.196	112.996	∞	∞		0.9557		0.957 ± 0.002[f]
∞ (fuel element + 1 in. sodium); axial blanket	∞	∞	54.407	88.697		1.0559		
37-element shipping cask	62.196	112.996	54.407	88.697		(0.805)[d]		
GE Follow-On design, inner element discharge[g]								
Fuel element; white boundary	7.536		∞		1.2217	1.2394		
Fuel element + 1 in. sodium; white boundary	7.536	10.163	∞	∞		1.1566		
Fuel element + 1 in. sodium; white boundary; homogeneous	10.163		∞			1.1535		
37 (fuel element + 1 in. sodium); 50.8-cm Fe reflector	61.819	112.619	∞	∞		0.8782		
∞ (fuel element + 1 in. sodium); axial blanket	∞	∞	38.10	68.58		0.8989		
37-element shipping cask	61.819	112.619	38.10	68.58		(0.683)[d]		
GE Follow-On design, outer element discharge[g]								
Fuel element; white boundary	7.536		∞			1.3544		
Fuel element + 1 in. sodium; white boundary	7.536	10.163	∞	∞		1.2629		
37 (fuel element + 1 in. sodium); 50.8-cm Fe reflector	61.819	112.619	∞	∞		0.9661		
∞ (fuel element + 1 in. sodium), axial blanket	∞	∞	38.10	68.58		0.9753		
37-element shipping cask	61.819	112.619	38.10	68.58		(0.746)[d]	0.7630	0.764 ± 0.004

[a]The hexagonal fuel element and sodium regions were approximated by circles of equal area.
[b]Atom densities taken from Table A-18, p. A-84, NAA-SR-MEMO-12604.
[c]Neutrons are reflected isotropically.
[d]Estimated from other calculations.
[e]Atom densities calculated from the fuel element description and loadings at mid-cycle, AI-AEC-12791, vol. 1.
[f]Hexagonal geometry used in the KENO calculation.
[g]Atom densities calculated from the fuel element description and loading at discharge, GEAP-5678.

by cylindrical geometry on an equal-area basis; the KENO calculation indicates that the effect of the cylindrical approximation is to cause an underestimation of k_∞ by about 0.1%. "Smeared" atom densities, based on volume fractions, were used for the fuel element and also for the fuel element and sodium annulus. When compared with a one-region calculation using smeared densities, a two-region calculation for a single fuel element surrounded by an annulus of sodium showed an increase in k_∞ of 0.3%.

For the AI Follow-On LMFBR, the substitution of six radial blanket elements for outer fuel elements in a 37-unit array reflected by iron reduces k_∞ (KENO calculations in hexagonal two-dimensional geometry) from 0.957 ± 0.002 to 0.848 ± 0.002. The substitution of natural lithium for sodium changed the value of k_∞ for the fuel element with 1 in. of alkali metal around it from 1.2528 to 0.7929 (ANISN calculations).

Fuel Storage Arrays. – Criticality calculations were made for infinite, one-tier arrays of FFTF and LMFBR fuel elements to establish the basis for the preliminary design of fuel element storage facilities (see Table 2.21). The elements were assumed to be spaced on a square pitch, with 12 in. between centers, in air, water, and sodium. Smeared atom densities were used to construct a simulation of the core and axial blanket regions filled with air, water, or sodium; these regions were then assumed to be surrounded by a region of air, water, or sodium. A concrete reflector was included adjacent to the axial blankets in the air-spaced case, but was not included for the water or sodium cases. The KENO Monte Carlo code with 16-group Hansen-Roach cross sections was used because of its applicability to the geometry of these problems.

Fuel Element Dissolvers. – Calculations were made with the ANISN program using the S_4 approximation and 16-group Hansen-Roach cross sections to estimate the critical mass and dimensions of PuO_2-water mixtures (Table 2.22). The plutonium was assumed to have the isotopic composition that is expected for fuel discharged from LMFBR's (i.e., 62% ^{239}Pu, 31% ^{240}Pu, 5% ^{241}Pu, and 2% ^{242}Pu).

Plutonium Solution Storage Tanks. – Large storage tanks packed with borosilicate glass provide an economical means for storing solutions of plutonium (as well as ^{235}U and ^{233}U). With the aid of C. L. Schuske of the Dow Chemical Company, a proposed American National Standards Institute standard was prepared on the use of borosilicate-glass raschig rings as a fixed neutron absorber in solutions of fissile material.

Table 2.21. Values of k_{eff} for Infinite Planar Storage Arrays of LMFBR and FFTF Fuel Elements Calculated by the KENO Monte Carlo Code

Fuel Element	k_{eff} for Infinite Planar Arrays Stored in:		
	Air	Water	Sodium
AI reference oxide	0.917 ± 0.007	0.617 ± 0.007	0.883 ± 0.005
AI Follow-On outer	0.835 ± 0.006	0.564 ± 0.005	0.750 ± 0.005
GE Follow-On outer	0.859 ± 0.007	0.562 ± 0.006	0.658 ± 0.004
FFTF outer	0.799 ± 0.005	0.599 ± 0.007	0.751 ± 0.005

Table 2.22. Results of Criticality Calculations for LMFBR Discharge PuO_2-Water Mixtures Reflected by 3 cm of Stainless Steel

H:(^{239}Pu + ^{241}Pu) Atom Ratio	(Pu+U)O_2 Volume Fraction	Density of ^{239}Pu + ^{241}Pu (g/cm^3)	Calculated Critical Parameter				
			Sphere			Infinite Cylinder Radius (cm)	Infinite Slab Thickness (cm)
			Radius (cm)	Volume (liters)	^{239}Pu + ^{241}Pu Mass (kg)		
1	0.79638	5.404	9.03	3.084	16.666	6.03	5.64
3	0.56592	3.840	10.70	5.131	19.705	7.23	6.98
10	0.28115	1.908	15.09	14.393	27.462	10.43	10.72
30	0.11533	0.7826	20.48	35.982	28.159	14.45	15.62
100	0.03764	0.2554	20.81	37.749	9.641	14.71	16.00
300	0.01287	0.0873	19.55	31.299	2.732	13.76	15.00
1000	0.00390	0.0265	23.05	51.298	1.359	16.52	18.68

This proposed standard, together with substantiating information, is to be published as a report in the Criticality Data Center series.[39]

2.8 ENGINEERING STUDIES

Reprocessing of LMFBR Fuel in an Existing LWR Facility

The reprocessing of fuel that has been discharged from test, demonstration, and early commercial LMFBR's will be desirable in order to make the contained fissile material available for useful purposes and to demonstrate the technology and potential economics of the fuel reprocessing portion of the LMFBR fuel cycle. A study was made to evaluate the potential of an existing commercial LWR fuel reprocessing plant [Nuclear Fuel Services, Inc. (NFS)] for accomplishment of these two purposes. The first phase of the study was the assessment of the capability of the facilities expected to exist in 1974 to perform the minimum function of separating fission products from fissile material. This assessment included both the process function and capacity (mass/time) limitations. In the second phase, the facilities required to enhance process and/or throughput capability were examined, and the feasibility of improving, or adding to, existing facilities was studied.

The possible presence of substantial amounts of metallic sodium in undetected failed fuel subassemblies was found to be the most serious of the currently unresolved problems connected with the treatment of LMFBR fuel in an existing LWR fuel reprocessing facility. Although there are a number of potential methods for harmless degradation of metallic sodium, none of them has been proved to be acceptable for use in the NFS complex. A development program is required for the satisfactory resolution of this problem.

Probably the second most difficult problem is the adequate disintegration of the sheathed LMFBR fuel subassembly into conveniently sized particles that can be processed without jamming or other mechanical difficulties while passing through the leaching train.

If we assume that the above-mentioned problems can be resolved and that the fuel is shipped by present LWR fuel shipment techniques, long-decayed LMFBR fuel can be processed in the NFS plant without significant modifications. Figure 2.24 shows the daily capacity of the various major equipment items for AI Follow-On fuel. The maximum processing rate is limited by the plutonium packaging facility to approximately 65 kg of plutonium per day. The solvent extraction system that is used for final plutonium purification is the limiting process complex in terms of throughput capability. Another major restriction in the daily capacity of the equipment is the dissolution system. Dissolution capacity could be improved by about 50% through the simple expedient of providing a third dissolver, as shown in the original plans. Increasing the plutonium purification and packaging capacities would probably require extensive modifications. For example, increasing the second and third plutonium cycle capacities would require installation of larger strip columns plus possible additional modifications. Increasing the capacity of the plutonium packaging system would probably involve construction of an additional facility.

The minimum acceptable decay time for LMFBR fuel after processing would be controlled both by the capacity for dissipating heat from chopped fuel and by the provisions for preventing the escape of radioiodine to the environment. The problems concerning the dissipation of heat from chopped fuel and the containment of radioiodine are interrelated. This interrelationship stems from the increased volatility of iodine with increasing temperature and from the nature of the existing process scheme. In this scheme, heat-producing chopped fuel is stored in non-gastight containers that are located in a cell through which a rather large volume (15,000 cfm) of air is passed to be discharged to the environment without benefit of iodine removal. We estimate that the minimum decay time for LMFBR fuels to be processed at NFS without any additions being made to the ventilation or vessel off-gas systems would be about 200 days. With the addition of iodine sorbers for the 15,000-cfm ventilation air stream (mentioned above) and a means for removing iodine from the condensate discharge, it is conceivable that the minimum decay time could be reduced by 50 days; however, expected temperatures in the chopped fuel baskets would be quite high at the reduced decay time. The effect of such temperatures cannot be predicted with confidence on the basis of information available at this time.

Operation of the NFS facility with LMFBR fuel feed, even though long-decayed, would be a significant demonstration. The capability of an aqueous processing system for accommodating the mechanical and chemical properties of irradiated fuel would be much more convincingly demonstrated in a large facility than

[39] J. P. Nichols, C. L. Schuske, and D. W. Magnuson, *Use of Borosilicate Glass Raschig Rings as a Fixed Neutron Absorber in Solutions of Fissile Material,* Criticality Data Center Report YCDC-8 (in press).

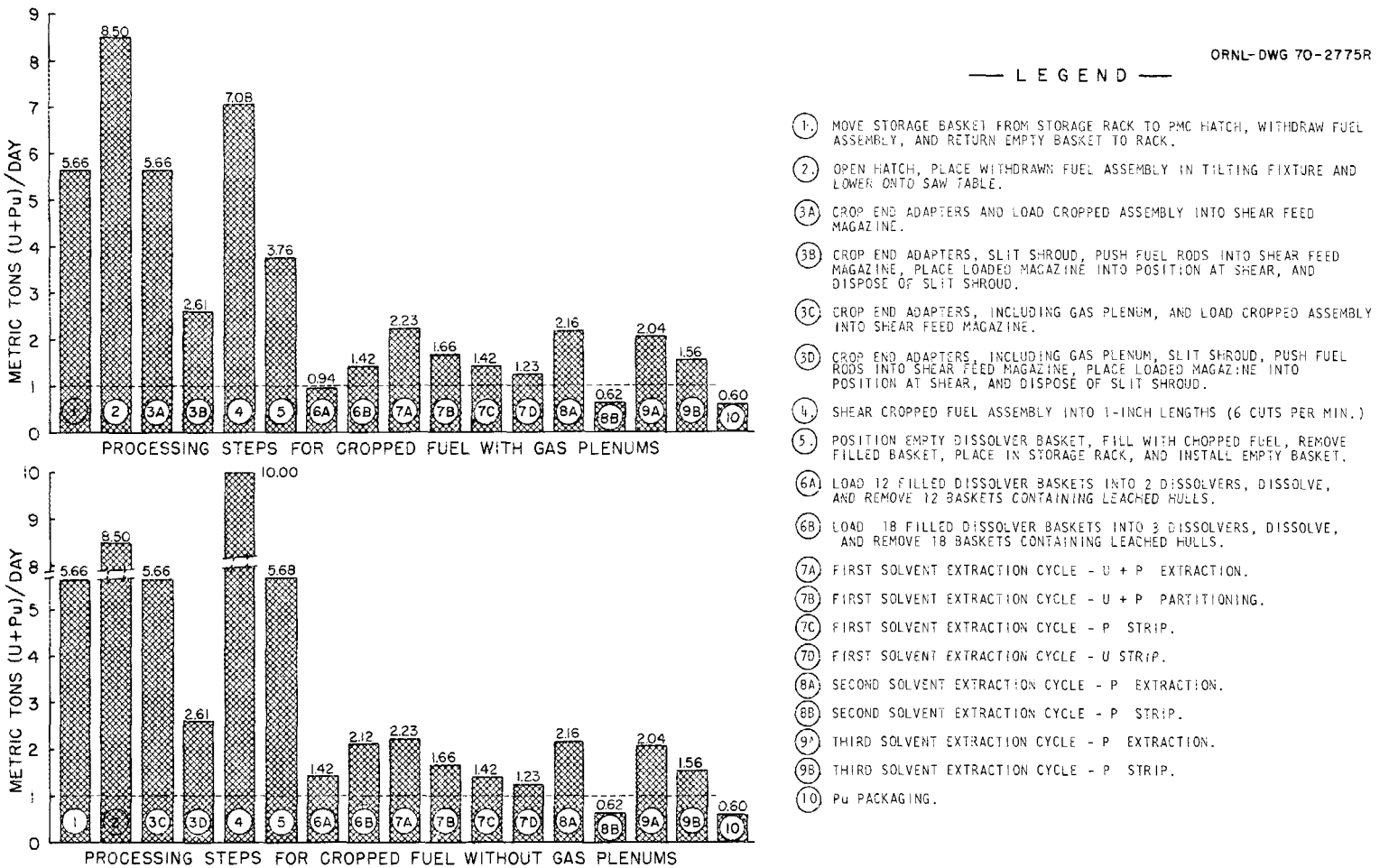

Fig. 2.24. Estimated Capacity of Major Processing Steps in an NFS-Type Plant for AI Fuel. A comparison of fuel throughput with and without gas plenums.

in a small system. Although short-decay processing in the NFS system was concluded to be impractical, this does not preclude demonstration of short-decay shipping and receiving, thereby providing convincing proof of their feasibility and economics. Receipt of short-decayed fuel shipped by advanced techniques would require a new receiving facility.

3. Development of Methods for Reprocessing HTGR Fuels

The High-Temperature Gas-Cooled Reactor (HTGR) is a promising thermal reactor for the conversion of ^{232}Th to ^{233}U and the production of economical electric power. Attaining the twin goals of economical electric power and improved utilization of uranium and thorium resources requires the development of an efficient fuel cycle, including fuel reprocessing and fabrication of recycle fuel.

Efforts to develop methods for reprocessing HTGR fuels have been continued. The current design for HTGR fuels includes the use of coated fuel particles bonded into graphite sticks and inserted into holes in large graphite blocks of hexagonal cross section. The use of fuel sticks rather than loose particles in the blocks represents a significant change made during the past year, and has had an important influence on head-end reprocessing. The reprocessing studies cover both the Ft. St. Vrain and the 1100-Mw (electrical) reference reactor fuels, since Ft. St. Vrain fuel will be the first to become available for use in recycle studies in the Thorium-Uranium Recycle Facility (TURF). The recycle fuel sticks for the Ft. St. Vrain reactor contain TRISO[1]-coated $^{235}UC_2$ fissile and $(Th,U)C_2$ fertile particles, which are expected to maintain their integrity throughout the block crushing and burning steps.

A method for separating the fertile from the fissile particles is being developed. This method is based on the difference in the sizes of the particles after the matrix carbon and the outer pyrolytic carbon layer are removed by burning. The reference 1100-Mw (electrical) reactor fuel uses TRISO-coated $^{235}UC_2$ fissile and BISO[1]-coated ThC_2 and $(U,Th)O_2$ fertile particles. Burning converts the ThC_2 fertile particles into finely powdered oxides, which must be separated from the fissile particles. The BISO-coated oxide particles may retain their shape after burning. The cleanup of the primary burner off-gas is more complicated in the case of the 1100-Mw (electrical) reactor fuel because fission product particulates and up to one-half of the total ^{85}Kr and ^{3}H must be removed from the large volume of off-gas produced when the matrix graphite and the recycle particles are burned together. The previously published reprocessing flowsheet[2] has been modified to reflect these changes (Fig. 3.1).

Emphasis has been placed on determining the efficiency of separation of the fertile and fissile particles in the engineering-scale and hot-cell tests. The lowest calculated power cost for an HTGR is obtained when only the bred uranium (^{233}U) is recycled.

Cost penalties accrue for "crossover" of ^{233}U and ^{235}U to the ^{235}U and the ^{233}U fractions respectively. Crossover can occur via particle breakage or inefficient particle separation. For example, the particles cannot be separated by screening if they stick together in small agglomerates after burning. Cost penalties of about 0.015 mill/kwhr have been calculated for a loss of 5% of the ^{233}U to the highly burned up ^{235}U waste fraction or for a retention of 10% of the ^{235}U (and attendant ^{236}U) by the ^{233}U recycle fraction.

3.1 HEAD-END REPROCESSING STUDIES WITH UNIRRADIATED HTGR FUELS

Resin-Bonded Fuel Stick from Early Ft. St. Vrain Reactor Prototype Fuel

A resin-bonded, unirradiated fuel stick obtained from Gulf General Atomic (GGA) was crushed, burned, and leached in order to test the head-end reprocessing characteristics of an unirradiated prototype Ft. St. Vrain reactor fuel. The fuel stick, enclosed in a graphite sleeve (1 in. in diameter, 15⅝ in. long, and weighing 379.21 g), was fabricated at GGA from TRISO-coated fertile (ThC_2) and fissile [$(Th,U)C_2$ with a Th/U ratio

[1] TRISO coatings consist of a porous carbon buffer layer on the fuel kernel, a thin sealer layer, and two outer isotropic pyrocarbon layers separated by a silicon carbide layer; BISO coatings consist of two pyrocarbon layers.

[2] *Chem. Technol. Div. Ann. Progr. Rept. May 31, 1968*, ORNL-4272, p. 57.

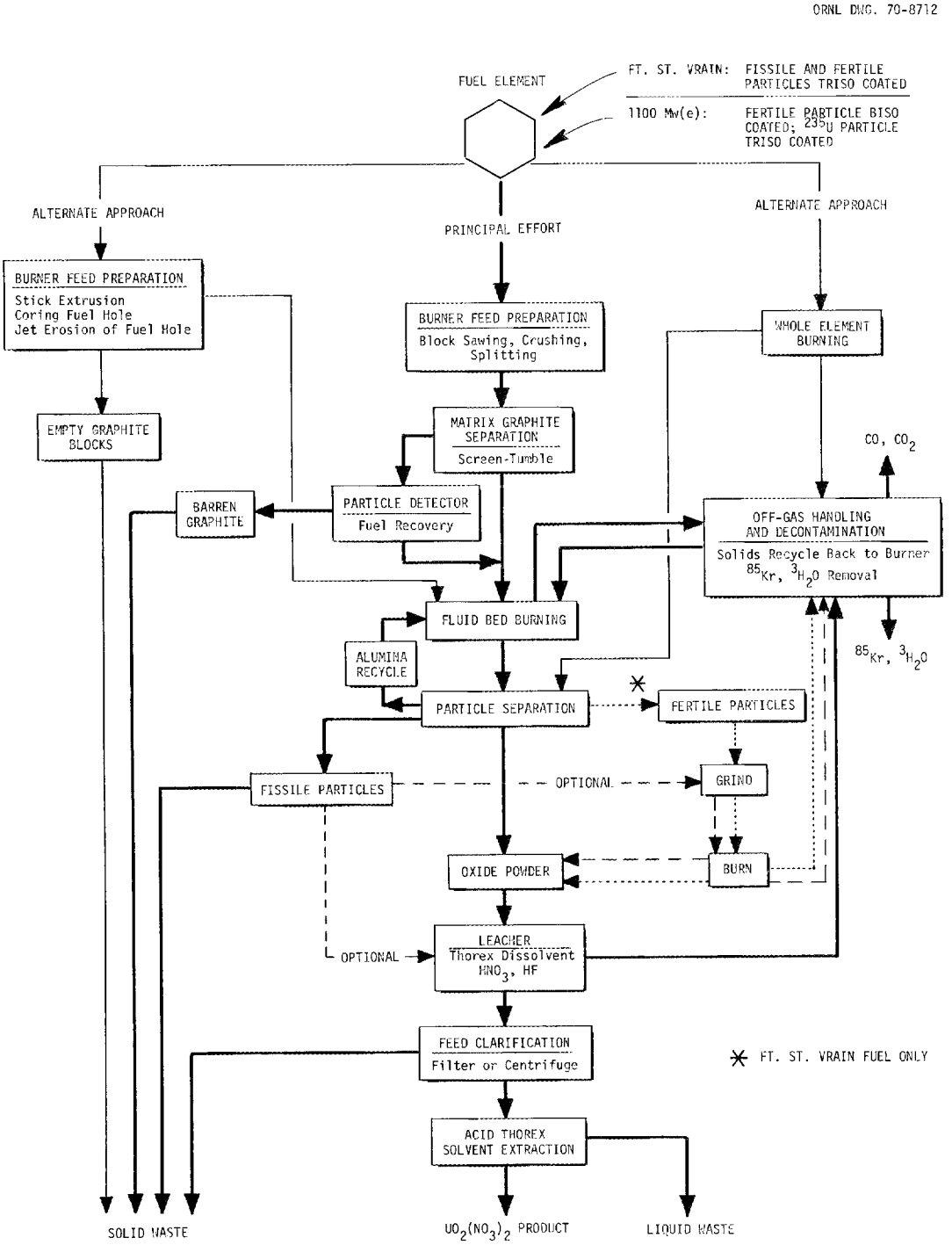

Fig. 3.1. Generalized Head-End Reprocessing Diagram.

of 4] particles bonded with a thermosetting resin and graphite filler. The coated particles are described in Table 3.1. Agglomeration of the particles occurred during the burning of the crushed fuel because a component in the bonding material formed a glassy surface on the SiC layer. Consequently, further grinding and leaching to determine ^{233}U-^{235}U crossover were omitted. Results showed that only limited success was achieved in tests in which leaching, tumbling, and screening were used to break up the small agglomerates and separate the fissile and fertile particles.

Crushing. – The fuel stick was crushed in the laboratory jaw crusher (DFC model 20830) at a $^5/_8$-in. jaw opening to simulate a large-scale crusher. Since the fuel stick was not bonded to the graphite sleeve, the crushed fuel was easily separated from most of the graphite splinters. The products were screened to give the following distribution of sizes: large pieces of sleeve (no fuel), 67.6%; +4 mesh (>4.76 mm), 16.5%; +9 mesh (>2.0 mm), 4.1%; +20 mesh (>84 μm), 2.8%; +42 mesh (>354 μm), 8.5%; +60 mesh (>250 μm), 0.58%; +100 mesh (>149 μm), 0.12%; and –100 mesh (<149 μm), 0.24%. Several larger lumps of fuel and one end plug were removed from the +4-mesh material for an archive sample. The fines fractions (–100 mesh) were combined for leaching tests. Each of the remaining sieve fractions was "split" (or divided) into eight equal portions, and these portions were combined to make eight random samples of crushed fuel (without the large sleeve fragments) for head-end tests. (This procedure has been standardized to give random samples of crushed HTGR fuels.) The samples weighed 14.29 ± 0.24 g. The median weight was 14.33 g. The material balance through the sample splitting step was 100.1%. The measured loss was 0.18 g (of a total of 379.2 g of original fuel plus sleeve).

Release of Broken Particles to the Crusher Fines. – Fines from the crushing step (1.42 g) were leached twice with 11 *M* HNO_3–0.05 *M* HF–0.1 *M* Al^{3+}. Soluble organic compounds colored the leach solutions dark brown. The total breakage in the –60 mesh fraction was 0.03% of the fissile particles and 0.25% of the fertile particles at a $^5/_8$-in. jaw spacing. This level of breakage is insignificant from a head-end processing standpoint. Additional broken particles were found after fluidized-bed burning studies were made (see below). In a second test, two of the samples (R3 and R4) were recrushed at a nominal $^1/_8$-in. jaw opening for small-scale burner tests. The distribution of sizes for the crushed product is given in Table 3.2. Estimates of breakage are given in the discussion of fluidized-bed burning studies (see below).

Tumbling to Subdivide Fuel Stick. – One sample of crushed fuel (R4) was tumbled in a $1^1/_4$-in.-diam by 12-in.-long Teflon pipe for 6120 revolutions (6 hr) and then rescreened. Since the fertile particle fraction (+35 mesh, 76.6 wt %) contained significant amounts of conglomerated fissile particles and resin, no further analysis of crossover was made. The total particle breakage in the –60 mesh fraction was less than 1.5% of the original sample weight – or an increase of 1%

Table 3.1. Description of the Coated Particles Contained in an Unirradiated Resin-Bonded Fuel Stick[a] Obtained from GGA

	Fertile Particle	Fissile Particle
Kernel composition	ThC_2	$(Th,U)C_2$; Th/U ratio of 4
Kernel diameter, μm	295–589	104–275
Thickness of TRISO coating (PyC/SiC/PyC), μm	86/21/43	55/19/28
Final TRISO diameter, μm	400–870	250–450
Weight of coated particles, g	51	44
Weight of SiC-coated particles, g[b]	41.97	31.91
Weight of U, g[b]	0.0	3.08
Weight of Th, g[b]	26.16	12.32

[a]The coated particles were bonded with a thermosetting resin and carbonized before insertion in the graphite sleeve.
[b]Calculated.

Table 3.2. Distribution[a] of Sizes of the Product Obtained from the Crushing Step

Screen (mesh)	Crushed Product (Total Fuel) Obtained at $^5/_8$-in. Jaw Opening	Recrushed Product Obtained at $^1/_8$-in. Jaw Opening	
		Sample R3	Sample R4
+4	50.7	1.6	1.3
+9	12.5	37.9	31.6
+20	8.5	18.7	21.7
+42	26.1	38.3	42.2
+60	1.2	2.3	2.6
+100	0.4	0.4	0.1
–100[b]	0.7	0.8	0.4
Total %	100.1	100.1	99.9
Total weight, g	123.43	14.39	14.25
Total weight after sieving	123.32	14.55	14.09

[a]Fraction, in percent, caught on a screen of a given mesh size.
[b]Fraction, in percent, passed by a 100-mesh screen.

due to the tumbling operation. We concluded that tumbling in this device is not effective for separating fertile and fissile particles.

Fluidized-Bed Burning. – Three samples (R1, R2, and R3) of crushed fuel were burned at 750°C in a fluidized-bed burner with 28 g of T-61 alumina screened to −80 +100 mesh. In each case, the burner product was free-flowing; however, the fertile and fissile SiC-coated particles adhered to each other to form small clusters, thus preventing separation by sieving. (Sticking is attributed to a glassy surface on the SiC layer caused by a component in the resin bonding agent.) Two of the samples were leached and resieved; then all three were tumbled and screened several times in an attempt to separate the two particle fractions. Although there was an improvement in separation after the leaching and tumbling operations, the combined treatment did not yield a clearly defined separation. In addition, some variability was noted in the three runs. The ratio of the weight of the +42 mesh fraction (fertile plus adhering fissile particles) to that of the −42 +60 mesh material (i.e., fissile plus broken fertile particles) is shown in Table 3.3.

The weight ratio of fertile to fissile particles in the original fuel stick was about 1.32.[3] A rough estimate of crossover may be made by dividing half the difference between the fertile-to-fissile-particle ratio for the final product and the original ratio (1.32) by the original ratio; for example, (100) (1.43 − 1.32)/2(1.32) = 4.2% crossover for sample R1 (see Table 3.3). The original crossover for the fluidized-bed burner product was about 28 to 42%. After the various steps and treatments described, this value was reduced to about 4 to 18%.

Alumina retentions were low; about 1% of the Al_2O_3 remained with the SiC-coated particles (0.02 g of Al_2O_3 per gram of SiC-coated particles).

Particle Breakage Due to Crushing and Fluidized-Bed Burning. – The leachable heavy metal content (a measure of particle breakage) in the coated particle and alumina fractions of the fluidized-bed burner product was determined by leaching the sieved products twice with 11 *M* HNO_3–0.1 *M* Al^{3+}–0.05 *M* HF (Table 3.4). The use of a $^5/_8$-in. jaw opening did not result in the breakage of more than about 1.5 to 2.0% of the fissile particles, whereas breakage in excess of 7.2% was obtained with a $^1/_8$-in. jaw opening. Breakage of the fertile particles was 0.1 to 0.2% with the $^5/_8$-in. jaw opening. An additional 0.03 to 0.25% breakage was found with the crusher fines (see above). Approximately 0.07% of the uranium and 0.01% of the thorium were lost to the alumina residues.

In summary, the bulk graphite was easily separated from the crushed unirradiated fuel. Particle breakage during crushing and fluidized-bed burning was greater than 7.2% using a $^1/_8$-in. jaw opening, but only 1.5 to 2% with a jaw opening of about $^5/_8$ in. Direct leaching of the crushed fuel yielded large quantities of dark-colored, soluble, organic degradation products. Fluidized-bed burning of resin-bonded fuel sticks of the Ft. St. Vrain reactor type (TRISO-coated particles) yielded small agglomerates of mixed fertile and fissile particles. Crossover for the fissile particles into the fertile fraction was 28 to 42% for the fluidized-bed burner product. After the leaching, tumbling, and sieving steps, and

[3] V. C. A. Vaughen, *Head-End Studies of SiC-Coated HTGR Fuels: Unirradiated Dragon Compact No. 8232,* ORNL-TM-2389 (February 1969).

Table 3.3. Comparison of Weight Ratios of +42 Mesh to −42 +60 Mesh Sieved Burner Products

Sieve analysis after each listed step

Sample	Fluidized-Bed Burner Product Ratio[a]	Original Crossover (%)	Separation Step			Final Product Ratio	Final Crossover[b] (%)
			Tumbler Product Ratio	Leacher Product Ratio	Tumbler Product Ratio		
R1	2.06	28		1.59	1.55	1.43	4.2
R2	2.20	33		1.84	1.82	1.60	10.6
R3	2.42	42	2.14			1.80	18.2
R4	Unburned		3.50				

[a]The original ratio of materials in the fuel stick was 1.32.

[b]^{235}U reporting to the thorium fraction.

Table 3.4. Particle Breakage[a] Due to Crushing and Fluidized-Bed Burning

Sample	Jaw Setting (in.)	Leachate from +42 Mesh Fraction		Leachate from −42 +60 Mesh Fraction		Al_2O_3 Leachate		Al_2O_3 Residue		Total Breakage	
		U	Th[b]	U	Th[b]	U	Th[b]	U	Th	U	Th[b]
R1	5/8	0.18	0.16	0.66	~0	1.1	0.05	0.06	0.01	2.0	0.2
R2	5/8	0.20	0.06	0.44	0.07	0.81		0.07	0.01	1.5	0.1
R3	1/8	c	c	c	c	7.1		0.07	0.02	>7.2	

[a]Expressed as percent of calculated total heavy metals.
[b]Corrected for thorium from fissile particles (Th/U ratio of 4).
[c]Not analyzed.

Table 3.5. Size Distribution of the Product Obtained by Crushing HTGR Graphite Fuel[a] in a Hammer Mill

Size Fraction	Hammer Mill[b] Product (wt %)			
	3/4-in. Grate Spacing[c]		3/8-in. Grate Spacing[c]	
+3/4 in.	2.2[d]	3.2[d]		
−3/4 +1/2 in.	9.0[d]	12.2[d]		
−1/2 in. +4 mesh	33.0[d]	30.8[d]d	14.4[d]	23.4[d]
−4 +12 mesh	14.5	14.6	27.6[d]	19.83[d]
−12 +20 mesh	11.1	11.7	14.5	11.72
−20 +35 mesh	19.8	18.0	10.7	19.7
−35 +50 mesh	3.6	2.6	8.5	6.6
−50 +80 mesh	2.5	2.5	7.4	5.4
−80 mesh	4.8[e]	4.4	16.7[e]	13.2[e]

[a]One-sixth section of a prototype Ft. St. Vrain fuel element containing TRISO-coated fertile and fissile fuel particles in resin-bonded fuel sticks.
[b]Type A Jeffrey swing hammer.
[c]Results shown are for duplicate runs.
[d]No fuel particles were found in these fractions.
[e]Contained only a few pieces of broken UO_2 and ThO_2 particles.

other handling, the crossover was reduced to 4 to 18%. Alumina retention by the SiC-coated particles was about 0.02 g of Al_2O_3 per gram of SiC-coated particles (~1% of the Al_2O_3 charged to the burner).

One-Sixth Section of a Prototype Ft. St. Vrain Fuel Element

Comminution Studies. – Unirradiated graphite fuel samples containing resin-bonded, TRISO-coated ThO_2 and UO_2 (ref. 4) particles were crushed in a hammer mill, using 3/4- and 3/8-in. grate spacings, and the crushed material was sieved to determine the particle size distribution (Table 3.5). No fuel particles were found in +4 mesh or larger size fractions with a 3/4-in. grate spacing, or in the +12 mesh or larger size fractions with a 3/8-in. grate spacing. Apparently, the increased time in the hammer mill with a 3/8-in. grate spacing freed the particles from the +12 mesh fractions so that the total amount of barren graphite (free from fuel particles) was about the same (~42 to 46%) for each spacing. Further treatment in a screen-tumbler should increase the amount of particle-free graphite. The barren graphite could be stored instead of burned if storage proves to be more economical.

[4]These particles were made and coated at ORNL.

Table 3.6. Fluidized-Bed Burning Tests with TRISO-Coated Fuel

	Run No.		
	BT-14	BT-15	BT-16
Burner charge			
Alumina,[a] g	1600	1600	1600
Crushed fuel,[b] g	2000	2038	1835
Reagent gas	20% O_2[c]	70% O_2, 30% N_2	100% O_2
Operating conditions			
Superficial gas velocity, fps	1.25	1.25	1.25
Temperature, °C	750 ± 25	750 ± 25	750 ± 25
Burning time, hr	14.75	7.25	4.25
Burner residue, g	1894	1954	1879

[a]–90 mesh Norton RR Alumina.
[b]Hammer mill set to produce –¾ in. product.
[c]Air.

The breakage of particle coatings was determined by leaching the hammer-mill product with Thorex dissolvent (13 M HNO_3–0.04 M F^-–0.10 M Al^{3+}). In two batches of graphite fuel, the coatings on 2.17% and 0.1% of the UO_2 particles and on 1.07% and 1.52% of the ThO_2 particles were broken by crushing at a ¾-in. grate spacing.

Fluidized-Bed Burning Studies. — Tests were made in a 2-in.-diam fluidized-bed burner using crushed graphite (material passing a ¾-in. grate spacing) containing TRISO-coated UO_2 and ThO_2 fuel particles to determine the direct and indirect effects of oxygen concentration in the reagent gas on particle-coating breakage (Table 3.6). The oxygen concentration was varied from 20% (air) to 100% while other operating conditions were held constant. Norton RR grade alumina was used as the heat-transfer medium. The bed temperature was 750°C. Operation was smooth, and no wall "hot spots" or plugs developed. Oxygen utilization averaged greater than 95% during the major portion of the burning period; the burner residue was free-flowing and had a carbon content of less than 1%. When the residue was screened, the ThO_2 particles reported to the +35 mesh fraction and the UO_2 particles reported to the –35 +50 mesh fraction.

The percentages of particles with broken coatings (as determined by leaching the product with Thorex dissolvent) are shown in Table 3.7. Breakage of the UO_2 particle coatings decreased from 6.09% to 2.97% as the oxygen concentration increased from 20% to 100%, primarily due to the decreased time in the fluidized bed. The breakage of the ThO_2 particle coatings decreased from 6.9% to 3.6% as the oxygen concentration increased from 20% to 70%, then increased sharply to 11.3% with 100% oxygen. However, since pure oxygen reagent can produce sintering of the bed, a feed containing 100% oxygen would probably not be used in a routine operation. If a 70% oxygen reagent is used, the overall coating breakage for both the crushing and the burning steps is 5.7% for UO_2 and 4.67% for ThO_2 particles.

Table 3.7. Breakage of Particle Coatings in Fluidized-Bed Burning Tests with TRISO-Coated Fuel

	Fraction of Particles with Broken Coatings (%)		
	Run BT-14	Run BT-15	Run BT-16
UO_2 particles, as charged	2.17	2.17	2.17
ThO_2 particles, as charged	1.07	1.07	1.07
UO_2 particles in burner ash	8.26	5.7	5.4
ThO_2 particles in burner ash	7.97	4.67	12.37
UO_2 particles broken in test	6.09	3.53	2.97
ThO_2 particles broken in test	6.90	3.6	11.30

3.2 HEAD-END REPROCESSING STUDIES WITH IRRADIATED HTGR FUELS

Flowsheet variables for the head-end reprocessing of HTGR fuels were tested on a small scale with irradiated HTGR fuels in a hot cell. The objectives of the hot-cell studies are: (1) to test the operational feasibility of the proposed flowsheets, for example, crush-burn-sieve-

grind-burn-leach; (2) to test the stability of coated particles in head-end steps; (3) to obtain information on releases of the fission products ^{3}H, ^{85}Kr, ^{90}Sr, ^{106}Ru, and ^{137}Cs in off-gases; (4) to obtain information for the design of a head-end pilot plant to be located at TURF; and (5) to obtain estimates of product losses and waste stream compositions. Unirradiated fuels were also studied in similar equipment to ensure that the results of the small-scale studies are comparable to those of the larger-scale studies with unirradiated fuels (see Sect. 3.1), and to permit evaluation of irradiation effects by comparison with the tests on unirradiated fuels.

Study of Dragon Compact 8375

Dragon compact 8375, a hollow cylinder, contained "standard" Dragon fuel with TRISO coatings of buffer pyrolytic carbon, silicon carbide, and isotropic pyrocarbon having thicknesses of 27, 17, and 64 μm respectively. Based on ^{137}Cs analyses, the compact was irradiated to a burnup of approximately 15,000 Mwd/ton. The purposes of the tests made with this compact were as follows: (1) to confirm that the crusher jaw opening was the major variable in the breakage of the SiC-coated particles, (2) to determine the extent of breakage during sawing, (3) to measure ^{85}Kr and ^{3}H releases during head-end reprocessing steps, and (4) to obtain data on leaching, fission product behavior, and uranium and thorium losses to residues. The experiments have been completed, but not all of the data have been analyzed. Details of the experimental procedures have been published.[3]

The Dragon compact was first sawed into two rings; then one of the rings was further sawed into four sections of about equal size. All of the sawdust was brushed off the cut edges and collected as fines for leaching. Two of the four sawed sections were burned as large pieces (in a static bed), and the residual fuel particles were leached to determine the fraction of particles broken during the sawing step. The final two sawed sections were crushed using a ⅛-in. jaw opening in the crusher, burned in a static bed, and leached to determine the amount of particle breakage. (It should be remembered that Ft. St. Vrain reactor-type fuel blocks can be cut without encountering fuel particles, whereas this is not possible with Dragon fuel compacts.)

The second ring was crushed into nine large pieces, using a ⅝-in. opening on the jaw crusher. Three samples (R5, R6, and R7) were burned in a fluidized bed with Al_2O_3, sieved to recover the SiC-coated particles from the Al_2O_3, ground to −60 mesh to break all the particles, burned again in a static bed, and leached to obtain the uranium, thorium, and fission product contents of the compact and the losses of these materials to the residue. The amount of ^{3}H and ^{85}Kr released in each step was also determined.

Crushing Studies. – The hot-cell crusher (DFC model 20830) has a nominal ⅝-in. jaw opening but was shimmed to a nominal ⅛ in. to produce a product suitable for small-scale burner tests.

With the ⅝-in. jaw opening, unirradiated compacts are crushed to a few large lumps, which are satisfactory feed for a 2-in.-diam fluidized burner (see Sect. 3.1). In the case of irradiated compact 8375, a quarter ring broke into nine pieces; consequently, size distribution of the product cannot be defined. However, two of the sawed sections (R3 and R4) were recrushed at a ⅛-in. jaw opening and analyzed by screening. The results, along with some earlier data for comparison, are given in Table 3.8. The important points are: (1) the fueled compacts release a larger fraction of +42 mesh material (free beads) than is obtained from machined cylinders, and (2) except for some variability in the amounts of +4 and +9 mesh material, the size distributions of the crushed product in each case are quite similar.

Breakage of Coated Particles During Size Reduction Studies. – Experiments with compact 8375 confirmed that the jaw crusher opening was a significant variable in the breakage of fuel particles. In general, the composition of the fines (−42 mesh) was representative of the composition of the compact. With unirradiated fuels (and compact 8368), significantly fewer particles were ruptured; hence, the fines were richer in graphite than the overall average composition of the fuel, indicating that the cleavage was around (rather than through) the particles dispersed in the hot pressed matrix.

The fraction of broken particles present in the original compact was estimated at 2.3% from static bed burn-leach tests on two sawed segments (R1 and R2). This fraction was considered to be broken prior to the sawing step since the sawed surfaces were brushed free of broken fines before burning and neither hacksawing nor static bed burning is expected to fracture particles that are surrounded by fuel matrix. The burner product was leached twice with 11 *M* HNO_3–0.1 *M* Al^{3+}–0.05 *M* HF without grinding the SiC-coated particles, and the uranium and thorium contents of this product were compared with the uranium and thorium contents of the crushed fuel samples as determined by analysis of fractions R5, R6, and R7.

Crushing with a ⅝-in. jaw opening produced a −42 mesh fines fraction containing 1.4% of the sample (by

weight) and about 1% of the calculated uranium and thorium present in the half cylinder. Crushing to a nominal $\frac{1}{8}$-in. jaw opening produced a fines fraction averaging 8.1% of the sample weight. After the crushed product was burned in a static bed and the residue was leached (without grinding), 13.6% of the calculated fuel particles present were found to be broken. Breakage due solely to crushing at a $\frac{1}{8}$-in. jaw opening is estimated at 11.3%, of which 28% was retained with the +42 mesh material. These results indicate that a significant number of fractured particles were retained with the larger lumps (+42 mesh) of fuel.

Release of ^{3}H and ^{85}Kr. – Three samples of fuel crushed at the $\frac{5}{8}$-in. opening (i.e., R5, R6, and R7) were put through the complete burn-grind-burn-leach flowsheet. In each step, a purge of either 4% H_2–argon or moist oxygen-nitrogen mixtures was used to provide adequate carrier water for trapping the ^{3}H on molecular sieves. The off-gases were passed over a hot copper oxide bed to convert all the hydrogen to water before trapping. The entire gas output was collected and analyzed for ^{85}Kr (Table 3.9). About 1% of the total ^{85}Kr was collected in the off-gas from the first burner; this represents a release of ^{85}Kr from broken particles. There was some variation in the amounts released during grinding and the second burning; however, the sum of these two steps averaged 98%. The remainder (~1 to 2%) was found in the dissolver off-gas. The fact that ^{85}Kr was found in the dissolver off-gas probably indicates that the burning conditions were not optimum for complete removal in this step.

Tritium release data are also given in Table 3.9. As reported previously,[5] a major fraction of the total

[5] *Chem. Technol. Div. Ann. Progr. Rept. May 31, 1969*, ORNL-4422, pp. 114–19.

Table 3.8. Size Distribution of Product Obtained with the Hot-Cell Crusher at $\frac{1}{8}$-in. Jaw Opening

	Fraction (%) of Total Product on Screen of Mesh Size:					
	+4	+9	+20	+42	+100	−100
Machined cylinders of graphite (no fuel)	~9	~60	12.6	6.6	4.9	6.9
Unirradiated compact 8232	2.6	62.6	9.1	18.1	2.9	4.8
Irradiated[a] compact 8368	5.9	48.0	12.2	22.8	3.8	7.3
Irradiated[a] compact 8375						
Sample R3	18.3	44.1	11.5	17.6	3.9	4.6
Sample R4	9.1	52.4	12.9	18.0	3.1	4.5

[a]Irradiated to a burnup of ~15,000 Mwd/ton.

Table 3.9. Release of ^{3}H and ^{85}Kr During Head-End Steps Performed on Samples of Dragon Compact 8375

	^{85}Kr Released from:			^{3}H Released from:		
	R5	R6	R7	R5	R6	R7
Fraction, %, present in off-gas from:						
First burning step	>0.4[a]	1.04	0.98	32.3	*b*	29.7
Grinding step	27.6	81.1	16.7	0.3		5.6
Second burning step	71.7	15.7	81.3	60.6		62.0
First leach	0.3	2.1	1.0	3.8[c]		2.2[c]
Fraction in first leach liquor, %				3.0		0.4
Total activity, dis/min	4.13×10^{10}	3.34×10^{10}	3.32×10^{10}	7.45×10^8	5.44×10^8	1.80×10^8
Sample weight, g	16.35	14.55	11.11	16.35	14.55	11.11

[a]Collected on dry ice–charcoal trap. CO_2 displaced some of the ^{85}Kr. Subsequent samples were taken from the collected gases.
[b]Percentage values were not realistic because the value for ^{3}H in the off-gas of the second burn cycle was very low.
[c]Accuracy is doubtful because of low counting rate.

tritium (~30 to 40%) exists outside the SiC-coated particles and is released in the first burning step. This tritium is believed to be a product of neutron reactions with materials in the bonding matrix and ^3He in the coolant gas. Most of the ternary-fission-produced tritium is thought to be retained with the SiC coating until the particles are crushed and heated or burned. Residual tritium (2.6 to 6.8%) in the second burner product was recovered during leaching. The presence of residual tritium also indicates a lack of optimum burning conditions.

In summary, studies on compact 8375, a "standard" Dragon fuel irradiated to a burnup of about 15,000 Mwd/ton, indicate that about 2.3% of the particles were broken in the as-received condition. Crushing the fuel at a ⅝-in. jaw opening gave a fines fraction of 1.4 wt % containing an additional 1% broken particles. Recrushing at a ⅛-in. jaw opening yielded 8.1 wt % of fines and a total breakage after all head-end steps of 13.6%. Assuming that the fines had the original fuel composition, the breakage would be characterized as follows: original broken fuel particles, 2.3%; fuel particles crushed and released as –42 mesh fines, 8.1%; fuel particles crushed and held with the +42 mesh material, 3.2%. Thus a total breakage of 11.3% was due to the crushing at the ⅛-in. opening.

Most (98%) of the fission gas ^{85}Kr was released during the grinding and burning steps. About 30 to 40% of the total recovered tritium was found outside the SiC-coated particles. As before,[5] most of the remainder (produced by ternary fission) was released when the SiC-coated particles were ruptured and burned. From 2.6 to 6.8% of the tritium was recovered on leaching the burner product, indicating that burning conditions were not optimum for complete removal.

3.3 PROCUREMENT OF IRRADIATED HTGR FUELS FOR HEAD-END STUDIES

We have requested additional samples of irradiated Dragon fuel compacts for head-end reprocessing tests. These compacts contain coated fuel particles similar to those proposed for the Ft. St. Vrain (Public Service of Colorado) and commercial 1100-Mw (electrical) HTGR's and will provide meaningful tests of reprocessing flowsheet concepts, even though the Dragon fuels differ[6] from GGA-HTGR fuels. A comprehensive study is also planned with prototype HTGR fuels as follows:

1. ORNL BISO-coated $(Th,U)O_2$ sol-gel microspheres, irradiated as compacts, in the Dragon reactor,
2. ORNL test capsules, to be irradiated in the ETR for combined head-end reprocessing and irradiation performance testing,
3. Recycle test elements (RTE's) fabricated jointly by GGA and ORNL for irradiation in the Peach Bottom reactor.

ORNL BISO-Coated $(Th,U)O_2$ Sol-Gel Microsphere Compacts

Several types of Dragon fuels of particular interest to our head-end work have been requested and should arrive in the early part of fiscal year 1971. These and ORNL sol-gel irradiated compacts are described in Table 3.10. Many important fuel types and head-end reprocessing steps can be simulated, as shown in the last column of this table.

ORNL Test Capsule

The irradiation performance and behavior of small quantities of three types of candidate coated-particle, 1100-Mw (electrical) HTGR fuels under proposed methods of head-end reprocessing will be studied jointly by the Metals and Ceramics and the Chemical Technology Divisions. The three types of fuel particle combinations that will be tested in small, loose beds and in fuel sticks (~2.5 in. long) are the alternate[7] block A recycle $[(4.2\ Th,U)O_2 + ThO_2]$, block B recycle $[UC_2(\text{TRISO-coated}) + ThC_2]$, backup block B recycle $[UO_2 + ThO_2]$ fuels, and the accelerated burnup alternate[7] block A recycle fuel $[(2Th,U)O_2 + ThO_2]$. Only the UC_2 particles have TRISO coatings. The particles in blended beds and in fuel sticks will be irradiated in two capsules at temperatures of 750, 950, 1050, and 1300°C to burnups of approximately (4 to 6) $\times\ 10^{21}$ fast fluence in the ETR. Although the quantities of fuel are quite small, they will be adequate for an early preliminary determination of the head-end reprocessing behavior of highly irradiated recycle and alternate fuels. They will be available before the first RTE's are removed from the Peach Bottom reactor (at about 1.4×10^{21} fast fluence). Studies will include the separation of fertile and fissile particles (BISO- and/or TRISO-coated), determination of uranium crossover, estimates of particle breakage, and measurement of the

[6] Hot pressed compact vs bonded fuel stick; particle kernel sizes; coating thickness; one-particle vs two-particle fuel, etc.

[7] This fuel would be the reference fuel if the fertile particle were thorium carbide rather than oxide.

Table 3.10. Irradiated Dragon Compacts[a] Requested for ORNL Head-End Studies

Experimental Fuel No.	Th/U Atom Ratio (93% ^{235}U)	Kernel Composition	Kernel Diameter (μm)	Type of Coating	Thickness of Coatings (μm)	Comments
2M4	10	$(U,Th)O_2$	500	BISO	130	Simulates ($^{233}U,Th)O_2$ reference (BISO) recycle particle for 1100-Mw (electrical) HTGR. Will be compared with ORNL sol-gel recycle particle.
2M7	10	$(U,Th)O_2$	500	TRISO	160	Simulates ($^{233}U,Th)O_2$ alternate (TRISO) recycle particle for 1100-Mw (electrical) HTGR.
2M10	10	$(U,Th)C_2$	500	TRISO	150	Suitable for comparison of carbides vs oxides in head-end studies. Simulates Ft. St. Vrain fertile-fissile particle.
3M	10	$(U,Th)C_2$	900	TRISO	50/30/80	Large kernel size; can be mixed with other fuels for particle separation studies of TRISO-TRISO and TRISO-BISO mixes (18M and ORNL sol-gel BISO-coated fuels).
18M		UC_{20}	500	TRISO	25/30/70	Simulates fissile (^{235}U) particle. Will be used in particle separation studies.
19M		ThC_2 UC_{10}	900 500	TRISO TRISO	25/30/70 25/30/70	Simulates Ft. St. Vrain fuel particles. Will be used in particle separation studies.
38M	5	$(U,Th)C_2$	500	BISO	40/80	1100-Mw (electrical) HTGR simulated fertile-fissile particle with accelerated burnup. Could be mixed with UC_{10} TRISO-coated particles (which are presently available) for separation studies.
ORNL sol-gel[b]	3, 4.5	$(U,Th)O_2$	290	BISO		1100-Mw (electrical) reference recycle fuel (fertile).

[a] To a burnup of about 7% fissions per initial metal atom and 2.5×10^{21} fast fluence.

[b] 12 to 18% fissions per initial metal atom.

Table 3.11. Fuel Combinations in the RTE Program and Justifications for Each

Particle Combination	Particle Makeup in Combinations		Justification
	Fissile Particle (and coating)	Fertile Particle (and coating)	
a	(Th, 20% U)O_2 (BISO)		1. Reference recycle fuel 2. Evaluate:[a] Equipment and chemical process checkout Bed sticking Metallic fission product behavior Kernel migration
b	UO_2 (BISO)	ThC_2 (BISO)	1. Backup fuel type if economics indicate that Th should be eliminated from recycle fissile particle
c	(Th, 33% U)O_2 (BISO)	ThO_2 (BISO)	1. Th/U ratio of 2 to obtain reference burnup in 3 years 2. ThO_2 backup if oxide process is adopted for economic reasons 3. Over a period of time, the desired Th/U ratio will move from 4 toward 2
d	(Th, 33% U)O_2 (BISO)	ThC_2 (BISO)	1. Reference-type recycle combination with a Th/U ratio of 2 for accelerated burnup in fissile particle
e	UC_2 (BISO)	ThC_2 (BISO)	1. Reference startup loading
f	UC_2 (TRISO)	ThC_2 (BISO)	1. Reference B block, makeup fuel loading 2. TRISO coating necessary to permit required separation of particles during reprocessing
g	UO_2 (BISO)	ThO_2 (BISO)	1. Backup fertile particle if thorium is eliminated from recycle particle 2. Backup fertile particle if sol-gel process is used
h	UC_2 (BISO)	ThO_2 (BISO)	1. Backup B block loading 2. Possible particle separation by chemical processes (e.g., selective burning or leaching)
i	UC_2 (TRISO)	ThC_2 (TRISO)	1. Needed if cleaner primary heat exchanger circuit becomes requirement 2. Ft. St. Vrain type fuel

[a]Applies to tests of all combinations.

release of volatile fission products such as ^{85}Kr, ^{3}H, ^{90}Sr, and ^{137}Cs in various head-end steps.

Recycle Test Elements

Eight RTE's will be inserted into the Peach Bottom reactor, six in the summer of 1970 and two in February of 1971, in a cooperative program between GGA and the ORNL Metals and Ceramics and Chemical Technology Divisions. Reference and advanced recycle and makeup fuel particle mixtures in these elements are being tested at operating temperatures (1050 to 2250°F) of interest for use in commercial HTGR's. Bonded beds and some loose particles (blended beds) will be irradiated for 1, 2, or 3 years at exposures of 1.4, 2.8, and 4.2×10^{21} fast fluence.

These irradiated elements will be more representative of the products of the large-scale production of fuel elements than the materials that are being used in capsule irradiation tests. In addition, they will provide significant quantities of irradiated fuels for head-end reprocessing studies and will probably be the first irradiated fuel used in a head-end process demonstration in TURF.

The types of fuel combinations in the RTE's and an indication of the reasons for their inclusion are given in Table 3.11. A more detailed breakdown of the loading combinations and irradiation conditions of the RTE's is given in Table 3.12. Odd-numbered RTE's are the primary source of material for the hot-cell head-end studies. The emphasis is on particle combinations a, c, f, and g, which are the reference candidates; however, all fuel combinations are covered in each odd-numbered element. The six 15-in. sections of the odd-numbered elements will be quartered lengthwise to obtain one sample of each fuel type (Fig. 3.2). Even-numbered RTE's will provide larger amounts of the various fuel combinations for additional hot-cell studies as necessary or desirable. They may also be the first irradiated specimens, representative of actual 1100-Mw (electrical) reactor fuel, that will become available for use in reprocessing studies in TURF.

Table 3.12. RTE Loading Combinations[a]

1-year elements will receive a maximum dose of $\cong 1.4 \times 10^{21}$ *nvt*
2-year elements will receive a maximum dose of $\cong 2.8 \times 10^{21}$ *nvt*
3-year elements will receive a maximum dose of $\cong 4.2 \times 10^{21}$ *nvt*

Position of Fuel Body in Element	Center-Line Temperature Range (°F)	First Discharge (1-Year Irradiation)		Second Discharge (2-Year Irradiation)		Final Discharge (3-Year Irradiation)			
		RTE 1	RTE 2	RTE 3	RTE 4	RTE 5	RTE 6	RTE 7	RTE 8
6 (top of reactor)	2050–1950	b d e i	f	b d e i	e[b]	b d e i	g	a c f g	f
5	2250–2050	b d e h	a[b]	b d e h	d	b d e h	f	a c f g	i
4 (max flux)	2250–2300	a c f g	e	a c f g	f	a c f g	f	b d g h	d
3 (max flux)	2050–2250	a c f g	f[b]	a c f g	a[b]	a c f g	d	b d g i	e
2	1650–2050	a c f g	d	a c f g	f[b]	a c f g	f	b d g i	i
1 (bottom of reactor)	1050–1650	a c f g	e[b]	a c f g	e	a c f g	e	b d g i	f[b]

[a]Loadings are indicated by letters a, b, c, d, e, f, g, h, and i, which are defined in Table 3.11.
[b]Blended beds.

ORNL-DWG 70-9214

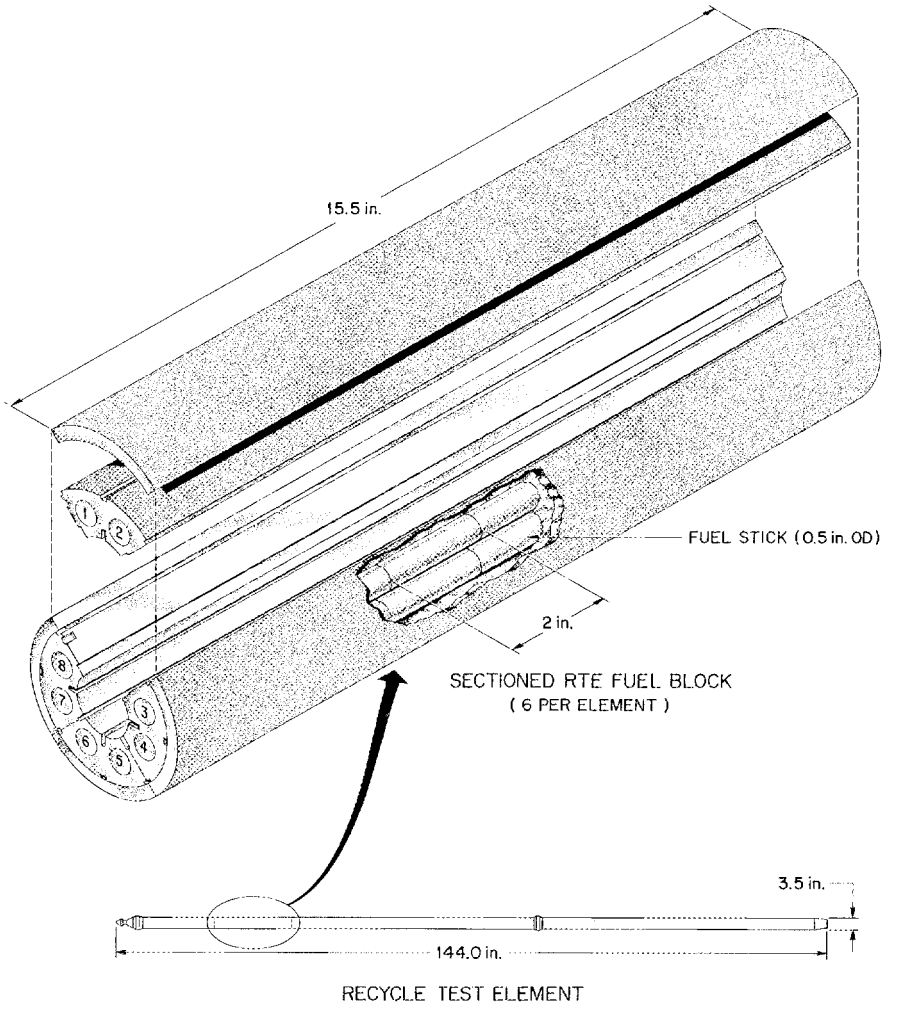

Fig. 3.2. Isometric Drawing of Sectioned RTE Fuel Block.

4. Waste Treatment and Disposal

The objectives of the waste treatment and development program are to develop a comprehensive waste management system for nuclear wastes, including final disposal of radioactive residues, and to estimate the cost of this operation. A comprehensive waste management flowsheet, which outlines the development program, was presented previously.[1] Progress is reported on: (1) the optimization of methods for estimating the costs of waste management, (2) an engineering survey and an experimental study of methods for the disposal of noble gases, (3) the development of an improved process for solidifying high-level wastes, and (4) the development of a process for isolating noble gases by the use of permselective membranes.

4.1 ENGINEERING, ECONOMIC, AND SAFETY EVALUATIONS

Survey of Fuel Processing Wastes

We have reviewed the wastes to be expected from the aqueous processing of fuels from three types of reactors – light water (LWR), liquid-metal-cooled fast breeder (LMFBR), and high-temperature gas-cooled (HTGR) – with a view to determining the most economical approaches to their management within the technology that is being developed. The initial part of this survey was devoted to the preparation of generalized fuel processing flowsheets and to the characterization of the principal liquid and solid wastes that are generated in each case.[2] Also, estimates were made of the probable characteristics of the solids that could be formed from the individual waste streams and from various combinations, or blends, of those streams that represent alternative methods of waste management.

To complete the study, an economic analysis was made to determine the optimal trajectories of waste management operations and to compute the costs involved in these operations. In order to limit the scope of the economic investigation, several assumptions were made, the most important of which are the following: the total on-site storage time of the wastes (i.e., liquids or solids, or a mixture of both) would be restricted to ten years; solidification would be carried out in containers no smaller than 6 in. in diameter by 10 ft long; and the solidified wastes would be shipped 1000 miles in lead-shielded casks to a government repository. The quantity of fuel processed was considered to be the amount necessary to generate 1.753×10^{11} kwhr of electricity annually, which corresponds to about 700, 550, and 275 tons of the reference LWR, LMFBR, and HTGR fuels respectively.

A computer code was written to calculate the cost of waste management, using the waste characteristics as input. The code is designed to provide capital costs, operating charges, and a capital equipment depreciation schedule for each of the following waste management operations: interim liquid storage of acid wastes, pot solidification, interim storage of solids, shipment, and final disposal in salt. Earlier studies[3,4] provided the basic design and cost information needed to construct a cost model for each operation. All costs were escalated to early-1970 dollars and then used in an economic model that is representative of corporate financing to

[1] *Chem. Technol. Div. Ann. Progr. Rept. May 31, 1969,* ORNL-4422.

[2] *Chem. Technol. Div. Ann. Progr. Rept. May 31, 1969,* ORNL-4422, pp. 120–36.

[3] J. J. Perona *et al., Evaluation of Ultimate Disposal Methods for Liquid and Solid Radioactive Wastes, I. Interim Liquid Storage,* ORNL-3128 (August 1961); *II. Conversion to Solid by Pot Calcination,* ORNL-3192 (September 1961); *III. Interim Storage of Solidified Wastes,* ORNL-3355 (October 1963); *IV. Shipment of Calcined Solids,* ORNL-3356 (October 1962); *VI. Disposal of Solid Wastes in Salt Formations,* ORNL-3358 (Rev.) (March 1969).

[4] J. O. Blomeke *et al., The Costs of Permanent Disposal of Power-Reactor Fuel-Processing Wastes in Tanks,* ORNL-2873 (September 1965).

determine the amount of income required, and hence the increment to the fuel cycle cost that is introduced, by each waste management operation.

The financing model is based on a discounted cash flow calculation that computes the income which is needed during the period of waste generation to pay all operating expenses, taxes, interest on bonds, retirement of equity and bonds, and the desired return on equity. Since interim storage causes a delay in the completion of some of the management steps, the income must also provide for the establishment of an escrow fund to pay for those commitments remaining to be completed after cessation of income.

For this study, it was assumed that: (1) income was received for 20 years; (2) 70% of the total capital investment was provided by equity and 30% by bonds; (3) the tax-deductible interest on bonds was 8%, and the after-tax return on equity was 16%; and (4) the income tax rate was 48%. The tax-exempt payments into the escrow fund were assumed to draw tax-free interest at an annual rate of 5%.

A brief description of the various waste streams from processing plant flowsheets for LWR, LMFBR, and HTGR fuels is presented in Table 4.1. Solidification of these wastes results in residues of two types: calcined oxides containing 70% voids, and dispersions of waste oxides in sodium tetraborate glass. The dispersions are formed in those cases where either sodium or boron is present in the liquid waste streams, and their relative proportions are adjusted to form thermally stable sodium tetraborate on solidification.

The optimum schedules and costs of management operations for the wastes derived from processing the three types of reactor fuels are given in Table 4.2. The characteristics of the solids that contain residues from solvent cleanup wastes have been modified from those presented last year[2] to reflect smaller volumes from this source than were shown on the original flowsheets.

LWR Fuel Processing Wastes. – For cases 1, 6, and 8, the series of operations are identical: interim storage of the waste as a liquid for 10 years, solidifcation in 6-in.-diam pots, followed by immediate shipment of the solid waste and final disposal in salt. The total costs for management of the wastes as solid dispersions (cases 6 and 8) are slightly higher than that for management as a calcine (case 1), primarily because the relatively low processing rates for making the dispersions required additional pot solidification units to be installed. This

Table 4.1. Description of the Waste Streams Used as Bases for Calculating Management Costs

Reactor Type	Case No.[a]	Description
LWR	1[b]	Fission product waste
	6[c]	Combination of fission product waste, alpha-contaminated wastes, and solvent cleanup waste
	7[c]	Combination of fission product waste, alpha-contaminated wastes, and caustic scrubber waste
	8[c]	Combination of case 7 and solvent cleanup waste
LMFBR	1[b]	Fission product waste, 1% cladding dissolved
	2[b]	Fission product waste, 10% cladding dissolved
	3[c]	Fission product waste containing boron, 1% cladding dissolved
	4[c]	Fission product waste containing boron, 10% cladding dissolved
	11[c]	Combination of fission product waste from case 1 with alpha-contaminated wastes, solvent cleanup waste, and caustic scrubber waste
	12[c]	Fission product waste of case 2 combined with the three streams as in case 11
	13[c]	Fission product waste of case 3 combined with the three streams as in case 11
	14[c]	Fission product waste of case 4 combined with the three streams as in case 11
HTGR	1[c]	Fission product waste
	4[b]	Fluidized-bed burner waste
	6[c]	Combination of cases 1 and 4 with solvent cleanup and caustic scrubber wastes

[a]Case numbers conform to those used in ref. 2.

[b]On solidification, calcined solids containing 70% voids are obtained.

[c]On solidification, a dispersion of waste oxides in a void-free sodium tetraborate matrix is obtained.

Table 4.2. Costs of Managing High-Level Waste Generated by the Processing of Reactor Fuels[a]

	LWR					LMFBR								HTGR		
Case No.[b]	1	6	7	7A	8	1	2	3	4	11	12	13	14	1	4	6
Interim Liquid Storage																
Storage time, years	10	10	2	0	10	10	10	10	10	10	10	10	10	0	0	0
Number of tanks	5	5	4	0	5	5	4	4	4	4	4	5	4	0	0	0
Tank size, 10^6 gal	0.88	0.88	0.29	0	0.88	0.73	1.07	1.07	1.07	1.07	1.07	0.73	1.07	0	0	0
Initial capital cost, $\$10^6$	12.2	12.2	7.8	0	12.2	14.1	15.5	15.5	15.5	15.5	15.5	14.1	15.5	0	0	0
Unit cost, 10^{-3} mill/kwhr	25.9	25.9	17.0	0	25.9	30.0	29.1	29.1	29.1	29.1	29.1	30.0	29.1	0	0	0
Pot Solidification																
Residual solids volume, $ft^3/10^4$ Mwd(thermal)	0.221[c]	0.291[d]	0.145[d]	0.35[d]	0.303[d]	0.252[c]	0.564[c]	0.467[d]	0.561[d]	0.345[d]	0.435[d]	0.485[d]	0.575[d]	0.575[d]	4.428[c]	3.24[d]
Solids conductivity, Btu $hr^{-1}ft^{-1}\,°F^{-1}$	0.26	1.20	2.03	2.03	1.06	0.26	0.26	1.02	1.41	1.34	1.87	1.09	1.46	2.27	0.26	2.27
Pot diameter, in.	6	6	6	6	6	6	6	6	6	6	6	6	6	12	24	24
Number of pot lines	2	14	7	17	15	2	3	18	22	14	17	19	23	6	9	8
Initial capital cost, $\$10^6$	3.7	5.8	4.8	7.3	6.0	3.6	3.8	6.4	7.0	5.7	6.2	6.5	7.2	4.7	0	5.1
Unit cost, 10^{-3} mill/kwhr	3.5	5.9	9.5	18.9	6.3	3.4	4.4	6.9	7.9	5.9	6.7	7.2	8.2	11.4	6.2	15.6
Interim Solid Storage																
Storage time, years	0	0	16	10	0	0	0	0	0	0	0	0	0	6	0	4
Initial capital cost, $\$10^6$	0	0	3.0	4.0	0	0	0	0	0	0	0	0	0	2.3	0	4.4
Unit cost, 10^{-3} mill/kwhr	0	0	5.2	7.8	0	0	0	0	0	0	0	0	0	4.8	0	7.4
Shipment																
Shipments per year	10	12	6	14	12	9	20	15	18	11	14	16	19	17	111	73
Number of casks, with spare	2	2	2	2	2	2	2	2	2	2	2	2	2	2	6	4
Initial capital cost, $\$10^6$	0.4	0.4	0.3	0.3	0.4	0.4	0.4	0.4	0.4	0.4	0.4	0.4	0.4	0.4	1.4	0.7
Unit cost, 10^{-3} mill/kwhr	0.4	0.4	0.1	0.4	0.4	0.4	0.6	0.5	0.5	0.4	0.5	0.5	0.5	0.7	7.9	2.7
Salt Mine Repository																
Unit cost, 10^{-3} mill/kwhr	6.6	6.6	3.7	4.4	6.6	3.1	2.5	3.5	2.5	3.5	3.5	2.3	2.5	4.1	0.4	3.2
Total Cost																
Maximum unrecovered capital, $\$10^6$	12.2	12.2	16.4	11.3	12.2	14.1	15.5	15.5	15.5	15.5	15.5	14.1	15.5	7.0	1.4	9.5
Unit cost, 10^{-3} mill/kwhr	36.4	38.8	35.5	31.5	39.2	36.9	36.6	40.0	40.0	38.9	39.8	40.0	40.3	21.0	14.5	28.9

[a]LWR fuel is continuously irradiated to 33,000 Mwd/metric ton at a specific power of 30 Mw/metric ton; LMFBR mixed core and blankets are continuously irradiated to an average burnup of 33,000 Mwd/metric ton at an average specific power of 58 Mw/metric ton; HTGR fuel is irradiated to an average burnup of 64,700 Mwd/metric ton at an average specific power of 44.4 Mw/metric ton.

[b]Case numbers correspond to those used in Table 4.1 and ref. 2.

[c]Calcined solid with 70% voids.

[d]Dispersion of waste oxides in sodium tetraborate matrix (void-free).

increased the cost of solidification and, in turn, the total costs.

In case 7, as calculated from the flowsheet characteristics, the volume of residual solids was so small that a minimum interim storage period of 18 years was required before the waste could be buried in salt. This, of course, violates our interim storage time limit of 10 years. However, by diluting the solids with a mixture of sodium tetraborate and Fe_2O_3, a larger residual volume can be achieved, and a much more desirable sequence of waste operations is obtained (case 7A, Table 4.2). Indeed, the cost resulting from this schedule is the lowest achieved. The principal advantage of the schedule used in case 7A is the elimination of the interim liquid storage step. Similarly, the need for interim liquid storage for cases 6 and 8 can be eliminated by diluting the waste to 0.5 ft^3 of solid per 10,000 Mwd (thermal). Implementing this modification reduces the total cost to 36.8×10^{-3} mill/kwhr for each case.

As seen in Table 4.1, cases 6, 7, and 8 represent combinations of various waste streams with the fission product waste of case 1. The costs for these combinations are less than 10% higher than that for the pure fission product waste. In fact, indications are that the total costs for the combinations can be reduced until they are equal to the cost, or less than the cost, of case 1 by increasing the volumes of the residual dispersions as required to permit immediate solidification.

LMFBR Fuel Processing Wastes. – In every case, the optimal schedule consists of storage of the liquid waste for 10 years, solidification in 6-in.-diam pots, and immediate disposal in salt. The two calcination cases (1 and 2) are somewhat less expensive than the dispersion cases (3, 4, 11, 12, 13, 14); again, this is due to the more favorable processing rates for calcination. Unlike the wastes from processing LWR fuels, those from LMFBR fuels cannot be immediately solidified by accepting a reasonable dilution of the residual solids. In fact, the dilution that would be required in order to make immediate solidification possible is so large that the increased costs of solidification would more than offset the advantages gained by eliminating the liquid storage step. This difference in the two types of wastes results from the short cooling period for the LMFBR fuels (30 days) as compared with the usual 150-day cooling period for LWR fuels.

Cases 11 through 14 represent combinations of other process effluent streams with fission product wastes. The costs for the combined waste streams are about 5 to 10% higher than those for the fission product wastes that do not contain boron (cases 1 and 2), but are virtually the same as those for the fission product wastes containing boron (cases 3 and 4).

HTGR Fuel Processing Wastes. – In this study, we assumed that the small, fissile (^{235}U) particles, which contain about 25% of the fission products in the HTGR fuel, are physically separated from the larger fertile particles (^{232}Th, ^{233}U) and are not further processed. About 93% of the waste obtained by processing the fertile particles (which contain the remaining 75% of the fission products) appears in the waste of case 1, which is derived from a Thorex solvent extraction flowsheet. Case 4 represents the residue from a fluidized-bed burner and contains the remainder of the fission products originally in the fertile particles. The solidification cost for case 4 consists only of the cost of the containers since no actual solidification process is needed. It can be seen from case 6 that it is clearly less expensive to combine the two waste streams (cases 1 and 4) than to process them separately (Table 4.2).

Conclusions. – All process waste streams containing long-lived radioisotopes can be combined with the first-cycle solvent extraction raffinates prior to solidification without increasing the total costs of managing only the raffinate wastes by more than 10%.

There is clearly an economic advantage in producing a high-thermal-conductivity solid dispersion from the combined wastes that are generated by the processing of 150-day-old LWR fuels. The advantage would be gained by increasing the volumes of these dispersions as necessary to permit immediate solidification. However, in the case of combined wastes from the processing of 30-day-old LMFBR fuels, it is not economically advantageous to increase the volumes of these dispersions to the magnitudes that would make immediate solidification possible. Indeed, an interim liquid storage time of at least 10 years prior to the solidification of LMFBR fuel-processing wastes is economically justified.

Comparison of the costs for managing wastes from processing LWR and LMFBR fuels is difficult since we do not have an exact correspondence of conditions among cases. In general, however, the cost of managing LMFBR wastes is approximately 10% higher than the cost of managing wastes generated by processing LWR fuels. Although the HTGR waste-management costs are lower than those for any of the LWR or LMFBR cases, it must be remembered that only the fertile particles in the irradiated HTGR fuel are processed. The fissile particles are almost completely burned, and processing these particles is not considered to be economically feasible.

Management of Noble-Gas Fission Product Wastes

In an expanding nuclear economy, it may become desirable to remove noble-gas fission products from the off-gases of fuel processing plants. Technology is presently available for the removal of krypton and xenon; thus a study was made to assess the practicability of managing these gases by encapsulating the krypton under pressure in standard gas cylinders (either mixed with xenon or separated from it) and subsequently shipping the cylinders to a salt-mine repository for permanent storage.[5]

A plant that annually processes 2800 tons of fuel would produce twenty-eight 50-liter gas cylinders of krypton per year. Each would contain about a million curies of ^{85}Kr and generate about 5800 Btu of heat per hour. If the krypton and xenon were not separated from each other, 160 cylinders of the combined gases would be produced per year. Each would contain 180,000 curies of ^{85}Kr and generate heat at the rate of 1000 Btu/hr.

The pressurized gas cylinders could be stored temporarily at the plant in water-filled canals and could then be shipped to a salt mine in specially designed casks containing from one to five cylinders each. A shipping cask that is adaptable for this purpose and that has already been shown to meet the impact, puncture, and fire-resistance specifications of AEC Manual, Chapter 0529, has been licensed for shipping capsules of curium oxide.[6] The probability of an accidental release during shipment is extremely small, and the consequences, while serious, would not be catastrophic.

At the mine, the cylinders could be stored above the floor in rooms that would be sealed to isolate them from the remainder of the mine. Under these conditions, the required space would be only about 1 to 2% of that required for the storage of solidified high-level wastes.

The cost of noble-gas management by this method, exclusive of the cost of separating the gases from the plant's process off-gas, is estimated to range from $190,000 to $220,000 per year. This corresponds to 0.0003 to 0.00035 mill per kilowatt-hour of electricity originally produced from the fuel. From the standpoints of the projected scale of operations, the estimated costs, and considerations of safety, the proposed method appears reasonable and manageable over the next several decades.

4.2 HIGH-LEVEL RADIOACTIVE WASTE

A few years ago, a process for solidifying waste by pot calcination was developed at ORNL[7] and demonstrated at Pacific Northwest Laboratory (PNL) with high-level radioactive wastes.[8] This process has recently been modified (at ORNL) to produce a superior product – a dispersion of calcine in glass. The improved process is scheduled for engineering evaluation and demonstration with high-level radioactive wastes at PNL in mid-1970. In the dispersion-in-glass process, high-level wastes are solidified and the solids are simultaneously dispersed in a glass matrix. Up to 60 wt % (43 vol %) solids from simulated wastes that arise from the processing of thermal and fast reactor fuels are dispersed in a borosilicate glass. About 50 wt % (33 vol %) was the highest loading of solids that this glass could accommodate and still yield a void-free product. This is about twice the volume of solids which can be dissolved in glass or ceramic products and is about equal to that possible for a calcined product. The thermal conductivity, namely, 1.25 Btu hr^{-1} ft^{-1} $°F^{-1}$, is about four times that of the calcined product, twice that of the glass product, and roughly equal to that of the ceramic product. Leach rates, expressed as the fraction leached $(cm^2/g)^{-1}$ day^{-1}, of these dispersions range from 10^{-4} to 10^{-5}. Thus, they are about a thousand times more insoluble than a calcined product, roughly equal in solubility to the ceramic product, and about 10 times more soluble than a glass product. The borosilicate matrix (45 wt % B_2O_3, 35 wt % SiO_2, and 20 wt % Na_2O) used in these dispersions has a softening point of about 750°C and a low corrosivity toward stainless steel. Laboratory tests carried out in a rising-level manner in a 6-in.-diam pot at 900°C demonstrated that feed rates as high as 5.5 liters/hr could be achieved in the absence of foaming, which is usually encountered in borate and borosilicate mixes. Corrosion of the pot during these tests was negligible.

---

[5] J. O. Blomeke and J. J. Perona, *Management of Noble-Gas Fission-Product Wastes from Reprocessing Spent Fuels,* ORNL-TM-2677 (Nov. 21, 1969).

[6] C. A. Wilkins *et al.,* "Design and Testing of Curium Shipping Capsule and Cask," *Proceedings of the Second International Symposium on Packaging and Transportation of Radioactive Materials,* CONF-681001.

[7] W. E. Clark, J. C. Suddath, C. W. Hancher, R. E. Blanco, H. W. Godbee, J. M. Holmes, and C. L. Fitzgerald, *Development of Processes for Solidification of High Level Radioactive Waste: Summary for Pot Calcination and Rising Level Potglass Processes,* ORNL-TM-1584 (August 1966).

[8] A. G. Blasewitz, J. E. Mendel, K. J. Schneider, and R. J. Thompson, *Interim Status Report on the Waste Solidification Demonstration Program,* BNWL-1083 (June 1969).

Chemical Development

Waste Solidification by the Dispersion-in-Glass Process. – In small-scale batch experiments, simulated high-level aqueous waste (Table 4.3) from the processing of fuels from light-water reactors (PW-4m) and from fast reactors (LMFBR) were solidified and dispersed in glass by evaporation, calcination, and liquefaction at 900°C. Sufficient quantities of glass-forming additives containing sodium, boron, and silicon were blended with the initial wastes to give final products containing 20 to 60 wt % waste solids (Table 4.4). The glassy nature of these products (Table 4.4) decreased as the solids content from waste increased until, at 60 wt %, there was not sufficient glass to fill the interstices between the solid particles; thus the product contained voids. The glass used as a matrix contained 45 wt % B_2O_3, 35 wt % SiO_2, and 20 wt % Na_2O, and had a softening point of about 750°C. This composition was selected by first studying the Na_2O-B_2O_3-SiO_2 system[9] to find compositions with low softening points (700 to 900°C) and low corrosiveness toward stainless steel. Then the selected compositions were tested to determine which one(s) would accommodate the largest volume of waste solids. The tendency of the melts to foam, a usual behavior of borates and borosilicates at 650 to 800°C, decreased as the percentage of waste oxides increased. No foaming was observed with melts containing 500 and 60 wt % waste solids.

The foaming and corrosive characteristics of borosilicate melts were evaluated in batch and semicontinuous experiments in 6-in.-diam pots that were 8 to 12 in. long. The pots were made of 304L stainless steel and were held in a 4-kw furnace with the pot wall temperature at a maximum of 900°C. The semicontinuous runs were made using a rising-level (RL) technique, that is, a mode of operation in which the pool of boiling liquid is kept small by controlling the rate of liquid feed. The liquid rises as calcine forms under it. In turn, part of the calcine melts to form the dispersion-in-glass product. This mode of operation is designed to obviate the foaming that is encountered with batch operations and viscous liquids by keeping the amount of viscous liquids (boiling solution, molten salt, or melting calcine) small so that gases from evaporation and denitration will not be trapped and produce a cellular mass which collapses slowly. Batch boildowns were made with PW-4m waste (Table 4.3) and sufficient additives to form 30/70 products (i.e., products containing 30 wt % waste and 70 wt % glass) and 50/50 products (see Table 4.4, No. 9 and No. 4). The 30/70 mixture foamed at temperatures between 650 and 800°C, while the 50/50 mixture exhibited no tendency to foam. In RL runs, PW-4m waste was mixed with additives to make a 30/70 product and then pumped to the pot at feed rates of 5 to 10 ml/min.

Table 4.3. Chemical Compositions of High-Level LWR and LMFBR Aqueous Wastes[a] Used for Dispersion-in-Glass Studies

Constituents	Substitute Chemical	Concentration (*M* at 100 gal/metric ton of U + Pu)	
		LWR Fuel (PW-4m)	LMFBR Fuel
From fuel processing			
H^+		0.5	0.5
Fe^{3+}		0.050	0.16
Cr^{2+}		0.012	0.046
Ni^{2+}		0.008	0.023
Al^{3+}		0.001	
Na^+		0.10	0.10
NO_3^-		2.4	4.7
PO_4^{3-}		0.003	0.060
SiO_3^{2-}		0.010	
From nuclear fission[b]			
Mo^{6+}		0.130	0.24
Sr^{2+}		0.036	0.040
Ba^{2+}		0.041	0.068
Cs^+	K^+	0.078	0.21
Rb^+	K^+	0.014	0.019
$(Y + RE)^{3+}$	La^{3+}	0.27	0.53
Zr^{4+}		0.14	0.22
Ru^{3+}	Fe^{3+}	0.082	0.22
Rh^{3+}	Co^{2+}	0.013	0.060
Pd^{2+}	Ni^{2+}	0.043	0.16
Ag^+	Cu^{2+}	0.0016	0.019
Cd^{2+}		0.0025	0.010
Sn^{4+}		0.0016	0.010
Sb^{3+}	As^{3+}	0.0004	0.003
Te^{4+}	S^{6+}	0.014	0.034
Se^{4+}	S^{6+}		0.005
Nb^{5+}	Zr^{4+}		0.002
La^{3+}			0.058

[a]More detailed information on these wastes is given in Sect. 2 of BNWL-1073, ed. by K. J. Schneider (August 1969).

[b]Burnup of PW-4m fuel: 45,000 Mwd/metric ton at a specific power of 30 Mw/metric ton; burnup of LMFBR fuel: 100,000 Mwd/metric ton at a specific power of 200 Mw/metric ton.

[9]G. W. Morey, *J. Soc. Glass Technol.* **35**, 270 (1951).

Table 4.4. Products Incorporating the Solids from High-Level Aqueous Wastes in Glassy Matrices

Component	Composition (wt %) of Products from LWR (PW-4m[a]) Wastes				
	(1)	(2)	(3)	(4)	(5)
Corrosion product oxides					
Fe_2O_3	0.66	0.99	1.31	1.64	1.97
Cr_2O_3	0.15	0.22	0.30	0.37	0.45
NiO	0.10	0.15	0.20	0.25	0.30
Al_2O_3	0.01	0.01	0.02	0.02	0.02
Na_2O	0.51	0.77	1.02	1.28	1.53
P_2O_5	0.03	0.05	0.07	0.09	0.10
SiO_2	0.10	0.15	0.20	0.15	0.30
Fission product oxides					
K_2O	0.72	1.08	1.44	1.80	2.15
SrO	0.61	0.91	1.22	1.52	1.82
BaO	1.04	1.55	2.07	2.59	3.11
La_2O_3	7.35	11.03	14.71	18.38	22.06
ZrO_2	2.90	4.35	5.81	7.26	8.71
MoO_3	3.82	5.73	7.63	9.54	11.45
Fe_2O_3	1.07	1.61	2.15	2.69	3.22
CoO	0.16	0.25	0.33	0.41	0.49
NiO	0.52	0.79	1.05	1.31	1.57
CuO	0.05	0.08	0.11	0.14	0.16
SO_3	0.19	0.28	0.38	0.47	0.57
Added oxides					
B_2O_3	36.00	31.50	27.00	22.50	18.00
SiO_2	28.00	24.50	21.00	17.50	14.00
Na_2O	16.00	14.00	12.00	10.00	8.00
Waste oxides	20	30	40	50	60
Density, g/cc	2.35	2.52	2.71	2.93	3.20
Comments	Glassy	Glassy	Oxide particles dispersed in glass	Oxide particles dispersed in glass	Too stiff for RL[b] operation

Component	Composition (wt %) of Products from LMFBR[a] Wastes				
	(6)	(7)	(8)	(9)	(10)
Corrosion product oxides					
Fe_2O_3	0.90	1.36	1.81	2.26	2.71
Cr_2O_3	0.25	0.37	0.49	0.62	0.74
NiO	0.12	0.18	0.24	0.30	0.36
P_2O_5	0.30	0.45	0.60	0.75	0.90
Fission product oxides					
SO_3	0.22	0.33	0.44	0.55	0.66
Cs_2O	2.28	3.42	4.56	5.70	6.84
SrO	0.29	0.44	0.59	0.73	0.88
La_2O_3	6.08	9.12	12.16	15.20	18.24
ZrO_2	1.93	2.90	3.87	4.83	5.80
Na_2O	1.31	1.97	2.63	3.29	3.94
MoO_3	3.05	4.58	6.11	7.63	9.16
Fe_2O_3	1.24	1.86	2.48	3.11	3.73
CoO	0.32	0.48	0.64	0.80	0.95
NiO	0.84	1.27	1.69	2.11	2.53
CuO	0.11	0.16	0.21	0.27	0.32
BaO	0.74	1.11	1.47	1.84	2.21
Added oxides					
B_2O_3	36.00	31.50	27.00	22.50	18.00
SiO_2	28.00	24.50	21.00	17.50	14.00
Na_2O	16.00	14.00	12.00	10.00	8.00
Waste oxides	20	30	40	50	60
Density, g/cc	2.34	2.50	2.68	2.90	3.15
Comments	Glassy	Glassy	Oxide particles dispersed in glass	Oxide particles dispersed in glass	Too stiff for RL operation

[a]Compositions of aqueous wastes given in Table 4.1. [b]Rising level.

PHOTO 98440

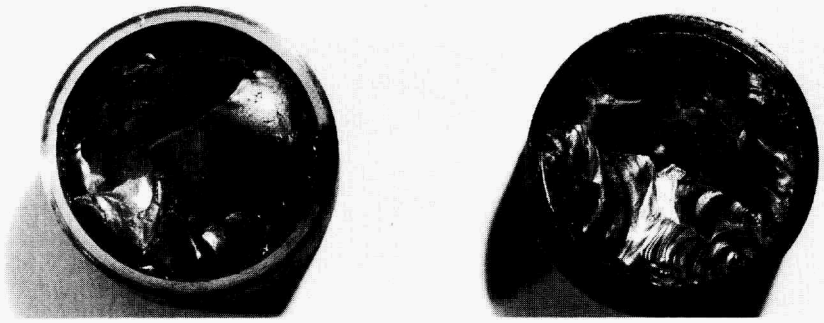

Fig. 4.1. Waste Product After 1000 hr at 850°C. Product contained 30 wt % (Table 4.4, No. 2) solids from waste (PW-4m in Table 4.3) and was held in a 304L stainless steel pot.

Foaming was not a problem at this low feed rate. In a final RL run, PW-4m waste and the additive stream (131 g of borosilicate glass per liter) were pumped separately at equal rates (44 ml/min for each stream) into the pot to make a 50/50 product. The mixture showed no tendency to foam. No corrosion of the pot was observed in any of these runs.

A series of pump-loop studies were made in an attempt to identify any problems that might occur in pumping waste solutions containing significant amounts of boron or cadmium. (Both of these elements may be used as soluble neutron poisons during fuel processing.) Three waste solutions – PW-4m waste (Table 4.3), PW-4m waste made 2.6 *M* in H_3BO_3 and then diluted with two volumes of water, and PW-4m waste made 0.9 *M* in $Cd(NO_3)_2$ and diluted with two volumes of water – were circulated continuously into and out of a tank, using either centrifugal or gear pumps. The mixtures were pumped at temperatures of 40 to 75°C at a flow rate of 1.3 gal/min through ¼-in. stainless steel tubing for 24 to 48 hr. No foaming, separation of solids from liquid, or other problems were observed in these tests. LMFBR fuel processing waste (Table 4.3) was diluted with 0.5 *M* HNO_3 to give mixtures comparable, in grams of solids per liter, to those with PW-4m (see above). These waste solutions were pumped under the same conditions used for the PW-4m waste solutions and gave similar results.

The corrosiveness of the dispersion-in-glass products toward 304L and 310 stainless steels was examined. In one study, ten samples of 30/70 product (Table 4.4, No. 2) were prepared in 1-in.-diam by 4-in.-high 304L stainless cylinders. These samples were held at 850°C for 100-hr intervals up to 1000 hr. No corrosion was visible, and the weight losses were not significant. A cross section of the 1000-hr sample is shown in Fig. 4.1. Coupons of 304L and 310 stainless steel were suspended in a 50/50 dispersion (Table 4.4, No. 4) at 900 and 1000°C. The penetration rate for the 310 stainless steel was 2 mils/month at 900°C and 6 mils/month at 1000°C. Some pitting of the 304L stainless steel occurred, and a penetration rate will not be reported. Apparently, the pitting was caused by small globules of a yellow substance, containing mainly sodium and molybdenum, which migrated toward the cooler regions of the system.

A dispersion is preferable to a single-phase glassy or crystalline product since it not only makes possible higher loadings of waste solids but it also has some of the desirable properties of each, namely, the lower leach rate of the glassy continuous phase and the higher thermal conductivity of the dispersed crystalline phase. For example, a British[10] borosilicate glass (containing 25 wt % waste solids) prepared at 1100°C had a conductivity of 0.62 Btu hr^{-1} ft^{-1} $°F^{-1}$ at 400°F. In comparison, the 30/70 product (Table 4.4, No. 2), which contained 15 vol % waste solids, had a conductivity of 0.85 Btu hr^{-1} ft^{-1} $°F^{-1}$ at 400°F. Previous studies[1] have shown that a product with about 30 vol % waste solids, similar to the 50/50 product

[10]D. B. Auty and J. R. Grover, *Thermal Conductivity of a Borosilicate Glass Suitable for Fission Product Wastes,* AERE-R4685 (December 1964).

given as No. 4 in Table 4.4, should have a conductivity of about 1.25 Btu hr^{-1} ft^{-1} $°F^{-1}$ at 400°F.

The initial leach rate of sodium and molybdenum from 30/70 products (Table 4.4, No. 2) ranged from 8×10^{-4} to 4×10^{-4} when expressed as fraction of original leached $(cm^2/g)^{-1}$ day^{-1}. Based on past experience, we would expect this rate to be lower by a factor of several hundred at the end of an initial transient period of one or two months. Analyses for lanthanum were at the limits of detection for this element (<3 ppm in the leachate).

These results are encouraging since they show that dispersion products with good physical and chemical properties can be prepared from LMFBR aqueous wastes. They also show that typical feed solutions can be pumped with conventional equipment, that reasonable feed rates can be attained with the RL dispersion-in-glass process, that the foaming characteristic of borosilicates can be circumvented, and that corrosion will not be a problem. Further studies are needed in order to: (1) find an additive that will prevent segregation of the low-melting yellow substance (apparently sodium molybdate) from dispersions containing high concentrations of waste oxides, and (2) extend the process to fluoride-bearing wastes containing calcium, which is added to complex the fluoride. The latter would serve to demonstrate the applicability of the borosilicate matrix to solids from all high-level wastes expected in the near future.

Encapsulation of Fission Product Gases. – The encapsulation of fission product gases in various solid media was studied as a possible method for immobilizing these gases during interim storage, transportation, and ultimate storage.[11] This type of immobilization would decrease the possibility of the uncontrolled release of such materials. Three media – glass, plastics, and metals – were investigated for use in encapsulation. The combination of known techniques and extrapolated test results showed that gas loadings of up to 50% of those currently obtained in cylinder storage can be achieved by using either pressurized steel bulbs or molecular sieves in a matrix of epoxy resin. Loadings of up to at least 7.5% should be obtainable by direct dispersion of the gases in glass. Other possible encapsulation methods were also considered.

Basic technology is already available for encapsulating radioactive gas in solid matrices to yield a final product containing 25 to 50%, by volume, of the gaseous component. Engineering and economic evaluations are needed to determine whether the added safety factor obtained by immobilizing such a gas warrants the additional expense.

[11] W. E. Clark and R. E. Blanco, *Encapsulation of Noble Fission Product Gases in Solid Media Prior to Transportation and Storage,* ORNL-4473 (February 1970).

4.3 SEPARATION OF RADIOACTIVE XENON AND KRYPTON FROM OTHER GASES BY USING PERMSELECTIVE MEMBRANES

A laboratory-scale process has been developed for separating krypton and xenon from other gases by the use of a cascade of permselective membranes.[12] Separation is based on the difference in the solubilities of the gases in, and the rates of transport of the gases through, a membrane. Applications of this process to the nuclear industry include the removal of radioactive noble gases from: (1) the air within a reactor containment building after an accidental release of fission products; (2) the off-gas from a processing plant for spent reactor fuels; and (3) the gas that blankets nuclear reactors, such as the molten salt or certain sodium-cooled breeder reactors which continuously vent volatile fission products. The advantages of this process include: (1) small equipment, (2) operation at ambient temperatures, (3) ease of placement in standby and prompt reactivation, (4) absence of materials that could contaminate coupled systems, (5) absence of explosion and fire hazards, and (6) competitive capital costs. Further development of the permselective membrane process has been terminated for the immediate future.

Effect of Carbon Dioxide on the Permeabilities of Krypton and Nitrogen

One of the favored types of reactor fuel is made by encasing fissile and fertile materials in graphite. A proposed method for processing this fuel is to burn the graphite in air or oxygen, thus releasing the noble gases along with carbon dioxide or nitrogen–carbon dioxide mixtures. Thin silicone-rubber membranes have been found to be more permeable to carbon dioxide, but less permeable to nitrogen, than to the noble gases. Thus, cascades of these membranes could be used to separate the noble gases from both carbon dioxide and nitrogen. When gas mixtures contained 1.5% CO_2, no appreciable change in the noble gas transport rate could be measured; however, when the mixture contained 15% CO_2, the transport rate was considerably suppressed.

[12] R. H. Rainey, W. L. Carter, and S. Blumkin, *Completion Report – The Use of Permselective Membranes for Removing Radioactive Xenon and Krypton from Various Off-Gas Streams in the Nuclear Industry,* ORNL-4522 (in preparation).

Degradation of Membrane Units Due to Irradiation

Five membrane units failed after irradiation doses varying from 1.4×10^8 to 1.7×10^8 rads. Failure was observed by a sudden increase in gas transport rate due to very small holes in the membrane. This increase in transport rate decreased the separation factor of the gases. The irradiation limit has been set at 1×10^8 rads since no adverse effects have been detected at this level.

As previously reported,[13] a radiation exposure of 1×10^8 rads does not seriously impair the usefulness of membranes for removing the noble gases from the off-gas from a reactor containment building or from a fuel processing plant. The membranes in the stage receiving the highest irradiation exposure would last longer than 150 days for fuels that had been cooled 60 days prior to processing. If the cover gas from an LMFBR[14] were to be processed immediately, the life of the membrane stage containing the highest concentration of noble gases would be less than one day. Since most of the noble gases are short-lived, a gas holdup time of 20 days would increase the life of this stage to more than 100 days, while a holdup time of 30 days would result in essentially unlimited life. Membrane stages are designed for easy replacement in installations requiring remote maintenance.

Estimated Cost of a Permselective Membrane Plant for Treatment of Off-Gas from a Fuel Processing Plant

The dissolver off-gas produced in the aqueous processing of reactor fuels contains nitrogen, oxygen, water vapor, nitrogen oxides, xenon, and krypton. This gas could be treated in a cascade of permselective membrane stages to reduce the concentration of radioactive constituents and thereby make discharge of the cleaned gas practical. The concentrated noble gases could be contained and sent to permanent storage (see Management of Noble-Gas Fission Product Wastes, Sect. 4.1).

The curves in Fig. 4.2 show the relationship between cost and plant size as a function of the volume of dissolver off-gas to be treated per minute. A 5-metric ton/day plant was assumed to generate about 100 scfm of off-gas. Costs are given for achieving off-gas decontamination factors (DF's) of 10, 100, and 1000; all values are based on a concentration factor of 100 for the recovered noble gases. For comparison, the estimated costs for a plant for absorbing noble gases by chlorofluoromethanes are included.[15] These costs are for fully equipped plants, but do not include allowances for building or for head-end treatment facilities to remove nitrogen oxides, water, etc.

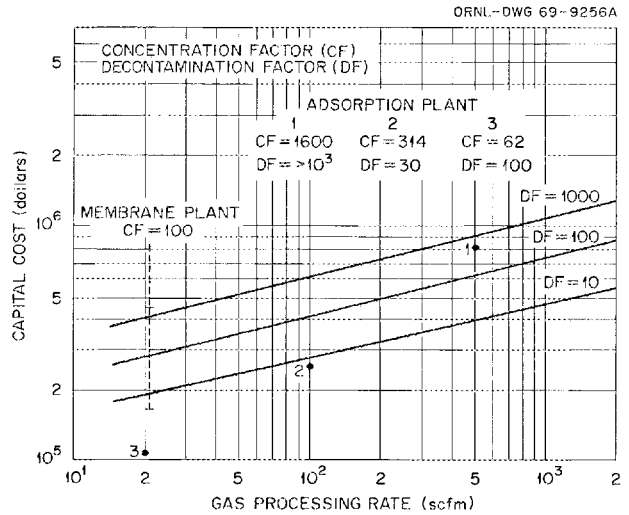

Fig. 4.2. Estimated Capital Cost for Removing Noble Gases from Fuel Processing Plant Off-Gas. Estimated rate: ~100 scfm ≈5 tons fuel/day.

Because of the delay between the discharge of fuel from the reactor and processing, DF's greater than 100 are probably unnecessary, using present-day release standards; for example, DF's of 10 may be sufficient for longer-cooled fuel (more than 60 days). Under these conditions, the cost of a gas-separation system for a 5-metric ton/day processing plant is in the range of $280,000 to $420,000. A plant designed to reduce the level of noble gases in the off-gas by a factor of 1000 would cost about $620,000.

4.4 RADIOACTIVE WASTE REPOSITORY IN SALT

The use of a bedded salt formation for the permanent storage of alpha-contaminated and solidified high-level beta-gamma wastes will be demonstrated in a waste repository that is being designed for construction in central Kansas. The repository will utilize an existing nonproducing salt mine and approximately 1000 acres

[13] *Chem. Technol. Div. Ann. Progr. Rept. May 31, 1969,* ORNL-4422, p. 151.

[14] *Chem. Technol. Div. Ann. Progr. Rept. May 31, 1968,* ORNL-4272, p. 89.

[15] J. R. Merriman and J. H. Pashley, *ORGDP Noble Gas Absorption Studies, Progress Report for Third Quarter FY 1969,* K-GD-2, Part 3 (June 9, 1969).

of adjoining salt mine area. This should provide sufficient space to store all of the alpha-contaminated wastes generated in AEC and privately owned installations, as well as all of the solidified high-level fuel-processing wastes projected for the civilian nuclear power industry over the remainder of this century. The principal components of the repository are as follows:

1. An alpha-contained, earthquake- and tornado-resistant building in which alpha-contaminated wastes shipped by rail and truck are unloaded, monitored, decontaminated, repackaged as required, and transferred to the mine.
2. A contained building and shielded hot cell equipped to receive the canned, solidified, high-level wastes, and to transfer the waste containers remotely from their shipping casks to the mine level.
3. Salt-excavating machinery for renovating the existing mine for storage of alpha-contaminated wastes, and for expanding the available mine area to permit burial of cans of high-level wastes in the salt formation.
4. Machinery for hauling the containers of alpha-contaminated waste to rooms in the existing mine area, storing them above the floor, and backfilling the storage areas with salt.
5. Machinery for transporting the cans of high-level waste to rooms prepared in the mine, depositing them in holes in the floor, backfilling the holes with salt, and eventually backfilling the rooms with salt.
6. A building to serve as a change house and headquarters for the mine crews, and to supply ventilation and other services and utilities to serve the mining and underground storage operations.

Because of designated priorities, the repository will be constructed in two phases. The initial phase will be concerned with providing an operating facility for accepting and storing alpha-contaminated waste in 1973; phase two will be directed toward completion of the high-level waste facility in 1975.

5. Transuranium-Element Processing

The Transuranium Processing Plant (TRU) and the High Flux Isotope Reactor (HFIR) are operated at ORNL as the primary production facility for the USAEC Heavy Element Program. During this report period, which corresponds to the fourth year of the operation of these facilities, the production of the actinide elements for research purposes continued at an accelerated pace. Quantities of recovered products approached three times the total production in prior years and included more than 50 mg of californium.

5.1 TRU OPERATIONS

The Transuranium Processing Plant (TRU) is operated in conjunction with the High Flux Isotope Reactor (HFIR) to produce large quantities of the transuranium elements for distribution to researchers. Since 1966, when it first began operation, TRU has been the only source of significant quantities of berkelium, californium, einsteinium, and fermium in the United States. The role of TRU as a production facility is unusual since many of the processes are actually being developed at the same time that they are being used routinely to separate and purify the transuranium elements.

The purpose of this section is to report the production of transuranium materials and to describe recent changes in the processes and equipment that are being used in TRU.

Status and Progress

During the first three years that TRU was in operation, we demonstrated all of the processing and recovery steps required to recover transuranium elements from irradiated HFIR targets and to purify the transcurium elements. Also, we fabricated curium oxide recycle targets, using the remote target fabrication line and oxide that had been produced in the sol-gel development program.

This year, for the first time, we operated the equipment for making americium and curium microspheres for use in fabricating recycle targets. We have now demonstrated all of the process steps that are required in TRU.

In three campaigns, in which HFIR-irradiated targets were processed, we recovered a total of about 7 mg of ^{249}Bk, 54 mg of ^{252}Cf, 380 μg of ^{253}Es, and 5×10^8 atoms of ^{257}Fm. These amounts are about three times the total amounts produced in the previous three years. Approximately 294 g of americium-curium oxide for use in fabricating recycle targets was produced this year. One hundred two shipments of transuranium elements were made to experimenters. One of these shipments, made to the European Transuranium Institute at Karlsruhe, Germany, contained 10 g of americium-curium oxide.

The previous difficulty with target failures during irradiation in the HFIR has apparently been resolved. Our solution was to press the target pellets to 80% or less of theoretical density (instead of the previous 90%), which leaves more space for fission products to accumulate and thereby reduces the internal stresses that are generated in the target.

During the three target-processing campaigns that we made this year, we performed some iodine evolution and retention experiments in conjunction with Liquid Metal Fast Breeder programs.

Production and Processing

A total of seven campaigns was made during this report period — three campaigns to process irradiated HFIR targets, two campaigns to produce americium and curium oxide from the Savannah River Plant (SRP) raffinate solution that had been previously purified to remove fission products, and two campaigns to prepare curium oxide for use in fabricating targets from curium scrap received from the ORNL Isotopes Division. The amounts of transuranium materials recovered in the target processing campaigns are listed in Table 5.1. The

Table 5.1. Amounts of Materials Recovered During Major Campaigns in the Transuranium Processing Plant During the Period June 1969 to May 1970

	Campaign 13	Campaign 16	Campaign 19	Total
Completion date	September 1969	January 1970	May 1970	
Material processed	7 plutonium targets 19 curium pellets	7 plutonium targets 18 curium pellets	7 plutonium targets 2 curium targets	
Quantities recovered				
^{242}Pu, g	3.0	3.5	1.1	7.6
^{243}Am, g[a]	0.8	1.2	0.7	2.7
^{244}Cm, g[a]	16.8	18.9	15.6	51.3
^{249}Bk, mg	2.1	1.9	2.6	6.6
^{252}Cf, mg	12.8	12.2	28.5	53.5
^{253}Es, μg	81.5	78	220	380
^{257}Fm, atoms	1.5×10^8	8.8×10^7	3×10^8	5×10^8

[a]Americium and curium are not usually separated from each other.

compositions of the processing loads for campaigns 13 and 16 were similar, namely, seven plutonium targets, each of which originally contained 8 g of plutonium in the form of PuO_2, and some curium pellets. Two irradiated curium targets and seven irradiated plutonium targets were processed in campaign 19. The curium targets contained oxide that was produced during sol-gel process development studies in Building 4507. Six of the seven plutonium targets were special targets, which were fabricated following the first target failures in order to determine what effects increasing the void volume and reducing the actinide content in targets would have on target life (see discussion of HFIR target failures).

Process Flowsheet

Figure 5.1 is a block diagram showing the processing steps that are being used for transuranium element production. These steps are: (1) the preparation of a feed solution by dissolving irradiated targets; (2) the recovery of plutonium; (3) the decontamination of the transplutonium elements; (4) the separation of americium and curium from the transcurium elements; (5) the separation and purification of berkelium, californium, einsteinium, and fermium; (6) the preparation of americium-curium microspheres; and (7) the fabrication of targets to be irradiated in the HFIR.

All of these steps are now performed routinely. The process and equipment used for each step, except step 6, are essentially as reported previously.[1]

In each of the three target processing campaigns that were made this year, the targets were first dejacketed with 3 *M* NaOH–1.5 *M* $NaNO_3$ and then the actinide oxides were dissolved in HNO_3. Nitric acid, instead of HCl, was used in order to accommodate an experimental effort for the LMFBR program (i.e., studying the behavior of iodine in radioactive nitric acid solutions and the treatment of off-gas from nitric acid solutions for iodine removal). This necessitated some alterations in the steps immediately following the actinide dissolution step. We used a combination of the Cleanex[2] and Pubex[3] processes to recover the plutonium and to convert the solution of transplutonium actinides from a nitrate to a chloride medium prior to the Tramex process step. In the combined Cleanex-Pubex process, the plutonium is extracted from an acid solution that is at least 1 *M* (to prevent polymerization of the plutonium). The acid concentration is reduced to about 0.03 *M*, which causes the transplutonium elements to be extracted. The aqueous raffinate, which contains the metallic impurities (such as the potassium that was added during the LMFBR iodine experiments), is discarded. The transplutonium elements are then stripped with 5 *M* HCl. We used HCl (although HNO_3 is also applicable) because the Tramex process, which is used in the subsequent step, requires a chloride-based feed solution. Plutonium in the organic phase is reduced using an organic-phase modifier, di-*tert*-butylhydro-

[1]*Chem. Technol. Div. Ann. Progr. Rept. May 31, 1969,* ORNL-4422, p. 156.

[2]*Chem. Technol. Div. Ann. Progr. Rept. May 31, 1968,* ORNL-4272, p. 96.

[3]*Chem. Technol. Div. Ann. Progr. Rept. May 31, 1967,* ORNL-4145, p. 132.

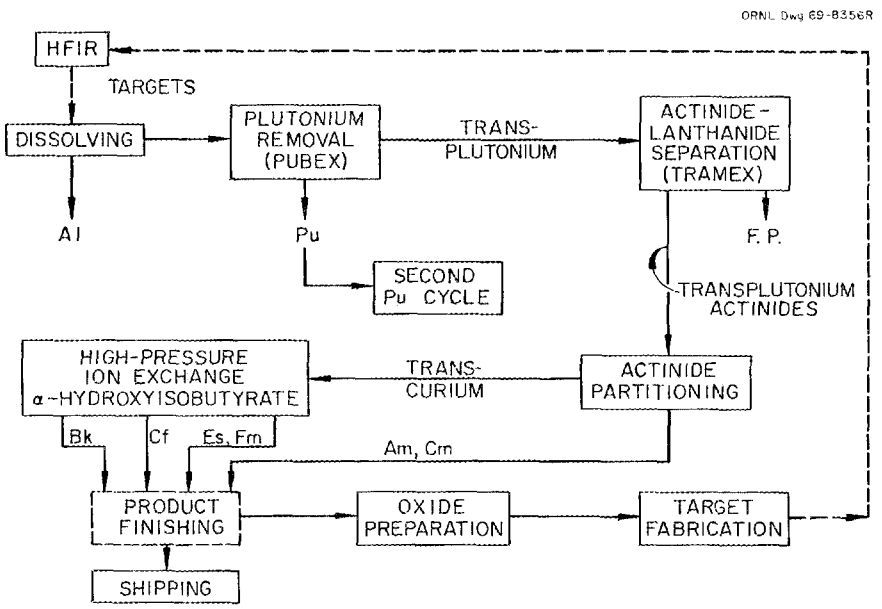

Fig. 5.1. Processing Steps Used for Transuranium Element Production.

quinone (DBHQ), in 2-ethylhexanol and then stripped with 6 *M* HCl–0.05 *M* hydroxylamine. Nitric acid interferes with the reducing power of the DBHQ and cannot be used.

We have installed a new Tramex feed system, which circumvents the difficulties that we had previously experienced in pumping the dense, viscous feed, which often contained solids. The pulsed-column contactors that we installed last year have performed satisfactorily. Both the equipment and the processes for the LiCl-based anion exchange process for separating the transcurium actinides from the americium and curium and the equipment and the procedure used for removing lithium from the americium-curium product, using oxalate precipitation, have also yielded satisfactory results.

The primary separation of the transcurium elements is still being carried out in equipment that is installed in the chemical development cell (cell 5) in TRU. Product finishing operations and special separations are also performed in this cell and in supporting shielded cave facilities. Californium purification and source fabrication procedures are being performed in a new facility that was installed in cell G of the neighboring TURF facility (see Sect. 5.6).

Preparation of Actinide Oxides

Most of the americium-curium product that is recovered from irradiated targets is purified, converted to oxide by a sol-gel technique, and then incorporated into recycle targets, which are subsequently irradiated in the HFIR to produce transcurium elements. We produced 294 g of oxide that was suitable for targets while, at the same time, we continued our attempts to improve the sol-gel process. Major problems remaining are: (1) high losses (up to 20%) during the washing of the americium-curium hydroxide in the conical washer during sol formation, (2) oversize oxide particles, which require a grinding and sizing step, and (3) low overall product yields, in the range of 50 to 70%.

The process involves treatment of the americium-curium product from the LiCl-based anion exchange process via oxalate precipitation to remove lithium and other impurities. This purified material is converted to a feed that is 0.1 *M* in HNO_3 and about 0.1 *M* in actinides. The feed solution is added to a 10 *M* NH_4OH solution to form a precipitate that is washed, using a fluidized-bed technique, and is concentrated and digested to form a sol. The sol is then converted to gel particles by agitation, in the presence of a drying solvent, in a stirred pot. The gel particles are calcined at 1150°C to give oxide particles, which are subsequently sized and incorporated into targets.

About 10 to 20% of the actinides are lost (to rework) during the fluidized-bed washing of the americium-curium hydroxides in the sol-forming step. This result represents a major difference from the results of the process development runs (reported last year) in which the losses were about 3%. We tried a number of

variations in the process to reduce the washing losses; however, none was effective.

The equipment rack that was installed in-cell last year contained a countercurrent, solvent drying column with a two-fluid nozzle for use in forming gel microspheres from the sol. Similar equipment had been used somewhat successfully during process development; however, we were not able to obtain satisfactory yields of gel microspheres because of excessive coalescence or clustering. Although several process variables were investigated, we were not able to pinpoint the cause of the difficulty.

We switched to a stirred-pot technique, after making preliminary studies with rare-earth sols. The change was made not only because of the problem with the sphere-forming column but also because it appeared less complicated and more straightforward for the scale of operations used. By adding the drying solvent directly to the sol in the conical vessel in which the sol is formed, no transfers of concentrated sols are required. The sol is dispersed in the drying solvent to form the gel particles.

In order for a batch of oxide (after calcination) to be acceptable for fabrication into targets, it must not contain any particles larger than 210 μ, and the fraction of the material that is smaller than 44 μ must be less than 15% (by weight). These limits are determined by considerations of heat transfer during irradiation of the targets.

We have made out-of-cell studies, using rare earths, of the effects of the physical characteristics of the mixing equipment (baffles in the apex of the conical vessel, agitator blade design, angle of the conical walls, and agitator speed) on particle size distribution. We have also tested a variety of drying solvent formulations. We found that, while the particle size in the nonradioactive tests could be controlled rather easily, production runs with curium behaved differently. In the latter runs, for example, usually only 20 to 30% of the original calcined oxide has been in the desired size range.

In the most recent series of sol-gel runs, which included eight sol-gel runs from a single batch of adjusted feed, the products from four of the runs contained the usual 20 to 30% in the desired size range; however, the products from the other four runs contained from 70 to 80% of the particles of the desired size. The drying solvent for this series of runs was the same as that used in several previous runs; it consisted of isoamyl alcohol that contained 0.6% Span 80, 0.6% Amine O, and 1% added water, and was 0.002 *M* in HNO_3. The sol was evaporated to a volume of 450 ml, as it had been in previous runs. From this point, three or four drying stages were required to remove all the water. In earlier runs, we had stirred the sol and drying solvent rapidly (200 to 225 rpm) to form discrete droplets in each of the drying stages. In this series, we concentrated the sol to about 100 ml in two stages of contact with drying solvent. During this concentration step, the agitator speed was kept low (60 to 90 rpm) in order to prevent the formation of droplets that might not coalesce on cessation of stirring. Then, in a final drying stage, the sol was dispersed in the drying solvent by stirring at 275 to 300 rpm. Although some improvement was made in controlling the particle size, we still do not know what caused the production of oversize particles in half of the runs.

Target Fabrication

Twelve targets containing americium and curium, one target containing plutonium, one special target, and numerous rabbits were fabricated this year.

HFIR targets must be fabricated in such a way that the center of the target pellets will not melt during irradiation. Normally, the maximum amount of actinide isotopes that can be loaded into a target is 10 g.

In addition to our "ordinary" curium product (i.e., curium containing 0.7% ^{245}Cm, recovered from HFIR targets), we recovered: (1) curium with a relatively high content of ^{240}Pu (formed by decay from ^{244}Cm) because it had not been purified from plutonium recently, and (2) curium with a relatively high ^{245}Cm content (this material had been produced in the original SRP irradiations). In these two batches, the heat generation rates during irradiation would be higher than in "ordinary" curium because of the increased rate of fissioning of ^{241}Pu (from neutron captures in ^{240}Pu) or ^{245}Cm. Targets fabricated exclusively from either of these batches would have to contain significantly less than 10 g of curium. The heat generation rate from ^{245}Cm is high at the very beginning of irradiation, but decreases to normal values in a few days. The heat generation rate due to the original ^{240}Pu content reaches a maximum three to six days after the beginning of the irradiation. Both of these effects occur only during the first few days of the first cycle in which the target is irradiated. Three alternatives are available to limit heat generation to safe levels: (1) targets containing less than 10 g of curium can be fabricated; (2) reactor power can be reduced for a week until the heat generation rate decreases; or (3) "ordinary" curium can be loaded in the center of the targets, with high-^{245}Cm-content and high-^{240}Pu-content pellets adjacent to the ordinary curium and at the ends of the

targets respectively. By using the third alternative, we have been able to make "fully loaded" targets (10 g of curium) and still operate the reactor at full power without exceeding permissible heat generation rates.

Iodine Studies

Last year we reported[4] that we had successfully demonstrated the use of an experimental off-gas treatment system, installed in cell 3, for limiting the release of radioiodine from TRU during the processing of short-cooled targets. This system, which treated 3 cfm of off-gas from the condensate collection system serving the dissolver and the seven process evaporators, consisted of a caustic scrubber to remove acid vapors, a heater, a bed of Hopcalite[5] to convert organic vapors to CO_2 and H_2O (thus protecting the charcoal bed from being poisoned), a cooler, and a bed of KI-impregnated charcoal. The off-gas was decontaminated from ^{131}I by a factor as high as 10^4. This is certainly satisfactory for processing short-cooled (three days) targets.

A larger system for treating the entire vessel and cubicle off-gas (450 cfm) is being fabricated.

During the three target-processing campaigns this year, we performed some iodine experiments in conjunction with Liquid Metal Fast Breeder (LMFBR) programs (see Sects. 2.3 and 2.6). We were able to approximate the proposed LMFBR dissolution process by making only minor changes in our dissolution and plutonium removal steps to allow us to dissolve in HNO_3 instead of HCl. A special equipment rack, which contained equipment to study iodine-removal techniques that are pertinent to LMFBR fuel processing, was installed in cubicle 7 in the dissolver off-gas line.

During the first campaign, about 3.3 curies of ^{131}I was collected in the effluent from the caustic scrubber in cell 3. In previous campaigns (in which the actinides had been dissolved using HCl), very little iodine had been collected in the scrubber. This clearly demonstrates that iodine in the off-gas can be present in different chemical forms, depending upon the medium in which it was generated.

After the first of the three campaigns, we inspected the experimental iodine removal system in cell 3 in order to locate and repair leaks that were causing loss of vacuum in the evaporator off-gas system. At this time, we found that the charcoal bed had burned, and subsequent examination showed that there was no charcoal present. We have been unable to determine what caused the ignition or at which period the burning occurred.

The system was found to contain numerous leaks resulting from corrosion of the stainless steel equipment. Evidently, HCl vapors had not been completely removed by the caustic scrubber. The entire system was removed and discarded. We were able to limit the release of iodine from TRU during the second and third target-processing campaigns by dissolving the targets in HNO_3 and using the LMFBR experimental iodine removal procedures and equipment. During the three- to four-week-long period required to complete each of the three campaigns, only 325, 52, and 40 mc of ^{131}I, respectively, were released from the HFIR stack.

HFIR Target Rod Failures

We believe that we have solved the problem of target failures in the HFIR.

The first targets that failed[6] during irradiation in the HFIR (in February and March 1967) had been irradiated for about one year in a Savannah River Plant reactor prior to the HFIR irradiation. They had each originally contained 10 g of plutonium (9.57 g of ^{242}Pu), in the form of PuO_2, in aluminum pellets that had been pressed to 90% of theoretical density. This left 10% void space in the pellets. The ruptured targets were examined, and an engineering model was developed to guide the development of a new target design. Hot-cell measurements showed that the exposure of the aluminum alloy cladding material to the high fast-neutron flux in the HFIR had caused a rapid decrease in ductility. Apparently, fission products had accumulated and filled the void volume in the pellets, and the fission gases had increased the pressure in the remaining voids. These effects then undoubtedly resulted in a gradual increase in the stresses in the cladding. When these stresses reached the yield point of the cladding, the embrittled cladding fractured instead of yielding.

The engineering model indicated that target life could be increased by decreasing the amount of target material, which would result in lower temperatures and thereby limit the internal pressure during irradiation, or by increasing the void space, which would likewise limit the internal pressure. With such modifications in mind, we fabricated three pairs of special targets, which

[4] *Chem. Technol. Div. Ann. Progr. Rept. May 31, 1969*, ORNL-4422, p. 161.

[5] Hopcalite, an oxidation catalyst, is a proprietary material of the Mine Safety Appliances Company.

[6] *Chem. Technol. Div. Ann. Progr. Rept. May 31, 1968*, ORNL-4272, p. 98.

contained: (1) 8 g of plutonium (95.82% ^{242}Pu) and 20% voids, (2) 8 g of plutonium and 25% voids, and (3) 6 g of plutonium and 20% voids. These targets were placed in the HFIR in June 1967. We continued to irradiate our existing HFIR targets, which contained 8 g of plutonium per target and only 10% voids.

The targets containing 8 g of plutonium and 10% voids were predicted, by the model, to have lifetimes that were approximately equal to the lifetime required for the desired irradiation-processing cycle. The validity of the model was demonstrated by the fact that some of these targets failed prior to scheduled processing times and some of them were processed before they ruptured. The engineering model predicted that all of the special test targets could be irradiated much longer than our specified period, based on production considerations, and the results confirmed this prediction. This year, the special targets were processed after having been irradiated for about two full-power years in the HFIR (equivalent to about 0.82 fission per original plutonium atom) without failure. Since, in the usual irradiation-processing cycle, a typical target would be dissolved and processed after being irradiated to only 0.6 fission per original actinide atom, we believe that targets containing 20% free voids should exhibit no failures.

Assay of ^{252}Cf Sources by Neutron Activation of Aluminum

We are using a nondestructive, neutron activation technique for assaying the ^{252}Cf contents of neutron sources and californium shipping containers. In this technique, a series of weighed aluminum disks is arranged in a linear array on each side of the source or shipping container. The disks become activated by fast neutrons, resulting in the (n,α) reaction to produce ^{24}Na. The threshold for this reaction is 3.25 Mev; however, because of the nature of the ^{252}Cf neutron flux distribution and the variation of the aluminum cross section as a function of energy, most of the neutrons causing the reaction are in the 7- to 9-Mev region. The probability that scattered neutrons will have an energy this high is extremely small; thus, there is no interference from neutrons that are scattered from nearby moderators. The activated disks are counted on a 200-channel pulse height analyzer, and the channels containing the 2.75-Mev photopeak of ^{24}Na are summed. There is no interference for this photopeak except from disks that are contaminated with ^{252}Cf. Gamma rays emitted by the spontaneous fission of ^{252}Cf increase the background in the region of the ^{24}Na photopeak, yielding high results. We prevent this by monitoring the disks for neutron emissions from ^{252}Cf contamination. The disks can easily be decontaminated.

Three uncertainties introduce errors in the method on an absolute basis: (1) uncertainty of the detailed neutron energy spectrum of ^{252}Cf, (2) uncertainty of the fine structure of energy dependence of the aluminum activation cross section, and (3) uncertainty of the geometry and efficiency of counting gamma-ray emissions from ^{24}Na. Calibration, by assaying a sample that was later dissolved and analyzed by ordinary analytical techniques, indicates that the uncertainties combine to give an overestimate. The actual ^{252}Cf content in the sample was only 75% of the amount indicated by the activation analysis. The precision is quite good for sources that contain at least 200 μg of ^{252}Cf. The standard deviation of the ^{252}Cf analysis for six disks irradiated simultaneously is normally 2 to 3% and has been as low as 1% (for a source that contained 2 mg of ^{252}Cf). At present, we are planning a program that will give a more accurate calibration of this technique.

5.2 ISOLATION AND PURIFICATION OF TRU PRODUCTS

Product finishing operations and the final purification and isolation of transplutonium elements are accomplished in equipment that is installed in cell 5 in TRU and in supporting shielded-cave facilities. When products reach certain levels of purity, they must be moved to progressively cleaner facilities that are used only for handling products.

Final Purification and Isolation of Transplutonium Elements

The purified products are obtained from two fractions that are produced routinely in the plant equipment: an americium-curium fraction, and a transcurium fraction. Final processing of these fractions is accomplished by procedures which have been previously described.[7,8]

Portions of the americium-curium fractions were processed to separate the contained elements by selectively precipitating americium as an Am(V)-potassium double carbonate. Berkelium was separated from residual actinides by oxidation to Bk^{4+} by $NaBrO_3$ and

[7] *Chem. Technol. Div. Ann. Progr. Rept. May 31, 1967*, ORNL-4145, pp. 136–51.

[8] *Chem. Technol. Div. Ann. Progr. Rept. May 31, 1968*, ORNL-4272, pp. 100–101.

Table 5.2. Summary of ^{248}Cm Products Isolated

Facility Used	Batch No.	^{248}Cm (μg)	^{248}Cm (at. %)	^{246}Cm (at. %)	^{244}Cm (at. %)
Cell 5, TRU	D-28	120	97.04	2.47	0.46
Cell 5, TRU	D-8	165	96.93	0.66	2.37
Cell 5, TRU	C-69	173	88.72	3.17	7.97
TRL	D-45	77	99.92	0.080	3.8×10^{-4}
TRL	D-9	120	99.93	0.071	8×10^{-5}
TURF	D-53	350	97.42	2.58	0.001

subsequent extraction from 8 *M* HNO_3 into di(2-ethylhexyl)phosphoric acid (HDEHP). Fermium, einsteinium, and californium were isolated from each other and from other residual actinides by selective elution from cation exchange resin with ammonium α-hydroxyisobutyrate.

Forty grams of ^{243}Am was prepared as highly pure AmO_2. The carbonate precipitation cycle was repeated three times to yield an americium product that contained less than 0.01% ^{244}Cm. The americium was additionally purified by three oxalate precipitation cycles and then calcined to the oxide at 800°C. Emission spectrographic analysis of the final product showed no detectable metal ion contaminants.

Isolation of Second-Growth Isotopes

Various special separations were also made; these included isolation of 60 μg of ^{253}Es (a daughter of ^{253}Cf) and about 1 mg of ^{248}Cm, both of which had grown into highly purified californium during storage. Sixty micrograms of ^{249}Cf that had grown into ^{249}Bk was also separated.

The isotope ^{248}Cm is of special interest in chemical experimentation because of its long half-life (3.52×10^5 years). Isotopically pure ^{248}Cm is obtained by the alpha decay of ^{252}Cf, which is originally isolated from large amounts of ^{244}Cm. In order to minimize the ^{244}Cm content in ^{248}Cm products, the ^{252}Cf must be highly purified, and special facilities must be used to prevent recontamination of the californium product.

Three facilities were used to isolate about 1 mg of ^{248}Cm from aged ^{252}Cf solutions. The processing was originally performed in cell 5, where the high ^{244}Cm contamination level limits the purity of the ^{248}Cm product. The ^{244}Cm contents in the products isolated in this cell varied from 0.5 to 8 wt %. In efforts to improve product purity, a hot cell located in the Transuranium Research Laboratory was used on an interim basis to recover about 200 μg of highly pure ^{248}Cm (see Table 5.2). New facilities have recently been installed in a hot cell at TURF to purify ^{252}Cf (see Sect. 5.6). The first operation to isolate curium in this facility produced about 350 μg of ^{248}Cm (^{244}Cm content, about 0.001%). A summary of the recovered ^{248}Cm products is given in Table 5.2.

In additional processing, a small quantity of isotopically pure ^{251}Cf was isolated for cross-section measurements. The origin of this product is as follows: The ^{253}Es produced at TRU contains a small amount of ^{254}Es and ^{255}Es, and the latter decays by beta emission to produce ^{255}Fm, which, in turn, decays (half-life, 20.07 hr) by alpha emission to ^{251}Cf. In this instance, the ^{255}Fm was separated by high-pressure ion exchange and was additionally purified to remove all traces of californium and einsteinium. The fermium was allowed to decay to ^{251}Cf, which was recovered ($\sim 4 \times 10^{-11}$ g) as an isotopically pure product. It was used to measure thermal capture and fission cross sections.

5.3 SPECIAL PROJECTS

The primary functions of TRU are: (1) to fabricate targets for irradiation in the HFIR to produce transuranium elements, and (2) to isolate and purify transuranium elements for use by research workers. The facilities that are available at TRU are also used for a variety of other purposes such as nonroutine productions, special preparations, and special irradiations in HFIR; in each case, a unique service can be provided to assist a research program at ORNL or another site.

Fabrication of Neutron Sources Using Californium

Data for the seven neutron sources that were fabricated in the past year, along with current data on the three sources made earlier, are listed in Table 5.3. A typical source is shown in Fig. 5.2. With the exception

Table 5.3. Neutron Sources Prepared at TRU

Source (NS-)	Date of Calibration	^{252}Cf Content (μg)	On Loan to: Individual	Site
1	8-28-68	311	J. L. Cason	PNL
2	8-28-68	268	J. E. Powell	Sandia
3	5-13-69	~90	H. E. Banta	ORAU
4	7-9-69	925	C. F. Masters	LASL
5	8-14-69	992	F. B. Simpson	INC
6	11-21-69	783	R. W. Hoff	LRL-L
7	1-21-70	807	T. F. Handley	ORNL
8	12-17-69	1927	H. Berger	ANL
9	4-17-70	1802	N. D. Wogman	PNL
10	3-11-70	118	J. P. Balagna	LASL

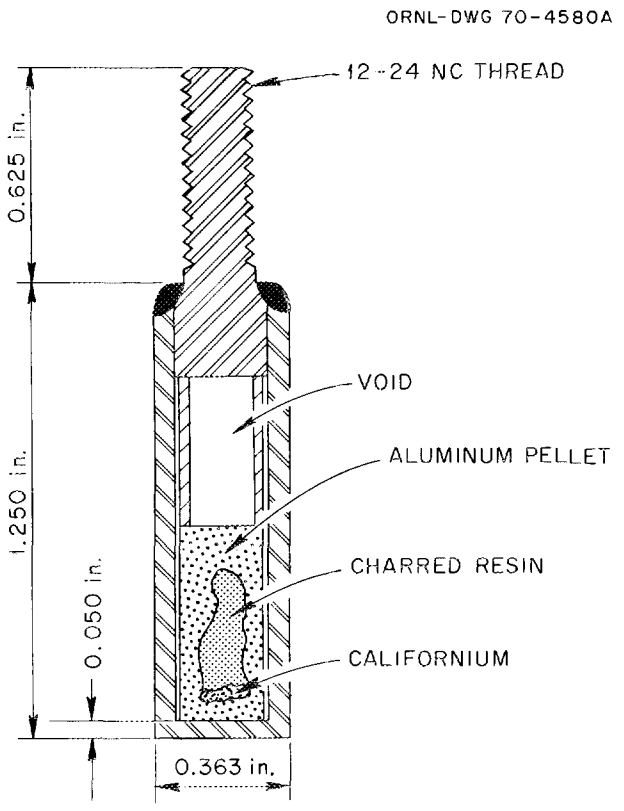

Fig. 5.2. Standard Neutron Source Using ^{252}Cf.

of NS-5, the sources that were fabricated during this report period were encapsulated in type 304L stainless steel. NS-5 was encapsulated in type 405 stainless steel, a low-nickel alloy, because nickel would interfere with some of the experiments for which the source will be used. In these experiments, which will involve the use of an iron "filter," the source will be surrounded by a massive block of iron, and many of the neutrons will be scattered into an energy region where iron has a very low cross section. Unfortunately, nickel has a strong resonance absorption in this energy region; therefore, an ordinary stainless steel capsule would be a significant sink for such neutrons and cause an undesirable flux depression.

One of the sources, NS-9, was doubly encapsulated to provide better containment for off-site use by the recipient.

All of the sources, except NS-1, have been calibrated by a neutron activation technique (see Sect. 5.1). Source NS-1 was calibrated for us by personnel from the Health Physics Division, using standardized long and proportional counters.[9]

Preparation of a High-Energy Gamma-Ray Source

An interesting new application of transuranium elements is a high-energy gamma-ray source (GS-1), which was fabricated in a manner similar to that of our neutron sources. The gamma radiation of interest (a monoenergetic 6130-kev gamma ray) arises from the reaction $^{13}C(\alpha,n)^{16}O$. The alpha particles are supplied by ^{244}Cm (α_0 = 5.802 MeV). This particular reaction is valuable because the 6130-kev gamma ray is produced from a metastable excited state of ^{16}O; the excited state has a half-life of 17 psec, which is sufficiently long to permit the recoil ^{16}O nucleus to come to rest before emitting the photon. In this way, the 6130-kev line is not broadened by the Doppler effect due to the motion of the nucleus.

The source was prepared by adding an alcohol solution of curium nitrate, containing 1 mg of ^{244}Cm, to 200 mg of carbon highly enriched (i.e., 92%) in ^{13}C

[9] D. W. Magnuson, *Thermal Neutron Flux Distribution from a ^{252}Cf Spontaneous-Fission Neutron Source*, Y-DR-1 (Oct. 17, 1968).

and subsequently converting the curium nitrate to curium oxide by heating the mixture in a stream of argon. The curium-impregnated carbon was then placed in an aluminum casing, and the resulting pellet was pressed to a minimum size. The pellet was encapsulated in a type 304L stainless steel can and welded shut to ensure complete containment.

The source strength of the 6130-kev gamma ray is about 3700 photons/sec. Undesired radiation arises from the spontaneous fission of the ^{244}Cm and from the decay of a few radioctive impurities that are present; however, this amounts to only about 5 millirems/hr at a distance of 2.5 cm from the source and does not interfere with the use of the source. The source is especially useful for calibrating high-quality Ge(Li) detector systems.

Irradiation of ^{252}Cf to Produce ^{253}Es

About 19.4 μg of isotopically pure ^{253}Es for use in an underground nuclear test, "Physics-8," was produced by irradiating and subsequently processing four ^{252}Cf rabbits that originally contained 6.01 mg of ^{252}Cf. Although the production method is the one normally used, this project was specially designed to meet the schedule of the customer's experiment.

The californium had been irradiated in the HFIR hydraulic rabbit facility and had been processed to remove the mixture of einsteinium isotopes produced by the irradiation. About 7.6 μg of ^{253}Es (in the mixture of isotopes) was distributed, and the purified californium was stored about one month to allow the ^{253}Cf (about 1% of the total californium) to decay to ^{253}Es. About 15 μg of pure ^{253}Es was recovered by "milking" the californium. When the Physics-8 shot was delayed, it became necessary to "milk" the californium a second time in order to obtain more ^{253}Es to replace part of the material lost by decay during the delay. About 4.4 μg of ^{253}Es was obtained from the second milking.

Other samples provided by TRU for "Physics 8" were: (1) 60 μg of ^{252}Cf (99.23% ^{252}Cf), (2) 41 μg of ^{245}Cm (~75% ^{245}Cm), (3) 21 μg of ^{247}Cm (~20% ^{247}Cm), and (4) 77 μg of ^{248}Cm (~90% ^{248}Cm).

Production of ^{250}Cf

Two batches of ^{250}Cf were prepared by irradiating ^{249}Bk in HFIR rabbits. This method permitted recovery of ^{250}Cf after a short irradiation, thereby minimizing the production of (and contamination with) higher isotopes of californium. Two test irradiations were made, for 5 and 29 hr respectively, to determine the optimum irradiation time to obtain the highest yield of good-quality product. For these irradiations, 5 μg of ^{249}Bk was sealed in quartz ampuls and welded into standard rabbits. The results allowed us to recalculate cross sections in this region. The best values are given in Table 5.4.

Table 5.4. Effective Cross Sections in HFIR for ^{250}Cf Production

Nuclide	σ_c	σ_f
^{249}Bk	1260	
^{250}Bk	294	2520
^{249}Cf	262	1430
^{250}Cf	1830	
^{251}Cf	2220	4410
^{252}Cf	18.2	

In the production irradiation, nearly 1.5 mg of ^{249}Bk was irradiated for 15.5 hr in a rabbit containing three pressed pellets made by the resin-loading technique. Forty-five minutes after discharge, the rabbit was transferred to TRU, using our new rabbit transfer line that connects directly to the shielded cave in laboratory 111. The initial separation was completed within 3 hr of discharge. About 155 μg of ^{250}Cf (87% purity) was recovered from the rabbit and shipped to Lawrence Radiation Laboratory at Berkeley. The ^{250}Cf is to be used as a target for transactinide element production in the Berkeley HILAC.

Four and one-half hours after the initial separation, the ^{250}Cf that had grown in from the ^{250}Bk ($t_{1/2}$ = 3.22 hr) was "milked." Nearly 6 μg of ^{250}Cf of high isotopic purity was obtained. A portion of this material was shipped to the Los Alamos Scientific Laboratory for fission cross-section studies; the remainder was retained at ORNL.

5.4 DEVELOPMENT OF CHEMICAL PROCESSES

Laboratory support was provided to assist high-activity-level processing in TRU. We investigated alternative processes for preparing oxides for HFIR targets and improved ^{252}Cf source and special target fabrication methods. In addition, we investigated new methods for isolating and partitioning actinides, developed an improved method for analyzing berkelium, and discovered that certain neutron capture reactions can be used to obtain products enriched in selected isotopes.

Status and Progress

To minimize the excessive recycle required in the preparation of americium-curium oxide microspheres for HFIR targets by sol-gel procedures, alternative preparation methods were investigated. A potentially simpler method that shows promise involves a resin-loading–calcination technique. In this process, uniform particles of curium oxide in the desired size range are produced by loading 50- to 100-mesh Dowex 50-X4 resin to saturation with americium and curium from a nitrate solution. After being loaded, the resin is carefully heated to decompose the resin matrix and then calcined at 1200°C to form the oxide. In studies to date, spherical particles of adequate strength have been produced; however, it has not been possible to consistently prepare material that is sufficiently dense to provide a satisfactory HFIR target loading.

A resin loading technique was also used as the primary method for preparing ^{252}Cf neutron sources. This procedure, reported last year,[10] was utilized during this report period to prepare six neutron sources. We also found that a modification of this technique provides a convenient means for preparing ^{252}Cf targets for irradiation in HFIR.

Laboratory studies were continued in an effort to improve the separation of actinides from fission product lanthanides by displacement elution with aminopolyacetic acids, and an interactinide separation method based on extraction chromatography was developed. Displacement elution can potentially accomplish both the actinide-lanthanide separations and the actinide partitioning since californium is eluted sufficiently far ahead of americium and curium to provide good separation from these elements. (Studies of this system are presented in Sect. 10.5.) Excellent separation (S.F. = 10^6) of ^{248}Cm from ^{252}Cf has been obtained by an extraction chromatographic technique in which di(2-ethylhexyl)phosphoric acid is held immobile on a porous glass matrix and is used in a multistage ion exchange mode. This technique also has potential application for actinide-lanthanide separations by utilizing the chemistry of the TALSPEAK[11] process. After the column has been loaded from a dilute acid medium, the actinides are preferentially eluted with a diethylenetriaminepentaacetic acid solution. Slow kinetics that are inherent in this procedure must be overcome to provide useful separations.

In our continued efforts to improve analytical procedures, a gamma counting method for berkelium analysis was developed. This method involves isolating and counting ^{245}Am from the alpha branching decay of ^{249}Bk. Another technique, which is based on the direct measurement of the 327.3-kev gamma associated with the alpha branching, was also developed. The gamma incidence per berkelium decay is 1.426×10^{-7}.

Work is presently in progress to develop a newly discovered method for producing selected, rare isotopes at greatly enriched concentrations into a practical process. The production of ^{247}Cm from ^{246}Cm is of particular interest. The method utilizes a molecular sieve (Linde X), which has the unique property of being able to incorporate ions, such as lanthanides or actinides, into its structure either at inaccessible locations or at sites from which they may be readily removed by ion exchange. Target material is loaded only at the inaccessible locations. Since the inaccessible locations are completely surrounded by ion exchange sites, the recoil energy from the nuclear reaction ejects the product nucleus to a site from which it may be selectively recovered by ion exchange. Although attempts to produce ^{247}Cm have not yet been made, the method has been tested with several lanthanide and actinide elements. Typically, about 50% of the product isotope, along with approximately 1% of the unreacted target isotope, is recovered. Products are enriched by a factor of about 50, as compared with products obtained from conventional irradiations. (This study is described in Sect. 13.)

Preparation of Actinide Oxides for HFIR Targets

Laboratory support was provided during plant operations to prepare americium-curium oxide microspheres. Although several equipment and process modifications led to the production of useful product, this process is still not satisfactory because of excessive curium recycle, which occurs primarily during the oxalate and hydroxide precipitation and washing steps (see Sect. 5.1). Because of these difficulties, studies were initiated to produce oxide particles by a resin-loading–calcination technique.

In this procedure, cation exchange resin is loaded to saturation from a metal nitrate solution. After being loaded, the resin is dried, heated to decompose the resin, and calcined to form the metal oxide. In order to

---

[10] *Chem. Technol. Div. Ann. Progr. Rept. May 31, 1969,* ORNL-4422, pp. 168–69.

[11] Boyd Weaver and F. A. Kappelmann, *Talspeak, a New Method of Separating Americium and Curium from the Lanthanides by Extraction from an Aqueous Solution of an Aminopolyacetic Acid Complex with a Monoacidic Organophosphate or Phosphonate,* ORNL-3559 (1964).

evaluate this technique, scouting runs were made with rare earths; two runs were made with curium.

In each case, the product consisted of free-flowing uniform particles of the desired size. The particles appear to have adequate strength for the required handling operations; however, it has not been possible, as yet, to consistently obtain particles of desired density. An oxide density at least 50% of the theoretical crystal density is required to provide a satisfactory loading in HFIR targets. This density has been approached in three experiments, but has not been obtained consistently.

Several series of experiments were performed with rare earths to evaluate process parameters such as resin cross-linkage, resin form, feed acidity, and calcination schedule. The results indicate that resin with low cross-linkage and feed of dilute acid concentration (approximately 0.005 *M*) are required. (In one experiment, excellent results were obtained with the NH_4^+ form, rather than the H^+ form, resin.) However, further studies will be required before any conclusions can be drawn. The results also suggest that it may be possible to improve particle density by careful regulation of calcination schedules.

In an initial curium experiment, particles with a density of about 4.9, which may be adequate for target preparation, were obtained (see Fig. 5.3). This material was prepared by loading 50- to 100-mesh Dowex 50-X4 resin to saturation with curium from a dilute nitric acid solution. The loaded resin was allowed to self-calcine overnight; then it was heated, slowly to 450°C at first and then rapidly to 1200°C. Unfortunately, we have not been able to produce material with this density in subsequent experiments; however, additional efforts are in progress.

^{252}Cf Target Preparation and Actinide-Source Fabrication Methods

Two techniques for the encapsulation of ^{252}Cf were described last year.[12] These techniques have been optimized to meet the increased demand for neutron sources and used to prepare a number of sources and californium targets for irradiation in HFIR.

One technique involved extracting californium with 2-ethylhexyl phenylphosphonic acid, which was absorbed on powdered quartz. The powdered quartz was packed into a quartz capillary tube, which, after loading, was fused into a sphere to effectively encapsulate the californium.

It was found that Bio-Glass 500[13] beads provide a much more effective support matrix for the organic extractant than powdered quartz. The use of Bio-Glass permitted faster flow rates through the column, higher loadings, and a significant reduction in the loss of organic extractant due to aqueous flow. A source containing approximately 20 μg of ^{252}Cf in a $^1/_{16}$-in.-diam sphere was prepared in this manner.

The resin-loading–encapsulation method has proved to be a versatile technique for ^{252}Cf handling. During this report period, it was used to prepare six neutron sources ranging in size from 100 μg to 2 mg of ^{252}Cf. The same general technique was modified for use in preparing ^{252}Cf targets for irradiation in HFIR, and a similar process is being investigated as a method for preparing actinides for shipment to other sites.

The preparation of a neutron source involves partially filling a specially constructed HFIR target pellet liner, containing a porous aluminum bottom, with 200 μl of cation exchange resin and then filling the remainder of the liner with aluminum powder. The pellet liner is subsequently used as a miniature ion exchange column. The required amount of californium, in dilute nitric acid solution, is pumped onto the resin. After being loaded, the resin is decomposed by calcination at 450°C for 2 hr. The resulting pellet is then compacted to reduce the dimensions of the active source region and, finally, sealed in a $^3/_8$-in.-diam stainless steel capsule.

In the preparation of ^{252}Cf targets, a uniform distribution of californium is required in each pellet to aid in heat removal during irradiation. A uniform distribution is accomplished by blending the cation exchange resin with aluminum powder and filling the pellet liner with this mixture. Results show that the californium loads uniformly over the entire length of the pellet. After resin decomposition, the pellet is pressed to 90% of theoretical density.

Separation of Actinides by Extraction Chromatography

A process that provides improved separation of ^{248}Cm from ^{252}Cf has been developed and is now in use. In this process, di(2-ethylhexyl)phosphoric (HDEHP) acid is sorbed on Bio-Glass 500 and used in an ion exchange mode. The actinides are loaded from 0.1 *M* HNO_3. Curium is selectively eluted with 0.5 *M* HNO_3, and the californium can then be stripped from

[12] *Chem. Technol. Div. Ann. Progr. Rept. May 31, 1969*, ORNL-4422, p. 168.

[13] Product of Bio-Rad Corp., Richmond, Calif.

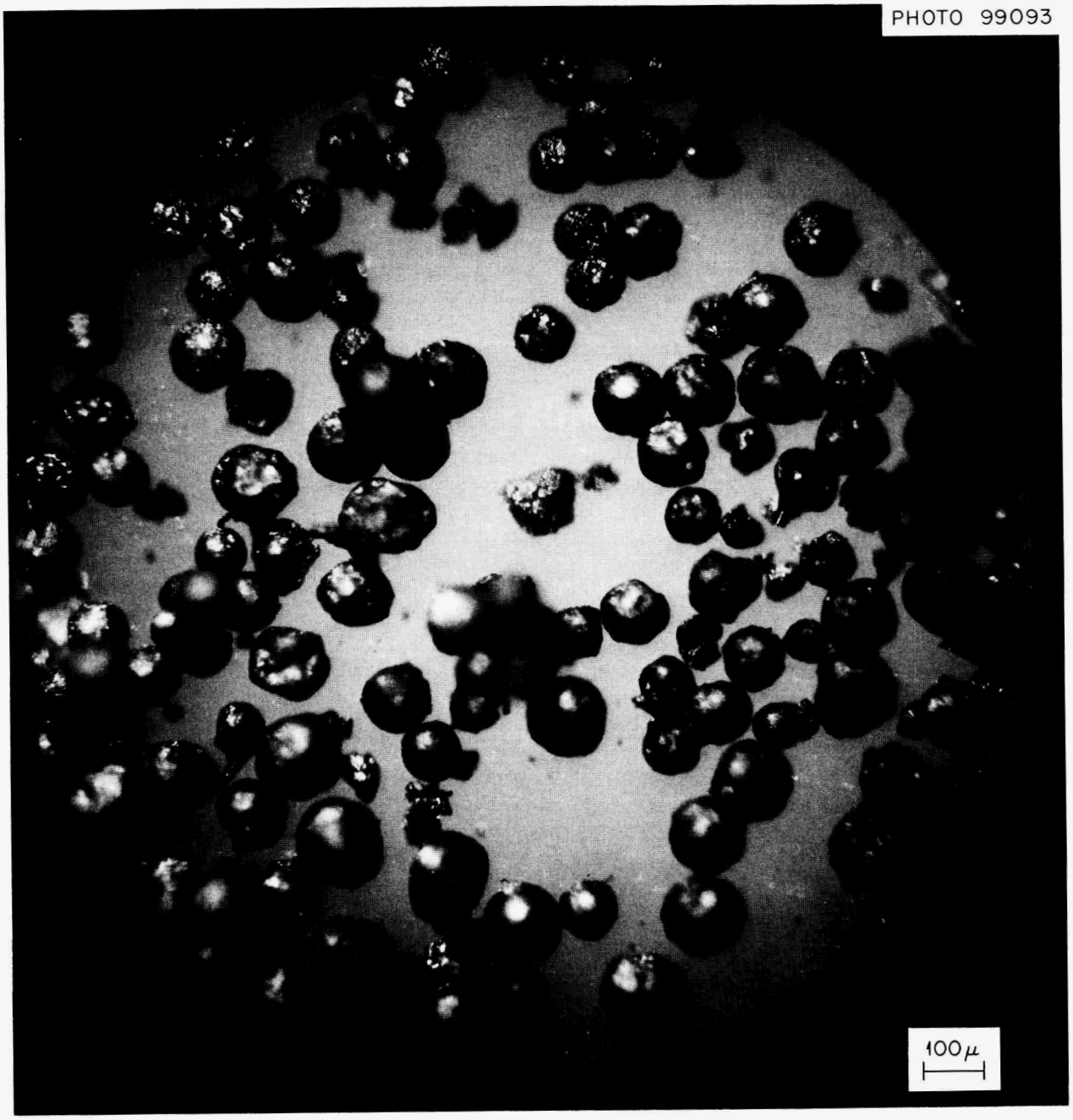

Fig. 5.3. Curium Oxide Microspheres Prepared by Resin Loading Technique.

the column with 2 *M* HNO_3. Curium-californium separation factors greater than 10^6 can be achieved.

The excellent operating characteristics of this system result from the properties of the support matrix. Bio-Glass 500 is porous glass, which has an internal void volume of about 30% and a controlled pore size of about 500 A. Because of this pore structure, the material will sorb larger quantities of organic extractant than other products tested; also, the tendency of the sorbed extractant to wash off the matrix during use is reduced, and product tailing during elution is minimized. After the glass is made hydrophobic by treatment with dimethylsilane, it will sorb 400 mg of HDEHP per gram of glass.

A flowsheet for this separation is shown in Fig. 5.4, and a typical elution curve is shown in Fig. 5.5. The actinides are loaded from dilute nitric acid feed solution, which can be pumped through the column at a flow rate of 10 ml cm^{-2} min^{-1}. The ^{248}Cm is eluted with about ten column displacement volumes of 0.5 *M* HNO_3. During this elution, the californium remains in the top 20% of the column. The californium is then stripped from the column with 2 *M* HNO_3 in about two column displacement volumes. The relatively fast flow

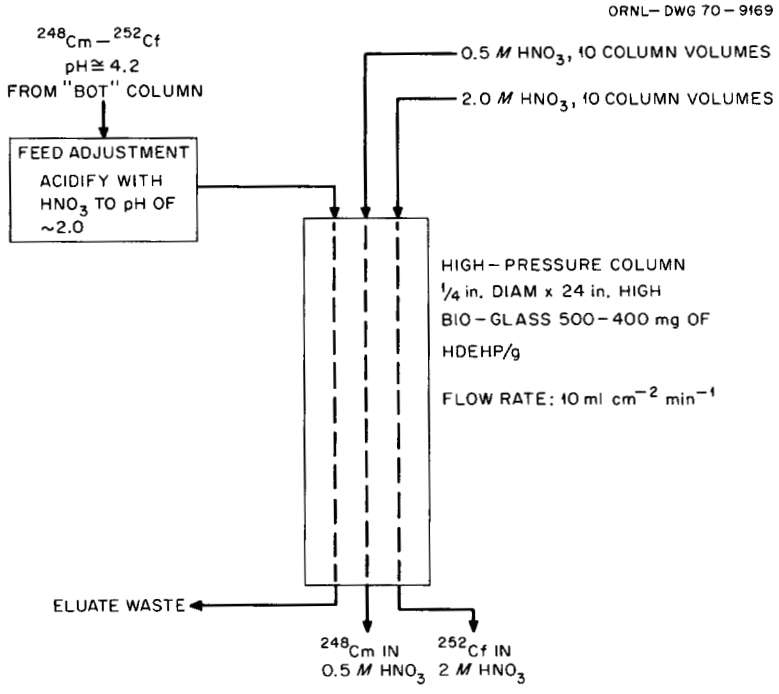

Fig. 5.4. Flowsheet for Separation of ^{248}Cm from ^{252}Cf by Extraction Chromatography.

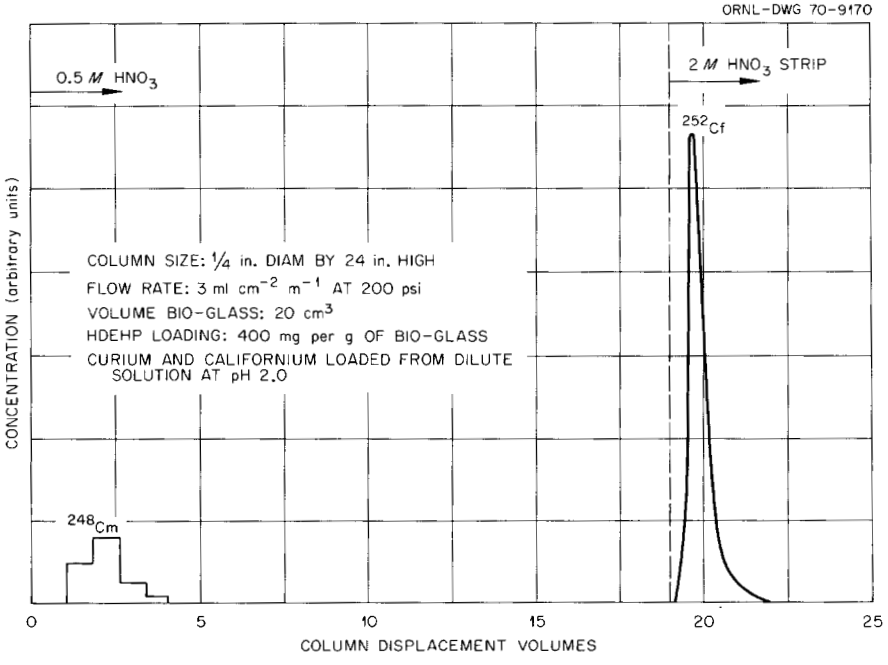

Fig. 5.5. Elution Curve for the Separation of ^{248}Cm from ^{252}Cf by Extraction Chromatography Using Bio-Glass.

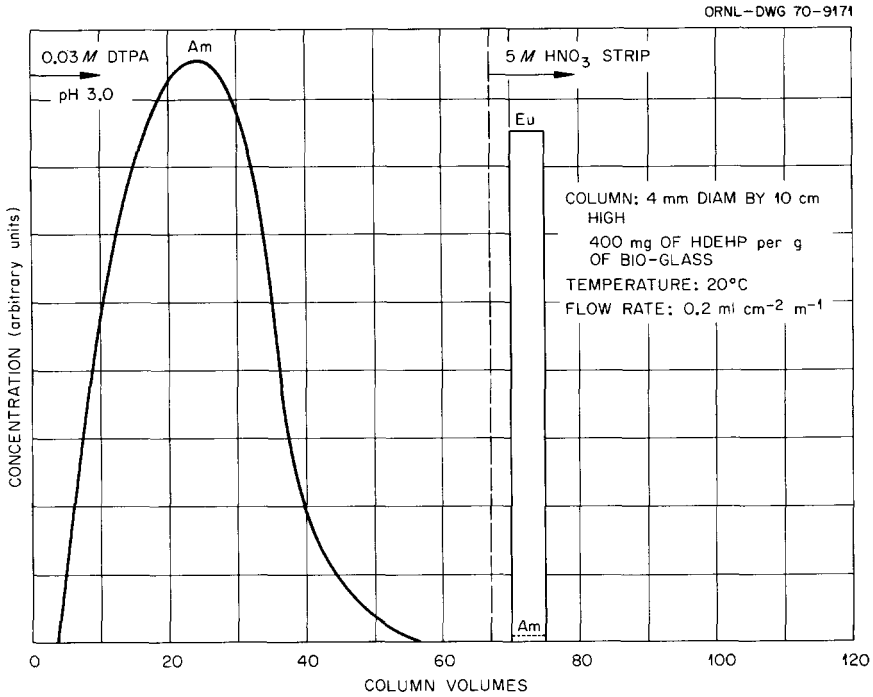

Fig. 5.6. Elution Curve for Actinide-Lanthanide Separation by Extraction Chromatographic Elution with DTPA.

rates and sharp elution bands are important characteristics of this separation.

Porous-glass–HDEHP columns of this type have also been used to study actinide-lanthanide separations. In such separations, the actinides and lanthanides are sorbed on the column from dilute acid solution, and the actinides are selectively eluted with a diethylenetriaminepentaacetic acid (DPTA) solution. In a demonstration run using ^{241}Am and ^{152}Eu, an americium recovery of 99% was achieved; the europium decontamination factor was 10^3. However, in order to make this process applicable for routine separations, we must find a means of circumventing the slow kinetics inherent in the system. Disadvantages of slow kinetics – americium tailing and an excessive volume of elutrient – are demonstrated in Fig. 5.6.

Analysis of Berkelium by Alpha Counting

Determination of the absolute quantity of berkelium in final purified products has been difficult since the most accurate method relies on the growth of the daughter product, ^{249}Cf, which is normally measured by alpha counting. (It may also be measured by counting the gamma associated with the alpha decay.) This method is somewhat disadvantageous in that it requires accurate sampling of a very small volume of a highly concentrated solution of berkelium and assaying the solution over a period of 7 to 15 days to determine the californium growth rate. In view of these drawbacks, we have developed an alternative method in which the berkelium can be determined by isolating and counting the ^{245}Am (half-life, 2.04 hr) daughter from the alpha branching decay of ^{249}Bk. By knowing the time at which the ^{245}Am is separated from its parent, the absolute quantity of berkelium may be determined when the ^{245}Cm daughter is in secular equilibrium with the berkelium. The ratio of the 252.7-kev gamma emission of the ^{245}Am to the beta emission of the ^{249}Bk is 5.79×10^{-7}. This method may prove to be more convenient and, hopefully, less time-consuming than the one previously used.

Another method for analyzing berkelium is by direct measurement of the 327.3-kev gamma ray associated with the alpha branching of ^{249}Bk. The 327.3-kev gamma/beta ratio is 1.426×10^{-7}. This gamma energy is in close proximity to a ^{249}Cf gamma emission at 333.4 kev; thus the measurement must be made within about two weeks from the time of ^{249}Bk purification.

Direct counting of the beta decay of ^{249}Bk is routinely done for process control and provides a much

more sensitive method than any of the product assay methods. The accuracy of the beta counting technique will be improved by using samples standardized by the above noted methods.

5.5 RECOVERY OF ^{252}Cf FOR THE USAEC MARKET EVALUATION PROGRAM

The Division of Production of the Atomic Energy Commission has undertaken a market evaluation program to estimate the long-term commercial demand for ^{252}Cf.[14] Californium is now being produced at the Savannah River Plant (SRP) by the irradiation of materials in two forms: (1) ^{242}Pu contained in 86 tubes that are 4 in. in diameter and have active lengths of about 4 ft, and (2) a mixture of americium and curium contained in 163 slugs that are 1 in. in diameter and 6 in. long. The latter slugs will contain about 400 mg of ^{252}Cf on discharge (about September 1, 1970), whereas the plutonium tubes will contain more than 2 g when discharged six months later.

Because of the unique services available at TRU and the present lack of similar facilities at SRP, arrangements have been made for the 163 americium-curium slugs to be processed in TRU during the coming year. No major modifications are required. A new carrier, which is similar to the existing "cannonball" carrier, is being designed and fabricated at ORNL to transport the irradiated slugs from SRP to TRU. The liquid wastes to be generated will contain significantly more fission products than those routinely handled at TRU; although they would create no unusual problems in processing, the containment of the Intermediate Level Waste transfer line to the Bethel Valley waste disposal facilities is not adequate to handle them. Therefore, the wastes will be transported in an existing carrier (after minor modifications) to the large stainless steel storage tanks in Bethel Valley. Loading and unloading stations are being provided for this operation.

Our original plans for processing irradiated HFIR targets have been revised somewhat in order to schedule the processing of the slugs. However, this revision will not reduce the availability of transuranium elements for research. The processing of targets will simply be accelerated before and after the slugs are processed in order that the total amount of californium recovered from HFIR targets in the next two years will remain essentially as estimated previously. The TRU operations group will be expanded by about 15% during fiscal year 1971 to handle the increased processing load. Research requirements for californium during the processing of the slugs will be satisfied by using the californium that will be recovered from the slugs. The total amounts of berkelium and einsteinium that will be recovered from the slugs (about 30 mg of ^{249}Bk and 600 μg of ^{253}Es) will be made available to researchers through the Transplutonium Committee.

5.6 CALIFORNIUM FACILITY AT TURF

One of the important special isotopes being recovered in significant quantities in TRU is ^{248}Cm, the alpha decay product of ^{252}Cf. This isotope is of particular interest because it has a very low specific activity (half-life, 3.52×10^5 years) and it can be easily recovered in relatively pure form. The ^{252}Cf product from each campaign can be purified and held for decay, following which pure ^{248}Cm can be recovered. In previous years, purity of the ^{248}Cm has been limited by the massive contamination levels of ^{244}Cm in the TRU production cells. No space exists in these cells in which clean equipment could be set up and used solely for this purification and separation. The following discussion will serve to illustrate the problems encountered with contamination.

About 10 g of ^{244}Cm and 10 mg of ^{252}Cf are processed in a typical processing campaign. To obtain high-quality ^{248}Cm, the ^{252}Cf should be purified until it contains only 1 ng of ^{244}Cm (i.e., equivalent to a curium DF of 10^7) prior to the decay period for ^{248}Cm production. Even if a product of this purity is obtained, measures to prevent recontamination in TRU are not practical. In addition to ^{244}Cm contamination from our ordinary mixture of californium isotopes, the alpha decay of ^{250}Cf leaves a contaminant isotope, ^{246}Cm, in the final product. The concentration of this product is such that its alpha emissions are about equal to those from ^{248}Cm. The highest-purity ^{248}Cm can be recovered only if the ^{250}Cf is burned out of our normal californium mixed isotopes by a short irradiation of the californium product.

To circumvent the ^{244}Cm contamination problem and provide badly needed space for handling californium, a new facility was designed, installed, and placed in operation in an unused cell (G) in the TURF facility. The plan view of this facility (Fig. 5.7) shows the three work stations located adjacent to three viewing windows in the single large cell. The three stations are used for: (1) final purification of the californium product from TRU; (2) milking of ^{248}Cm

[14] F. P. Baranowski, "Development and Production of Californium 252," pp. 201–11 in *Californium-252*, CONF-681032 (1969).

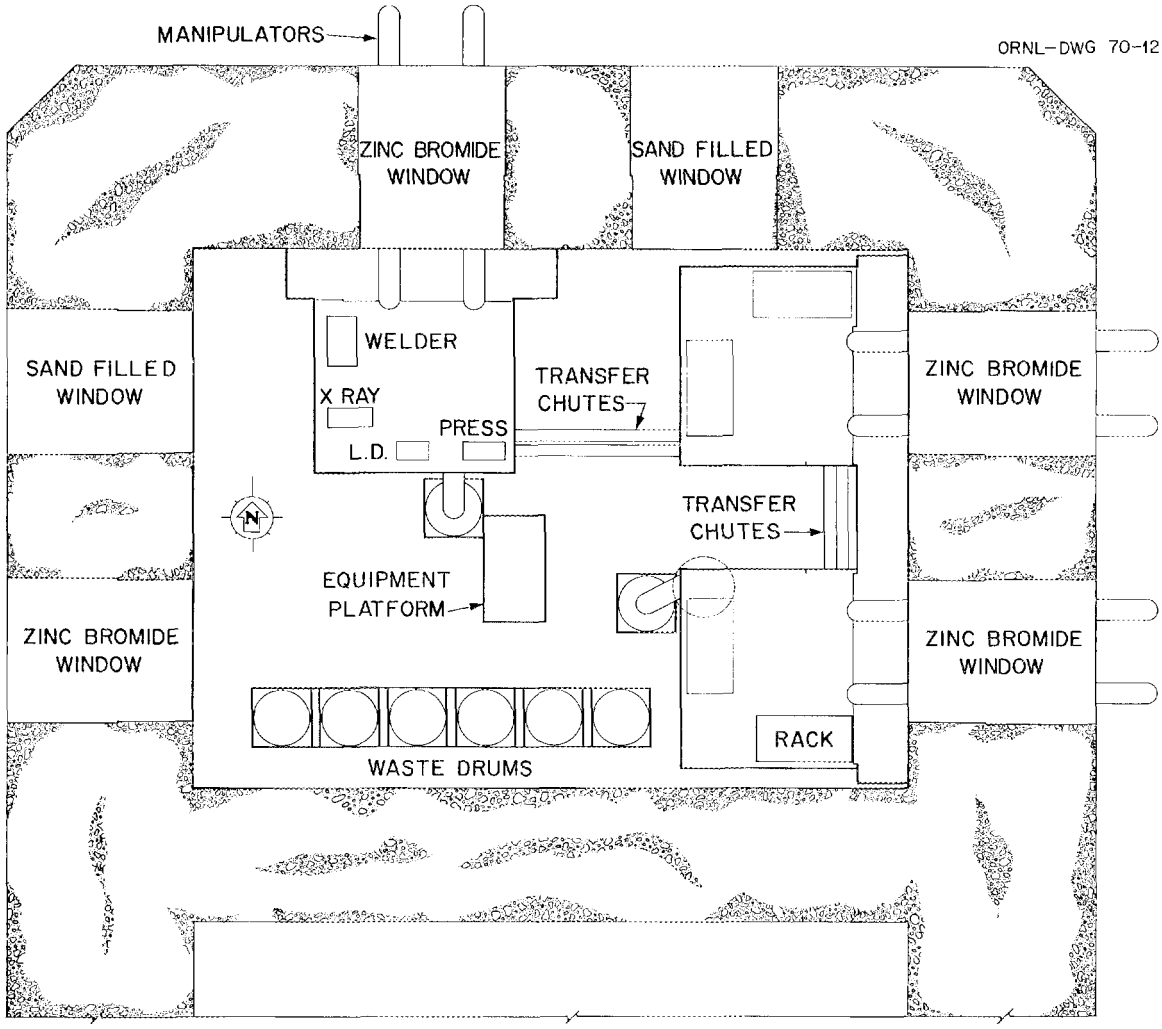

Fig. 5.7. Plan View of the Californium Facility at TURF.

from used sources or stored solutions; and (3) source fabrication and packaging operations. All of the processing steps and techniques used in this facility duplicate those used previously in TRU and described in previous reports or in other sections of this report. Following its first-stage purification in TRU, californium is processed and handled exclusively in the new facility.

Cell G in TURF was originally intended to be used as a high-level gamma-shielded cell; thus no particular consideration was given to neutron shielding in the design of the facility. Calculations indicated that at least 25 mg of ^{252}Cf could be adequately shielded, whereas results of initial operations show that the levels could be increased to at least 100 mg without problems. The zinc bromide shielding windows, not the concrete cell walls, are the weak points in the neutron shielding. The windows are built of heavy steel sections without offsets, which permit some streaming when sources are aligned with these steel sections. In addition, activation of the zinc bromide near the inside of the cell can cause problems as the solution is circulated slowly to the cold side of the window by action of the argon sparge and purge system or simple thermal convection.

The facility was placed in operation in March 1970, after about a five-month period of fabrication and construction. To date, 35 mg of ^{252}Cf has been handled in the facility; no shielding problems have been encountered.

5.7 TRANSPLUTONIUM-ELEMENT RESEARCH

A systematic study of actinide element chemistry and of comparative lanthanide chemistry is being made as significant quantities of new isotopes become available.

Such a study materially increases our basic understanding of actinide systems. This part of the USAEC Heavy Element Program includes work on problems involving solution chemistry, with particular emphasis on complex formation, and the preparation of solid actinide compounds that will be characterized by x-ray diffraction, electron microscopy, thermogravimetry, differential thermal analysis, and metallographic examination.

Lanthanide and Actinide Sulfate Complexes

Studies of the sulfate complexes of europium[15] and americium[16] reported earlier have now been extended to include curium, berkelium, californium, and einsteinium. In each case, the expected but previously unreported trisulfate species has been found and confirmed as an important aqueous-phase species at relatively high sulfate ion concentrations. Thermodynamic formation constants for the mono-, di-, and trisulfate species have been calculated for each element.

A survey of the literature has revealed a number of studies of the sulfate complexes of europium,[17-19] americium,[17,18,20-23] and curium,[17,23,24] one of californium,[17] but none of berkelium and einsteinium. Most of these studies have been done by solvent extraction or ion exchange methods at constant ionic strength. The use of these experimental methods imposes an upper limit on the ligand concentration of 20 to 30 equivalent percent of the ionic strength chosen, which is usually 1 or 2 *M*. Observation of the higher complexes at these low ligand concentrations would be difficult. Earlier work with thorium and uranium[25-27] suggested that higher complexes (in this case, trisulfate species) might be found by using a system in which sulfate is the only anion and in which higher sulfate concentrations can be reached by allowing the ionic strength to vary.

A series of Na_2SO_4-H_2SO_4 solutions varying in sulfate concentration, but constant in sulfuric acid activity, were equilibrated with a reference phase that extracts only neutral or anionic species and in which the organic phase metal extract species is always stoichiometrically equivalent to the neutral aqueous species. An organic liquid anion exchanger, 1-nonyldecylamine sulfate in benzene, was used as the reference phase. The metal concentration in the reference phase was kept constant throughout each run, and the concentration in each equilibrated aqueous solution was determined by liquid scintillation counting (cf. Sect. 10.6). The change in ratios of activity coefficients of the different species as the ionic strength varies is accounted for by using an extended Debye-Hückel equation,

$$\log G = 0.509\, \Delta Z_i^2 \sqrt{I}/(1 + B\sqrt{I})\,, \qquad (1)$$

which has been found to fit sodium sulfate activity coefficients up to 0.5 *M*. Thermodynamic equilibrium constants for zero strength are calculated directly by this approach. These experiments, as well as earlier studies at ORNL and work by others,[28] have shown that this method is superior to the constant-ionic-strength method for defining the higher complexes.

As previously described and illustrated for europium,[15] the experimental results for each actinide gave a smooth curve of aqueous metal-ion concentration (or $1/E_a^o$, since the metal-ion concentration in the organic phase is constant) vs aqueous sulfate ion concentration. This curve has a minimum (the extraction coefficient E_a^o is maximum) at the sulfate concentration, where the aqueous metal species average neutral. At lower sulfate concentrations, cationic species predominate, and, at higher sulfate concentrations, anionic species predominate, in each case resulting in increased aqueous actinide concentration. The set of material balance equations relating the experimental results to the

[15] *Chem. Technol. Div. Ann. Progr. Rept. May 31, 1968*, ORNL-4272, pp. 116–18.

[16] *Chem. Technol. Div. Ann. Progr. Rept. May 31, 1969*, ORNL-4422, pp. 176–77.

[17] R. G. De Carvalko and G. R. Choppin, *J. Inorg. Nucl. Chem.* 29, 725, 737 (1967).

[18] T. Sekine, *Acta Chem. Scand.* 19, 1469 (1965).

[19] P. G. Manning and C. B. Monk, *Trans. Faraday Soc.* 58, 938 (1962).

[20] G. M. Naire, *Radiochim. Acta* 10, 116 (1968).

[21] I. A. Lebedev, S. V. Priozhkov, and G. N. Lakovlev, *Akad. Nauk SSSR*, USAEC Trans. Tr. 4275 (1960).

[22] P. K. Khopkar and H. D. Sharma, unpublished work quoted by B. M. L. Bansal, S. K. Patri, and H. D. Sharma, *J. Inorg. Nucl. Chem.* 26, 993 (1964).

[23] I. A. Lebedev, S. V. Priozhkov, and G. N. Lakolev, *Radiokhimiya* 2, 549 (1960).

[24] A. Aziz, J. S. Lyle, and S. J. Naqui, *J. Inorg. Nucl. Chem.* 30, 1013 (1968).

[25] K. A. Allen and W. J. McDowell, *J. Phys. Chem.* 67, 1138 (1963).

[26] K. A. Allen, *J. Am. Chem. Soc.* 80, 4133 (1958).

[27] W. J. McDowell and C. F. Baes, *J. Phys. Chem.* 62, 777 (1958).

[28] Y. Marcus and C. D. Coryell, *Bull. Res. Council Israel, Sect. A* 8, 1 (1959).

Table 5.5. Formation Constants[a] of Selected Lanthanide and Actinide Sulfate Complexes

Element	K_{01}	K_{02}	K_{03}	K_{12}	K_{23}
Eu	7.21×10^3	5.55×10^5	1.15×10^5	78.1	0.204
Am	6.40×10^3	4.15×10^5	2.22×10^5	66.8	0.534
Cm	4.83×10^3	5.29×10^5	1.51×10^5	65.9	0.284
Bk	4.18×10^3	3.72×10^5	8.76×10^4	89.3	0.234
Cf	7.33×10^3	6.44×10^5	1.63×10^5	74.0	0.256
Es	6.49×10^3	4.59×10^5	1.17×10^5	70.7	0.257

[a]These are thermodynamic constants calculated to zero ionic strength. The first number in each subscript indicates the number of sulfates in the reacting species, and the second number indicates the number of sulfates in the product species.

activity coefficients of Eq. (1) and the formation constants for the series of sulfate complexes were solved by a least-squares fitting program, NLL2,[29] with appropriate subroutines. A value of 1.5 was used for B in Eq. (1). Values of 1.0 to 2.0 were found to make little difference in the fit, and the value of B to fit the mean activity coefficients of Na_2SO_4 was also in this range. The formation constants are summarized in Table 5.5. Each set is the average of at least two runs.

Curves for the distribution of einsteinium among its various species are shown in Fig. 5.8. The corresponding curves for europium[15] and for americium,[16] curium, berkelium, and californium are closely similar.

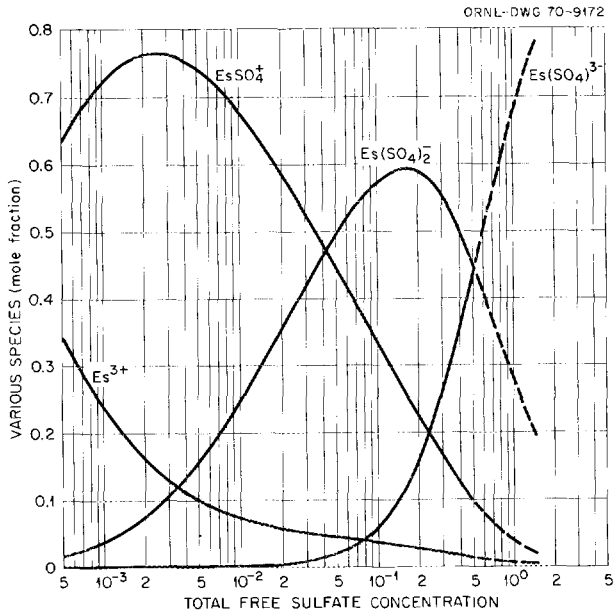

Fig. 5.8. Mole Fraction of Aqueous Einsteinium Species as a Function of Total Free Sulfate Concentration at pH 3. Calculated by means of the formation constants evaluated from solvent extraction equilibria over the range 0.0005 to 0.5 M sulfate. Free sulfate includes H_2SO_4 and Na_2SO_4 but not sulfate in the complex species.

Preparation of Anhydrous Chlorides

The preparation of actinide compounds of interest frequently requires anhydrous chlorides as starting materials. Past experience with the related lanthanides[30] has shown that the preparation of anhydrous chlorides completely free of oxychlorides is difficult, especially for the heavier lanthanides.

We reviewed and tested several methods of preparing anhydrous lanthanide chlorides, taking into consideration the problems involved in applying them to the actinides. Heating oxides with ammonium chloride in an open container, although often used, is unsatisfactory because oxychloride is formed when air contacts the hot chloride. Oxychloride impurities can be removed, on a large scale, by vacuum sublimation of anhydrous chloride; however, this technique is probably not applicable to actinides on a micro scale. Although certain aprotic solvents (e.g., dimethyl sulfoxide) remove water effectively from hydrated chlorides, removal of the solvents from the products is difficult.

We tested several methods in which hot chlorinating gases are passed over lanthanide oxides. Temperature programming proved to be helpful in preventing the production of oxychloride at high initial temperatures. The best results were obtained by passing hot anhydrous hydrogen chloride over a mixture of oxide and

[29]E. Schonfeld, private communication, June 20, 1968; a least-squares program for ORNL computers, adapted from a program by D. W. Marquardt, *J. Soc. Ind. Appl. Math.* **11**, 431 (1963).

[30]*Chem. Technol. Div. Ann. Progr. Rept. May 31, 1969*, ORNL-4422, p. 178.

ammonium chloride, although recondensation of the ammonium chloride can present problems. Chlorination with phosgene was more effective in a fluidized bed than in a boat, but this technique may not be generally applicable to the actinides. However, it should give satisfactory results for most applications at the Transuranium Research Laboratory (TRL). Chlorination by any method is more effective when the oxides have not been ignited at high temperatures. Regardless of the method used, the product must not be exposed to hot or moist air. In a comparison of all the lanthanides, the heavier elements were more difficult to chlorinate; pure ytterbium chloride was never successfully prepared.

Several of the anhydrous lanthanide chlorides prepared in this study were used in the Chemistry and Analytical Chemistry Divisions in the preparation of organic compounds. On the basis of the results of this work, smaller-scale equipment is being assembled in TRL to prepare protactinium and americium chlorides.

Actinide and Lanthanide Hydrides

We have begun a study of the preparation and properties of actinide hydrides; subsequently, the hydrides of these elements will be used in the preparation of other actinide compounds. The design of the system for preparing the hydrides and measuring their dissociation pressures was based on current experience in the preparation and handling of hydrides in various laboratories, together with the limitations required for rigorous alpha containment. The system consists of two sections, with ancillary high vacuum and temperature control. In the first section, hydrogen will be purified by diffusion through a palladium-silver membrane[31] and then passed through a liquid-nitrogen cold trap to a glass transfer bulb of known volume. The bulb will be transferred to the second section, via glove-box containment, which has a temperature control up to 1000°C and provisions for measuring pressures from 0.01 to 1000 mm Hg. Pressures above 1 mm Hg will be measured by a quartz Bourdon-tube gage;[32] lower pressures will be measured by a diaphragm-capacitance meter.[33]

The first section has been fabricated and is now undergoing tests. Some difficulty has been experienced in obtaining a leak-tight arrangement because of poor seal construction on the U-tube and well-type manometers. Members of the Health Physics Division favor catalytic oxidation for disposing of the bleed hydrogen gas, with open burning as an alternative; the final selection has not been made. All equipment for the pressure measuring section has been received and is now being installed. The total volume of this section is designed to be less than 25 ml. Preliminary tests of the quartz Bourdon-tube gage have shown it to be satisfactory. Upon completion, the hydride preparation and measuring system will be checked for safety and accuracy by measurements of the well-documented erbium-hydrogen system.[34,35]

Thermal Analysis of the Lanthanides and Actinides

Previously described[36,37] equipment for thermogravimetric analysis (TGA) and differential thermal analysis (DTA) has been used to evaluate the thermal stabilities of lanthanide and actinide compounds. The materials investigated include hydroxides of the lanthanide elements and yttrium, gel microspheres of the lanthanide hydroxides prepared by the sol-gel process, plutonium carbides, and uranium-plutonium carbides. Special handling techniques for use in studying the transcurium elements have also been developed. Interest in the hydroxides of the lanthanides is based on two factors: (1) colloidal solutions of the hydroxides are used for preparing dense ceramic bodies, and (2) knowledge of the lanthanide behavior is important for comparative studies of the actinides. The study of the carbothermic reduction of $(U,Pu)O_2$ and PuO_2 with carbon is of value in understanding the preparation of carbides and carbonitrides of these elements by a sol-gel procedure.

The hydroxides of the lanthanides have been studied by electron microscopy, electron and x-ray diffraction, thermogravimetry, and DTA. A study of all the lanthanide hydroxides, using electron microscopy and

[31] Serfass Hydrogen Purifier, Milton Roy Company, Philadelphia.

[32] Texas Instruments Inc., Industrial Products Division, Houston.

[33] *MKS Baratron Electronic Pressure Meter,* Bulletin 90, MKS Instruments, Inc., Burlington, Mass.

[34] C. E. Lundin, *Trans. Met. Soc. AIME* 242, 903-7 (1968).

[35] C. E. Lundin, *The Use of Thermodynamic Properties of Metal-Gas Systems as Reduced-Pressure Standards,* NASA Report CR-1271 (January 1969).

[36] C. A. Blake, Jr., K. B. Brown, and D. J. Crouse, *Chemical Applications of Nuclear Explosions (CANE): Progress Report for July 1 to September 30, 1966,* ORNL-TM-1688 (November 1966).

[37] *Chem. Technol. Div. Ann. Progr. Rept. May 31, 1968,* ORNL-4272, pp. 127–28.

electron diffraction, was previously reported.[38,39] In this study,[38,39] it was found that a freshly precipitated lanthanide hydroxide gave an amorphous-like pattern using both x-ray and electron diffraction. However, after sufficient aging in water, the original precipitate converted to a crystalline form. The microstructure of the material also changed during the conversion to a crystalline state. All of the lanthanide hydroxide preparations consisted of 20- to 50-A symmetrical particles immediately after precipitation; however, on aging in water, the lighter lanthanides (lanthanum through dysprosium) formed rod-like structures, while the heavier elements formed platelets and/or fibrous rods. The study of the thermal stabilities of the preparations was concerned with the general decomposition pattern and with determining what differences existed between the elements. Two objectives of special interest were: (1) to compare the thermal decomposition of the amorphous and crystalline forms, and (2) to determine whether any trends or changes in decomposition behavior could be related to ionic radii. A comparison of the elements preceding and following the dysprosium-holmium region was also of special interest since a noticeable change in the crystallization behavior was observed at this region in the series.[38,39]

A comparison of the TGA and DTA curves for amorphous and crystalline hydroxide preparations showed that there is a distinct difference between the two forms with regard to thermal decomposition. Curves for the amorphous and crystalline hydroxide preparations of gadolinium and for $Gd(NO_3)_3 \cdot 4H_2O$ are given in Fig. 5.9. The latter material was included for comparison with the hydroxides. The decompositions in Fig. 5.9 were carried out in a flowing air stream; for gadolinium, similar results were obtained in argon or helium. The TGA curve for the amorphous preparation is characterized by an essentially continuous weight loss, showing only small inflections to indicate successive reactions. The curve for the crystalline preparation shows more distinctive weight changes, with a sharp transition at 250°C. Although the different weight losses were not isolated by plateaus, the data can be extrapolated to give reasonable estimates for the magnitude of the changes. The TGA curve for $Gd(NO_3)_4 \cdot 4H_2O$ shows the loss of water up to 400°C and the two-step decomposition of nitrate, in which

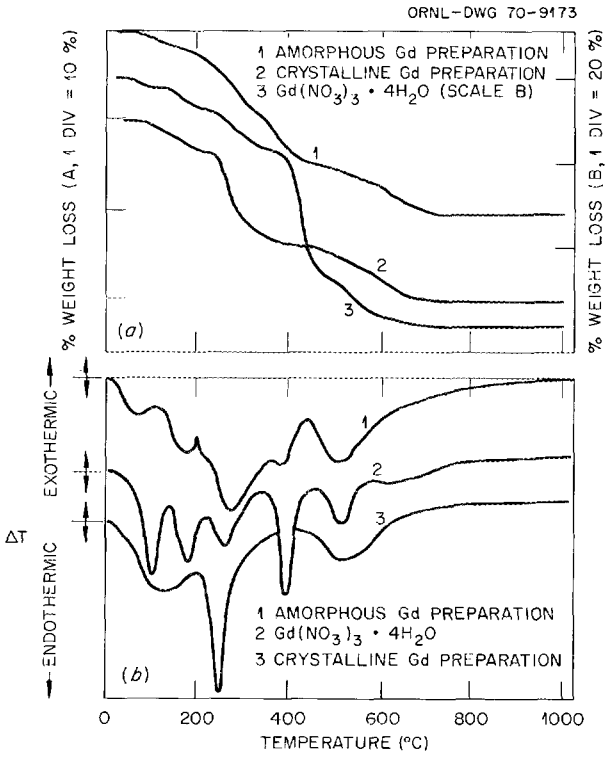

Fig. 5.9. Thermal Decomposition of Gadolinium Preparations as Shown by (*a*) TGA and (*b*) DTA Curves.

$Gd(NO_3)_3$ first forms $GdONO_3$, which then decomposes to the sesquioxide. The residual nitrate contained in the hydroxide preparations was also found to decompose in the region where the oxynitrate decomposed. Differences between the amorphous and crystalline hydroxide preparations were also observed in the DTA curves (Fig. 5.9). The curve for the amorphous form contains more peaks, but these appear as shoulders of a large endotherm that extends up to 700°C. This type of DTA curve is consistent with the continuous weight-loss curve for the same material. The DTA curve for the crystalline hydroxide preparation has three, more clearly defined peaks, plus a large endothermic peak that corresponds to the weight loss at 250°C. The DTA curve for the nitrate salt shows endotherms for the loss of water and for the two-step decomposition of nitrate.

In general, the TGA and DTA curves for the gadolinium preparations presented in Fig. 5.9 are typical for all of the other lanthanide hydroxide preparations. Some differences in behavior were observed for the individual lanthanides, but these could be interpreted in terms of the varying ionic radii and the change in complexing ability of the lanthanides. In the

[38] *Chem. Technol. Div. Ann. Progr. Rept. May 31, 1969,* ORNL-4422, pp. 178–81.

[39] R. G. Haire and T. E. Willmarth, *Trends and Differences in the Crystallization Behavior of Lanthanide Hydroxide Preparations,* ORNL-TM-2387 (October 1968).

cases of cerium, praseodymium, and terbium, the higher oxides were formed in air, but oxidation was incomplete in inert atmospheres. The preparation of the amorphous hydroxide samples of lanthanum, cerium, praseodymium, and neodymium required special handling procedures in order to avoid partial conversion to the crystalline state. In some of the hydroxide preparations, small amounts of carbonate were present (generally less than 0.1 mole of CO_3^{2-} per mole of metal), and, in several cases, the decomposition of the carbonate was detected between 600 and 900°C.

Extrapolation of the inflections in the TGA curves permitted an estimation of the stoichiometry for each weight change. In the case of the amorphous hydroxide preparations, each of the first three weight changes corresponded to 0.5 mole of H_2O per mole of metal. Curves for the crystalline forms indicated dehydration changes of 0.5 and 1.0 mole of H_2O per mole of metal. We conclude that the thermal decomposition of the amorphous and crystalline hydroxide preparations is different but that the decomposition of each form is similar for all the lanthanides. Extension of this work to the actinides has shown that americium behaves in a similar manner. Further studies to fully characterize the lanthanide and actinide compounds are planned.

An examination of the high-temperature reactions between $(U,Pu)O_2$ and carbon has been initiated; the results will yield information for optimizing procedures to prepare carbides and carbonitrides by a sol-gel process. The small size of the primary particles (<400 A) and the intimate mixture of the reactants provide conditions favorable for rapid reaction. The carbothermic reductions have been studied at temperatures up to 1650°C, in vacuum and argon, by thermogravimetry. As expected, the reaction in vacuum started at a temperature approximately 200°C lower than that for the same reaction in argon. The reaction of $(U,Pu)O_2$ or PuO_2 with carbon was rapid at 1550 to 1600°C, whereas the reaction of PuO_2 with carbon was significant at a temperature as low as 1100°C in vacuum. Figure 5.10 shows TGA curves for the carbothermic reduction of material obtained from a $(U,Pu)O_2$-C sol in which the U/Pu atom ratio was 4. The weight loss below 900°C was due to residual water and nitrate in the gel. Further studies are in progress to examine some of the variables associated with preparations of the carbides and carbonitrides.

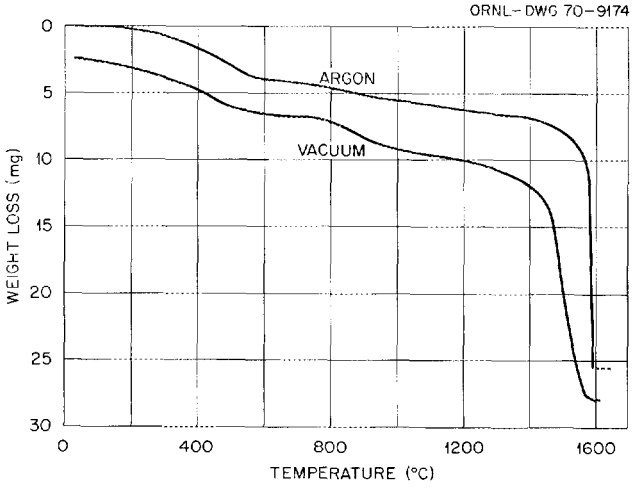

Fig. 5.10. Carbothermic Reduction of $(U,Pu)O_2$-C Sol-Gel Material.

Investigation of Lanthanides and Actinides by Electron Microscopy

The hydrous oxides and hydroxides of the lanthanides and actinides have been studied by means of electron microscopy, x-ray diffraction, and electron diffraction. These compounds are of interest because of their utility in sol-gel processes as well as in comparative studies of the two series of elements. Previous work on uranium, plutonium, americium, curium, and the lanthanides has been reported.[40,41] Because of their scarcity and their higher specific activities, the transplutonium elements present special experimental problems.

Examination of hydroxide preparations of the lanthanide and actinide elements has shown that the initial precipitates give amorphous-like x-ray or electron diffraction patterns. The primary particles in the fresh precipitates are less than 50 A in diameter (less than 25 A for uranium and plutonium). Following a sufficient period of aging in water, the precipitates become crystalline. A change in the physical microstructure accompanies the crystallization; rods or platelets are formed in the case of the lanthanides and transplutonium elements; however, with uranium and plutonium precipitates, the particles increase in size but retain their original symmetry.

The general crystallization behavior of the lanthanide hydroxides has been reported.[41] It was found that both the time required for conversion and the crystalline microstructure which is obtained can be used to divide the series of elements into two groups – one preceding and one following the dysprosium-holmium region.

[40] *Chem. Technol. Div. Ann. Progr. Rept. May 31, 1968,* ORNL-4272, pp. 123–27.

[41] *Chem. Technol. Div. Ann. Progr. Rept. May 31, 1969,* ORNL-4422, pp. 178–82.

Earlier work with the transplutonium elements showed that these elements behaved in a manner characteristic of the lighter lanthanides. However, the crystallization behavior of the transplutonium elements is complicated by their radioactive characteristics and a scarcity of material. The heat and radiolysis accompanying the radioactive decay present variables that are not encountered with the lanthanides. In recent studies with ^{253}Es, the rate of destruction was found to be very high; there was some indication that the destruction rate was greater than the rate of conversion from the amorphous to a crystalline form. In addition, the scarcity of the transplutonium elements has required that preparations be made on a micro scale. These problems have made it necessary to perform additional studies with the lanthanides in order to determine how preparation conditions affect the crystallization behavior and the type of microstructure that is obtained.

Experiments with 0.5 to 1.0 μg of lanthanides have shown that the microstructures are altered from the familiar rod and platelet forms. In general, we have observed sheet-like material or very thin rod structures, which tend to give single crystal patterns. These forms are more difficult to differentiate from small amounts of inorganic salts and other impurities, which are sometimes present in the preparations. To date, the diffraction patterns obtained from these micro preparations have not been as useful as those obtained by the standard preparations.

To better understand the effect that the method of preparation has on the morphology of the products, additional experiments with gram quantities of lanthanides have been made. In the initial experiments, we used more extreme conditions for aging the washed lanthanide hydroxide precipitate (i.e., 1 *M* NH_4NO_3 and 4 *M* NH_4OH were employed as aging media) than would be expected in the micro preparations. These reagents were chosen since they are encountered in the normal preparation procedure. It was found that both of the reagents inhibit the formation of the rod and platelet forms that are routinely produced by the standard aging procedure in water. Instead, either irregularly shaped sheet structures or rudimentary rods were observed. The degree of crystallinity was much less than that of the normal rod or platelet structures aged in water for the same period of time.

The effects of the aging conditions on the morphology of holmium hydroxide preparations are shown in Fig. 5.11. Four samples were aged for the same length of time (approximately three months) in different media: water (at two holmium concentrations), 1 *M* NH_4NO_3, and 8 *M* NH_4OH. These samples were initially prepared from the same washed precipitate. The material that was aged in water formed the expected fibrous rods, while the sample that was aged in NH_4NO_3 formed large sheet-like structures. In NH_4OH, an agglomerated form of the original particles was obtained. Similar results were found with several of the other lanthanides. The effects of the aging media on the morphology of the lanthanide hydroxides are more readily studied with the lighter lanthanides, because of their shorter conversion times. In experiments with praseodymium, sheet-like structures were also observed in hydroxide samples that were aged in NH_4NO_3. However, if the portion of the precipitate that was aged in NH_4NO_3 was separated from the salt solution and then aged further in pure water, the platelets were converted into rod-like structures. This sequence is shown in Fig. 5.12. The rod structures in Fig. 5.12*d* are about the same as those found in precipitates aged only in water.

A thorough knowledge of the morphology of the hydroxide products is important for isolating and identifying products made from the transcurium elements. An understanding of how the aging medium affects the microstructures is also necessary for the successful preparation of identifiable products on a microgram level.

Since electron diffraction plays a vital role in the identification of the products, a thorough understanding of the lanthanide hydroxide diffraction patterns is required. To complement the electron diffraction work, x-ray powder patterns have been made for all of the lanthanide hydroxide preparations. The x-ray patterns are especially useful for the heavier lanthanides, where preferred orientation of the platelet structures[41] can affect the electron diffraction patterns obtained. Analysis of the x-ray powder patterns is in progress; preliminary conclusions are that the lighter members (up to terbium or dysprosium) form hexagonal patterns, while the heavier members contain more than one crystalline phase. The x-ray diffraction pattern for $Am(OH)_3$ has also been obtained and is in excellent agreement with the electron diffraction results previously reported.[40,41]

Electron microscopy has also been used to examine $(U,Pu)O_2$-C and PuO_2-C sols, which are employed in preparing carbides and carbonitrides by a sol-gel process. The examination of UO_2 and PuO_2 sols has been previously reported.[42] The intimate contact of

[42] *Chem. Technol. Div. Ann. Progr. Rept. May 31, 1968,* ORNL-4272, pp. 125–26; *Chem. Technol. Div. Ann. Progr. Rept. May 31, 1969,* ORNL-4422, pp. 208–10.

PHOTO 93154

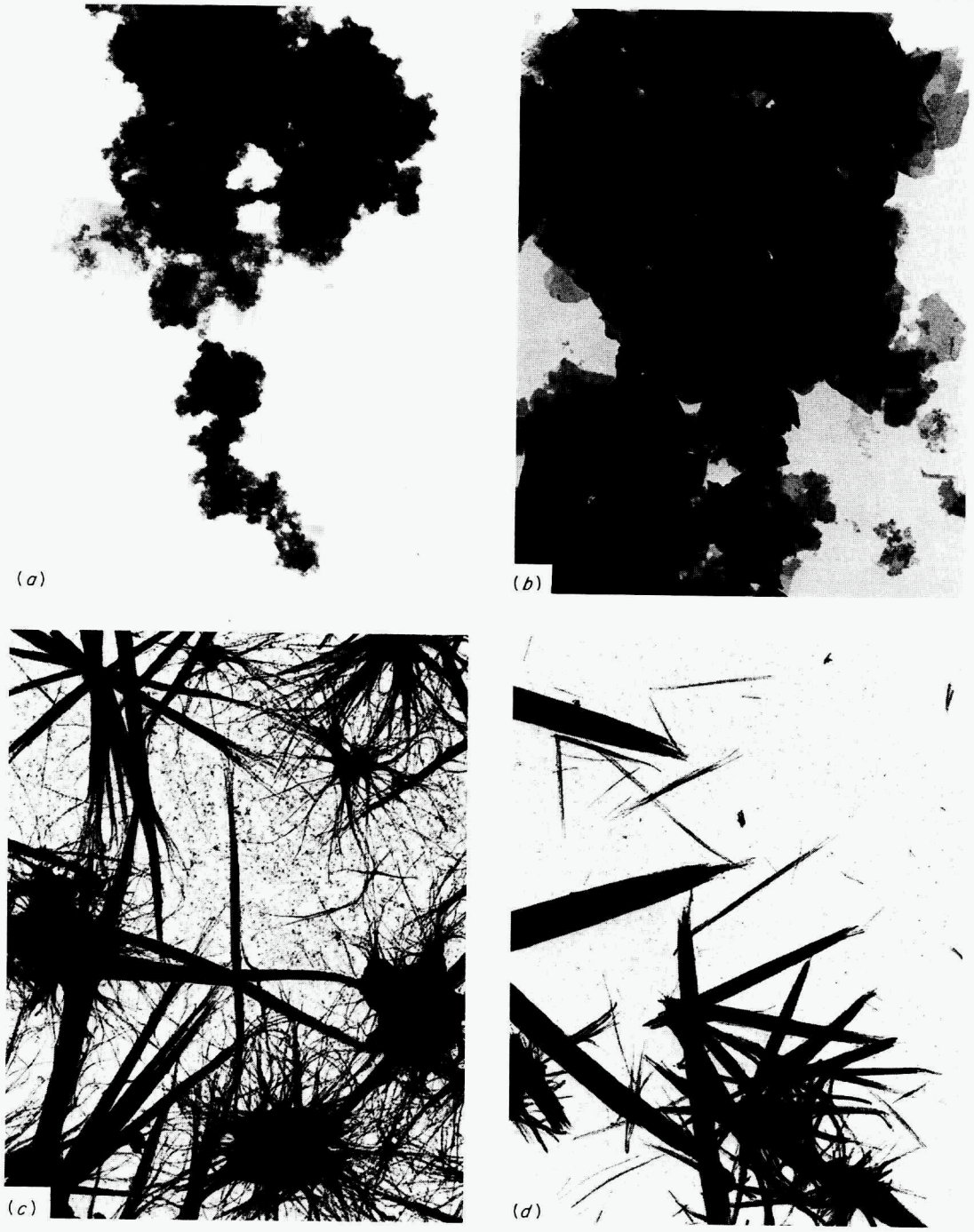

1585 Å

(a) HOLMIUM AGED IN 8 *M* NH_4OH
(b) HOLMIUM AGED IN 1 *M* NH_4NO_3
(c) HOLMIUM (0.02 *M* Ho) AGED IN WATER
(d) HOLMIUM (0.5 *M* Ho) AGED IN WATER

Fig. 5.11. Electron Micrographs of Holmium Precipitates Aged in Different Media.

PHOTO 99831

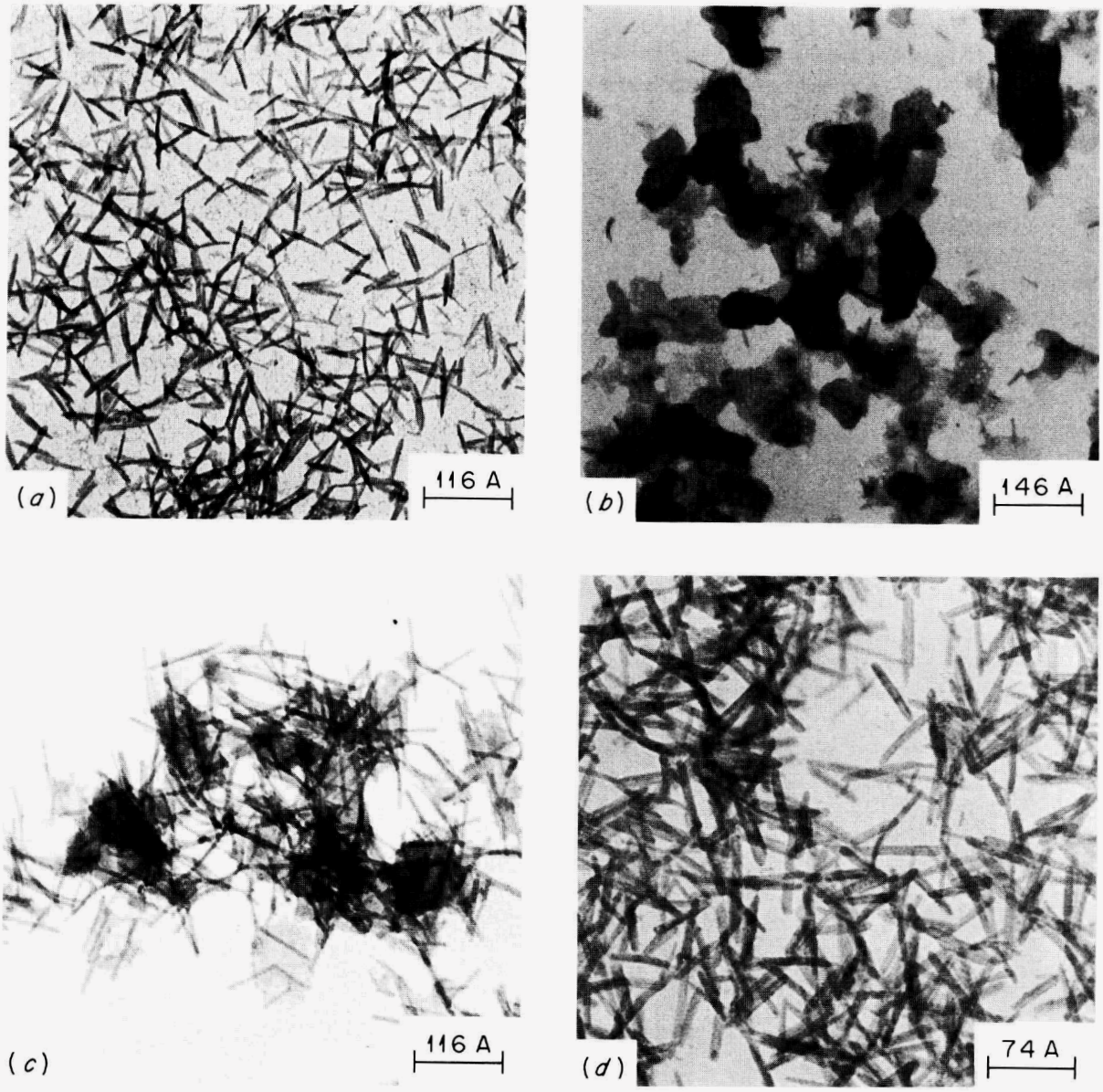

Fig. 5.12. Aging of $Pr(OH)_3$ in Various Media. (*a*) Water, one day; (*b*) NH_4NO_3, one day; (*c*) NH_4NO_3 for one day, then water for one day; (*d*) NH_4NO_3 for one day, then water for three days.

the particles in the sols can be seen in Fig. 5.13. An electron micrograph of a PuO_2 sol is shown in Fig. 5.13*a*; the structure of the carbon black alone is shown in Fig. 5.13*b*; and the particles present in the mixed sol can be seen in Fig. 5.13*c*. The primary particles of the PuO_2 sol are approximately 80 A in diameter, whereas a colloidal solution of the carbon black is composed of 400-A particles aggregated to form larger units. In the PuO_2-C sol, the carbon structure is essentially the same, but the PuO_2 particles are closely associated with the carbon surface. With $(U,Pu)O_2$ + C mixtures, a similar condition was observed. In the case where CUSP-prepared sols were used, it was possible to differentiate between the urania aggregate[42] and the PuO_2 particles[40] in the UO_2-PuO_2-C mixtures.

PHOTO 99953

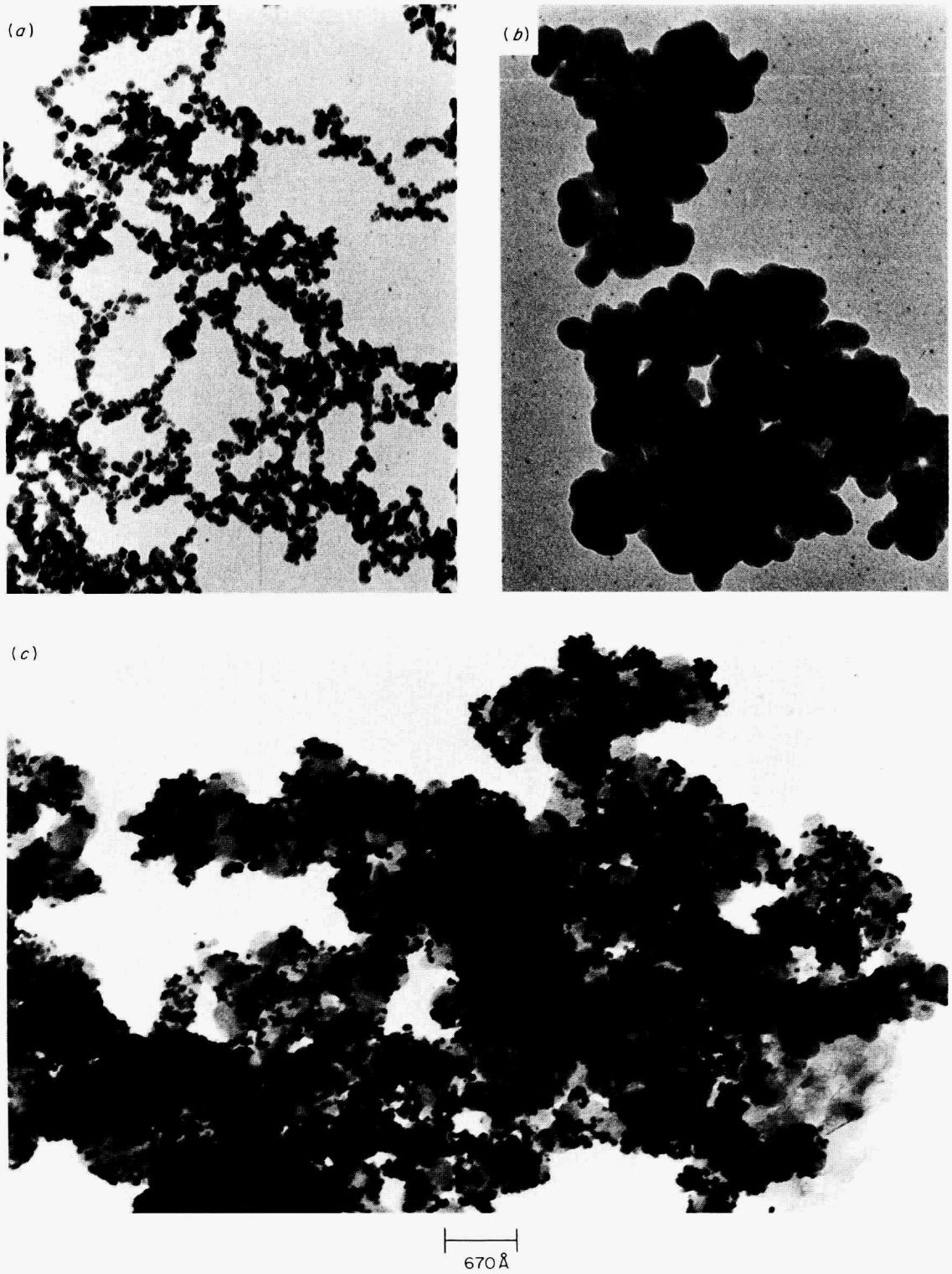

Fig. 5.13. Electron Micrographs of (*a*) PuO_2, (*b*) Carbon, and (*c*) PuO_2–C Sols.

5.8 COLLABORATIVE RESEARCH WITH THE TRANSURANIUM RESEARCH LABORATORY

Several research projects are being carried out in collaboration with personnel at the Transuranium Research Laboratory (TRL). This work is summarized briefly here. More detailed information can be obtained in annual reports published by the Chemistry Division.

The thermal neutron capture and fission cross sections for ^{251}Cf in the HFIR were determined. These measurements were made with isotopically pure ^{251}Cf, which was obtained as a decay product from purified ^{255}Fm. The capture cross section, σ_c, and the fission cross section were determined to be 2700 barns[43] and 3200 barns respectively; hence, the depletion cross section is the sum of these two, or 5900 barns. A similar experiment with ^{257}Fm was performed, and the depletion cross section in the HFIR, along with the thermal and resonance integrals in the ORR, was determined. The depletion cross-section value obtained in the HFIR is approximately 6100 barns. This is the highest mass isotope for which a neutron cross-section determination has been made.

The method of determining the II-III oxidation potentials of the actinide and lanthanide elements by correlation of the electron transfer bands to known redox potentials[44] was extended to the III-IV couple for the two series of elements. The electron transfer and the $f \rightarrow d$ absorption bands of the oxidizable lanthanides (cerium, praseodymium, and terbium) and the actinide elements (plutonium, americium, and berkelium) were determined with the tribromides in absolute ethanol, and with the hexabromides in acetonitrile saturated with tetraethylammonium bromide. From the position of the absorption bands, it was possible to determine the constants for Jørgansen's refined spin-pairing electronic energy theory and to calculate the III-IV oxidation potentials for the entire lanthanide and actinide element series. The correlation between the electron transfer bands and the oxidation potentials has made it possible to estimate the formal potentials of couples that are unstable in aqueous media. The III-IV oxidation potentials[45] for americium, curium, berkelium, californium, and einsteinium are calculated to be −2.0, −3.1, −1.6, −3.3, and −4.6 v respectively.

The formal potential for Bk(III-IV) oxidation in a variety of solutions was determined by direct potentiometry. The potentials[44] vs the H_2 electrode in 7 M H_3PO_4, 1 M $HClO_4$, 1 M HNO_3, 1 M H_2SO_4, and 3 M K_2CO_3 were −1.10, −1.61, −1.51, −1.36, and −0.10 v respectively. Significant differences between the potentials of Ce(III-IV) and Bk(III-IV) were noted. In most systems, the potential for berkelium was 40 to 100 mv greater than that for cerium [i.e., since Bk(III) was less negative, it was more easily oxidized than Ce(III)].

The investigation of the properties of berkelium metal has continued, and additional preparations of high-purity metal have been made. Two forms of the metal have been identified: the high-temperature form of the metal, which is a face-centered cubic form with a = 4.9948 ± 0.0016 A; and the low-temperature form, which is a double hexagonal close-packed structure with a = 3.411 ± 0.001 A and c = 11.057 ± 0.006 A. Berkelium also forms a monoxide with a face-centered cubic form with a = 4.964 ± 0.002 A.

[43]This value is somewhat in disagreement with the results calculated from the irradiation of ^{249}Bk (see sect. 5.3).

[44]L. J. Nugent, R. D. Baybarz, and J. L. Burnett, *J. Phys. Chem.* 73, 1177 (1969).

[45]Convention used in W. M. Latimer, *Oxidation Potentials*, p. 293, Prentice-Hall, Inc., New York, 1938.

6. Development of the Thorium Fuel Cycle

6.1 RECYCLE OF THE ALCOHOL USED IN THE MICROSPHERE-FORMING COLUMN

Our previous studies have shown that the pH, surfactant concentration, and water content of 2-ethyl-1-hexanol (2EH) are important variables in the microsphere-forming process. We are presently examining methods for improving the control of pH and surfactant concentration during the continuous operation of microsphere-forming columns.

Our present method for controlling the water content of the 2EH is adequate. This method involves heating a portion of the used solvent at 150 to 160°C to remove most of the water and mixing this relatively dry 2EH with the remaining wet solvent to obtain the desired water content. However, the removal of nitric and formic acids from 2EH prior to distillation is desirable (and probably necessary). Nitric acid accelerates solvent and surfactant degradation during the distillation step in which water is removed, and formic acid interferes with long-term column operation with urania sols by promoting clustering. Therefore, the use of caustic scrub solutions and of ion exchange resins for removing these acids from 2EH is being investigated. We are also studying a total 2EH purification method in which the 2EH is recovered by distillation, the used surfactants are discarded, and the 2EH is recycled to the forming column after desired amounts of surfactants, water, and nitric acid have been added.

Laboratory studies have shown that the reactions of nitric acid with 2EH and surfactants during distillation could essentially be eliminated by removal of the acid prior to the distillation step by contacting the 2EH with alkaline solutions or ion exchange resin. The acid content of the alcohol could then be maintained at the desired level by adding nitric acid to the alcohol after the water has been removed by distillation. We tested the caustic scrubbing method as a means of controlling the pH and surfactant concentration during continuous operation of the microsphere-forming column used in engineering development studies. Scrubbing with alkaline solutions[1] was found to be unsatisfactory because of difficulties with emulsification and entrainment. Emulsification problems were reduced, but not eliminated, by carrying out the scrubbing process in a packed column with the organic phase continuous. A liquid-liquid membrane separator (Selas Corporation) used in conjunction with the packed column was found to be unsatisfactory due to plugging. Therefore, we are now evaluating anion exchange resins as a means of removing nitric and formic acids prior to distillation. No phase separations are required in the ion exchange approach; hence emulsion and entrainment are avoided.

Use of Anion Exchange Resins

Laboratory studies showed that a weak-base resin (Amberlite IRA-93) is almost as effective as a strong-base type (Amberlite IRA-900) for the removal of both nitric and formic acids. The nitric acid is removed in preference to the weaker formic acid, and the formic acid breaks through first as the column becomes loaded by a mixture of both acids. With the macroreticular (highly porous) weak-base resin, even formic acid was removed at a fairly rapid rate; at a flow rate of four bed volumes per hour, removal was quantitative up to the bed capacity. At 16 bed volumes per hour, removal was still quite satisfactory. Although a strong-base resin should be more effective than the weak-base type for removing weak acids (e.g., formic acid), regeneration, particularly from the nitrate form, is more difficult for a strong-base resin. Therefore, both chemical types were evaluated. Only macroreticular resins were tested initially.

We have installed a resin-bed column in the circuit of our engineering development sphere-forming equipment, and anion exchange resins are being evaluated for the removal of nitric and formic acids. Also, the degree

[1] *Chem. Technol. Div. Ann. Progr. Rept. May 31, 1969*, ORNL-4422, pp. 197–99.

of removal of nitric and formic acids that is required for satisfactory microsphere forming is being determined.

The surfactants (Span 80 and Ethomeen S/15) do not appear to interfere with acid removal. Losses of surfactants to the resin have not been determined.

Use of Distillation

The recovery of 2EH from surfactants requires fewer distillation stages when water is present than when it is absent. Also, considerably less decomposition of surfactants occurs, as compared with our previously reported data,[1] which were obtained in the absence of water. We have carried out laboratory studies of the recovery of 2EH at distillation temperatures of 100°C when two phases are present and at distillation temperatures of 150 and 180°C when a single phase is present. We have determined both the maximum initial rate of distillation of surfactant-free 2EH that could be attained with our laboratory equipment at several temperatures and the volume of water that is required per volume of purified 2EH. The results for the two-phase distillation at 100°C are shown in Table 6.1; those for single-phase distillation at 150 and 180°C are presented in Table 6.2.

The distillations at 100°C and 150°C were carried out by metering the used 2EH and water into a distilling pot, collecting the condensate, and then separating the 2EH and water phases in the condensate. The distillation at 180°C was done in the same manner as the 100°C and 150°C distillations except that two cycles of distillation were used. All of the recovered 2EH was free of surfactant (<0.005 vol %). The rate of distillation was varied by varying the applied voltage to the

Table 6.1. Two-Phase Distillation of Used 2EH and H_2O at 100°C

Conditions: The 2EH feed contained surfactants and had been used in microsphere-forming columns. An electrically heated (600 w, max) five-liter still pot was used.

Rate of Collection of Distillate (ml/min)	2EH in Distillate (vol %)	Rate of 2EH Recovery (ml/min)
3.55	28	0.99
3.55	20	0.71
3.60	20	0.72
3.40	24	0.82
4.80	21	1.00
8.30	19	1.58
12.6	16	2.02

Table 6.2. Single-Phase Distillation of Used 2EH-Water Solutions

Conditions: The 2 EH feed contained surfactants and had been used in microsphere-forming columns. An electrically heated, one-liter still pot was used.

Temperature (°C)	Rate of Distillate Collection (ml/min)	2EH in Diphasic Distillate (vol %)	Rate of 2EH Recovery (ml/min)
150[a]	8.0	68	5.4
	8.0	73	5.8
	11.0	79	8.7
	12.0	77	9.2
	12.5	76	9.5
155[a]	15	78	11.7
180[b]	15	~100	15.0
	27.5	~100	27.5
	45.0	~100	45.0

[a]Water and used 2EH were metered into the distillation pot at 2EH/H_2O volume ratios of ~4.

[b]Used 2EH that had been saturated with water (2.5% water) at room temperature was metered into the distillation pot.

electrical heaters. The rates attained at 100°C cannot be directly compared with those obtained at 150°C and 180°C. A five-liter round-bottom flask heated by a 600-w heater was used in the 100°C distillation, whereas a one-liter flask heated by a 380-w heater was used at the other temperatures.

Simple prorating of the volume-power ratio of the five-liter flask to the one-liter flask indicates that rates of 2EH recovery in the 100°C distillation would have been about a factor of 0.55 smaller if the experiment had been performed in the same equipment as the 150°C and the 180°C distillations.

6.2 DEVELOPMENT OF TECHNIQUES FOR DRYING AND FIRING GEL MICROSPHERES

Batch, fixed-bed dryers with capacities up to 20 kg were used earlier for successfully drying ThO_2 gel spheres; however, they were not suitable for use with ThO_2-UO_2 spheres because of the uncontrollable, deleterious temperature excursions that occurred.[2] Exothermic reactions (which have been observed previously) occur between the nitric acid in the gel and the sorbed alcohol from the microsphere-forming column. Additional studies were made to determine the proper methods and equipment for controlling these exothermic reactions so that excessive temperature rises and breakage of spheres are prevented during drying. Twenty-kilogram-capacity dryers of improved design for ensuring controlled heat input were built, installed, and used successfully to dry 20-kg batches of ThO_2-UO_3 spheres under a steam purge flow.[3]

Gel drying studies showed that the heating rates of fixed beds being purged with steam must be both slow and uniform so that the chemical reaction rate of nitric acid with the alcohol, and hence the rate of heat liberation by the reaction, can be controlled. A purge of steam through the bed of spheres enhances the desorption and vaporization of the organic reactants and thus serves to reduce the quantity of organic materials that are available for reaction with the nitric acid. Washing the gel spheres in NH_4OH solutions prior to drying was successful in removing the nitric acid and preventing the nitrate-organic reaction; however, this washing process caused about 50% breakage of the spheres.

Steam drying to 200°C does not remove all of the carbon-bearing materials. The spheres still contain about 1% carbon, which is subsequently removed in the calcination step by combustion in air. Firing studies showed that the carbonaceous materials and other volatiles (nitrates and water) remaining after drying are removed before any appreciable shrinkage or densification of the ThO_2-UO_3 gel spheres occurs; thus, no problems are encountered in attaining the density and chemical concentrations specified for calcined products. Dried ThO_2-UO_3 gel spheres were successfully fired to 1150°C in 10-kg fixed beds, and satisfactory product was obtained.

Drying Studies

Further laboratory studies of the drying of ThO_2-UO_3 gel spheres were required because the spheres that were produced in the 10-day continuous demonstration of the ORNL ThO_2-UO_2 sol-gel process were much more sensitive to the initiation of deleterious, exothermic reactions than had been anticipated on the basis of earlier, smaller-scale work.[3] Also, the gel spheres prepared in the demonstration run had a higher thorium content (Th/U atom ratio of 4.5) than had been used in our earlier developmental work (i.e., a Th/U ratio of 3). The spheres with the higher thorium content were considerably more sensitive to drying conditions.

Even when the temperature was increased as slowly as 25°C/hr during the drying of gel spheres (Th/U atom ratio = 4.25) in a 2-in.-diam fixed bed, exothermic reactions began to occur at 190 to 200°C and cause significant breakage (>50%) of the spheres during the almost instantaneous temperature rise to 250–300°C. We observed that, at a temperature rise rate of 25°C/hr in the 100–200°C range, the central-bed temperature lagged the heated dryer wall temperature by 10 to 20°C. Introductions of soaking periods in the 100–200°C range were found to prevent the exothermic reaction, and no breakage of the spheres resulted. However, the nitrate-to-metal ratio was substantially decreased by the process [from an initial value of 0.1 to as low as 0.005 (see Table 6.3)], indicating that an organic–nitric acid reaction occurred at rates that did not liberate excessive amounts of heat. Conductivity measurements on the effluent steam condensate showed that material producing a conducting electrolyte was liberated throughout the course of the drying in the 100–200°C range. This probably indicates the presence of dissolved NO_2 or NO in the condensate. Steam purge flow rates as low as 0.1 g/min

---

[2] *Chem. Technol. Div. Ann. Progr. Rept. May 31, 1969*, ORNL-4422, pp. 187–90.

[3] C. C. Haws, W. D. Bond, and B. C. Finney, *Engineering Scale Demonstration of the Sol-Gel Process: Preparation of 100 kg of ThO_2-UO_2 Microspheres at a Rate of 10 kg/day*, ORNL-4544 (in press).

Table 6.3. Effects of Soaking Times at Various Temperatures on Steam Drying of ThO_2-UO_3 Gel Spheres

Conditions: Initial NO_3^-/Th + U mole ratio of gel spheres = 0.105

100-g samples heated to 100–110°C in argon (0.7 std ft^3/hr) at 50°C/hr

Steam flow rate was 1 g/min, and the temperature rise rate was 25°C/hr between holding temperatures

	Sample							
	1-26-69	1-26-69	1-27-69	1-27-69	GB	GB[a]	GB	GB
	Soaking Time (hr)							
Holding temperature, °C								
110	2	16	2	2	3.5	3.5	16	16
125	2	0	16	2	16	16	0	2
150	16	2	2	16	1	1	2.5	16
175	13	16	3	3	2.5	2.5	16	2
200	2.5	4	2	3	2	2	4	3
	Analysis of Dried Gel							
NO_3^-/Th + U mole ratio	0.024	0.025	0.009	0.022	0.006	0.005	0.008	0.027
NO_3^- content, %	0.54	0.56	0.20	0.48	0.14	0.11	0.17	0.60
C content, %	1.14	0.92	0.73	0.85	0.96	1.99	0.76	0.97
O/U atom ratio	2.95[b]	2.81	2.93[b]	2.93[b]	2.96	2.72	2.84	2.94

[a]0.1 g/min used instead of usual 1 g/min.
[b]Samples were exposed to air during the unloading step after firing.

were effective in preventing the exothermic reaction. The 16-hr soaking period was used in some cases because it was convenient to carry out this stage of the drying overnight and resume drying the next day.

Washing the spheres in NH_4OH solution prior to drying was very effective in removing nitrate and preventing an exothermic reaction during drying. However, this washing step caused spalling and cracking of the spheres. The cracking and spalling were independent of NH_4OH concentration from 0.1 to 15.0 *M* and of addition of NH_4NO_3 to the NH_4OH prior to washing. Separation of the cracked spheres with a roundometer showed that 50 to 60% of the spheres were broken or chipped in the washing step. For this reason, washing with NH_4OH was given no further consideration as a process step.

The essential features of the improved dryer that was built for drying ThO_2-UO_3 spheres are shown in Fig. 6.1. An array of tubular heating elements is employed throughout the bed for good heat input distribution. Thermocouples welded to the surfaces permit temperature rise rates to be carefully monitored and controlled. External cooling coils are provided so that an exothermic reaction, if initiated, can be suppressed by air or water cooling.

Firing Studies

To effect carbon removal and densification, the dried gel spheres were fired in fixed beds in air to 1150°C. The oxide was then reduced in Ar–4% H_2 to the desired O/U atom ratio. The calcined spheres were cooled to room temperature in argon. On calcination, the gels underwent about 65% shrinkage in volume and a 30% reduction in diameter.

The calcination procedure has been used throughout our work on ThO_2-UO_3 gels, beginning with the Kilorod Program.[4] A few test firings of gel microspheres with the ThO_2 and UO_2 compositions used in the present study were made in the laboratory prior to the beginning of the campaign. In the laboratory studies, several samples of the dried gel spheres were heated to 1150°C at the rate of 300°C/hr in air and held for 1 hr at 1150°C. They were then heated for 3 hr in Ar–4% H_2. The products had densities of 95 to 98%

[4]C. C. Haws, J. L. Matherne, F. W. Miles, and J. E. Van Cleve, *Summary of the Kilorod Project — a Semiremote 10 kg/day Demonstration of $^{233}UO_2$-ThO_2 Fuel Element Fabrication by ORNL Sol-Gel Vibratory-Compaction Methods*, ORNL-3681-A (Mar. 23, 1965).

ORNL DWG 69-12117R

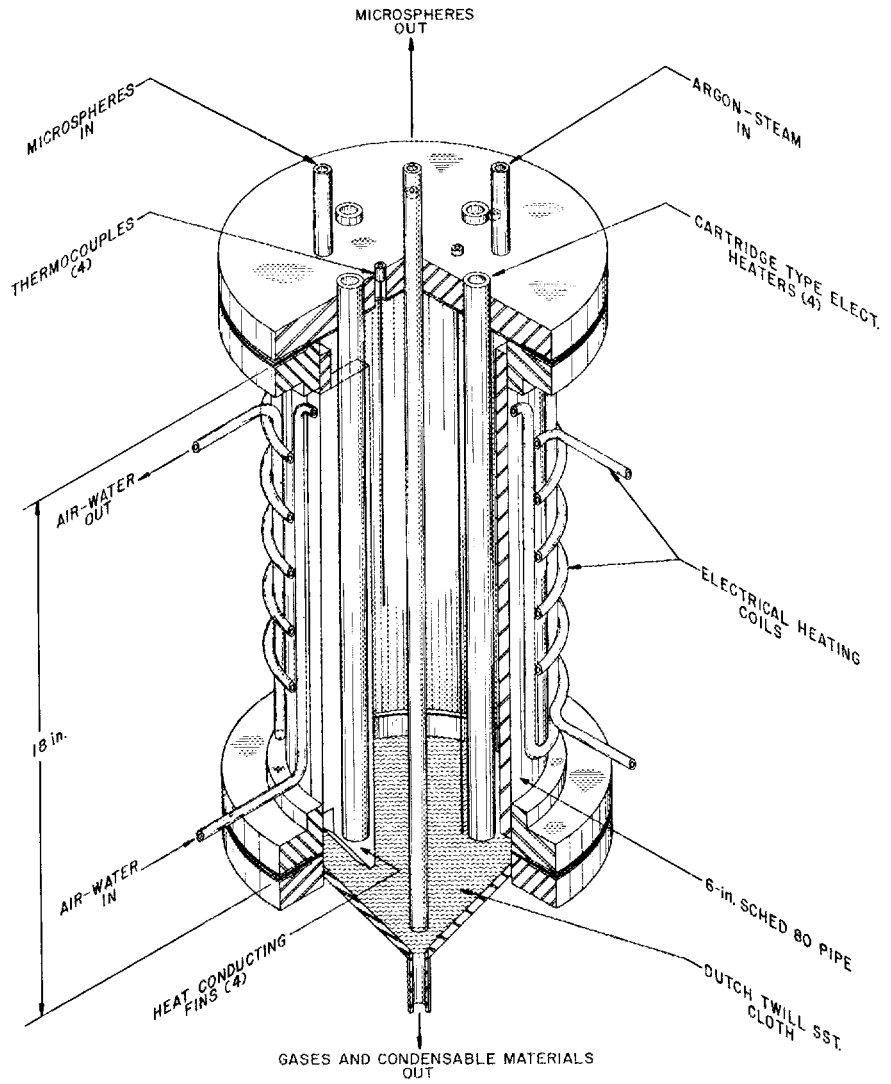

Fig. 6.1. Improved Internal Arrangement of the Microsphere Dryer.

Table 6.4. Analytical Evaluation of the ThO_2-UO_2 Product from the Vertical-Bed Calciner

Calciner Batch No.	O/U Atom Ratio	Surface Area (m^2/g)	Hg Density (at 15,000 psi)	Carbon (ppm)	Gas Release (cc/g to 1200°C)
1	2.004	0.017	10.17	40	0.026
2	2.010	0.005	10.19	40	0.009
3	2.011	0.122	10.11	30	0.030
4	2.015	0.009	10.22	40	0.019
Specifications:	<2.03		9.67[a]	<500	≤0.3

[a]Theoretical density = 10.18.

of theoretical, carbon contents of 20 to 40 ppm, and O/U atom ratios of 2.001 and 2.020. The products were solid solutions of UO_2 in ThO_2, as determined by x-ray lattice parameter measurements, and had a crystallite size of 1000 to 2000 A. The gel spheres used in these studies had a good shrinkage pattern for ease of removal of the remaining volatiles. The density was only about 40% of theoretical at 850°C, and all the pores were open. Thus, the sorbed carbon-bearing materials, nitrates, and water could be removed easily before pore closure occurred.

A vertical-bed calciner with a capacity of 10 kg was used for firing the ThO_2-UO_3 gel microspheres produced in a 10-day demonstration run of microsphere forming (Fig. 6.2). Product having the desired properties was produced (Table 6.4). The jet transfer method for loading dried gel spheres and removing the product was entirely satisfactory.

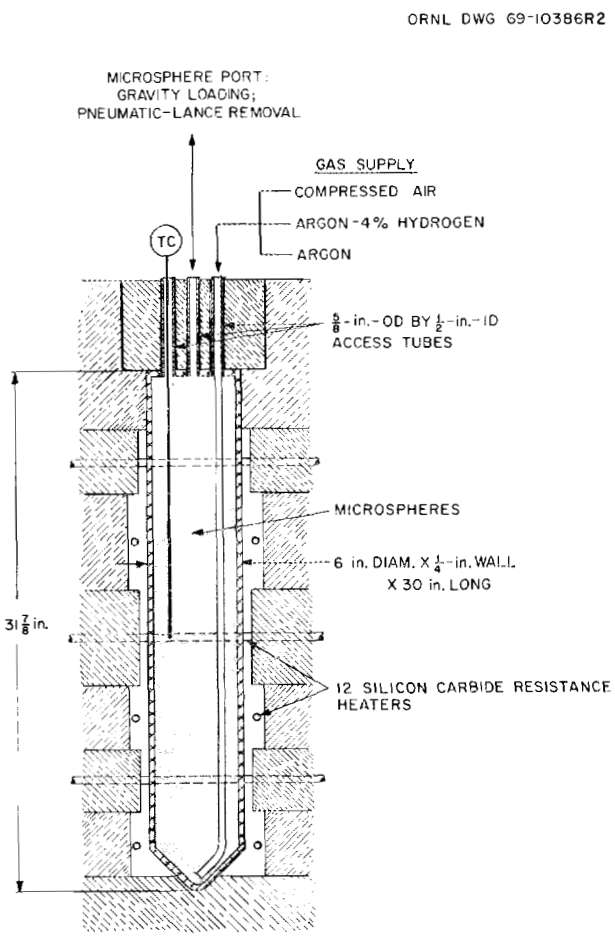

Fig. 6.2. Vertical-Bed Calciner Tested in Extended Operating Test with ThO_2-UO_2 Microspheres. Capacity, 10 kg.

6.3 DEVELOPMENT OF FLUIDIZED-BED COLUMN EQUIPMENT

A report that presents information for designing and operating fluidized-bed columns for gel sphere preparation was published during this report period.[5] In this report, emphasis is on factors such as the premature discharge of incompletely gelled particles from the sphere-forming column, the formation of nonspherical gel particles, and the capacity limitations of the equipment. Briefly, the report can be summarized as follows. The correct column configuration and the use of a bottom, tangential fluid inlet to create a swirling motion of the liquid are important factors in ensuring good sphere fluidization. Successful continuous operation requires control of the composition of the fluidizing mixture of alcohol and minor constituents and the operation of a still to remove the water and other materials from the sphere-forming alcohol. Capacities under normal conditions, expressed in terms of grams of oxide spheres per hour, are estimated to range from 100 for dilute sols, using a 1-in.-ID (minimum) column, to 9000 for concentrated sols, using a 3-in.-ID (minimum) column. The dispersion of sol into uniform drops is also important in maintaining continuous, efficient, high-yield operation. Four useful dispersion techniques are described. The composition and size of the product spheres must be specified before equipment and procedures can be optimized.

The use of standard pH electrodes in the forming alcohol gives a meaningful and reliable pH measurement that is useful for controlling the composition of alcohol in the column. Such electrodes were installed in the columns used in engineering development studies after laboratory studies had demonstrated their application over the usual range of alcohol compositions. The pH readings are reproducible between instruments and are close to those of aqueous solutions in equilibrium with the alcohol. The electrodes are less reliable for alcohol solutions with low electrical conductivities, that is, those containing unusually low concentrations of water and nitric acid, as well as formic acid and Ethomeen S/15.

6.4 PREPARATION OF MICROSPHERES IN NONFLUIDIZED-BED COLUMNS

The requirements with respect to control of the forming alcohol (2EH) and sol flow rates, the surfactant

[5] P. A. Haas, *Sol-Gel Preparation of Spheres: Design and Operation of Fluidized Bed Columns*, ORNL-4398 (September 1969).

concentrations, and the uniformity of sol droplets are much less restrictive in the absence of fluidization; however, the maximum sphere diameter that can be produced is typically 200 μ or less for simple, nonfluidized systems. Materials that were prepared in our equipment were used for development studies at ORNL and elsewhere. These materials included about 50 kg of ThO_2 spheres, 10 kg of UO_2 spheres, 10 kg of UO_2-C spheres, and smaller amounts of spheres of other compositions. Both the ThO_2 and UO_2 spheres densified to greater than 9.9 g/cc on firing to 1150°C.

The sol droplets that are introduced into a nonfluidized column must be small enough to gel before they settle to the bottom. This is the principal limitation on nonfluidized preparation of spheres. The required column heights are dependent on mass transfer and the settling velocity. Mass transfer, as a function of sol droplet and organic liquid variables, has been investigated and correlated by Clinton.[6] The settling behavior of droplets or spheres is easily calculated using Stokes' settling velocity equation for laminar conditions and a drag coefficient for larger Reynolds numbers. Both the sol droplet size and the density vary with time. Thus, mass transfer and the settling velocity vary with time, and analytical solutions of the equations for settling velocity and mass transfer are not possible. However, the mass transfer and settling velocity correlations are easily combined using a computer program[7] to give time and free-fall distance as functions of sol droplet variables and organic-phase variables. As an example, Fig. 6.3 gives the settling velocity, droplet diameter, sol droplet molarity, and free-fall distance vs time for specified values of initial sol droplet size and organic-phase composition.

The free-fall distance (or column height) for gel formation with nonfluidized column operation (neglecting any flow of alcohol) is shown in Fig. 6.4 as a function of initial sol droplet diameter for four sets of organic-phase compositions and temperatures. Experimental results for three of the conditions show reasonable agreement with the calculated values. These curves show the largest sol droplet that can be gelled for the corresponding combination of organic-phase properties and column length. Larger droplets would reach the

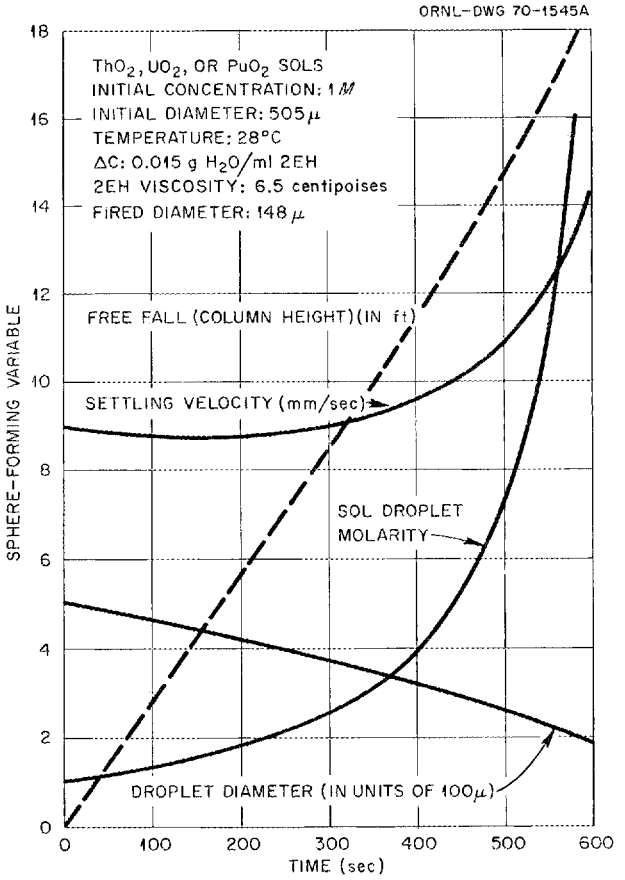

Fig. 6.3. Changes in Sphere-Forming Variables with Time, as Determined from Mass-Transfer Calculations.

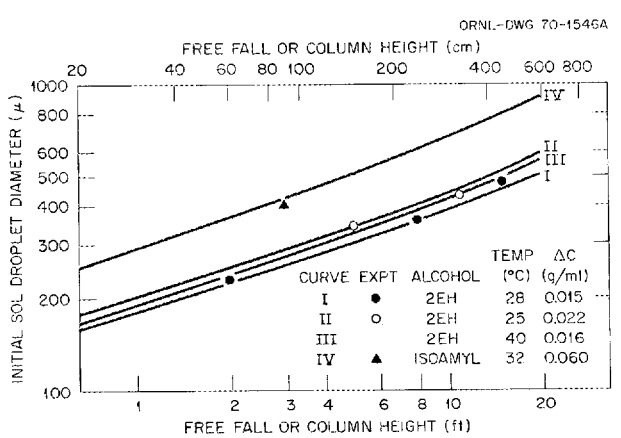

Fig. 6.4. Initial Sol Drop Diameter vs Column Height Required for Gelation.

[6] S. D. Clinton, *Mass Transfer of Water from Single Thoria Sol Droplets Fluidized in 2-Ethyl-1-hexanol*, M.S. thesis, University of Tennessee, Knoxville (1968); also issued as ORNL-TM-2163 (June 1968).

[7] D. A. Schneider and N. I. Salas, *Gelation of Small Diameter Thoria Sol Microspheres in Nonflowing Alcohols*, ORNL-MIT-95 (in press).

bottom of the column before gelation was complete, resulting in clumping or coalescing of the ungelled droplets. (The mass-transfer calculations do not predict whether the gel particle will be a sphere, or will merely be spheroidal.)

The use of isoamyl alcohol (see curve IV of Fig. 6.4) commonly results in distorted particles when the initial sol droplet has a diameter larger than 300 μ. While the calculated values of Fig. 6.4 are for 2 *M* ThO_2 sols, UO_2 or PuO_2 sols should give essentially the same values. The initial diameter for a sol droplet that can be gelled in a specified height of alcohol varies less than ±5% over the initial sol concentration range of 1 *M* to 8 *M*. A droplet of less-concentrated sol has a longer gelation time; however, because of the lower density of the sol, the average settling velocity is smaller. Thus, the result represents a nearly exact compensation of one effect by the other.

6.5 PREPARATION OF TEST MATERIAL FOR RECYCLE TEST ELEMENTS

Experimental fuel elements, called Recycle Test Elements (or RTE's), are being fabricated for irradiation in the first Peach Bottom reactor. The RTE's constitute an important part of the National HTGR Recycle Program. They will provide prototype 1100-Mw (electrical) HTGR fuel in sufficient quantities for use in hot-cell studies of head-end reprocessing operations and of equipment simulating that to be used in the Thorium-Uranium Recycle Facility (TURF).

The task of the Chemical Technology Division was to prepare oxide kernels for use in fabricating the RTE's and deliver them to the Metals and Ceramics Division for pyrocarbon coating. The requirements were as shown in Table 6.5. The preparation of these kernels is described below.

The ThO_2 microspheres were selected from the product from the thorium engineering-scale development run reported previously.[8]

Table 6.5. Oxide Kernels for Fabricating RTE's

Material	Quantity (g)	Size (μ)	Density (g/cc)
ThO_2	1300	400 ± 100	>9.50
ThO_2-$^{235}UO_2$ (Th/U = 4.2)	1000	350 ± 100	*a*
ThO_2-$^{235}UO_2$ (Th/U = 2.0)	2700	350 ± 100	*a*
$^{235}UO_2$	300	100 ± 30	>10.20

[a]>95% of theoretical.

The ThO_2-$^{235}UO_2$ material was prepared in the engineering-scale sol-gel facility that was operated previously to prepare 32 kg of ThO_2-$^{233}UO_2$ (Th/U atom ratio = 3) for use in tests in the High Temperature Lattice Test Reactor.[9-11]

A total of eight batches (1 kg of metal per batch) of ThO_2-$^{235}UO_2$ (Th/U atom ratio = 4.2) was processed through the solvent extraction equipment[12] for the preparation of hydrosol having a NO_3^-/metal mole ratio of 0.1. The first run was necessary in order to obtain equilibrium, and the sol was of poor quality. Excessive amounts of nitrate ion were extracted. In order to prevent overdenitration of the sol, it was necessary to reduce the flow rate of the extractant (Amberlite LA-2 in an *n*-paraffin diluent) by 15% from the established rate used for the HTLTR Program.

Microsphere forming was accomplished in the cell 4 facility. The drying agent was 2EH containing 0.1% Ethomeen S/15 and 0.1 *M* HNO_3. The two-fluid nozzle was replaced with a perforated plate (bucket type),[13] which permitted the use of an air-lift feed device rather than the syringe pump. However, it became obvious that the microspheres were not being dried sufficiently in the column, and a new column with a smaller throat diameter was installed. An increased solvent velocity corrected the difficulty, and operation was excellent during the remainder of the program. A total of 6.98 kg of ThO_2-UO_2 microspheres was transferred to the Metals and Ceramics Division for coating.

The material containing Th and ^{235}U at a Th/U atom ratio of 2.0 required the preparation of sol by solvent extraction of nitrate from four batches (1 kg of Th + U in each) of thorium nitrate–uranyl nitrate solution. The denitration procedure used in the sol-forming equipment was the same as that used for the material with a

[8] *Status and Progress Report for Thorium Fuel Cycle Development for 1967 and 1968*, ORNL-4429 (August 1969), pp. 62–69.

[9] *Chem. Technol. Div. Ann. Progr. Rept. May 31, 1969*, ORNL-4422, pp. 183–86.

[10] *Status and Progress Report for Thorium Fuel Cycle Development for 1967 and 1968*, ORNL-4429 (August 1969), pp. 3–10.

[11] J. R. Parrott *et al.*, "Demonstration of $^{233}UO_2$-ThO_2 Microsphere Production by the Sol-Gel Process," presented at the 1969 Winter Meeting of the American Nuclear Society, Seattle, Wash., November 1969.

[12] J. W. Snider, *The Design of Engineering-Scale Solex Equipment*, ORNL-4256 (April 1969).

[13] P. A. Haas *et al.*, *Engineering Development of Sol-Gel Processes at Oak Ridge National Laboratory*, ORNL-TM-1978 (January 1968), pp. 37–40.

Th/U ratio of 4.2. However, the preparation of spheres from sol with a Th/U ratio this low had not been tried on a large scale, and initial efforts to form the material into spheres were unsuccessful. Various combinations of surfactants and sol "aging" steps failed to reduce the degree of cracking during drying in the sphere-forming column. The direct method, that is, the formation of microspheres directly from ThO_2-UO_3 sol (commonly called "red sol"), was abandoned in favor of an indirect method that involved adding carbon to the oxide sol prior to sphere forming. This method was adopted in order to eliminate cracking since past experience had shown that cracking tendencies were greatly minimized when carbon was present. The carbon can then be burned out prior to final densification.[14]

Preliminary laboratory tests indicated that a ratio of at least three moles of carbon per mole of oxide was necessary to obtain good spheres and that a ratio of four moles of carbon per mole of oxide was desirable. The carbon was added by ultrasonic agitation of the oxide sol containing the weighed amount of carbon black. Microspheres were formed from the carbon-oxide sols by maintaining the following surfactant, water, and HNO_3 concentrations in the 2EH:

0.3–0.4% Ethomeen S/15
0.004 *N* HNO_3
0.2–0.4% Pluronic L-92
0.5–1% H_2O

The carbon can cause a number of exothermic reactions during drying and calcining. Therefore, the microspheres were allowed to dry in air overnight, and were then heated slowly in argon to 300°C over a period of 8 hr. This treatment was followed, successively, by an 8-hr heating period at a decreased argon flow, an 8-hr cooling period, and calcination to 1000°C, at the rate of 300°C/hr, in air. After calcination, the carbon content was found to be 0.003 wt %. The product microspheres are not true spheres, but are spheroidal, and their surfaces are rough. They retain their general shape during calcination, and require sintering at 1450°C to attain a density greater than 95% of the theoretical value. A photograph of these sintered spheres is shown in Fig. 6.5. Approximately 4.6 kg of this material was transferred to the Metals and Ceramics Division for coating and subsequent use in preparing RTE's.

Although the above technique provided material acceptable for use in preparing the RTE's, frequent plugging of the sol disperser and other handling problems led to a desire to produce microspheres directly from the red sol. Toward this end, nine experimental runs, varying in size from 10 to 100 g (as metal), were made in the laboratory. The results of these runs showed that a satisfactory yield (71%) could be attained by forming microspheres directly from the red sol if the Ethomeen S/15 content were maintained at 0.2 vol %, the water content at 1.5 vol %, and the pH of the alcohol between 3.5 and 4.5. Modifications to the cell 4 facility were made to incorporate the necessary controls to meet these requirements. A total of 5.7 kg of material made in the facility was transferred to the Metals and Ceramics Division. A representative sample of this material, after rounding and screening, is depicted in Fig. 6.6.

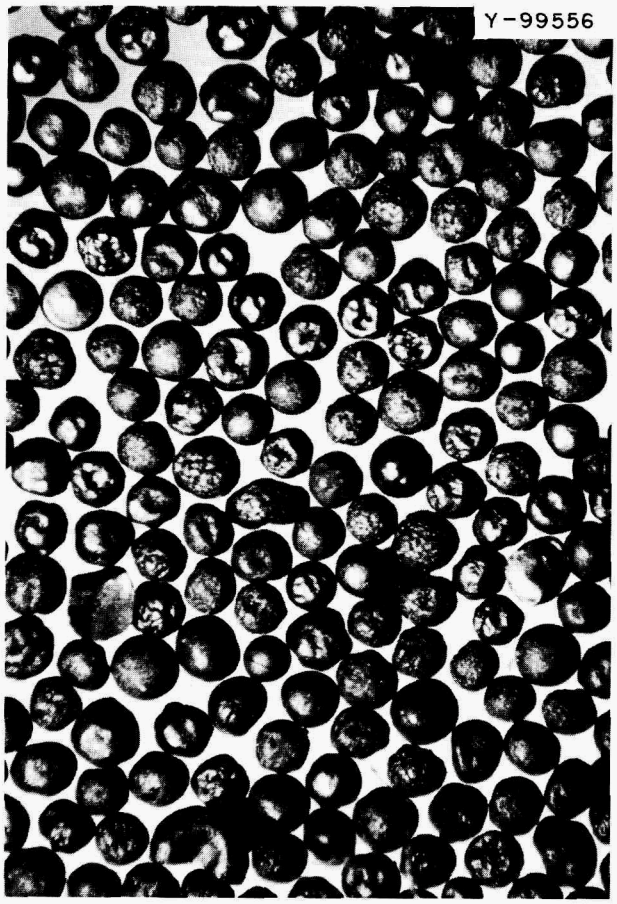

Fig. 6.5. Photograph of ThO_2-$^{235}UO_2$ Microspheres (Th/U Atom Ratio = 2) Formed by Carbon Incorporation Technique. Magnification, 17×.

[14] K. J. Notz, *Preparation of Porous Thoria by Incorporation of Carbon in Sols,* ORNL-TM-1780 (December 1968).

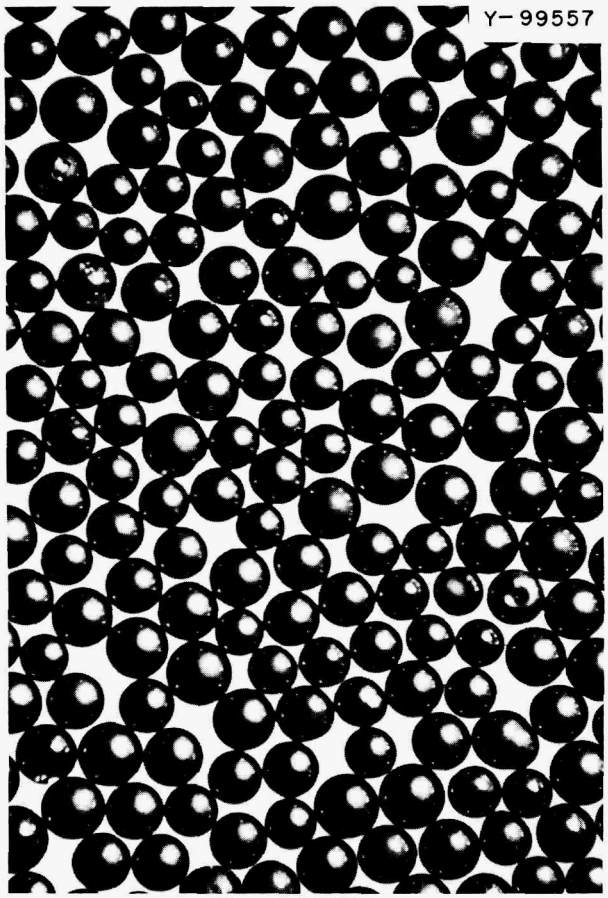

Fig. 6.6. Photograph of ThO_2-$^{235}UO_2$ Microspheres (Th/U Atom Ratio = 2) Formed Directly from Red Sol. Magnification, 17×.

Table 6.6. Enriched Urania Sols Prepared for Use in the RTE Program

Lot No.	U Content		U(IV)	Mole Ratio	
	(g)	(g/liter)	(%)	NO_3^-/U	$HCOO^-/U$
93-21	277.5	245.5	90	0.14	0.24
93-26	286.0	280.4	92	0.15	0.42
93-30	295.8	197.4	88	0.14	0.24
93-31	295.3	190.6	79	0.15	0.27

The $^{235}UO_2$ material was prepared from sols produced using the previously described[15] precipitation-peptization technique. The data relating to these sols are given in Table 6.6. Operation of the microsphere column during sphere forming was quite satisfactory; however, interparticle sintering was severe during the 1150°C calcination of the first two batches, resulting in a low (46%) yield. The final two batches were first fired to 800°C, cooled and stirred thoroughly, and then refired to 1100°C. The yield for the final two batches was 81%. A total of 635 g was transferred to the Metals and Ceramics Division for coating.

Six of the eight RTE's have been fabricated using the materials described above. The remaining two will be fabricated late in 1970.

6.6 ^{233}U STORAGE, PURIFICATION, AND DISTRIBUTION

Oak Ridge National Laboratory serves as a national distribution center for ^{233}U. The facility includes shielded wells for storing up to 168 kg of ^{233}U in solid form and tanks (containing borosilicate glass for neutron poisoning) that can store 500 kg of ^{233}U in uranyl nitrate solutions at ^{233}U concentrations up to 250 g/liter. Also, a shielded interim storage vault (located in Building 3100) can hold up to 70 kg of ^{233}U or ^{239}Pu in shipping containers. At present, nine wells for storing solids and five tanks for storing solutions are being added to increase our capacity for solids and for solution by 80% and 100% respectively. Both of the new facilities are needed for the storage of feed material for the Light Water Breeder Reactor (LWBR) support program; later, the solids storage facility will be required for the storage of 200 kg of ^{233}U from the Elk River reactor (after recovery and conversion to oxide at the Italian CNEN Plant).

The storage facility accepts ^{233}U as uranyl nitrate solution or as properly packaged solids. The solids may consist of uranium metal or uranium compounds that can be readily and safely dissolved in stainless steel equipment.

The purification facilities in the center include a single-cycle solvent extraction system that is capable of purifying ^{233}U at the rate of 25 kg/week. At present, all the ^{233}U that is processed in the facility is shipped as nitrate solution. The system is presently being modified to increase its reliability and flexibility, and a complete nitrate-to-oxide conversion line with a capacity of 22 kg of ^{233}U per week is being installed for the LWBR support program.

Summary of Distribution Activities

During the past year, 18 shipments containing 44 kg of ^{233}U were received by the facility. Twenty-three shipments, amounting to 7 kg of ^{233}U, were made

[15] J. P. McBride, *Laboratory Studies of Sol-Gel Processes at Oak Ridge National Laboratory*, ORNL-TM-1980 (September 1967), pp. 25–29.

from the facility. The largest single shipment received was 13 kg of ^{233}U (as UO_3) from Nuclear Fuel Services at Erwin, Tennessee, for the LWBR support program. The largest single disbursement was 1 kg of ^{233}U [as $UO_2(NO_3)_2$] to the Los Alamos Scientific Laboratory. The activity of the facility for each calendar year from 1960 to the present is shown in Fig. 6.7. Table 6.7 shows the inventory of ^{233}U (exclusive of Consolidated Edison fuel) in the facility as of March 31, 1970; the form, isotopic purity, and ^{232}U content are also given.

The TRUST (Thorium Reactor Uranium Storage Tank) facility was placed in operation last year. The receipt of material, accountability, radiation exposure during unloading, and other pertinent information were reported earlier.[16] However, experience gained in the storage of a large volume of fissile solution, using soluble neutron absorbers for criticality control, is felt to be of sufficient interest to the industry to warrant a detailed report of our first year's operation, including all aspects of nuclear safety.

The increase in the number of operating power reactors will result in the reprocessing of spent fuels having isotopic contents relatively undesirable for immediate recycle; hence, provision must be made for the interim storage of large volumes of aqueous nitrate fissile solutions. In such instances, there is incentive to use soluble neutron absorbers for criticality control since these absorbers provide a safe, inexpensive means of storage and can be separated from the fissile material in the solvent extraction purification process.

The facility consists of a charging glove box in the area above the cell, an unloading and sampling facility located in a processing cell, and a 5000-gal storage tank in an underground pit adjacent to the building (Fig. 6.8). The tank was originally filled with borosilicate-glass raschig rings to give initial criticality control. At present, we have 1047 kg of uranium (76.5% ^{235}U, 9.7% ^{233}U) stored in the facility.

Calculations performed with the ANISN program (a one-dimensional, multigroup neutron transport code) using the S_4 approximation and the 16-group cross sections of Hansen and Roach are shown in Table 6.8. The results are given as values of k_∞, the neutron

Table 6.7. ^{233}U Inventory as of March 31, 1970

Form	Isotopic Purity (wt %)	^{232}U Content (ppm)	Quantity (kg)
Nitrate	91	13	24.8
	97	5	2.2
	97	9	45.8
	97	42	17.9
	98	6	34.3
Oxide	84	6	7.6
	91	250	61.7
	97	<5	13.4
	97	50	11.0
	98	6	35.6
Fluoride	91	250	1.9
Metal	98	42	5.1
Total			261.3

[16] *Chem. Technol. Div. Ann. Progr. Rept. May 31, 1969*, ORNL-4422.

Table 6.8. Calculated k_∞ for Systems Containing UNH Solution or Precipitate and Borosilicate-Glass Raschig Rings

Solution Composition				Volume Fraction (%)			k_∞	
Uranium (g/liter)	HNO_3 (*M*)	$Cd(NO_3)_2$ (*M*)	$Gd(NO_3)_2$ (*M*)	Solution	Precipitate[a]	Raschig Rings	Calculated	Experimental
415 (93% ^{235}U)	<1			78	0.0	22	1.04	1.0
330 (98% ^{233}U)	<1			62	0.0	38	0.98	0.97
250[b]	6.5	0.0	0.0	66	0.0	34	0.63	
250[b]	6.5	0.33	0.0	100	0.0	0.0	0.81	
200[b]	6.5	0.0	0.028	100	0.0	0.0	1.00	
0.0	6.5	0.33	0.028	50	16[b]	34	0.56	
0.0	6.5	0.33	0.028	41	25[b]	34	0.76	
0.0	6.5	0.33	0.028	33	33[b]	34	0.91	
0.0	6.5	0.33	0.028	25	41[b]	34	1.03	
0.0	6.5	0.33	0.028	16	50[b]	34	1.14	

[a] Precipitate is $UO_2(NO_3)_2 \cdot 6H_2O$ at 2.807 g/cm^3.
[b] Uranium contains 75% ^{235}U, 12% ^{233}U, and 13% ^{238}U.

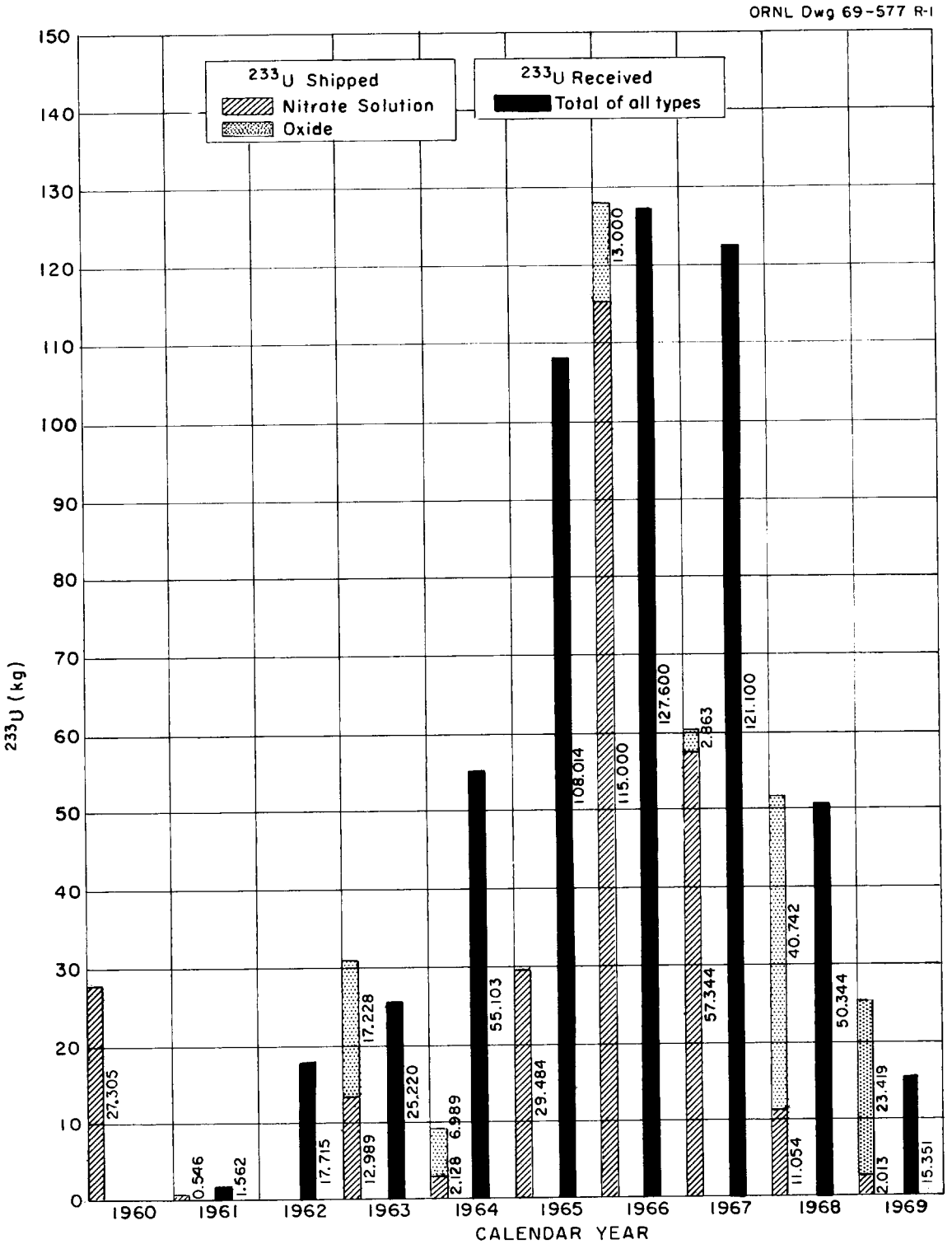

Fig. 6.7. ^{233}U Receipts and Shipments, Building 3019 Dispensing Facility.

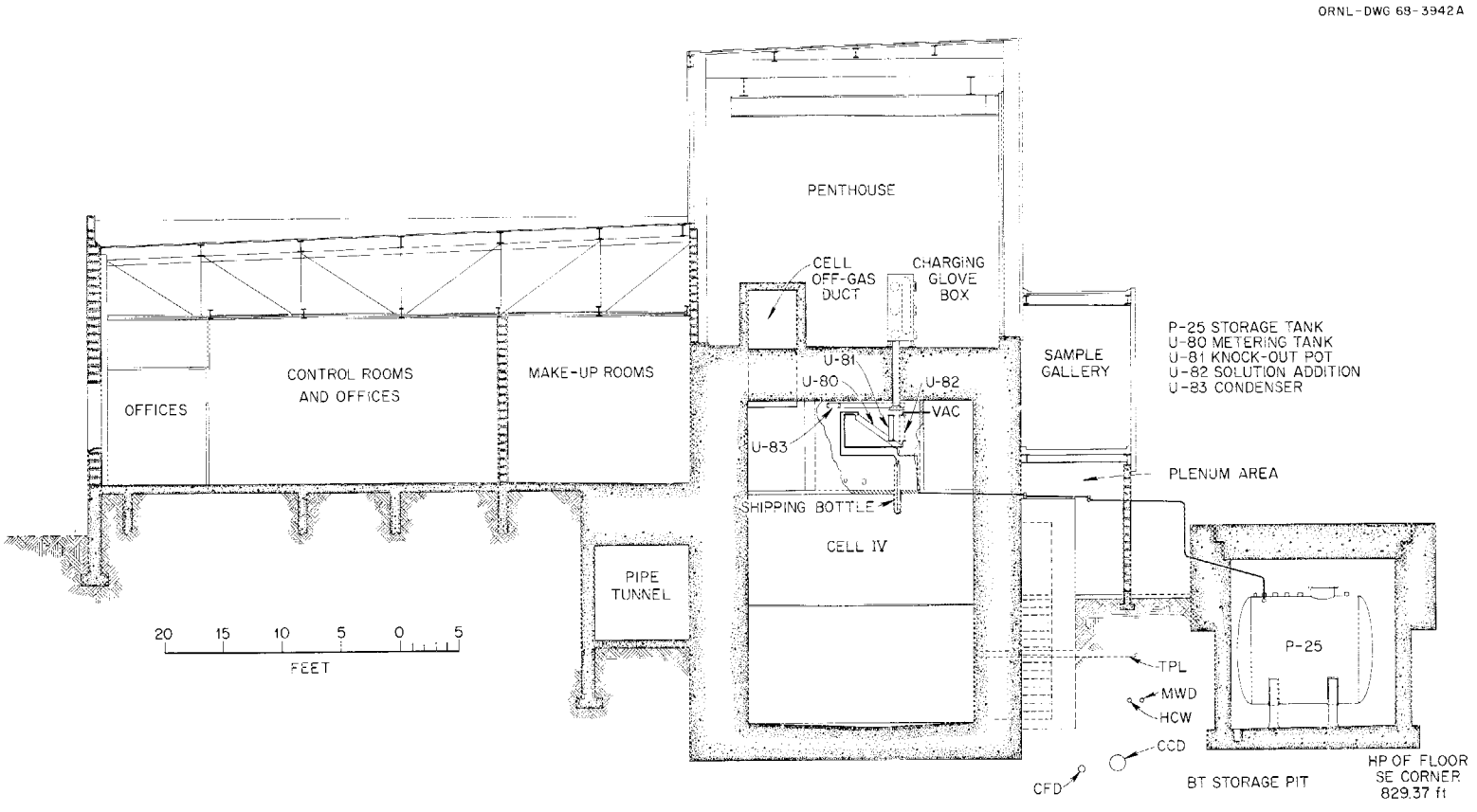

Fig. 6.8. Cross-Section Drawing of TRUST Facility.

multiplication factor for systems of infinite dimensions containing solutions, precipitates, and raschig rings.

The method and the geometrical model tend to slightly overestimate the results of ORNL critical-mass experiments, as shown in the first two lines of Table 6.8. These two cases are results of critical-mass experiments with solutions of ^{235}U and ^{233}U in vessels packed with borosilicate-glass raschig rings. The effect of the raschig rings (line 3), assuming that no cadmium or gadolinium is in solution, is to cause a neutron multiplication factor of 0.63 or less for solutions containing no more than 250 g of uranium per liter. The multiplication factor calculated on line 5 shows that a gadolinium concentration of 0.028 *M*, without cadmium or rings, would result in a marginally subcritical limit system with a maximum uranium concentration of 200 g/liter. Lines 6 through 10 show that, if all the uranium was *selectively* precipitated and if the volume fraction of precipitate was less than or equal to 40%, an infinite system would remain subcritical. This situation is overly pessimistic because of the following:

1. Our experience indicates that a precipitate would deposit uniformly on all the surfaces of the rings.
2. The precipitate would probably carry down gadolinium and cadmium, rendering the mixture subcritical.
3. A precipitation would successively occur slowly and be detected well before 40% of the column contained precipitate.
4. A dense precipitate located near the bottom of the tank would have enough neutron leakage to reduce the multiplication factor by 10 to 15%.

Several laboratory experiments were performed to determine the stability of the solution containing uranium and the neutron absorbers. By slowly evaporating the solution in a stream of air at room temperature, we found that a precipitate did not begin to form until the solution was concentrated to about 370 g of uranium per liter. Results showed that the solution began to freeze at approximately 13°C. Analysis of the "ice" crystals and supernatant liquid indicated that the solution does not change composition upon freezing.

Based on these calculations, the uranium concentration is expected to be maintained between 100 g/liter and 200 g/liter, the cadmium will be maintained at a concentration of at least 0.3 mole per mole of uranium, and the gadolinium will be maintained at a concentration of at least 0.025 mole per mole of uranium.

Analyses of samples of the solution withdrawn at intervals during the past 13 months are presented in Table 6.9. The average uranium content is 1045 kg, as compared with 1047 kg determined by analyses of the individual shipments received. Discrepancies in the soluble poison content are probably due to inadequate mixing of the solution prior to sampling; however, the possibility of analytical error or deposition of the poisons should not be overlooked. Initial efforts to sparge the solution for a long period of time resulted in excessive radiation exposures from the off-gas piping and filter. This system was redesigned with a deentrainment separator and small filter, which will permit more effective mixing for future samples.[17]

[17] W. L. Carter and R. G. Nicol, ORNL, private communication, Nov. 18, 1969.

Table 6.9. Analyses of Solution in TRUST Tank

Date Sampled	Solution Volume (liters)	U (kg)	HNO_3 (*M*)	Soluble Poison Content			
				Cd		Gd	
				kg	mole/mole U	kg	mole/mole U
9-11-68	1110	0	0.11	164.2		21.4	
2-20-69	6970	1040	2.72	164.2	0.33	16.2	0.023
3-28-69	7100	1036	2.57	142.4	0.29	14.8	0.021
4-17-69	7240	1039	2.66	144.8	0.29	15.1	0.022
7-29-69	7300	1053	2.59	142.4	0.28	14.6	0.021
10-10-69	7280	1055	2.46	143.4[a]	0.28[a]	15.3[a]	0.021[a]
11-11-69	7030	1041	2.51	152.9	0.31	17.8	0.025
4-6-70	7085	1020	2.65	145.3	0.30	16.6	0.024

[a] A total of 14.2 kg of cadmium and 3.8 kg of gadolinium was added to the tank on Oct. 3, 1969.

7. Sol-Gel Processes for the Uranium Fuel Cycle

Sol-gel processes are ideally suited for the preparation of LMFBR fuel since they can be readily adapted to continuous and remote operations for processing materials behind shielding. In the processes under development, sols are prepared by the controlled extraction of nitrate from uranium nitrate and plutonium nitrate solutions, which are the products from fuel reprocessing plants. The sols are then converted into the desired form required for subsequent fabrication into recycle fuel elements; this form usually consists of high-density oxide microspheres for use in Sphere-Pac operations.

Emphasis during the past year has been on the CUSP (*C*oncentrated *U*rania *S*ol *P*reparation) process for preparing urania sols by solvent extraction. The preparation of sols by this process is one step in the production of UO_2-PuO_2 for spheres and pellets. In addition, the UO_2 sols are used in sphere-forming studies that serve as a base line for evaluating the behavior of mixed sols. The CUSP process is amenable to scaleup and remote operation. It has been operated throughout the past year in engineering-scale equipment.

A solvent extraction process for preparing plutonia sol (i.e., the APEX process) has been developed and tested in the laboratory. The formation of microspheres from mixed sols prepared by the CUSP and APEX processes has also been studied on a laboratory scale. Results have been encouraging. Additional investigation and scaleup of the APEX process and preparation of $(U,Pu)O_2$ microspheres are required. Much of the mixed $(U,Pu)O_2$ for irradiation testing is still prepared by precipitation-peptization processes since equipment is not yet available for the production of enriched urania sols by the CUSP process or for plutonia sols by the APEX process. A series of factorial-design experiments to determine optimum conditions for forming sols prepared by the CUSP process (called CUSP sols) into microspheres is under way.

7.1 PREPARATION OF UO_2 SOL BY THE CUSP PROCESS

The CUSP process for preparing concentrated ($\geqslant 1\ M$) urania sols directly by solvent extraction, which was described last year,[1] has proved to be a reliable and easily controlled method for the routine preparation of urania sol. This process is being operated at two levels, 1 kg and 4 kg of UO_2 per batch, and sols containing more than 230 kg of UO_2 have been prepared.

In the CUSP process, nitrate is extracted continuously at a controlled rate from a U(IV) nitrate-formate solution with an organic solution of Amberlite LA-2 (a high-molecular-weight secondary amine). By following a prescribed conductivity-temperature-time path, a highly crystalline, stable, approximately 1 *M* urania sol with a high U(IV) content is produced. During the past year (1) laboratory-scale equipment with a capacity of 1 kg of UO_2 per batch was constructed for studying process variables, (2) engineering-scale equipment with a capacity of 4 kg per batch was operated routinely, and (3) laboratory support was provided for the engineering operations and to characterize sol products. Engineering studies with the large-scale equipment included a sol production demonstration covering 26 runs, numerous other sol production runs, and an investigation of several different types of nitrate-extraction contactors.

Laboratory Development

In addition to the construction of laboratory equipment for producing sol, we carried out laboratory work including sol preparation, aging and characterization studies, and an investigation of various methods for

[1] *Chem. Technol. Div. Ann. Progr. Rept. May 31, 1969*, ORNL-4422, pp. 203–10.

cleaning up the solvent used in producing sol in the engineering equipment.

Laboratory-Scale Equipment for the Preparation of Urania Sol. – Equipment for preparing urania sols at a 1-kg-per-batch level by the CUSP process was assembled to test variations in chemical and operating process conditions. This equipment will allow us to reduce the large amount of material and manpower usually necessary for engineering-scale operations. The equipment is illustrated schematically in Fig. 7.1. The feed reduction and extraction equipment is a scaled-down version of the equipment used in the large-scale sol preparations. The major differences in the process conditions used for laboratory-scale equipment, as compared with those used for engineering-scale equipment, are: (1) the Amberlite LA-2 extractant is 0.46 *M* rather than 0.25 *M*, and (2) the extractant is regenerated batchwise by scrubbing with caustic rather than continuously by scrubbing with HNO_3–acetic acid, water, and Na_2CO_3-NaOH. A minor difference is noted in the location of the heating and cooling coils in the laboratory-scale equipment; that is, they are in the phase separation section instead of in a separate chamber in the loop through which the aqueous phase is recirculated. The normal feed capacity is 4 liters of uranous nitrate solution with NO_3^-/U and $HCOO^-/U$ mole ratios of 2 and 0.5 respectively.

Two individuals operated the laboratory equipment during the first four startup (shakedown) runs (Table 7.1); however, it is now possible for one person to prepare 1 kg of UO_2 as sol in three 8-hr days, with the operations being distributed as follows: one day for feed reduction, one day for sol making, and one day for solvent regeneration and equipment cleanup. With continuous, round-the-clock operation, it is estimated that one man per shift can produce 1 kg of UO_2 as 1 *M* sol every 16 hr.

Improved Solvent Cleanup and Regeneration Treatment. – During the engineering-scale operations of the CUSP process, solvent regeneration has been compli-

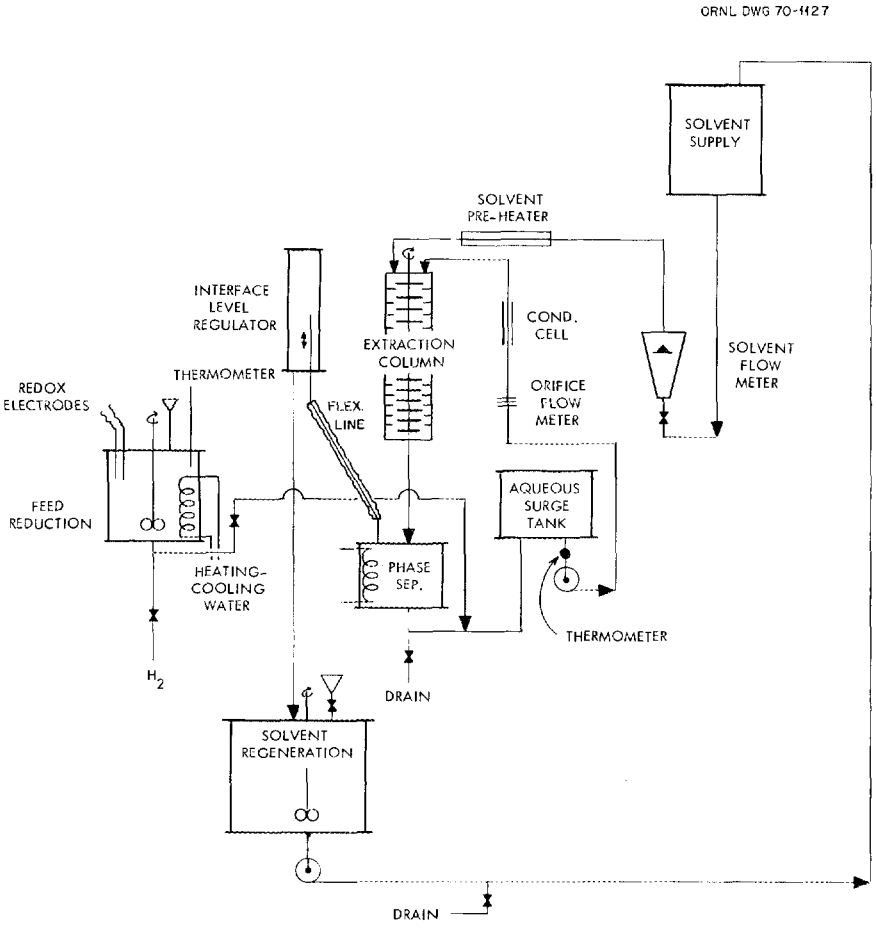

Fig. 7.1. Schematic Diagram of Laboratory-Scale Equipment for the Preparation of Urania Sol.

cated by the presence of small quantities of colloidal uranium, amounting to about 0.5% of the total uranium in a given run, in the solvent. These particles are well suspended, carry a slight negative charge, cannot be removed by filtration or adsorption on silica gel or activated charcoal, and are not effectively removed by the standard solvent treatments. The bulk of the suspended UO_2 accumulates in the caustic-carbonate scrub. We have developed a method for removing most of the uranium from the solvent in an easily recoverable form; this method involves treating the solvent with a nitric acid–acetic acid scrub prior to regeneration. In the normal engineering operation used previously, the spent solvent was contacted with a water scrub, a caustic-carbonate scrub, and then an additional water scrub.

With a three-stage solvent treatment system, uranium recovery and recycle would be simplified if the uranium could be scrubbed out in the first column in a readily recoverable form; then the second and third columns could be used solely for amine regeneration. Several scouting experiments were made with various oxidizing agents in the first scrubber to oxidize the suspended UO_2 to uranyl ion, which could then be readily scrubbed from the solvent into dilute nitric acid (Table 7.2). Of the scrub solutions tested, the most effective was a solution of 1 *M* HNO_3–0.4 *M* $HC_2H_3O_2$, which removed 96% of the uranium when four volumes of the solvent were contacted with one volume of scrub for 5 min. It was postulated that the UO_2 particles exist as an aqueous-in-oil type of suspension in which the particles are stabilized by an organic film. Hence, acetic acid was added to penetrate the film and to expose the UO_2 to stripping by nitric acid.

With the previously used standard solvent treatment, much of the uranium is scrubbed into the caustic-carbonate solution; however, 18% remains in the regenerated solvent (see Table 7.2). Hydrogen peroxide mixed with nitric acid performed poorly as an oxidant, and 67% of the uranium remained in the regenerated solvent. Sodium nitrite added to 1 *M* HNO_3 proved quite effective; 89% of the uranium was recovered in

Table 7.1. Properties of Sols Prepared by the CUSP Process in Shakedown Runs in the Laboratory Equipment

Sol Run No.	Uranium Concentration (*M*)	U(IV) Content (% of total U)	NO_3^-/U Mole Ratio	$HCOO^-$/U Mole Ratio	Density (g/cc)	Conductivity at 25°C (micromhos/cm)
CUSP-45-1	0.98	88	0.10	0.51	1.278	2430
CUSP-45-2	1.02	88	0.13	0.43	1.258	3820
CUSP-45-3	0.90	88		0.43	1.228	3980
CUSP-45-4	0.97	85	0.12	0.45	1.247	4000

Table 7.2. Tests of Various Solvent Treatments for Recovering Uranium in the CUSP Process

Conditions: 80 ml of solvent; 20 ml of reagent contacted 5 min at 25°C; solvent originally contained 0.79 mg of uranium per ml

Run	Uranium Distribution						
	Scrub 1		Scrub 2		Scrub 3		Treated Solvent, % U
	Reagent	% U	Reagent	% U	Reagent	% U	
Standard	H_2O	4	1 *M* NaOH–1 *M* Na_2CO_3	76	H_2O	Negligible	18
Nitrite	1 *M* HNO_3–0.4 *M* HNO_2	89	1 *M* NaOH–1 *M* Na_2CO_3	10	H_2O	Negligible	2
Peroxide	1 *M* HNO_3–1 *M* H_2O_2	2	1 *M* NaOH–1 *M* Na_2CO_3	9	H_2O	Negligible	67
Acetic acid	1 *M* HNO_3–0.4 *M* $HC_2H_3O_2$	96	1 *M* Na_2CO_3	3.7	H_2O	Negligible	0.4

the first scrub. Although equally good recovery was realized in engineering tests, the treatment caused destruction of about 25% of the amine per run.

An engineering test incorporating scrubbing with an acetic acid–nitric acid mixture gave favorable results. The system will be more completely evaluated when a series of runs is made to produce large quantities of sol for use in sphere-forming development studies.

Engineering Development and Sol Production

Urania sols containing more than 230 kg of UO_2 have been prepared in engineering-scale equipment. The most recent equipment and chemical process flowsheets are given in Figs. 7.2 and 7.3. The method presently used for solvent cleanup and regeneration is outlined in Fig. 7.4, and a typical conductivity-temperature path and time schedule is shown in Fig. 7.5. The process was operated batchwise in these runs, and 4 to 5 hr was required to produce a 15-liter batch of 1 *M* urania sol. The results showed that process control was relatively simple and that high-quality 1 *M* urania sols with shelf lives of 3 months or longer were prepared consistently. Furthermore, these sols could be concentrated to 2 *M* urania if desired.

Chemical data relevant to some of the sols produced in the production runs are summarized in Table 7.3. While x-ray diffraction data were not available to permit determination of the average crystallite size or the degree of crystallinity of the sols, the long shelf lives and relatively small changes in conductivity on aging indicate that the sols were highly crystalline. X-ray data obtained on sols produced in the early stages of the engineering development work indicated that they had an average crystallite size of 40 A, and electron micrographs showed uniform, spherical micelles with average sizes varying between 250 and 350 A.

Nitrate-Extraction Contactor Development. — Equipment improvements and modifications were made during the engineering-scale test runs to improve the operation and reliability of the process. The principal equipment item being studied was the type of contactor used for extracting nitrate. Three types of contactors were evaluated during the preparation of 1-kg batches of UO_2 as sol (4 liters of 1 *M* sol) to replace the mechanically stirred contactors in use at that time. These included a column packed with ceramic berl saddles, a free-fall column with a perforated plate, and a column with a spray header to disperse the aqueous phase into the organic solvent. The mode of operation

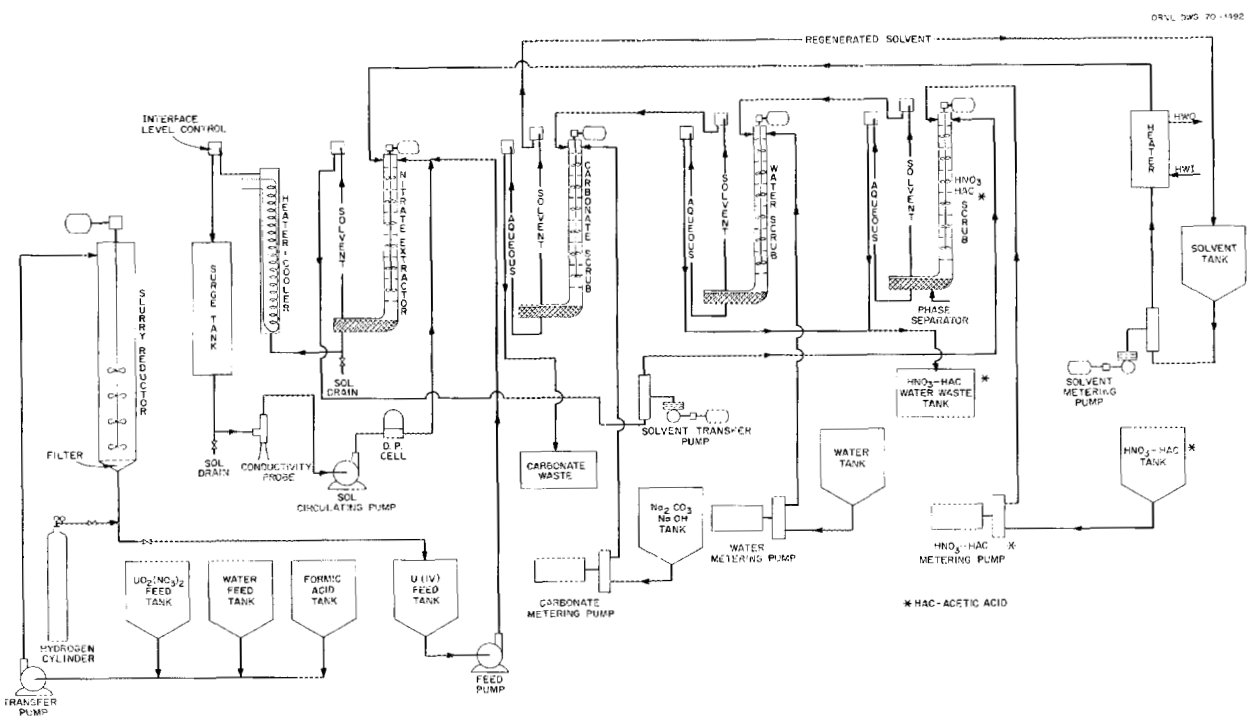

Fig. 7.2. Equipment Flowsheet for Preparing UO_2 Sol by the CUSP Process.

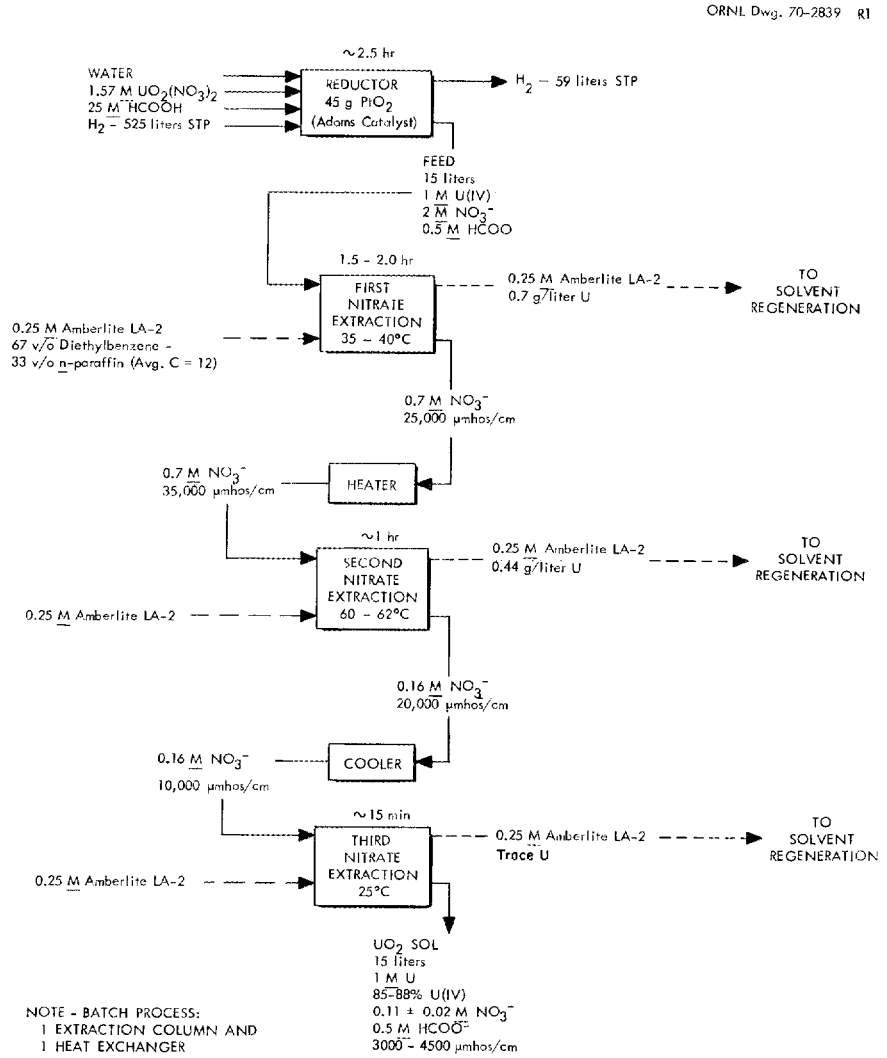

Fig. 7.3. Chemical Flowsheet for Preparing UO_2 Sol by the CUSP Process.

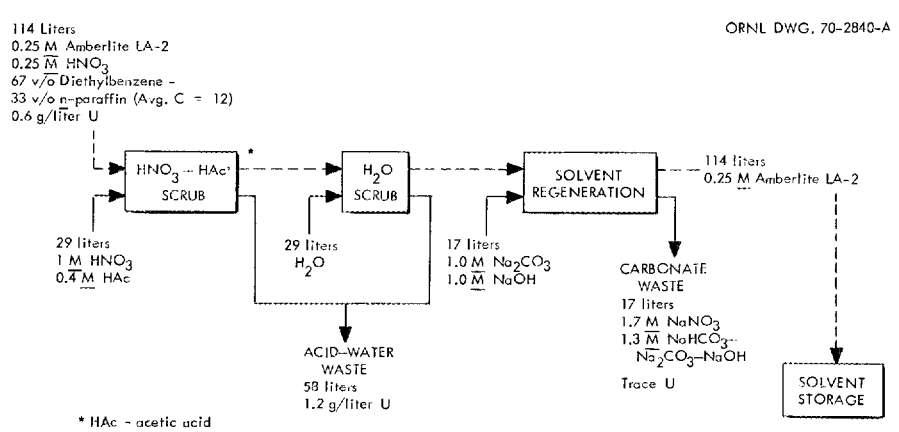

Fig. 7.4. Chemical Flowsheet for Solvent Regeneration in the CUSP Process.

was organic phase continuous with cocurrent flow downward through the column. The spray column operation was the most satisfactory.

Hydraulic difficulties were encountered with the packed column and perforated plate due to vapor locking, which was caused by the release of gas during the crystallization stage of sol preparation. Operation of the spray column (Fig. 7.6) was quite satisfactory; no operational difficulties were encountered. Gas that was released during crystallization was vented through the annulus between the spray header and the column wall. A scaled-up version of the spray column is now being considered for use with the large-scale sol-making equipment.

A summary of selected properties of the sols produced in four spray column runs (SCHB-9 through -12) are presented in Table 7.4. These sols were of very good quality and had U(IV) contents of 85 to 90%; they were still very fluid after more than 3.5 months.

Table 7.3. Selected Properties of 1 *M* UO_2 Sols Prepared in Engineering-Scale Process Equipment by the CUSP Process

Run No.	U(IV) Content (% U)	NO_3^-/U Mole Ratio	$HCOO^-$/U Mole Ratio	NH_4^+/U Mole Ratio[a]	Conductivity at 25°C (micromhos/cm)	Aging Time to Gelation (months)
					$\times 10^3$	
7	93	0.12	0.45	0.0017	3.02	>9
8	85	0.11	0.32	0.0019	3.75	2
9	87	0.09	0.35	0.0015	3.10	4
10	86	0.10	0.41	0.0017	3.10	3
23	88	0.11	0.49	0.0008	3.99	>5
24	88	0.11	0.45	0.0012	4.30	>4
31	88	0.09	0.46	0.0012	4.10	>8
38	84	0.10	0.45	0.0012	5.90	5
43	88	0.11	0.46	0.0012		6
44	88	0.08	0.48	0.0008		>6
45	86	0.11	0.50	0.0009	3.56	>6
46	86	0.10	0.52	0.0017	3.89	>6
47	86	0.10	0.37	0.0008	3.31	6
48	84	0.11	0.43	0.0017		3
49	84	0.11	0.43	0.0016	3.75	3
52	86	0.13			4.24	4
53	84	0.11			3.65	4
54	83	0.10	0.44	0.0012	3.94	>3

[a]The NH_4^+/U mole ratio was determined for the uranous nitrate feed.

Table 7.4. Selected Properties of UO_2 Sols Prepared in a Spray Column Nitrate-Extraction Contactor by the CUSP Process

Run No.	U (mg/ml)	U(IV) Content (%)	NO_3^-/U Mole Ratio	Conductivity at 25°C (micromhos/cm)	Aging Time to Gelation (months)
SCHB-9	239.8	86	0.12	4275	>3.75
SCHB-10	238.3	88	0.11	3329	>3.75
SCHB-11	240.3	85	0.106	4184	>3.5
SCHB-12	239.3	90	0.07	2668	>3.5

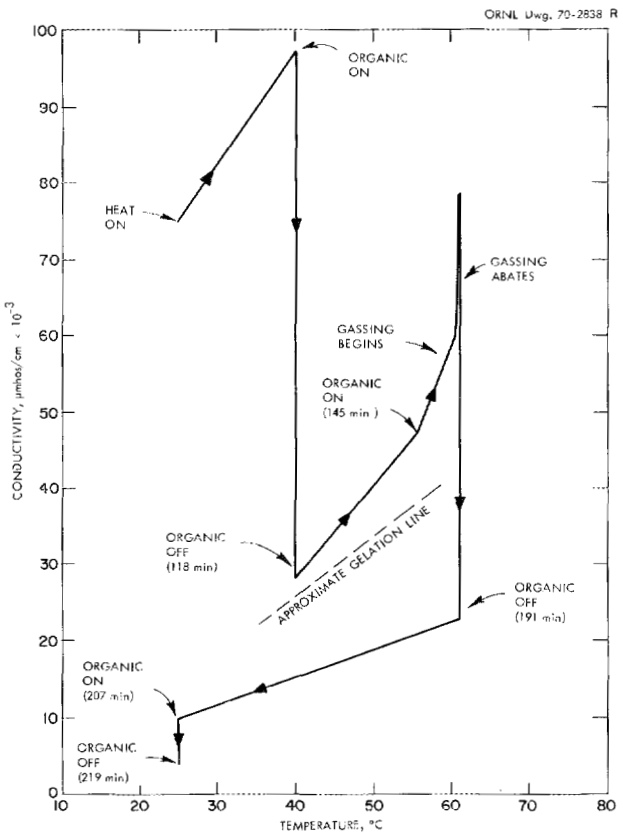

Fig. 7.5. Operating Path for Production of Urania Sol in Engineering Equipment by the CUSP Process.

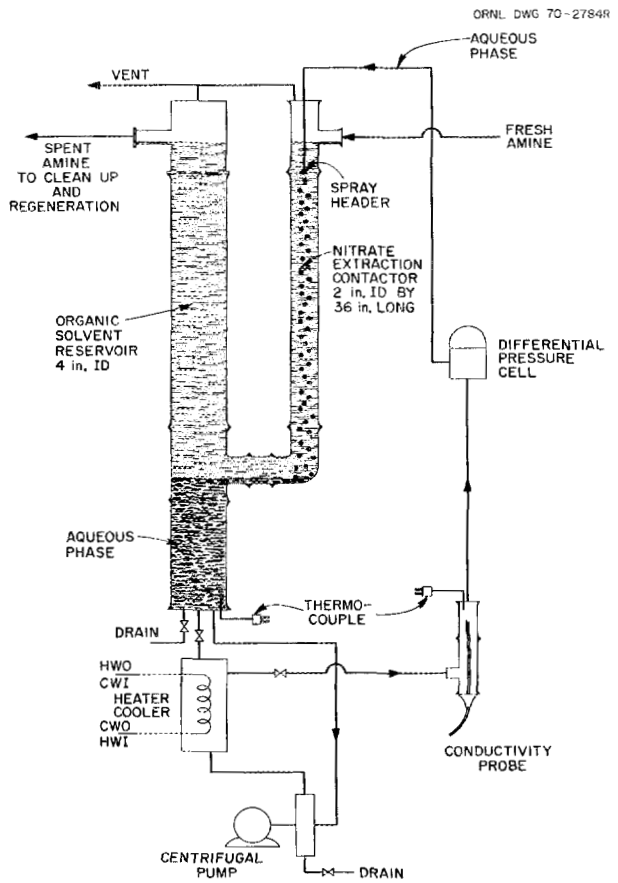

Fig. 7.6. Engineering-Scale Spray Column for Preparing UO_2 Sol. Aqueous-phase capacity, 4 liters.

7.2 DEVELOPMENT OF THE UO_2-PuO_2 SOL-GEL PROCESS

During the past year, laboratory work to develop a solvent extraction process for the preparation of mixed UO_2-PuO_2 sol was continued. Emphasis was centered on solvent extraction since this type of process should be readily amenable to scaleup and to the remote operations necessary for fabricating LMFBR recycle plutonium into reactor fuel. In the process selected for study, CUSP-prepared urania sol is pretreated to remove excess formate and is then mixed in the proper proportions with a high-nitrate plutonia sol prepared by an alcohol extraction process (i.e., APEX). No additional studies have been made with high-nitrate plutonia sols prepared by amine extraction since extraction with *n*-hexanol presents fewer operational difficulties and produces a sol that is more compatible with CUSP-prepared urania sols. During this report period, development efforts were concentrated on: (1) evaluation and optimization of the APEX process, (2) mixed-sol compatibility studies, with particular emphasis on increasing our ability to control the factors responsible for gelation in sols prepared by the CUSP and APEX processes, and (3) an extended series of laboratory experiments to prepare UO_2-PuO_2 microspheres by the CUSP-APEX mixed-sol process. The purpose of these experiments was to demonstrate the reproducibility and reliability of the process on a laboratory scale and to increase our understanding of the importance and the interaction of the many process variables.

The results of these studies have been encouraging. Good yields of product microspheres were obtained in a series of experiments, and the techniques that were developed to prolong the stability of the mixed sols appear to be adequate for process needs. Continued investigation is required, however, since variations in product yields and microsphere characteristics indicate subtle variations in sol properties and sphere-forming variables which are not adequately understood.

Evaluation and Optimization of the APEX Process

Plutonia sols with NO_3^-/Pu mole ratios of 0.6 to 0.8 can be prepared by the APEX process. (These sols are called APEX sols.) The procedure requires several steps. First, nitric acid is extracted into *n*-hexanol from a dilute solution of $Pu(NO_3)_4$ in nitric acid to decrease the NO_3^-/Pu mole ratio to about 2.5. Then the solution is digested at 100°C to hydrolyze the plutonium, thus releasing more nitric acid. After cooling to room temperature, the aqueous phase, which is already a high-nitrate sol, is reextracted with *n*-hexanol to produce a sol having a NO_3^-/Pu mole ratio of approximately 1.0. The sol can then be concentrated, via evaporation, until it is greater than 1 *M* in plutonium, and additional nitrate can be extracted to provide a final NO_3^-/Pu mole ratio of 0.6 to 0.8. Very stable, highly crystalline sols containing very little ionic plutonium (less than 1%) are prepared by this procedure.

Chemical Studies. – The chemical and physical factors involved in the operations described above have been studied so that process parameters can be optimized. Spectrophotometric studies and distribution coefficient data have shown that the chemical mechanisms include initial disproportionation of Pu(IV), subsequent recombination of Pu(III) and Pu(VI), and, finally, hydrolysis and polymerization of Pu(IV).

During the initial process step in which nitric acid is extracted from the feed solution, most of the tetravalent plutonium disproportionates to tri- and hexavalent plutonium according to the following reaction:

$$3Pu(NO_3)_4 + 2H_2O \rightleftharpoons 2Pu(NO_3)_3 + PuO_2(NO_3)_2 + 4HNO_3 \,. \quad (1)$$

Disproportionation decreases the concentration of tetravalent plutonium to a very low value and releases a large amount of HNO_3, which can be extracted before the tetravalent plutonium hydrolyzes, as in the following reaction:

$$Pu^{4+} + H_2O \rightleftharpoons Pu(OH)^{3+} + H^+ . \quad (2)$$

Digestion at 100°C promotes hydrolysis, and, as the tetravalent plutonium hydrolyzes, the tri- and hexavalent plutonium recombine to produce more ionic tetravalent plutonium; in turn, the newly formed tetravalent plutonium hydrolyzes, etc. These reactions continue until essentially all of the plutonium is converted to Pu(IV) polymer. Probably the most significant aspect of this procedure is that the hydrolysis and polymerization of plutonium occur at low acid concentrations under relatively constant conditions that are conducive to the formation of highly crystalline polymer.

In initial studies, nitrate and plutonium extraction coefficients were determined for several different alcohols at various plutonium concentrations. Data obtained for a series of seven successive extractions with about eight volumes of *n*-hexanol per volume of plutonium nitrate solution are given in Table 7.5. During the first five extractions, both the plutonium and the total nitrate extraction coefficients decreased as the NO_3^-/Pu mole ratio decreased. After these extractions, digestion at 100°C was carried out to promote plutonium hydrolysis and polymerization and to release additional nitrate. In the subsequent extractions (Nos. 6 and 7), the plutonium extraction coefficients were substantially decreased and the nitrate extraction coefficients were substantially increased. The nitrate extraction behavior for this series of runs indicates that nitrate is extracted primarily as HNO_3. The decrease in plutonium extraction coefficients appears to reflect the extent of hydrolysis that occurs, since extraction coefficients for polymer were determined to be about a factor of 10 lower than those for ionic plutonium species. It has also been determined, in other experiments, that extraction coefficients for Pu(III), Pu(IV), and Pu(VI) are all about the same order of magnitude (from $\sim 5 \times 10^{-5}$ to 1×10^{-3}) but that Pu(VI) extraction coefficients are typically 20 to 30% higher than those for Pu(IV).

For all of the extractants tested, both the nitrate and the plutonium extraction coefficients increased as the water solubility in the alcohol extractant increased. The order of extraction into some of the alcohols studied was as follows: *n*-butanol > *n*-hexanol > 2-ethyl-1-hexanol (2EH). In the *n*-hexanol system, at constant NO_3^-/Pu mole ratio, plutonium extraction coefficients increased as the plutonium feed concentration increased; however, the nitrate extraction coefficient remained nearly constant. This effect limits the plutonium feed concentration to about 0.1 to 0.2 *M* in order to prevent excessive plutonium extraction.

APEX Process Demonstrations. – Solvent extraction equipment with a capacity of 10 g of plutonium was fabricated for use in laboratory studies of the APEX process. The apparatus consists of two identical contactor-separator sections. In the first section, nitric acid is extracted from aqueous $Pu(NO_3)_4$ solution with *n*-hexanol. After phase separation, the alcohol is pumped to the second section, where the acid is stripped from the alcohol into water. The regenerated alcohol is then recycled to the first section for reuse in

Table 7.5. Extraction of Plutonium and Nitrate into *n*-Hexanol from Plutonium Nitrate Solution

Initial feed: 0.14 *M* $Pu(NO_3)_4$ – 1.0 *M* HNO_3

Extraction Number[a]	NO_3^-/Pu Mole Ratio in Extracted Aqueous Phase	Extraction Coefficients	
		Plutonium[b] E_a^o	Nitrate E_a^o
1	6.10	0.0037	0.067
2	4.47	0.0029	0.042
3	3.94	0.0029	0.041
4	2.98	0.0017	0.044
5	2.85	0.0014	0.029
6[c]	2.02	0.0003	0.057
7[c]	1.40	0.0001	0.067

[a]A series of seven successive batch extractions, each with about eight volumes of *n*-hexanol per volume of plutonium nitrate solution, were made.

[b]Extraction coefficients are for total plutonium concentrations, regardless of the valence state or species.

[c]Solutions heated to 100°C prior to extraction.

extraction. The plutonium nitrate solution is circulated through the extraction section only, and the water strip is circulated through the stripping section only. All of the liquids are circulated by means of gas-lift pumps, which use argon as the pumping gas. The net result of this extraction-stripping cycle is to transport HNO_3 from the plutonium nitrate solution into the water strip, which must be changed periodically in order to maintain satisfactory extraction rates. The progress of the extraction is monitored by a conductivity probe located in the circulating plutonium nitrate stream. This instrument is useful in following the progress of the extraction; however, since the measured conductivity varies with both plutonium and nitrate concentrations, it is necessary to determine total nitrate by acid-base titrations of feed samples. This latter technique has been used to determine the proper end points in the extraction.

Eighteen runs have been made in this equipment. During the first seven runs, acceptable process parameters were determined by spectrophotometric analysis and electron microscopic examination of key samples. It was found that a careful selection of end points is required to produce sol that is highly crystalline and has a low Pu(VI) content. This information was used to establish the procedure given below.

The process as described here cannot be considered to be fully optimized. It should be possible to simplify the procedures for scaleup purposes; however, any major deviation will require careful study in order to prevent adverse effects on crystallinity, crystallite size, or other sol characteristics. The process consists of the following steps:

1. Adjust the feed solution (~500 ml) to a plutonium concentration of 0.07 to 0.13 *M* and a total nitrate concentration of 1.0 to 1.25 *M*. This provides a free acid concentration of less than 1 *M* in all cases.
2. Extract continuously with *n*-hexanol until the NO_3^-/Pu mole ratio is 5 to 6; then replace the water in the stripping contactor with fresh water. (Since the volume of the water strip is three times that of the plutonium nitrate feed, the strip is about 0.2 *M* in HNO_3 when it is replaced.)
3. Continue extraction until the NO_3^-/Pu mole ratio is 2 to 3.
4. Remove the sol from the extraction equipment and digest by heating at approximately 100°C for 1 hr; then allow the sol to cool. (It is important that the first four steps be done continuously and as rapidly as possible, since allowing the plutonium solution to age at any intermediate stage can alter the final characteristics. There are no indications that continuous operations are required after this digestion step.)
5. Replace the water in the stripping contactor with fresh water, and add the digested sol to the extraction contactor.
6. Extract until the NO_3^-/Pu mole ratio is reduced to 0.9 to 1.1.
7. Remove the sol from the extraction equipment and concentrate by evaporation at 80 to 100°C. The sol

can be evaporated to a plutonium concentration of about 1.1 *M* without incurring colloidal instability.

8. Batch extract the sol with water-saturated *n*-hexanol (organic/aqueous volume ratio = 10). This will reduce the NO_3^-/Pu mole ratio to approximately 0.75. (A second batch extraction will reduce the NO_3^-/Pu mole ratio to 0.60 to 0.65 without adversely affecting the stability of the sol.)

Eleven sols, all of which were uniform in behavior and performance characteristics, were prepared using this procedure. The plutonium concentrations and NO_3^-/Pu mole ratios were intentionally varied within the ranges of 0.8 to 1.1 *M* and 0.61 to 0.79 respectively. A sample of each sol was held at room temperature to determine the useful shelf life. All of the sols gelled within 30 to 42 days. Sols with plutonium concentrations greater than 0.95 *M* gelled within 30 to 34 days, whereas 0.8 to 0.9 *M* plutonia sols remained fluid for 40 to 42 days. Thus there appears to be a correlation between sol concentration and shelf life.

The primary plutonium recycle stream in this process results from the plutonium extraction prior to the first digestion step. The amount of plutonium that is extracted depends on both the plutonium and the acid concentrations of the feed. Losses as high as 25% were obtained when 0.22 *M* $Pu(NO_3)_4$ in 1.1 *M* HNO_3 was used as feed. In the 11 demonstration runs with $Pu(NO_3)_4$ concentrations of 0.07 to 0.13 *M* and HNO_3 concentrations of 0.75 to 0.85 *M*, the amount of plutonium extracted was 13.0 ±1%.

In a recent demonstration run, plutonium extraction was reduced to approximately 7% by continuously processing the aqueous stripping solution. A side stream from the stripping section was continuously circulated through two ion exchange columns connected in series. The first column, which contained Dowex 50 cation exchange resin, sorbed plutonium. The second column, which contained Dowex 1 anion exchange resin in the hydroxide form, sorbed nitrate. This arrangement worked extremely well in that the amount of extracted plutonium was reduced, the aqueous stripping solution did not have to be changed during the run, and all of the extracted plutonium was readily recovered by eluting the cation exchange resin.

Mixed-Sol Compatibility Studies

Since thickening or gelling limits the useful shelf life of mixed UO_2-PuO_2 sols, studies were continued in an effort to understand the variables that affect the shelf life of mixed sols and the mechanisms that are responsible for gelation. Several techniques were used to evaluate the effects of adding HNO_3, HCOOH, CH_3CH_2COOH, and $CH_3(CH_2)_2COOH$ to UO_2 or PuO_2 sols as well as to mixed sols. Particular emphasis was placed on determining the affinity of specific sol components for a given anion. It was demonstrated that mixed-sol stability is a function of formic acid concentration. The extraction of formic acid from urania sol prior to mixing this sol with plutonia sol increases the time that the mixed sol remains fluid. Additions of nitric acid also increase the shelf lives of mixed CUSP-APEX sols. In addition, it was found that both temperature and sol concentration have pronounced effects on mixed-sol stability. The period during which a sol remains fluid increases rapidly as the temperature and/or the sol concentration decrease. It was found that a significant change occurs in the typical plutonium(IV) polymer absorption spectrum of a PuO_2 sol when small amounts of formic acid are added to the sol. Spectrophotometric studies have shown that the hydrolytic behavior of plutonium(IV) formate is strikingly different from the behavior of plutonium(IV) nitrate solutions. From these studies, it appears that the PuO_2 component in a mixed sol has an affinity for, or reacts with, formate (formic acid). This, in turn, could promote anion imbalance in the mixed-sol system by several mechanisms and thus result in colloid instability. Fortunately, we have always been able to find combinations of conditions that will produce sols of more than adequate stability for use in the formation of microspheres.

Effects of Temperature and Concentration on Mixed UO_2-PuO_2 Sol Stability. – The effects of temperature and sol concentration on the gelation time for UO_2-PuO_2 sols are shown in Fig. 7.7. The stability of mixed sols is highly temperature dependent; for example, the shelf life of a mixed CUSP-APEX (0.8 *M* UO_2 – 0.2 *M* PuO_2) sol increased from 5 min at 38°C to 1 hr at 25°C, and to more than 5 hr at 0°C. Longer shelf lives can be obtained by partial removal of formate from the CUSP-prepared sol just prior to mixing the sols. Preextraction of formate from the CUSP-prepared sol with an equal volume of *n*-hexanol increased the shelf life of the CUSP-APEX sol described above to 4 hr at 24°C and to approximately 30 hr at 0°C. The time required for gelation of the mixed sol was also found to be a function of sol concentration. Dilute sols require a longer time for gelation; the period of fluidity is approximately inversely proportional to the sol concentration (Fig. 7.7).

Effect of Additives on the Stability of UO_2, PuO_2, and UO_2-PuO_2 Sols. – Various nitrate and formate

compounds, as well as nitric acid and formic acid, were added to UO_2, PuO_2, and UO_2-PuO_2 sols that had been prepared by the CUSP, APEX, and CUSP-APEX processes, respectively, and the effects on colloidal behavior were observed.

We found that, when HNO_3 was added to UO_2-PuO_2 sols, the shelf life of each sol increased linearly as the HNO_3 concentration increased; however, when HCOOH was added, the time to gelation decreased linearly with the logarithm of the HCOOH concentration. Similarly, the addition of other nitrates (Table 7.6) increased, and the addition of formates decreased, the time prior to gelation.

Results of a series of tests showed that the shelf life of CUSP-APEX UO_2-PuO_2 sol (0.57 *M* UO_2, 0.14 *M* PuO_2) decreases as the concentration of $UO_2(OOCH)_2$ increases; for example, it decreased from 3 hr to 1.5 hr as the $UO_2(OOCH)_2$ concentration was increased from 0.05 *M* to 0.20 *M*. The addition of either propionic or butyric acid also adversely affected the mixed sol (see Table 7.6); however, it caused thickening rather than gelation.

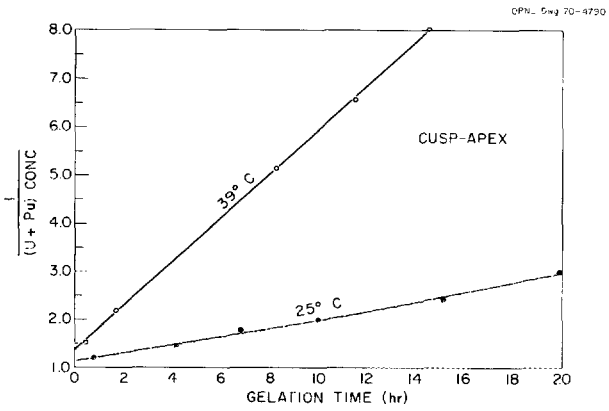

Fig. 7.7. Effect of (U + Pu) Concentration on Gelation Time for Sols with a U/Pu Atom Ratio of 4.

Additives that have caused gelation of PuO_2 sols include HNO_3, HCOOH, and $UO_2(OOCH)_2$. In one series of tests in which HCOOH was added to an APEX-prepared sol (0.45 *M* PuO_2, 0.3 *M* NO_3^-), the shelf life decreased linearly with the logarithm of the HCOOH concentration. Gelation occurred 2 min and 210 min after HCOOH was added to obtain concentrations of 0.33 *M* and 0.0333 *M* respectively. The addition of HNO_3 also promotes gelation of sols prepared by the APEX process; the dependence is about the same as that for HCOOH addition. The addition of $UO_2(OOCH)_2$ caused gelation at a more rapid rate than either HNO_3 or HCOOH at comparable concentrations. Similar results were obtained with three other APEX sols; however, a recently prepared APEX sol was considerably more stable, and the addition of significant quantities of both HNO_3 and HCOOH did not cause sol instability. The reason for this is not known, but it is apparently the result of an interaction of the nitrate and the formate in the sol. To study the effect of formic acid on this more stable APEX sol, which was 0.53 *M* in plutonium and 0.36 *M* in NO_3^-, varying amounts of HCOOH were added to a series of sol samples. (See Table 7.7 for the range of HCOOH/Pu mole ratios investigated.) None of these samples gelled

Table 7.6. Effect of Additives on the Stability of UO_2-PuO_2 Sols

Mixed CUSP-APEX Sol		Additive	Concentration of Additive (*M*)	Shelf Life (hr)
UO_2 (*M*)	PuO_2 (*M*)			
0.571	0.142	None		3¾
0.571	0.142	HNO_3	0.07	5½
0.571	0.142	HCOOH	0.07	1
0.571	0.142	$UO_2(OOCH)_2$	0.10	2
0.590	0.188	None		5½
0.590	0.188	$UO_2(NO_3)_3$	0.09	Did not gel
0.590	0.188	$Pu(OOCH)_2$	0.02	3½
0.590	0.188	CH_3CH_2COOH	0.5	2½[a]
0.590	0.188	$CH_3(CH_2)_2COOH$	0.5	2½[a]

[a]The mixed sols with the added CH_3CH_2COOH and $CH_3(CH_2)_2COOH$ became viscous but did not gel.

Table 7.7. Effect of HCOOH on the Stability of APEX Sols

HCOOH/Pu Mole Ratio	pH[a] at Which Gelation Occurred
0	>4.2
0.23	3.8
0.52	3.4
1.04	2.8
1.22	2.4

[a]The pH was adjusted by the slow addition of 0.09 *M* Amberlite LA-2 in dodecane to extract HNO_3.

Table 7.8. Effect of $PuO_2/(UO_2 + PuO_2)$ Mole Ratio at a Fixed Total Molarity on the Stability and the pH of CUSP-APEX Sols[a,b] at 25°C

$PuO_2/(UO_2 + PuO_2)$ Mole Ratio	Gelation Time	Initial pH[c]	pH After 4 Days
0.05	>10 days	2.4	2.60
0.10	~4 days	2.4	2.70
0.20	11 hr	2.2	2.72
0.30	8.5 hr	2.1	2.70
0.40	4 hr	1.8	2.60
0.50	3.1 hr	1.8	2.60

[a]CUSP-LS-1 was used as feed: pH = 2.40 for 0.4 *M* UO_2; APEX [64-2] was used as feed: pH 1.70 for 0.33 *M* PuO_2.
[b]Total (U + Pu) concentration in each mixed sol was 0.41 *M*.
[c]After mixing.

within 48 hr; however, gelation was promoted by the amine extraction of HNO_3.

The effects of adding HCOOH to CUSP sols were studied in a series of isomolar tests in which the sum of the UO_2 and the added HCOOH concentrations was 1.0 *M*. In these tests, the concentration of UO_2 ranged from 0.8 to 0.2 *M*. No gelation occurred, although thickening sufficient to impair the usefulness of the sols did occur in tests in which more than 0.25 mole but less than 4 moles of HCOOH per mole of uranium were added. The thickening occurred initially and most seriously in tests in which the quantity of formic acid present exceeded two HCOOH molecules for each uranium atom at the surface of the sol crystallites. This result may indicate that the interaction of two or more HCOOH molecules with each surface UO_2 molecule is involved in the mechanism which causes thickening. It is of interest that results of studies with plutonia sols seem to indicate that two or more $HCOO^-$ ions (or HCOOH molecules) interact with each surface plutonium atom (see the next two sections).

The effect of the $PuO_2/(UO_2 + PuO_2)$ mole ratio at a fixed total molarity on mixed CUSP-APEX sol stability is shown in Table 7.8. In the series of experiments summarized in this table, the total metal concentration was kept constant at 0.41 *M* while the plutonium content was varied from 5 to 50%. The addition of PuO_2 was found to produce gelation at a rate that increased with increasing PuO_2 concentration (i.e., from 3.1 hr with 50% plutonium to more than 10 days with 5% plutonium). This behavior is consistent with the hypothesis that the gelation of mixed sols involves an interaction between HCOOH and the PuO_2 component; however, other factors may also be (and probably are) involved.

Effect of Additives on the pH of UO_2 and PuO_2 Sols. – This study was designed to evaluate the relative affinities of UO_2 and PuO_2 for NO_3^- and $HCOO^-$ ions (or HNO_3 and HCOOH). Since HNO_3 is a much stronger acid than HCOOH, a change in pH would be expected if the addition of one acid resulted in the displacement of the other acid (or its anion) from the surface of the colloidal particles. The results obtained indicate that formate preferentially displaces nitrate from the surface of a PuO_2 colloid, while UO_2 colloids do not exhibit preferential affinity for either HNO_3 or HCOOH.

The data obtained in this study were plotted as titration curves showing pH as a function of the titrant volume added. In order to isolate pH changes that resulted from dilution of the sol and the addition of acid to the system, control curves were obtained by titrating water that had been adjusted with HNO_3 to the pH of the starting sol. When the curves obtained by titrating sol and water are similar, it is assumed that there is little or no interaction between the sol components and the acid used as a titrant. For purposes of illustration, a control titration curve and an APEX sol titration curve are shown in the lower part of Fig. 7.8. The pH of the control sample was adjusted to 1.55 with HNO_3 before titration with 0.2 *M* HNO_3. The close similarity of the two curves indicates that the PuO_2 sol did not sorb significant quantities of additional HNO_3. Similarly, the other curves in Fig. 7.8 suggest that there was little or no sorption of HNO_3 by either CUSP sol or formate-free UO_2 sol. The curves also indicate that HNO_3 did not displace formate, since this would have resulted in higher pH values than those obtained in the control curve. Similar data obtained in other tests indicated that there is little or no interaction between a formate-free urania sol (0.1 *M* in U, 0.05 *M* in HNO_3) and a 0.5 *M* HCOOH solution used as the titrant.

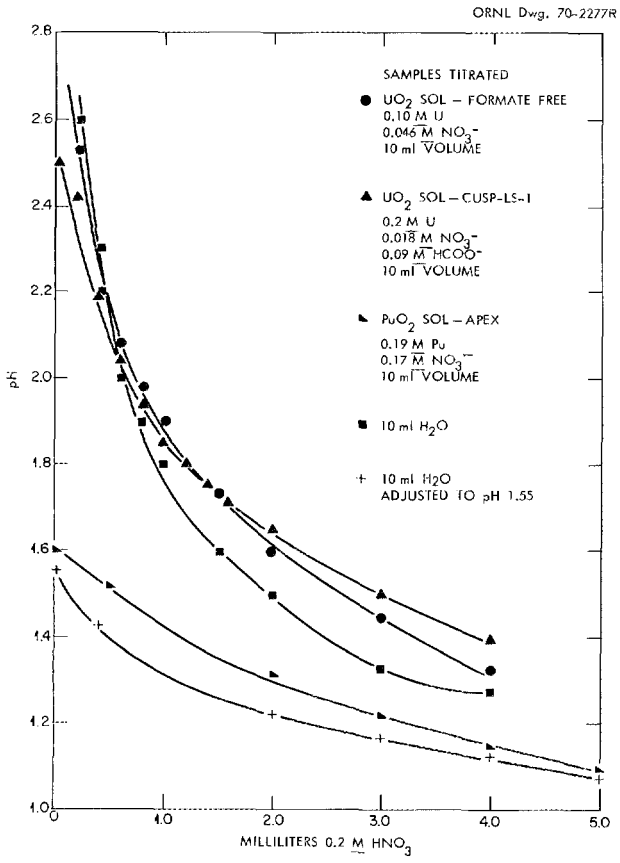

Fig. 7.8. Change of pH as a Function of 0.2 *M* HNO_3 Addition to UO_2 Sols, PuO_2 Sol, and H_2O.

The titration of an APEX sol with 0.5 *M* HCOOH indicates a striking interaction between PuO_2 sol and HCOOH. A typical curve, which is shown in Fig. 7.9, demonstrates the sharp decrease in pH as 0.5 *M* HCOOH is added to the sol. The decrease in pH indicates that NO_3^- associated with the surface of the PuO_2 particles of the sol was liberated by the addition of HCOOH. If it is assumed (1) that both a decreasing and a constant pH during titration with HCOOH reflect the release of sorbed nitrate, and (2) that all of the nitrate has been removed from the PuO_2 particle surfaces when the pH starts to increase, then it appears that about 2 millimoles of formate is required to replace 1 millimole of nitrate on the particle surfaces. Stated in another way, these results can be interpreted to indicate that the PuO_2 sol capacity to sorb $HCOO^-$ is about twice its capacity to sorb NO_3^- under the conditions investigated. The upper curve in Fig. 7.9 is a control curve, which was obtained by titrating water into a second sample of the PuO_2 sol. The later portion of the HCOOH curve parallels the control curve, indicating that this pH increase is essentially due to a dilution effect.

In additional studies, a PuO_2 sol with an initial pH of 1.73 was titrated with water to a pH of 2.5; then the titrant was changed to 0.5 *M* HCOOH. The curve that developed during the addition of HCOOH was almost identical in shape to the HCOOH titration curve shown in Fig. 7.9. A PuO_2 sol was also titrated with CH_3CH_2COOH; again, the pH changes were almost identical to those obtained by titration with HCOOH.

Affinity of UO_2 and PuO_2 Slurries for HCOOH. – In additional efforts to investigate the affinities of UO_2 and PuO_2 sols for HCOOH, the individual sols were precipitated via the addition of NaOH, washed free of anions, and then equilibrated with solutions containing various concentrations of HCOOH. After equilibration, the solids were allowed to settle, and the supernate was analyzed for HCOOH. Formate associated with the solids was determined by difference. The data obtained are shown in Fig. 7.10, where the mole ratio of sorbed HCOOH to metal oxide is plotted as a function of the HCOOH concentration in the supernate. The curve for PuO_2 shows a rapid increase in HCOOH sorption until a sorbed-HCOOH-to-PuO_2 mole ratio of approximately 2 is reached. Then no further sorption occurs until the HCOOH concentration reaches 0.75 to 1.0 *M*. The UO_2 behavior appears to be similar, although there are insufficient points to describe the extent of the plateau. Sorption of formic acid on UO_2 occurred fairly rapidly until a sorbed-HCOOH-to-UO_2 mole ratio of approximately 0.7 was reached.

The sorption capacity of these oxides appears to be nearly identical when sorption is related to crystallite surface area. Since crystallites in PuO_2 sol are very small (10 to 15 A), a high percentage of the plutonium atoms are located on the surface, and the sorbed-HCOOH-to-surface-PuO_2 mole ratio will still be nearly 2. The crystallites of the UO_2 sol, however, are about 40 A, and only about one-third of the molecules are surface oriented. Therefore, the sorbed-HCOOH-to-surface-UO_2 mole ratio would also be very close to 2. These values are consistent with the ratios indicated by previously described techniques.

Spectrophotometric Studies of Plutonium Formate and the PuO_2–Formic Acid System. – Results of laboratory studies in which PuO_2 and UO_2-PuO_2 sols were thickened or gelled by HCOOH and in which gelation of the mixed sol could be delayed by reducing the HCOOH concentration in the UO_2 sol prior to mixing it with PuO_2 sol seem to indicate that the interaction of formate with PuO_2 sol is involved in

gelation. Thus spectrophotometric studies were made of the PuO_2-HCOOH system in an effort to obtain further evidence of this interaction. In these studies, spectral changes were noted when HCOOH was added to APEX sol. The normal spectrum for an APEX sol is the same as that observed for typical plutonium(IV) polymer (which has a characteristic absorption peak at approximately 610 nm). Although several subtle changes in the spectrum occur when HCOOH is added to an APEX sol, the principal change is the appearance, between 610 and 620 nm, of a shoulder on the polymer peak. This shoulder occurs immediately upon addition of HCOOH and does not change with time. It can be detected at very low HCOOH concentrations (HCOOH/Pu mole ratio = 0.01), and its height and breadth increase as the HCOOH concentration increases, as shown in Fig. 7.11. These studies also demonstrated that the addition of HCOOH to plutonium polymer does not promote depolymerization or result in any detectable plutonium valence change. Such spectral behavior indicates that formic acid or the formate ion interacts with plutonium atoms on the surface and is consistent with the hypothesis that this interaction is one of the factors involved in the gelation of mixed sols.

Other studies were made in which HCOOH was extracted with *n*-hexanol from Pu(IV) formate solu-

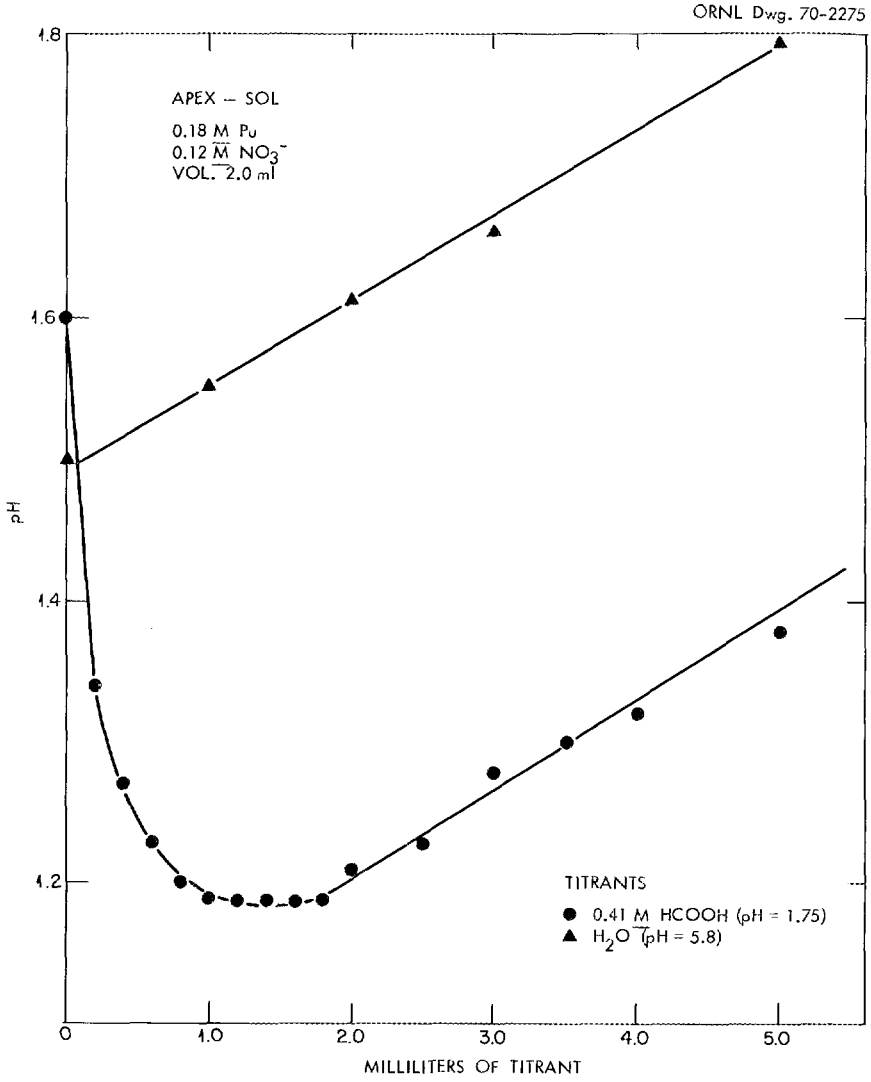

Fig. 7.9. Change of pH as a Function of 0.41 *M* HCOOH or H_2O Addition to PuO_2 Sol.

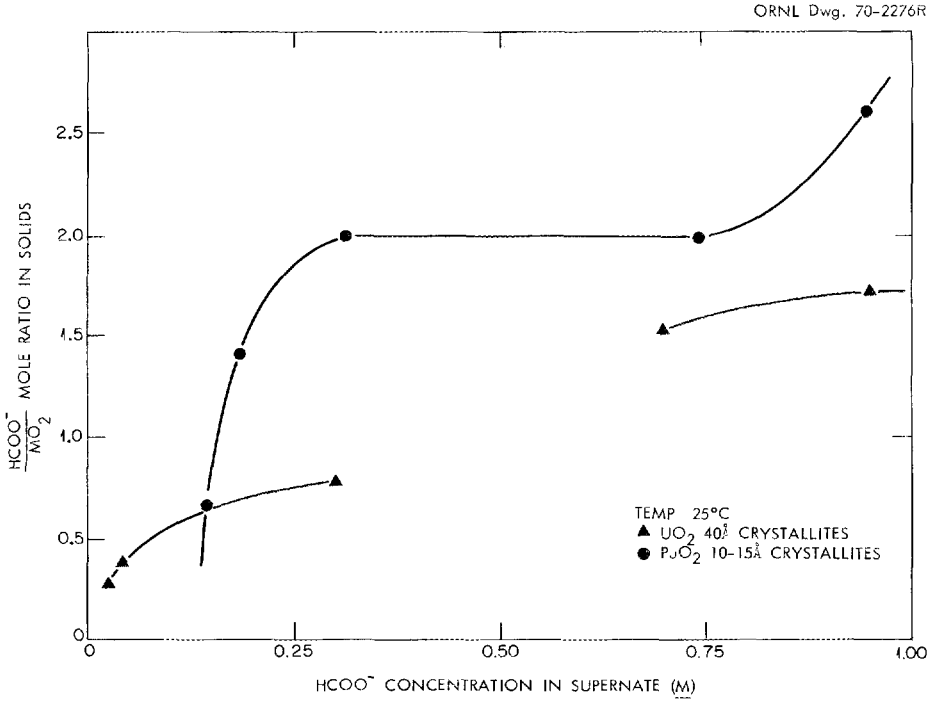

Fig. 7.10. Sorption of Formate on UO_2 and PuO_2 Solids.

tions containing excess formic acid ($HCOO^-$/Pu mole ratio = 10). Successive batch extractions were made until the $HCOO^-$/Pu mole ratio was reduced to 2.0. The absorption spectra of these solutions were determined and compared with plutonium spectra obtained from comparable experiments in nitrate media.

Changes in the Pu(IV) spectrum indicate that, as acid is extracted in the nitrate system, the plutonium disproportionates to form Pu(III) and Pu(VI). With continued extraction, these species recombine to form Pu(IV), which hydrolyzes and forms polymer. When sufficient HNO_3 has been extracted (NO_3^-/Pu mole ratio $\cong$ 3), essentially complete plutonium polymerization will occur slowly upon standing (and rapidly if the solution is heated). In the formate system, on the other hand, very little change occurs in the Pu(IV) spectrum when HCOOH is extracted. In acid-deficient solution ($HCOO^-$/Pu mole ratio = 2), the spectrum is still predominantly that of ionic Pu(IV) and shows no similarity to the absorption spectrum of polymeric Pu(IV). The spectrum is not changed by heating the solution or by extracting below a $HCOO^-$/Pu mole ratio of 2; however, the solution is not stable when heated, and solids eventually precipitate at mole ratios of less than 2. Acid-deficient plutonium formate solutions are reddish brown and very transparent; polymeric plutonium solutions are a dark emerald green.

Conclusion. – Considered collectively, the data from these tests indicate that the instability of UO_2-PuO_2 sols prepared by the CUSP and APEX processes is related to a redistribution of the nitrate and formate anions when the UO_2 and PuO_2 sols are mixed. The initiating step appears to involve a preferential association of $HCOO^-$ (or HCOOH) with PuO_2 crystallites and a release of NO_3^-. Following this reaction, colloid instability and gelation could result from several mechanisms. For example, the PuO_2 component could become unstable by virtue of association with formate through loss of colloidal charge or formate bridging. The UO_2 sol stability could be adversely affected by anion imbalance resulting from formate loss, even if the NO_3^- released from the PuO_2 is sorbed on the UO_2, since the data indicate that PuO_2 can sorb more than twice as much $HCOO^-$ as NO_3^-.

Some understanding of the chemical reactions and the causes of mixed-sol instability has been obtained through these studies. Even though we still lack a complete understanding of the mixed CUSP-APEX systems, good results have been obtained in laboratory-scale preparations of microspheres by close adherence

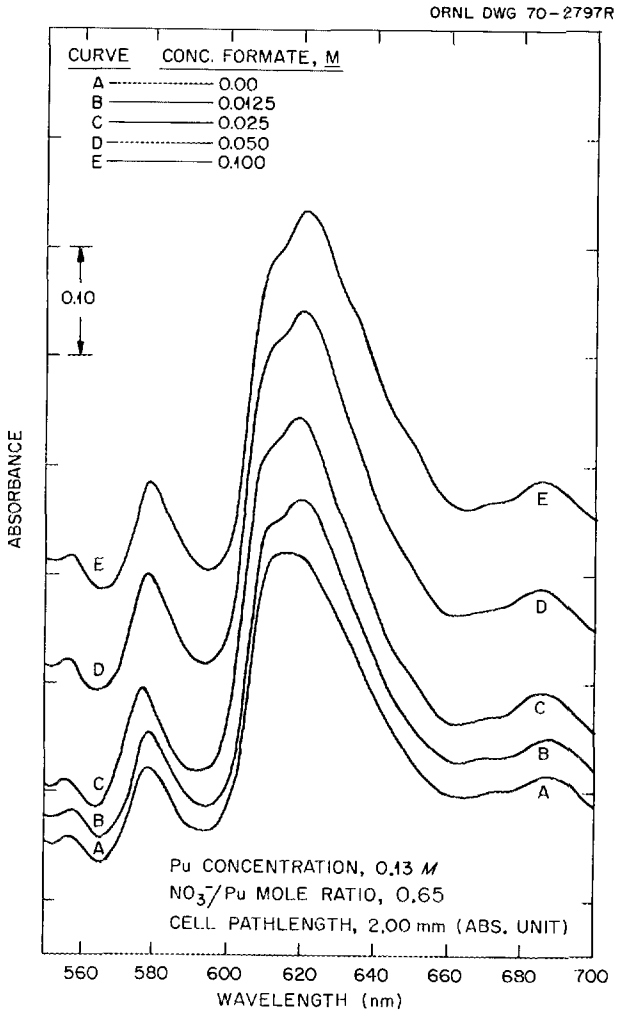

Fig. 7.11. Effect of Formate Ion on the Absorption Spectrum of Polymeric Plutonium(IV). Successive spectra, *B* through *E*, are arbitrarily plotted 0.05 absorbance unit higher than the previous spectrum in order to display the entire spectrum at each formate concentration.

to practices suggested by the results obtained in this study (see next section).

Laboratory-Scale Demonstration of $(U,Pu)O_2$ Microspheres by the CUSP-APEX Mixed-Sol Process

In numerous small-scale experiments, it was demonstrated that one part of an APEX sol (NO_3^-/Pu mole ratio of about 0.7) can be mixed with four parts of a CUSP sol (NO_3^-/U and $HCOO^-$/U mole ratios of about 0.1 and 0.5, respectively) and formed into microspheres by virtue of two expedients that prolong the time to gelation after mixing and prevent extensive cracking of gelled microspheres during drying and calcining. The first expedient is the partial removal of formic acid from the CUSP sol prior to mixing the sols. The second is reducing the temperature of the mixed sols to 5°C. Other experiments indicated that, in some cases, microsphere cracking problems can be eliminated by making minor modifications in the microsphere forming and drying procedures. It was found that both sparging the sphere-forming alcohol with argon and limiting the contact time between the microspheres and the drying alcohol were effective in decreasing or eliminating sphere cracking.

In laboratory-scale demonstrations of the CUSP-APEX mixed-sol flowsheet, two series of microsphere-forming experiments were made. The results obtained were quite encouraging in that good yields of product microspheres were made in consecutive runs in each series of experiments. However, variations in product yields and microsphere characteristics indicate the presence of subtle variations in sol properties and sphere-forming variables.

In the first series of experiments, four APEX sols were prepared; each of these sols was blended with three different CUSP sols to yield three mixed sols. About 10 g of microspheres were formed, dried, and calcined from each mixed sol. In the first three experiments in this series, one of the APEX sols was mixed with each of the three CUSP sols to standardize sphere-forming and handling procedures; these experiments will not be described here. In the other experiments of this series, good yields of product microspheres were obtained in six consecutive runs with mixed sols prepared from two of the CUSP sols and the three APEX sols. Satisfactory yields were not obtained with the third CUSP sol; the reasons for its adverse behavior are not understood.

The APEX sols used in these experiments had NO_3^-/Pu mole ratios of 0.74, 0.75, and 0.71 at plutonium concentrations of 0.60, 0.87, and 0.90 *M*. The properties of the urania sols used are given in Table 7.9. All three sols exhibited good characteristics of fluidity and showed no tendency to gel or thicken throughout the course of these experiments.

Three batches of microspheres were formed from each mixed sol. Each batch required about 12 min to form, and, after all the sol had been introduced into the column, an additional residence time of 35 min was allowed to completely set the gel spheres. The spheres were then removed from the column and dried.

Two drying conditions were evaluated. The first two batches from each run were placed in fritted glass filters and purged continuously with argon. This resulted in

rapid removal of residual solvent. The third batch was placed on filter paper and allowed to dry slowly in air. This resulted in prolonged contact of the gel spheres with solvent as well as exposure to air. All batches were dried overnight and then calcined in 4% H_2–Ar at 1150°C. The microsphere products were examined microscopically before and after calcination to evaluate cracking behavior and surface appearance.

In each case, mixed sols that were maintained at about 0°C remained fluid during the 4- to 6-hr period required for the experiment, and flow characteristics to the forming column and in the two-fluid nozzle were excellent. Sol samples that were allowed to warm up to room temperature gelled in about 1 hr. Column behavior under the selected forming conditions was excellent, except for coalescence of a few of the wet spheres. In several runs, this was the only source of product loss.

The feed sol characteristics and the product yields for microspheres dried in argon are shown in Table 7.10. Product yields for microspheres dried slowly in air were generally much lower, since this drying procedure promoted a distinctive type of microsphere cracking that can be described as surface peeling. This cracking occurred during drying and tended to "heal" (i.e., to be repaired) during calcination. Previous work indicates that this effect results primarily from prolonged contact of the gel spheres with solvent rather than from exposure to air; however, additional study of this problem is needed.

Product yields were good for six consecutive experiments when CUSP sols LS-1 and LS-1HN were used. While this demonstrates satisfactory reproducibility of the process, some of the results cannot be satisfactorily explained. The very poor yields obtained from CUSP-PCHB-5 mixtures do not appear to be related to the nitrate concentration, formate concentration, U(VI) concentration, crystallite size, or micelle structure of the sol; furthermore, the appearance and the handling characteristics of this urania sol were essentially the same as those for the other sols. The lower yields are attributed to microsphere cracking that occurred during both drying and calcining. The unusual behavior of the CUSP-PCHB-5 mixtures may be related to the presence

Table 7.9. Composition of Urania Sols Used in CUSP-APEX Runs

	Urania Sols		
	CUSP-PCHB-5[a]	CUSP-LS-1[b]	CUSP-LS-1HN[c]
Total U concentration, *M*	0.99	1.05	1.03
U(IV) content, % of total U	87.4	86.0	86.0
NO_3^-/U mole ratio	0.13	0.09	0.12
$HCOO^-$/U mole ratio	0.47	0.45	0.45

[a]CUSP-PCHB-5 sol was prepared in experimental engineering equipment.
[b]CUSP-LS-1 sol was prepared in laboratory-scale equipment.
[c]CUSP-LS-1HN sol was prepared from CUSP-LS-1 sol by adding sufficient HNO_3 to increase the NO_3^-/U mole ratio from 0.09 to 0.12.

Table 7.10. Properties of CUSP-APEX Mixed Sols and Microsphere Products

	Mixed Sols								
	APEX-39 plus CUSP-			APEX-42 plus CUSP-			APEX-46 plus CUSP-		
	PCHB-5	LS-1	LS-1HN	PCHB-5	LS-1	LS-1HN	PCHB-5	LS-1	LS-1HN
Pu + U concentration, *M*	0.86	0.91	0.89	0.97	1.01	1.0	0.98	1.02	1.0
Pu content, %	14.0	13.3	13.5	15.5	14.8	15.0	16.4	15.6	15.9
NO_3^-/(Pu + U) mole ratio	0.22	0.21	0.21	0.22	0.19	0.22	0.22	0.19	0.21
pH of alcohol	2.0	3.0	3.1	2.0	1.7	2.7	2.5	2.5	2.3
Yield as calcined microspheres, %	22	65	80	4.2	75	90	2.5	95	85
Appearance of product surface	Fair	Very good	Good	Very good	Poor	Poor	Good	Very good	Very good
Cracks[a] present?	Yes	Yes	No	Yes	Yes	No	Yes	No	No

[a]Small cracks that are not visible at 60× but can be detected at 250×.

of amorphous particles in the urania sol; thus this factor is being investigated. Also, it is interesting to note that, with this material, less cracking occurred and higher yields (up to 40%) were obtained when the microspheres were dried slowly in air rather than rapidly in argon.

The results obtained during the six runs that gave good product yields point out one or more variables which are not understood. Product yields improved in each series of runs (APEX-39 < APEX-42 < APEX-46) although, with the exception of sol concentration, there were no known variations in the APEX sols, sphere-forming procedure, or drying techniques that would adequately explain the observed differences in product yields and surface appearance of the microspheres.

In the second series of experiments, seven additional APEX sols were mixed with three different CUSP sols and formed into microspheres. The procedures used in the first series were followed, except that all products were dried in argon. Two of the CUSP sols, LS-1 and SCHB-12, had aged for three to five months by the time they were used in these experiments; the third sol, CUSP-SCHB-19, was less than one month old when used.

Consistently high yields of product microspheres were again demonstrated when CUSP-SCHB-19 sol was mixed with several of the APEX sols. For example, in four consecutive experiments, product yields of 93, 93, 90, and 94% were obtained from mixed sol containing 20% PuO_2 and 80% UO_2. These products were crack-free, highly lustrous, and had a density 96% of the theoretical crystal density. In a single scouting experiment, a good yield (80%) of crack-free microspheres was also obtained from mixed sol containing 30% PuO_2 and 70% UO_2.

Good results were not obtained consistently with the two older sols; thus it appears that the age of the sol may be involved, since excellent results were obtained with the CUSP-LS-1 sol in the first series when it was less than 1½ months old. Although, from a process standpoint, it is not necessary or desirable to allow sols to age 3 to 5 months, a large number of runs were made with these sols in an effort to understand the high degree of variability observed. It was impossible to obtain consistent results with either of the older sols. Yields of good product varied from as low as 20% to as high as 90% even though the operating conditions were essentially identical. This difference in yields was primarily due to variation in microsphere cracking. A second type of particle distortion, which had not been previously observed with CUSP-APEX mixed sols, sometimes occurred in these runs. This distortion, termed a "raisin" effect, was invariably accompanied by an extremely dull particle surface. The distortion could be partially controlled by varying the sol temperature, since the effect was generally reduced or eliminated if the sol was allowed to warm up to approximately 20°C prior to sphere forming. However, several exceptions to this (i.e., the distortion sometimes occurred even though the sol was warmed) indicate that additional factors are involved. To date, the effect has not been observed for CUSP sols less than 2 months old.

7.3 MICROSPHERE FORMING STUDIES

The optimum conditions for forming a sol into gel microspheres change in a complex manner as the properties of the sol vary. A complete understanding of these relationships has not yet been attained, especially for urania sols. Often, only qualitative results and, in some cases, even conflicting results have been obtained. Since the CUSP process now makes it possible to prepare sols reproducibly, we are in a position to study the details of sphere forming. When a complete understanding of sphere forming from a particular sol has been obtained, it will then be possible for us to use this operation as a test procedure for determining optimum sol properties.

When a sol with specified properties is formed into gel spheres, the composition of the organic drying medium is the principal operating variable. The successful continuous operation of a sphere-forming column requires that the alcohol composition be controlled within satisfactory ranges. This is still largely empirical and requires demonstration in three stages:[2] (1) satisfactory operating conditions, (2) control of surfactant depletion, and (3) control of excessive accumulations of surfactants, degradation products, or impurities.

Tests to develop and demonstrate the stages listed above were continued for the UO_2 sols prepared by the CUSP process (see Sect. 7.1). The results obtained to date show that the formation of microspheres from CUSP sols is more complex than for ThO_2 or ThO_2-UO_3 sols. Quantitative measurements are difficult to make, and the interactions between variables are complex. This can be illustrated by generalized diagrams showing the four most common operating problems as functions of the Span 80 vs Ethomeen S/15 concentration (Fig. 7.12*a*–*d*). These curves are based on data obtained in numerous runs from the Unit Operations

[2]P. A. Haas, *Sol-Gel Preparation of Spheres: Design and Operation of Fluidized Bed Columns,* ORNL-4398 (September 1969).

ORNL DWG 70-2R

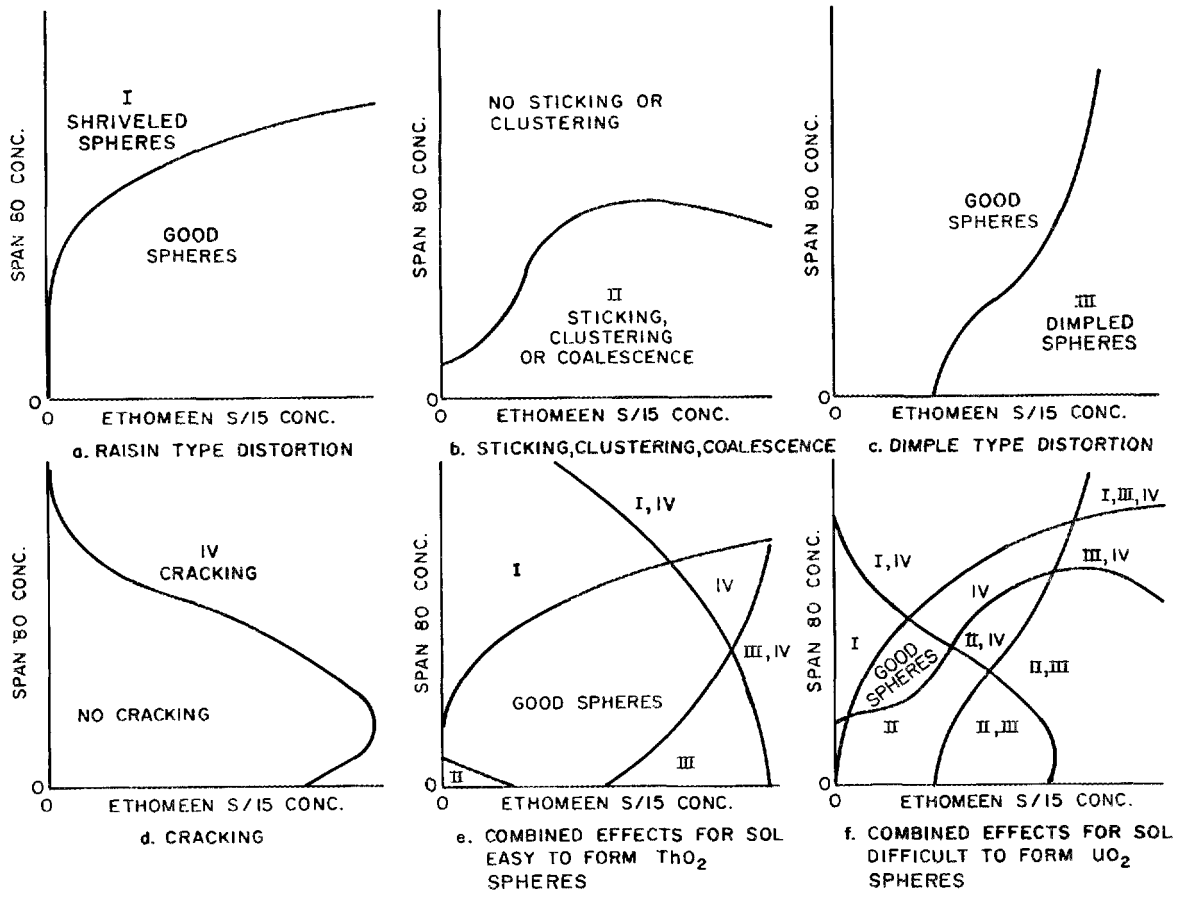

Fig. 7.12. Conceptual Graphs Showing Effects of Ethomeen S/15 and Span 80 on the Formation of Gel Spheres. Changes in other variables such as pH, NO_3^-/metal ratio, sol concentration, etc., would materially change the shapes and locations of the curves.

Section continuous sphere-forming column and from the laboratory batch-operated columns. The curves shown in Fig. 7.12 give the most commonly observed trends. However, the sol characteristics, the pH of the 2-ethyl-1-hexanol (2EH), and other variables result in large changes in numerical values or in distortions of the curve shape. Therefore, numerical values of the surfactant concentrations are not given in Fig. 7.12 since they would apply only if all other variables were fixed and since sufficient quantitative information has not yet been obtained for CUSP sols. When sufficient information is available, it should be possible to superimpose these curves to define a region of conditions for the preparation of satisfactory microspheres. This has been indicated in a qualitative manner in Fig. 7.12*e* for thoria sols that are generally easy to form and in Fig. 7.12*f* for urania sols that are difficult to form.

The effects of variables on the formation of gel spheres from UO_2 sols prepared by the CUSP process are being investigated by a series of factorial-design experiments. Secondary variables are checked by simple comparisons. Unless otherwise specified, the conditions selected as standard as variables include:

Sol: 1 *M* UO_2 sol prepared in batch equipment (4 kg of UO_2) under the standard CUSP flowsheet conditions

Age of sol: 5 to 20 days after sol preparation

Drying alcohol: 2EH containing 0 to 0.9 vol % Span 80 and/or Ethomeen S/15

H_2O content of drying alcohol: 1.0 ± 0.2 vol %

pH of drying alcohol: 4.5 ± 0.5

Temperature of drying alcohol: 28 ± 2°C

Size of gel spheres: 700 μ in diameter

Other conditions: argon blanket and 2EH pretreatment to reduce oxidation of UO_2

Although further work remains to be done, qualitative conclusions about the effects of some of the variables can be made on the basis of the work performed thus far. Good yields of gel spheres were obtained from sols formed in 2EH containing 0.2 vol % Span 80, 0.05 or 0.20 vol % Ethomeen S/15, and about 1.0 vol % H_2O, and having a pH of 4.5.

We plan to continue our sphere-forming studies by performing factorial experiments during the coming year. This will allow us to obtain a complete picture of the solvent composition variables. The experiments will be expanded to include determination of the primary effects and cross effects of solvent impurities, such as formic acid, that build up during continuous operation.

7.4 PREPARATION OF UO_2-PuO_2 MATERIALS

Significant quantities of sol-gel materials have been prepared for use in the LMFBR fuel cycle program. The required materials include such items as normal and enriched urania sols, plutonia sols, and microspheres prepared from individual or mixed sols. Most of these products are used by the Metals and Ceramics Division for irradiation tests and for development of fuel fabrication techniques such as Sphere-Pac or pellet formation from gel spheres or shards. Although solvent extraction processes amenable to scaleup are being developed, plutonia and enriched urania sols are still being prepared by precipitation-peptization processes because facilities are not available for forming adequate quantities of these sols by the solvent extraction processes. As soon as such facilities are provided, we plan to use the extraction processes to prepare all test materials.

Preparation of Sols

Plutonia Sol. – During the past year, approximately 3 kg of plutonium was converted into stable, high-quality PuO_2 sol by the standard precipitation-peptization-baking process reported previously.[3] About half of this material was blended with enriched urania sols, and the other half was mixed with CUSP natural urania sols. The mixed sols were used to prepare irradiation capsules of both pellets and Sphere-Pac microspheres for testing in the TREAT, ORR, and EBR reactors.

[3]M. H. Lloyd and R. G. Haire, "A Sol-Gel Process for Preparing Dense Forms of PuO_2," *Nucl. Appl.* 5, 114–22 (1968).

Urania Sols. – Natural urania sols were prepared by the CUSP process (Sect. 7.1). A total of 14 kg of enriched uranium was converted from uranyl nitrate solution into urania sols by the standard precipitation-peptization process. Enrichments of 9% and 20% were obtained by blending natural and 93% enriched uranyl nitrate solutions prior to sol preparation. A summary of the sols that were prepared and their properties is given in Table 7.11.

Preparation of Microspheres

A total of 3.1 kg of $(U,Pu)O_2$ microspheres was prepared from UO_2 and PuO_2 sols mixed in the proper proportions to obtain the desired Pu/U atom ratio. Prior to blending, all urania sols were decanted from any settled solids (even though, in all cases, very little or no settling was noted), and each sol was then contacted with dry *n*-hexanol to remove the extractable formate. Blends of these sols with plutonia sols were stable for several days before gelling occurred. Urania sols prepared by the precipitation-peptization process were used in all blends with enriched uranium, and urania sols that had been prepared in engineering-scale equipment by the CUSP process were used in all blends with natural uranium.

Microspheres of Natural Urania–Plutonia. – The following quantities of 80% UO_2–20% PuO_2 microspheres were prepared in two size ranges: less than 44 μ in diameter, 160 g; and 425 to 595 μ in diameter, 440 g. These microspheres were formed from a mixed sol (a blend of a PuO_2 sol with a UO_2 sol that had been prepared by the CUSP process and extracted with *n*-hexanol) in the usual manner; that is, droplets of the mixed sol were dried in a column of 2EH containing about 0.5 vol % each of Span 80 and Pluronic L-92. The gel microspheres were removed from the 2EH and dried to approximately 170°C in a stream of mixed steam and argon. The dried gel beads were then fired successively in wet argon to 600°C and in argon–4% H_2 to 1290°C. Although a significant fraction of the 425- to 595-μ-diam product spheres had surface cracks to a depth of about one-fourth of the sphere radius, they were satisfactory for the Sphere-Pac preparation of irradiation specimens. Personnel in the Metals and Ceramics Division adjusted the oxygen/metal atom ratio by treatment of the microspheres in argon–4% H_2 at 1450°C and then prepared Sphere-Pac beds with a "smear" density equal to approximately 85% of the theoretical density of the mixed $(Pu,U)O_2$.

Microspheres of Enriched Urania–Plutonia. – About 1.4 kg of 425- to 595-μ-diam spheres and 364 g of smaller (<44-μ-diam) spheres of 80% $^{235}UO_2$–20%

PuO_2 were prepared for use in the EBR II, series 2 irradiation tests. The Pu/(Pu + U) ratio for the large spheres was 0.200 for one lot and 0.203 for a second lot. The tap density was 6.3 to 6.5 g/cc, which is indicative of satisfactory sphere density. The Pu/(Pu + U) ratio for the small spheres was 0.204. Autoradiographs showed no variation in alpha activity throughout samples of the material, indicating that the product was completely homogeneous. These materials were delivered to the Metals and Ceramics Division for use in Sphere-Pac test rods to be included in the EBR II, series 2 irradiations.

Table 7.11. Enriched UO_2 Sols for Fuel Fabrication

Lot Designation	Number of Batches[a]	U Enrichment (%)	Uranium		U(IV) (% of total U)	NO_3^-/U Mole Ratio	$HCOO^-$/U Mole Ratio
			Total Product (g)	Conc. (g/liter)			
REQ-72	3	9	575	192	88	0.12	
PUM-9	3	20	820	195	89	0.12	0.2
MP-2	1	93	300	250	88	0.07	
REQ-93	16	93	1750	200	88	0.12	0.25
REQ-93	14	93	3900	240	89	0.12	0.30
GGA	6	93	1735	240	88	0.12	0.30
REQ-93A	4	93	1155	240	89	0.15	0.30

[a]Each batch was prepared from uranyl nitrate solution containing 325 g of uranium.

8. Conversion Studies in the LMFBR Fuel Cycle

8.1 COST STUDIES

Estimated Costs for LMFBR Fuel Material Conversion

Four conceptual plants to convert depleted UF_6 and $Pu(NO_3)_4$ solution to completed LMFBR core fuel assemblies were studied to determine the cost differences among them.[1] The basic processes used by the four plants are: (1) "Mechanical Blend Pellet," in which UO_2 and PuO_2 powders are prepared separately, mechanically blended, and then subjected to conventional pellet preparation, rod loading, and element assembly; (2) "Coprecipitation Pellet," in which aqueous uranium and plutonium nitrate solutions are mixed and oxide powder is prepared by coprecipitation prior to conventional pellet preparation and element assembly; (3) "Sol-Gel Pellet," in which uranium and plutonium oxide sols are prepared and mixed and then converted to mixed oxide powder, which is used in conventional pellet preparation and element assembly; (4) "Sol-Gel Sphere-Pac," in which uranium and plutonium sols are prepared, mixed, and converted to mixed oxide microspheres, the microspheres are loaded into fuel rods using gentle vibration, and conventional element assembly is carried out.

Each conceptual pellet plant starts with UF_6 from diffusion plant tails and plutonium nitrate solution from aqueous processing plants and produces Atomics International Reference LMFBR (oxide) core fuel elements. The Sphere-Pac plant produces an equivalent element, differing in that pellets are replaced by spheres. Each plant produces 500 kg of heavy-metal core material in finished elements each day for 260 days each year. Remote operations and maintenance are used for all operations involving recycle plutonium. A plant throughput of three metric tons of heavy-metal core material per day has also been studied to provide a guide for the effect of plant size.

Estimating Procedure

Costs are estimated only for areas of difference among the competing processes. The estimating procedure was a modification of FABCOST 9,[2] a computer code used to calculate complete fabrication costs. The following procedure was used: (1) prepare process flowsheets for the required operations; (2) determine, in detail, the equipment that is required for each process step not common to all processes; (3) estimate the equipment purchase price, required daily operating manpower, and fuel material loss and scrap generation associated with each of the foregoing disparate steps; and (4) utilize approximate factors to convert the estimates to differential plant costs (i.e., the sum of all steps).

FABCOST 9 classifies plant types as contact, hooded, semiremote, and remote, and presents factors to convert estimated operator man-hours and equipment price for contact operations to operating and capital costs for the type of operation involved. In this study, operations are classified as contact (operations involving no plutonium), easily remote, or difficultly remote. The last two classifications reflect the fact that certain types of equipment are less expensive to install, operate, and maintain than others. Modified FABCOST 9 factors are developed for these classifications. When each proved step is estimated separately, the estimate reflects the mode of operation for the step.

The plutonium loss and the scrap that is generated are also estimated for each process step. Fuel loss is evaluated on the basis of $10 per gram for fissile plutonium, and scrap recovery is priced at one-tenth the value of the plutonium content.

[1] F. E. Harrington *et al.*, *Cost Study of Four Alternate Routes for LMFBR Fuel Material Preparation Fabrication*, ORNL-TM-2813 (February 1970).

[2] A. L. Lotts *et al.*, *FABCOST 9, A Computer Code for Estimating Fabrication Costs for Rod-Bundle Fuel Elements*, ORNL-4287 (August 1968).

Resulting Estimates

Table 8.1 summarizes the results of combining the detailed estimates and factors mentioned above for the plant producing 500 kg of heavy-metal core material per day.

Table 8.2 summarizes the fuel fabrication costs for 0.5- and 3-metric ton/day plants to illustrate the effect of scale of operation on fabrication cost.

Table 8.1. Summary of Differences in the Costs[a] of Fabricating AI[b] Reference LMFBR Oxide Core Fuel Elements by Four Fuel Preparation Methods

Type of Cost	Fuel Preparation Method			
	Mechanical Blend Pellet	Coprecipitation Pellet	Sol-Gel Pellet	Sol-Gel Sphere-Pac
Capital	11.23	12.91	11.74	9.51
Operating	31.58	35.37	32.27	24.68
Loss	19.47	17.77	17.77	10.20
Scrap	8.20	6.52	5.93	2.60
Total	70.48	72.57	67.71	46.99

[a]Estimated in dollars per kilogram.
[b]Atomics International.

Table 8.2. Effect of Fabrication Plant Size on the Costs[a] for the Four Fuel Fabrication Processes

Fuel Fabrication Process	Plant Capacity	
	500 kg/day	3000 kg/day
Mechanical Blend Pellet	70.48	61.22
Coprecipitation Pellet	72.57	62.62
Sol-Gel Pellet	67.71	58.65
Sol-Gel Sphere-Pac	46.99	40.31

[a]In dollars per kilogram.

Discussion

The results indicate that the Sol-Gel Sphere-Pac operation offers appreciable potential savings over the three pellet processes, despite the assumption of higher operating and capital costs ($2.58/kg and $0.61/kg respectively) for the Sphere-Pac rod loading operations over loading rods with pellets.

In detailing the Sphere-Pac plant in this study, all the plutonium was assumed to be contained in large microspheres of PuO_2-UO_2; the fines fraction was assumed to be pure UO_2. With this approach, the following advantages are foreseen:

1. Weld contamination would be minimized.
2. One infiltration would be required for the core and blanket.
3. Loose-fitting UO_2 pellets could be used in the blanket region, eliminating centerless grinding and reducing blanket pellet fabrication costs.
4. Controlled, sharp cutoffs between core and blanket would be readily obtainable.
5. The UO_2 could be made in an unshielded facility.

The development of this approach is continuing; indications are that the cost penalty assumed in rod loading, as cited above, would be eliminated.

The costs associated with plutonium loss and scrap recovery make up a large fraction of the total cost difference between Sol-Gel Sphere-Pac and the pellet methods. Earlier cost comparison methods, which assumed a constant plutonium loss and scrap generation rate, overlooked this area of possible major cost differences.

The high cost of hardware for LMFBR oxide fuel elements clearly points to the use of other fuel materials, such as carbides, nitrides, and carbonitrides, which have characteristics that allow for larger rod diameter, in order to achieve a major reduction in conversion-fabrication costs.

Estimated LMFBR Fuel Shipping Costs

The plutonium product of fuel processing plants is plutonium nitrate solution, which is usually concentrated to about 1 *M* for storage or shipment. The LMFBR, using plutonium as the fissile material, will both require and produce larger quantities of plutonium than previously encountered in the fuel cycle. The storage and shipping of plutonium will significantly influence fuel cycle costs. This study considers both the direct costs of shipping and storage and the relative safety of alternative approaches.

Safety Considerations in Shipping Plutonium. – Plutonium compounds present four types of hazards to be considered in shipping or storage practice. These are: (1) the biological hazard due to ingestion or inhalation, (2) the possibility of a nuclear excursion, (3) the presence of electromagnetic and neutron radiation, and (4) the radiolytic decomposition of water when solutions are handled. The use of solid forms, such as dry oxide or dried gel, for shipping eliminates radiolytic decomposition and significantly increases the quantity of material that can be handled without the possibility

of nuclear excursion. The oxide can be sealed in metal containers (because there is no gas evolution) to reduce the contamination hazard. The radiation hazard is about the same for both liquid and solid forms, but is dependent on the isotopic composition of the plutonium. Recycle plutonium will require more shielding for both gamma and neutron radiation than is the case for the plutonium presently being produced. Gas production by radiolysis is largely a function of the total alpha-decay energy. The present plutonium product contains about 10% ^{240}Pu and very small amounts of ^{238}Pu and ^{242}Pu, whereas the recycle product is expected to be about 25% ^{240}Pu and contain 4 to 5% ^{242}Pu plus up to 1% ^{238}Pu. The gas evolution rate for the present product is about 0.05 cc per gram of plutonium per day in 4 *M* HNO_3 solution. The rate of gas production for recycle material is expected to be 0.45 cc per gram of plutonium per day, on the basis of the difference of activities of present vs recycle products (i.e., 1220 vs 11,500 curies/kg).

Table 8.3. Estimated Costs[a] for Shipping Plutonium Products Round Trip by Rail from Buffalo to Denver[b]

	Plutonium Nitrate[c] Packages		Plutonium Oxide[d] Packages
Class and size	I-3	I-10	I
Costs per shipment			
Container	59.86	30.50	1.45
Filling	68.12	43.91	20.09
Analysis	76.50	22.50	40.00
Transportation	99.60	66.23	6.11
Receiving	123.24	36.70	19.43
Total round-trip costs	427.32	199.84	87.08

[a]In dollars per kilogram of plutonium.

[b]Data as reported in ref. 3.

[c]Twenty kilograms of plutonium in the form of $Pu(NO_3)_4$, shipped as solution containing 200 g of plutonium per liter and having a specific gravity of 1.5.

[d]Twenty kilograms of plutonium in the form of PuO_2, shipped in cans containing 2 kg of material each.

Costs of Shipping Plutonium Products. — The shipping costs used in this study were based on shipment between Buffalo, New York, and Denver, Colorado, by common carrier at published rates (see Table 8.3). Results of the study show that shipping dense, solid oxide is significantly lower in cost (based on current charges) than shipping a nitrate solution.

To assist in estimating costs, we have specified the sizes for several components of the shipping system, using data from the Dow Chemical Company and the Atlantic Richfield Company[3,4] and taking into account a discussion of criticality considerations for FFTF fuel.[5] The containers chosen have been approved for shipment of fissile materials and have been in actual service. The approved dimensions and loading limits allow larger masses of dense products such as microspheres to be loaded in a single container. This has a significant effect on cost since the loading, unloading, sampling, and accountability inspections make up a large part of the shipping cost.

[3]F. E. Adcock *et al.*, *Plutonium Oxide Shipping Packages*, RFP-501, Rocky Flats Division, Dow Chemical Co. (1965).

[4]J. T. Byrne *et al.*, *Measurements Involved in Shipping Plutonium Oxide*, RFP-502, Rocky Flats Division, Dow Chemical Co. (1965).

[5]C. L. Brown, "Criticality Safety Considerations in the Fabrication of 25 wt % PuO_2–UO_2 FFTF Fuel," from BNWL:SA-1388, Battelle Northwest (1967).

Table 8.4. Shipping Costs[a] for Four Types of Plutonium Product as a Function of Plant Capacity

Plant Capacity (kg Pu/day)	Cost ($/kg) of Shipping Four Types of Plutonium Product			
	PuO_2 Powder[b]	PuO_2 Microspheres[c]	PuO_2-UO_2 Powder[b]	PuO_2-UO_2 Microspheres[c]
100	87	87	87	87
200	43.50	43.50	70.50	43.50
600	32.50	23.50	41.50	23.50

[a]In dollars per kilogram of plutonium.

[b]Density, 3 g/cc.

[c]Density, 7.4 g/cc.

Table 8.4 shows the final results of these shipping concepts in terms of the cost per kilogram of plutonium for the four product forms and for three different plant sizes. Examination of the table leads to two tentative conclusions: (1) microspheres (or other dense oxides) represent a more economic form for shipping either pure or mixed oxides, and (2) the unit costs are very reasonable when one considers that inspection costs make up about 45% of the total cost. Inspection costs were not included in earlier studies, which have indicated costs ranging from \$50 to \$425 per kilogram of plutonium. It should be pointed out that the cost of converting plutonium to dense oxide has not been included. Also, if the oxide is not used in the as-shipped form (as microspheres could be, via Sphere-Pac fabrication), the cost of putting the oxide back into solution would have to be added.

8.2 PREPARATION OF SINTERABLE UO_2 FINES

Small $(U,Pu)O_2$ gel spheres offer potential advantages as a source of sinterable powder for pellet pressing. They have the potential of possessing a more uniform composition than a mixture of UO_2 and PuO_2 powders, and of flowing more easily than either conventional powders or crushed gel. Small spheres that are very free flowing and have the desired mean diameter can be prepared, thus eliminating slugging and granulating operations.

The procedures for preparing small spheres in non-fluidized columns (see Sect. 6.4) are preferred for preparing sinterable gel spheres. Among the possible disadvantages in using these procedures is that carbon is picked up from the sol and from the sphere-forming steps. Carbon is more easily removed from the gel when isoamyl alcohol is used as the drying alcohol than when 2-ethyl-1-hexanol (2EH) is used. The carbon remaining in the dried gel is probably present as formate; the carbon analyses (Table 8.5) are in agreement with the $COOH^-/U$ ratio of the sol. The optimum firing conditions prior to pelletizing will have to be determined experimentally. The surface area, 86 to 446 m^2/g, and the reactivity (the UO_2 spheres burn in air) are both undesirably high after the drying step at 225°C.

Further studies are needed to evaluate this method for preparing powders that are suitable for pelletizing.

Table 8.5. Properties of UO_2 Gel Microspheres Prepared as Sinterable Fines

Drying conditions: in Ar or Ar-H_2O to ~225°C

Drying Alcohol Used	UO_2 Sol No. (CUSP-)	Properties of Gel Microspheres				
		Mean Diameter (μ)	C (wt %)	U (wt %)	Surface Area (m^2/g)	Bulk Density (g/cc)
2-Ethyl-l-hexanol	32	35	1.60	81.2	446.0	1.8
Isoamyl	28	35	1.52	83.4	86.9	1.6
Isoamyl	35 and 36	50	2.20	83.1	94.5	1.4

9. Preparation of $^{233}UO_2$ for Light Water Breeder Reactors

ORNL participation in the Light Water Breeder Reactor (LWBR) Program, under contract with Bettis Atomic Power Laboratory, involves: (1) the receipt and storage of approximately 640 kg of ^{233}U (400 kg as UNH and 240 kg as UO_3), (2) the purification of this material in small batches (~20 kg of ^{233}U per week) to remove ^{232}U daughters, (3) the conversion of this UNH to ceramic-grade UO_2 powder at the rate of about 20 kg of ^{233}U per week, (4) the packaging and shipping of the UO_2 to BAPL for blending with thoria and pressing into pellets, and (5) the recovery of 175 to 225 kg of ^{233}U from an estimated six to seven tons of urania-thoria scrap from the Bettis operation.

This program will require additional storage facilities for both oxide and solution, a new dissolver for recovering ^{233}U from the thoria-urania scrap, modifications to the present purification system, and a complete oxide conversion line. The facility is presently scheduled to begin production in October 1971.

9.1 PROCESS DEVELOPMENT AND FLOWSHEETS

Although the feed for the program will consist of ^{233}U (^{232}content, eight parts per million parts uranium) that has been decontaminated by solvent extraction, it will be necessary to purify this material immediately prior to conversion to remove the high-energy ^{232}U daughters that continually grow in. Purification may be achieved by processing through the standard solvent extraction cycle that has been used in the Kilorod[1] program and the ^{233}U Purification and Dispensing Facility.[2] However, since most of this material would meet product specifications if the ^{232}U daughters were removed, we have the option of using a recently developed ion exchange process which effectively reduces the radioactivity to less than 1% of that of ^{233}U containing 8 ppm of ^{232}U in equilibrium with its daughters (i.e., to less than 1 mr per hour per mg of ^{232}U at the distance of 1 ft). This process consists of pumping the uranium feed solution, which is less than 0.5 *N* in HNO_3 and contains 110 g of ^{233}U per liter, through 6 liters of Dowex 50-X12 resin at the rate of 53 liters/hr. The uranium saturates the resin and then breaks through, free of most of the ^{232}U daughters which are more strongly absorbed. The removal of the ^{228}Th and ^{224}Ra results in rapid decay of the other daughter products. The quantities of daughter products in the feed, as compared with the quantities in the product immediately after ion exchange processing and after four days decay, are shown in Fig. 9.1.

Purification of a 20-kg batch of ^{233}U requires 4 hr of process time and provides a week's supply of feed to the oxide conversion line. After purification of each batch, the ion exchange column is eluted with 1.5 *M* HNO_3, and the eluate is recycled to the subsequent batch of feed. This method has proved effective and reproducible during multiple runs in the laboratory. An elution technique for ensuring complete removal of the thorium is presently being developed. Tests have shown that a small volume of fairly concentrated (7.5 *M*) HNO_3 will remove 60% of the thorium, but the volume required to remove 90% of the thorium would be prohibitive.

The advantages of using the ion exchange technique are twofold; first, the six or seven tons of thorium scrap expected to be received from the pellet fabrication line at Bettis can be recovered and purified through the solvent extraction system at the same time that the ion exchange purification step is being carried out; second, the effort required for operations will be reduced by a

---

[1] C. C. Haws, J. L. Matherne, F. W. Miles, and J. E. Van Cleve, *Summary of the Kilorod Project – a Semi-Remote 10 kg/day Demonstration of $^{233}UO_2$-ThO_2 Fuel Element Fabrication by the ORNL Sol-Gel Vibratory Compaction Method*, ORNL-3681 (1965).

[2] J. R. Parrott and R. E. Brooksbank, "The Handling of Kilogram Quantities of ^{233}U by Direct and Remote Methods at the ORNL Central Dispensing Facility," *Proceedings of the 15th Conference on Remote Systems Technology*, American Nuclear Society, Seattle, Wash., 1967.

factor of 3 for the material that can be processed directly through ion exchange. Some ^{233}U feed will contain excessive metallic impurities and thus must be treated, via solvent extraction, in order to meet specifications. The resulting product must, of course, still be processed through the ion exchange system to meet the required specifications regarding thorium content of the product (≤300 ppm).

ORNL Dwg 70-3681-R2

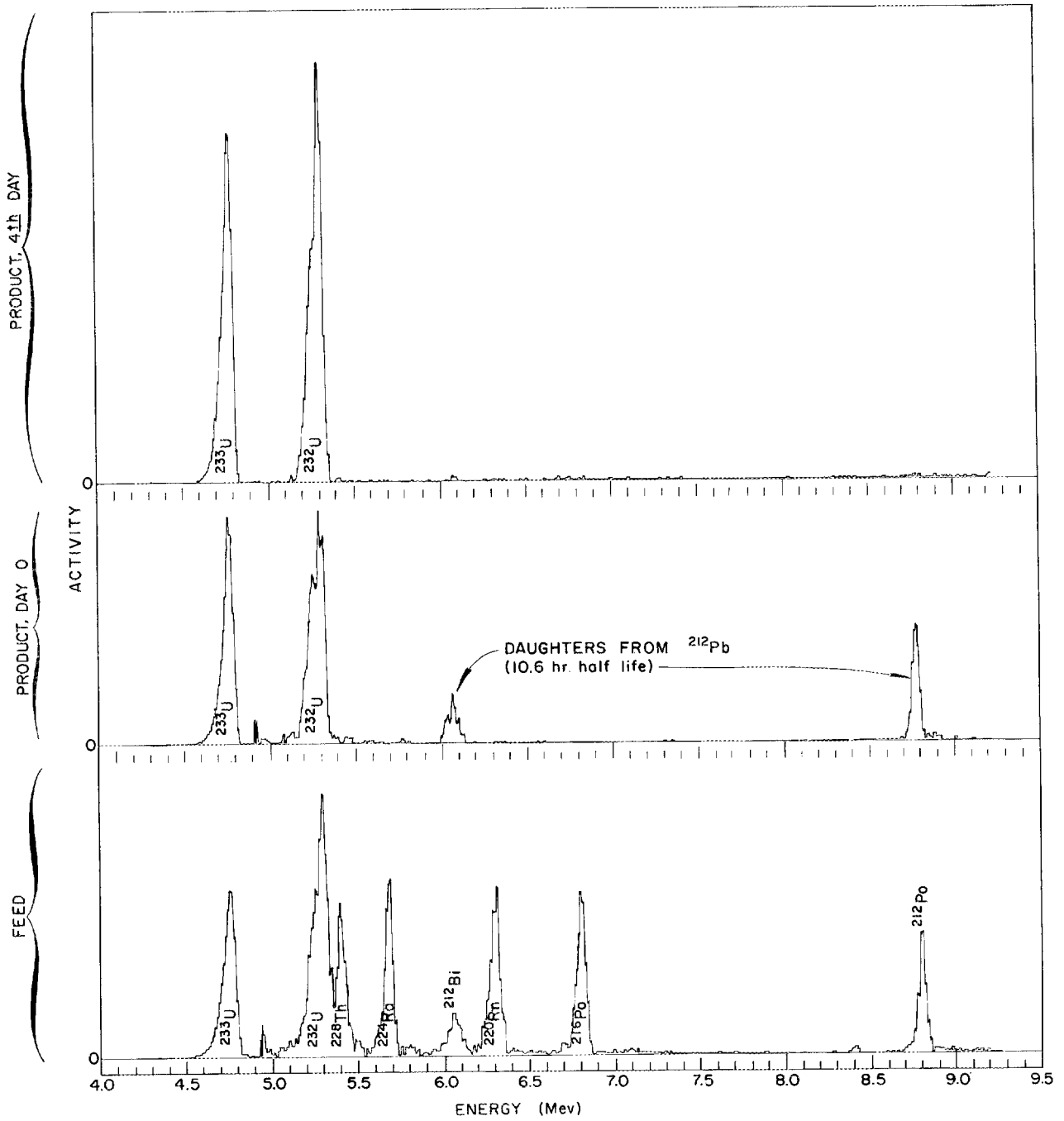

Fig. 9.1. Alpha Energy Spectrum of ^{233}U Solution Containing 8 ppm of ^{232}U Before and After Passage Through Ion Exchange Resin.

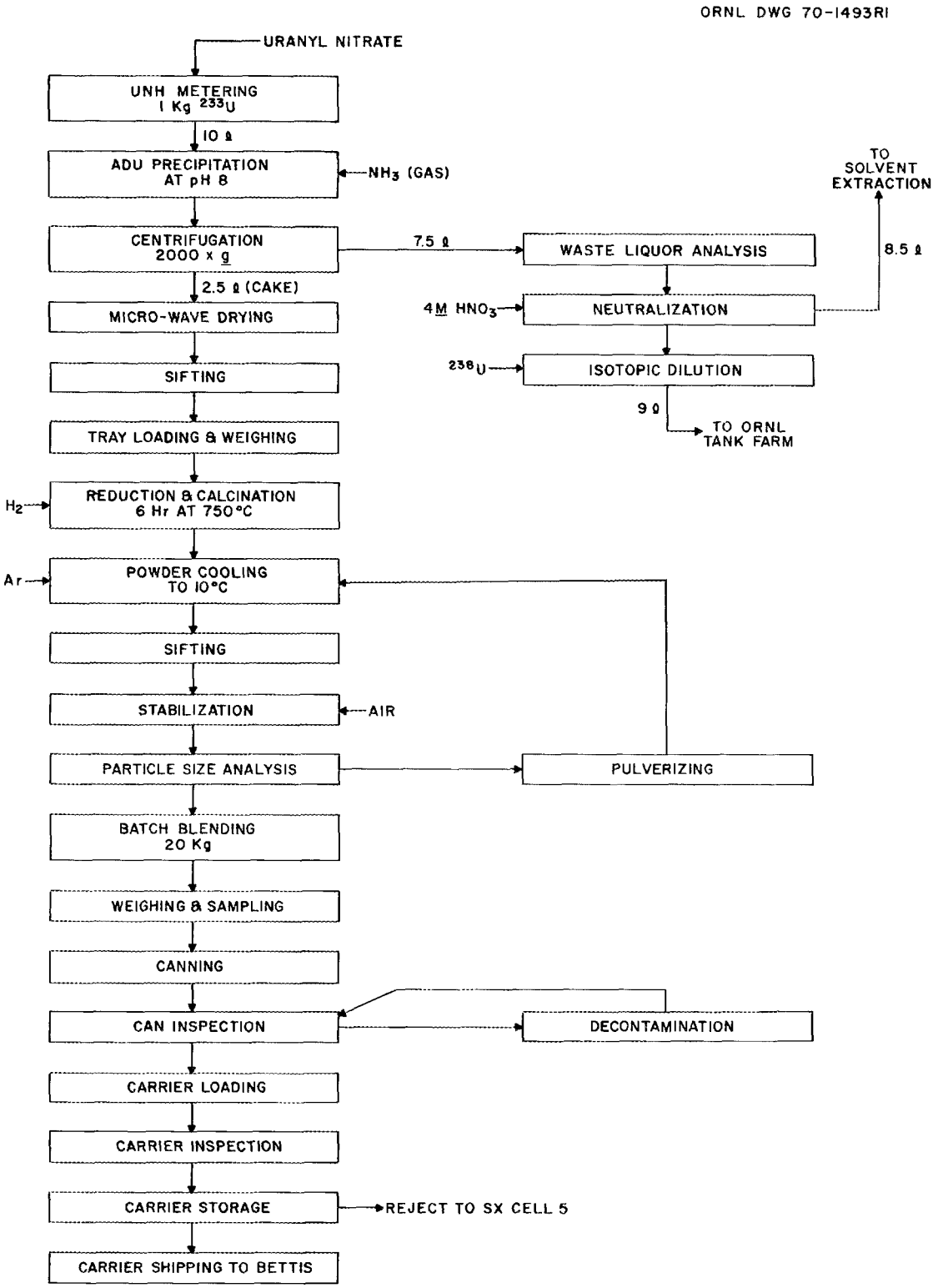

Fig. 9.2. Simplified Chemical Flowsheet for Oxide Conversion.

The development of the flowsheet for the oxide conversion line is the responsibility of the Metals and Ceramics Division, whereas the detailed design of the equipment and the establishment of the operating philosophy are the responsibilities of the Chemical Technology Division. Studies with ^{238}U and ^{235}U indicate that the "standard conversion process," which has been in use for many years at other facilities, can be used to make ceramic-grade $^{233}UO_2$ of satisfactory quality for blending with thoria powder and pressing homogeneous pellets. To date, a total of 2 kg of $^{235}UO_2$ has been shipped to Bettis, where it was made into pellets having desired characteristics. Principal changes that we propose to make in the flowsheet are: (1) the substitution of gaseous ammonia for liquid ammonium hydroxide to facilitate handling and to provide increased purity, and (2) the development and design of a continuous stabilization device following calcination to replace the crude dry-ice technique presently being used. The chemical flowsheet for the oxide conversion line is shown in Fig. 9.2.

9.2 PLANT MODIFICATIONS

Proposed modifications to the existing solvent extraction plant, located in three 20 X 20 X 27 ft cells in Bldg. 3019, are as follows: (1) the design, fabrication, and installation of a scrap dissolver for dissolving the ThO_2-$^{233}UO_2$ scrap from Bettis; (2) the design, fabrication, and installation of the ion exchange thorium-removal system; (3) modifications to existing equipment to provide a solvent wash system; (4) the replacement, or overhaul, of principal pumps and instruments to ensure reliability; and (5) the design, fabrication, and installation of tanks and piping to connect the purification system to the oxide conversion equipment.

The conceptual design of the scrap dissolver is complete, and a review by the ORNL Criticality Review Committee has been requested prior to beginning the detailed design. The proposed batch size is 48.9 kg of thorium, which will contain a maximum of 3.25 kg of ^{233}U at a concentration of 15.4 g/liter. The time required for dissolution is 12 hr, using a 13.0 M HNO_3–0.04 M NaF dissolvent. Computer calculations indicate that a dissolver with a 9-in. diameter is "ever-safe" for thorium scrap containing up to 5.8 wt % ^{233}U, whereas our maximum will be 5.5 wt %.

The design of the vessels, ion exchange column, and piping for the thorium removal system is complete, and fabrication is under way. This system will purify ^{233}U at the rate of 5 kg/hr, but will require complete elution after each 20-kg batch. Four additional vessels will be required.

The requirements for the solvent wash system will be minimal since degradation of the solvent will be negligible. However, it is anticipated that solvent cleanup will be required to remove impurities after every two or three purification runs (25 kg of ^{233}U each). An existing batch mixer will be modified to provide sufficient contact and phase separation.

Replacement pumps and instruments were ordered for the pumps and instruments that perform strategic operations. Replacement transmitters and recorders also have been ordered to replace the outdated ones now in service.

The fabrication of surge tanks to connect the purification system to the oxide conversion line is under way, and the design of the piping has been started.

9.3 DESIGN OF EQUIPMENT FOR THE UO_2 CONVERSION LINE

The UO_2 conversion line, which will be located in alpha enclosures in the basement of Bldg. 3019, will have a capacity of 22 kg of ^{233}U per week and will be operated on a 5-day-per-week, 24-hr-per-day schedule. A schematic diagram of the proposed equipment is shown in Fig. 9.3.

Conceptual drawings of the equipment for precipitation and centrifugation, the furnace tray-loading equipment, the furnace, the furnace unloading station, the powder stabilization equipment, and the solid waste-burning equipment have been prepared. Preliminary operating flowsheets were prepared for each of the above items as well as for the liquid waste-handling equipment. The design of the equipment for the liquid waste-handling enclosure is now complete; fabrication of this enclosure is scheduled to begin shortly.

9.4 STORAGE SYSTEMS

The Savannah River Plant will provide 240 kg of $^{233}UO_3$ and the Hanford Plant will provide 400 kg of ^{233}U as uranyl nitrate solution for the LWBR Program. The material from both plants will be received during 1970; therefore, sufficient storage capacity for this material must be provided at ORNL.

Five additional storage tanks, each with a capacity of 100 kg of ^{233}U at a concentration of 250 g/liter, are presently being installed adjacent to the existing tanks. These tanks (denoted as U-6 through U-10 in Fig. 9.4) will utilize borosilicate-glass raschig rings for neutron absorbers.

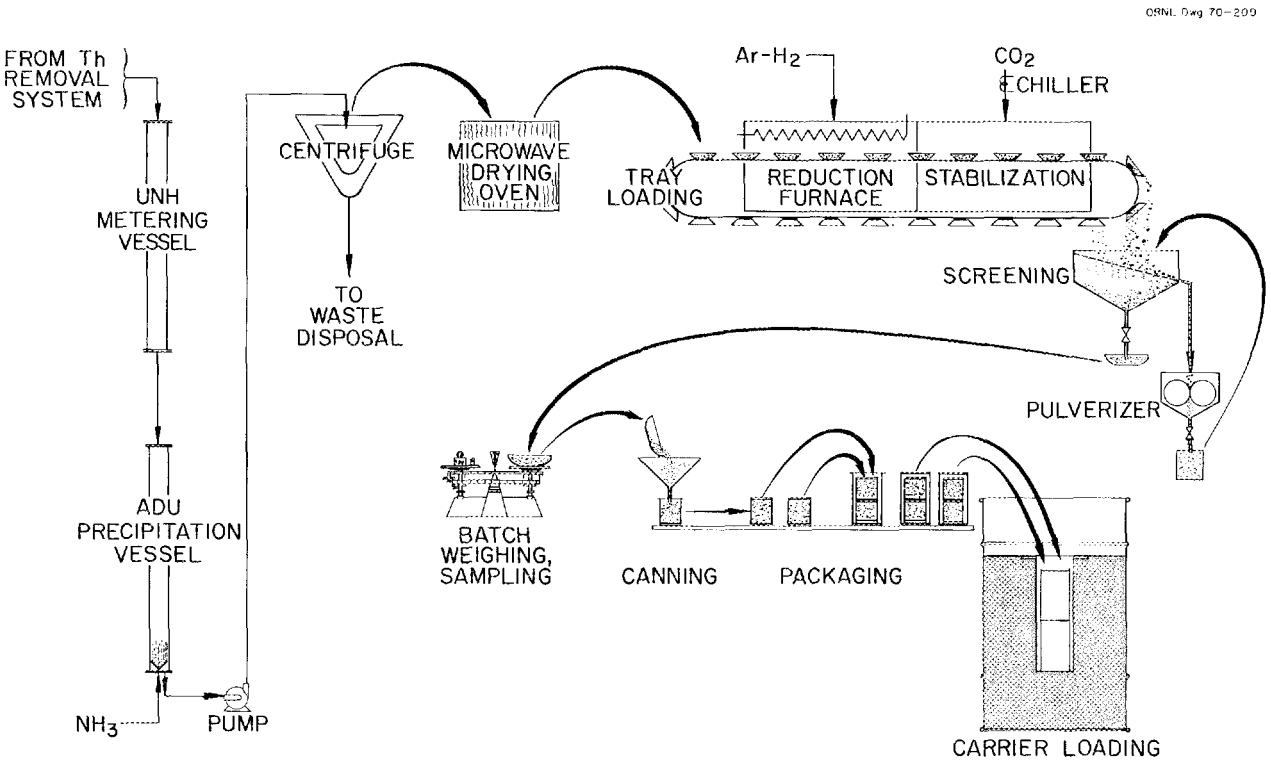

Fig. 9.3. Proposed Equipment for the UO_2 Conversion Line, Bldg. 3019.

The $^{233}UO_3$, which will be received in aluminum cans (900 g of ^{233}U per can) will be stored in nine 4-in.-diam, 15-ft-deep vertical holes that have recently been drilled into the shielding wall between processing cells 2 and 3, Bldg. 3019 (see Fig. 9.5). These holes, which are lined with 4-in.-diam stainless steel pipe, are approved by the ORNL Criticality Committee for the storage of up to 1.5 kg of ^{233}U per linear foot of low-density (1 g/cm^3) powder.

9.5 SITE PREPARATION

The UO_2 conversion line will be located adjacent to the purification system in Bldg. 3019. However, this area presently houses plutonium fuels fabrication equipment, which must be moved to an area in Bldg. 4508 that is presently being renovated for a plutonium fuels fabrication laboratory. The scheduled completion date for the renovation is July 15, 1970.

Modifications to the ^{233}U facility in Bldg. 3019 will include construction of a product storage vault, a new glove-box off-gas system including fan and filters, a chiller for the stabilization system, and miscellaneous minor modifications to the doors, walls, etc. A cost estimate for these modifications is being made.

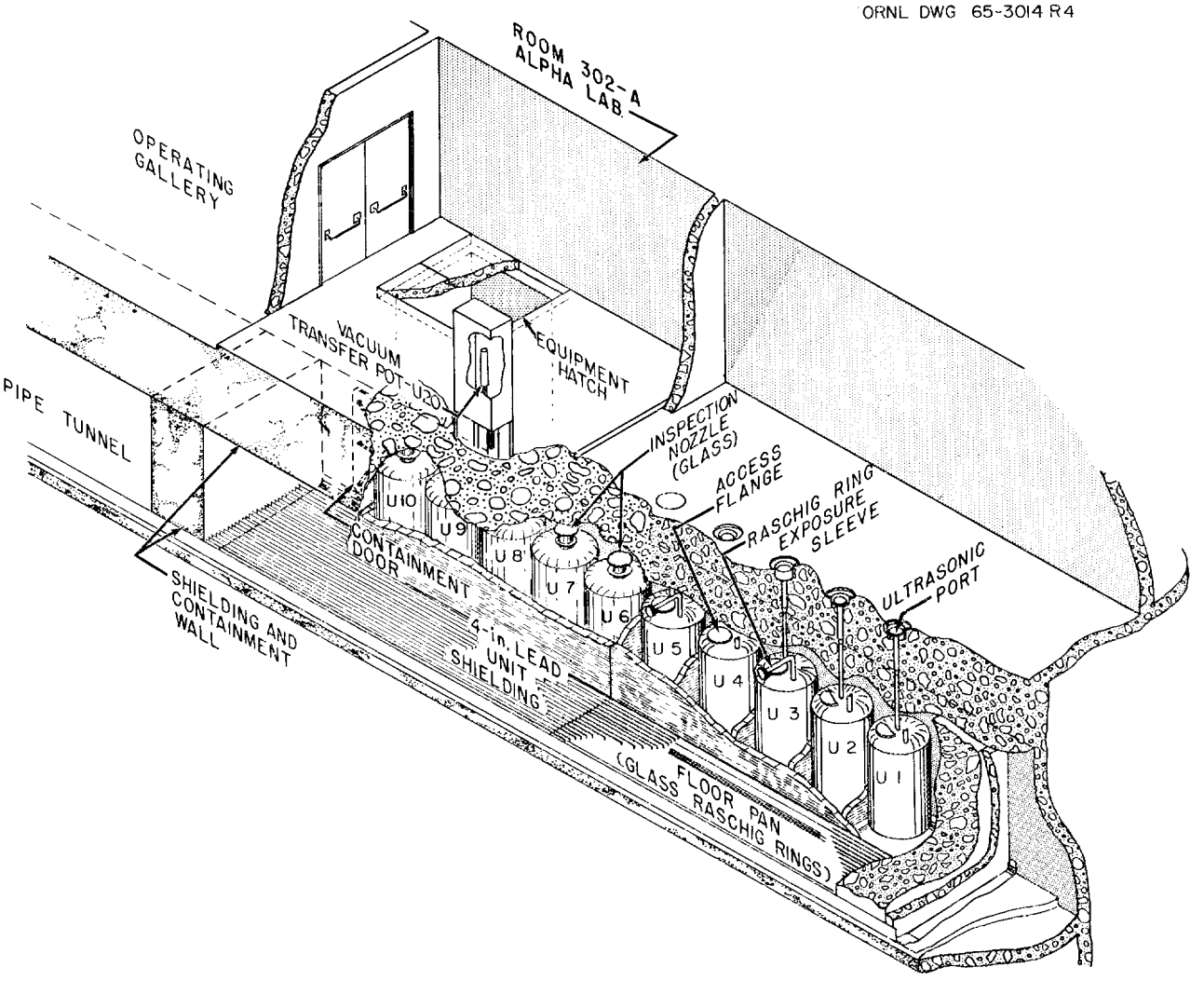

Fig. 9.4. Artist's Conception of ^{233}U Liquid Storage and Related Handling Facilities, Bldg. 3019.

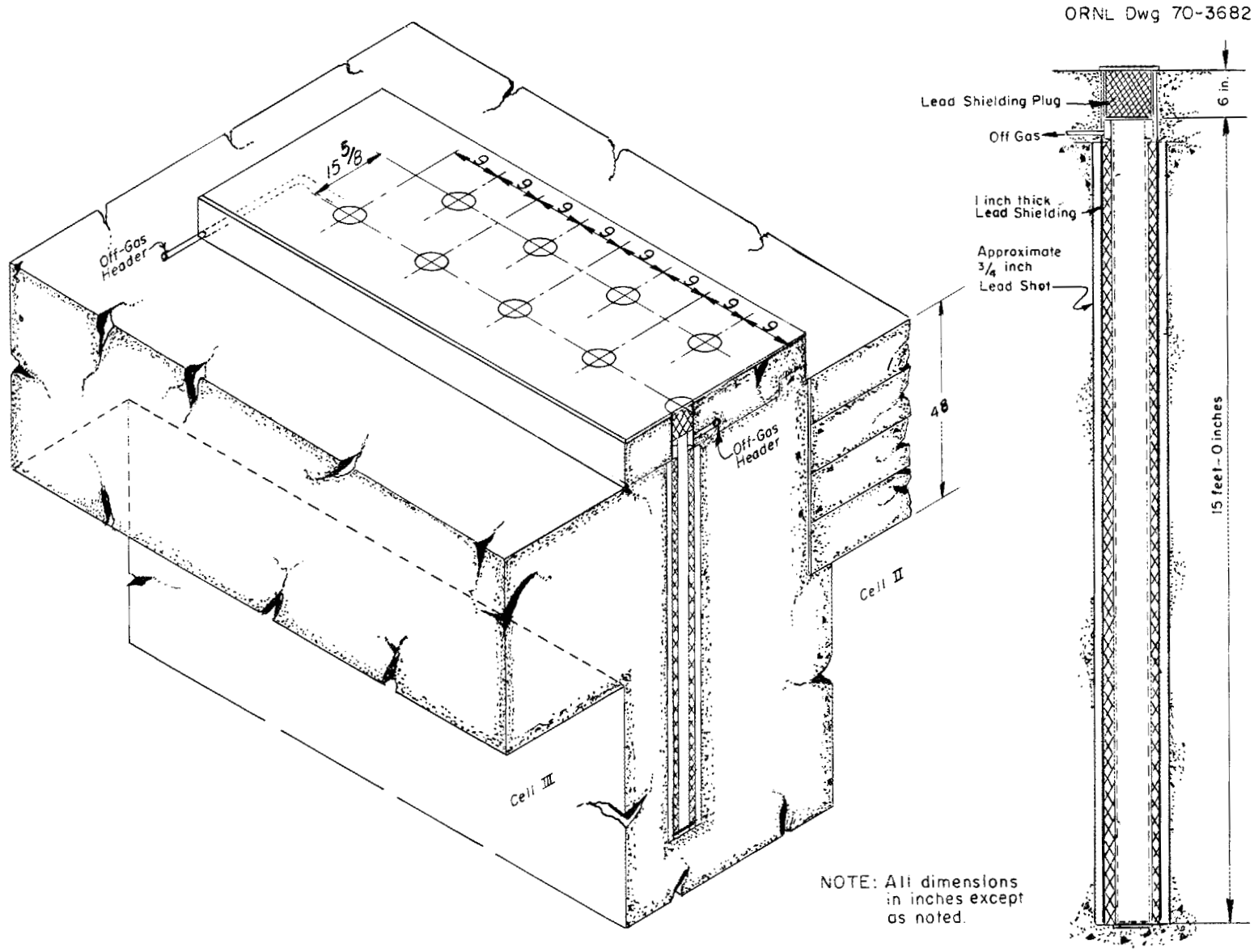

Fig. 9.5. ^{233}U Storage Holes in Cells 2-and 3, Building 3019.

10. Separations Chemistry Research

10.1 EXTRACTION OF METAL SULFATES AND NITRATES BY AMINES

A systematic survey of the extraction of metals from acidic solutions with representative amines was completed. Data for the extraction of selected metals from hydrochloric acid and from acidified lithium chloride solutions were reported previously,[1] while data for acidified lithium sulfate and lithium nitrate solutions were only partially reported.[2–4] The studies reported here complete the work planned for the sulfate and nitrate systems.

Figure 10.1 shows data for the extraction of 19 metals from Li_2SO_4 – 0.2 N H_2SO_4 solutions (ranging from 0.3 to 5 N total sulfate) with 0.1 M solutions of representative primary, secondary, tertiary, and quaternary amines in diethylbenzene. Metals for which extraction coefficients exceeded 1 were: Ru(III), In(III), Sn(II), Ta(V), W(VI), Re(VII), Os(IV), Pt(IV), Au(III), Bi(III), and Th(IV). In a majority of cases, the extraction coefficients were higher for the primary amine than for the other amines, and were not greatly affected by changes in sulfate concentration.

In the $LiNO_3$–0.2 N HNO_3 system (0.5 to 10 N nitrate), the highest extraction coefficients were obtained with the quaternary amine in most cases. The coefficients showed a somewhat stronger dependence on salt concentration in this system than in the sulfate system. Extraction coefficients higher than 1 were obtained only for Ru(III), Re(VII), Os(IV), Pt(IV), Au(III), Bi(III), and Th(IV) (Fig. 10.2). As in the sulfate system, Au(III) was extracted more strongly than any of the other elements.

[1] F. G. Seeley and D. J. Crouse, *J. Chem. Eng. Data* 11(3), 424 (1966).

[2] *Chem. Technol. Div. Ann. Progr. Rept. May 31, 1967*, ORNL-4145, pp. 208–9.

[3] *Chem. Technol. Div. Ann. Progr. Rept. May 31, 1968*, ORNL-4272, p. 174.

[4] *Chem. Technol. Div. Ann. Progr. Rept. May 31, 1969*, ORNL-4422, pp. 252–54.

10.2 NEW SEPARATIONS AGENTS

Methyltrioctylphosphonium (MTOP) Salts

The properties of the dimethylphosphate salt of MTOP and its ready conversion to other salts were reported previously.[5] The extraction of uranium(VI) from acid lithium chloride, nitrate, and sulfate solutions by 0.1 N solutions of the corresponding MTOP salts in 95% diethylbenzene–5% tridecanol was qualitatively similar to extractions with the nearly analogous Adogen 464 (methyltrialkylammonium) compound. The curves of the extraction coefficients obtained with the two extractants vs the lithium salt concentration were closely parallel. The extraction coefficients were higher with the phosphonium compound by a factor of about 10 from chloride and nitrate solutions, but lower by a factor of about 3 from the sulfate solution, than with the ammonium compound. The maximum extraction coefficients with the MTOP salts were about 2×10^4 at the highest chloride (5 to 10 N) and nitrate (8 to 10 N) concentrations tested, but about 10 at the lowest sulfate concentration (0.3 N H_2SO_4). Coefficients for the extraction of U(VI) and Pu(IV) from 3 M nitric acid solution by 0.1 N MTOP nitrate in 92% n-dodecane–8% tridecanol were 0.6 and 20, respectively, as compared with approximately 1 and approximately 100 with Adogen 464 nitrate. This indicates relatively more impairment by free acid of extraction with the phosphonium compound than with the ammonium compound.

Quaternary Ammonium Salt in Polystyrene

A scouting test was made to determine the feasibility of fixing a quaternary ammonium salt in plastic. This test was directed toward obtaining a permanent stationary phase of high-surface, but nonporous, particles for

[5] *Chem. Technol. Div. Ann. Progr. Rept. May 31, 1969*, ORNL-4422, p. 252.

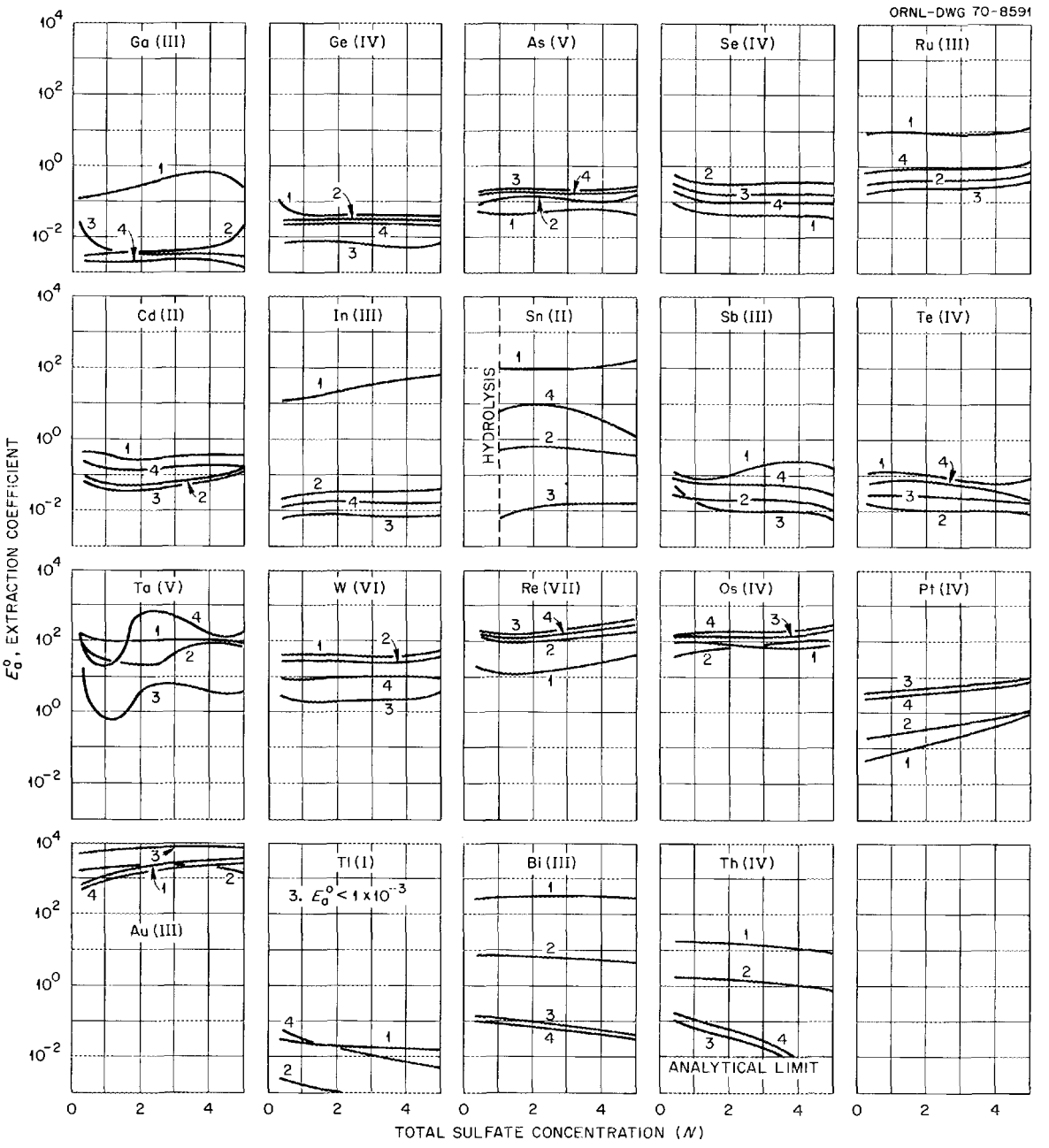

Fig. 10.1. Extraction of Metals from Sulfate Solutions with Amines. Organic phase: 0.1 *M* solutions of (1) Primene JM (RR'R" CNH_2, 18 to 22 carbon atoms), (2) Amberlite LA-1 (RR'R" $CNHC_{12}H_{23}$, 24 to 27 carbon atoms), (3) Adogen 364 (R_3N, R = *n*-octyl, *n*-decyl mixture), (4) Adogen 464 [$R_3(CH_3)N^+$, R = *n*-octyl, *n*-decyl mixture] in diethylbenzene. With Adogen 464, 3 vol % of tridecanol was added to the solvent to prevent the formation of a third phase. Amines were in the sulfate form. Aqueous phase: 0.01 *M* metal ion in Li_2SO_4–0.2 *N* H_2SO_4. Contact: 10 min at a phase ratio of 1:1.

use in the anion exchange chromatography of macromolecules. Hexadecyltrimethylammonium bromide was dissolved in a chloroform solution of polystyrene to give a solution containing 0.25 meq of the bromide per gram of plastic. This solution was then dispersed in a violently stirred aqueous sodium chloride solution. We wanted to test our hypothesis that the ammonium salt would concentrate at the aqueous-organic interface as a surfactant and thus stabilize microdroplets, and then remain trapped at the surface of the resulting plastic microspheres as the chloroform escaped. Although most of the plastic agglomerated, a small

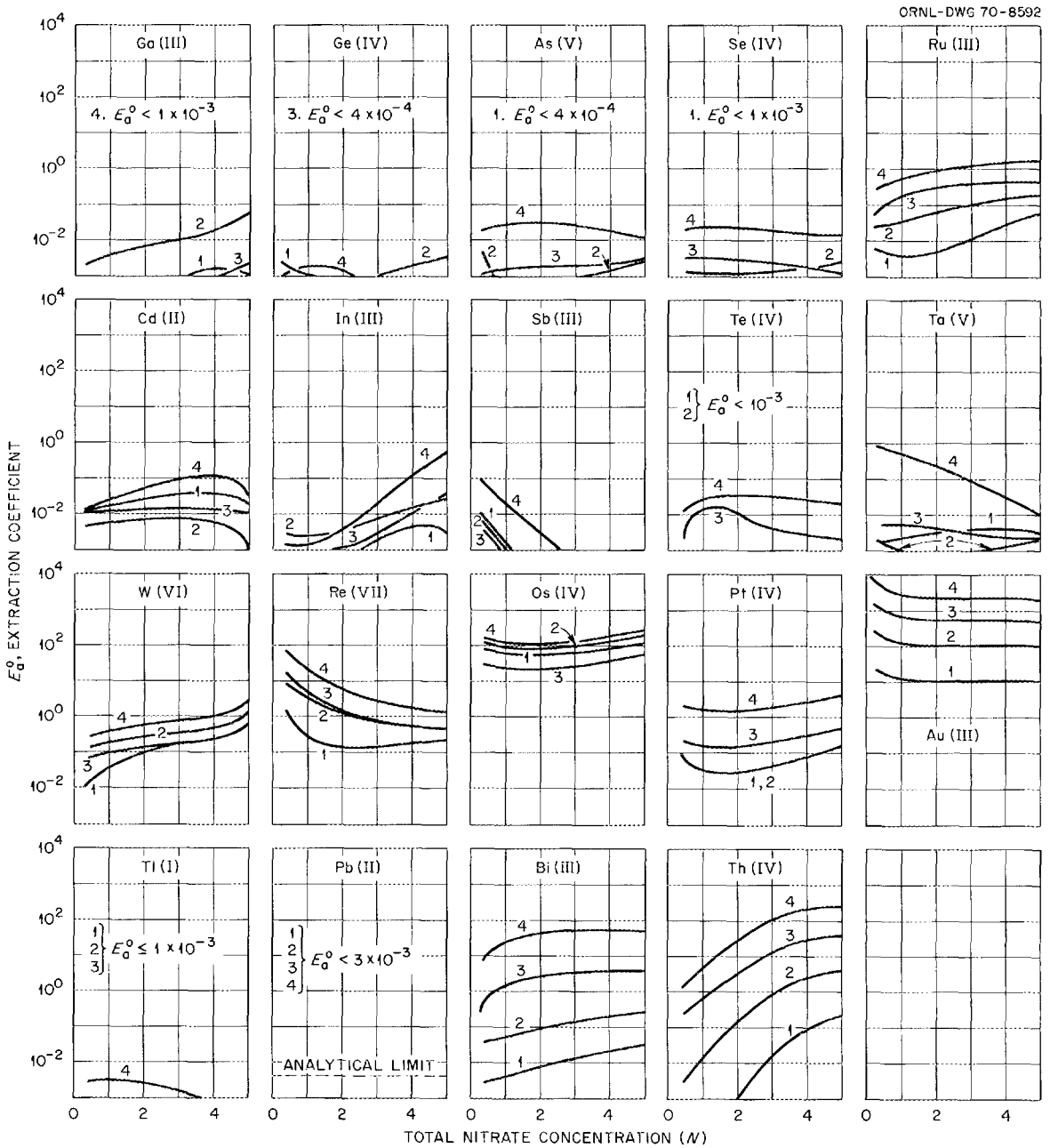

Fig. 10.2. Extraction of Metals from Nitrate Solutions with Amines. Organic phase: 0.1 *M* solutions of (1) Primene JM, (2) Amberlite LA-1, (3) Adogen 364, (4) Adogen 464 in diethylbenzene. With Adogen 464, 3 vol % of tridecanol was added to the solvent to prevent the formation of a third phase. Amines were converted to the nitrate form just prior to use in the extraction tests. Aqueous phase: 0.01 *M* metal ion in $LiNO_3$–0.2 *N* HNO_3. Contact: 10 min at a phase ratio of 1:1.

quantity of nonsettling microbeads or granules that appeared to be near 10 μ was obtained. After all the sodium halide had been removed by dialysis, the dried and weighed fines fraction was slurried in glacial acetic acid and titrated with perchloric acid/dioxane in the presence of mercuric acetate. The content of quaternary ammonium halide was found to be 1.2 meq per gram of plastic; this shows that the halide had been concentrated into the fines, presumably as a surfactant. Also, the amount detected had to be present at the surface of the plastic, since other tests have shown that the plastic does not dissolve in the titration medium. This result is encouraging for further tests of a finely divided surface-ion-exchange material.

Infrared Spectra of Dialkyl Sulfoxides

The synthesis of three unsymmetrical dialkyl sulfoxides (methyl 3-ethylheptyl, methyl 4,8-dimethylnonyl, and methyl pentadecyl sulfoxide) was previously reported.[5] Infrared spectra of these compounds have now been obtained, both as 0.1 *M* solutions in *n*-octane and as undiluted thin films. The spectra are rather simple, showing the symmetric and asymmetric CH stretch and the symmetric and asymmetric CH_3 deformation bands that are characteristic of all organic compounds containing these groups. The S-O stretch frequency appeared at 1065 cm^{-1} for the *n*-octane solutions and at 1040 cm^{-1} for the undiluted compounds. There were no meaningful differences in these band positions among the three compounds. Although differences were observed in the CH_3 rocking frequencies[6] at 900 to 1200 cm^{-1}, we found no differences in any position of the spectra which could correlate with the large difference in extraction observed for these compounds (Sect. 10.6). However, the absence of dissimilarities in bands does not necessarily imply a similarity in the electron donating ability of the donor group. Examination of the spectra of the metal complexes of these compounds should resolve this uncertainty.

10.3 BERYLLIUM PURIFICATION BY SOLVENT EXTRACTION

New and potentially less-expensive methods are being investigated for preparing high-purity beryllium compounds for reactor use, starting with beryllium concentrates such as those obtained by amine extraction or di(2-ethylhexyl)phosphoric acid extraction of low-grade beryllium ore leach liquors. Major emphasis has been on the development of a purification process[7-9] that uses quaternary alkylammonium extractants to recover beryllium from a carbonate solution of the beryllium concentrate. The beryllium is stripped from the solvent with 2 to 2.5 *M* NH_4HCO_3 and is precipitated as the hydroxide from this solution by heating.

The development of the quaternary ammonium extraction process has been completed. Results of recent tests show that the relatively high boron content of the beryllium products[9] is significantly decreased by adding a boron complexing agent to the process solutions.

Effect of Boron Complexing Agents

Since polyhydroxy alcohols are known to complex boron, we tested several compounds of this type in various stages of the beryllium purification flowsheet. Mannitol was found to be the most effective. With a feed solution containing 50 to 100 parts of boron per million parts of BeO, making the feed and scrub solutions 0.0005 to 0.001 *M* in mannitol reduced the boron content of the product to 5 ppm. This is a significant decrease over the content found (30 ppm) when mannitol was not added.

10.4 RECOVERY OF URANIUM FROM COMMERCIAL PHOSPHORIC ACID

Promising solvent extraction processes, using di(2-ethylhexyl)phosphoric acid (D2EHPA) plus trioctylphosphine oxide (TOPO) as the extractant, were developed and tested for recovering uranium from wet-process phosphoric acid. Commercial phosphoric acid produced from Florida phosphate rock contains 0.1 to 0.2 g of uranium per liter and represents a potential source of about 2000 tons of U_3O_8 per year.

Good results were obtained in bench-scale continuous tests of the original process,[10] which uses ammonium carbonate solution for stripping uranium from the solvent extract. However, a new process, using reductive stripping, appears to have considerable economic advantage over the original method. In the new process, the uranium is reduced with Fe(II) and stripped from the solvent to give a relatively concentrated uranium solution that is highly amenable to processing in a second extraction cycle.

Carbonate Stripping Process

Continuous demonstrations of the process flowsheet were made in a mixer-settler test array, using 0.5 *M* D2EHPA–0.125 *M* TOPO in kerosene to recover uranium from samples of wet-process acid obtained from two commercial phosphate plants. The samples ranged from 5.4 to 5.9 *M* in H_3PO_4 and contained 0.14 to 0.17 g of uranium per liter, plus the following

[6] The original assignments of bands in sulfoxide were made by F. A. Cotton, R. Francis, and W. D. Horrocks, *J. Phys. Chem.* **64**, 1534 (1960).

[7] *Chem. Technol. Div. Ann. Progr. Rept. May 31, 1967*, ORNL-4145, pp. 215–17.

[8] *Chem. Technol. Div. Ann. Progr. Rept. May 31, 1968*, ORNL-4272, pp. 175–77.

[9] *Chem. Technol. Div. Ann. Progr. Rept. May 31, 1969*, ORNL-4422, pp. 255–56.

[10] *Chem. Technol. Div. Ann. Progr. Rept. May 31, 1969*, ORNL-4422, pp. 256–59.

impurities (concentration in g/liter): 6 to 12 Fe, 3.5 to 5 Al, 27 to 33 SO_4, and 26 to 30 F. From 0.3 to 0.8 g of iron per liter was divalent, and about 50% of the uranium was present as U(IV). Prior to extraction, the liquors were treated with one-sixth mole of $NaClO_3$ per mole of Fe(II) to ensure complete oxidation of the uranium to U(VI), its most extractable form.

Typically, about 90% of the uranium was recovered in four extraction stages at 40°C, using an organic/aqueous phase ratio of 3. The extract was scrubbed with water (equivalent to one-fifth the volume of the extract) in two stages to remove extracted phosphoric acid and was then stripped in two stages with ammonium carbonate–ammonium hydroxide solution at 45°C.

Physical operation of the system has been encouraging. To avoid emulsions, the extraction contactors are operated with the organic phase as the continuous phase; the stripping contactors are operated in the aqueous-continuous mode. Under these conditions, primary separation of the phases in both systems is reasonably rapid. Solids accumulate at the aqueous/organic interface in the extraction settlers but do not interfere with the operation. Although the band of solids at the interface appears soon after the start of the run, the thickness of the band reaches a certain level and then increases very slowly with extended operation. Eventually some provision would have to be made for removing the solids from the settlers.

Measurements showed that about 0.2 gal of solvent was lost by entrainment per 1000 gal of raffinate; passing the raffinate continuously through a vessel with a 0.5-hr solution holdup capacity decreased the entrainment loss to less than 0.1 gal per 1000 gal of raffinate. These measurements are encouraging since they are at the low end of those used for preliminary estimates[11] of the process reagent costs.

The strip product solutions, which contained about 5 g of uranium per liter, were filtered to remove precipitated iron and then heated to the boiling point to volatilize ammonia and carbon dioxide and to precipitate uranium. After being washed and calcined at 850°C, the precipitates were analyzed and found to contain 85.6 to 92.3% U_3O_8, 2.8 to 4.6% PO_4, and 1.7 to 3.9% Fe_2O_3. The product recovery portion of the flowsheet, as presently developed, is not wholly satisfactory. Filtration of the colloidal iron precipitate from the solution prior to uranium precipitation is slow and difficult. In addition, the recovery of uranium from the strip solution is hampered by the presence of dissolved organic matter (presumably humates, which complex uranium and prevent its complete precipitation) that is extracted from the wet-process phosphoric acid and accumulates in the strip product solution. Uranium recoveries have been in the range of 90 to 95% in most of the precipitation tests. The relatively high phosphate contamination of the products is also a disadvantage.

[11] F. J. Hurst, D. J. Crouse, and K. B. Brown, *Solvent Extraction of Uranium from Wet-Process Phosphoric Acid*, ORNL-TM-2522 (April 1969).

Reductive Stripping Process

Based on initial results, the reductive stripping process avoids many of the problems associated with the carbonate stripping flowsheet. The uranium is first reduced to the less-extractable tetravalent state by contact with a solution that is about 6 *M* in H_3PO_4 and contains 10 to 20 g of Fe(II) per liter. We have found it convenient (and inexpensive) to borrow a small volume of the raffinate from the extraction system for stripping since this solution is suitably concentrated in H_3PO_4 and, after reduction with iron metal, contains a suitable concentration of Fe(II). For best results, excessive contact of the solutions with air must be avoided. Under the proper conditions, uranium product solutions containing about 12 g of uranium per liter are readily obtained. Intrastage recycle of the aqueous phase from the settler to the mixer is provided in order to give an aqueous/organic phase ratio of about 2 in the mixer. This provision and operation at 45 to 50°C ensure that a sufficient fraction of the U(VI) in the solvent phase will be transferred to the aqueous phase [and will be made available for reaction with Fe(II)] to give suitably rapid reduction kinetics.

Figure 10.3 shows the solution flow rates and the distribution of uranium in the system at steady state in a typical continuous run. Uranium recovery in four extraction and two strip stages was about 96%. In this run, the aqueous solution that was recycled from the settler to the mixer of the first stripping stage was passed through an electrolytic cell to maintain the iron in the solution in the divalent state. Subsequent tests have shown that the electrolytic cell is not necessary.

The uranium in the strip product solution is oxidized electrolytically or with air to the hexavalent state and then extracted with 0.25 *M* D2EHPA–0.05 *M* TOPO. The extract is scrubbed with water (to remove phosphoric acid) and then stripped with an ammonium carbonate–ammonium hydroxide solution under conditions that result in direct precipitation of rapid-filtering ammonium uranyl tricarbonate (AUT) from the

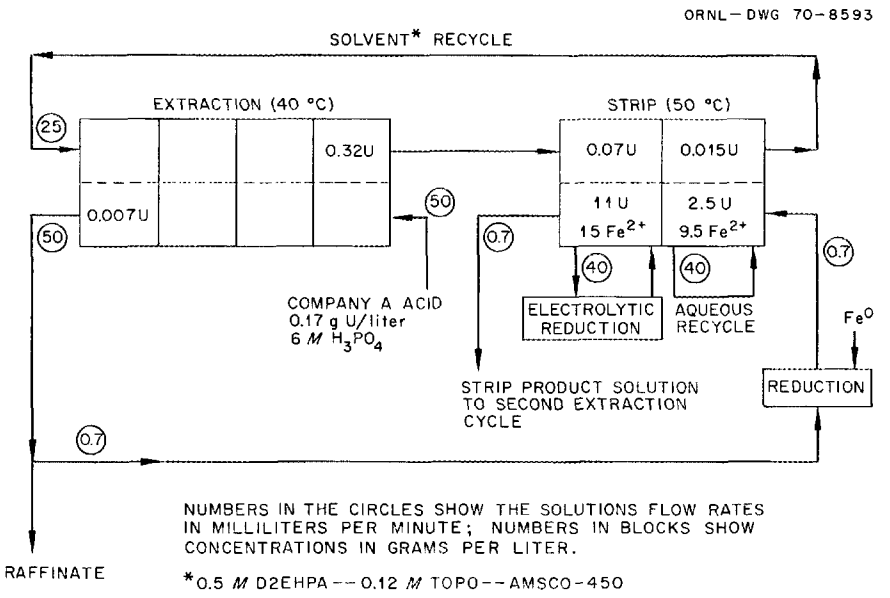

Fig. 10.3. Continuous Mixer-Settler Demonstration of Uranium Recovery from Phosphoric Acid, Utilizing a Reductive Strip.

solvent.[12] The AUT is calcined to U_3O_8. Because the concentration of uranium in the feed solution is high (11 g/liter), the solvent can be efficiently loaded with uranium, and the uranium can be more effectively separated from contaminants than in the first extraction cycle. Therefore, the consumption of ammonia per pound of uranium in stripping is much (about a factor of 20) lower than when the first-cycle extract is stripped directly with a carbonate solution.

Chemical reagent costs for the reductive stripping process, unlike those for the carbonate stripping process, are not very sensitive to the uranium content (loading) of the solvent that is achieved in extraction. Consequently, lower loadings, which result in better uranium recoveries at the higher solvent pumping rates, can be accepted. The higher recoveries, lower reagent costs, easier product recovery, and higher-purity products give the reductive stripping process a significant economic advantage over the carbonate stripping process.

10.5 DISPLACEMENT ELUTION OF TRANSPLUTONIUM ACTINIDES FROM ION EXCHANGE RESINS

We have continued our work aimed at the development of a process for separating the transuranium elements from the fission product lanthanides by displacement elution with aminopolyacetic acids.[13] The process consists of elution of the elements from a cation exchange resin with an aminopolyacetic acid in which the stability constants of the transplutonium elements are somewhat greater than those of the lanthanides. Three eluting agents were employed in the most recent tests: iminodiacetic acid (IDA), nitrilotriacetic acid (NTA), and hydroxyethylethylenediaminetriacetic acid (HEDTA). A combination of either IDA or NTA with HEDTA was found to give enhanced separation of the transplutonium elements from the fission product lanthanides.

Tests of the elution of californium, curium, and americium from a hydrogen-form cation exchange resin column by HEDTA have shown that californium is eluted slightly ahead of curium, decontaminated from americium and curium by a factor of about 10^3. This is adequate for an initial separation technique. Approximately 80% of the curium and the americum were obtained as relatively pure ($\geq$95%) products; the remaining 20% was in the area between the two bands. The transplutonium elements were eluted slightly ahead of the lanthanides; however, the tail of the americium contained a small amount of ^{152}Eu.

Attempts were made to improve the californium separation by means of a "wedge," that is, by the

[12] F. J. Hurst and D. J. Crouse, *Recovery of Uranium from Di(2-ethylhexyl) Phosphoric Acid (DAPEX) Extractant with Ammonium Carbonates*, ORNL-2952 (June 1960).

[13] *Chem. Technol. Div. Ann. Progr. Rept. May 31, 1969*, ORNL-4422, pp. 261–62.

presence of a metal ion with a stability constant between that of curium and californium. Lead, which has a stability constant in this region, was used in an attempt to achieve such a wedge. Although lead was eluted between curium and californium, it did not increase the separation of the latter elements; it merely spread between and overlapped onto their positions.

The initial work with the aminopolyacetic acids as displacement elution agents has been promising; thus equipment is being built for an equipment rack in cell 5 of the Transuranium Processing Plant (TRU) to further evaluate the possibilities of using this class of eluting agents for primary separations at TRU.

10.6 DISTRIBUTION EQUILIBRIA AND MECHANISMS

Extraction by Dialkyl Sulfoxides

The current study of extractions by dialkyl sulfoxides was completed, and a paper was prepared for submission to the *Journal of Inorganic and Nuclear Chemistry*. Its abstract follows:

"Unsymmetrical Dialkylsulfoxides as Extractants: I. Preparation and Extraction Surveys with Three Sulfoxides. II. Equilibria and Species in Iron(III) Extraction by Methyl-4,8-dimethylnonylsulfoxide," by W. J. McDowell and H. D. Harmon. *Abstract:* Methyl-3-ethylheptyl sulfoxide (Me-3EHSO), methyl-4,8-dimethylnonyl sulfoxide (Me-4,8-DMNSO), and methyl pentadecyl sulfoxide (Me-PDSO) were synthesized and their extraction properties were studied. The extraction of iron, cobalt, manganese, sodium, calcium, and europium from concentrated HCl solutions was investigated. The metals were extracted in the order Fe $\gg$ Co $>$ Mn $>$ Ca $>$ Na $>$ Eu. Extraction peaks came at 8 to 10 *M* HCl. By extraction power, the sulfoxides ranged Me-4,8-DMNSO $>$ Me-3EHSO $>$ Me-PDSO. A detailed study of the extraction of iron by 0.100 *M* Me-4,8-DMNSO in *p*-xylene indicated that 2 to 3 molecules of sulfoxides are associated with each iron (as $FeCl_3$ or $HFeCl_4$) in the organic phase.

Aqueous Americium Thiocyanate Complexes

We are investigating the aqueous thiocyanate complexes of trivalent actinides (and lanthanides). In a preliminary examination, contradictory qualitative results were obtained from distribution methods vs electromigration and spectrophotometry. From published information,[14-16] we would expect to find cationic, neutral, and anionic complexes. Distribution measurements (TBP extraction, liquid anion exchange extraction, and resinous anion exchange sorption) gave distribution coefficients for americium that continually increased as the thiocyanate concentration increased. This is the behavior expected when only cationic species predominate. On the other hand, electromigration showed significant proportions of americium traveling toward the anode, and spectrophotometric measurements of americium solutions showed plateaus or inflections (in the plot of peak wavelength vs thiocyanate concentration) that are consistent with the successive formation of cationic, neutral, and anionic complexes. At this point, it appears certain that neutral and anionic americium thiocyanate complexes do exist, and that the distribution behavior is perturbed by factors which can be ignored in some cases but not in this system. Such results may raise a question as to the general validity of accepted methods for investigating complexes by distribution; therefore, studies will be made to resolve this point.

Distribution Equilibria. – Two extractants, tributyl phosphate and Adogen 464 (methyltrialkylammonium) thiocyanate, were tested. (Nonyldecylamine, an excellent extractant for americium sulfate, is ineffective for americium thiocyanate.) Both of these extracted negligible amounts of KSCN but considerable amounts of HSCN. Extractions with "constant" organic-phase compositions[17] gave the following extraction coefficients (together with resin distribution coefficients described below):

Aq. KSCN (*M*)	E_{Am}		D_{Am}
	0.5 *M* TBP	0.2 *M* Adogen·SCN	Dowex-1·SCN
0.13	0.15	0.6	
1.0	6	2.5	10
2.0	24	120	50
5.0	140	1400	600
10.0	240	3400	4800

The resulting equilibrium aqueous pH's ranged from 1.4 to 3.3 with both extractants.

The resin sorption coefficients tabulated above were from distributions into Dowex 1-X8 from aqueous thiocyanate solutions at an equilibrium pH of 2.0. Results were similar when the initial aqueous solutions were uniform at 0.01 *N* HSCN (equilibrium pH, 2.2 to 2.8) and also with Dowex 1-X10 (Bio-Rad AG1-X10).

[14] T. Sekine, *Acta Chem. Scand.* **19**, 1519 (1965).

[15] G. R. Choppin and J. Ketels, *J. Inorg. Nucl. Chem.* **27**, 1335 (1965).

[16] I. A. Lebedev and G. N. Yakovlev, *Radiokhim.* **4**, 3042 (1962).

[17] Extraction with a "constant" organic-phase composition means that each aqueous solution was equilibrated with a succession of portions of the same organic solution until no further transfer of acid occurred.

If neutral and anionic americium thiocyanate complexes do exist, the failure of the extraction coefficients to reach a maximum and decrease with increasing thiocyanate concentration may result from failure of either or both of the assumptions that (1) the equilibrium organic-phase compositions depend only on the thiocyanic acid activity, or (2) the activity coefficient of a neutral complex is independent of the ionic strength. (Both of these assumptions appear to be valid in several sulfate systems.) Assumption (2) also applies to resin sorption, while (1) must be replaced by a partially analogous assumption involving Donnan invasion. Hence, the similar behavior in extraction and sorption suggests that (2) may be more important than (1).

Electromigration. – A cell (three compartments separated by medium-porosity glass frits) was filled with 0.1, 1.0, or 10 *M* KSCN solution; then a small amount of $^{241}Am(SCN)_3$ was added to the center compartment, and sufficient current was passed through the cell to produce noticeable electrolysis of the water. Drop-size samples were removed at intervals until enough americium had migrated for accurate analysis; this never required more than 30 min. Parallel tests indicated that transport by diffusion was negligible. In each case, migration occurred toward both electrodes. The results, which were only qualitative and provided no information on transference numbers, suggest that anionic species are significant at 0.1 *M* KSCN and predominate at 10 *M* KSCN.

Spectrophotometry. – A stock solution of 0.0110 *M* $^{243}Am(ClO_4)_3$ (containing 0.17 mole % ^{241}Am and 0.02 mole % ^{244}Cm) was diluted to 0.001 *M* with 0 to 10 *M* KSCN solutions at pH 2. Spectral scans from 4800 to 5300 A at 1-cm path length were made with a Cary model 14 spectrophotometer modified for alpha containment. Both the peak wavelength and the molar absorptivity of the 5029-A americium band increased with increasing thiocyanate concentration, indicating continuously increasing formation of complex. The peak wavelength shift, from 5029 A for less than 0.05 *M* KSCN to 5092 A for 10 *M* KSCN, showed definite plateaus at 5034 and 5038 A, and inflections near 5045, 5055, and 5075 A. If these indicate predominance of successive complex species, they presumably correspond to $AmSCN^{2+}$, $Am(SCN)_2^+$, $Am(SCN)_3$, $Am(SCN)_4^-$, and $Am(SCN)_5^{2-}$. On this basis, the formation constant for the first complex, $AmSCN^{2+}$, was evaluated, by the method described by Delle Site and Baybarz,[18] from absorbances at 5029 A in the presence of 0.0084, 0.084, and 0.18 *M* KSCN. The average of the results, individually corrected to zero ionic strength by the Debye-Hückel equation, compare as follows with published values which we have similarly adjusted to zero ionic strength:

K_1	Original Medium	Ref.
50 ± 12		Present work
261	5 *M* $NaClO_4$	14
52.9	1 *M* $NaClO_4$	15
51.2	0.5 *M* NH_4ClO_4	16
64.1	5 *M* $NaClO_4$	16

We expect the continuing spectral study to permit evaluation of additional formation constants.

Liquid-Scintillation Analysis of Heavy Actinides

The use of solvent extraction equilibria to study the solution chemistry of the transplutonium actinides (cf. the preceding section, and the discussion on actinide sulfate complexes in Sect. 5.7) requires a large number of analyses; hence an analytical method that is simple and rapid, while also accurate and highly sensitive, is needed. To date, the only analytical method to meet these requirements is liquid scintillation counting. An essential part of the development of this method was the incorporation of an organic extractant in the organic scintillator solution to extract the actinide ions from aqueous samples. This eliminates the need for solubilizers or emulsifiers for aqueous samples. A paper has been prepared for presentation at the International Conference on Liquid Scintillation, San Francisco, 1970. Its abstract follows:

"Liquid Scintillation Counting Techniques for the Higher Actinides," by W. J. McDowell. *Abstract:* Liquid scintillation counting procedures developed in studies of the aqueous complexes of the trivalent transplutonium actinides and having 100 percent counting efficiency, high accuracy and very simple, convenient sample preparation are described. Liquid scintillation spectra are presented for ^{233}U, ^{241}Am, ^{243}Am, ^{244}Cm, ^{249}Bk, ^{252}Cf, and ^{252}Es taken both on a commerical liquid scintillation detector (Packard Tri-Carb) and a single phototube instrument built according to a recently published design for optimum energy resolution.[19] Both instruments give a linear relationship between alpha energy peak and channel number. The commercial instrument gave an average alpha energy resolution of 26 percent while the ORNL-built detector gave 8.2 percent. Under some favorable conditions it was possible to count one actinide in the presence of others or in the presence of other radiotracer impurities. Conditions for and examples where this was done are given. A simple extractive scintillator

[18] A. Delle Site and R. D. Baybarz, *J. Inorg. Nucl. Chem.* **31**, 2201 (1969).

[19] D. L. Horrocks, *Rev. Sci. Instr.* **35**, 334–40 (1964).

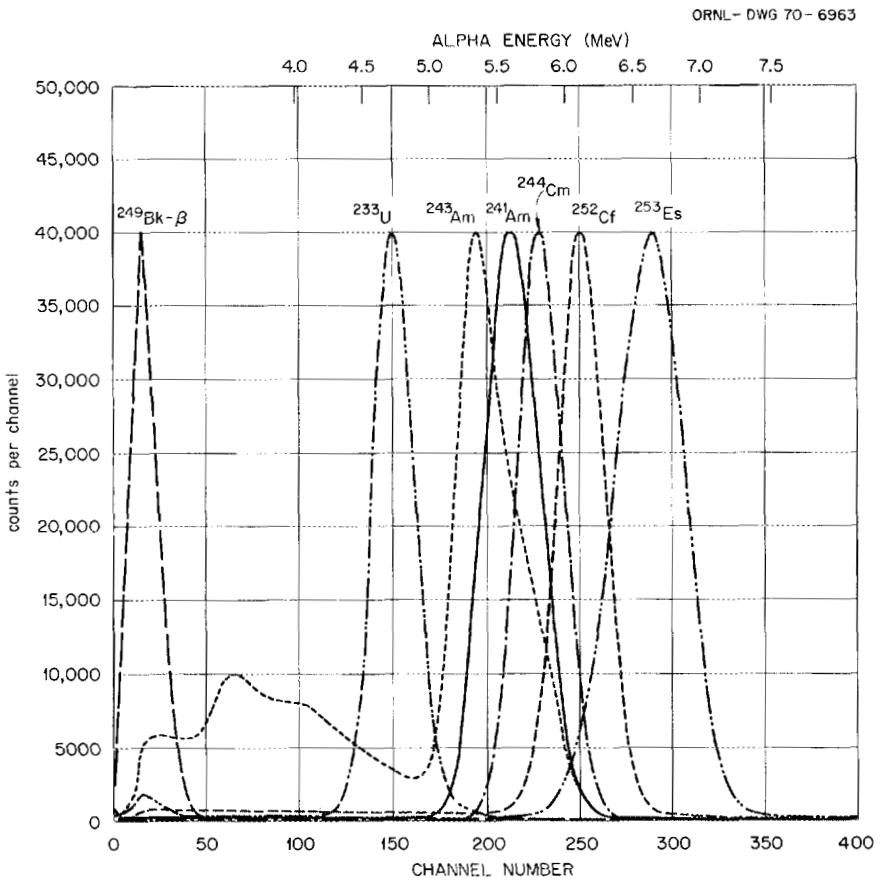

Fig. 10.4 Liquid Scintillation Spectra of Selected Actinide Nuclides Using a Single-Phototube Detector.

consisting of PPO and Me_2POPOP plus a suitable extractant[20] in toluene was shown to be an effective means of placing the aqueous actinides and other radionuclides in the scintillation medium. It was demonstrated that subsequent removal of the barren aqueous phase from contact with the scintillator was not necessary, that the same counting efficiency was obtained with and without bulk water present and that liquid scintillation spectra obtained with bulk water present gave as good, or better, resolution than those taken from dry scintillation solutions.

In order to make certain that the counting was reflecting only the concentration of the desired nuclide and that no interferences from other radioelements or from background were present, both surface barrier detector (electroplated plate) spectra and liquid scintillation spectra were obtained for the elements under examination. Liquid scintillation spectra were obtained using both the commercial detector (which was used to count most of the routine samples) and the single-phototube detector, which was designed to give improved energy resolution at the expense of low-energy sensitivity. A multichannel analyzer was used to analyze and record the spectra from both detectors. Figure 10.4 shows the spectra obtained with the single-phototube detector; ^{233}U was included to aid in the calibration of the alpha energy—channel number scale. The linear relationship between alpha energy and channel number is shown by the two abscissas of Fig. 10.4.

Pure alpha emitters with no interfering daughters presented no counting problems. These included ^{241}Am, ^{244}Cm, and ^{253}Es. However, the nuclides ^{249}Bk and ^{252}Cf had interferences that required special counting techniques, and ^{243}Am was not used because its beta-emitting daughter, ^{239}Np, gave non-resolvable interferences and because a suitable alternative, ^{241}Am, was available. In counting the primarily low-energy beta emitter, ^{249}Bk, there were increased problems due to background and alpha- and gamma-emitting contaminants. These problems were resolved

[20] PPO = 2,5-diphenyloxazole; Me_2POPOP = 1,4-bis(4-methyl-5-phenyloxazolyl)benzene. The extractant for the trivalent actinides in aqueous sulfate samples is 1-nonyldecylamine sulfate.

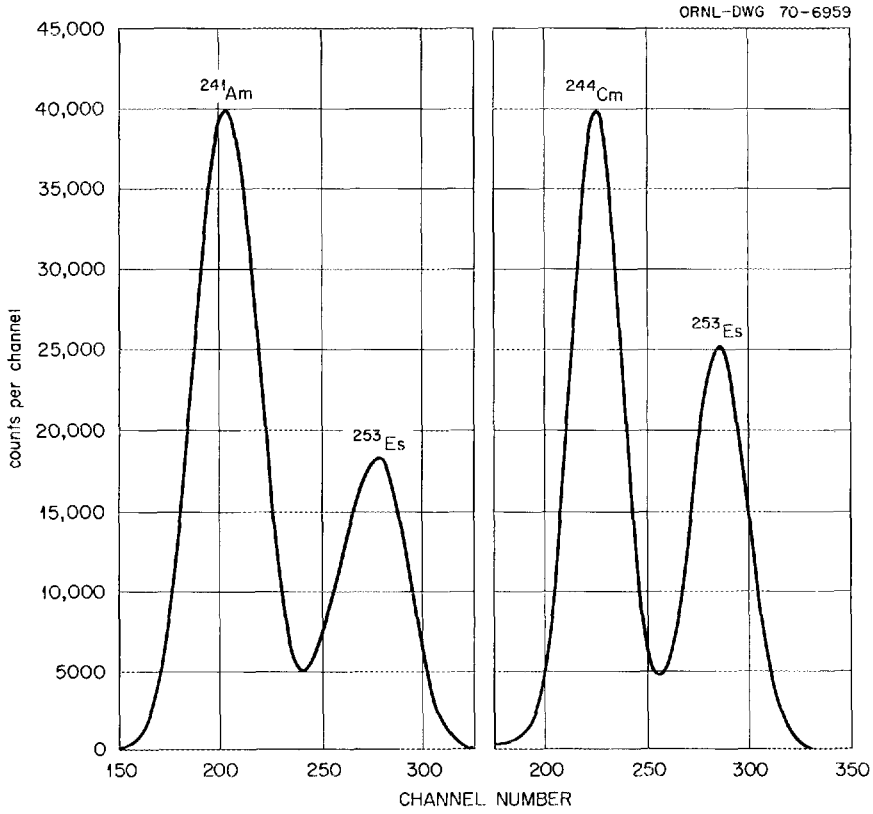

Fig. 10.5. Examples of Resolution of Pairs of Transplutonium-Element Alphas by Liquid Scintillation Counting.

by counting at a higher gain (10% gain instead of 1%) through a window that eliminated the lowest-energy region and the small amount of higher-energy alpha counts. In the case of ^{252}Cf, it was necessary to count only the alpha peak for californium and to subtract the contribution from the fission product beta emitters by counting portions on either side of the peak and correcting to an adjusted base line.

Although energy resolution in liquid scintillation cannot approach that of a surface barrier detector (~600 kev vs 20 kev), quantitative discrimination between isotopes is possible in a number of cases. Figure 10.5 shows the liquid scintillation spectra of ^{244}Cm + ^{253}Es and of ^{241}Am + ^{253}Es, as obtained with the single-phototube detector. Also, as may be seen from Fig. 10.4, some discrimination between alpha and beta emitters is possible, and some qualitative identifications of nuclides can be made even when quantitative counting of one nuclide in the presence of another is not.

Lanthanide Loading of Molecular Sieves

The reversible capacity of molecular sieves for the various lanthanides was examined in support of the study of enrichment of isotopes produced by nuclear reactions (the Campbell reaction, Sect. 13). The molecular sieves of present interest are those with the faujasite zeolite structure, containing both large and small interconnected pores. To date, only Linde X has been studied. The zeolites are cation exchangers; thus, ions such as sodium, lithium, calcium, and the lanthanides can be readily and reversibly interchanged, but large ions exchange readily only within the larger pores. On appropriate heat treatment of a Linde X sieve loaded with a lanthanide (a "LanX"), the lanthanide ions move into the smaller pores, where they can no longer be readily eluted or exchanged. The loadings attainable and the degree of resistance to elution are important factors in the Campbell reaction.

Molecular Sieves Containing Binder. — A weighed portion of hydrated Linde X molecular sieve with binder (a clay-like component used in the manufacture of the sieve) was contacted with hot aqueous solution containing a known amount of a lanthanide. The amount of lanthanide that was reversibly absorbed was determined by gravimetric analysis of the depleted solution. The analytical results for cerium and europium were checked by radiotracer analysis. In this first series of tests, the apparent loading capacities ranged from 0.7 to 1.0 milligram-atom of lanthanide per gram of molecular sieve, but there was no trend that could be correlated with the known chemical properties of the lanthanide series. In view of subsequent findings (see below), it seems likely that the large variation in results may have been caused by some excess base (probably alkali carbonate) in the zeolite.

Molecular Sieves Without Binder. — A supply of Linde X crystals that had been prepared without a binder initially gave inconsistent results because of the presence of excess alkali. The alkali was removed by leaching with very dilute ammonium formate, followed by redrying to the constant-weight zeolite hydrate. After this treatment, the observed reversible loading capacities for all the natural lanthanides (omitting cerium) and yttrium were within the range of 0.91 to 1.05 milligram-atom per gram of molecular sieve.

The capacity for americium is considerably lower, that is, about 0.3 milligram-atom per gram of Linde X. At first, it was thought that the lanthanides might be showing a regularly decreasing series of capacities, so that the lower capacity for americium might fit a downward extension; however, the possibility that such a relationship exists is eliminated by the present finding of nearly uniform loading capacities for all the lanthanides.

10.7 RELATIVE POTENTIALS OF THE Bk(IV)-Bk(III) AND Ce(IV)-Ce(III) COUPLES

The study of the difference between the potentials of the Bk(IV)-Bk(III) and Ce(IV)-Ce(III) couples in aqueous solutions by solvent extraction methods was continued. This method requires only tracer amounts of berkelium, since individual potentials are not measured. Values were obtained for $HClO_4$ solutions, and data for HNO_3 solutions were extended and refined after improvements were made in the experimental techniques and in the measurement of relative berkelium concentrations in a wide variation of acid concentrations.

The method depends on the application of a form of the Nernst equation. When berkelium is introduced into a solution containing Ce(III) and Ce(IV), oxidation of the berkelium proceeds until an equilibrium is reached. At equilibrium,

$$\Delta E \text{ (in volts)} = E_{Ce} - E_{Bk} = 0.059 \log \frac{[Bk(IV)]}{[Bk(III)]} - 0.059 \log \frac{[Ce(IV)]}{[Ce(III)]}$$

Thus the Bk(IV)/Bk(III) concentration ratio is a function of the Ce and Bk potentials and the experimentally fixed Ce(IV)/Ce(III) ratio. The Bk(IV)/Bk(III) ratio is measured by quantitatively extracting the Bk(IV) and the Ce(IV) into an equal volume of extractant, leaving the Bk(III) quantitatively in the aqueous solution, and then determining the relative beta activities of the two

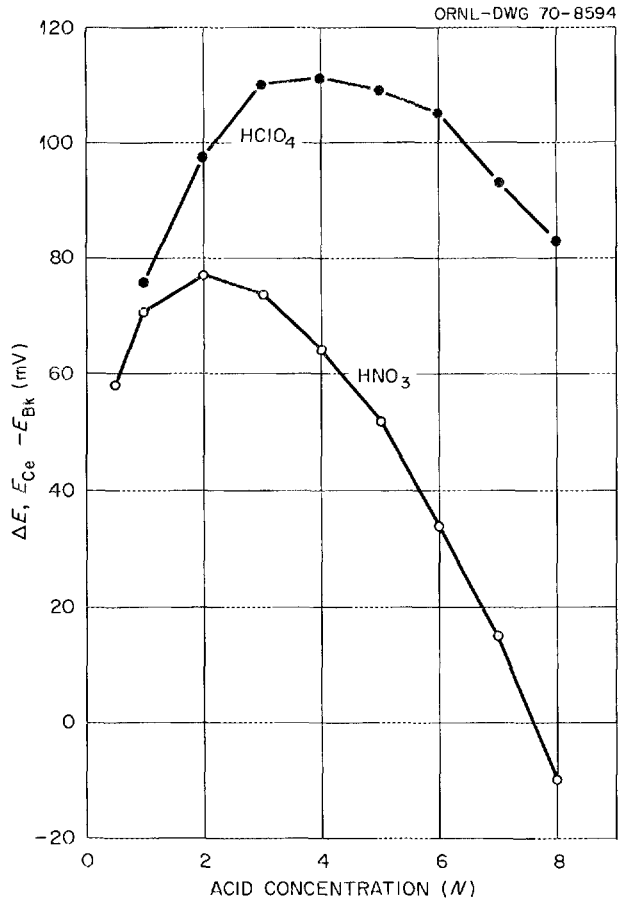

Fig. 10.6. Differences Between Oxidation Potentials of Bk(IV/III) and Ce(IV/III) in Nitric and Perchloric Acid Solutions. ΔE, $E_{Ce} - E_{Bk}$, is positive when Bk(III) is more easily oxidized than Ce(III).

phases. Appropriate concentrations of di(2-ethylhexyl)phosphoric acid in *n*-dodecane were found for extracting Bk(IV) and Ce(IV) from all concentrations of HNO_3 and $HClO_4$. After preliminary approximations, ratios of Ce(IV)/Ce(III) were used which would give Bk(IV)/Bk(III) ratios not greatly different from the reciprocals of the Ce(IV)/Ce(III) ratios. Adherence to the Nernst equation is best under these conditions.

Data for ΔE in $HClO_4$ and HNO_3 are given in Fig. 10.6. The value of ΔE is maximum near 0.11 v in 4 *N* $HClO_4$ and 0.08 v in 2 *N* HNO_3, and decreases at higher acid concentrations. The potential of the Ce(IV)-Ce(III) couple actually becomes less than that of the Bk(IV)-Bk(III) couple in 8 *N* HNO_3.

Preliminary work with H_2SO_4 over the same acidity range indicates nearly constant values of ΔE around 0.05; however, inconsistencies, possibly due to subsidiary equilibria, prevent assignment of exact values at present. Because of interference by the strongly complexing H_2SO_4, it was necessary to use the stronger extractants 1-methylheptyl and 2-ethylhexyl phenylphosphonic acids as extractants from H_2SO_4.

10.8 RELATIVE BASICITIES OF LANTHANIDES AND ACTINIDES

The basicities of the lanthanides are known to decrease as the atomic numbers of these elements increase and their ionic radii decrease. Parallel behavior was expected for the trivalent actinides. One method for comparing basicities consists in observing the hydrolytic behavior as solutions of salts are titrated with sodium hydroxide. In an early study of this type,[21] Pu(III) was found to behave very much like Pr(III). We have compared americium and curium with all the natural lanthanides, except cerium and lutetium, in nitrate solutions which were at least an order of magnitude more dilute than any previously used for this purpose. This dilution causes hydrolysis to take place at pH values 0.5 to 1.0 unit higher than those previously observed.

[21] K. A. Kraus and J. R. Dam, "Hydrolytic Behavior of Plutonium(III)," pp. 466–77 in *The Transuranium Elements*, ed. by Glenn T. Seaborg *et al.*, National Nuclear Energy Series Vol. 14B, McGraw-Hill, New York, 1949.

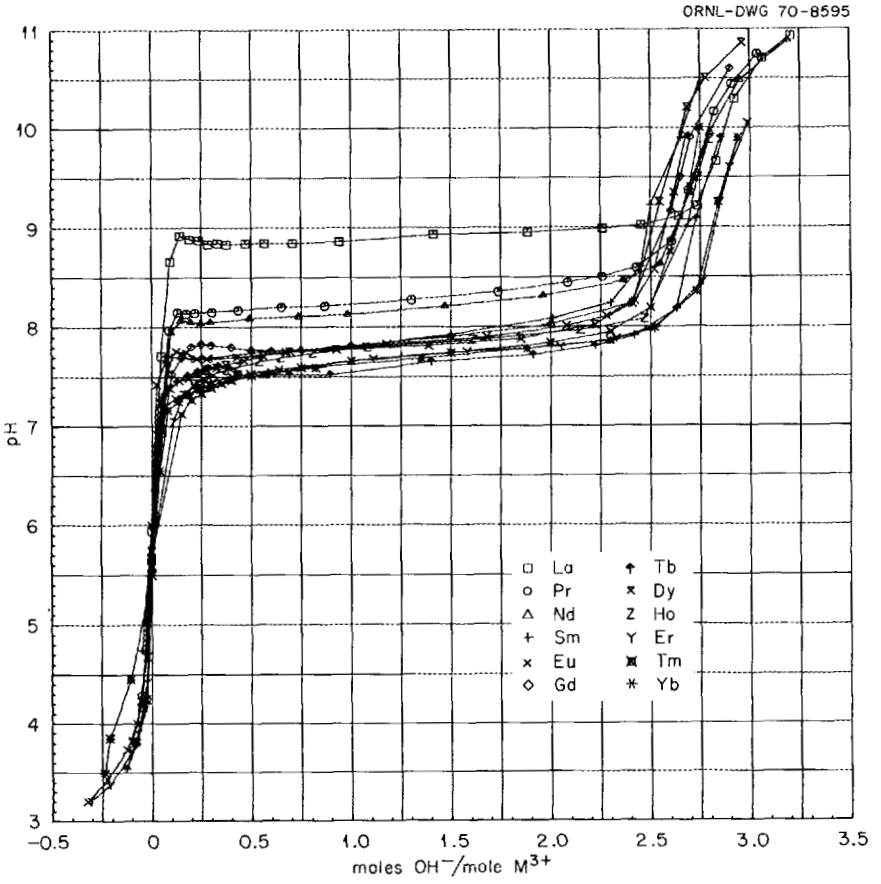

Fig. 10.7. Titration Curves Showing the Relative Basicities (and Nonstoichiometry of Precipitation) of Lanthanides. Initial concentration, ~0.002 *M* $Ln(NO_3)_3$; titrated with 0.05 *M* NaOH.

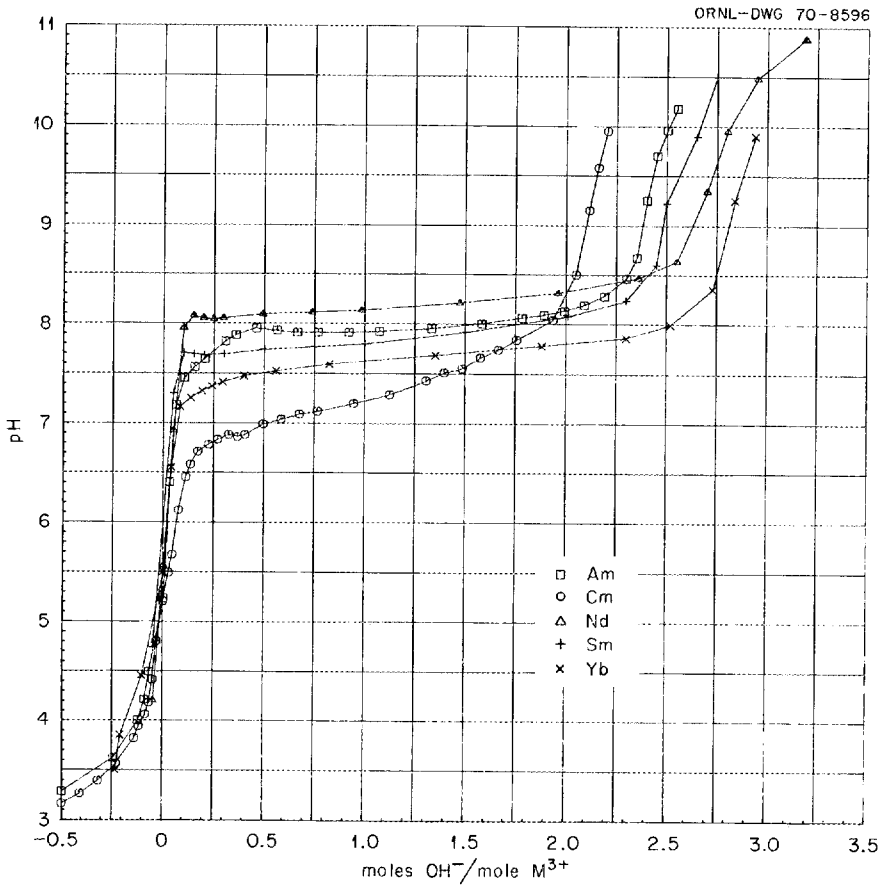

Fig. 10.8. Relative Basicities (and Nonstoichiometry of Precipitation) of Americium and Curium, as Compared with Selected Lanthanides. Initial concentration, ~0.002 *M* $Ln(NO_3)_3$; titrated with 0.05 *M* NaOH.

Results of titrating approximately 0.002 *M* nitrate solutions of the lanthanides with 0.05 *M* NaOH are shown in Fig. 10.7. The basicities of the elements decrease as the atomic numbers increase, although the differences between successive elements decrease as the series progresses. This is in accord with their relative atomic radii. Approach to a constant pH is less abrupt as basicity decreases.

Previous workers[21,22] have observed that the titration of lanthanides and Pu(III) with alkali is not stoichiometric, indicating the formation of some basic salts. In the present instance, the lowest equivalent base/lanthanide ratio (~0.85) for complete removal from solution occurs near the middle of the series, while the ratio for ytterbium used approximately 0.95 of the nominal stoichiometry.

[22]Therald Moeller and H. E. Kremers, *J. Phys. Chem.* **48**, 395 (1944).

Corresponding data for americium and curium are compared with those for neodymium, samarium, and ytterbium in Fig. 10.8. The basicity of americium lies between the basicities of neodymium and samarium, and is about equivalent to that of the missing element, promethium. In titrations of americium and neodymium, no visible precipitates were observed. Precipitates were evident in all other cases. The basicity of the next actinide, curium, is much lower than that of americium, and is even lower than that of any of the lanthanides tested. A constant pH was never achieved in its titration.

In deviations from nominal stoichiometry, the actinides are notably lower than even the lanthanides. For example, the fractions of the nominal stoichiometry for americium and curium were about 0.80 and about 0.70 respectively. The result obtained for curium is nearly consistent with the composition $CmNO_3(OH)_2$.

10.9 KINETICS OF METAL ION EXTRACTIONS BY ORGANOPHOSPHORUS ACIDS

Beryllium Extraction by HDEHP

We previously reported (Fig. 10.9 of ref. 23) that, after the first few hours of each run, the initially low rate of beryllium extraction by di(2-ethylhexyl)phosphoric acid (HDEHP or HA) gradually increased, and then leveled off at a significantly higher rate after an additional 10 to 15 hr. We have now determined that this "induction" period resulted from catalysis by a substance, presumably a plasticizer, that was leached from the plastic tubing in the peristaltic continuous sampling pump.[23,24] Accordingly, the peristaltic pump has been replaced by a metal bellows pump in an all-glass and -metal continuous sampling system for the rate measurements. In addition, the nature and the mechanism of the catalysis are being studied as an additional probe into the beryllium extraction mechanism, especially to see if it can provide an improvement in beryllium processing.

Recognition of the foregoing catalysis showed that only initial slopes, about the first hour, of the previously obtained curves were pertinent to the direct beryllium extraction kinetics. In spite of the poor precision of the results from such relatively short intervals, these curves indicated that the power dependence of the first-order extraction rate constant on the concentration of HA is between $\frac{1}{2}$ and 1 below 0.1 *M* HA and between 1 and $\frac{3}{2}$ above 0.1 *M* HA, and that its dependence on the concentration of aqueous perchloric acid is between 1 and $\frac{3}{2}$. Subsequent runs in the all-glass and -metal system (20 hr and longer) showed power dependences on the HA concentration of near $\frac{3}{4}$ below and $\frac{5}{4}$ above about 0.2 *M* HA (Fig. 10.9). There is considerable scatter below 0.005 *M* HA, possibly masking a further change of slope. If the extraction mechanism for beryllium resembles that of iron, the $\frac{3}{4}$ slope would result from simultaneous parallel reaction paths involving A^- (slope $\frac{1}{2}$) and HA_2^- (slope 1).

One step of the mechanism of iron extraction by HA proves to be zero order instead of first order with respect to iron concentration.[23] Accordingly, tests using varying beryllium concentrations have been made in order to look for a similar step in the beryllium extraction mechanism. The first results do not indicate any zero-order component in the beryllium kinetics.

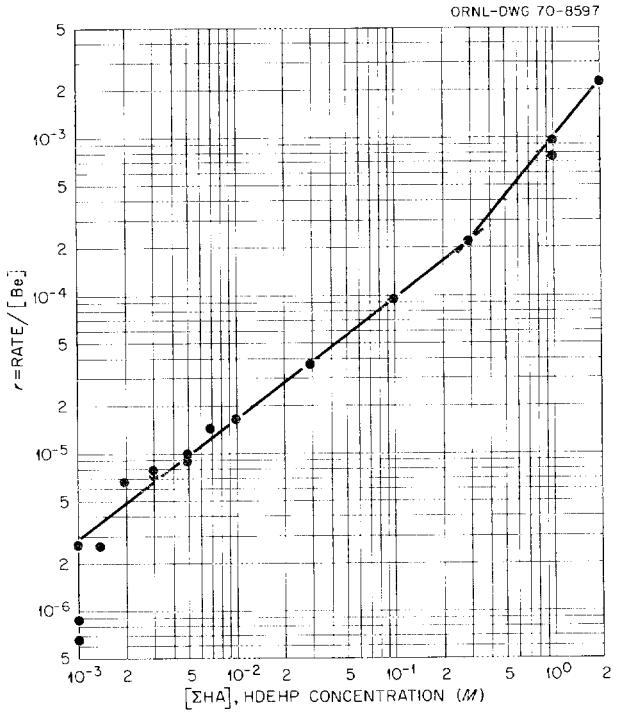

Fig. 10.9. Kinetics of the Extraction of Beryllium from Acid Perchlorate Solution by HDEHP (HA) in *n*-Octane. Initial conditions: 0.002 *M* Be, 0.1 *M* $HClO_4$, 1.9 *M* $NaClO_4$, 25°C.

Iron Extraction by HDEHP

We previously reported considerable increases in the rate of iron extraction when proton-accepting complexers were added to the aqueous phase.[24] Extraction of contaminant iron has been found to be fairly rapid in the extraction of uranium from commercial phosphoric acid (cf. Sect. 10.4). In a test made under the same conditions as were used to study the other complexers[24] (i.e., 2 *M* $NaClO_4$–$HClO_4$, pH 1, 0.002 *M* Fe^{3+}, with 0.1 *M* HA), 0.1 *M* phosphate increased the iron extraction rate constant by a factor of 12, from 6×10^{-4} to 70×10^{-4} cm/min. For comparison, 0.1 *M* nitrate, dichloroacetate, and acetate increased the rate constant from 6×10^{-4} to 30×10^{-4}, 85×10^{-4}, and 105×10^{-4} cm/min respectively. We plan to examine this effect to learn whether iron extraction follows the same or a different mechanism in phosphoric acid medium.

---

[23] *Chem. Technol. Div. Ann. Progr. Rept. May 31, 1969*, ORNL-4422, pp. 267–69.

[24] *Chem. Technol. Div. Ann. Progr. Rept. May 31, 1967*, ORNL-4145, p. 230.

10.10 AGGREGATION AND ACTIVITY COEFFICIENTS IN SOLVENT PHASES

As previously reported,[25] the installation of new diaphragm-manometer indicator heads[26] in an improved all-metal vapor-pressure system gave the most accurate vapor-pressure data we have been able to obtain. With these new components, temperature control proved to be the limiting variation. Accordingly, further improvement in accuracy has been achieved by replacing the previous thermostatic controls with a commercial solid-state temperature controller[27] that is nearly an order of magnitude better with regard to long-term stability (±0.001°C).

Benzophenone was "calibrated" as a reference standard solute in dry carbon tetrachloride by means of the improved vapor-pressure system. The measured values of the osmotic coefficient are fitted by the equation

$$\phi = 0.5637 - 0.0165m + 0.2003/(0.4591 + m) ,$$

which is valid up to 6.1 m benzophenone, with a standard deviation of fitting of 0.0139. The benzophenone in carbon tetrachloride deviates from ideality by 8% at 0.1 m and 26% at 1 m.

The previous "calibration" of three reference standard solutes in benzene was completed, and a paper has been accepted for publication in the *Journal of Inorganic and Nuclear Chemistry*. The abstract follows:

"Reference Solutes for Isopiestic and Dynamic Vapor Pressure Osmometry in Organic Solvents: Triphenylmethane, Azobenzene, and Benzil in Dry Benzene," by J. W. Roddy and C. F. Coleman. *Abstract:* The vapor pressure lowering of benzene solutions of azobenzene (AZO), triphenylmethane (TPM), and benzil (BZL) was measured at 20°C by two methods, one a direct differential measurement of the difference between vapor pressure of the solution and solvent, and the other a direct measurement of the total vapor pressure of the solution. The results were cross-checked by isopiestic measurements at 25°C on the three pairs of benzene solutions, AZO-TPM, AZO-BZL, and TPM-BZL. Each solute-benzene system shows some deviation from ideality. The osmotic coefficients are well-fitted by:

$$\phi_{TPM} = 0.9847 - 0.1120m_{TPM} + 0.00077/(m_{TPM} + 0.0504)$$

$$\phi_{AZO} = 0.8795 - 0.0530m_{AZO} + 0.0520/(m_{AZO} + 0.4313)$$

$$\phi_{BZL} = 0.7713 - 0.0112m_{BZL} + 0.1200/(m_{BZL} + 0.5247) .$$

The nonideality of these solutions is not accounted for by regular solution theory, and only partially by assumption of association. With TPM (but not with AZO or BZL) it is well-accounted for by Guggenheim's lattice model.

Attempts to measure the aggregation of methyltrioctylphosphonium dimethylphosphate (cf. Sect. 10.2) in benzene by means of a matched-thermistor dynamic osmometer were unsuccessful because of persistent drifting. Isopiestic balancing against azobenzene as a reference indicated that this extractant is nearly a dimer. The aggregation number, $\bar{n}$, is 1.8 at 0.5 m and changes only slightly over the range of 0.1 to 0.5 m. It is not affected by the presence of water.

The average aggregation of mixtures of di(2-ethylhexyl)phosphoric acid with its lithium salt (HA + LiA, 0.125 M ΣA in benzene) was measured, by isopiestic balancing against triphenylmethane as reference, at three different ratios of salt to acid. The results, $\bar{n}$ = 2.7, 4.0, and 7.8 at LiA/ΣA = 0.125, 0.25, and 0.5, respectively, match very closely the aggregation of corresponding mixtures of the acid with its sodium salt.[28] The results validate the previously tentative conclusion obtained from extraction equilibria[29] that the specific organic-phase species at low loading is LiA·3HA (analogous to NaA·3HA, ref. 28).

[25] *Chem. Technol. Div. Ann. Progr. Rept. May 31, 1969*, ORNL-4422, p. 268.

[26] *MKS Baratron Electronic Pressure Meter*, Bulletin 90, MKS Instruments, Inc., Burlington, Mass.

[27] Model PTC-1000, Tronac, Inc., Provo, Utah.

[28] W. J. McDowell and C. F. Coleman, *J. Inorg. Nucl. Chem.* 27, 117 (1965).

[29] *Chem. Technol. Div. Ann. Progr. Rept. May 31, 1966*, ORNL-3945, p. 183.

11. Chemical Applications of Nuclear Explosions

The purpose of this program is to provide research and development in selected areas of the Plowshare Program, especially those areas requiring knowledge of chemical or metallurgical engineering to determine feasibility. Areas in which research was performed during the past year included: (1) studies of the behavior of radionuclides in the recovery of copper from ore deposits that have been fractured with nuclear explosives, and (2) studies of the behavior of radionuclides in the recovery of oil from shales.

11.1 COPPER ORES

Fracturing of copper ore deposits with nuclear explosives, followed by leaching in place, is being studied by the Division of Peaceful Nuclear Explosives of the USAEC and by associated contractors. The Oak Ridge National Laboratory is cooperating in this program by studying potential problems that might arise from the presence of radioactive contaminants in the processing cycle. The proposed flowsheet for recovering copper involves percolating dilute sulfuric acid down through the nuclear-broken ore to dissolve the copper, collecting the leach liquor at the bottom of the ore body and pumping it to the surface, recovering a copper concentrate from the solution by cementation on iron, and recycling of the barren solution (after fortifying it with acid) for use in the leaching step.

Previous test results showed ^{106}Ru to be the most troublesome isotope with respect to radioactive contamination of the cement copper. Some of the ruthenium is dissolved by the leaching solution and cements with the copper on sheet iron. Changing the oxidation state of the iron or the pH of the liquor in recent batch cementations had little effect on the ^{106}Ru content of the cement copper. When copper was cemented from ^{106}Ru-traced liquors that contained 2 g of copper and 4 g of total iron per liter, varying the initial pH from 1.6 to 2.2 or varying the ferric iron concentration from 0 to 2 g/liter caused a maximum variation of only about 10% in the ^{106}Ru concentration in the cement copper.

Cement copper can be purified by melting it into a consumable anode and electrolytically converting the anode to cathode copper metal or by dissolving it in dilute sulfuric acid and electrolytically depositing (i.e., electrowinning) the copper metal from the solution. Both of these treatments provide effective separation of copper from ^{106}Ru. Most of the ^{106}Ru accumulates in the cell electrolyte and eventually must be removed. The ^{106}Ru contamination of copper products prepared in recent electrowinning tests was proportional to the ^{106}Ru concentration in the cell electrolyte. Increasing the concentration of ^{106}Ru in the electrolyte from 0.0027 to 0.43 μc/ml increased the amount in the products from 0.0014 to 0.20 μc per gram of copper. In these tests about 14% of the copper and about 0.2% of the ruthenium were deposited from the electrolyte solutions in 1 hr at a current density of about 10 amp/ft^2 and a cell potential of 2 v. The solutions, prepared by dissolving ^{106}Ru-contaminated copper in hot aerated 1 M sulfuric acid, initially contained 25 g of copper per liter.

Behavior of Tungsten

Tungsten-185 is a neutron activation product that is normally produced in significant amounts in nuclear detonations. Studies of the behavior of ^{185}W in the copper recovery process indicated that contamination of the cement copper with this isotope should be very low. About 28% of the ^{185}W cemented from a simulated leach liquor with about 77% of the copper. However, we found that the tungsten was strongly adsorbed ($K_D > 50$) from the liquor by Safford ore tailings. Therefore, the amount of ^{185}W in the leach liquor would be limited to a very low level by this mechanism. The ^{185}W concentration would be further limited by its 74-day half-life; less than 4% of the ^{185}W initially present in the chimney would remain one year after the detonation.

Solvent Extraction of Copper

The recovery of copper from ore liquors by solvent extraction is a potential alternative to the cementation process. The extracted copper can be stripped from the solvent with sulfuric acid and fed directly to an electrowinning operation. A new copper extractant, Kelex 100-25, was received and tested to determine if it will provide separations of copper from radionuclides comparable to those obtained with LIX-64 in earlier tests.

Kelex 100-25, as received from the Ashland Chemical Company, is a mixture of 25% active reagent and 75% tridecanol by volume. Titration of the mixture with standard NaOH gave a curve with a single large break, indicative of a strong monobasic acid. An isotherm for the extraction of copper from a simulated leach liquor, initially containing 2 g of copper per liter at pH 2, with a solution of 15 vol % Kelex 100-25 in kerosene indicated that about 97% of the copper could be recovered in three ideal extraction stages while loading the organic phase to 2 g of copper per liter. The copper can be stripped with 2 *M* H_2SO_4 to give a product solution containing 25 to 30 g of copper per liter.

The relative extractabilities of copper and some of the radionuclides that might be present in the copper recovery system were measured with the 15% Kelex 100-25–kerosene solution. In 10-min extractions from simulated leach liquors, the extraction coefficient for copper was 8 at a pH of 0.9 and more than 200 at pH 2.3 and above. Extraction coefficients in the pH range of 0.9 to 2.6 were less than 0.01 for ^{106}Ru, ^{134}Cs, and ^{144}Ce, and between 0.01 and 0.05 for ^{60}Co, ^{85}Sr, and ^{125}Sb. Extraction coefficients were about 30 for ^{95}Zr-Nb, from 2 to 5 for ^{110}Ag, and 0.1 for ^{59}Fe; fortunately, the concentrations of these radionuclides in copper leach liquors should be extremely low. As compared with LIX-64, Kelex is a stronger extractant for copper and fission products. Apparently both of these extractants would give copper products that are essentially free of radionuclides.

11.2 RECOVERY OF OIL FROM SHALE

The feasibility of recovering oil from Green River oil shales by using a nuclear device to fracture the shale and then retorting the oil in place is being studied by several government agencies and commercial companies. The Oak Ridge National Laboratory is participating in this program by studying the oil recovery system with regard to the behavior of the radioactive contaminants that would be formed in the nuclear detonation.

Behavior of Tritium

Studies made this year continued to show that tritium is a major potential contaminant of oil that is recovered from nuclear-fractured shale. Contamination is more rapid when the shale is exposed to tritiated water or tritiated hydrogen than when exposed to tritiated hydrocarbons. In these exposure tests, samples of oil shale were heated in closed vessels with tritiated compounds, using about 1 μc of tritium per gram of shale. Before being retorted the shale was washed thoroughly with water and dried with warm air.

The tritium concentrations of oil products derived from shale that had been exposed to tritiated water or tritiated hydrogen for about a week at 85°C and 560 psig were 0.57 and 0.24 μc/g respectively (Table 11.1).

Table 11.1. Effect of Tritium Species on Contamination of Shale and Oil

Procedure: 120 g of oil shale was heated in small pressure vessels for six to seven days at 85°C and 560 psig (pressurized with nitrogen) with 1.2 ml of water containing about 120 μc of tritiated water or with 130 ml of hydrogen, methane, or ethane containing about 100 μc of the corresponding tritiated gas. After the shale was washed with water and dried at 65°C, oil was retorted from a 100-g sample, and the oil was washed six times with an equal volume of water to remove entrained tritiated water.

Tritiated Compound Added	Tritium Concentration (μc/g)	
	In Dried Shale	In Washed Oil
Water	0.37	0.57
Hydrogen	0.19	0.24
Methane	0.013	0.023
Ethane	0.037	0.024

The tritium concentration of oil from shale that had been exposed to tritiated methane or ethane under these conditions was about an order of magnitude lower.

The tritium concentration of oil recovered from shale that had been exposed for one year to tritiated water vapor at 85°C and atmospheric pressure was about the same as that found for oil obtained from shale exposed for 30 days (Fig. 11.1). The tritium concentration of oil obtained from shale exposed to tritiated hydrogen increased from 0.10 μc/g to 0.81 μc/g as the exposure time was increased from 1 to 44 days. For short exposure times at high pressure, contamination from tritiated water was considerably higher than from tritiated hydrogen.

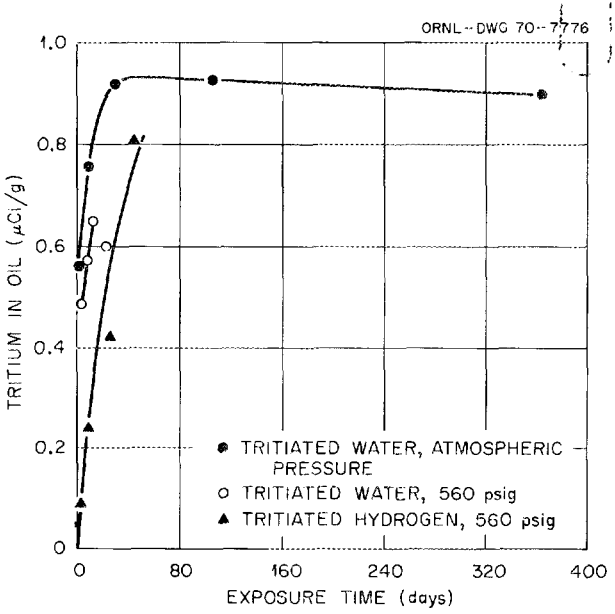

Fig. 11.1. Effect of Exposure Time on Tritium Contamination of Oil. Procedure: 120 g of oil shale was heated at 85°C with 1.2 ml of water containing about 115 μc of tritiated water or with 130 ml of hydrogen containing about 100 μc of tritiated hydrogen. After the shale was washed with water and dried at 65°C, oil was recovered from a 100-g sample, and the oil was washed six times with an equal volume of water to remove tritiated water.

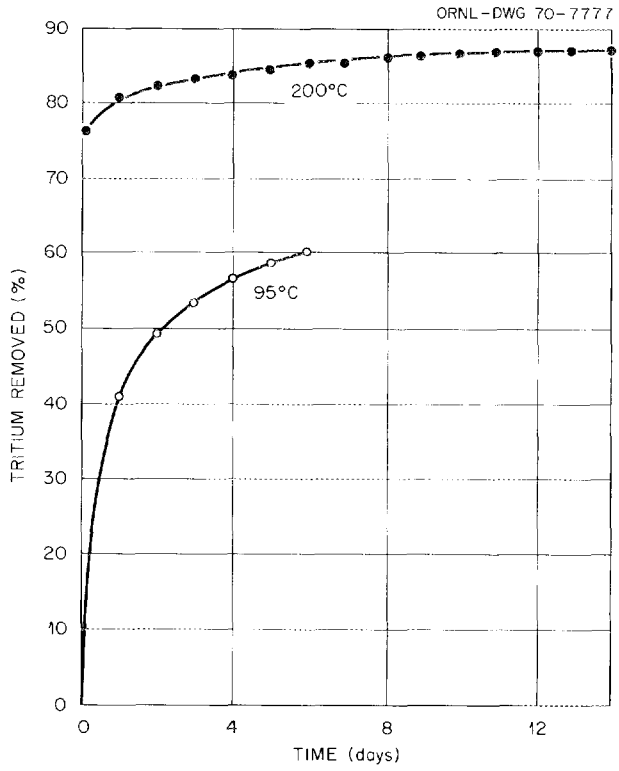

Fig. 11.2. Removal of Tritiated Hydrogen from Shale. Procedure: shale that had been contaminated by exposure to tritiated hydrogen was heated in a humid gas (50% N_2–50% CO_2) stream. The shale treated at 200°C initially contained 0.26 μc of tritium per gram, and the shale treated at 95°C contained 0.13 μc/g.

Removal of Tritium from Shale

Earlier tests[1] with shale that had been exposed to tritiated water showed that treating the shale at elevated temperatures with a moist gas stream significantly reduces the tritium contamination. In recent tests this method was used to remove tritium from shale that had been contaminated by exposure to tritiated hydrogen. More than 87% of the tritium was removed by slowly passing a gas stream (saturated with water at 38°C) through a column of contaminated shale for 14 days at 200°C (Fig. 11.2). About 76% of the tritium was removed in the 4-hr period that was required to heat the shale from room temperature to 200°C; 81% of it was removed in the first day of treatment. The oil retorted from the shale at the end of the test contained 0.11 μc of tritium per gram. The results obtained at 95°C were less impressive; 41% and 60% of the tritium were removed in one day and six days respectively. More than 99% of the tritium that was removed from the shale in these tests was caught in a cold trap located immediately downstream of the treatment vessel. This indicates that, although the shale was initially exposed to tritiated hydrogen, the tritium was released from the shale as tritiated water. Apparently, a significant fraction of the tritiated hydrogen is converted to water during the exposure.

[1] *Chem. Technol. Div. Ann. Progr. Rept. May 31, 1969,* ORNL-4422, p. 272.

12. Biochemical Technology

MACROMOLECULAR SEPARATIONS

12.1 EFFECT OF DIVALENT METAL IONS ON REVERSED-PHASE CHROMATOGRAPHIC (RPC) SEPARATION OF TRANSFER RIBONUCLEIC ACIDS

Magnesium ion has dramatic effects on the properties of tRNAs in solution. For example, at least two tRNAs have active and inactive forms, and conversion between these forms can be achieved by the addition or removal of Mg^{2+}. The presence of Mg^{2+} "protects" tRNAs from nuclease degradation; therefore, 0.01 *M* Mg^{2+} is usually added to aqueous solutions of tTNAs. Further, tRNAs that have been digested with ribonuclease to form two fragments can be annealed in the presence of Mg^{2+} to yield tRNA that is active in the aminoacylation reaction. The helix-coil transition of tRNAs is affected by Mg^{2+}, and the tRNA structure is stabilized in the

ORNL DWG. 70-81R

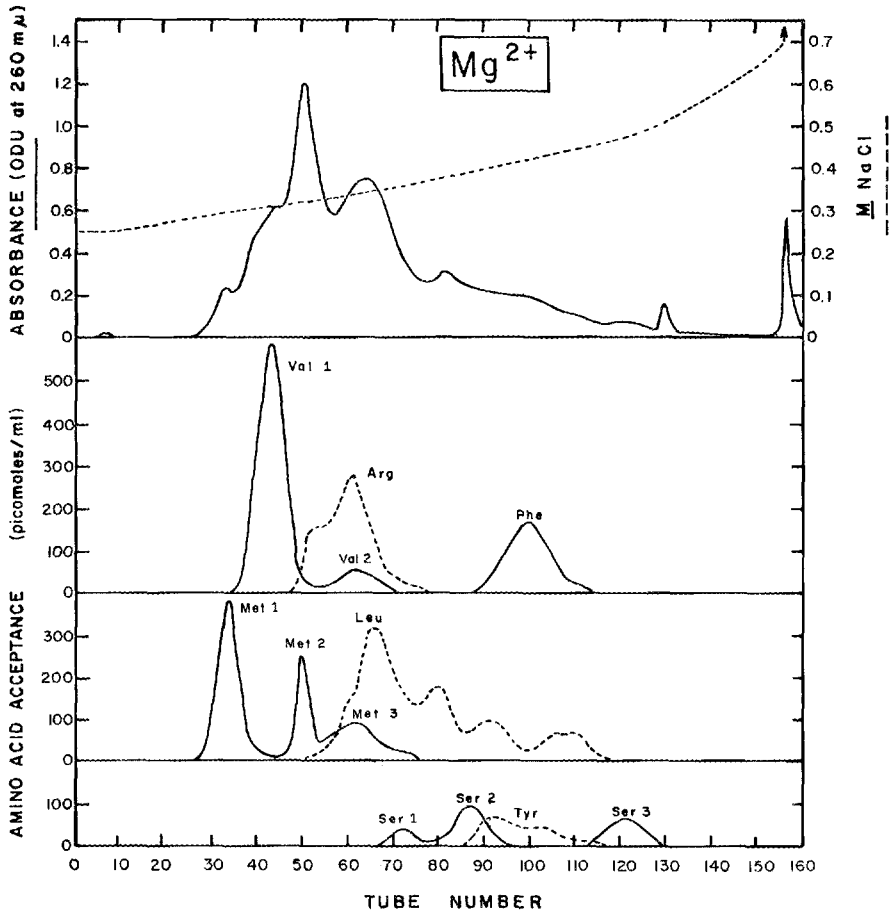

Fig. 12.1. RPC-3 Separation of tRNAs in the Presence of 0.01 *M* Mg^{2+}.

presence of Mg^{2+}, as measured by a marked increase in "transition temperature" T_m and sharpening of the thermal denaturation profile.

Less attention has been given to other divalent ions. Salts of metals such as zinc, copper, cobalt, calcium, and iron are essential for growth of *E. coli*. It has been shown that the intracellular concentration of Mg^{2+} in *E. coli* is the same as the extracellular concentration; thus it seems probable that the intracellular concentrations of other divalent metal ions are also significant.

A series of experiments was carried out to investigate the effects of group IIA ions (Mg^{2+}, Ca^{2+}, Sr^{2+}, and Ba^{2+}), and of certain transition elements (Mn^{2+}, Co^{2+}, and Ni^{2+}) on the chromatographic resolution of tRNAs on RPC-3 columns. The RPC-3 system was selected for this series of tests since it gives the greatest resolution in the early portion of the chromatogram, where the largest number of tRNAs are grouped, and has proved to be practical for the large-scale production of purified tRNAs (see Sect. 12.5).

A series of runs was made with buffers containing either 0.01 *M* $MgCl_2$, $CaCl_2$, $SrCl_2$, or $BaCl_2$. Since the results were quite similar, only those for Mg^{2+} (Fig. 12.1) and Ba^{2+} (Fig. 12.2) are shown. In each figure, the upper panel shows the absorbance trace and the calculated sodium chloride concentration of the eluate.

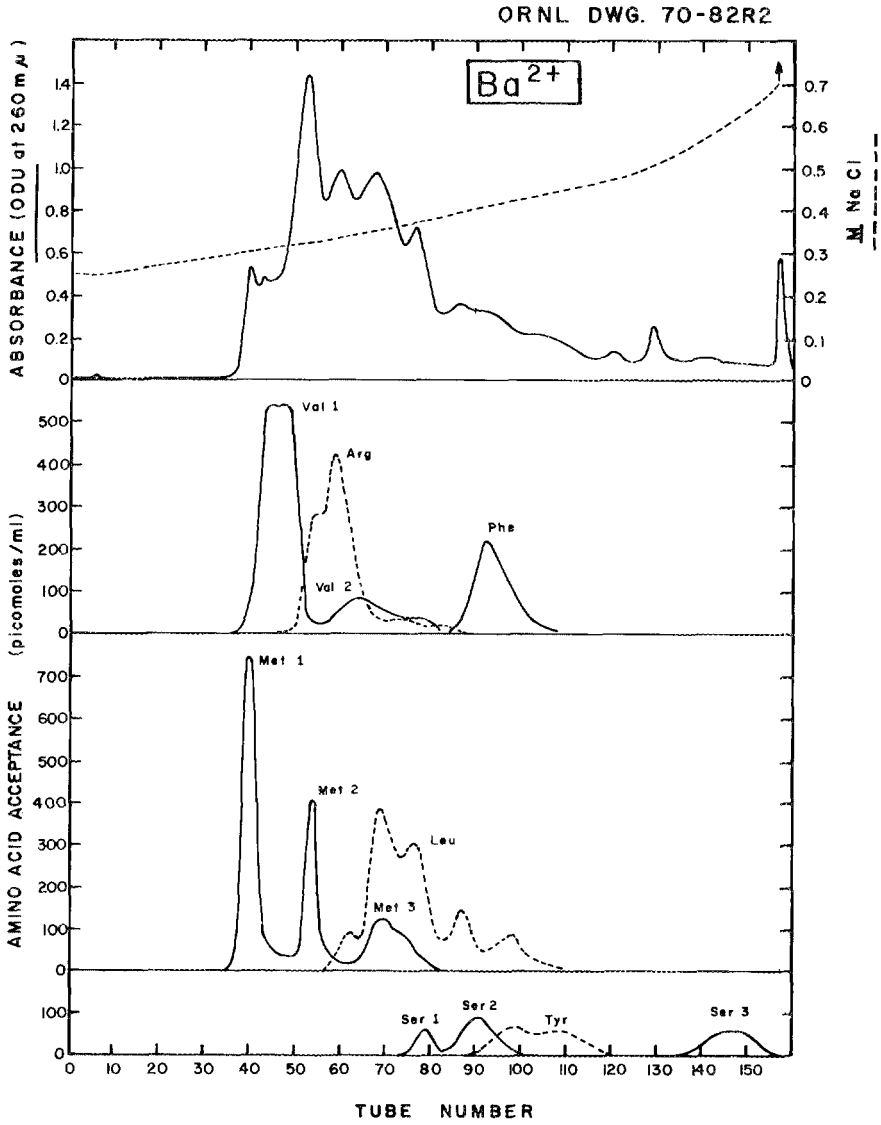

Fig. 12.2. RPC-3 Separation of tRNAs in the Presence of 0.01 *M* Ba^{2+}.

The lower panels show the position of arginine, leucine, methionine, phenylalanine, serine, tyrosine, and valine tRNAs. Sharp chromatographic peaks were obtained for all of the tRNAs except tyrosine; multiple peaks were obtained in most cases. Good recoveries, that is, 85 to 115% of the total tRNA (in the feed) accounted for after each run, were recorded for all tRNAs except tyrosine for the runs with Mg^{2+}, Ca^{2+}, Sr^{2+}, or Ba^{2+}. The tRNA elution positions, measured in terms of the NaCl concentration of the eluent at the center of the peak, were similar for all the group IIA ions.

Results for a reference RPC-3 run in which no divalent ion was present are shown in Fig. 12.3. The entire chromatogram was shifted to higher NaCl concentrations, and substantial changes occurred in the number and shape of the chromatographic peaks, as compared with the runs with group IIA ions. The methionine, valine, and leucine tRNAs were much

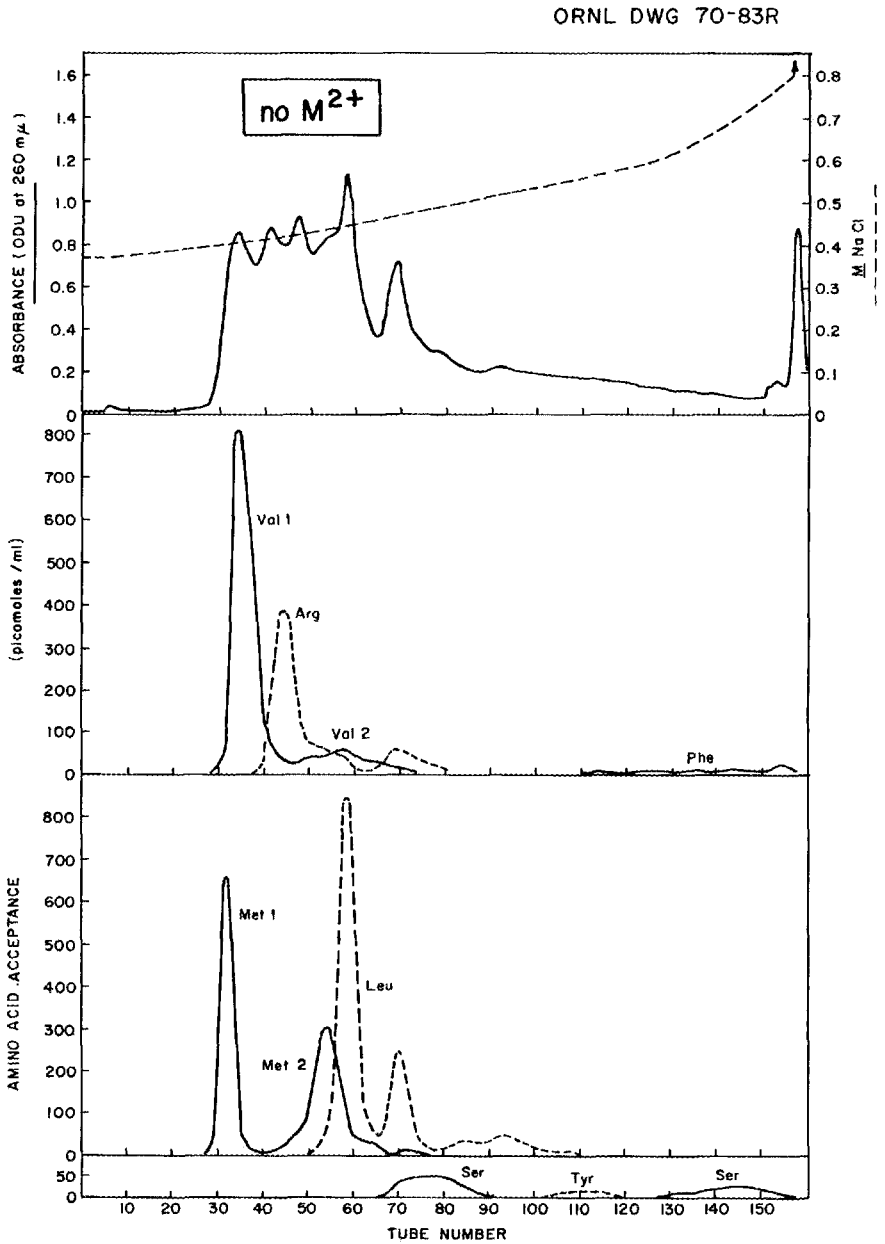

Fig. 12.3. RPC-3 Separation of tRNAs with No Divalent Metal Ion Present.

sharper, the serine tRNAs were broad and ill-defined, and the phenylalanine and tyrosine tRNAs were scarcely evident.

Runs were also made with buffers containing 0.01 *M* $MnCl_2$, $CoCl_2$, or $NiCl_2$. In general, the chromatographic peaks produced in these runs were broader and less clearly defined, and tRNA recoveries were lower, than in runs made without these elements.

Although the atomic weights and crystal radii increase substantially in the group IIA elements from magnesium through barium, the size of the hydrated divalent ions does not vary greatly. One set of calculated hydrated radii shows a systematic decrease from Mg^{2+} (4.28 A) through Ba^{2+} (4.04 A). Since the sizes of the hydrated ions are similar, large differences in chromatographic behavior in the presence of group IIA ions would not be expected, and did not occur. However, the addition of any divalent ion decreased the concentration of NaCl required to elute a given tRNA.

The tRNAs that were eluted late in the chromatogram – phenylalanine, tyrosine, and serine – were stable under chromatographic conditions only when a divalent ion was present. Since these tRNAs are not denatured in the presence of group IIA ions or Mn^{2+}, such ions serve to stabilize a specific region. It is interesting to note that these tRNAs are known to contain a unique modified nucleoside, 2-methylthio-N^6-(Δ^2-isopentenyl)adenosine, next to the anticodon.

The RPC-3 chromatograms obtained in this study suggest a number of practical considerations for the preparation of samples of purified tRNAs. Previously, during rechromatography, purification of a specific tRNA was achieved by changing the pH of the feed or shifting from an RPC-3 to an RPC-4 system. The experiments made in this study show that changes in the concentration of a divalent metal ion can also be effective. The peaks for the tRNAs that were resolved in the early part of the chromatogram were sharpest when no metal ion was present, while the tRNAs that were eluted late in the run required the presence of a divalent metal ion for stability. In general, the multiplicity of isoaccepting tRNAs diminished in the absence of metal ions.

12.2 SEPARATION OF ISOACCEPTING TRANSFER RIBONUCLEIC ACIDS FOLLOWING CHEMICAL DERIVATIZATION

Extensive experience with reversed-phase chromatographic separations of transfer ribonucleic acids has demonstrated the difficulty of separating the majority of the tRNAs that fall in the envelope, or middle, of the chromatogram. It is necessary to devise, by trial and error, a unique combination of experimental variables for each desired product. The benzoylated DEAE-cellulose system devised by Tener[1] and associates offers a first step for reducing the complexity of these separations problems and, further, provides a possible means for recovering families of isoaccepting tRNAs. The BD-cellulose packing is produced by substituting aromatic groups (from benzoyl chloride) for some of the hydroxyl groups of DEAE-cellulose. When a family of isoaccepting tRNAs has been aminoacylated and chemically derivatized, these tRNAs adhere more strongly to the packing (because of ionic attractions and hydrophobic forces) so that they tend to become the last tRNAs to be eluted from the column.

In the aminoacylation reaction, the crude tRNA is mixed with the desired amino acid, its aminoacyl-tRNA synthetase, and requisite cofactors. A crude enzyme (one containing all of the activating enzymes) is acceptable, but it should be free of endogenous amino acids. The removal of such amino acids may be accomplished by gel filtration of the enzyme immediately before use. Optimal concentrations of reagents and enzyme to achieve complete aminoacylation at the chosen tRNA concentration are found by preliminary experiments. The aminoacyl-tRNA is derivatized by either a phenoxyacetyl or a naphthoxyacetyl ester of *N*-hydroxysuccinimide, with the substitution occurring at the α amino group of the amino acid. For best results, the amino group should be uncharged; hence the reaction must be performed at a pH near the p*K* of that amino group. In addition to its buffering action, triethanolamine-HCl will limit the derivatization of hydroxyl groups in the tRNA.

The crude tRNA containing the derivatized aminoacyl-tRNA is applied to a BD-cellulose column in a small volume of the equilibrating solution, 0.30 *M* NaCl (this solution is 0.01 *M* in $MgCl_2$, 0.01 *M* in sodium acetate, and 0.002 *M* in $Na_2S_2O_3$, and has a pH of 4.5). The column is then washed with one to two column volumes of equilibrating solution, followed by a 1.0 *M* NaCl step elution for a duration of five to seven column volumes. This step elution removes 80 to 85% of the initial crude tRNA. The individual tRNAs on the column are then eluted with a salt-ethanol solution of gradually increasing concentration (1.0 *M* to 2.0 *M* in NaCl and 0 vol % to 35 vol % ethanol). As shown in Fig. 12.4, the tRNAs that naturally adhere to the BD-

[1] G. M. Tener *et al.*, *Biochemistry* 7, 3459 (1968).

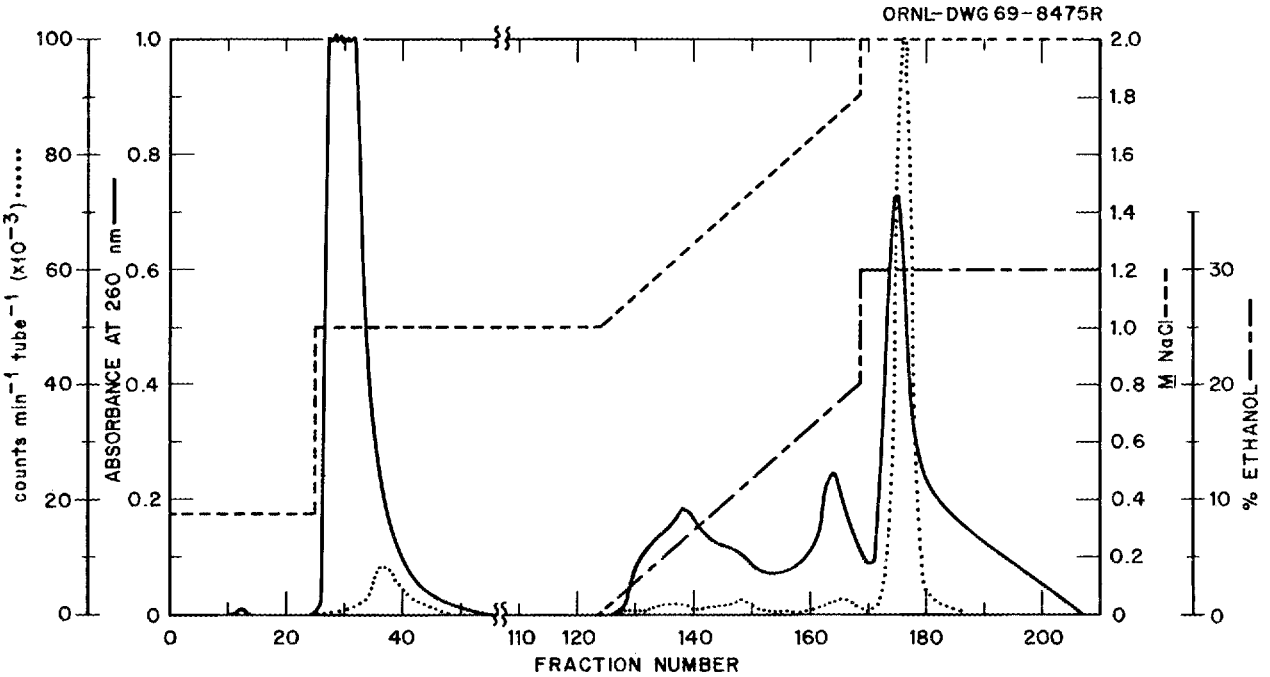

Fig. 12.4. Separation of Napthoxyacetyl Derivative of Arginyl-tRNA on a Benzoylated DEAE-Cellulose Column.

cellulose are eluted in low concentrations of ethanol, while the derivatized aminoacyl-tRNA is eluted last.

Initial runs employing the BD-cellulose column were made with small samples of crude tRNA (100 to 1000 A_{260} units) to ascertain the applicability of the method to *E. coli* K-12 MO tRNAs. Recoveries of purified tRNAs were found to be sufficiently high to justify scaleup of the process; therefore, an intermediate-size run (run 105-BD-10) was undertaken using 40,000 A_{260} units of crude tRNA. The crude tRNA, initially discharged to remove endogenous amino acids, was aminoacylated with ^{14}C- and ^{12}C-arginine in a reaction volume (800 ml) containing 50 A_{260} units of crude tRNA per milliliter. This tRNA concentration was previously determined to be the maximum that could be optimally charged with the available crude enzyme. The arginyl-tRNA was derivatized with the naphthoxyacetyl ester in a volume based on 200 A_{260} units of crude tRNA per milliliter, employing 1 mg of ester per 80 A_{260} units of crude tRNA. The volume of the BD-cellulose column was chosen to approach, but not exceed, a value based on a loading capacity of 80 A_{260} units of crude tRNA per milliliter of packing. The recovery of the ethanol-gradient fraction of arginine tRNA after discharge and reaminoacylation was low, as might be expected, considering the several reactions and handling procedures involved.

It was determined, based on the radioactivity of the ^{14}C-arginine tracer, that about 70% of the arginine tRNAs initially present in the crude tRNA were isolated in the ethanol-gradient eluate from BD-cellulose. However, after basic discharge and reaminoacylation, only about 30% of the arginine tRNAs could be recovered from this fraction. From the location of the ^{14}C label, we concluded that initial derivatization was relatively efficient (70%). Subsequently, on the BD-cellulose column, discharge of the aminoacyl bond occurred so that unlabeled arginine tRNA was removed in the 1 *M* NaCl eluent; then both the derivatized arginyl-tRNA and the liberated derivatized arginine were eluted together in the ethanol gradient. Hence, recoveries cannot be calculated using the tracer, but must be calculated from subsequent reaminoacylation.

Table 12.1 lists the recoveries (in percent) of purified tRNAs from run 105-BD-10, along with those of several other runs. In run 105-BD-10, only 28% of the original arginine tRNAs was recovered; however, the arginine tRNAs had an acceptable specific activity of 1045 picomoles/A_{260}. The largest losses were realized by discharge from the BD-cellulose column (described above) and by incomplete derivatization. The overall accountability of arginine tRNAs for aminoacylation, derivatization, BD-cellulose chromatography, and discharge has ranged from 80 to 85%; thus, the 1 *M* NaCl

Table 12.1. Results for BD-Cellulose Runs Using Naphthoxyacetyl Ester for Derivatization

Run No.	tRNA Pool	Crude Feed (A_{260} Units)	Feed Assay (picomoles/A_{260})	Product		Recovery of Purified tRNAs (%)	Accountability of $tRNA^{Arg}$ (%)
				A_{260} Units	Picomoles/A_{260}		
105-BD-3	Leucine	200	140	11.7	750	31	
105-BD-5	Arginine	500	95	16.0	1000	34	
105-BD-7	Arginine	1,000	95	36.0	920	35	
105-BD-10	Arginine	40,000	95	1040.0	1045	28	82
105-BD-13	Arginine	10,000	95	282.0	710	21	80

fraction probably could be recycled through these steps to achieve a greater recovery of arginine tRNAs in subsequent ethanol-gradient fractions. Further, none of the other tRNAs were damaged (as measured by amino acid acceptance) by these processing steps. It follows then, theoretically at least, that the 1 *M* NaCl fraction from a crude tRNA sample could be repeatedly aminoacylated, derivatized, and chromatographed on BD-cellulose to achieve high yields of many different tRNAs.

Future efforts will be oriented toward scaleup of runs to separate families of isoaccepting tRNAs from 10^5 to 10^6 A_{260} units of crude tRNA in both *E. coli* K-12 MO and beef liver. Also, experiments will be made in an attempt to improve low-recovery steps in the BD-cellulose process.

The leucine and arginine pools from runs 105-BD-3 and 105-BD-10 had activities of 750 and 1045 picomoles/A_{260} respectively (see Table 12.1). Each of these products is a mixture of several isoaccepting species (i.e., at least five species of leucine and five species of arginine) and other contaminating tRNAs or materials. It was possible that one or more of the species could have been damaged in the process up to this point, or that the isolation was selective for only certain of the isoaccepting tRNAs. In order to investigate this possibility, a small sample of the leucine pool was aminoacylated with ^{14}C-tagged leucine, and a sample of crude tRNA was aminoacylated with ^{3}H-tagged leucine. The two samples were mixed and cochromatographed on an RPC-2 column (see Fig. 12.5). Each of the isoaccepting species of the BD-cellulose product is seen in the same position and in the same ratio as is the case for the crude tRNA. It is obvious that no damage or fractionation occurred. Similarly, the cochromatography of the arginine pool and a sample of crude tRNA on an RPC-4 column showed coincidence of the peaks in the crude tRNA and BD-cellulose-purified arginine tRNAs.

Table 12.2. Separation of Isoaccepting Arginine tRNAs by RPC-4 Chromatography

Peak	Specific Activity (picomoles/A_{260})	A_{260} Units	Total Quantity of Material Recovered (picomoles)
1	718	9.11	6,541
2	1270	33.78	42,901
3	700	11.50	8,050
4	530	10.39	5,507
5	308	12.52	3,856
Total		77.30	66,855
Feed	885	100.00	88,500
Recovery		(77.0%)	(75.5%)

The conditions for separation of the individual isoaccepting species of the arginine pool have been determined. A total of 100 A_{260} units was loaded on a 1- by 240-cm RPC-4 column at 37°C and chromatographed. One major and four minor peaks of arginine were separated and pooled, as seen in Fig. 12.6. Total recoveries and final specific activities are tabulated in Table 12.2. Successful separation is dependent on a carefully constructed 2-liter gradient extending from 0.45 to 0.80 *M* NaCl (Fig. 12.6). Work is now under way to obtain similar data for 100-A_{260} samples of the leucine pool obtained after BD-cellulose chromatography.

We have found that RPC-3 and RPC-4 columns are also applicable to the separation of naphthoxyacetyl tRNAs from nonderivatized tRNAs. Specifically, when either RPC-3 or RPC-4 columns are loaded with a mixture of derivatized and nonderivatized tRNAs, it is possible to separate the two species using the normal NaCl gradients employed with these systems. In each column system, the derivatized aminoacyl-tRNA is held back and eluted at higher NaCl concentrations than

ORNL DWG 69-8479R

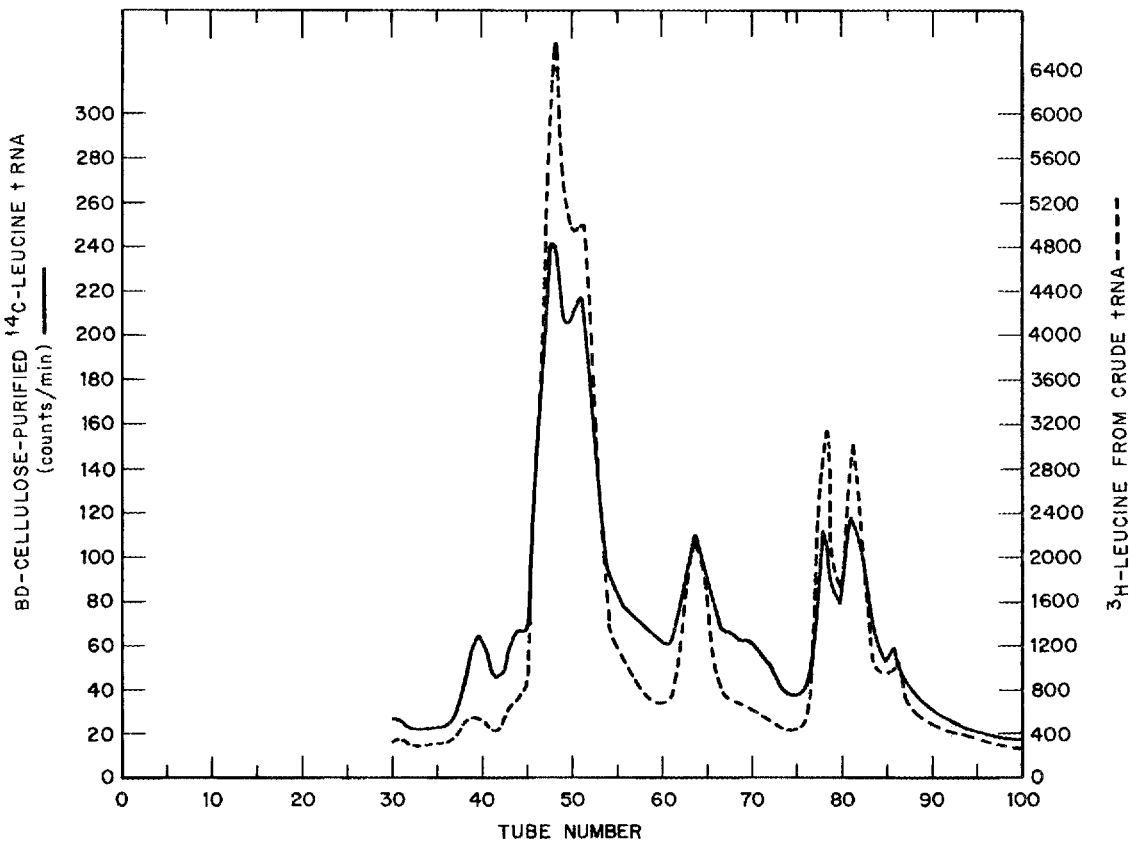

Fig. 12.5. Cochromatography of Leucyl-tRNAs, Isolated by BD-Cellulose Techniques, and Crude tRNA.

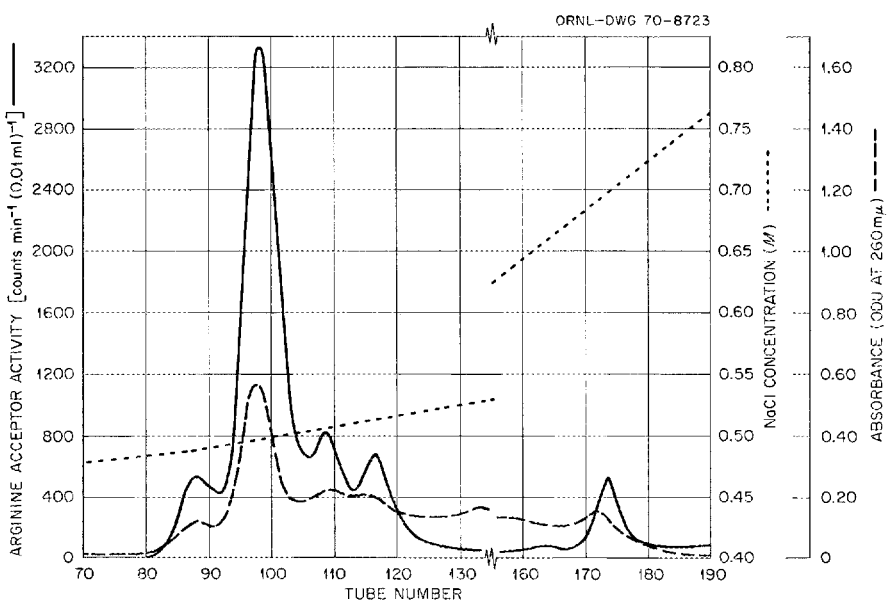

Fig. 12.6. Separation of Arginine tRNAs by RPC-4 Chromatography.

those at which the underivatized material is eluted. In addition, preliminary work seems to indicate that the recoveries of specific tRNAs may be more complete on these columns than on BD-cellulose columns. Work will be continued to determine if the purities and recoveries obtainable using these methods justify their use instead of BD-cellulose columns in the scheme of tRNA isoacceptor separations.

12.3 PREPARATION OF TRANSFER RIBONUCLEIC ACIDS FROM BEEF LIVER

Experimental work has been initiated to prepare samples of crude tRNA from mammalian sources and to subsequently purify the individual tRNAs by reversed-phase chromatography. The use of a tissue source instead of bacterial cells will necessitate some changes in the initial processing steps; however, based on experience in the Biology Division, no major problems are anticipated in RPC separation of the tRNAs. Beef liver has been selected as the source since it is readily available and should contain appreciable quantities of tRNAs. In each case, the liver is removed immediately after an animal is killed, chopped into small chunks, and then frozen in liquid nitrogen within 2 or 3 min.

Several methods of recovering tRNA from the frozen liver chunks are being evaluated. One method that appears promising involves grinding the beef liver in liquid nitrogen in a Waring Blendor and then pouring the frozen liver "dust" into a stirred tank containing phenol and aqueous buffer. The crude RNA mixture is recovered from the buffer by ethanol precipitation and

Table 12.3. Crude tRNAs Obtained from Beef Liver

Batch No.	1	2	3	4
Batch size, kg/liver	4	0.5	4	4
Method	(1) Grind in liquid nitrogen	(1) Grind in mixture of buffer and phenol	(1) Grind in liquid nitrogen	(1) Grind in mixture of buffer and phenol
	(2) Disperse in buffer	(2) Centrifuge	(2) Disperse in mixture of buffer, phenol, and 1 *M* NaCl	(2) Centrifuge
	(3) Disperse in phenol	(3) Precipitate with ethyl alcohol	(3) Precipitate with ethyl alcohol	(3) Precipitate with ethyl alcohol
	(4) Precipitate with ethyl alcohol	(4) Carry out batch DEAE	(4) Carry out batch DEAE	(4) Carry out batch DEAE
	(5) Lyophilize	(5) Precipitate with isopropanol	(5) Lyophilize	
	(6) Carry out batch DEAE	(6) Lyophilize		
	(7) Lyophilize			
Yield				
mg/kg	260	394	500	1578
A_{260}/kg	4316	6186	3403	18,157
Purity, A_{260}/mg	16.6	15.7	6.8	11.5
Visual appearance	Hazy	Clear	Very milky	Hazy
Aminoacylation of tRNAs, picomoles/A_{260}				
Arginine	3	20	18	18
Glutamic acid	1	4	3	3
Leucine	2	13	18	8
Lysine	3	21	18	11
Methionine	1	8	12	4
Phenylalanine	2	7	8	1
Serine	3	33	30	17
Valine	3	27	25	18

is further purified by batch DEAE or RPC-3 chromatography. Crude tRNA prepared by this method is being compared with tRNA prepared from rat liver by the method of Rogg, Wehrli, and Staehelin,[2] and also with tRNA prepared from mouse tumor by the method of Yang and Novelli.[3] Active beef liver tRNA preparations have been obtained, and process variables are being evaluated. Active beef liver aminoacyl-tRNA synthetase, used in the aminoacylation assays, was prepared by the method of Yang and Novelli.[3]

Table 12.3 shows analyses of four preparations of beef liver tRNA. Samples of the higher-quality products are being processed on RPC columns for the separation of individual tRNAs. Larger batches are planned for the future.

12.4 SEPARATION OF RIBOSOMAL RIBONUCLEIC ACIDS

The reversed-phase chromatographic technique was extended to the separation of ribosomal ribonucleic acids (rRNAs) from *E. coli* and RNAs from mammalian sources. The system previously described,[4] consisting of tricaprylymethylammonium chloride extractant (Adogen 464) dissolved in tetrachlorotetrafluoropropane (Freon 214) and supported on Chromosorb W, has proved to be the most successful. Therefore, it has been studied in detail.

The RNAs are eluted from the column with an eluent of increasing NaCl concentration, buffered with 0.05 *M* Tris-HCl at a pH of 7.2 to 7.5. In addition, this eluent is 3 *M* in urea and 0.01 *M* in $MgCl_2$. The column is maintained at 5°C. The 3 *M* urea is necessary in order to obtain good RNA recovery. A higher column temperature (25°C) causes the tRNAs to elute at higher salt concentrations. The lower temperature serves to suppress RNA degradation.

Since Freon 214 is no longer readily available, other solvents have been sought. Good separation of 16S and 23S rRNAs has been obtained with benzene, carbon tetrachloride, or diisopropylbenzene; however, all of these solvents are slightly soluble in the aqueous phase. Also, benzene and diisopropylbenzene have absorption bands in the 260-mμ region, where the RNA concentration is usually monitored. On the other hand, the

[2] H. Rogg, W. Wehrli, and M. Staehelin, *Biochim. Biophys. Acta* 195, 13–15 (1969).

[3] Wen-Kuang Yang and G. D. Novelli, *Proc. Nat. Acad. Sci. U.S.* 59(1), 208–15 (1968).

[4] *Chem. Technol. Div. Ann. Progr. Rept. May 31, 1969*, ORNL-4422, p. 283.

ORNL DWG 70-2764R

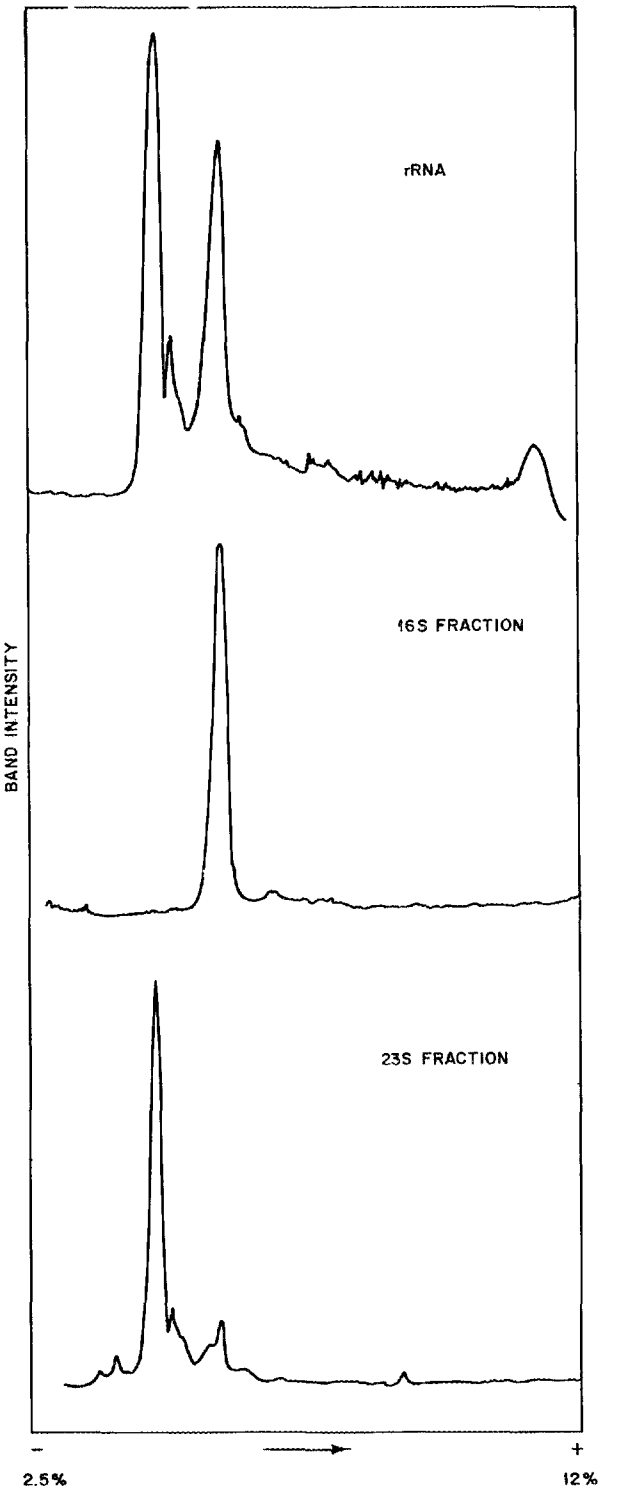

Fig. 12.7. Polyacrylamide Gradient Gel Electrophoresis of Fractions Obtained by Reversed-Phase Chromatography of *E. coli* Q13 rRNA.

availability and the low cost of these solvents are significant advantages.

Electrophoretic analysis of the 16S and 23S rRNA products was improved by the development of a continuous gradient polyacrylamide gel technique, which allows the determination of RNAs ranging in size from 4S to 28S on a single gel. The validity of the technique was verified by ultracentrifugation. Although ultracentrifugation does not give the resolution that is obtainable by electrophoresis, it is more useful for determining the actual sizes of the RNAs present. Several variables were studied in order to determine the optimal conditions for maximum resolution of the rRNAs in the Spinco L-2 ultracentrifuge. We found that the best results were obtained with a 6 to 24% glycerol gradient (in 0.01 *M* Tris, pH 7.0, and 0.001 *M* $MgCl_2$) at 39,000 rpm for 4 hr at 12°C.

Typical patterns obtained by scanning the dyed gels after electrophoresis are shown in Fig. 12.7. The top part of the figure shows the rRNA sample before reversed-phase chromatography. The major peaks correspond to 23S rRNA, 16S rRNA, and tRNA. The 16S fraction obtained by reversed-phase chromatography is shown in the center part of the figure. The 23S fraction still contains a small amount of 16S material after a single chromatographic run, as shown in the lower part of Fig. 12.7. However, the 16S material can be removed by rechromatography, as shown in Fig. 12.8.

End-group analysis of the 16S product by anion exchange chromatography after alkaline hydrolysis gave

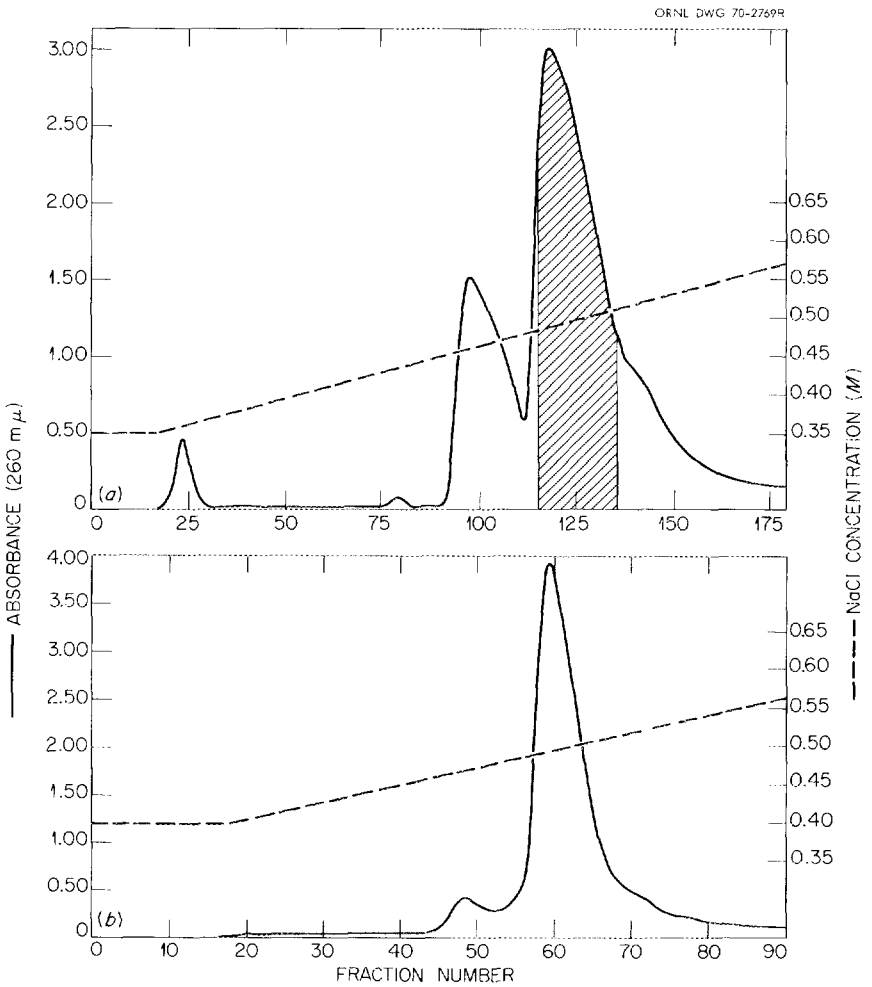

Fig. 12.8. Purification of 23S rRNA by Rechromatography. (*a*) Chromatogram from reversed-phase chromatography of about 50 mg of *E. coli* Q13 rRNA on a 1- by 240-cm column. (*b*) Rechromatography of the 23S fractions, shown by the cross-hatching, after precipitation with ethanol.

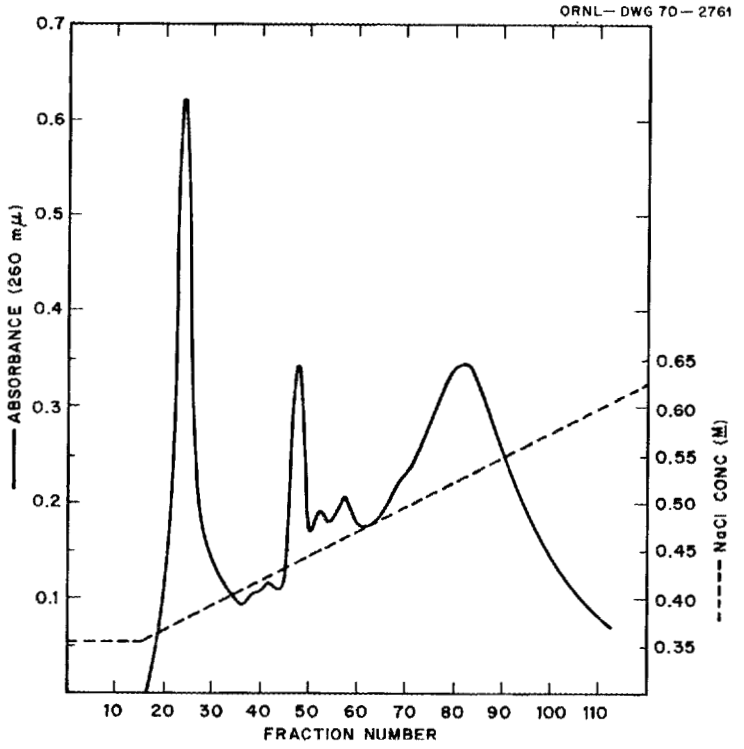

Fig. 12.9. Chromatogram of Rat Spleen RNA.

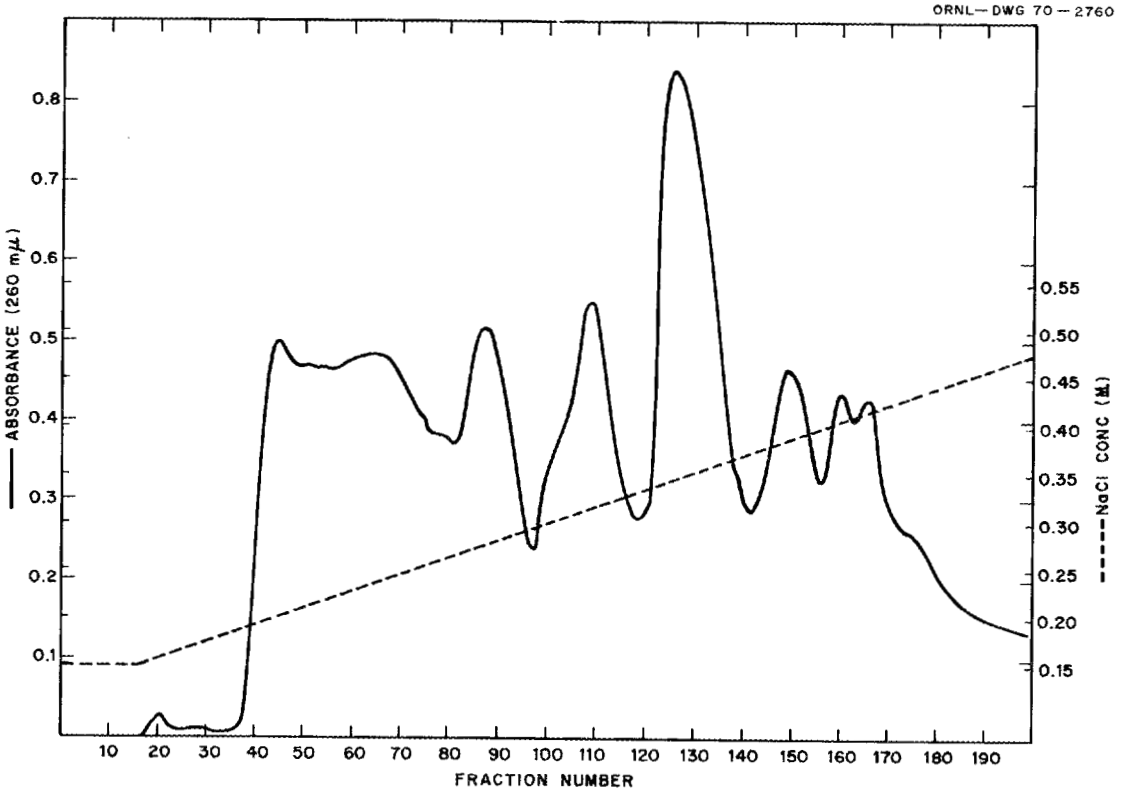

Fig. 12.10. Chromatogram of 4–8S Nuclear RNA from a Novikoff Hepatoma.

a molecular weight of 532,000, with adenosine as the 3′-terminal end group. Although electrophoresis and reversed-phase chromatography indicated a pure 23S product, more than one end group and a correspondingly low value for the molecular weight of the 23S product were repeatedly obtained. Other investigators have reported similar behavior for 23S rRNA.

Figures 12.9 and 12.10 demonstrate the applicability of the reversed-phase chromatographic system to the separation of other RNAs. Figure 12.9 is a chromatogram of a sample of rat spleen RNA, showing several 260-mμ-absorbing peaks. Although the peaks were not analyzed further, rRNAs are expected to occur in the rear region; the first peak probably contains 4S to 5S RNA. Figure 12.10 shows a chromatogram obtained from a sample of 4S to 8S nuclear RNA from a Novikoff hepatoma. Again, several 260-mμ-absorbing peaks were obtained using a 0.15 to 0.55 *M* NaCl gradient.

This chromatographic system should prove useful for separating a variety of RNAs ranging in size from 4S to 28S, including messenger RNAs.

12.5 ENGINEERING SCALEUP AND PREPARATION OF PURIFIED *E. COLI* TRANSFER RIBONUCLEIC ACIDS

Purification of Formylmethionine, Valine, Glutamic Acid, and Arginine tRNAs from *E. Coli* K-12 MO7

Last year, mixed tRNAs were recovered from 52 kg of *E. coli* K-12 MO7 cells and were further purified and divided into three pools by using DEAE-cellulose column chromatography. Phenylalanine tRNA was recovered from the middle pool. During the current report period, the front pool was processed to yield four purified tRNAs: formylmethionine, valine, arginine, and glutamic acid. This is the first time we have recovered the last two products in large quantities. The recovery of arginine is particularly significant because it is found near the middle of most chromatograms. In fact, it was divided nearly equally between the first and second pools on the DEAE-cellulose columns.

Preliminary testing of RPC-3 columns showed that some of the tRNAs from strain K-12 chromatographed in different positions from those previously processed from strain B. Results of flowsheet development tests showed that the elution sequence of tRNAs was dependent on the pH and on the extent of the tRNA loading on the column. As the pH was decreased from 8 to 4.5, the relative positions of the early-eluting tRNAs were shifted. A second formylmethionine was moved forward from a position between valine and arginine until it was nearly coincident with the first formylmethionine. Glutamic acid was moved to the front of the chromatogram.

As the load was increased from 10 to 50 A_{260} units per milliliter of packing, glutamic acid and arginine were moved forward relative to formylmethionine and valine. The best separation of the four tRNAs from each other was achieved with a 1-in.-diam by 30-in.-long column loaded with about 30 A_{260} units per milliliter. This procedure was successfully scaled up to either a 2-in.-diam by 96-in.-long or a 4-in.-diam by 30-in.-long column. A typical chromatogram, obtained at pH 4.5 with a load of 32 A_{260} units per milliliter of packing on a 4-in.-diam by 30-in.-long column, is shown in Fig. 12.11. The sequence of elution of tRNAs at the front of the chromatogram is glutamic acid, formylmethionine, arginine, and valine. The formylmethionine product pool was obtained directly from the RPC-3 column eluate. The amounts recovered and the purities are shown in Table 12.4. Three additional pools were obtained: one that contained a mixture of glutamic acid and formylmethionine; one that contained arginine and formylmethionine; and one that contained valine and the remaining tRNAs. Glutamic acid was recovered by rechromatography on a small RPC-3 column at pH 4.0. Nearly complete separation from methionine was obtained; the activity was 83%. Arginine was purified by rechromatography on RPC-4 at pH 7.0 and was well separated from three methionine peaks; the final arginine product had an activity of 70%. Valine was recovered by rechromatography on RPC-3 at pH 8. It was well separated from all the other tRNAs, except alanine, and was 82% pure. The tRNA recoveries were as follows: 3.3 g of formylmethionine, 0.86 g of glutamic acid, 0.88 g of arginine, and 1.3 g of valine.

The tRNA products were concentrated by sorption on a small DEAE-cellulose column from dilute sodium chloride (0.2 *M*) solution, followed by desorption with an 0.8 *M* salt solution. This yielded a solution in which the concentration of tRNA was about 50 A_{260} units/ml. A fibrous form of DEAE-cellulose (DE-23) was used because the pressure drop is much lower with this type than with the microgranular form (DE-52).

Reliability and Reproducibility of Large-Scale Production of Purified tRNAs from *E. coli* K-12 MO

The reliability and reproducibility of the large-scale processing methods for recovery and purification of formylmethionine, arginine, and phenylalanine tRNAs were demonstrated with three batches of *E. coli* K-12

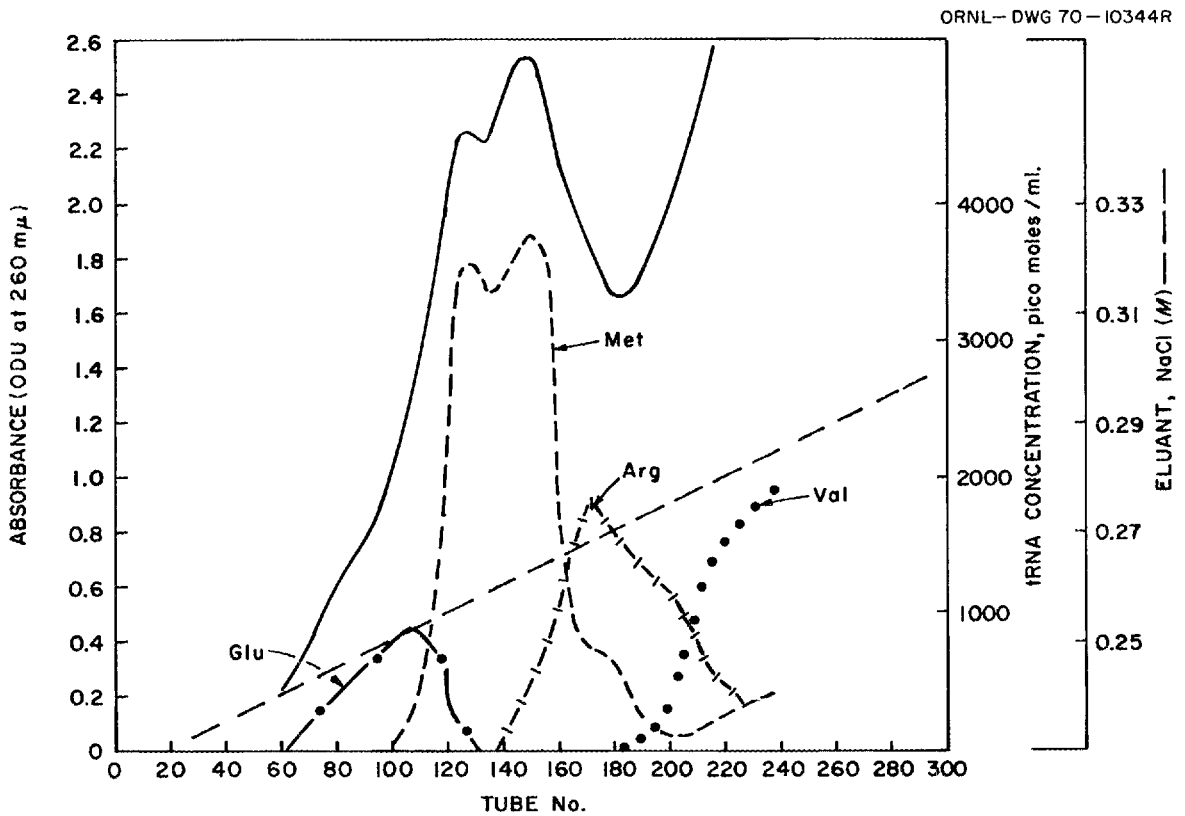

Fig. 12.11. RPC-3 Column Chromatogram.

Table 12.4. Summary of tRNA Products from *E. coli*

tRNA	*E. coli* Strain	Weight (g)	Amino Acid Acceptance (picomoles/A_{260})	Terminal Adenosine (picomoles/A_{260})	Activity[a] (%)
fMet	K-12 MO	1.63	1435	1570	92
	K-12 MO7	3.32	1413	1452	97
Arg	K-12 MO	0.84	1345	1343	100
	K-12 MO7	0.88	1266	1798	70
Phe	K-12 MO	0.20	1300	1450	90
	K-12 MO	0.45	720	1450	50
	K-12 MO7	0.92	995	1270	78
Val	K-12 MO7	1.27	1310	1590	82
Glu	K-12 MO7	0.86	1450	1749	83

[a]Amino acid acceptance per terminal adenosine.

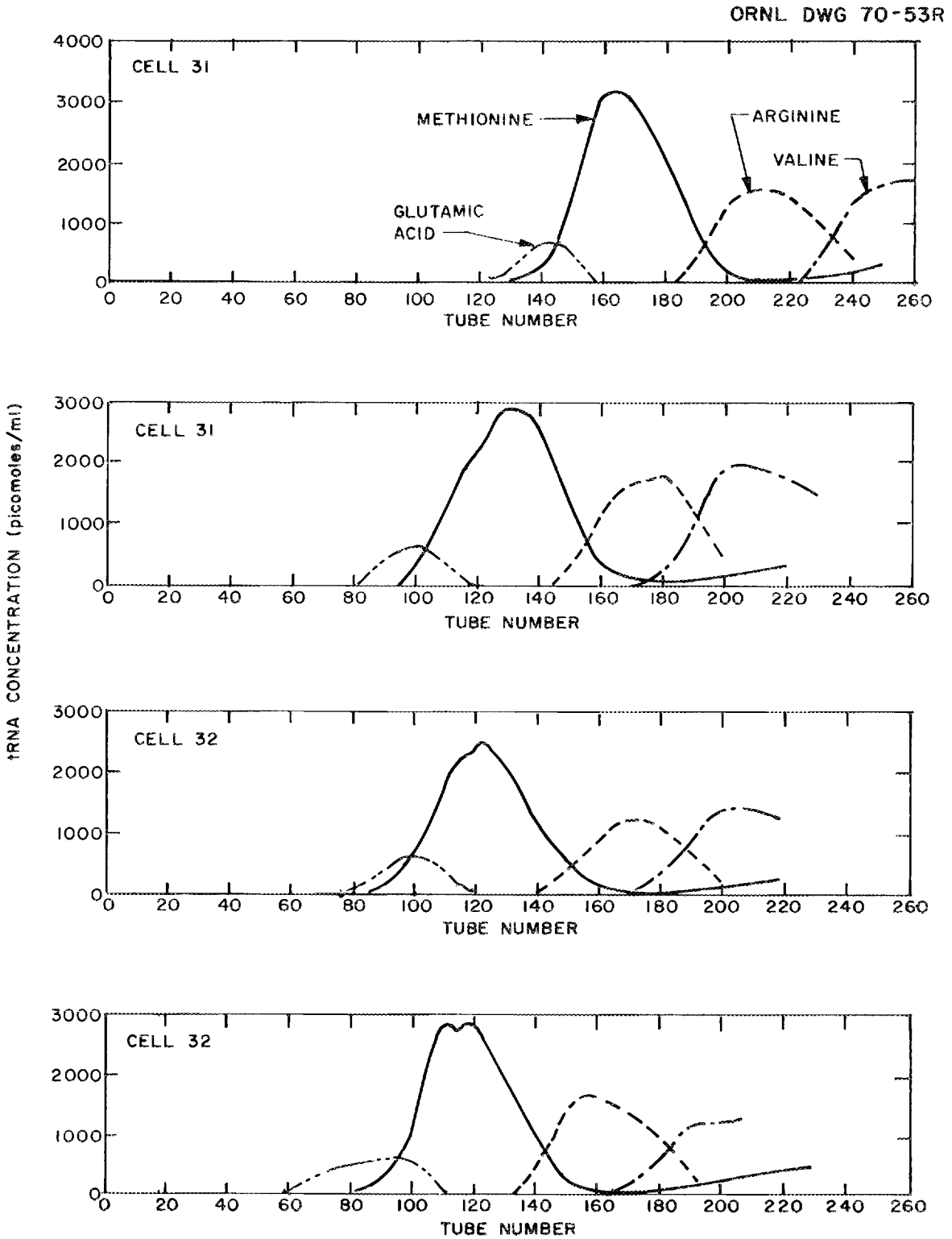

Fig. 12.12. Chromatograms from Duplicate Runs Made with tRNAs from Two Batches of *E. coli* Cells.

MO cells grown in successive weeks. Each batch, which consisted of about 17 kg of wet cells, was harvested by centrifugation; then the mixed tRNAs were recovered in a phenol-extraction step, purified by a double ethanol precipitation, and further refined and separated into pools of tRNA by chromatography on 6-in.-diam by 30-in.-long DEAE-cellulose columns. The front pool was rechromatographed on RPC-3 columns (4 in. in diameter and 30 in. long) to isolate the formylmethionine product and to produce an arginine-rich pool from which the arginine was recovered by subsequent chromatography on RPC-4 columns. Phenylalanine tRNA was recovered from the rear DEAE pool by chromatography on 2-in.-diam by 96-in.-long RPC-4 columns. The products were concentrated to about 50 A_{260} units/ml by sorption-desorption on a 2-in.-diam by 10-in.-long DEAE-cellulose column.

Except for a few delays in the product concentration steps, each step in the flowsheet was accomplished according to a preestablished six-week operating schedule. With minor exceptions, the reproducibility of the processing methods was found to be good. There was some indication of a pattern in the rate of growth of different batches of cells that persisted throughout the subsequent processing steps. The last two batches were quite similar (but were different from the first batch) as to rate of cell growth, yield of tRNAs, and purity of the isolated products. In general, duplicate runs on the reversed-phase columns from a given batch of cells showed good replication of yield and purity (see Fig. 12.12). The summary of the products is shown in Table 12.4. The following quantities of purified tRNAs were obtained: 1.6 g of formylmethionine, 0.8 g of arginine, and 0.6 g of phenylalanine. The total direct operating cost, including manpower, overhead, analytical services, support craft, and chemicals, was $40,800, which is equivalent to $13.20 per milligram of total purified tRNAs. No charges were included for amortization of the capital equipment or buildings. The major cost item was manpower. The total labor required for the demonstration was 214 man-days. The distribution of manpower was as follows: preparations, 30%; recovery of mixed tRNAs, 25%; DEAE-cellulose chromatography, 10%; reversed-phase chromatography, 25%; and concentration of products, 10%.

12.6 DISTRIBUTION OF PURIFIED TRANSFER RIBONUCLEIC ACIDS

Gram quantities of individual tRNAs have been prepared as by-products of the engineering scaleup and flowsheet demonstration for the purification of tRNAs. In January 1970, an inventory of our products showed that we had on hand five different purified tRNAs from *E. coli* B, K-12 MO, or K-12 MO7, in a total of 13 different samples. These samples were equivalent to almost 10 g of purified tRNAs.

After public announcement of the availability, without charge, of these tRNAs was made in *Science* and in *Chemical and Engineering News* in January 1970, requests for samples have averaged one to two per day. These requests are reviewed by a committee of the National Institute of General Medical Sciences, and shipments are made in accordance with the committee's recommendations. Shipments to recipients in this country are made by air express in containers packed with dry ice. Samples to locations abroad are dialyzed against distilled water, lyophilized to a dry powder, and then sent via air parcel post. A total of 103 investigators in 10 countries have received samples of these purified tRNAs over the past three years. Eighty-six of these investigators were in the United States, principally in biology departments and medical schools of universities. The foreign recipients were in England, West Germany, the U.S.S.R., Poland, Japan, Spain, France, Norway, and Canada. The areas of interest of these investigators cover many fields – X-ray crystallography, conformation in solution, nucleotide composition, protein chain initiation, etc. In most cases, these investigators are dependent upon our supply of tRNAs.

BODY FLUIDS ANALYSES

In order to take advantage of recent advancements in the medical sciences, the supporting clinical laboratory must have more selective and more sensitive analytical techniques. Increasing demands for medical services will also require that these techniques and other laboratory procedures be highly automated, accurate, and as rapid as is practical. The development of instrumentation to meet these needs is the objective of the Body Fluids Analyses Program.

At present, our efforts are directed toward the development of high-resolution automated analyzers for clinical application; emphasis is on techniques that result in the determination of a large number of constituents. The initial effort has involved the determination of low-molecular-weight constituents of body fluids and has resulted in the development of two separate analytical systems: an analyzer for ultraviolet (UV)-absorbing constituents and an analyzer for carbohydrates.

12.7. PROTOTYPE ANALYZERS

The carbohydrate analyzer and three UV-analyzer model II prototype systems have been undergoing evaluation at three other laboratories – the Clinical Center of the National Institutes of Health, Johns Hopkins Medical Center, and the Duke University Medical Center. Although some problems have been experienced, the operability of the machines has proved to be very good. For example, the UV-analyzer at the Johns Hopkins Medical Center has operated for over 400 hr with less than 5% downtime.

Model Mark II and Mark II-A Analyzers

The design and construction details of the Mark II prototypes of both the UV-analyzer and the carbohydrate analyzer have been previously discussed.[5,6] Two of the Mark II UV-analyzers have been upgraded to the Mark II-A version by installation of a new, small sample injection valve and a new, miniaturized UV-photometer. A Mark II-A UV-analyzer has been built for Eli Lilly and Company using their funds. This analyzer will be used at the Lilly Laboratory for Clinical Research to determine the excretion of drugs and drug metabolites by subjects whose diets and drug intakes are carefully controlled.

Model Mark III Analyzer

The miniaturized, advanced UV-analyzer, designated as Mark III,[7] has been modified and repackaged (Fig. 12.13), and an advanced version of the carbohydrate

[5] C. D. Scott *et al.*, *Body Fluid Analysis Program. Progress Report for the Period March 1 to August 31, 1968*, ORNL-TM-2372 (January 1969).

[6] C. D. Scott, R. L. Jolley, W. W. Pitt, and W. F. Johnson, *Am. J. Clin. Pathol.* 53(5) (Suppl.), 701–12 (1970).

[7] C. D Scott *et al.*, *Body Fluids Analyses Program. Progress Report for the Period September 1, 1968 to February 28, 1969*, ORNL-TM-2551 (July 1969).

Fig. 12.13. Miniaturized Mark III UV-Analyzer.

analyzer has been designed and built. Each of the new prototypes is completely contained in a 32½-in.-high, 25½-in.-wide, and 22-in.-deep metal cabinet which can be placed on the top of a laboratory bench. The analyzers yield results comparable to those obtained with the larger Mark II analyzer. The quantities of ion exchange resin and the volumes of eluent and sample that are required for these advanced prototypes are only 13% of those required for the earlier models. The fabrication costs have been reduced by about 30%.

12.8 SEPARATION SYSTEMS

The availability of a miniaturized double-beam photometer with flow cells that cause very little backmixing of the eluent stream has made it possible to evaluate small-diameter ion exchange columns (i.e., columns with an inside diameter as small as 0.1 cm) and to establish operating parameters for their use in chromatographic systems. These columns gave results comparable to the larger (0.62-cm-ID) columns when both were tested in a straight, vertical configuration.

To reduce the size of the instrument package, it was desirable to decrease the overall height of the column without decreasing its length. Several different column configurations were tested before a successful design was evolved. A coiled column (1-in.-diam coils) was found to significantly reduce chromatographic resolution, while a single loop (15 in. in diameter) was somewhat more effective. Three 50-cm-long straight columns were connected with short U-shaped sections of capillary tubing to give a 150-cm-long column with an external length of only about 55 cm. This segmented configuration provided essentially the same resolution as a straight column; however, the pressure drop was excessive at comparable flow rates since it had three additional sintered metal filters.

A fourth configuration, called a folded column, yielded the desired results of high resolution and low pressure drop. This configuration consists of a single length of tubing, 150 cm long, bent at 180° about 50 cm from each end (Fig. 12.14). The pressure drop of the folded column is sufficiently low to permit the flow rate in the UV-analyzer to be doubled and, in turn, the analysis time to be decreased from 40 hr to 20 hr, with only a slight loss in resolution.

Cation Exchange Systems

Coupled anion and cation exchange columns are being studied in an attempt to improve chromatographic resolution and decrease analysis time. The chromatograms obtained from the anion column and from the coupled columns were quite similar, except that improved resolution was observed in the front portion of the chromatogram from the coupled (anion followed by cation) system.

The use of a cation exchange column for the rapid separation of nucleosides[8] was investigated, and a method that is suitable for use with the Mark II and Mark III UV-analyzers has been developed. The separation of uridine, guanosine, adenosine, and cytidine in 50 min is illustrated in Fig. 12.15.

Fundamental Studies

Fundamental studies of gradient elution chromatography are continuing. We have developed a mathematical model[9] that shows good correlation, in regard to both peak position and shape, between predicted and actual experimental data. This model has enabled us to make optimization studies of chromatographic systems, since the effect of individual parameter changes can be investigated on the computer without the accompanying effects of other induced system variations that are usually observed with operating experimental systems.

The mathematical model was used to predict the effect of initial eluent concentration and the steepness of the gradient on the positions and the shapes of two representative adjacent peaks. Comparison of these model-predicted chromatograms with chromatograms predicted for isocratic elution (constant concentration), but with the same elution volumes, shows that gradient elution has virtually no effect on the shapes of the peaks but does shift the elution positions of the peaks (i.e., the gradient affects only the distribution coefficient of the solute – not the mass-transfer coefficient).

The overall mass-transfer coefficient, K_2 (refs. 7 and 10), was calculated from experimental peak dispersion data for ten urinary constituents. A plot of the reciprocal of K_2 vs the reciprocal of the dynamic distribution coefficient, λ (refs. 7 and 10), indicates that there is very little, if any, resistance to mass transfer in the fluid phase.

---

[8] M. Uziel, C. K. Koh, and W. E. Cohn, *Anal. Biochem.* 25, 77 (1968).

[9] W. W. Pitt, Jr., *Gradient Elution Chromatography of Urinary Constituents. Mathematical Analysis of the Kinetics of Gradient Elution Chromatography,* ORNL-TM-2870 (April 1970).

[10] C. D. Scott *et al., Body Fluids Analyses Program. Progress Report for the Period March 1 to August 31, 1969,* ORNL-TM-2779 (December 1969).

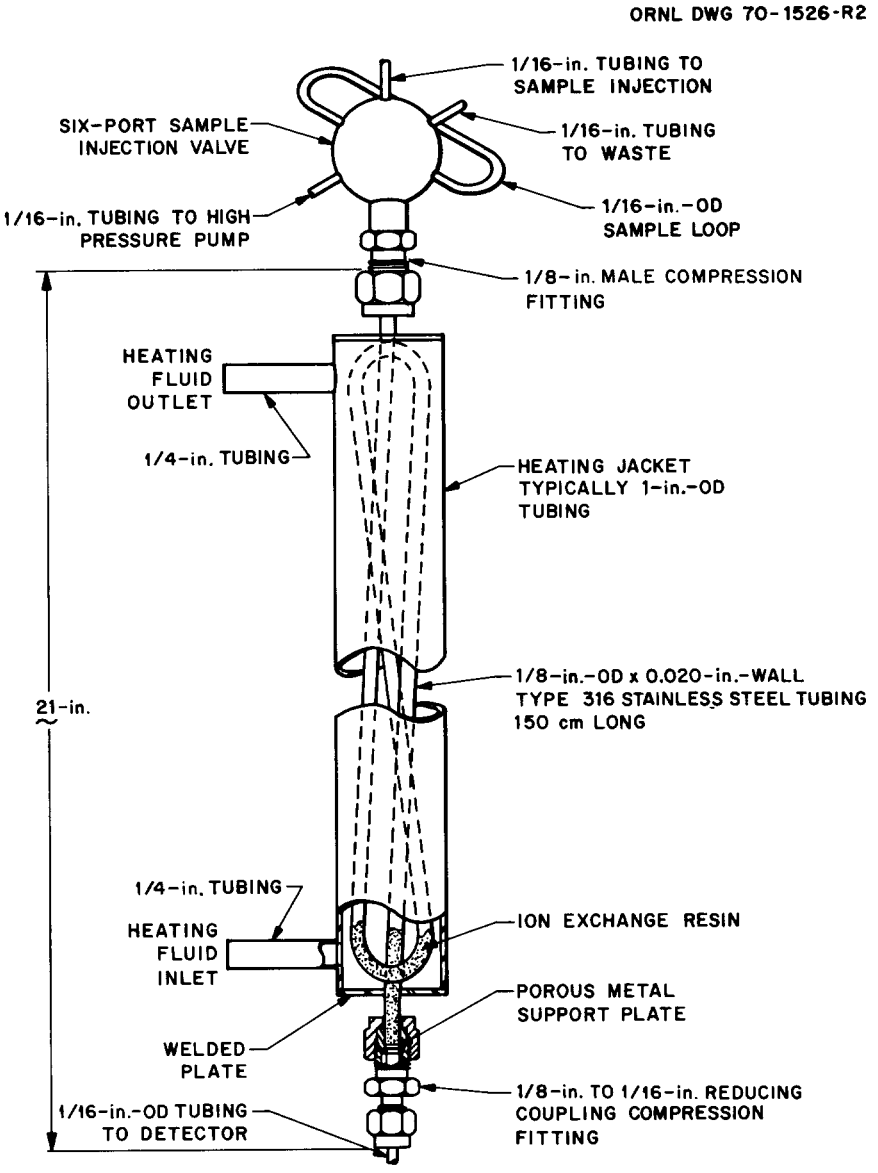

Fig. 12.14. Folded High-Pressure Chromatographic Column.

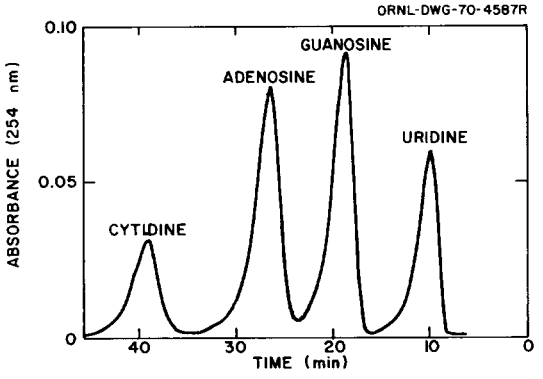

Fig. 12.15. Separation of Nucleosides Using Cation Exchange Resin. Conditions: ammonium acetate–acetic acid buffer (NH_4^+ = 0.3 *M*, pH = 4.65); temperature = 50°C; flow rate = 41 ml/hr; 50 nanomoles of each nucleoside.

12.9 SYSTEM COMPONENTS

UV-Photometer

The ORNL UV-photometer is a dual-beam, dual-wavelength flow photometer that operates at 254 nm and 280 nm by using a low-pressure mercury lamp (254 nm) and a phosphor rod (280 nm) as light sources. The flow cells are 3-mm-ID quartz tubes that actually form part of the flow line. The Mark II UV-photometer, an improved version of the previously reported Mark I model,[7] is of modular construction and has most of its electronics on printed circuit cards inside the end cap of the detector head (Fig. 12.16).

Colorimeter

A flow colorimeter based on the same general design (with the exception of the light source) as the UV-photometer is being evaluated as the detector for both prototype versions of the carbohydrate analyzer. An incandescent light coupled with interference filters is utilized to achieve the desired wavelengths, which are 480 and 490 nm for the carbohydrate analyzer. The electronic noise of the colorimeter has proved to be low enough to permit operation at an electronic gain of 10; that is, full-scale deflection on the recorder corresponds to an absorbance of 0.046.

Automated Gradient Generator

The two-chamber (each chamber being wedge-shaped) gradient generating device that is used on the Mark II and Mark II-A prototypes has proved to be unsatisfactory for the smaller Mark III prototype system. Mild gradient changes, apparently caused by surface tension effects, create only small artifacts in chromatograms on the larger Mark II system; however, they become more severe on the miniaturized Mark III system. To solve this problem, a dual-chamber, controlled-stroke gradient generator for the Mark III UV-analyzer has been constructed and is currently undergoing developmental testing (Fig. 12.17). It consists of two spring-loaded, 100-ml syringes filled with acetate buffer – one with dilute (0.015 *M*) buffer and the other with a more concentrated (6.0 *M*) buffer – coupled together by means of a sliding cam arrangement.

Difficulty has been encountered in obtaining syringes and sliding cams that have sufficiently low friction to permit springs of low tension (10-lb pull) to force the solutions out of the syringes at the desired low flow rate (10 ml/hr).

12.10 IDENTIFICATION OF BODY FLUID CONSTITUENTS

Identification of the molecular constituents of physiologic body fluids has been aided by the interchange of information with the investigators that are evaluating prototype UV-analyzers in laboratories at other locations.

Positive identification of constituents in normal or pathologic urine samples requires separation and identification by at least two of the following methods: ultraviolet spectroscopy, gas chromatography, and mass spectrometry. To date, 35 UV-absorbing components of

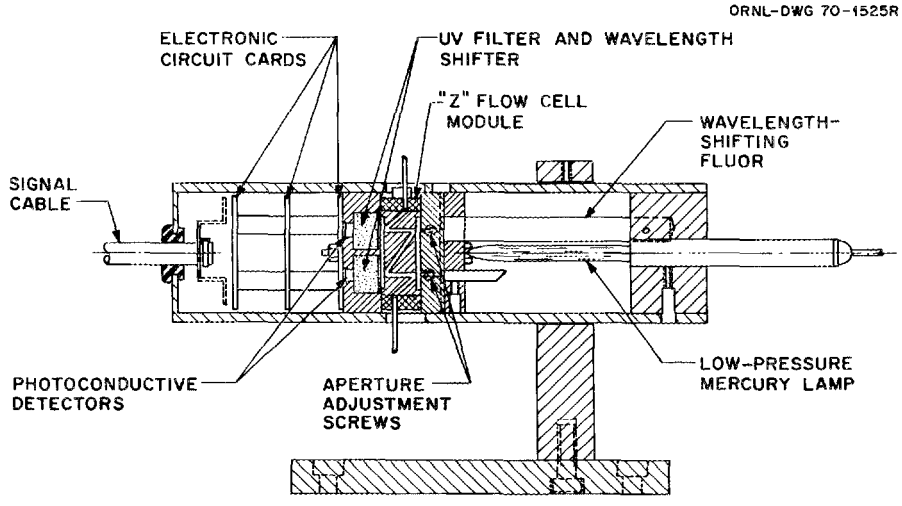

Fig. 12.16. The Mark II UV-Photometer, Showing Modular Construction.

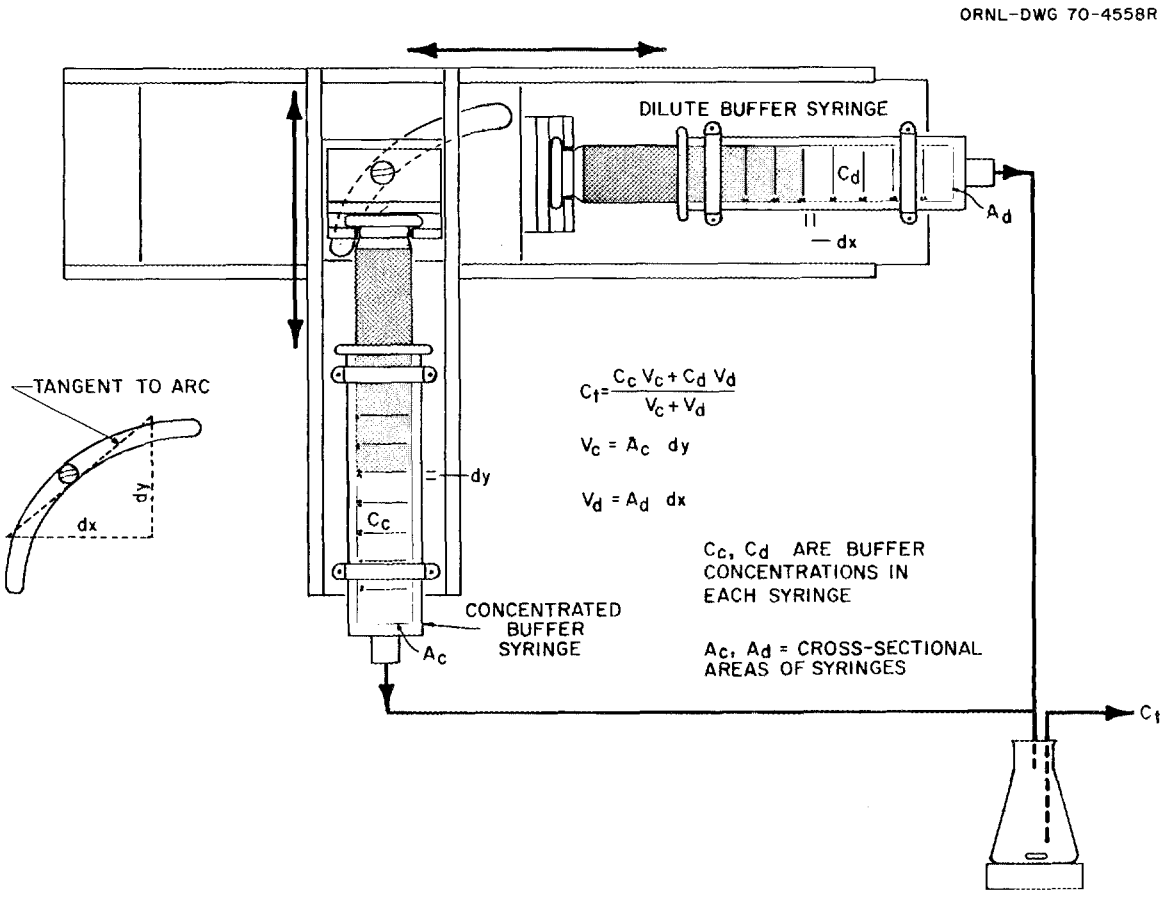

Fig. 12.17. Gradient Generating Device.

body fluids have been positively identified: 16 compounds in normal urine,[11] 12 compounds in pathologic urine, and 7 drugs or drug metabolites. The elution positions of many of the 70 additional cochromatographed standards are shown in Fig. 12.18.

Positive identification has been established for ten carbohydrates in the normal reference urine, and tentative identification has been established for eight additional compounds by cochromatography with reference standards. Positive identification of carbohydrates is based on elution position and relative gas chromatographic retention times for the separated constituents of the carbohydrate chromatogram. Some of the more significant work in identification is given below.

Identification of Orotidine

An abnormal metabolite was identified with the UV-analyzer in studies of patients undergoing allopurinol or oxypurinol (oxidation product of allopurinol) therapy. Three patients, each in a different pathologic state, were found to be excreting abnormal amounts of orotidine (50 to 133 mg/day as compared with the normal rate of 2 to 4 mg/day)[12] and orotic acid. The normal metabolic pathway, shown in Fig. 12.19, involves the conversion of orotic acid to orotidine-5′-phosphate, catalyzed by the enzyme orotidylic pyrophosphorylase (OPP), and the subsequent decarboxylation of orotidine-5′-phosphate. Apparently the decarboxylation, catalyzed by the enzyme orotidylic decarboxylase (OD), is being inhibited by one of the metabolites of allopurinol, either the ribosyl derivative or oxypurinol. High-resolution techniques are expected to provide information on possible metabolic changes induced by therapy using new drugs and thus, hopefully, to aid in preventing unwanted side effects.

[11] A composite sample of urine from eight normal males, 25 to 40 years of age.

[12] M. Lotz, H. J. Fallon, and L. H. Smith, Jr., *Nature* 197, 194 (1963).

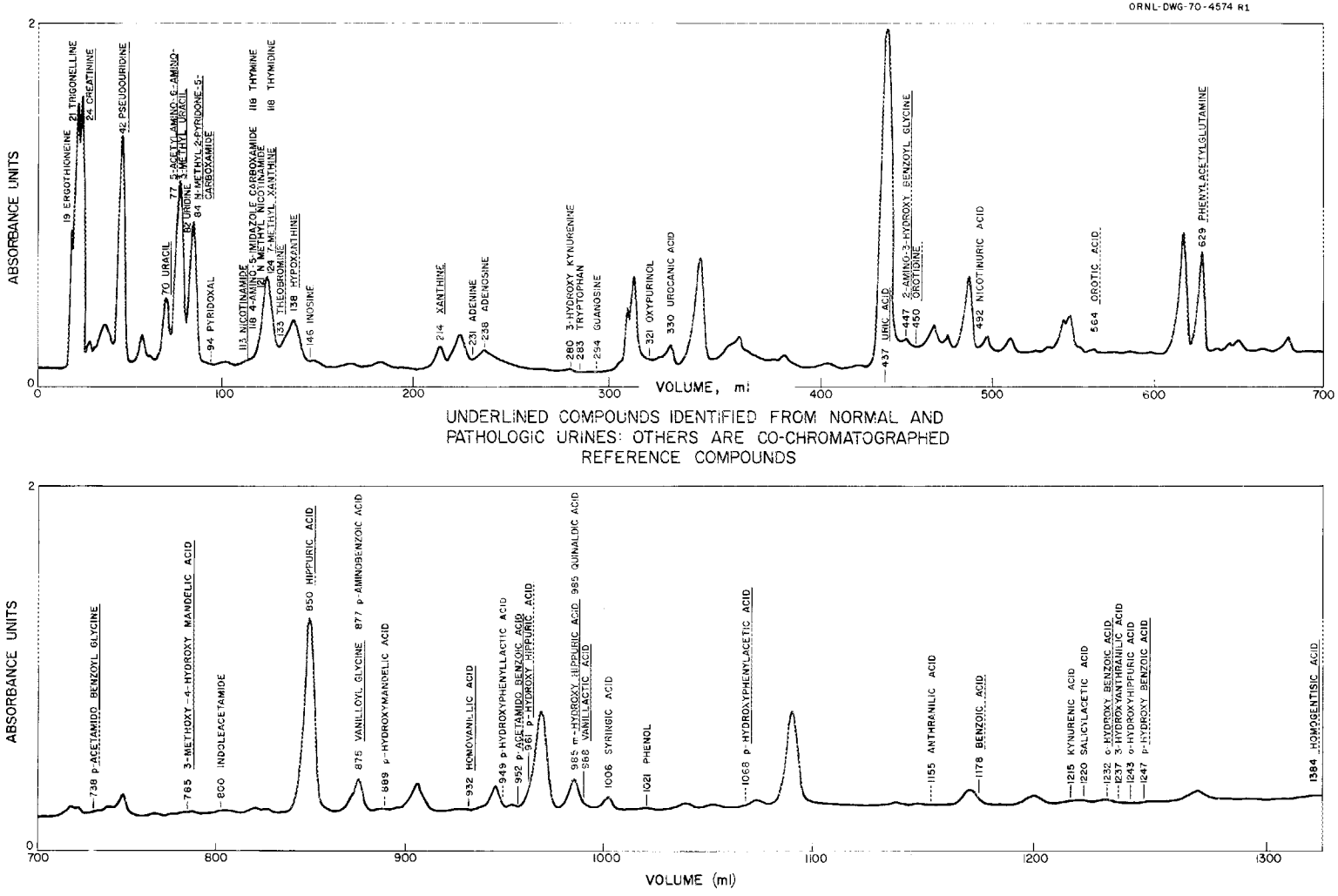

Fig. 12.18. UV Chromatogram of Normal Reference Urine Showing Elution Positions of Positively Identified Compounds and Selected Reference Compounds.

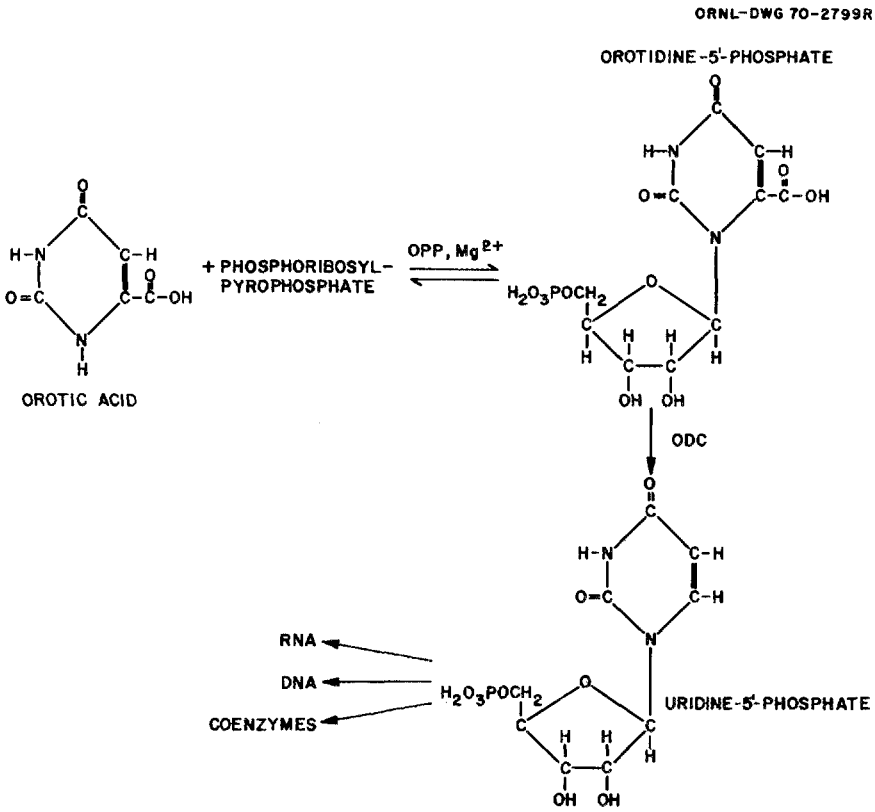

Fig. 12.19. Normal Metabolic Pathway for Orotic Acid and Orotidine.

Identification of Aromatic Acids and Their Glycine Conjugates

Gas chromatographic data have been gathered on several aromatic carboxylic acids (and their glycine conjugates) isolated from urine. Trimethylsilyl derivatives were prepared in order to impart the necessary volatility to these polar compounds to permit gas chromatographic analysis. An approximately constant increase of 5.76 ± 0.07 in methylene unit (MU) retention values was observed for the glycine conjugates of the nine acids studied when the conjugates were compared with the free acids. This relationship has proved useful in identification since reference glycine conjugates are not usually available commercially.

Gas Chromatography of Carbohydrates

The various classes of carbohydrates are eluted within relatively distinct ranges of retention times (retention times, in MU values, are relative to standard C_nH_{2n+2} hydrocarbons). The pentoses, hexoses, disaccharides, and trisaccharides have MU values of 16.44 to 17.94, 18.15 to 20.31, 27.34 to 29.94, and 35.60 to 36.55 respectively. Multiple peaks are observed for the anomeric forms of the reducing sugars, while nonreducing carbohydrates such as sucrose and raffinose give only a single gas chromatographic peak.

12.11 APPLICATIONS AND EXPERIMENTAL RESULTS

Concurrent with progress in engineering developments for the UV- and carbohydrate analyzers, a program is being conducted to evaluate applications of these instruments to the investigation of various etiologies of disease. Some of the pathologic states that have been studied include schizophrenia, ataxia telangiectasia, microcephaly, alkaptonuria, maple syrup urine disease, hereditary nephritis, and Lesch-Nyhan syndrome. Physiologic body fluids other than urine that have been investigated include blood, cerebrospinal fluid, amniotic fluid, perspiration, and kidney tubal fluid. Preliminary evaluation of several of these analyses is given below.

The analytical determination of the individual molecular constituents of physiologic body fluids by peak

area measurement is a very important aspect in determining the utility of the UV- and carbohydrate analyzers in the clinical laboratory. This has been studied by the addition of known amounts of standard compounds, together with a small amount of standard reference urine to provide matrix effects. Quantification of the chromatograms for 12 urinary excretion products by peak area measurement gave analytical results that agreed to within ±10% of the known amounts placed on the column. These results will undoubtedly be improved upon when on-line computer evaluation of each chromatogram becomes a reality.

Analyses of Other Body Fluids

Amniotic Fluid. – A specimen of amniotic fluid[13] from a normal subject was analyzed on both the UV- and carbohydrate analyzers. Both chromatograms contained fewer peaks than are normally observed in urine samples and, in general, were similar to those obtained for blood serum. The UV chromatogram contained 3 major peaks (two of which were tentatively identified as urocanic and uric acids) and 25 minor peaks. The carbohydrate chromatogram contained 1 major peak (glucose) and 13 minor peaks (one of which was tentatively identified as fructose).

Cerebrospinal Fluid. – Cerebrospinal fluids[14] from three patients afflicted, respectively, with muscular dystrophy, cerebral hemorrhage, and a brain tumor were examined by the UV-analyzer; the sample from the patient with muscular dystrophy was also analyzed on the carbohydrate analyzer.

The chromatogram of the fluid from the patient with a brain tumor comtained 4 major peaks (two of which were tentatively identified as uric acid and creatinine) and 29 minor peaks. The chromatogram of the sample of fluid from the patient with the cerebral hemorrhage contained 8 major peaks (two of which were creatinine and uric acid) and 40 minor peaks, and appeared qualitatively to contain approximately the same peaks as the chromatogram of the fluid from the patient with a brain tumor. Creatinine in these two samples appeared to be significantly higher than that reported in the literature.

The UV chromatogram of the fluid from the patient afflicted with muscular dystrophy generally indicated very low concentrations of molecular constituents when compared with the other two samples of fluid. It contained 3 major peaks (one of which was uric acid) and 15 minor peaks. A very large unidentified peak was eluted after uric acid; this peak did not appear in the chromatograms of the other two samples. The carbohydrate chromatogram of this sample contained one major peak (glucose) and five minor peaks (three of which were tentatively identified as mannose, fructose, and ribulose).

Analyses of Pathologic Urine Samples

Lesch-Nyhan Syndrome. – A 24-hr urine sample[14] obtained from a 14-year-old boy afflicted with Lesch-Nyhan syndrome (manifestations are a strong tendency for self-destruction and aggressive behavior) was analyzed on the UV- and carbohydrate analyzers. The sample was collected while the patient was undergoing allopurinol therapy. Although the carbohydrate chromatogram appeared to be normal, the UV chromatogram had many abnormal aspects. Notable among the absent urinary constituents was hippuric acid, the glycine conjugate of benzoic acid, which has been found in every human urine sample analyzed to date except urine from subjects afflicted with acute lymphocytic leukemia. The glycine conjugates of vanillic acid and *m*- and *p*-hydroxybenzoic acids (Fig. 12.20) were also absent or only present in very small amounts.

The absence of the conjugated compounds would lead one to expect to find benzoic acid and related compounds, possibly conjugated with glucuronic acid, in the urine. Both benzoic and *p*-hydroxybenzoic acids were identified and were present in relatively high concentrations, suggesting an inhibition or complete lack of the normal glycine detoxification mechanism in this patient.

Both orotidine and orotic acid were excreted in significant amounts by this patient as the result of the allopurinol therapy (see Sect. 12.10).

Alkaptonuria. – Alkaptonuria is a metabolic disorder caused by lack (or inhibition) of the enzyme homogentisic acid oxidase. Inhibition of this enzyme prevents the normal metabolic breakdown of homogentisic acid (HGA) and, consequently, causes elevated urinary excretion of the latter toxic compound.

A study was made in which ^{14}C-labeled HGA was given to a control patient and two patients afflicted with alkaptonuria.[15] Results of the study showed that

[13] Courtesy of Dr. R. Rodney Howell, The Johns Hopkins Medical Center.

[14] Courtesy of Dr. Donald S. Young, Clinical Center, National Institutes of Health.

[15] Samples were obtained through the courtesy of Dr. J. E. Seegmiller, Department of Medicine, University of California at San Diego.

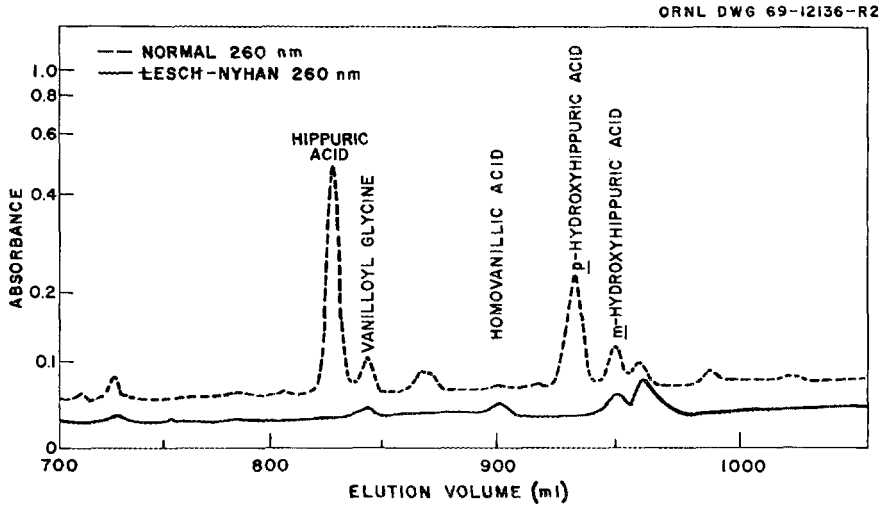

Fig. 12.20. Comparison Between Normal Reference Urine and Urine from a Patient Afflicted with Lesch-Nyhan Syndrome.

homogentisic acid was the only ^{14}C-containing constituent present in the urine samples from the two alkaptonuric patients. No ^{14}C activity was found in the urine of the nonalkaptonuric control patient, thus indicating that only the normal degradative metabolism of HGA was occurring in this patient.

The presence of ascorbic acid is believed to be necessary in order for homogentisic oxidase to function; therefore, further studies were conducted to determine the effect of ascorbic acid on HGA excretion in the two alkaptonuric patients. One week after the above study was made, ^{14}C-labeled HGA was again administered to the two alkaptonuric patients, this time following pretreatment with ascorbic acid. A reduction in the excretion of HGA of about 30 to 60% was observed. The reduction appeared to be relatively long-lived, since the excretion rate of one of the patients (only one patient was checked) was still depressed four days later.

12.12 DATA ACQUISITION AND ANALYSIS

A small digital computer (PDP-8/I) with a core memory of 8000 words is now being used on-line to acquire and analyze the chromatographic data from one UV-analyzer. A simple but efficient method for analyzing complex envelopes of peaks has been devised and is currently in use.

The small computer with its limited core memory is unable to utilize normal nonlinear least-squares programs for on-line operation because of the memory space required. A modified nonlinear least-squares method has been devised in which an envelope is analyzed by fitting the data with the number of individual peaks corresponding to the number of pairs of inflection points detected within the envelope. Inherent in the stripping procedure is the assumption that the chromatographic envelope can be described as the summation of a series of Gaussian peaks, as follows:

$$A = \sum_{j=1}^{n} \overline{A}_j \exp\left[-(T - \overline{T}_j)^2 / 2\sigma_j^2\right] , \qquad (1)$$

where

A = total absorbance at T,

T = elution time,

$\overline{A}_j$ = maximum absorbance of peak j,

$\overline{T}_j$ = value of T at $\overline{A}_j$,

σ_j = standard deviation or one-half the peak width at $e^{-1/2}\overline{A}_j$.

Initial estimates of the parameters $\overline{A}_j$ and $\overline{T}_j$ are obtained using the inflection point pairs. Since it has been observed that near-neighbor chromatographic peaks have almost identical peak widths, the simplifying assumption is made that each peak in a given envelope has the same σ. This is determined using the inflection points on either side of the envelope maximum absorbance. Corrections to the initial estimates of the parameters are obtained by expanding about each parameter

in a truncated Taylor series (discarding all but the linear terms) and solving the set of linear algebraic equations by successive elimination.

For evaluation purposes, the computer program was used to analyze envelope data synthesized by summing overlapping Gaussian peaks. We found that the program is capable of analyzing envelopes of up to three Gaussian peaks, with errors of less than 5% (based on peak area).

WATER POLLUTION STUDIES

Because water resources in densely populated areas are frequently reused, there is a danger of buildup of potentially hazardous levels of soluble chemical contaminants in the water. This is particularly true of refractory organic compounds, which are found in the effluents from municipal sewage plants. If contamination from such compounds becomes too great, additional processing steps may be necessary before the sewage plant effluent can be released to the environment. To date, the identification of refractory organics on a molecular level has been relatively unsuccessful; however, it must be accomplished if efficient treatment processes are to be developed and evaluated.

In recent years, several ORNL research and development programs have dealt with similar problems in the biological and biomedical sciences. Scouting tests were made in which effluent streams from a municipal sewage treatment plant were analyzed for UV-absorbing constituents. The results suggest that a similar technique can be used for the analysis of more than 100 of the individual refractory organic pollutants.

12.13 PREPARATION OF SAMPLES

The initial effort of this program has been directed toward comparing several methods for concentrating secondary sewage effluent for subsequent analysis, and determining what degree of concentration is required for an adequate analysis. Secondary effluent from the East Waste Treatment Plant of Oak Ridge, Tennessee, was used as starting material in all the tests.

In tests of various vacuum evaporation and freeze drying techniques, a combination of vacuum evaporation (as a first step to remove the largest fraction of water) followed by freeze drying (as the final concentration step) was found to be the most economical method for obtaining concentration factors of several hundred. In each case, several passes through the equipment were required to obtain the desired concentration factor. A comparison of the chromatograms obtained from samples concentrated by factors of 200 to 600 indicates that a concentration factor of at least 500 would be desirable.

12.14 ANALYTICAL SYSTEMS

The high-resolution UV-analyzer, which was developed in the Body Fluids Analyses Program,[6,10] was used in two scouting tests in which samples of the effluents of primary and secondary treatment steps in a typical municipal sewage plant were examined. In each case, a 300-cc volume of the solution was filtered and concentrated by a factor of 100, via vacuum evaporation, prior to analysis. More than 100 chromatographic peaks were detected in the primary effluent sample, and more than 70 peaks were detected in the secondary effluent (Fig. 12.21). These peaks represent UV-absorbing molecular constituents, many of which are probably the same as those found in human body fluids. Results from the two samples could be used to evaluate the efficiency of the secondary treatment step.

We have initiated a program that will include development of the techniques and automated instrumentation for separating and identifying, on the molecular level, pollutants in sewage both before and after various treatment steps. The development of automated, high-resolution, analytical systems for sewage effluent and other polluted streams will be based on the analyzers presently being used in the Body Fluids Analyses Program. This effort will proceed through design, building, and field-testing of prototype instruments. Automated, on-line monitoring of treatment processes will also be considered. As the program progresses, separated pollutants will be identified by isolation, purification, and spectral and chemical methods. Later in the program, a preliminary evaluation will be made of the environmental effect of each identified pollutant.

ORNL DWG. 69-10413R1

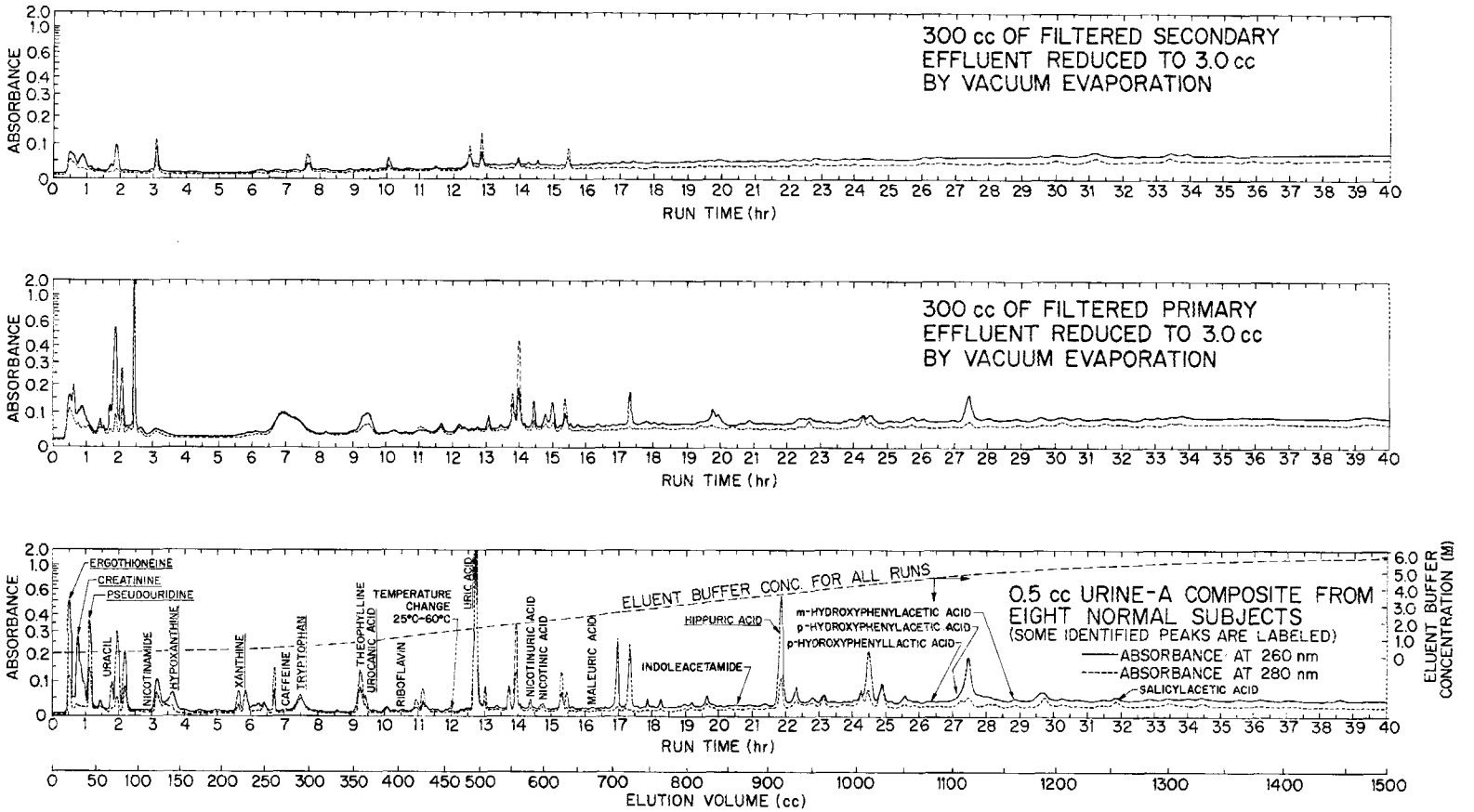

Fig. 12.21. Comparison Between Some of the Molecular Constituents of Human Urine and Those of Effluent Streams of the Primary and Secondary Stages of a Typical Municipal Sanitary Sewage Plant. Analysis was made using the ORNL UV-analyzer and an acetate buffer with a pH of 4.4.

13. Irradiation Effects on Heterogeneous Systems

13.1 ISOTOPE ENRICHMENT BY (n,γ) REACTIONS IN MOLECULAR SIEVES: THE CAMPBELL REACTION

There are numerous programs in which artificial isotopes are produced by neutron irradiation, in quantities ranging from tracer to multigram amounts. For example, the production of artificial heavy isotopes is the primary objective of the HFIR-TRU complex. In nearly all cases, single isotopes of high purity are required or desired as products. However, the target material and the product cannot be separated chemically when they are isotopes of the same element; also, the long irradiation periods required to produce appreciable amounts of product can result in mixtures of several isotopes. Of course, a pure isotope can be obtained from such mixtures by physical methods (e.g., electromagnetic separation), but these methods are slow and expensive. For years there has been a need to obtain selectively enriched products from irradiations. For example, ^{247}Cm would be a very valuable material because of its long half-life, but it cannot be produced at a concentration greater than about 2% by conventional reactor irradiation (see Sect. 5).

In principle, the Szilard-Chalmers reaction can result in enrichment of the product isotope of a nuclear reaction.[1] This reaction depends on physical effects resulting from recoil of the product nucleus after nuclear reaction, for example, from the emission of gamma rays after thermal-neutron capture. In instances when the recoil energy is sufficient to break a chemical bond and the recoil atom does not recombine or exchange with the target material, the product may be substantially separated from the target.

The actinides and lanthanides, which are the elements of principal interest to our programs, do not readily form appropriate compounds or complexes for the Szilard-Chalmers reaction. Further, such compounds, including covalent organic compounds and Werner complexes, are generally not sufficiently stable to radiation to permit production of useful amounts of product. As a result, the Szilard-Chalmers reaction has not proved satisfactory for solving our production problems.

Recently, a new reaction that offers considerable promise for producing useful amounts of neutron capture products has been observed. This reaction, called the Campbell reaction, involves incorporation of the target metal ion into a zeolite (i.e., an inorganic aluminosilicate) having two systems of interconnected pores, one large and one small. With appropriate treatment, the target ions may be concentrated in the small pore system, from which they are not readily removed subsequently. The product atoms may be selectively eluted from the zeolite after irradiation, probably from the large pores into which they have recoiled during irradiation. Zeolites have sufficient resistance to radiation damage[2] to promise useful production.

Description of Zeolite

The zeolite Linde X has been used in nearly all our work to date; however, all zeolites of the faujasite structure, and possibly a few closely related structures, may be equally satisfactory. The structure of Linde X is known;[3] its most important characteristic is the dual pore system, which consists of two sizes of interconnected pores (Fig. 13.1). These zeolites are cation exchangers, and Linde X can be exchanged with certain metal ions to yield a family of catalysts that are valuable for a number of industrial processes. During the last few years, considerable attention has been given to Linde X and Linde Y. When these zeolites are

[1] L. Szilard and T. A. Chalmers, *Nature* **134**, 462 (1934).

[2] L. V. C. Rees and C. J. Williams, *Trans. Faraday Soc.* **61**, 1481 (1965).

[3] P. V. Venuto and P. S. Landis, *Advances in Catalysis*, vol. 18, p. 263, Academic, New York, 1968.

ORNL-DWG 69-10103

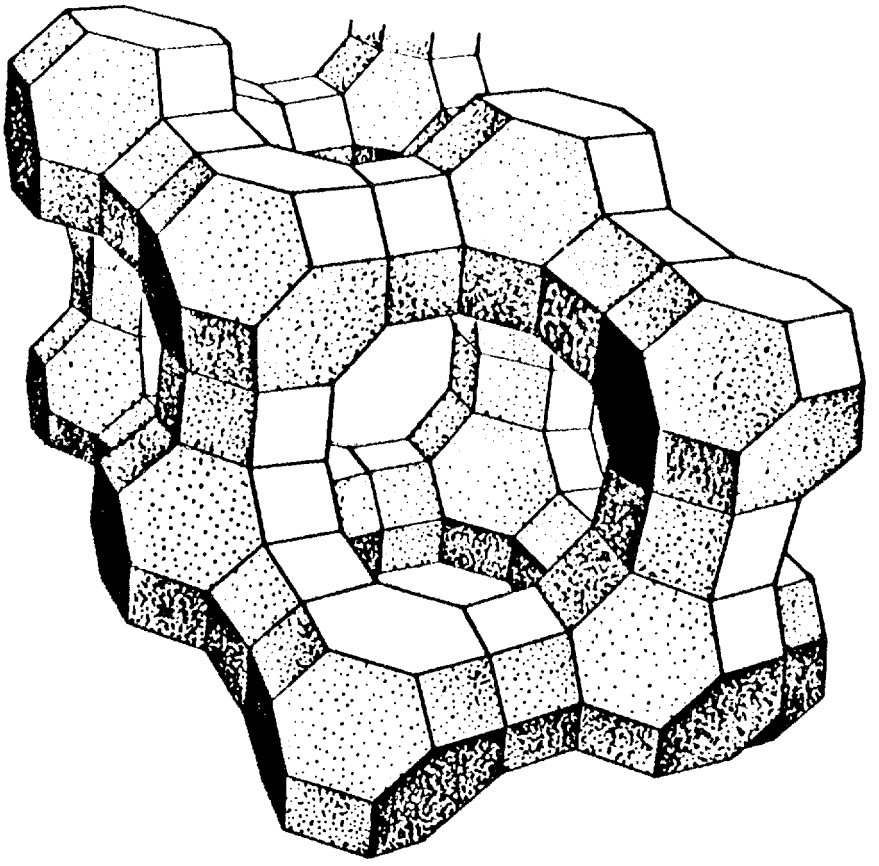

Fig. 13.1. Structure of Linde X.

contacted with an aqueous lanthanide solution, the lanthanide ions are strongly absorbed, readily displacing alkali metal and alkaline-earth ions.[4] The lanthanide ions enter the large supercages. When such an exchanged zeolite is heated to dehydrate the system (350 to 700°C), the lanthanide ions move into the small pore system,[5,6] and they are not readily exchanged back out of the crystal.

Experimental Results

Several rare earths including praesodymium, neodymium, erbium, and thulium, yttrium, actinides including americium and curium, and certain mixtures of these have been exchanged into Linde 13X by contacting the zeolite with an aqueous solution of the metal nitrate at a pH of about 4 to 5. The exchanged zeolite is washed, dried, and heated to about 500°C to fix the target ions in the small pores. The procedure is usually repeated in order to approach maximum loading. Before irradiation, the zeolite is eluted or leached with an appropriate solution (usually 10 to 11 *M* LiCl) to remove any readily exchangeable target material, washed with calcium or magnesium nitrate solution to displace the fissionable lithium ion, and dried.

Irradiations have been carried out with the assistance of Bruce Ketelle of the Chemistry Division, using that Division's pneumatic tube facility in the ORR. The thermal-neutron flux is 4 to 5 $\times$ 10^{13} neutrons cm^{-2} sec^{-1}, and irradiation times have varied from 15 sec to 10.5 min.

After irradiation, the zeolite is leached with the selected eluent, and the activated product in both the zeolite and a sample of the eluate is determined by gamma counting. In many cases, the amount of target

[4] H. S. Sherry, *J. Colloid Interface Sci.* 28, 288 (1968).

[5] D. H. Olsen, G. T. Kokotailo, and J. F. Charnell, *J. Colloid Interface Sci.* 28, 305 (1968).

[6] J. V. Smith, J. M. Bennett, and E. M. Flanigen, *Nature* 215, 241 (1967).

material that is eluted with the product was determined by activation analysis after the product had decayed.

Typical results (Table 13.1) for Linde X show generally similar response from both light and heavy rare earths. Approximately 40 to 60% of the neutron capture product, along with about 1% of the target material, was eluted. Thus enrichment factors are in the vicinity of 50. In two cases (A and C, Table 13.1), the target zeolite was recovered after the first irradiation, reirradiated, and eluted again. Yields were similar in the second cycle, showing that the same zeolite may be reused, at least with short irradiations such as these.

The amount of stable target material present in the activated product was usually less than 1%. Higher values, which were occasionally obtained, could result from inadequate elution of the zeolite before irradiation, entrainment of some of the zeolite with the eluate, or effects of temperature, gamma irradiation, etc., on target ions. However, we have been unable to reduce the amount of eluted target material to less than a few tenths of a percent, and thus far this places the limit on attainable enrichment.

Partial loading of the zeolite markedly decreased the yield (Table 13.2). In this case, only enough praseodymium to exchange 25% or 40% of the total zeolite capacity was used; the remaining exchangeable ions were mostly calcium (plus a small amount of sodium and lithium). The yield was only a few percent at 25% loading, even after elution was carried out over a weekend. The yield was much higher at 40% loading,

Table 13.1. Enrichment of Neutron Capture Product by Zeolite Elution
(Ca. 3 meq of lanthanide per gram of Linde X)

Description of Procedure	% of Isotope in Fraction	
(A) Irradiate 100 mg of PrX for 0.5 min	^{141}Pr	^{142}Pr[a]
Elute with:		
1 ml 11 *M* LiCl, 10 min, 25°C	0.76	49.
1 ml 11 *M* LiCl, 15 min, 90°C	0.54	13.
Remaining in PrX	98.	38.
Wash PrX, ignite to 450°C, reirradiate 1 min		
Elute with:		
1 ml saturated Na_2SO_4, 10 min, 25°C	0.52	40.
1 ml 11 *M* LiCl, 15 min, 90°C	0.59	18.
Remaining in PrX	*b*	42.
(B) Irradiate 52 mg of NdX for 15 sec	^{148}Nd	^{149}Nd[a]
Elute with:		
1 ml saturated Na_2SO_4, 10 min, 90°C	0.75	17.
1 ml 10 *M* LiCl, 5 min, 90°C	0.8	25.
1 ml 10 *M* LiCl, 5 min, 90°C	0.5	6.
Remaining in NdX	*b*	52.
(C) Irradiate 100 mg of ErX for 15 sec	^{170}Er	^{171}Er[a]
Elute with:		
1 ml 10 *M* LiCl, 5 min, 25°C	1.5	36.
1 ml 10 *M* LiCl, 10 min, 90°C	0.8	10.
1 ml 10 *M* LiCl, 20 min, 90°C	3.6	8.
Remaining in ErX	94.	46.
Wash ErX, ignite to 500°, reirradiate 2 min		
Elute with:		
1 ml 10 *M* LiCl, 1.5 min, 25°C	0.8	25.
1 ml 10 *M* LiCl, 15 min, 25°C	0.6	11.
Remaining in ErX	*b*	64.
(D) Irradiate 50 mg of TmX for 10 min	^{169}Tm	^{170}Tm[a]
Elute with:		
3 ml 10 *M* LiCl, 15 min, 25°C	*b*	36.
3 ml 10 *M* LiCl, 15 min, 25°C	*b*	4.
3 ml 10 *M* LiCl, 18 hr, 25°C	*b*	3.
Remaining in TmX	*b*	57.

[a]Radioactive neutron capture product.
[b]Not determined.

Table 13.2. Yield of ^{142}Pr from Partially Loaded Zeolite

Material	Description of Procedure	% of Isotope in Fraction		Cumulative % Yield of Product	Cumulative Enrichment Factor
		^{141}Pr	$^{142}Pr^a$		
(A) Linde X, 25% saturated with Pr	Irradiate 100 mg for 1 min; then elute with:				
	1 ml 10 *M* LiCl, 4 min, 25°C	0.2	3.2	3.2	16
	1 ml 10 *M* LiCl, 2 min, 25°C	0.2	1.6	4.8	12
	1 ml 10 *M* LiCl, 66 hr, 25°C	0.1	3.2	8.0	16
	Remaining in PrX	*b*	92.		
(B) Linde X, 40% saturated with Pr	Irradiate 100 mg for 1 min; then elute with:				
	1 ml saturated Na_2SO_4, 5 min, 25°C	0.34	14.1	14.1	41
	1 ml 10 *M* LiCl, 5 min, 25°C	0.36	9.7	23.8	34
	Remaining in PrX	*b*	76.2		

[a]Neutron capture product.
[b]Not determined.

but was still less than that obtained with highly loaded zeolites. In each case, the eluate was enriched.

A high yield of enriched product is obtained with high lanthanide loadings, even if a rare earth other than the chosen target is used to provide part of the loading. This is shown in Table 13.3 for three zeolites, which were all partially loaded to the same praseodymium content. When the remainder of the exchange capacity was loaded with calcium, the yield was low, as shown in Table 13.2. When the zeolite was highly loaded with lanthanide by adding erbium or yttrium, a high yield of enriched product was obtained. With the PrErX zeolite, it was practicable to determine the behavior of both ^{142}Pr and ^{171}Er. It is interesting that the yield of erbium was lower than that of praseodymium; in fact, both elements behaved very much as each does alone at full loading (Table 13.1). Perhaps the lower yields of erbium reflect a lower fraction of neutron capture reactions in which the product atom has enough recoil energy to be freed.

A number of variables have been tested in the hope of achieving a higher enrichment factor, but no significant improvement has been demonstrated. Since the product recovery is already high, a significantly higher enrichment factor can be obtained only by decreasing the amount of target material that is simultaneously eluted. Variables that have been studied include the extent of hydration of the zeolite during irradiation, the ignition procedure and temperature (up to 750°C), the method and extent of loading, the order of loading and igniting with two lanthanides, and elution reagents and procedures. There is evidence that the very high loadings used in most of the work are not optimum, and that an intermediate loading, probably in the 50 to 75% range, may be the best compromise between high yield of product and low amount of eluted target.

In order to separate the possible effects of gamma and beta irradiation from direct and indirect effects of neutron irradiation on the leachability of the target ions, small samples of Linde X loaded with neodymium and with erbium were irradiated in a ^{60}Co source (estimated temperature, 70°C) and a ^{90}Sr source (70°C) to doses of about 10^9 rads. These samples, together with control samples that had been held at 25 and 100°C, were then leached with 10 *M* LiCl, and the leach solution was analyzed spectrophotometrically. The amounts of target ion leached, 1 to 3%, showed no correlation with either irradiation or temperature, indicating that no large effect is to be expected from either beta or gamma irradiation or from a moderate temperature rise during neutron irradiation.

Experiments have been done with both ^{241}Am and ^{243}Am targets, and also with a mixed ^{244}Cm-^{141}Pr loading to test the effect of the effect of the intense alpha activity of curium. The yield of the neutron capture product of each of the americium isotopes is easily measured, whereas the yield of the neutron capture product of curium is not. Typical results with americium are given in Table 13.4. High zeolite loadings have not been achieved with either americium or curium. At about 30% loading, product yields are low (i.e., about 4%), as they were with lanthanides at similar low loading. When a high total loading is used, by adding yttrium or praseodymium after the americium, yields (e.g., 58%) are comparable to those with lanthanides.

Table 13.3. Effect of Mixed Loading on Yields

Materials: PrX – zeolite, Linde 13X; loading, 30% Pr–70% Ca
PrErX – zeolite, Linde 13X; loading, 30% Pr–70% Er
PrYX – zeolite, Linde 13X; loading, 30% Pr–70% Y

Procedure: irradiate 50 mg each for 1 min; then elute with:
L1 – 1 ml 10 *M* LiCl, 5 min, 25°C, followed by:
L2 – 1 ml 10 *M* LiCl, 16 hr, 25°C

Description	Element Analyzed	% of Isotope in Fraction		Cumulative % Yield of Product	Cumulative Enrichment Factor
		Target	Product		
PrX					
L1		0.7	15.1	15.1	22
L2	Pr[a]	0.6	15.5	30.6	24
Zeolite			69.4		
PrErX					
L1		0.5	50.8	50.8	102
L2	Pr[a]	0.4	13.2	64.0	71
Zeolite			36		
PrErX					
L1		0.8	34.6	34.6	43
L2	Er[b]	0.8	16.1	50.7	32
Zeolite			49.3		
PrYX					
L1		1.2	57.4	57.4	48
L2	Pr[a]	0.5	9.2	66.6	39
Zeolite			33.4		

[a]The target is ^{141}Pr; the product is ^{142}Pr.
[b]The target is ^{170}Er; the product is ^{171}Er.

The larger amount of actinide target material that is eluted, as compared with lanthanide target material, may be an effect of the alpha radiation of the actinides. However, this is not directly related to either the exposure time or the intensity of the alpha radiation, since similar behavior was observed for the curium and the americium isotopes. Typically, target elution of actinides is 3 to 5% as compared with less than 1% for lanthanides.

13.2 CAMPBELL REACTION BY ALPHA BOMBARDMENT IN A MOLECULAR SIEVE

Nuclear recoil reactions for the separation of radiation-produced nuclides from targets are applicable to materials produced in cyclotrons as well as in nuclear reactors. Therefore, the Campbell reaction has been tested for use in the recovery of lanthanide nuclides produced by the Oak Ridge Isochronous Cyclotron. Targets of enriched gadolinium isotopes (masses 156, 157, and 158) absorbed in Linde X molecular sieves were bombarded with 40- to 60-MeV alpha particles at intensities up to 5 μa for periods up to 1 hr. The induced ^{157}Dy and ^{159}Dy were then leached from the targets. Although yields of up to 50% of the product nuclides have been obtained, 5 to 8% of the target

Table 13.4. Results of the Campbell Reaction with an Actinide

Materials: AmX – zeolite, Linde X; loading, 30% Am–70% Na
AmYX – zeolite, Linde X; loading, 30% Am–70% Y
(0.8 meq of americium per gram of Linde X)

Procedure: Irradiate 10 mg of each for 1 min; then elute with 11 *M* LiCl for 20 min

Description	% of Isotope in Fraction		Enrichment Factor
	^{241}Am	^{242}Am	
Eluate from AmX	0.31	3.6	12
Zeolite	99.7	96.4	
Eluate from AmYX	4.4	58	13
Zeolite	95.6	42	

material has also been leached by the methods used thus far. We have not determined whether this large percentage of eluted target material is attributable to the effects of the intense alpha bombardment. Further attention is being given to the entire loading and leaching procedure in order to minimize the amount of target material that is dissolved, since this method should provide a rapid and useful means for preparing short-lived nuclides for physics experiments. However, the products will have utility only if they are essentially free from weighable amounts of any other material, including the target material.

14. Spectrophotometric Studies of Solutions of Lanthanides and Actinides

The major objective of this program is to develop and exploit spectrophotometric techniques for studying the chemical properties of aqueous solutions, especially in comparisons of the lanthanide and actinide elements, over wide ranges of experimental conditions. Some studies extend to nonaqueous and to solid solutions. The usual spectrophotometric techniques are used wherever materials and experimental conditions permit. A specially modified Cary model 14 spectrophotometer system has been built for use in extreme conditions and to permit study of the more highly alpha-active actinides. This system can be alpha-contained and is capable of operating at temperatures up to the critical point of water (374°C) and at pressures up to 10,000 psi. At present, it is installed in a standard laboratory, where it is used for test purposes and for making measurements on non- and low-alpha-active solutions. In conjunction with the spectrophotometric studies, the densities of aqueous solutions are being measured over the temperature range of 25 to 400°C to determine the concentration changes needed in the spectrophotometric studies and to obtain fundamental information.

14.1 HIGH-ENERGY ABSORPTION BANDS VS CONCENTRATIONS OF H_2O AND D_2O TO 380°C

Two new absorption bands, at 6050 A and at 6600 A, for H_2O have been observed by virtue of the long-path-length cells (21 cm) used in this program. These bands occur at higher energies than the normally studied bands of H_2O and represent a continuation of the series of near-infrared absorption bands of H_2O. Two comparable bands and a third band, which has no H_2O counterpart, were observed for D_2O. These bands for H_2O and for D_2O occur at wavelengths that interfere with the spectral studies of lanthanides and actinides. Therefore, the effects of temperature on the new bands, as well as on the two previously known highest energy bands of H_2O and of D_2O, were observed to 380°C for both the liquid and vapor phases.[1]

The band energies and the molar absorptivities of the absorption bands between 5800 and 8600 A (17,200 and 11,600 cm^{-1}) for H_2O, and between 7200 and 12,000 A (13,900 and 8300 cm^{-1}) for D_2O increase as the temperature of the liquid state is increased from 25°C to the critical point (374.2°C for H_2, and 371.5°C for D_2O). Similar and more dramatic changes occur when the bands for the liquids are compared with the corresponding bands of the vapor states (Fig. 14.1). Since these changes in band parameters result from a degradation of the H_2O or D_2O structures, the parameters have been plotted as functions of the H_2O or D_2O concentrations. The resulting plots show that the changes in the band parameters are linear functions of the H_2O or D_2O molar concentrations throughout the liquid and vapor states. (The concentration range for liquid H_2O or D_2O is 55 to 17 *M*, and the lower concentrations occur in the vapor state.) This relationship indicates that the molecular association of H_2O or D_2O is a continuous and constant function of the concentration, regardless of whether the state is liquid or vapor.

14.2 EFFECTS OF TEMPERATURE ON AQUEOUS Am^{3+} COMPLEXES

Thermodynamic quantities for the reaction of Am^{3+} with the monoacid form of iminodiacetic acid, IDA^-, to form a 1:1 complex have been determined from

[1] J. T. Bell, N. A. Krohn, and D. M. Helton, "New Absorption Bands for H_2O and D_2O, and the Effects of Temperature to 380°C on the Near-IR Bands of Liquid and Vapor H_2O and D_2O," submitted for publication in the *Journal of Molecular Spectroscopy*.

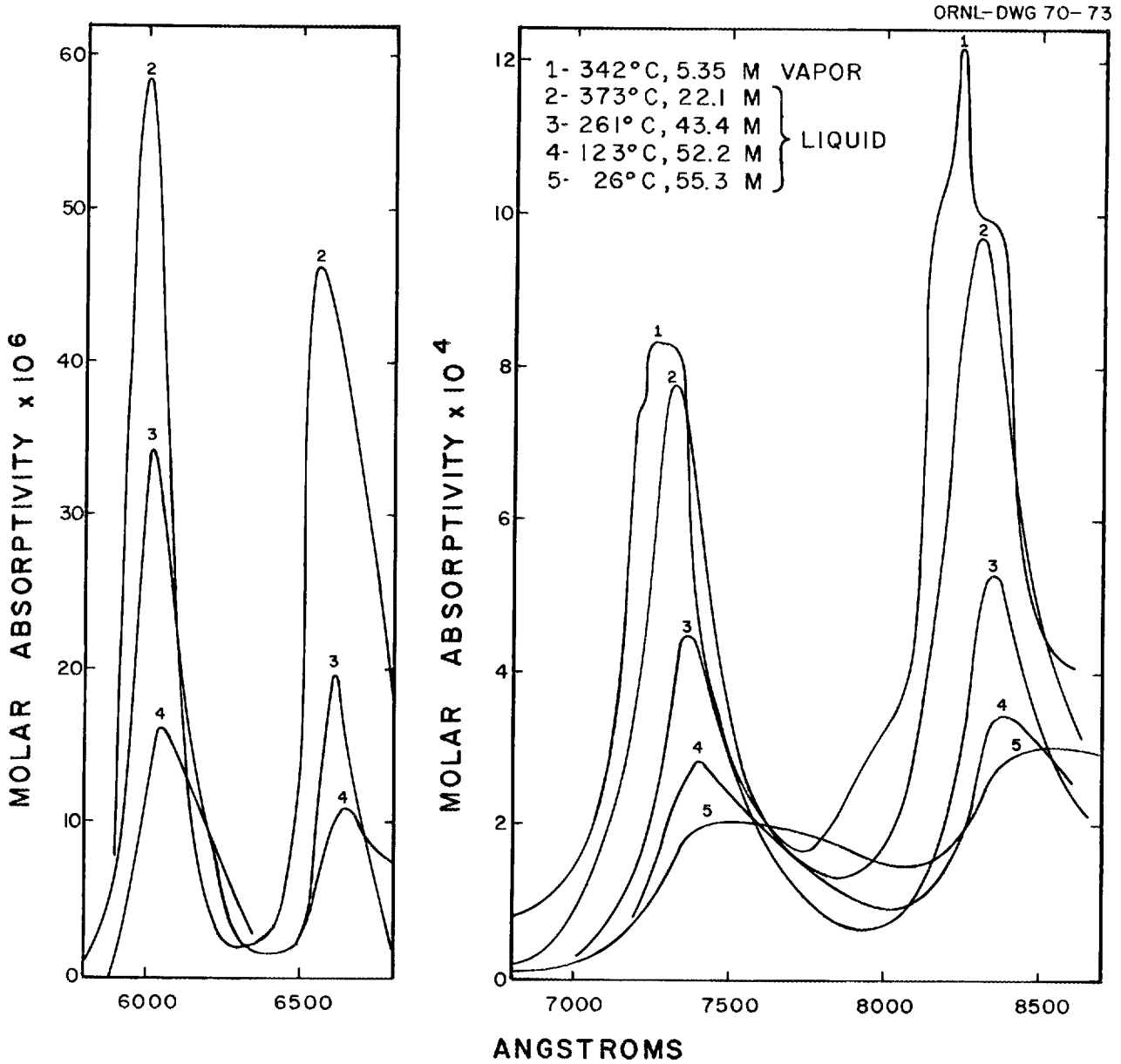

Fig. 14.1. The Four Highest Energy Absorption Regions of the Water Spectrum at 25 to 373°C, 55.3 to 5.35 *M* H_2O.

spectroscopic and pH data over the 17 to 90°C temperature range.[2] The effects of temperature on the spectra are shown in Fig. 14.2. The enthalpy change for the reaction

$$Am^{3+} + IDA^- \rightarrow AmIDA^{2+} + H^+$$

is 6.9 ± 1.2 kcal. The endothermic character of this reaction is explained by the high entropy change, 13.2 ± 1.2 entropy units, and the entropy change probably results from the complex binding of the IDA^- ligand. The formation of the 1:2 and the 1:3 complexes also

[2] J. T. Bell, R. D. Baybarz, and D. M. Helton, "The Thermodynamics for the Reaction of Americium (III) with Iminodiacetic Acid," submitted for publication in the *Journal of Inorganic and Nuclear Chemistry*.

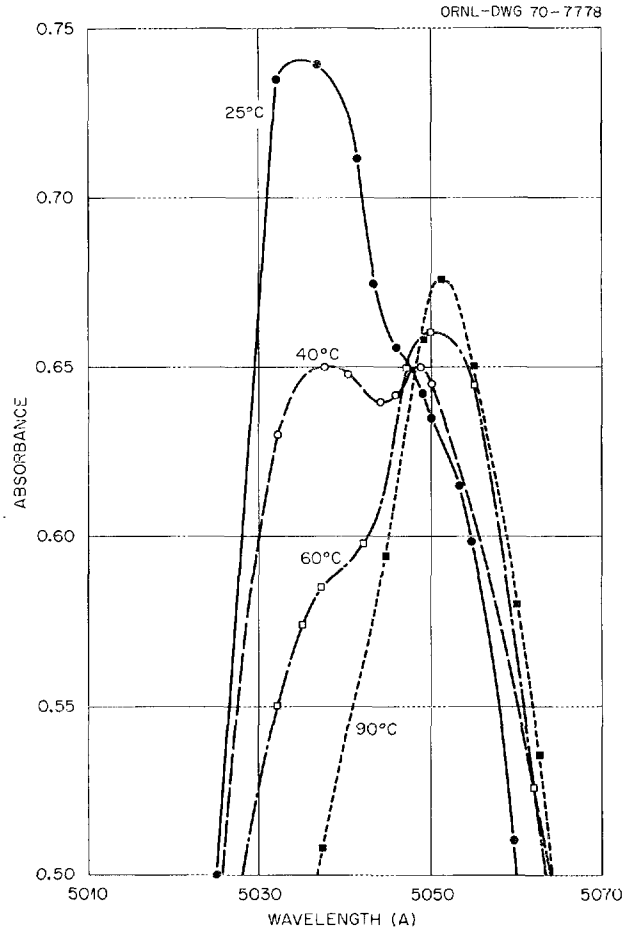

Fig. 14.2. Effect of Temperature on the Spectrum of the Complex of Americium with Iminodiacetic Acid. Path length, 2.5 cm; 8.4×10^{-4} *M* Am^{3+}. (Intensities were not normalized for the effect of thermal expansion on concentration.)

appears to be endothermic, while the formation of the 1:5 complex appears to be exothermic. However, the spectral bands for the 1:2 and 1:3 complexes cannot be adequately resolved for conclusive thermodynamic studies, and the measured pH levels of the solutions containing the 1:5 complex (pH 7) are too uncertain because of the effect of carbon dioxide.

14.3 EMISSION SPECTRA OF THE TRANSURANIUM ELEMENTS

The absorption and emission spectra and the theoretical electronic energy levels for Am^{3+} indicate that this ion has laser potentiality comparable to the ruby laser. Laser solutions of Nd^{3+} have been prepared by dissolving $Nd(ClO_4)_3$ in $POCl_3$ and adding $TiCl_4$ or $ZrCl_4$ as Cl^- ion scavenger.[3] Similar techniques for preparing a liquid laser of Am^{3+} in $POCl_3$ are being developed.

14.4 DENSITIES OF AQUEOUS RARE-EARTH SOLUTIONS TO 374°C

The densities of various concentrations (0.05 to 0.44 *M*) of $Pr(NO_3)_3$ at various acidities (0.1 to 0.63 *M*) were measured from 25 to 370°C.[4] The molar volumes of the solutions at 25°C increase with the mole fraction of $Pr(NO_3)_3$, while at 300°C the molar volumes decrease as the $Pr(NO_3)_3$ mole fraction increases. At each temperature the extrapolation of the molar volumes to a mole fraction of unity gives the partial molar volume of $Pr(NO_3)_3$. It is 98 cc/mole at 25°C and continuously decreases to −160 cc/mole at 300°C.

14.5 PROTONIC WAVE FUNCTIONS AND SPECTRA

The method used almost exclusively for the theoretical study of molecular structure is based on the Born-Oppenheimer approximation. The procedure is to solve for the electronic motion with all the nuclei fixed. Then approximate equations for the nuclear motion are solved using the solution for the electronic motion obtained from the fixed nuclei approximation. The model for vibrating and rotating nuclei is based on this procedure. This model has been, and continues to be, very successful; however, there are some problems to which it has not given a satisfactory solution. Among these are the descriptions of the hydrogen bond and the ground state of the ammonia molecule. The work to be described here began as an effort to obtain a more accurate description of the ground state of ammonia; however, its consequences now appear to be of fundamental importance to quantum chemistry. Its logical development will obviously extend beyond the normal scope of the Chemical Technology Division; hence, we will develop the concept far enough to ensure its recognition, but further ramifications will not be pursued within our program.

Our method for the study of molecular structure is simply to solve Schrödinger's equation as accurately as possible.[5,6] That is, we use the correct nonrelativistic and spin-free Hamiltonian and find the wave function

[3] C. Brecher and K. W. French, *J. Phys. Chem.* 73, 1785 (1969).

[4] J. T. Bell and D. M. Helton, "The Partial Molal Volumes of Aqueous Pr and Nd Nitrates to 370°C," submitted for publication in the *Journal of Physical Chemistry.*

[5] I. L. Thomas, "The Protonic Structure of Methane, Ammonia, Water, and Hydrogen Fluoride," *Chem. Phys. Letters* 3, 705 (1969).

[6] I. L. Thomas, "The Protonic Structure of Molecules. I. The Ammonia Molecule," *Phys. Rev.* 185, 90 (1969).

that gives the lowest ground-state energy using the variational method. The procedure is straightforward. Consider a molecule that consists of n electrons, m protons, and a heavier atomic nucleus of charge $n - m$ and mass m_a. The Hamiltonian, in Hartrees, is:

$$H = \sum_i \left(\frac{-1}{2m_i} \nabla_i^2 + \sum_{j>i} \frac{q_i q_j}{r_{ij}} \right),$$

where m_i and q_i are the mass and charge of the ith particle. We transform to center-of-mass coordinates to obtain:

$$H = \frac{-1}{2M} \nabla_R^2 + \sum_k \left(\frac{-1}{2\mu_k} \nabla_k^2 - \frac{1}{m_a} \sum_{l>k} \nabla_k \cdot \nabla_l \right) + \sum_k \left(\frac{q_k q_a}{R_k} + \sum_{l>k} \frac{q_k q_l}{R_{kl}} \right),$$

where M is the total mass of the molecule, R is the vector to the center of mass, $\mu_k = m_a m_k/(m_a + m_k)$ is the reduced mass of the kth particle, m_a is the mass of the most massive nucleus, and $R_k = r_k - r_a$. Since the motion of the center of mass is separable, the solution of Schrödinger's equation with this Hamiltonian is of the form

$$\Psi = \Phi(R)\, \psi(R_1, \ldots, R_{n+m}) .$$

We are interested only in ψ, which gives the molecular structure in terms of n particles of mass μ_e (the electronic reduced mass) and m particles of mass μ_p (the protonic reduced mass) moving about particle a. Since we do not have analytical solutions for such a system, we use the variational method to obtain a solution as accurate as we like. Our trial (or initial guess) for the true ψ is:

$$\psi = \sum_i \sum_a C_{ia} F_i G_a ,$$

where F_i is a Slater determinant of Slater functions representing the n electrons and G_a is a Slater determinant of Slater functions representing the m protons.

So far we have studied CH_4, NH_3, H_2O, HF, LiH, and H_2. Of these, only the studies of CH_4, NH_3, and H_2O are complete. Figure 14.3 shows a probability density plot along an N-H bond in ammonia, and Table 14.1 gives the protonic spectra of methane, ammonia, and water. This is the first time it has been theoretically demonstrated that such spectra may exist; surprisingly, they are very similar to electronic spectra.

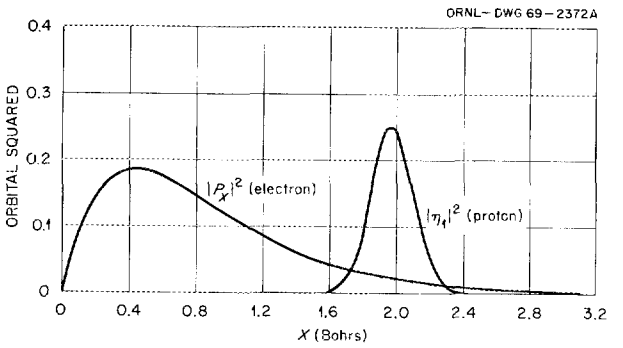

Fig. 14.3 Probability Plot of the Density of the P_x Electronic Orbital and the η_1 Protonic Orbital Along the X-Axis in Ammonia. The nitrogen nucleus is at the origin. (1 Bohr = 0.529167 A.)

Table 14.1. Calculated Protonic Energy Levels of CH_4, NH_3, and H_2O in Hartrees

Molecule	Configuration[a]	Multiplet	Energy
CH_4	sp^3	^5S	−39.13764
		^3D	−38.86341
		^3P	−38.86338
		^3S	−38.59223
		^1D	−38.59070
		^1P	−38.59067
	s^2p^2	^3P	−38.84821
		^1D	−38.75626
		^1S	−38.71031
	p^4	^3P	−38.72845
		^1D	−38.63651
		^1S	−38.59059
NH_3	sp^2	^4P	−55.44522
		^2D	−55.19149
		^2P	−55.14043
		^2S	−54.99058
	p^3	^4S	−55.31222
		^2D	−55.15900
		^2P	−55.15897
	s^2p	^2P	−55.20868
H_2O	sp	^3P	−75.50005
		^1P	−75.17450
	p^2	^3P	−75.42833
		^1D	−75.31884
		^1S	−75.26413
	s^2	^1S	−75.31884

[a]Each configuration was diagonalized separately.

We have also shown that the intensities and selection rules of the protonic transitions are the same as those for electrons.[7] This fact makes it difficult to verify these results experimentally using light. However, since neutrons will selectively excite protons, we plan to do experiments with neutron beams in the near future. We also plan to study deuterated molecules, which are especially interesting because deuterons are bosons and do not conform to the same statistics as protons (fermions) do.[8]

[7] I. L. Thomas, "Selection Rules and the Protonic Spectrum of Molecules," *Phys. Rev.* (in press).

[8] I. L. Thomas, "Hamiltonian Matrix Elements from a Symmetric Wave Function," *Phys. Rev.* (in press).

15. Reactor Evaluation Studies

This program, which is a joint effort with other ORNL Divisions, especially the Reactor Division and the Metals and Ceramics Division, has the primary purpose of assisting the USAEC in evaluating the technical feasibility and economics of various nuclear power concepts being developed, or being considered for development, under the U.S. civilian power program. Work in this Division during the past year was devoted primarily to the development of computational models for use in the planning of optimal electrical power systems in the United States. Accomplishments included the completion of the Oak Ridge Systems Analysis Code, the development of a dynamic programming algorithm for the dispatching of power generating plants, and the completion of a study of the feasibility of applying advanced dynamic programming procedures to the expansion planning of nuclear power generation systems and the fuel reprocessing industry.

15.1 THE OAK RIDGE SYSTEMS ANALYSIS CODE

The Oak Ridge Systems Analysis Code, which was described in last year's report,[1] is a linear programming computational model that was developed for use in planning optimal nuclear electric power systems in the United States. In the past year, we completed work on the code by adding a number of improvements and preparing a user's manual[2] to facilitate the implementation of the code at other sites. The code was tested by comparison of a series of bench-mark problems in cooperation with the Pacific Northwest Laboratory and the Los Alamos Scientific Laboratory. A copy of the code was transmitted to the Argonne National Laboratory for their use in LMFBR evaluation studies.

[1] D. E. Ferguson *et al.*, *Chem. Technol. Div. Ann. Progr. Rept. May 31, 1969*, ORNL-4422, pp. 309–11.

[2] F. G. Welfare *et al.*, *The Oak Ridge Systems Analysis Code (ORSAC)*, ORNL-4546 (in preparation).

15.2 OPTIMAL DISPATCHING OF ELECTRIC POWER GENERATION PLANTS

The Joint Systems Analysis Study Group was formed in the spring of 1969 with representation of the following utilities and Governmental agencies: Tennessee Valley Authority, Commonwealth Edison, Atomic Energy Commission, Argonne National Laboratory, Pacific Northwest Laboratory, and Oak Ridge National Laboratory. The purpose of this group is to investigate the feasibility of using modern optimization techniques for modeling some of the long-range planning problems of the utility industry.[3]

Two problems were formulated in order to familiarize members of the group with some of the constraints that are characteristic of the utility industry. The first problem required optimal dispatching of six coal-fired plants over a one-week period. A dynamic programming solution of this problem is described in ORNL-TM-2881.[4] The second problem was an expansion of the first. The period of optimization in the second problem was also taken to be one week, but the system included gas-turbine, pumped-storage, and conventional hydroelectric plants as well as coal-fired plants. The generating plants are described in Table 15.1.

Several constraints are placed on the system and the operation of the individual units. Sufficient energy must be generated to meet the system load; however, additional energy can be generated in order to pump water into the pumped-storage reservoir. A minimum amount of spinning reserve (i.e., excess capacity that is committed but is not generating power) must also be

[3] R. T. Jenkins, S. W. Anderson, D. S. Joy, E. T. Merrill, and T. D. Wolsko, "Methods of Planning Generating Unit Operation," presented at the American Power Conference, Chicago, Ill., Apr. 21–23, 1970; published in the *Proceedings* (May 1970).

[4] D. S. Joy, *A Dynamic Programming Solution of the Electric Generating System Unit Commitment Problem*, ORNL-TM-2881 (April 1970).

Table 15.1. Characteristics of Generating Plants

Plant Type	Capacity (Mw)		Costs		
	Min	Max	Fuel (¢/10^6 Btu)	Startup ($)	Operation and Maintenance ($/hr)
Coal-fired					
B1	90	250	20.0	750.0	85.0
B2	110	350	21.0	900.0	115.0
B3	100	250	23.0	700.0	87.5
B4	65	200	27.0	600.0	66.3
B5	50	150	31.0	500.0	50.0
Gas turbine[a]		45	30.0	50.0	75.0
Pumped storage	0	250[b]		0.0	9.0
Hydroelectric	75[c]	175		0.0	2.0

[a]All peaking plants are identical.
[b]Represents maximum generating capability and maximum pumping load.
[c]Run-of-the-river hydroelectric power.

supplied. This reserve can quickly assume the load in the event of a forced outage of a unit and thus ensure continuity of service. The model also assumes that the power demands in the previous week and the following week are identical to those of the week being studied.

A coal-fired plant must either be shut down or operated at some level between the minimum and maximum capacities. A minimum shutdown time is also specified for each plant. When in operation, the gas-turbine peaking plants must be operated at their rated capacity. These plants are generally characterized by high fuel costs and low startup requirements.

The usual method of operation of the pumped-storage hydroelectric plant consists of releasing water for generating power during periods of high system load and pumping the water back into the reservoir during the off-peak periods. The efficiency of this unit is assumed to be independent of the amount of energy in storage. The quantity of energy that can be stored is limited by the size of the reservoir. If the quantity of energy in storage falls below a specified level, this unit cannot contribute to the spinning reserve of the system. This constraint arises from the fact that, in order to be considered as spinning reserve, the unit should be capable of generating a significant amount of energy.

The conventional hydroelectric plant operates in two power-generating modes. The minimum capacity represents run-of-the-river hydroelectric power, and the unit must continuously generate this amount of power. Additional hydroelectric power may be generated using water from the reservoir. The amount of hydroelectric energy that is available during a given week is determined by long-range predictions of precipitation and system load.

A dispatching schedule that minimizes system operating coasts was determined using a dynamic programming formulation with a successive approximations technique. The results are shown in Fig. 15.1, where the run-of-the-river hydroelectric power has been subtracted from the system load. The identical problem was solved by the Tennessee Valley Authority with a standard production cost program, using a "peak shaving" method to determine the hydroelectric energy allocation and pumped-storage operation. The dynamic programming formulation treats hydroelectric usage, pumped-storage operation, and fossil unit commitment as variables and does not decide on the optimum path until all combinations have been investigated. In the dynamic programming solution, the distribution of the conventional hydroelectric energy was distorted in order to obtain a more efficient use of the pumped-storage capability. Also, the pumping duty was shifted in such a manner that some of the fossil plants could be shut down. The calculated operating costs from the two solutions were as follows:

Production cost program	$487,518
Dynamic programming solution	485,327
Savings	$ 2,191

Dynamic programming, with its ability to handle discrete variables, nonlinear system equations, and stochastic events, appears to be an attractive method for determining optimal planning and operating policies for utility systems.

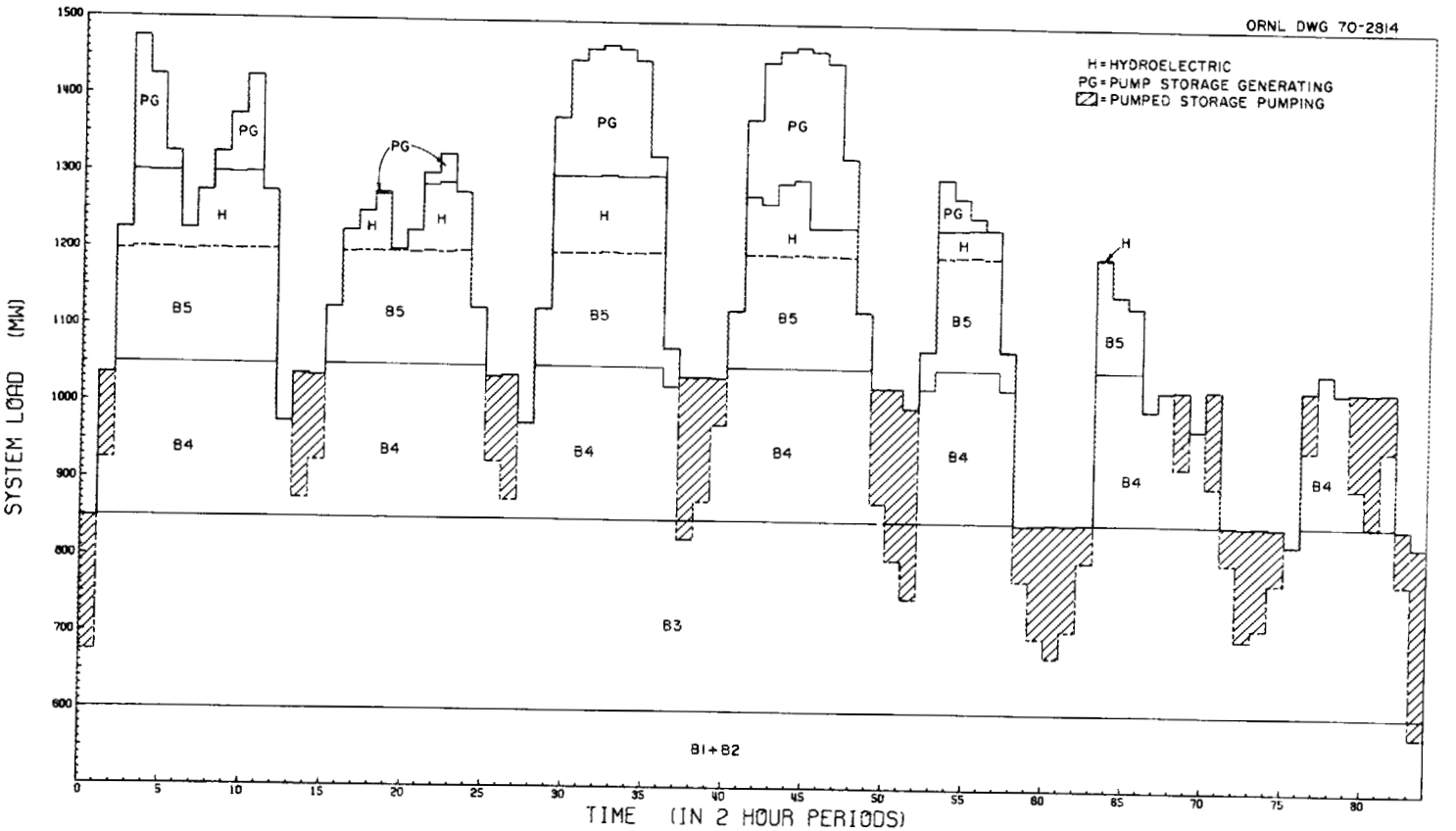

Fig. 15.1. Optimal Operating Schedule for the System of Coal-Fired, Gas Turbine, Pumped-Storage, and Hydroelectric Plants.

15.3 DYNAMIC PROGRAMMING FOR EXPANSION PLANNING OF THE NUCLEAR POWER INDUSTRY

With the assistance of Systems Control, Inc., a study was made of the feasibility of applying advanced dynamic programming computational procedures to expansion planning problems in nuclear power generation systems and the spent-fuel processing industry. Results of these studies were presented in a topical report[5] and in papers before the American Nuclear Society.[6,7]

Expansion Planning of Nuclear Power Generation Systems

Much of the demand for low-cost electric power over the next several decades will be satisfied by nuclear power generation plants. Present nuclear power plants are fueled with enriched uranium (uranium of enhanced ^{235}U content made by gaseous diffusion of natural uranium) and consume more fissile material (^{235}U) than they produce (as plutonium or ^{233}U). Since the amount of natural uranium that can be mined at low cost is limited, other nuclear reactor types are being developed that will be able to use the plutonium or ^{233}U as the primary fissile material and produce more of these materials by transmutation of natural thorium or the depleted uranium tailings resulting from gaseous diffusion. A study was made of the feasibility of applying advanced dynamic programming computational procedures[8] to the problem of planning the expansion of the nuclear power industry so that the long-term demand for electric power can be satisfied by the available low-cost uranium.

The optimization problem is to select the combination of plant types to be installed during the planning period such that the present-worth cost of reactor construction, operation, and fuel is minimized and specified capacity additions, as a function of time, are met. The cost of operating a plant over the remainder of a planning period is combined with the cost of construction and projected fuel cycle costs in an expanding nuclear industry to produce a single present-worth cost of adding that plant during a particular year. These overall cost coefficients, as well as the production and consumption of commodities (natural uranium, separative work, depleted uranium, fissile plutonium, and ^{233}U) in each year of operation of the reactor, may be estimated using the Oak Ridge Systems Analysis Code.

A straightforward dynamic programming solution of the problem is computationally infeasible because a state variable is required for each year (or biennium) in the life of each plant type. Several few-state approximate models of the problem were formulated using advanced dynamic programming techniques; these techniques were evaluated using a simple linear test problem devised such that an exact global optimum solution could be calculated with a linear program. The most promising techniques for rapid and accurate solution of the problem utilized a single-state method and a method of successive approximations.

The single-state method, using fissile plutonium inventory as the state variable, was formulated to determine the optimal plutonium inventory in each time stage consistent with the minimum cost of all construction and operations through that time stage and with projections of future fuel requirements. This method produced a total cost that was 0.07% higher than the linear programming result.

The method of successive approximations, using one state variable per plant type, was formulated to determine the optimal number of additions of a plant type in each time stage consistent with projections of future fuel requirements, startups of that plant type, and estimates of the optimal startup schedule of all other plant types. The algorithm then proceeded iteratively, using single-state dynamic programming for each plant type, until the solution converged. The total cost was 0.2% higher than the result obtained by linear programming.

In "real world" problems, the costs of construction and operation of nuclear reactors, gaseous diffusion plants, and other fuel cycle plants vary nonlinearly with the size of the plants. The dynamic programming techniques described can consider such nonlinearities explicitly and generate a reasonable solution with essentially no penalty in speed of computation. By contrast, the approximations that must be made to

---

[5] R. E. Larson and F. J. Rees, *Application of Advanced Dynamic Programming Computational Procedure to the Planning of Nuclear Fuel Reprocessing Plants and Nuclear Power Reactors*, ORNL Subcontract 3240 (November 1969).

[6] R. E. Larson, F. J. Rees, and J. P. Nichols, "Dynamic Programming for Expansion Planning of the Fuel Reprocessing Industry," presented at the Sixteenth Annual Meeting of the American Nuclear Society, Los Angeles, Calif., June 28–July 2, 1970.

[7] R. E. Larson, F. J. Rees, and J. P. Nichols, "Dynamic Programming for Expansion Planning of Nuclear Power Generation System," presented at the Sixteenth Annual Meeting of the American Nuclear Society, Los Angeles, Calif., June 28–July 2, 1970.

[8] R. E. Larson, *State Increment Dynamic Programming*, American Elsevier Publishing Co., Inc., New York, 1968.

formulate a linear programming model can sufficiently change the problem so as to produce results of doubtful validity.

Expansion Planning of the Fuel Reprocessing Industry

One problem facing the expanding industry for processing spent fuel from nuclear reactors is determination of a schedule for plant construction (by year, site, and size), fuel processing, fuel storage, and fuel shipping that results in a minimum discounted cost over a defined period. The fuel can be assumed to be generated at a number of discrete sources; similarly, plants can be built at a number of discrete sites. These plants are characterized by high capital cost, pronounced economy of scale, and a developing technology that may limit the maximum size of plant that can be built at a given time. Fuel may be stored and the construction cost may be deferred; however, the storage cost will be substantial. Shipping spent fuel to a distant plant with excess capacity is another alternative, although the additional cost over shipment to a local plant is significant.

The feasibility of applying advanced dynamic programming procedures to this problem was studied by developing methods to solve a sample problem and then evaluating the applicability of these methods to an actual problem. The full-scale problem might involve fuel reprocessing plant expansion in the United States over a 30-year period, assuming sources of fuel and potential sites in eight geographical regions. The sample problem has two sources of fuel and two potential sites; fuel load, unit costs, allowable plant size, and other data are defined in Table 15.2.

A dynamic programming technique that appears to be suitable for solution of a large problem utilizes the method of successive approximations.[8] With this method, the problem is subdivided into a series of coupled single-state (one-dimensional) dynamic programming problems that are solved iteratively intil the solution converges. The time-dependent state variables are considered to be the quantities of processing

Table 15.2. Input Data and Solution of Sample Problem

Assumptions: Present-worthed plant capital and operating cost = ($9.0 × 10^6) (tons/year of capacity)$^{0.35}$
Supplementary plant operating cost = $500/ton
Storage cost = $10,600/ton
Round-trip shipping costs:
Source 1 to Site 1 = $1625/ton
Source 2 to Site 2 = $2000/ton
Source 1 to Site 2 = $4060/ton
Source 2 to Site 1 = $4060/ton
Discount rate = 12%
Plant life = 10 years
Constraint: No fuel storage in last year

Year	Allowable Plant Capacity (tons/year)	Fuel Generated (tons)		New Capacity Installed		Fuel Storage (tons)		Fuel Processed (tons)	
		Source 1	Source 2	Site 1	Site 2	Source 1	Source 2	Site 1	Site 2
1	260	94	0	0	0	94	0	0	0
2	520	228	86	0	0	322	86	0	0
3	780	370	285	780	0	0	283	780	0
4	1040	529	455	0	0	0	487	780	0
5	1300	781	684	0	0	0	1171	780	0
6	1560	1204	1090	0	1560	425	701	780	1560
7	1820	1694	1589	1820	0	0	249	2600	1560
8	2080	2079	2002	0	0	0	170	2600	1560
9	2080	2694	2674	0	2080	0	0	2600	2938
10	2080	3525	3602	0	0	887	0	2600	3640
11	2080	4358	4633	2080	2080	0	0	4680	5198
12	2080	4860	5400	0	0	0	0	4680	5580
13	2080	5370	6090	2080	0	0	0	5740	5720
14	2080	5910	6770	0	2080	0	0	5910	6770
15	2080	6510	7640	520	0	0	0	6500	7650

capacity at each site. Other potential state variables – the quantities of storage at each site – can be eliminated by an inventorying policy that considers the relative costs of processing, shipping, and storage. A difficulty associated with finite plant lifetimes can be obviated by using forward dynamic programming as opposed to the traditional backward method.

The successive approximations solution of the sample problem (Table 15.2) was obtained in 20 sec on a UNIVAC 1108 computer using 40,000 words of core memory. This technique appears to be suitable for solving a problem having at least eight fuel sources and eight potential processing sites on the basis that computing time and core storage requirements increase approximately linearly with the number of state variables. While it cannot be proved that the resulting solution is the global optimum, no better solutions of the sample problem could be obtained with a variety of initial conditions and alternative dynamic programming formulations.

16. Preparation and Properties of Actinide Oxides

16.1 MATHEMATICAL MODELS OF COLLOIDAL SYSTEMS

In our continued theoretical analysis of colloidal particles, we have completed the study of aggregation and flocculation of 80-A-diam particles dispersed in a solution of a singly charged electrolyte. The mathematical model and the assumptions were described previously.[1] Briefly, it is assumed that the individual Verwey-Overbeek attractive and repulsive potentials sum linearly to give the overall attractive and repulsive potentials around an aggregate. The shape of the potential barrier calculated in this manner and its height relative to kT (the average thermal energy of a particle) show that, under conditions for stability and slow aggregation, linear strings of particles will be the favored shape of the aggregate. Under conditions that are conducive to rapid flocculation, aggregates will tend to be spherical. Both of these conclusions agree with the observed behavior of thoria sols.[2]

A zeta potential of about 25 mv and an electrolyte concentration of about 0.01 M at 25°C are typical values for a thoria sol that is subject to rapid flocculation. Figure 16.1 shows a contour map of the potential barrier (against the approach of a single unattached particle) around a "string" of two particles under these conditions. (Only one-fourth of the map and of the two-particle string is shown since the system is symmetric above and below, as well as right and left.) The barrier is highest at the middle of the string, and drops to a minimum at the end. Figure 16.2 shows cross sections of the potential barrier at those two positions. The minimum is about half (54%) as high as the maximum, and it is farther out from the nearest particle surface than is the maximum. The dotted line located above both cross sections is drawn at the average thermal energy, kT. Since kT is higher than the barrier, there should be practically no hindrance to rapid flocculation from any direction of approach; hence this provides an explanation for the observation that thoria sols with these characteristics undergo rapid flocculation, showing little tendency to form strings.

A zeta potential of approximately 70 mv and an electrolyte concentration of approximately 0.001 M are typical values for a stable thoria sol. For this case we found that the barrier maximum was ten times as high as it was in the preceding case, and that the minimum was about 60% as high as the maximum. Thus since the barrier is everywhere much higher than kT, few approaching particles can cross it; consequently, most of those that are successful will cross at the minimum and will preferentially attach at the ends, thereby extending the string. These conclusions would explain why such sols are extremely stable. For example, some of these sols have aged for more than five years without showing any substantial flocculated sediment, and the flocculation which does occur is oriented into strings.[2]

Our calculations show that, as the size of the string increases, the barrier height increases everywhere, including at the minimums. This result indicates that the length of the string should be self-limiting as the height of the minimum increases and thereby inhibits the attachment of more particles. The length of the string is also limited because strings are broken by thermal energy, at some finite rate, due to the smaller binding energy between particles as compared with kT.

We estimate that our calculation using the 70-mv zeta potential is in error by about 5 to 10% because the potentials are derived from a linearizing approximation to the differential equation that describes the double layer. This limit of error was estimated by comparing the numerical solution of the exact differential equation of the one-particle case with the approximate solution. Since the experimental particle size and the zeta potential values are only accurate to within 5 to 10%, the accuracy of our calculations should be sufficient for most purposes.

---

[1] *Chem. Technol. Div. Ann. Progr. Rept. May 31, 1969*, ORNL-4422, pp. 312–15.

[2] K. H. McCorkle, *Surface Chemistry and Viscosity of Thoria Sols*, ORNL-TM-1536 (July 1966).

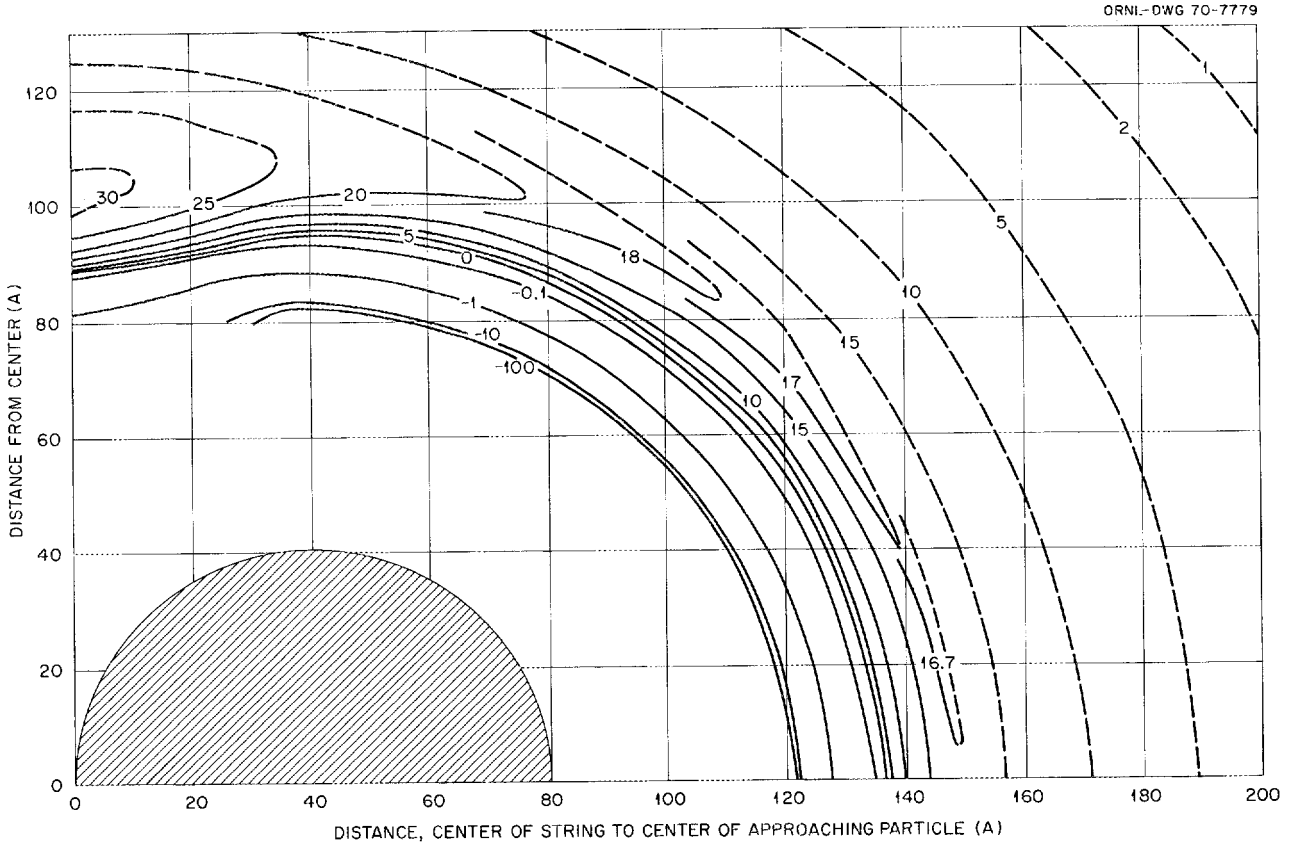

Fig. 16.1. Contour Map of the Potential Energy Barrier Against the Approach of an 80-A Particle to a "String" of Two 80-A

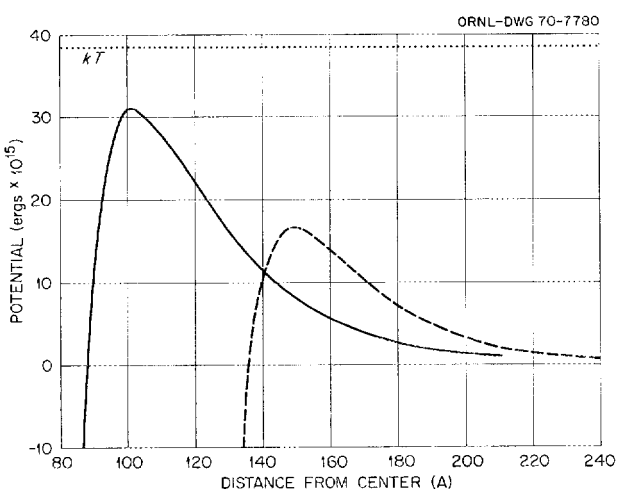

Fig. 16.2. Cross Sections of the Potential Barrier of Fig. 16.1. The solid line shows a cross section through the maximum, in the radial direction. The dashed line shows a cross section through the minimum, in the axial direction.

16.2 OXIDATION OF UO_2 SOLS

One particularly important variable that must be considered in the study and use of urania sols is the extent of oxidation of the U(IV) to U(VI). Moreover, it is presumably not only the amount of excess oxygen (over UO_2) that is important but also the distribution of this oxygen between the surface and the interior of crystallites (and possibly its effects on the surface structure and the adsorptive properties of the crystal). In one area of study of this variable, we are examining the kinetics of oxidation of urania sols under various conditions and the resulting effect on the properties of the sols.

The rate of oxidation of UO_2 sols was measured at room temperature in air and in pure oxygen at 1 atm. The sols were stirred gently with a magnetic stirrer. The surface-to-volume ratio of the sol was about 1 (i.e., 1 cm^2 of exposed surface per 1 cm^3 of sol). Some typical results are shown in Fig. 16.3.

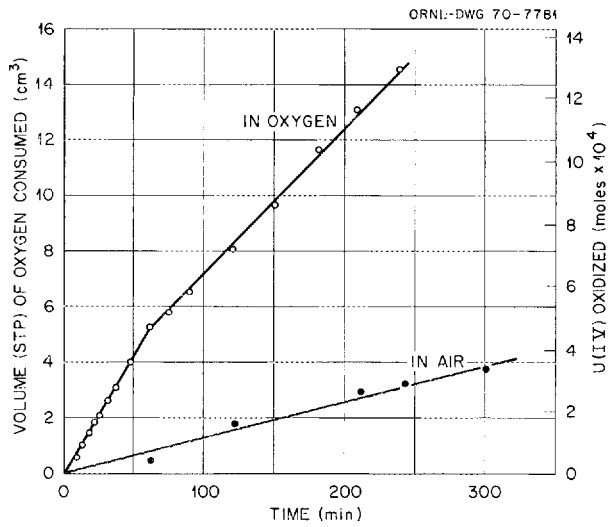

Fig. 16.3. Rate of Oxidation of a 1 *M* UO_2 Sol (CUSP-ES-7). Conditions: total pressure, 1 atm; room temperature.

The initial oxidation rates were found to be proportional to the partial pressure of oxygen and independent of the uranium concentration, although, at the lower concentrations, an induction period was noted under the experimental conditions used. After a total of about 25.5% of the U(IV) had been oxidized (including that oxidized during preparation), a decrease in oxidation rate was observed. We interpret this decrease to represent the completion of oxidation of the urania surface. This interpretation is supported by the fact that the results were reproducible with various sols having initial U(VI) contents of 14.0 to 16.6%. In one test, in which the specific surface area of the sol was decreased by boiling the sol to grow larger crystallites, the decrease in rate occurred when 17.4% of the U(IV) had been oxidized. This reflects a lower number of metal atoms on the surface.

The concept of oxidation of a surface layer is also supported by evidence from titration with hydrogen peroxide, using sol conductivity to detect the end point. The conductivity decreases sharply until the surface is oxidized, and then levels off. A decrease in the electrical charge of the sol particles, as determined by measurement of the streaming current, can also be used to follow the titrations; however, the end point for this type of measurement is less sharply defined.

16.3 ADSORPTION OF CO_2 BY SOLS

Previous work on the adsorption of CO_2 by nitrate-stabilized thoria and urania sols has been reported.[1] In this work, it was found that adsorbing CO_2, removing

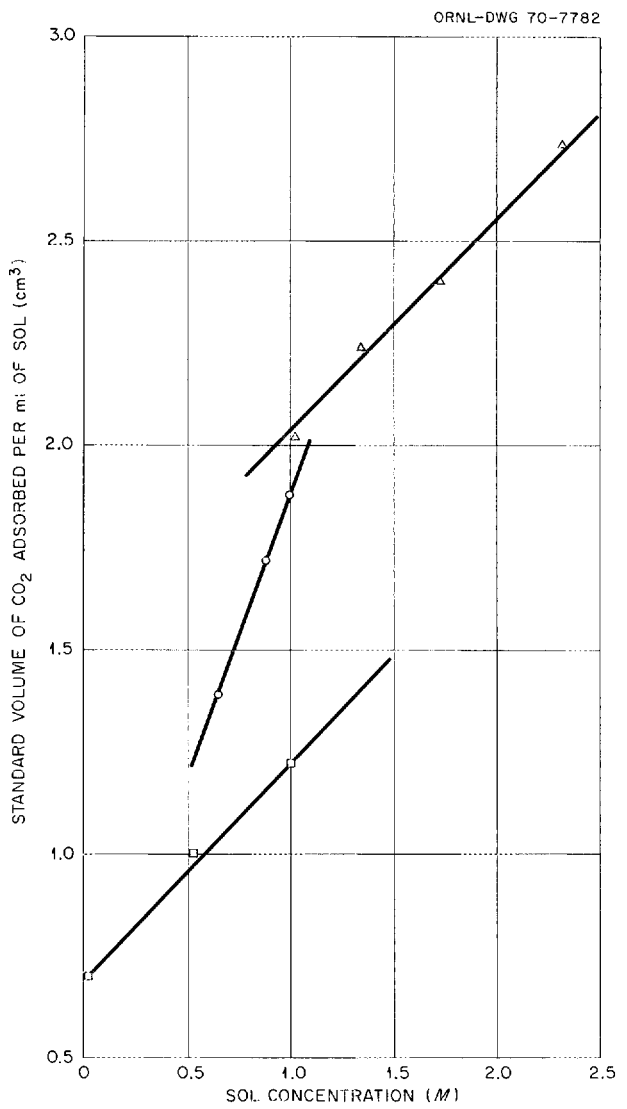

Fig. 16.4. Adsorption of Carbon Dioxide by Three Thoria Sols. Sols prepared from: Δ, steam-stripped $Th(NO_3)_4$; ○, oxalate-derived ThO_2, fired at 500°C; □, oxalate derived ThO_2, fired at 700°C. Lower concentrations of each series were achieved by dilution with intermicellar solution obtained by centrifugation.

the displaced nitrate from solution, and repeptizing the oxide with another mineral acid constituted a convenient method for changing the sol-stabilizing anion.[1,3] It was also proposed that this method might afford a means of measuring the surface areas of sols in situ without the necessity of drying the samples (and perhaps altering them in the process). Specific testing to determine the validity of such a proposal has now been

[3] I. L. Thomas, "Methods for Exchanging Counterions in a Sol," U.S. patent applied for.

started; results obtained thus far have been partially encouraging but show that not all of the pertinent variables have been recognized.

Thoria sols were used for the first tests, since they have been thoroughly studied[2] and do not exhibit problems of oxidation as urania sols do. In each test, 10 ml of a thoria sol was added to a 25-ml Erlenmeyer flask (attached to a gas burette) after the system had been filled with CO_2. The amount of adsorbed CO_2 was measured while the sol was stirred with a magnetic stirrer. Equilibrium was reached in 20 to 25 min. Sols of various ThO_2 contents were prepared by combining stock sols with diluted sol obtained by centrifugation. Attempts were also made to attain higher concentrations by resuspending centrifuged solids in a smaller-than-original volume of fluid; however, the sol would not completely repeptize in these cases.

Results of the measurements are shown in Fig. 16.4. Two of the sols were made with oxalate-derived thoria, and one was made with steam-stripped thorium nitrate. In the first two cases it was found that each CO_2 molecule occupied 70 A^2. Using similar sols, McCorkle[2] has shown that a nitrate ion occupies about 30 A^2. Although these data are not very precise, they are consistent with the displacement of two nitrate ions by one carbonate ion. However, results for the thoria prepared by steam stripping showed only one CO_2 molecule adsorbed per 150 A^2, which does not fit any convenient picture. Perhaps the concentration of the electrolyte is involved, since the solubility of CO_2 in the intermicellar fluids is strongly affected by a salting-out effect (as shown in Fig. 16.4, by extrapolating the lines to zero thoria).

The amount of CO_2 that dissolved was inversely related to the electrical conductivity and directly related to the pH of the intermicellar fluids. Thus it seems that more variables must be investigated before the adsorption of CO_2 can become a useful tool for measuring the surface of sols in situ.

16.4 ELECTROKINETIC STUDIES OF LANTHANIDE SOLS

The study of the hydroxide (or hydrous oxide) sols of the lanthanides was continued. Emphasis was on the effects of electrolytes on their electrokinetic behavior. The sols were prepared as described previously.[1] Reported discrepancies in the behavior of such sols upon aging at 80°C (i.e., that the usual positive charge of the sols sometimes would change, but at other times would not change, to a negative charge) were resolved. This behavior was found to be related to the pH at which the sol had been aged. For example, the charge consistently remained positive for sols aged at pH levels of 7 to 9, although the value of the charge did generally decrease. On the other hand, aging at a pH near 11 always caused the positive charge to be reversed to negative.

Sols of several of the lanthanides were titrated to their isoelectric points with a 1 *N* sodium hydroxide solution. Several concentrations of each sol (prepared by diluting the sol with distilled water to preserve a constant nitrate/metal mole ratio) were used, and the hydroxide demand was determined from the slope of a graph of the hydroxide required vs the metal concentration. The results (Table 16.1) show that, at least for the lighter, more-crystalline lanthanides, the amount of hydroxide required to reach the isoelectric point increases with the nitrate/metal mole ratio. Other results showed that reducing this ratio increased the zeta potential of the sols of the lighter lanthanides but had little effect on the heavier ones, that the dilution with distilled water also had little effect, and that sulfate ion was approximately twice as effective as hydroxide ion in reducing the zeta potential to zero.

While the value of the zeta potential is one criterion for the stability of hydrophilic sols such as these, the hydration sheath around the particles must also be taken into consideration. By observing changes caused by the addition of various electrolytes and reactive gases such as CO_2 or NH_3, we hope to learn more about the nature of the double layer and the water sheath.

Table 16.1. Amount of Hydroxide Required to Neutralize the Charge of Lanthanide Hydroxide Sols

Lanthanide	(meq OH^-/meq metal)[a]	(meq NO_3^-/meq metal)[b]	meq OH^- / meq NO_3^-
Pr	0.043	0.043	1.0
	0.095	0.107	0.9
	0.099	0.082	1.2
	0.121	0.118	1.0
Nd	0.049	0.039	1.3
	0.124	0.090	1.4
	0.128	0.112	1.1
Sm	0.171	0.092	1.9
Ho	0.131	0.099	1.3
	0.178	0.062	2.9
Er	0.094	0.110	0.9
Yb	0.083	0.063	1.3
	0.084	0.095	0.9
	0.091	0.080	1.1

[a]From NaOH titration to the isoelectric point.
[b]Nitrate in the original preparation, after dialysis, or after addition of ammonium nitrate.

16.5 PREPARATION OF CARBIDES AND CARBONITRIDES

During the past year, the preparation of uranium and plutonium carbides[4] has been extended to include the preparation of monocarbides and carbonitrides. The primary objective has been to form dense microspheres or shards by a single conversion-sintering step. Powders were prepared for comparative purposes.

The general preparation scheme is outlined in Fig. 16.5. Low-nitrate plutonia sols were mixed with urania sols that had been prepared either by batch precipitation or by the CUSP process[4,5] at a Pu/(U + Pu) mole ratio of approximately 0.2. The $(U,Pu)O_2$-C sols were 1 to 1.5 *M* in metal, 0.1 to 0.15 *M* in NO_3^-, and 0.3 to 0.5 *M* in formate. The carbon/metal mole ratios in the sols to be used for preparing the monocarbides and carbonitrides ranged from 2.2 to 3.1.

Microspheres were formed from the metal oxide-C sols by the standard ORNL technique. Shards and powders were prepared by evaporating the sols under argon. Volatile materials such as water, formate, nitrate, and residual organic material (when a drying solvent was used) were removed by heating to 800°C in a nonoxidizing atmosphere. A 4% H_2–argon mixture was preferred, since it reduces the higher oxides of uranium

[4] *Chem. Technol. Div. Ann. Progr. Rept. May 31, 1968,* ORNL-4272, pp. 158–60; *Chem. Technol. Div. Ann. Progr. Rept. May 31, 1969,* ORNL-4422, pp. 223–28.

[5] *Chem. Technol. Div. Ann. Progr. Rept. May 31, 1967,* ORNL-4145, pp. 180–207.

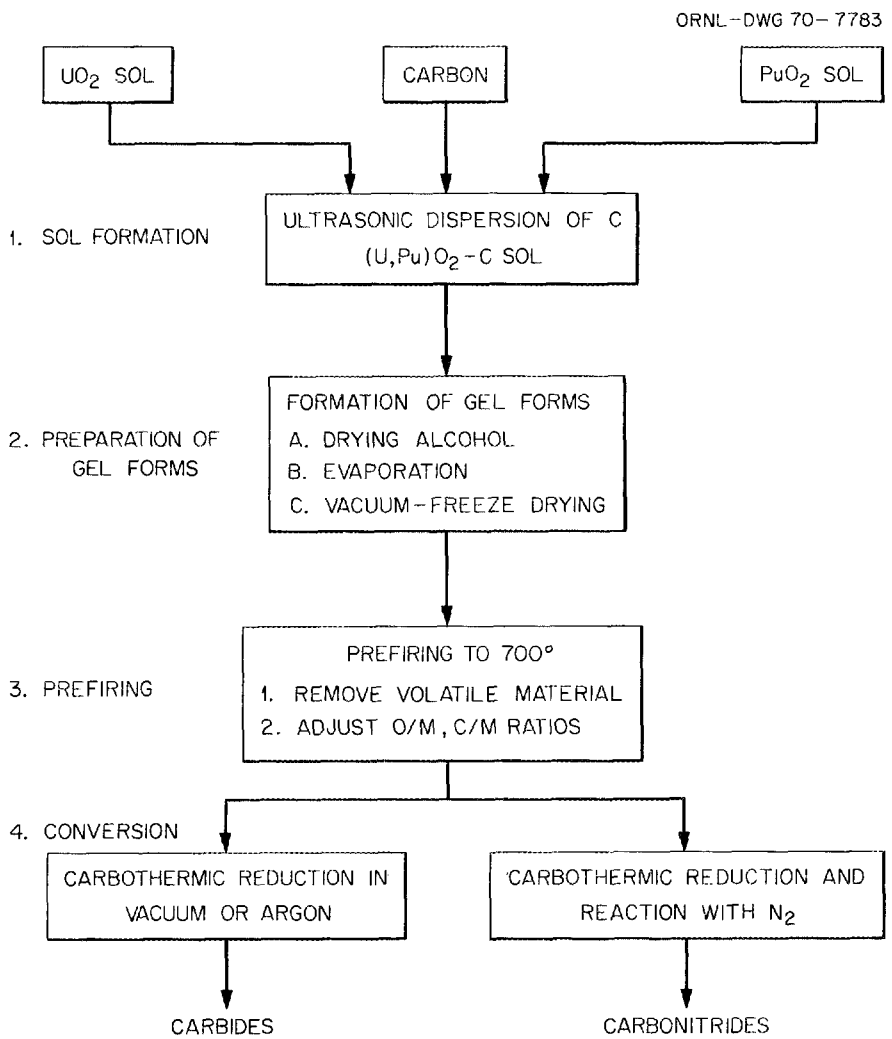

Fig. 16.5. General Flowsheet for Preparing (U,Pu)C and (U,Pu)C,N by a Sol-Gel Process.

to UO_2 and preserves the carbon/metal mole ratio present in the material. Although the prefiring and reduction steps could be combined into a single operation, there are several advantages in using two separate steps. These include: (1) better control of low-temperature firing parameters, and (2) the availability of a single batch of analyzed, prefired material for evaluating variables in the reduction step.

The prefired material was converted to the carbide or carbonitride at 1500 to 2000°C in tantalum containers. The procedure for preparing the carbonitrides differed from that for preparing carbides in that a nitrogen atmosphere was used during the carbothermic reduction. The conversion cycle consisted of a moderately rapid heatup in argon (20 to 40°C/min) to the reaction temperature of 1500° and then holding at 1500 to 1600°C for 2 to 4 hr in argon (for monocarbides) or nitrogen (for carbonitrides). The conversions were completed by heating in argon or vacuum for several hours at 1600 to 1700°C; evacuation aids in removing the last traces of oxygen and, with the carbonitrides, in decomposing higher nitrides that may have formed.

In the preparation of monocarbides, the carbon/metal mole ratio must be carefully controlled if a single-phase (U,Pu)C product is to be obtained. Even with the proper stoichiometry, other phases can form if equilibrium is not achieved. The crucial nature of this ratio requires that higher oxides of uranium, which would consume carbon above 800°C, be absent or reduced before the reduction step. It also prohibits the use of a slight excess of carbon to aid in decreasing the oxygen contents of the products. The oxygen content of the prepared monocarbides has ranged as high as 4000 ppm for products made from prefired material having carbon/metal mole ratios of 2.9 to 3.0 (stoichiometrically, a ratio of 3.0 yields monocarbide from dicarbide). With the optimum conditions described, it has been possible to decrease the oxygen content to 1000 ppm or less. X-ray analyses showed the presence of M_2C_3 in some of the monocarbide preparations; however, free metal was not detected, and traces of oxide were observed only in products that were made from feed material having low carbon/metal mole ratios (oxycarbides). Lattice parameters of the monocarbide products ranged from 4.94 to 4.96 A. Metallographic examination of the microspheres indicated that all of the products had high densities and that several of the preparations were essentially single phase. Measurement of the density of the products by mercury porosimetry gave values 90 to 95% of theoretical, based on the value calculated from the lattice parameter. Figure 16.6 *a* shows a metallograph of a monocarbide microsphere and indicates the type of porosity that is present in the products. A product microsphere that had been etched with a mixture of HNO_3, H_2O, and acetic acid shows the presence of a metallic phase at the grain boundaries (Fig. 16.6 *b*). Some needle-like forms, which can also be seen in the metallograph, are believed to be dicarbide. It is very difficult to avoid the presence of small amounts of other phases in the monocarbides.

Sols with carbon/metal mole ratios of 2.2 to 2.8 were produced for use as feed material in the preparation of carbonitrides. The advantage of the carbonitride system is that a single-phase product should be obtained from starting materials with this range of carbon/metal ratios; also, small changes in the carbon/metal ratio prior to the carbothermic reduction step are not detrimental. Even some air oxidation of the UO_2 can be tolerated, as long as the carbon/metal ratio does not fall below 2.2. In general, we use sols with carbon/metal mole ratios of 2.4 to 2.6, which allow changes as large as ±0.2 in the ratio during preparation and handling.

The oxygen content of the products prepared from sols with carbon/metal mole ratios of 2.4 to 2.8, using several different procedures, was usually less than 3000 ppm and could be decreased to less than 1000 ppm under optimum conditions. The oxygen contents were generally higher for products made from sols with carbon/metal ratios of 2.2 to 2.4 if the same length of time was allowed for conversion. X-ray analysis indicated only an MCN-type structure for most of the products. In some early preparations, higher nitrides and/or carbides were detected; metallographic examination also showed the presence of two phases in these products. It is believed that the recent preparations are single phase, but our failure to etch products with compositions close to $MC_{0.5}N_{0.5}$ has made metallographic analysis more difficult. X-ray lattice parameters for all of the carbonitride products have ranged from 4.90 to 4.96, and are in agreement with the literature values.[6] Densities measured by mercury porosimetry ranged from 90 to 95% of theoretical (based on the value calculated from the lattice parameter); the measurements also indicated a surface-connected porosity of up to 5%. Figure 16.7 presents some metallographs of a carbonitride product, showing the type of porosity that is present in such products.

To date, monocarbide and carbonitride microspheres up to approximately 400 μm in diameter have been prepared. In general, the surface quality is only slightly

[6] R. Lorenzelli, *Contribution to the Study of the System (U,Pu)C,N*, CEA-R-3536 (May 1968).

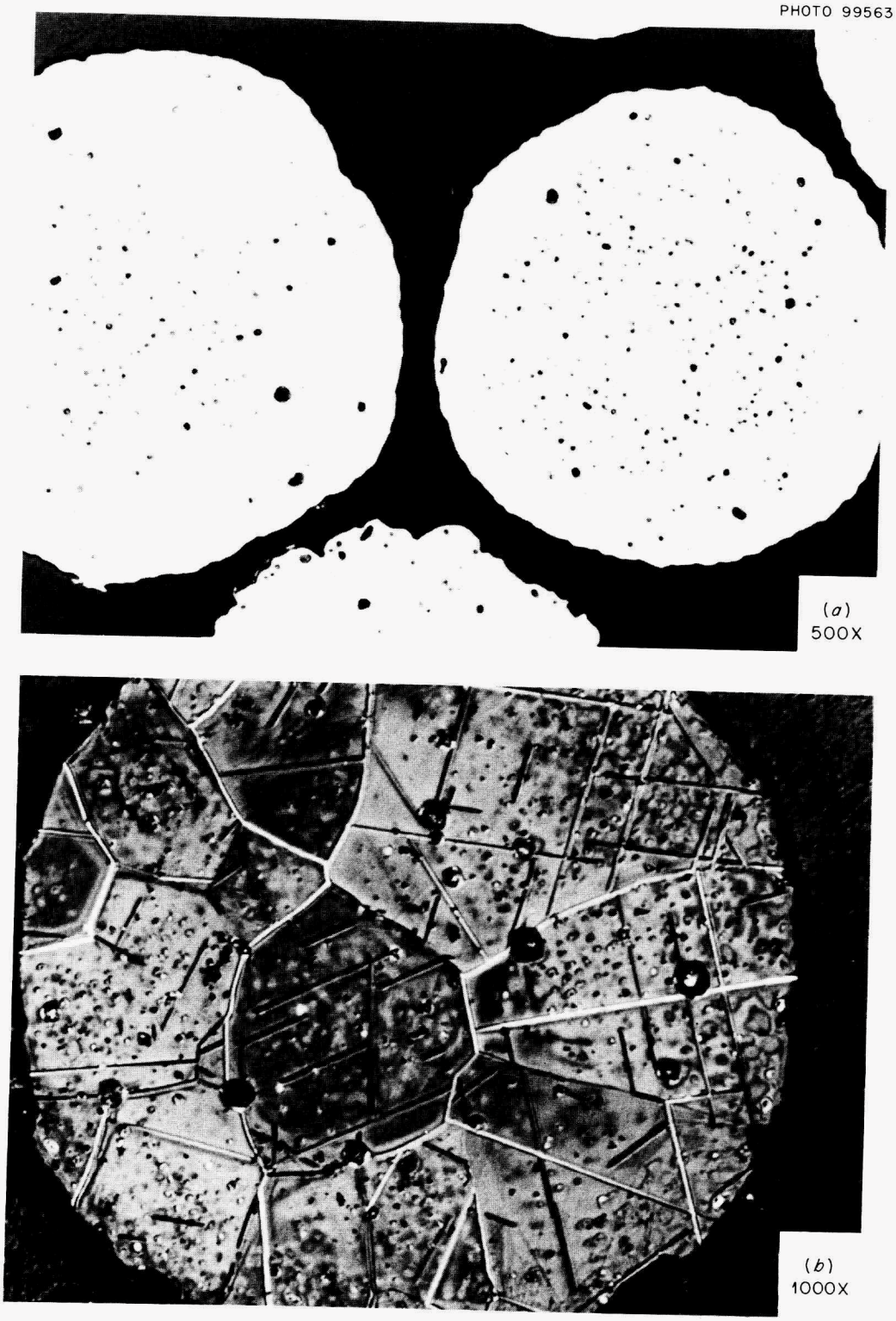

Fig. 16.6. Metallographs of (U,Pu)C. (*a*) As polished. (*b*) Etched with a mixture of water, nitric acid, and acetic acid. Reduced 22.5%.

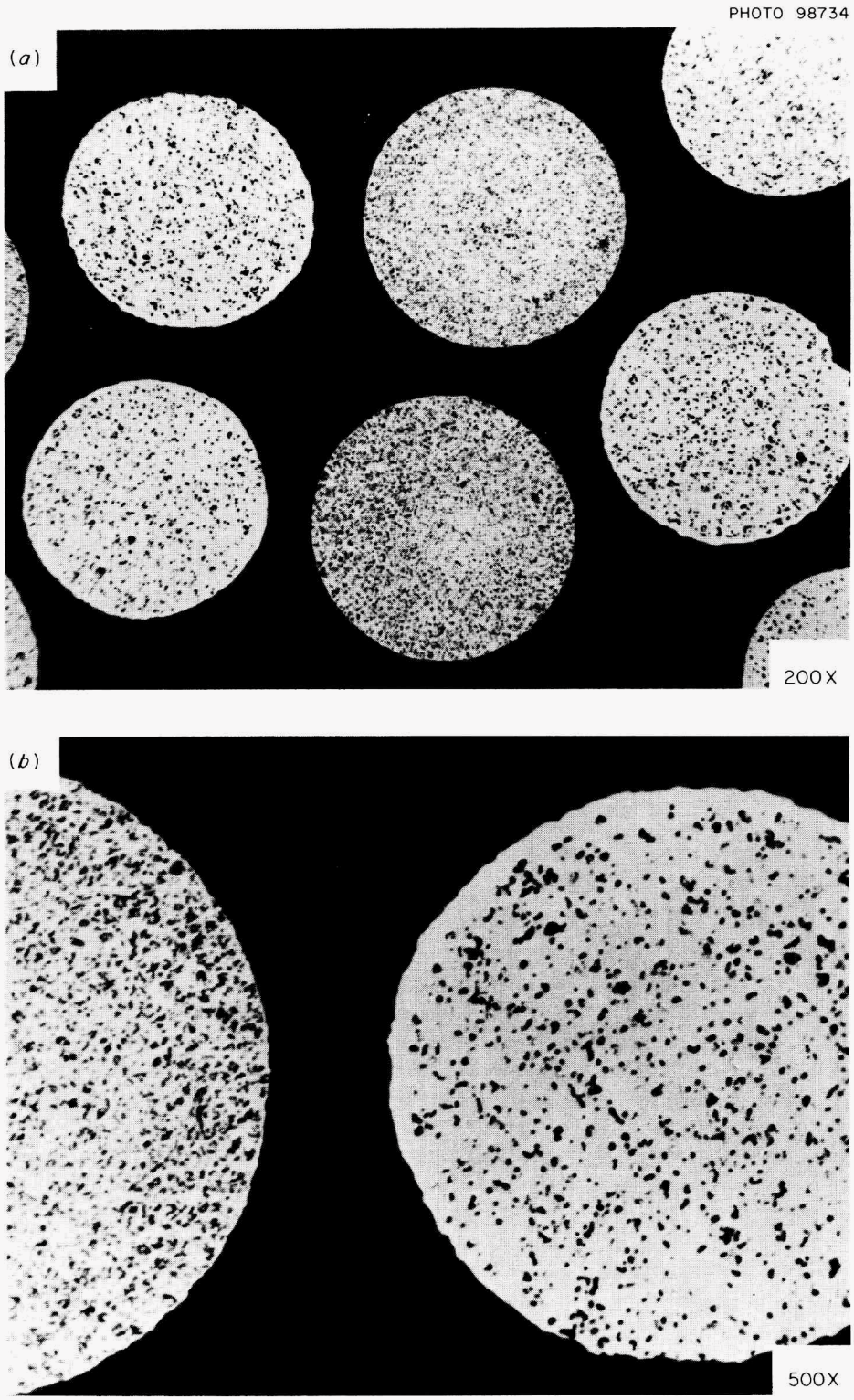

Fig. 16.7. Metallographs of (U,Pu)$C_{0.4}N_{0.6}$ Microspheres (As Polished). Reduced 22%.

inferior to that of oxide microspheres prepared by a sol-gel process. With regard to density and porosity, better-quality products have been obtained in microspheres than with shards.

Kinetic Studies of the Carbothermic Synthesis of Carbides, Nitrides, and Carbonitrides[7]

The studies of the kinetics[4] of the carbothermic synthesis of carbides, nitrides, and carbonitrides of uranium, plutonium, and their solid solutions are being continued. Oxide-carbon gels produced by the sol-gel process can be conveniently used as feed material for the synthesis of these fuels. Generally, carbon has been found to play a vital role in reactions in the U-C-O-N system.[8] This has been demonstrated by extensive studies of the kinetics and thermodynamics of reactions in the system from 1400 to 2000°C, including those of UO_2 with carbon,[9] UC with nitrogen,[10] and UC_2 with nitrogen.[11] Carbon can act as a reductant, or it can control the reaction rate by means of diffusional processes, by the distribution of free carbon within the solid reactants, by the formation of compounds that are richer in carbon, or by the formation of a nonequilibrium type of free carbon. In each case, the role of carbon is dominant.

This information has been used, in part, to analyze the carbothermic synthesis of advanced fuels in a fluidized bed.[12] The analysis considers the interrelationship of the kinetics of the oxide-carbon reaction studied previously,[9] the carbon monoxide pressures obtained via thermodynamic calculations, and the operational parameters of a fluidized bed. The conclusions of the analysis provide a means for optimizing the operation of the process for the synthesis of the fuels.

[7]This work was performed by T. B. Lindemer of the ORNL Metals and Ceramics Division.

[8]T. B. Lindemer, J. M. Leitnaker, and K. E. Spear, *The Role of Carbon in Reactions in the U-C-O-N System*, ORNL-TM-2715 (November 1969).

[9]T. B. Lindemer, M. D. Allen, and J. M. Leitnaker, "Kinetics of the Graphite-Uranium Dioxide Reaction from 1400 to 1756°C," *J. Am. Ceram. Soc.* **52**, 233–37 (1969).

[10]J. M. Leitnaker, T. B. Lindemer, and C. M. Fitzpatrick, "The Reaction of UC with Nitrogen from 1475 to 1700°C," submitted for publication in the *Journal of the American Ceramic Society*.

[11]T. B. Lindemer, J. M. Leitnaker, and M. D. Allen, "Kinetics of the Reaction of UC_2 and Nitrogen from 1500 to 1700°C," submitted for publication in the *Journal of the American Ceramic Society*.

[12]T. B. Lindemer, "Factors That Control the Carbothermic Synthesis of Advanced Fuels," presented at the Symposium on Sol-Gel Processes and Reactor Fuel Cycles, Gatlinburg, Tenn., May 4–7, 1970; published in the *Proceedings*.

17. Chemical Engineering Research

Chemical engineering research is an aggregate of studies which, while generally pertinent to the applied programs of the Chemical Technology Division, are fundamental in nature or pursue attractive new ideas. The fundamental studies usually arise from interesting effects noted during work on programs with more specific commitments. On the other hand, work begun on new ideas frequently becomes part of applied programs as the work matures.

This year we are reporting work associated with the sol-gel, the LMFBR, and the MSR programs. Although much of the work that is embraced by chemical engineering research is more conveniently reported as parts of the applied programs with which they are associated, four particular studies have been isolated for presentation here.

17.1 MASS TRANSFER OF WATER FROM SOL DROPLETS

The microsphere forming operation in the ORNL sol-gel process for the fabrication of nuclear reactor fuels has provided a system that is amenable to unusually precise mass-transfer measurements. Three years ago, a fundamental study was undertaken to provide information for the design of columns in which sol droplets would be gelled. The technique consists of fluidizing a single droplet of either water or thoria sol with 2-ethyl-1-hexanol (2EH) in a small, carefully machined, tapered Plexiglas chamber (see Fig. 17.1). The hydrodynamics in the convergent-divergent flow channel are stable and well defined, and the parallel outer faces of the plastic block make the system ideal for optical measurements. As the water from each suspended drop is transferred into the organic phase, the sphere shrinks, and successive optical measurements of the diameter at a magnification of about 20X permit an accurate measure of the mass-transfer rate. Since the water concentration inside the sol droplet is very high, the resistance to mass transfer exists exclusively in the organic-phase film through which the water is being transferred.

A linear relationship was found for the water and sol droplet data, using the classical correlation in which the Sherwood number is proportional to the product of the square root of the Reynolds number (for the sphere) and the cube root of the Schmidt number.[1] It was possible to devise a simple expression involving the physical properties of the sol and the organic solvent, along with the concentration at which the sol was known to gel, to predict the time required for gelation. The original study was restricted to 2EH as the organic phase and to a temperature of 25°C, which limited the Schmidt number to the single value of 35,700.

These earlier results were interesting enough to motivate us to extend the studies to encompass a wider range of Schmidt numbers (from 5000 to 35,000) and Reynolds numbers for the sphere (from 0.2 to 30). Mass-transfer data have been obtained for single water and thoria sol droplets fluidized in 2EH at temperatures of 25, 40, and 50°C, and in 2-methyl-1-pentanol and *n*-hexanol at 25°C. In the majority of the runs, a surface-active agent, Ethomeen S/15, was added to the alcohols in order to prevent internal circulation of the fluidized drop; however, about ten runs were made using 2EH with no added surfactant.

Starting with the convective diffusion equation and the continuity equation in natural curvilinear coordinates for a rigid drop, a relationship involving the Sherwood number, the Reynolds number, the Schmidt number, and the tangential velocity gradient at the drop interface has been derived. By relating the velocity gradient to the sphere drag coefficient (which is solely a function of the Reynolds number), the Sherwood number has been found to be proportional to the

[1] S. D. Clinton, *Mass Transfer of Water from Single Thoria Sol Droplets Fluidized in 2-Ethyl-1-hexanol*, M.S. thesis, University of Tennessee, Knoxville; also published as ORNL-TM-2163 (June 1968).

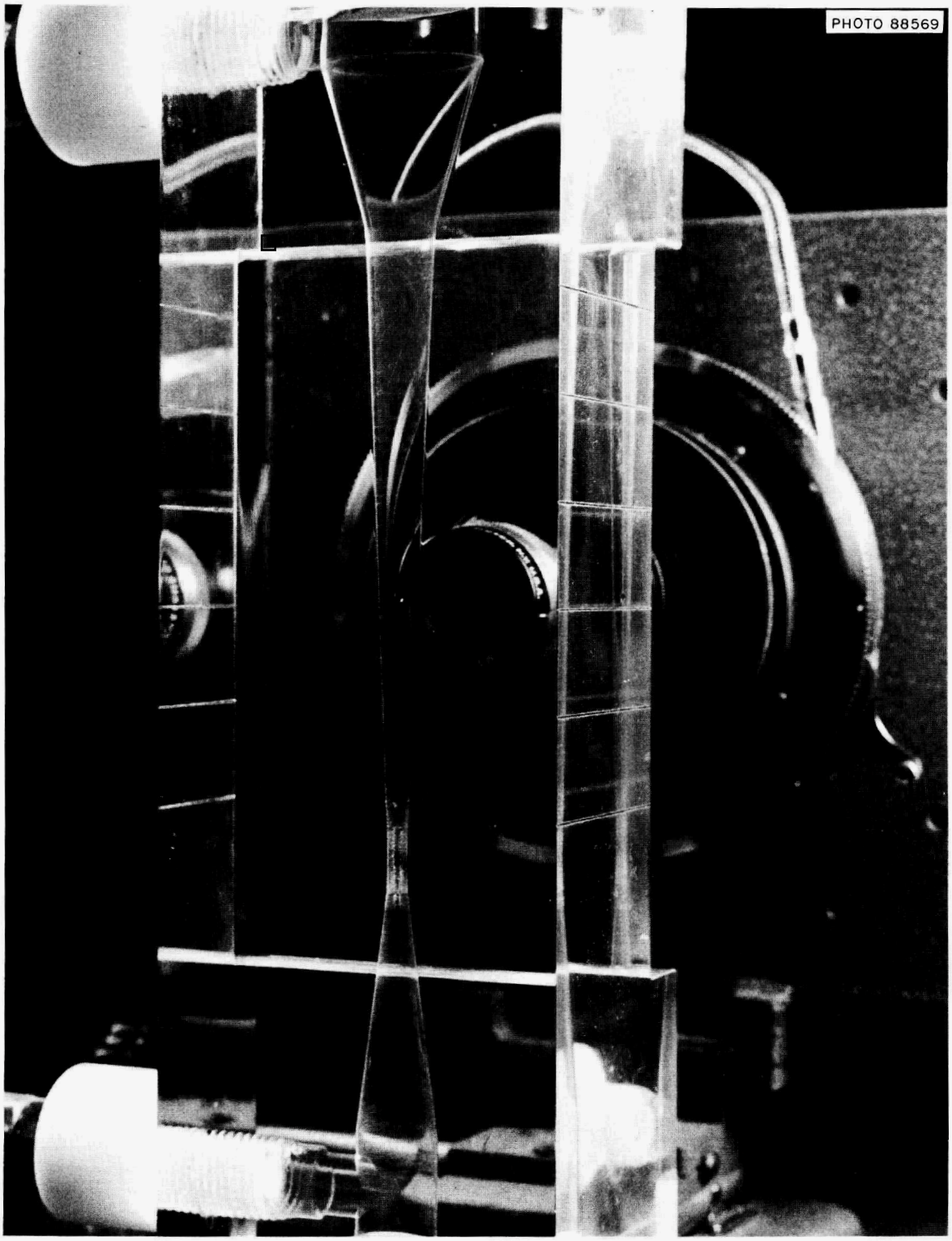

Fig. 17.1. Fluidization of a 0.0625-in.-diam Sapphire Sphere in the Tapered Plexiglas Column.

sphere Reynolds number raised to a variable exponent ranging from $1/3$ for the region in which Stokes' law is applicable to $2/3$ for the fully turbulent region. Hopefully, enough rate data for single fluidized drops have been accumulated to allow a positive statement to be made in the near future on the proposed mass-transfer correlation involving the appropriate dimensionless groups and drag coefficients.

17.2 PRODUCTION OF SOL-GEL MICROSPHERES OF SMALL UNIFORM SIZE

Our present techniques for forming sol-gel microspheres with diameters of 100 μ and larger are quite satisfactory. Currently, we are studying methods for producing uniform microspheres with diameters as small as 20 μ. One of these methods involves the use of ultrasonic vibrations to pace the breakaway of droplets from a jet or nozzle.

Devices based on the use of ultrasonic vibrations are of two types: nonresonant and resonant. In each case, either the alcohol or the nozzle through which the sol is injected, or both, would be caused to vibrate at ultrasonic frequencies. In the nonresonant case, the nozzle and attached structures would have to be light and pliant; that is, this assembly would need to have a higher natural frequency than the applied ultrasonic frequency which would apply the forcing function. Prior art indicates that droplets can be formed by vibrating the nozzle either transverse to the direction of sol injection or in the direction of sol injection. In the first case, one droplet is formed every half cycle; in the second, a droplet is formed every full cycle.

In a resonant device, the nozzle would be contained in a bar of metal that is dimensioned, or tuned, to resonate (or "ring") at the applied ultrasonic frequency. In a novel form of such a resonant structure, the injection nozzle would look into an alcohol-filled cavity in the bar proportioned in such a way that it, too, was tuned to the applied frequency. By a proper selection of materials and dimensions, the standing waves in the metal bar would be approximately 180° out of phase with the standing waves in the alcohol-filled cavity. Such a situation should give maximum encouragement to a droplet of sol to break away from the injection nozzle at exactly the correct time.

17.3 AXIAL DISPERSION IN PACKED COLUMNS FOR CONTACTING LIQUIDS WITH A HIGH DENSITY DIFFERENCE

The probable need for packed columns in which molten fluoride salts can be contacted with molten bismuth for the on-line processing of molten salt breeder reactors has prompted basic studies with high density difference systems. The work includes measurements of flooding, mass transfer, and axial dispersion. Flooding studies have been performed with mercury-water systems in towers packed with raschig rings. Correlations from these studies have predicted rather accurately the flooding points in small towers operated with a molten fluoride salt and bismuth. Although this work was supported largely from research funds, it is discussed in detail in Sect. 1 of this report. In the work reported here on axial dispersion in packed columns, mercury and water were used to simulate the salt-bismuth system.

Measurement of Axial Dispersion in Packed Columns

We have initiated an experimental program in which axial dispersion coefficients in packed columns are measured under conditions similar to those expected in the proposed reductive extraction processes; mercury and water are used to simulate bismuth and molten salt. The measured axial dispersion coefficients have been used to estimate column performance in the proposed systems. When a tracer material is introduced near the column exit, the tracer diffuses upstream. At steady state, the concentration of tracer is given by the relationship:

$$\ln \frac{C}{C_1} = \frac{v}{E}(Z - Z_1) ,$$

where

E = axial dispersion coefficient,

C = tracer concentration at position Z,

v = superficial fluid velocity, and

Z = position along column.

Thus, a semilogarithmic plot of C/C_1 vs Z should yield a straight line having a slope of $-v/E$.

The experimental technique for measuring the concentration at several points down the column is as follows. A small stream of water (flow rate, ~1 ml/min) is withdrawn from the column, circulated through a photocell containing a light source and a photoresistor, and then returned to the column at the same elevation. This circulating side stream is driven by a small centrifugal pump containing a magnetically coupled impeller. The photocell is cylindrical in shape, with a $1/2$-in. inside diameter and a $3/4$-in. path length. The light

source is a GE No. 253X lamp, and the detectors are Clairex CL707L photoresistors.

The tracer material, cupric nitrate solution, is injected near the top of the column with a syringe pump. The solutions to be analyzed are very dilute, and the response of the photoresistors is essentially linear (a limited form of Beer's law) as confirmed by experiment.

The results of a typical run are shown in Fig. 17.2. In this case, the column was packed with $\frac{3}{8}$-in.-diam raschig rings, and the mercury and water flow rates were 29.1 and 9.1 ft/hr respectively. The axial dispersion coefficient is calculated from the slope of the line drawn through the data. Results obtained in seven runs indicate that the axial dispersion coefficient is approximately 3.5 cm^2/sec. The data include results obtained at several water flow rates (as well as several mercury flow rates). The conditions used in the runs are given in Table 17.1. It is possible that the axial dispersion coefficient increases as the flow ratio increases; however, if this is true, the increase is relatively small and cannot be confirmed by the data. It should be emphasized that, although the water and mercury flow rates were varied, the data were, in all cases, taken at less than 50% of the estimated flooding rate. Therefore, these data should not be extrapolated to near-flooding conditions, where holdup and drop sizes change significantly.

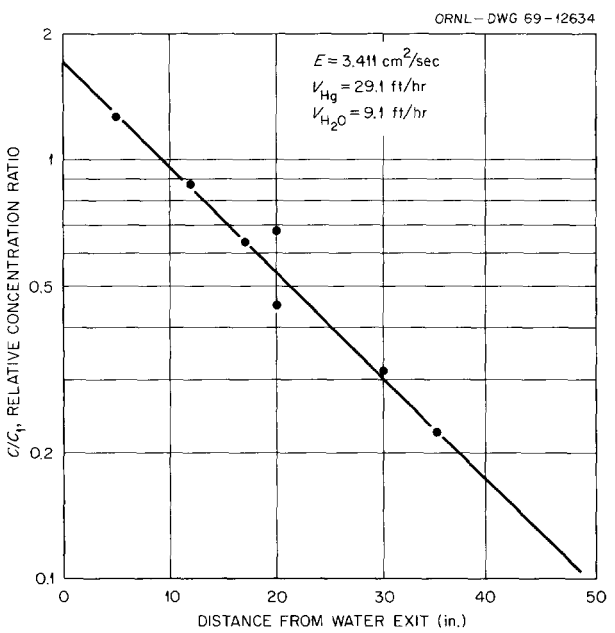

Fig. 17.2. Variation of Relative Concentration with Column Height.

Table 17.1 Summary of Axial Diffusion Data Obtained for Columns Packed with $\frac{3}{8}$-in.-diam Raschig Rings

Run No.	Superficial Velocity of Water (ft/hr)	Superficial Velocity of Mercury (ft/hr)	Mercury-to-Water Flow Ratio	Axial Diffusivity (cm^2/sec)
1	13.1	87.4	6.67	3.7
2	2.33	29.1	12.5	3.84
4	4.56	58.3	12.7	2.68
5	4.56	87.4	19.1	3.07
6	2.28	121.4	53.2	4.33
8	9.13	29.1	3.19	3.41
11	4.56	116.6	25.5	4.03

Reduction of Axial Dispersion in Packed Columns

We are also studying column modifications that will decrease the effect of axial dispersion. The proposed modifications involve placing devices that reduce or prevent axial dispersion, or backflow, along the column. If these devices are separated by a distance equivalent to one theoretical extraction stage, the calculated stage efficiency of the columns in a typical system will be greater than 75% when less than 15% of the salt flowing through a segment is recycled or back-mixed to the segment below. As will be shown, these conditions are not difficult to achieve and will result in satisfactory column heights (probably less than 3 ft per theoretical stage).

The type of device under investigation is illustrated in Fig. 17.3. The metal flows down the annular section of the upper piece into what is effectively an inverted bubble cap. As the metal flows over the weir in the lower piece, it forms a seal that forces the salt to pass upward through a sieve plate in the center of the column. The sieve plate is a restriction to provide a reasonably high salt velocity, which allows very little back diffusion of salt through the openings.

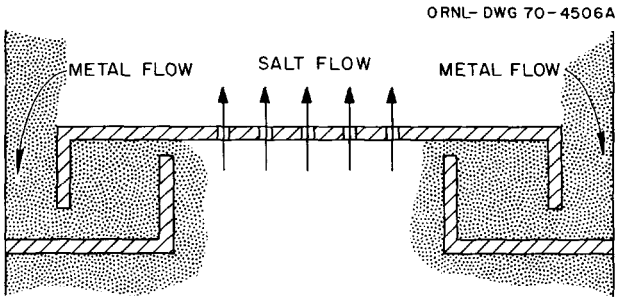

Fig. 17.3. Schematic Diagram of an Axial Mixing Preventer.

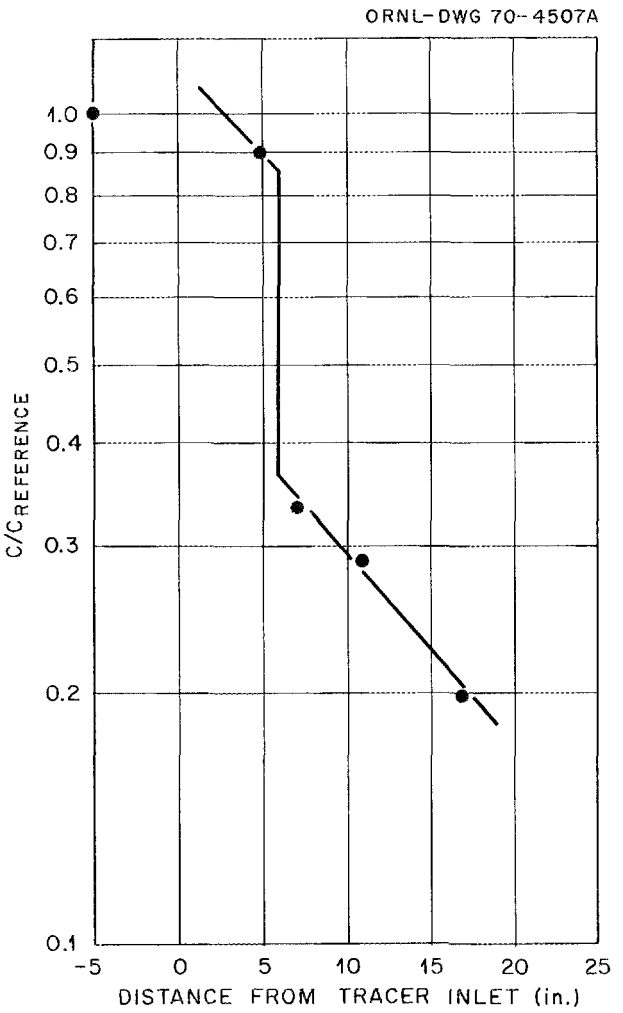

Fig. 17.4. Concentration Profile Using a Backflow Preventer with a Single $^3/_8$-in. Sieve Opening. Mercury flow rate, 400 ml/min; water flow rate, 115 ml/min.

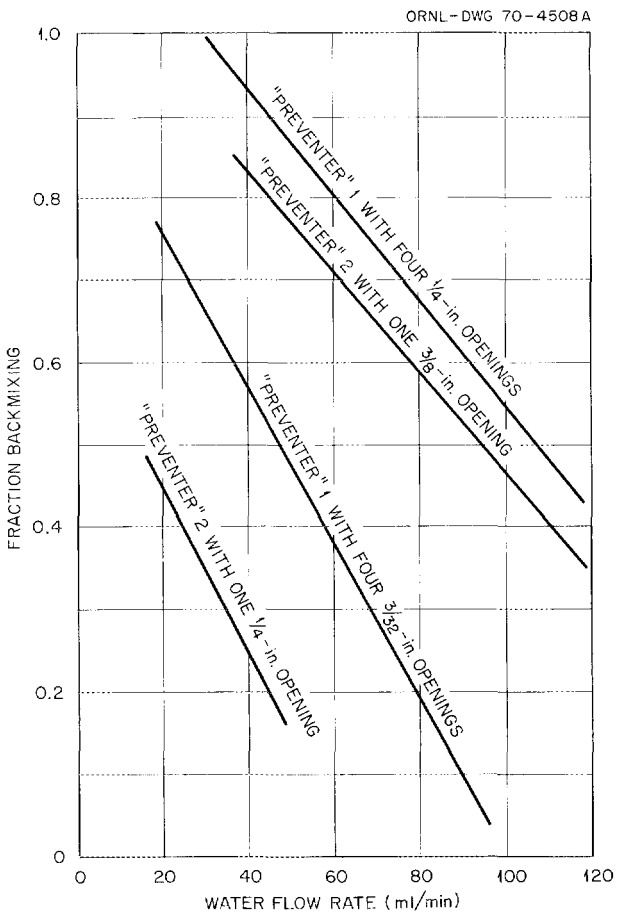

Fig. 17.5. Summary of Backflow Preventer Results.

Two designs of "backflow preventers" have been tested using mercury and water. In the tests, the column was packed with $^3/_8$-in.-diam raschig rings, and at least one backflow preventer was inserted near the middle of the column. The countercurrent flow of mercury and water was established, and an aqueous solution containing a tracer (cupric nitrate) was injected near the top of the column at a constant rate. The solution in the column was analyzed for tracer at several points down the column on both sides of the backflow preventer(s). If the logarithm of the tracer concentration is plotted as a function of distance down the column, a discontinuity is observed at the location of the preventer, as illustrated in Fig. 17.4. At the discontinuity, the ratio of the tracer concentration below the preventer to that above the preventer is then a measure of the fraction of solution back-diffusing through the preventer.

The fraction of backflow through a preventer appears to be principally a function of the water velocity through the sieve openings and the diameter of the sieve openings. No dependence of back-mixing on mercury flow rate was evident; however, the relatively few changes in mercury flow rate and the usual data scatter make this conclusion tentative. It is expected that a significant dependence on metal flow rate would be observed if this rate were increased sufficiently to prevent complete coalescence in the metal downcomer.

Data obtained with the backflow preventers are presented in Fig. 17.5. Although there is considerable scatter in the points through which the lines were drawn, the lines are believed to be representative. The backflow preventer used in the first test contained a $^1/_2$-in.-deep bubble cap and a $^1/_8$-in.-thick sieve plate with four $^3/_{32}$-in.-diam holes. Backflow decreased as the water flow rate was increased. The openings were then

drilled out to ¼ in. in diameter, and the results obtained with these larger openings are also shown in Fig. 17.5. The backflow did not reach an acceptably low level with the larger openings; however, an extrapolation of the curve predicts that it would become less than 15% at water flow rates between 150 and 200 ml/min (approximately 50 ml/min per hole). A second preventer, which had a 2-in.-deep bubble cap and only a single 1/16-in.-diam opening in the orifice, was tested; however, no backflow could be detected at the lowest measurable water flow rate (23.5 ml/min). The opening was increased to ⅛ in. in diameter, but again no backflow was detected. When the opening was increased further to a diameter of ¼ in., the results shown in Fig. 17.5 were obtained. The backflow is less than 15% when the water flow rate is greater than 50 ml/min. This value agrees with the results estimated by extrapolating results from the first preventer with four ¼-in. holes. When the diameter of the sieve opening was further increased to ⅜ in., the percentage backflow was increased considerably (see Fig. 17.5); however, it is known that the percentage backflow can be reduced to any desired value at sufficiently high water flow rates.

The only undesirable feature of these backflow preventers (other than adding complexity to simple packed columns) is their reduction of the column capacity. It is unlikely that a device which will accommodate the unmodified column capacity will be developed. The devices just discussed were operated at metal flow rates as high as 94 ft/hr (column superficial velocity), which is approximately 15% of the flooding rate for a column packed with ⅜-in.-diam raschig rings. Future designs are expected to perform effectively at much higher throughputs.

Estimating the Effect of Axial Dispersion on the Height of Extraction Columns

Axial dispersion (or longitudinal mixing) is detrimental to equipment performance in countercurrent operations. This situation has been understood since Miyauchi and Vermeulen[2] and Sleicher[3] developed solutions for systems with constant distribution coefficients. These solutions are, however, complex and difficult to use; apparently, they have been used quantitatively in only a few recorded instances. We have found that the following simple, empirical equation approximates the complex exact solutions over a wide range of conditions:

$$\eta \approx 1 - \frac{1}{N_{\mathrm{Pe}x} + 1 - F + 1/\mathrm{NTU}} - \frac{F}{N_{\mathrm{Pe}y} - 1 + F + 1/\mathrm{NTU}},$$

where

η = length of the column without back-mixing, divided by the length of the column with back-mixing,

$N_{\mathrm{Pe}x}$ = Peclet number in the reference phase = $U_x(\mathrm{HTU_p})/E$,

$\mathrm{HTU_p}$ = height of a transfer unit with plug flow,

U_x, U_y = superficial velocity of the reference and second phases respectively,

E = axial diffusion coefficient,

m = distribution coefficient,

F = extraction factor = mU_x/U_y,

NTU = number of transfer units calculated as if the phases were in plug flow.

This equation predicts efficiencies to within approximately 0.07 (e.g., the difference between the estimated and the calculated efficiency will be less than 0.07) when

$$\mathrm{NTU} \geqslant 2\,,$$

$$\eta \geqslant 0.2\,,$$

$$N_{\mathrm{Pe}x} \geqslant F - \frac{1}{\mathrm{NTU}}\,,$$

and

$$N_{\mathrm{Pe}y} \geqslant 1.5\,.$$

17.4 DEVELOPMENT OF THE STACKED-CLONE CONTACTOR

A stacked-clone contactor is a multistage, countercurrent solvent extraction device capable of performing liquid-liquid mass-transfer operations efficiently and rapidly.[4] A low stage-inventory-to-throughput ratio

[2] T. Miyauchi and T. Vermeulen, *Ind. Eng. Chem., Fundamentals* 2, 113 (1963).

[3] C. A. Sleicher, *A.I.Ch.E. J.* 5, 145 (1959).

[4] M. E. Whatley and W. M. Woods, *The Performance of an Advanced Experimental Stacked-Clone Contactor: A High-Performance Solvent Extraction Machine with Potential for Application to Very Highly Radioactive Solutions*, ORNL-3533 (April 1964).

permits rapid response to process control signals and hastens the approach to steady-state operation. Thus, radiation and chemical degradation of the organic solvent is minimized, and the performance during short processing campaigns is efficient. This contactor design occupies less physical space than any other known solvent extraction device of similar capacity, and is inherently safe from a nuclear standpoint because of its geometry.

The most recent design of a centrifugal-pump-driven hydroclone contactor is the multiclone contactor, which contains nine separate hydroclones in each of its 12 stages. All of the hydroclones are driven by the same pump. This machine was designed to test the concept of manifolding hydroclones, which will be necessary in large applications. Results of the initial testing were reported last year.[5]

As fabricated, the multiclone contactor did not produce the expected flow capacity. The particular pump design that was chosen for this machine imparted undue shear and shock to the fluids and thus emulsified the two phases to a greater degree than is normal in this type of operation. To circumvent these problems, we shrouded the impellers and increased the clearances between the impeller vane tips and the casings by machining. These steps alone represent a significant improvement since they gave a 20% increase in flow capacity. In any future design, other considerations of fluid flow characteristics can be taken into account to provide even better performance.

The hydroclones in the multiclone contactor are three-eighths the size of the "standard" hydroclones used in the development programs. Based on scaling studies, nine of these hydroclones were expected to have a combined flow capacity that was 1.85 times greater than that observed in a single standard hydroclone. We currently observe flows that are 1.07 times greater, which is equivalent to 3.06 liters/min (A/O = 3) for the system 1 *M* $NaNO_3$–18% TBP in Amsco at 40°C, with the aqueous phase continuous. In its present form, the multiclone stacked-clone contactor has a shorter residence time per theoretical stage than any other existing solvent extraction device.

Additional developments, especially those involving the pumps, are desirable to advance stacked-clone contactor technology. Although we have reported the advantages of hydroclones on several occasions, have proved the concept of manifolding hydroclones, and have demonstrated the higher performance of small hydroclones, efforts to reduce fabrication costs and to improve pump performance are needed. However, a lack of specific application at this time probably means that such efforts will be delayed. A stainless steel prototype contactor containing a single full-sized hydroclone in each of its 18 stages still exists for possible inclusion in a hot cell for radiochemical testing. The multiclone contactor is also available for further modifications.

The prototype centrifugal pump for the full-scale stainless steel stacked-clone contactor failed after 34,931 hr (i.e., four years) of continuous operation. The failure was not related to wear or any mechanical characteristics of the pump, but resulted from the fracture of a plastic line. This fracture drained the system of fluid. Consequently, the pump ran dry and overheated, causing an impeller to bind and the housing to fracture. A pressure switch, installed expressly for the purpose of cutting off the pump motor in case a leak developed, also failed to operate. A critical examination of all the parts of the pump showed that wear surfaces had not changed more than 5 mils during the testing period. Radial wear did not exceed 1 mil. Extrapolation of these figures indicates that a total life of from 8 to 12 years would probably have been attained if the pump had continued to operate normally.

[5] *Chem. Technol. Div. Ann. Progr. Rept. May 31, 1969,* ORNL-4422.

18. Miscellaneous Programs

18.1 QUALITY ASSURANCE PROGRAM

Quality assurance is defined as the total planned and systematic action necessary to provide adequate confidence that a material, component, system, or facility will perform satisfactorily in service. Quality assurance procedures are now being applied, under the auspices of the Quality Assurance Program, to important projects in the Laboratory at the request of the USAEC. The Program is being administered by an organization, composed of representatives from most of the divisions, that reports to the Laboratory Coordinator for Quality Assurance.

In the Chemical Technology Division, the Quality Assurance Program is being developed along two lines. First, formal quality assurance procedures are presently being applied to some projects that are now in progress. Second, plans are being made to extend the application of these procedures to future projects.

We have been fortunate in that fairly extensive informal quality assurance procedures have been applied to most of the projects carried out in the Chemical Technology Division in the past. These procedures are now being written and compiled in a systematic form, patterned after the *Quality Assurance Program Requirements, RDT F2-2,* which was written for the Division of Reactor Development and Technology, USAEC. We will maintain formal records for significant projects, thus enabling meaningful audits to be carried out. Of the projects that were already in progress when the Quality Assurance Program was initiated, the LMFBR 37 Assembly Shipping Cask Experiment is the first to be involved with quality assurance procedures. A detailed report on this experiment has been written.

Another project, called Solex 2, was audited to determine the extent to which this project had been subjected to informal quality assurance procedures. The results of this audit were encouraging and have been discussed in a chapter of the forthcoming Safety Analysis Report on the Project.

Other projects that are currently being subjected to more formalized quality assurance procedures include the Continuous Salt Purification Experiment and the Radioactive Waste Repository Project.

18.2 EVALUATION OF THE RADIATION RESISTANCE OF SELECTED PROTECTIVE COATINGS (PAINTS)

Tests to evaluate commercial protective coatings for potential use in various nuclear facilities have been continued. Eighty-seven coating systems (115 specimens of ten different types), supplied by 13 manufacturers, are being tested by exposure to a ^{60}Co source with an intensity of 6×10^5 r/hr at a temperature of 40 to 50°C. Current exposure data on coatings that were gamma irradiated in air and submerged in deionized water are presented in Table 18.1. Tests of these coatings systems will be continued until the systems have failed or until they have received an accumulated exposure of 1×10^{10} rads.

The epoxies, modified phenolics, and phenolics exhibited an average failure level of 1.6×10^9 rads in deionized water, with maxima above 3×10^9 rads; exposures in air show failures at doses ranging from 2×10^9 to 1×10^{10} rads. The polyurethanes, vinyls, and chlorinated rubbers that had been exposed in deionized water had average failures at 1.1×10^9, 4.4×10^8, and 5.2×10^8 rads respectively; the average failure levels of these systems when exposed in air were 3×10^9, 2.9×10^9, and 6.8×10^9 rads respectively.

An American Nuclear Standards Institute standard, ANSI 101.5-1970, "Protective Coatings (Paints) for Light Water Nuclear Reactor Containment Facilities," has been written and is in the process of being approved. The N101.5 subcommittee that produced the standard was comprised of reactor designers, protective coatings manufacturers, USAEC site contractors, architect-engineers, private consultants, and representatives from TVA and one private utility company.

Table 18.1. Gamma Radiation Resistance of Several Protective Coatings

Radiation source: ^{60}Co with an intensity of 6×10^5 r/hr
Temperature: 40 to 50°C

Coating	Type	Manufacturer[a]	Substrate	Exposure[b] in Demineralized Water		Exposure in Air[b]	
				Dose (rads)	Effect[c]	Dose (rads)	Effect[c]
Amercoat No. 90	Modified phenolic	1	Steel	$>5 \times 10^9$		$>5 \times 10^9$	
Amercoat-90/Dimetcote-6	Modified phenolic	1	Steel	$>5 \times 10^9$		$>5 \times 10^9$	
Q-Kote	Phenolic	2	Steel	3.4×10^9	C	$>3.6 \times 10^9$	
	Phenolic		Concrete	3.4×10^9	C,D	2.4×10^9	C,D
Epoxy-Polyamide	Epoxy	2	Steel	$>4.3 \times 10^9$		$>3.6 \times 10^9$	
	Epoxy		Concrete	3.4×10^9	C	$>2.9 \times 10^9$	
Chem-Thane	Urethane	2	Steel	$>4.3 \times 10^9$		$>3.6 \times 10^9$	
	Urethane		Concrete	$>4.3 \times 10^9$		$>2.9 \times 10^9$	
Silicone-Alkyd	Alkyd	2	Steel	1×10^8	B	$>3.6 \times 10^9$	
	Alkyd		Concrete	1×10^8	B	$>2.9 \times 10^9$	
68-139A (Epolon AE-7/Epolon Multi-Mil)	Epoxy	3	Concrete			$>3.3 \times 10^9$	
68-139B (Vinyloid AE-98/Epolon Multi-Mil)	Vinyl	3	Concrete			$>3.3 \times 10^9$	
69-138A (Vinyloid AE-98/Vinyloid and Vinyl Grip)	Vinyl	3	Steel	2.5×10^8	B	2.0×10^9	B,C
69-138B (Vinyloid AE-98/Vinyl Grip)	Vinyl	3	Steel	2.5×10^8	B	2.0×10^9	B,C
68-121A (Epolon/Epolon Primer)	Epoxy[d]	3	Steel	8.0×10^8[e]	B	$>9.5 \times 10^9$	
68-121B (Epolon/Metal Bond Primer)	Epoxy[d]	3	Steel	1.9×10^9[e]	B	$>9.5 \times 10^9$	
Epoxy-Phenolic (Rust-Ban EP6846/EP6841)	Modified phenolic	4	Steel	$>4.5 \times 10^9$		4.59×10^9	C
	Modified phenolic		Concrete	3.3×10^9	B,C		
Epoxy-Polyamide (Rust-Ban EX6671/EX6664)	Epoxy[d]	4	Steel	$>4.5 \times 10^9$		4.59×10^9	C
	Epoxy		Concrete	$>4.0 \times 10^9$		4.1×10^9	A
Epoxy-Polyamide (Rust-Ban EX6671/EX6664 and No. 191)	Epoxy[d]	4	Steel	9.0×10^8	B	$>4.5 \times 10^9$	
No. 1 (Vinyl Y-5280/Y-5296, Y-5295, Y-5290)	Vinyl	5	Steel	7.0×10^8	B	$>1.5 \times 10^9$	
No. 2 (Nu-Pon Y-5240, Y-5242/Glid-Zinc 103)	Epoxy	5	Steel	1.9×10^9	B	$>1.5 \times 10^9$	
No. 3 (Nu-Pon Y-5240, Y-5242/EGL-69722)	Epoxy	5	Steel	$>1.5 \times 10^9$		$>1.5 \times 10^9$	
No. 4 (Nu-Pon Y-5240, Y-5242/Chromate Primer)	Epoxy	5	Steel	$>1.5 \times 10^9$		1.49×10^9	B
No. 5 (Glid-Tile Y-5596/Nu-Pon Cote Y-5240)	Epoxy	5	Steel	3.8×10^8	B	$>1.5 \times 10^9$	
No. 6 (Nu-Pon Y-5240, Y-5242/Nu-Pon Mastic Y-5256)	Epoxy	5	Steel	$>1.5 \times 10^9$		$>1.5 \times 10^9$	
No. 7 (water reducible enamel EGL-68144, -68146/EGL-68145, -68146 primer)	Epoxy	5	Steel	$>1.5 \times 10^9$		1.49×10^9	D
Nos. 2 and 9 [No. 7230, Hi-build (HB) stainless steel flake enamel]	Phenolic	6	Concrete	2.3×10^9[e]	A	9.0×10^9	A
	Phenolic		Steel	4.0×10^8[e]	B	1.0×10^{10}	D
No. 11 (No. 7230/No. 6820 zinc-rich chlorinated rubber primer)	Phenolic	6	Steel	4.0×10^8[e]	B	$>1.0 \times 10^{10}$	
No. 12 (No. 7230/No. 6040 oxidized alkyd primer)	Phenolic	6	Steel	4.0×10^8[e]	B	1.0×10^{10}	A,D
No. 1 (84-F-15/89-F-34, Mobilzinc-7)	Epoxy[d]	7	Steel	1.6×10^9[e]	A,B	$>9.0 \times 10^9$	
No. 3 (78-D-7/Mobilzinc-7; amine cured)	Epoxy	7	Steel	1.6×10^9[e]	A,B	$>9.0 \times 10^9$	
No. 5 (80-F-15/83-F-34, Mobilzinc-7)	Vinyl	7	Steel	3.8×10^8[e]	B	5.0×10^9	C
No. 6 (28-F-15/27-F-34, Mobilzinc-7)	Chlorinated rubber	7	Steel	3.8×10^8[e]	B	$<6.3 \times 10^9$[f]	C,D
No. 7 (84-F-15/89-F-34)	Epoxy[d]	7	1-steel	1.6×10^9[e]	A,C	$>9.0 \times 10^9$	
	Epoxy[d]		2-steel	3.8×10^9	A,B		
No. 9 (28-F-15/27-F-34)	Chlorinated rubber	7	Steel	3.8×10^8[e]	B	$<6.3 \times 10^9$[f]	C,D

Table 18.1 (continued)

Coating	Type	Manufacturer[a]	Substrate	Exposure[b] in Demineralized Water		Exposure in Air[b]	
				Dose (rads)	Effect[c]	Dose (rads)	Effect[c]
No. 11 (80-F-15/83-F-34)	Vinyl	7	Steel	1.1×10^{8}[e]	B	5.0×10^{9}	C
No. 15 (78-D-7, amine cured)	Epoxy	7	1-steel	1.6×10^{9}[e]	A,C	$>9.0 \times 10^{9}$	
	Epoxy		2-steel	1.2×10^{9}	B,C		
No. 17 (Val-Chem/89-F-34)	Polyurethane	7	Steel	7.8×10^{9}	C	$>9.0 \times 10^{9}$	
No. 19 (84-F-15/89-F-34)	Epoxy[d]	7	1-concrete	3.8×10^{8}[e]	B	$>9.0 \times 10^{9}$	
	Epoxy		2-concrete	2.0×10^{9}	A,B		
No. 19-1 (84-F-15/89-F-34 and latex filler)	Epoxy[d]	7	1-concrete	1.1×10^{8}[e]	B	1.9×10^{9}[c]	C,D
	Epoxy[d]		2-concrete	1.7×10^{9}	B		
No. 20 (28-F-15/27-F-34)	Chlorinated rubber	7	1-concrete	3.8×10^{8}[e]	B	7.8×10^{9}	C,D
	Chlorinated rubber		2-concrete	9.5×10^{8}	B		
No. 21 (80-F-15/83-F-34)	Vinyl	7	1-concrete	3.8×10^{8}[e]	B	2.0×10^{9}	B,C
	Vinyl		2-concrete	2.0×10^{9}	B,C		
No. 23 (78-D-7, amine cured)	Epoxy	7	1-concrete	5.9×10^{8}[e]	B	$>9.0 \times 10^{9}$	
	Epoxy		2-concrete	1.2×10^{9}	B		
No. 24 (Val-Chem/89-F-34)	Polyurethane	7	1-concrete	3.1×10^{8}[e]	B	$>9.0 \times 10^{9}$	
	Polyurethane		2-concrete	$>8 \times 10^{8}$			
No. 25 (LM-115, "water dispersed")	Epoxy	7	Concrete	3.4×10^{8}	B	$>4.5 \times 10^{9}$	
No. 26 (78-W-102)	Modified phenolic	7	Steel	1.2×10^{9}	B,C		
	Modified phenolic		Concrete	$>8 \times 10^{8}$			
No. 27 (LM-809, w/fiberglas cloth backing)	Epoxy	7	Concrete	$>8 \times 10^{8}$			
N-1-S (No. 5671 thixopoxy)	Epoxy	8	Steel[g]	1.0×10^{9}[e]	B	$>7.5 \times 10^{9}$	
N-1 (No. 5671 thixopoxy)	Epoxy	8	Steel[h]	1.0×10^{9}[e]	A,B	$>7.5 \times 10^{9}$	
N-1-C (No. 5671 thixopoxy)	Epoxy	8	Concrete	1.3×10^{9}[e]	A,B,C	$>7.5 \times 10^{9}$	
N-2-C (No. 5697, polyamid epoxy)	Epoxy[d]	8	Concrete	4.6×10^{9}	C	$>7.5 \times 10^{9}$	
N-3-S (Nos. 5673 and 5627)	Epoxy	8	Steel[g]	1.0×10^{9}[e]	A,B,C	$>7.5 \times 10^{9}$	
N-3 (Nos. 5673 and 5627)	Epoxy	8	Steel[h]	1.0×10^{9}[e]	A,B,C	$>7.5 \times 10^{9}$	
N-4-S (No. 1371, "4Z")	Inorganic	8	Steel[g]	1.0×10^{9}[e]	E	$>7.5 \times 10^{9}$	
N-5-S (No. 5627/5673/1371)	Epoxy	8	Steel[g]	1.0×10^{9}[e]	B	$>7.5 \times 10^{9}$	
N-6-S (No. 1357, "5Z")	Inorganic	8	Steel[g]	$>7.5 \times 10^{9}$		$>7.5 \times 10^{9}$	
N-6 (No. 1357, "5Z")	Inorganic	8	Steel[h]	$>7.5 \times 10^{9}$		$>7.5 \times 10^{9}$	
N-7-S (No. 5697/1357, "5Z")	Epoxy[d]	8	Steel[g]	$>7.5 \times 10^{9}$		$>7.5 \times 10^{9}$	
N-7 (No. 5697/1357, "5Z")	Epoxy[d]	8	Steel[h]	1.0×10^{9}[e]	A,B,C	$>7.5 \times 10^{9}$	
N-8-S (No. 5627/5673 and 1357 "5Z")	Epoxy	8	Steel[g]	1.0×10^{9}[e]	A,C	4.6×10^{9}	C
N-8 (No. 5627/5673 and 1357 "5Z").	Epoxy	8	Steel[g]	1.0×10^{9}[e]	B	4.6×10^{9}	C
Series-1 (DD-82/DD-82 primer)	Polyurethane	9	Steel	1.0×10^{8}	B	2.8×10^{9}	A
	Polyurethane		Concrete	$>8.0 \times 10^{8}$			
Series-2 (DD-82/DD-81 primer)	Polyurethane	9	Steel	1.0×10^{8}	A,B	2.8×10^{9}	A
	Polyurethane		1-concrete	1.0×10^{8}	A,B		
	Polyurethane		2-concrete	$>8 \times 10^{8}$			
Series-3 (100% solids epoxy)	Epoxy	9	Steel	2.7×10^{9}	C	2.8×10^{9}	A
	Epoxy		Concrete	1.0×10^{8}	A,D		
Series-4 (DD82/HB epoxy primer)	Polyurethane	9	Steel	1.0×10^{8}	B	2.8×10^{9}	A
	Polyurethane		Concrete	6.0×10^{8}	B		
System-1 (No. 545 and 520/545 primer)	Epoxy	9	Steel	1.4×10^{9}	A	$>5.0 \times 10^{9}$	
	Epoxy		Concrete	4.3×10^{9}	B	$>5.0 \times 10^{9}$	

Table 18.1 (continued)

Coating	Type	Manufacturer[a]	Substrate	Exposure[b] in Demineralized Water		Exposure in Air[b]	
				Dose (rads)	Effect[c]	Dose (rads)	Effect[c]
System-2 (HSA/P-62 primer)	Vinyl	9	Steel	1.0×10^8	B	4.6×10^9	A,C
	Vinyl		Concrete			1.4×10^9	C
System-3 (HSA and A-series/P-62 primer)	Vinyl	9	Steel	1.0×10^8	B	2.0×10^9	A,C
	Vinyl		Concrete			2.0×10^9	A,C
System-4 (Epoxy-polyester/No. 545 epoxy primer)	Epoxy-polyester	9	Steel	2.0×10^8	B	9.6×10^8	B
	Epoxy-polyester		Concrete	$>4 \times 10^9$		1.7×10^9	A,B
System-5 (styrene copolymer/P-50, alkyd-phenolic)	Styrene-copolymer	9	Steel	2.0×10^8	B	$>4.6 \times 10^9$	
	Styrene-copolymer		Concrete	1.0×10^8	A,D	1.7×10^9	C,D
System-6 (Zp-200)	Inorganic	9	Steel			3.8×10^9	C,D
	Inorganic		Concrete	$>4 \times 10^9$		3.8×10^9	C,D
System-7 (No. 520/Epoxy Primastic and ZP-200	Epoxy	9	Steel	2.0×10^8	B	$>4.6 \times 10^9$	
	Epoxy		Concrete	6.0×10^8	B		
ME-1022 (Kem Cati-Coat Enamel and Primer)	Epoxy	10	Steel	$>6.5 \times 10^9$		$>6.5 \times 10^9$	
ME-1023 (Rexthane Enamel/Kem Cati-Coat Primer)	Polyurethane	10	Steel	$>6.5 \times 10^9$		$>6.5 \times 10^9$	
ME-1024 (Kem Cati-Coat Enamel/Zinc Clad-7)	Epoxy	10	Steel	8.0×10^8[e]	B	7.0×10^9	D
ME-1025 (Rexthane Enamel/Zinc Clad-7)	Polyurethane	10	Steel	3.0×10^8[e]	B	$>6.5 \times 10^9$	
ME-1026 (Rexthane Enamel/latex-cement filler)	Polyurethane	10	Concrete	5.0×10^8[e]	B	$>6.5 \times 10^9$	
ME-1027 (Rexthane Enamel/B44 VA21 Conditioner)	Polyurethane	10	Concrete	5.0×10^8[e]	D	3.5×10^9	C,D
X-430 A(Capox EP System)	Modified phenolic	11	Steel	1.2×10^9	A	$>8.5 \times 10^9$	
X-430 B (Capox A HB System)	Epoxy	11	Steel	1.5×10^9	B	$>8.5 \times 10^9$	
X-430 D (Capox EP inorganic zinc system)	Modified phenolic	11	Steel	1.2×10^9	A	$>8.5 \times 10^9$	
X-430 F (Capox A HB system w/fiberglas)	Epoxy	11	Concrete	1.2×10^9	B	$>8.5 \times 10^9$	
System-1 (No. 92 Tnemec Zinc)	Inorganic	12	Steel	3.0×10^8	E	$>7.0 \times 10^9$	
System-2 (HB Epoxoline)	Epoxy[d]	12	Concrete	2.1×10^9	B	$>7.0 \times 10^9$	
System-3 (HB Epoxy/No. 92 Zinc)	Epoxy[d]	12	Steel	3.0×10^8	B	$>7.0 \times 10^9$	
System-4 (HB Epoxy/HB Epoxy Primer)	Epoxy[d]	12	Steel	$>7.0 \times 10^9$		$>7.0 \times 10^9$	
System-5 (Vinoline/33-1211 Primer)	Vinyl	12	Steel	1.0×10^8	B	2.9×10^9	B,C,E
System-1A (No. 368 urethane/67-1241 epoxy)	Polyurethane	12	Concrete	1.8×10^9	B	$>7.0 \times 10^9$	
System-2B (Vinoline/zinc primer)	Vinyl	12	Steel	1.0×10^8	B	2.9×10^9	A,C
Plasite (1120/1100, water-base zinc system)	Inorganic	13	Steel	$>1.0 \times 10^{10}$		$>1.0 \times 10^{10}$	
Plasite (9009/1100 system)	Epoxy	13	Steel	1.9×10^9	B	9.7×10^9	C

[a]Manufacturer: (1) Amercoat Corp.; (2) Chemline Div., Dixie Paint and Varnish Co., Inc.; (3) Con-Lux Paint Products, Inc.; (4) Enjay Chemical Co.; (5) Glidden-Durkee Div. of SCM Corp.; (6) Keeler and Long, Inc.; (7) Mobil Chemical Co.; (8) NAPCO, Inc.; (9) Prufcoat Div., Grow Chem. Coatings Corp.; (10) Sherwin-Williams Co., Inc.; (11) Subox Division, Wyandotte Chemical Corp.; (12) TNEMEC Co.; (13) Wisconsin Protective Coatings Co.

[b]The coatings were inspected for radiation damage at various exposure levels: ($\sim 1 \times 10^8$, 3×10^8, 5×10^8, and each additional 5×10^8 rads exposure thereafter). The values listed represent the cumulative dose that had been received at the time adverse effects were observed. If no effects are entered, the exposure test is continuing.

[c]Radiation effects: A, chalked; B, blistered; C, embrittled; D, loss of adhesion; E, "sweating."

[d]Polyamide-cured epoxy.

[e]Previously reported in ORNL-4422.

[f]Earlier failure not detected. Appearance indicates that resistance is less than that given.

[g]Sandblasted steel.

[h]Pickled steel.

19. Nuclear-Powered Agro-Industrial Complexes: Special Studies

Work by the Chemical Technology Division on studies of Nuclear-Powered Agro-Industrial Complexes has been described in detail in monthly reports issued by the Nuclear Desalination Program and also by separate ORNL reports on aquaculture and nutrition economics, which are to be published;[1,2] consequently, only an abstract appears in this report (see the Summary).

[1] W. C. Yee, *Potential of Aquaculture at Nuclear Energy Centers*, ORNL-4488 (to be published).

[2] W. C. Yee, *Nutrition Economics for Desalination Agriculture*, ORNL-4489 (to be published).

Publications, Speeches, and Seminars

BIOCHEMICAL TECHNOLOGY

Burtis, C. A.,[1] G. Goldstein,[2] and C. D. Scott, "Fractionation of Human Urine by Gel Chromatography," *Clin. Chem.* **16**, 201 (1970).

Butts, W. C., and C. D. Scott, "Gas Chromatographic Identification of Urinary Carbohydrates Isolated by Anion Exchange Chromatography," presented at the 2nd Annual Symposium on Automated, High-Resolution Analyses in the Clinical Laboratory, ORNL, Mar. 12–13, 1970.

Egan, B. Z., J. E. Caton,[2] and A. D. Kelmers, "Separation of *E. coli* Ribosomal RNAs and Mammalian RNAs by Reversed-Phase Chromatography," presented at the 54th Annual Meeting of the Federation of American Societies for Experimental Biology, Atlantic City, N.J., Apr. 13–17, 1970.

Hancher, C. W., "A Simple 50-Bottle Fraction Collector for Volumes up to 350 Liters," *Biotechnol. Bioeng.* **XI**, 1033 (1969).

Hancher, C. W., "Recovery of Crude Mixed tRNAs," presented at the Industrial Conference on Production Methods for Purified Transfer Ribonucleic Acids, Oak Ridge, Tenn., May 11–12, 1970.

Hancher, C. W., E. F. Phares,[3] G. D. Novelli,[3] and A. D. Kelmers, "Large Scale Production of Transfer Ribonucleic Acids from *E. coli* K-12 M07," *Biotechnol. Bioeng.* **XI**, 1055–70 (1969).

Jolley, R. L., "Interesting Experimental Results from High-Resolution Analyses of Body Fluids," presented at the 22nd National Meeting of the American Association of Clinical Chemists, Buffalo, N.Y., July 1970.

Jolley, R. L., W. W. Pitt, Jr., and C. D. Scott, "Nonpulsing Reagent Metering for Continuous Colorimetric Detection Systems," *Anal. Biochem.* **28**, 300 (1969).

Jolley, R. L., and C. D. Scott, "Preliminary Results from High-Resolution Analyses of UV-Absorbing and Carbohydrate Constituents in Normal and Pathological Body Fluids," presented at the Southeast Section of the American Association for Clinical Chemists, Nashville, Tenn., Nov. 14–15, 1969.

Jolley, R. L., and C. D. Scott, "Preliminary Results from High-Resolution Analyses of UV-Absorbing and Carbohydrate Constituents in Several Pathological Body Fluids," presented at the 2nd Annual Symposium on Automated, High-Resolution Analyses in the Clinical Laboratory, ORNL, Mar. 12–13, 1970.

Jolley, R. L., and C. D. Scott, "Use of Normalization Techniques for Establishing Elution Positions of Chromatographic Peaks," *J. Chromatog.* **47**, 2772 (1970).

Kelmers, A. D., "Separations Technology," presented at the 5th Annual Conference on Engineering at ORNL, ORAU Library, Apr. 7, 1970.

Kelmers, A. D., "Product Distribution and Shipping Procedures," presented at the Industrial Conference on Production Methods for Purified Transfer Ribonucleic Acids, Oak Ridge, Tenn., May 11–12, 1970.

---

[1] Present address: Varian Aerograph, Walnut Creek, Calif.

[2] Analytical Chemistry Division.

[3] Biology Division.

Kelmers, A. D., and M. P. Stulberg,[3] "Purified Transfer RNAs Available" (Letter to the Editor), *Science* **167**, 238 (1970).

Mrochek, J. E., "Techniques for Fractionation of Low Molecular Weight Constituents of Physiologic Body Fluids," presented at the 5th Annual Conference on Engineering at ORNL, ORAU Library, Apr. 7, 1970.

Mrochek, J. E., R. L. Jolley, and C. D. Scott, "Recent Developments in High-Resolution Analyses of Body Fluids," presented at the Spring Meeting of the Southeast Section of the American Association of Clinical Chemists, Emory School of Medicine, Atlanta, Ga., Apr. 3–4, 1970.

Phares, E. F.,[3] and C. W. Hancher, "Automation of Semi-Continuous Fermentation," presented at the Industrial Conference on Production Methods for Purified Transfer Ribonucleic Acids, Oak Ridge, Tenn., May 11–12, 1970.

Pitt, W. W., W. F. Johnson,[4] and C. D. Scott, *Operation Manual for the UV-Analyzer, Prototype Mark II,* ORNL-TM-2593 (August 1969).

Pitt, W. W., Jr., and C. D. Scott,, "Computer Solution of a Multichambered Gradient Device with Non-Equal Chamber Cross-Sectional Areas and Variable Fluid Properties," *Anal. Biochem.* **30**, 58 (1969).

Pitt, W. W., Jr., C. D. Scott, and W. F. Johnson,[4] "A Bench Top, Automated, High-Resolution Analyzer for UV-Absorbing Constituents of Body Fluids," presented at the 2nd Annual Symposium on Automated, High-Resolution Analyses in the Clinical Laboratory, ORNL, Mar. 12–13, 1970.

Ryon, A. D., "Discussion of Flowsheets, Recoveries, and Costs," presented at the Industrial Conference on Production Methods for Purified Transfer Ribonucleic Acids, Oak Ridge, Tenn., May 11–12, 1970.

Ryon, A. D., C. W. Hancher, H. O. Weeren, and E. F. Phares,[3] *Demonstration of the Reliability and Reproducibility of Large-Scale Production of Purified tRNAs from* E. coli *K-12 MO,* ORNL-TM-2904 (April 1970).

Scott, C. D., "Automated, High-Resolution Analysis of Body Fluids by High-Pressure Anion Exchange Chromatography," presented at the 19th Annual Symposium on Recent Developments in Research Methods and Instrumentation, NIH, Bethesda, Md., Oct. 6–9, 1969.

Scott, C. D., "A Chemical Profile of Man. Development of High-Resolution Analytical Systems for Body Fluids," presented to the Department of Biochemistry, State University of New York at Buffalo, Jan. 6, 1970.

Scott, C. D., "A Chemical Profile of Man. Development of High-Resolution Analytical Systems for Body Fluids," presented to the Northeast Section of the American Chemical Society, Boston, Mass., Jan. 8, 1970.

Scott, C. D., "A Chemical Profile of Man. Development of High Resolution Analytical Systems for Body Fluids," presented to the Department of Chemical Engineering, University of Tennessee, Knoxville, Jan. 19, 1970.

Scott, C. D., "A Chemical Profile of Man. Development of High Resolution Analytical Systems for Body Fluids," presented to the Department of Biochemistry and the Child Development Center of the University of Tennessee Medical Unit, Memphis, Tenn., Jan. 20, 1970.

Scott, C. D., "High-Pressure Ion Exchange Chromatography as Applied to Body Fluids Analyses," presented at the 1970 Pittsburgh Conference on Analytical Chemistry and Applied Spectroscopy, Cleveland, Ohio, Mar. 1–6, 1970.

Scott, C. D., D. D. Chilcote, and W. W. Pitt, Jr., "A Method for Stripping Interfering Peaks from Chromatographic Data by an On-Line Computer with Limited Storage Capability," presented at the 2nd Annual Symposium on Automated, High-Resolution Analyses in the Clinical Laboratory, ORNL, Mar. 12–13, 1970.

Scott, C. D., W. F. Johnson,[4] and V. E. Walker,[5] "A Sample Injection Valve for Use in High-Pressure Liquid Chromatography," *Anal. Biochem.* **32**, 182 (1969).

Scott, C. D., and N. E. Lee, "Dynamic Packing of Ion Exchange Chromatographic Columns," *J. Chromatog.* **42**, 263 (1969).

---

[4] Instrumentation and Controls Division.

[5] Plant and Equipment Division.

Scott, C. D., W. W. Pitt, Jr., W. F. Johnson,[4] and L. H. Thacker,[4] "A Small, Automated, High-Resolution Analyzer for Quantifying the UV-Absorbing Constituents of Body Fluids," presented at the 21st National Meeting of the American Association of Clinical Chemists in Denver, Colo., Aug. 17–22, 1969.

Thacker, L. H.,[4] C. D. Scott, and W. W. Pitt, Jr., "Miniature Photometers for Liquid Chromatography," presented at the 2nd Annual Symposium on Automated, High-Resolution Analyses in the Clinical Laboratory, ORNL, Mar. 12–13, 1970.

Warren, K. S., and C. D. Scott, "Interfering Ultraviolet-Absorbing Compounds as Sources of Error in Common Clinical Chemistry Tests," *Clin. Chem.* **15**(12), 1147–56 (1969).

Weeren, H. O., "Preparatory Scale Reversed-Phase Chromatography," presented at the Industrial Conference on Production Methods for Purified Transfer Ribonucleic Acids, Oak Ridge, Tenn., May 11–12, 1970.

Wymer, R. G., "Bioengineering: The Application of Chemical Engineering Operations to the Separation of Biological Macromolecules," presented at Lowell Technological Institute, Lowell, Mass., Apr. 24, 1970.

CHEMICAL ENGINEERING RESEARCH

Long, J. T., *Rational Development of Solvent-Extraction Separations Processes,* ORNL-TM-601 (May 1969).

Whatley, M. E., "Solvent Extraction Applications in the Nuclear Industry," presented at a Symposium on Liquid-Liquid Extraction, sponsored by the Cincinnati Section of the American Chemical Society, Cincinnati, Ohio, Mar. 25, 1970.

CHEMICAL PROCESSING FOR MOLTEN-SALT BREEDER REACTORS

Bell, M. J., *Calculated Radioactivity of MSRE Fuel Salt,* ORNL-TM-2970 (May 1970).

Chandler, J. M., and R. B. Lindauer, "Preparation and Processing of MSRE Fuel," presented at the 1969 Nuclear Metallurgy Symposium, "Reprocessing of Nuclear Fuels," Ames Laboratory, Ames, Iowa, Aug. 25, 1969.

Ferris, L. M., J. C. Mailen, J. J. Lawrance,[6] F. J. Smith, and E. D. Nogueira,[7] "Chemistry Relating to a Reductive-Extraction Process for MSBR Fuels," presented at the 15th American Nuclear Society Meeting, Seattle, Wash., June 15–19, 1969; published in *Trans. Am. Nucl. Soc.* **12**(1), 26–27 (1969).

Lindauer, R. B., *Processing of the MSRE Flush and Fuel Salts,* ORNL-TM-2578 (August 1969).

Mailen, J. C., L. M. Ferris, and E. D. Nogueira,[7] "Estimate of the Solubility of Protactinium in Liquid Bismuth," *Inorg. Nucl. Chem. Letters* **5**, 869–72 (1969).

Schilling, C. E., and L. M. Ferris, "The Solubility of Thorium in Liquid Bismuth," *J. Less-Common Metals* **20**, 155 (1970).

Smith, F. J., L. M. Ferris, and C. T. Thompson, *Liquid-Vapor Equilibria in LiF-BeF_2 and LiF-BeF_2-ThF_4 Systems,* ORNL-4415 (June 1969).

Whatley, M. E., "Reductive Extraction Separation Processes for Molten Salt Reactors," presented at the Third Joint Puerto Rico AIChE/IIQPR Meeting, sponsored by the American Institute of Chemical Engineers, New York City, May 20, 1970.

Whatley, M. E., L. E. McNeese, W. L. Carter, L. M. Ferris, and E. L. Nicholson, "Engineering Development of the MSBR Fuel Cycle," presented at the 1969 Nuclear Metallurgy Symposium, "Reprocessing of Nuclear Fuels," Ames Laboratory, Ames, Iowa, Aug. 25, 1969.

Whatley, M. E., L. E. McNeese, W. L. Carter, L. M. Ferris, and E. L. Nicholson, "Engineering Development of the MSBR Fuel Recycle," *Nucl. Appl. Technol.* **8**(2), 170 (1969).

---

[6] Australian Atomic Energy Commission, Lucas Heights, Sydney, Australia.

[7] Junta de Energia Nuclear, Madrid, Spain.

MISCELLANEOUS

Arnold, W. D., and D. J. Crouse, "Radioactive Contamination of Oil Produced from Nuclear-Broken Shale," presented at the Fourth Plowshare Symposium, Las Vegas, Nev., Jan. 14–16, 1970.

Bell, J. T., "High Temperature Spectroscopy of Aqueous Solutions," presented in a seminar series at Murray State University, Murray, Ky., Mar. 6, 1970.

Bell, J. T., "High Temperature Spectroscopy of Aqueous Solutions," presented in a seminar series at Memphis State University, Memphis, Tenn., May 1, 1970.

Bell, J. T., R. E. Biggers,[8] T. G. Rogers,[9] and A. M. Rom, "A Dilatometer Method for the Precision Measurement of the Densities of Liquids to 400°C and 5000 psi," *Rev. Sci. Instr.* **40**(8), 985–91 (1969).

Bell, J. T., D. M. Helton, and T. G. Rogers,[9] "Densities of Aqueous KCl and UO_2SO_4 from 25° to 374°C," *J. Chem. Engr. Data* **15**(1), 44–46 (1970).

Bell, J. T., C. C. Thompson,[10] and D. M. Helton, "The High Temperature Spectra of Aqueous Transition Metal Salts. Part I. Praseodymium and Neodymium Nitrate to 356°C," *J. Phys. Chem.* **73**, 3338–45 (1969).

Bell, M. J., *Heavy Element Composition of Spent Power Reactor Fuels,* ORNL-TM-2897 (May 1970).

Bell, M. J., and J. P. Nichols, "Penetrating Radiation Dose Rates and Shield Requirements in Fabrication of Fuels Containing ^{233}U and High Exposure Plutonium," presented at the Sol-Gel Processes and Reactor Fuel Cycles Symposium, Gatlinburg, Tenn., May 4–7, 1970; published in the *Proceedings.*

Brooksbank, R. E., "Licensing of Reprocessing Plant Operators," presented at the Fifteenth Annual Meeting of the American Nuclear Society, Seattle, Wash., June 15–19, 1969.

Brooksbank, R. E., and W. H. Carr, *Material Form for Maximum Safety in the Shipping of Alpha-Emitting Materials,* ORNL-4554 (April 1970).

Brooksbank, R. E., D. J. Skovholt,[11] and W. H. Lewis,[12] *Licensing of Reprocessing Plant Operators,* ORNL-TM-2573 (June 1969).

Campbell, D. O., "Isotopic Enrichment of the Product of a Lanthanide Neutron Capture Reaction," presented at the 8th Rare Earth Research Conference, Reno, Nev., Apr. 19–22, 1970.

Campbell, D. O., "Isotopic Enrichment of Neutron Capture Product by Elution from a Faujasite Zeolite," *Inorg. Nucl. Chem. Letters* **6**, 103 (1970).

Crouse, D. J., W. D. Arnold, and F. J. Hurst, "Radioactive Contamination of Copper Produced Using Nuclear Explosives," presented at the Fourth Plowshare Symposium, Las Vegas, Nev., Jan. 14–16, 1970.

Goeller, H. E., "Energy Intensive Industry," presented at the Atlanta National Meeting of the American Institute of Chemical Engineers, Feb. 13–18, 1970.

Joy, D. S., *A Dynamic Programming Solution of the Electric Generating System Unit Commitment Problem,* ORNL-TM-2881 (April 1970).

Joy, D. S., *et al.,* "Methods of Planning Generating Unit Operation," in the *Proceedings of the American Power Conference, Chicago, Illinois, April 21, 1970* (May 1970).

Klima, B. B., *Analysis of the Oak Ridge National Laboratory Garden Carrier No. 2,* ORNL-TM-2531 (September 1969).

Klima, B. B., *DOT Specification 7A Container Designed for Use by Chemical Technology Division,* ORNL-TM-2731 (November 1969).

---

[8] Coca-Cola Research Laboratory, Atlanta, Ga.

[9] Department of Chemistry, University of California, Riverside.

[10] Department of Chemistry, Memphis State University.

[11] Atomic Energy Commission.

[12] Nuclear Fuel Services, Inc.

Klima, B. B., *DOT Specification 6M Shipping Container for Use by Chemical Technology Division,* ORNL-TM-2784 (February 1970).

Klima, B. B., and E. L. Youngblood, "Poor Man's Model," presented at the American Engineering Model Society Meeting, New York City, June 6–8, 1969.

Landry, J. W., "Constructive Nuclear Explosions for Industry and Science," presented to exhibit managers of This Atomic World, Oak Ridge Associated Universities, Oak Ridge, Tenn., Aug. 7, 1969.

Mrochek, J. E., J. M. Holmes, and W. C. Yee, "The Role of Electricity-Intensive Industries on the Economics of Nuclear Power," presented at the Symposium on Nuclear Energy Costs and Economic Development, Istanbul, Turkey, October 20–24, 1969.

Parrott, J. R., J. P. Nichols, and R. G. Nicol, "Operating Experience in a Facility Utilizing Soluble Neutron Absorbers for Storage of Fissile Solution," presented at the 1969 Winter Meeting of the American Nuclear Society, San Francisco, Calif., Nov. 30–Dec. 4, 1969; published in *Trans. Am. Nucl. Soc.* **12**(2), 450 (1969).

Salmon, Royes, *A Revision of Computer Code POWERCO (Cost of Electricity Produced By Nuclear Power Stations) to Include Breakdowns of Power Cost and Fixed Charge Rates,* ORNL-4116 (August 1969).

Sears, M. B., *Rates of Gas Evolution from the Reactions of Uranium Nitride and Carbonitrides with Nitric Acid,* ORNL-4505 (February 1970).

Sears, M. B., and L. M. Ferris, *Rates of Gas Evolution from the Reactions of Uranium and Thorium Carbides with Aqueous Solutions of HCl, H_2SO_4, NaOH, and NH_4F,* ORNL-4381 (June 1969).

Sears, M. B., and L. M. Ferris, "Studies on the U-C Constitutional Diagram Between UC and UC_2," *J. Nucl. Mater.* **32**, 101–12 (1969).

Thomas, I. L., "The Protonic Structure of Methane, Ammonia, Water, and Hydrogen Fluoride," *Chem. Phys. Letters* **3**, 705 (1969).

Thomas, I. L., "The Protonic Structure of Molecules. I. The Ammonia Molecule," *Phys. Rev.* **185**, 90 (1969).

Thomas, I. L., "The Protonic Structure of Molecules," presented at: Villanova University, Villanova, Pa., Sept. 30, 1969; Argonne National Laboratory, Argonne, Ill., Oct. 21, 1969; University of South Florida, Tampa, Nov. 24, 1969; Instituto Technologico y De Estudios Superiores De Monterrey, Monterrey, N.L., Mexico, Apr. 2, 1970.

Watson, C. D., H. B. Graham, *et al.,* "American National Standard Protective Coatings (Paints) for Light Water Nuclear Reactor Containment Facilities," proposed ANSI N101.5-1970 standard (April 1970).

Yee, W. C., "Seawater Utilization in an Energy Center," presented at the 67th National Meeting of the American Institute of Chemical Engineers, and the Biennial Materials Sciences and Engineering Division Conference, Atlanta, Ga., Feb. 15–18, 1970.

Yee, W. C., "Economic Assessment of Littoral Interactions at Energy Centers," presented (as part of the course on "Special Studies in Systems Engineering") at the Massachusetts Institute of Technology, Cambridge, Mass., Mar. 5, 1970.

Yee, W. C., "Aquaculture Economics Using Shrimp as a Model," presented at the Conference on Beneficial Uses of Waste Heat, ORNL, Oak Ridge, Tenn., Apr. 20–21, 1970.

Yee, W. C., "Nutrition Economics for Nuplexes," presented to the Nutritionists and Economists of Vanderbilt University, Nashville, Tenn., May 8, 1970.

Yee, W. C., "Nuclear Energy Centers and Food Production Potential," presented at the Symposium on Chemistry and the World Food Problem (a joint meeting of the American Chemical Society and the Chemical Institute of Canada), Toronto, Canada, May 24–29, 1970.

Yee, W. C., and J. E. Mrochek, "Industrial Complexes Based on Nuclear Desalting Waste Brines," presented at the Symposium on Nuclear Energy Costs and Economic Development, Istanbul, Turkey, Oct. 20–24, 1969.

POWER REACTOR FUEL PROCESSING

Crouse, D. J., J. M. Schmitt, and F. G. Seeley, "Scrubbing of Iodine and Organic Iodides from Gas Streams," presented at the National American Chemical Society Meeting, New York City, Sept. 7–12, 1969.

Davis, Wallace, Jr., *Thermal Reactions of Iodine with Olefins, and Radiation-Induced Reactions with Paraffins. A Brief Literature Survey Pertinent to LMFBR Fuel Processing,* ORNL-TM-2772 (December 1969).

Ferris, L. M., "Head-End Processes for Graphite-Base and Carbide Reactor Fuels," pp. 121–70 in vol. 4 of *Progress in Nuclear Energy,* series III, ed. by C. E. Stevenson, A. T. Gresky, and E. A. Mason, Pergamon, Oxford, 1970.

Finney, B. C., B. A. Hannaford, G. A. West, and C. D. Watson, *Shear-Leach Process: Semicontinuous and Batch Leaching of Sheared, Unirradiated Stainless-Steel-Clad and Zircaloy-2-Clad* UO_2 *and* UO_2-ThO_2, ORNL-3984 (July 1969).

Goode, J. H., and V. C. A. Vaughen, *ORNL Experiments on the Behavior of Tritium During Head-End Processing of Irradiated Reactor Fuels,* ORNL-TM-2793 (February 1970).

Harrington, F. E., R. W. Horton, R. B. Pratt, and J. D. Sease, *Cost Study of Four Alternate Routes for LMFBR Fuel Material Preparation and Element Fabrication,* ORNL-TM-2813 (February 1970).

Mann, S., and A. R. Irvine, *A Study of Plutonium Polymer Formation and Precipitation as Applied to LMFBR Fuel Processing,* ORNL-TM-2806 (December 1969).

Rollins, J. D., and R. E. Best,[13] "Neutron Shielding Problems Associated with the Shipment of High-Burnup LWR Fuel," *Trans. Am. Nucl. Soc.* **12**(2), 970 (1969).

Rollins, J. D., and J. L. Ridihalgh,[13] "Evaluation of the Criticality Problem in Irradiated Fuel Shipment," *Trans. Am. Nucl. Soc.* **12**(2), 892 (1969).

Shappert, L. B., "Irradiated Fuel Shipping Today and Tomorrow," presented at the 15th Annual Meeting of the American Nuclear Society, Seattle, Wash., June 15–19, 1969.

Shappert, L. B., "Transporting Radioactive Material," *ORNL Review* (Summer 1969).

Shappert, L. B., "Containers for Shipment of Radioactive Material," presented at the University of Virginia, Charlottesville, Oct. 26–28, 1969; published in the *Proceedings,* CONF-UVA-TRM-01 (1970).

Shappert, L. B., *et al., Cask Designers Guide: A Guide to the Design, Fabrication, and Operation of Shipping Casks for Nuclear Application,* ORNL-NSIC-68 (February 1970).

Unger, W. E., R. E. Blanco, A. R. Irvine, D. J. Crouse, and C. D. Watson, "Application of Aqueous Reprocessing to Liquid Metal Fast Breeder Reactor Fuel," presented at the 1969 Nuclear Metallurgy Symposium, Ames Laboratory, Iowa State University, Ames, Iowa, Aug. 25, 1969; to be published in the *Proceedings.*

Vaughen, V. C. A., J. P. Flanary, J. H. Goode, and H. O. G. Witte,[14] *Hot-Cell Evaluation of the Burn-Leach Method for Reprocessing Irradiated Graphite-Base HTGR Fuels,* ORNL-4120 (February 1970).

PROGRESS REPORTS

Arnold, W. D., and D. J. Crouse, *Chemical Applications of Nuclear Explosions (CANE): Progress Report for April 1 to June 30, 1969,* ORNL-TM-2689 (Aug. 25, 1969).

Arnold, W. D., and D. J. Crouse, *Chemical Applications of Nuclear Explosions (CANE): Progress Report for July 1 to September 30, 1969,* ORNL-TM-2756 (Oct. 30, 1969).

Arnold, W. D., and D. J. Crouse, *Chemical Applications of Nuclear Explosions (CANE): Progress Report for October 1 to December 31, 1969,* ORNL-TM-2888 (Feb. 27, 1970).

Burch, W. D., J. E. Bigelow, and L. J. King, *Transuranium Processing Plant Semiannual Report of Production, Status, and Plans for Period Ending December 31, 1968,* ORNL-4428 (November 1969).

[13] Battelle Memorial Institute, Columbus, Ohio.

[14] Present address: KFA-heisse Zellen, Juelich, Germany.

Burch, W. D., J. E. Bigelow, and L. J. King, *Transuranium Processing Plant Semiannual Report of Production, Status, and Plans for Period Ending June 30, 1969,* ORNL-4447 (March 1970).

Ferguson, D. E., and staff, *Chemical Technology Division Annual Progress Report for Period Ending May 31, 1969,* ORNL-4422 (October 1969).

Scott, C. D., and Sidney Katz, *Body Fluids Analyses Program Progress Report for the Period September 1, 1968 to February 28, 1969,* ORNL-TM-2551 (July 1969).

Scott, C. D., *Body Fluids Analyses Program Progress Report for the Period March 1 to August 31, 1969,* ORNL-TM-2779 (December 1969).

Staffs of the Chemical Technology and Metals and Ceramics Divisions, *Thorium Fuel Cycle Development Progress Report, September 1969, No. 2,* ORNL-TM-2705 (September 1969).

Staffs of the Chemical Technology and Metals and Ceramics Divisions, *Thorium Fuel Cycle Development Progress Report, October 1969, No. 3,* ORNL-TM-2739 (October 1969).

Staffs of the Chemical Technology and Metals and Ceramics Divisions, *Thorium Fuel Cycle Development Progress Report, November 1969, No. 4,* ORNL-TM-2765 (November 1969).

Staffs of the Chemical Technology and Metals and Ceramics Divisions, *Thorium Fuel Cycle Development Progress Report, December 1969, No. 5,* ORNL-TM-2792 (January 1970).

Staffs of the Chemical Technology and Metals and Ceramics Divisions, *Thorium Fuel Cycle Development Progress Report, January 1970, No. 6,* ORNL-TM-2846 (January 1970).

Staffs of the Chemical Technology and Metals and Ceramics Divisions, *Thorium Fuel Cycle Development Progress Report, February 1970, No. 7,* ORNL-TM-2886 (March 1970).

Staffs of the Chemical Technology and the Metals and Ceramics Divisions, *Aqueous Processing of LMFBR Fuels Progress Report, May 1969, No. 3,* ORNL-TM-2624 (June 1969).

Staffs of the Chemical Technology and the Metals and Ceramics Divisions, *Aqueous Processing of LMFBR Fuels Progress Report, June 1969, No. 4,* ORNL-TM-2650 (July 1969).

Staffs of the Chemical Technology and the Metals and Ceramics Divisions, *LMFBR Fuel Cycle Studies Progress Report, No. 5,* ORNL-TM-2671 (August 1969).

Staffs of the Chemical Technology and the Metals and Ceramics Divisions, *LMFBR Fuel Cycle Studies Progress Report for August, No. 6,* ORNL-TM-2710 (October 1969).

Staffs of the Chemical Technology and the Metals and Ceramics Divisions, *LMFBR Fuel Cycle Studies Progress Report for September, No. 7,* ORNL-TM-2748 (November 1969).

Staffs of the Chemical Technology and the Metals and Ceramics Divisions, *LMFBR Fuel Cycle Studies Progress Report for October, No. 8,* ORNL-TM-2764 (November 1969).

Staffs of the Chemical Technology and the Metals and Ceramics Divisions, *LMFBR Fuel Cycle Studies Progress Report for November 1969, No. 9,* ORNL-TM-2795 (December 1969).

Staffs of the Chemical Technology and the Metals and Ceramics Divisions, *LMFBR Fuel Cycle Studies Progress Report for December 1969, No. 10,* ORNL-TM-2819 (January 1970).

Staffs of the Chemical Technology and the Metals and Ceramics Divisions, *LMFBR Fuel Cycle Studies Progress Report for January 1970, No. 11,* ORNL-TM-2871 (February 1970).

Staffs of the Chemical Technology and the Metals and Ceramics Divisions, *LMFBR Fuel Cycle Studies Progress Report for February 1970, No. 12,* ORNL-TM-2918 (March 1970).

Staffs of the Chemical Technology and the Metals and Ceramics Divisions, *LMFBR Fuel Cycle Studies Progress Report for March 1970, No. 13,* ORNL-TM-2949 (April 1970).

Staffs of the Chemical Technology and the Metals and Ceramics Divisions, *LMFBR Fuel Cycle Studies Progress Report for April 1970, No. 14,* ORNL-TM-2996 (May 1970).

Whatley, M. E., *et al., Unit Operations Section Quarterly Progress Report, July–September 1967,* ORNL-4234 (July 1969).

Whatley, M. E., *et al., Unit Operations Section Quarterly Progress Report, October–December 1967,* ORNL-4235 (October 1969).

Whatley, M. E., *et al., Unit Operations Section Quarterly Progress Report, January–March 1968,* ORNL-4364 (October 1969).

Whatley, M. E., *et al., Unit Operations Section Quarterly Progress Report April–June 1968,* ORNL-4365 (February 1970).

Whatley, M. E., *et al., Unit Operations Section Quarterly Progress Report, July–September 1968,* ORNL-4366 (April 1970).

Wymer, R. G., and A. L. Lotts, *Status and Progress Report for Thorium Fuel Cycle Development for 1967 and 1968,* ORNL-4429 (August 1969).

SEPARATIONS CHEMISTRY

Coleman, C. F., "Amine Extraction in Reprocessing," pp. 233–85 in Vol. 4 of *Progress in Nuclear Energy,* Series III, ed. by C. E. Stevenson, A. T. Gresky, and E. A. Mason, Pergamon, Oxford, 1970.

Davis, W., Jr., J. Mrochek, and R. R. Judkins, *J. Inorg. Nucl. Chem.* **32**(5), 1689–1702 (1970).

Delle Site, A.,[15] and R. D. Baybarz, "A Spectrophotometric Study of the Complexing of Am^{3+} with Aminopolyacetic Acids," *J. Inorg. Nucl. Chem.* **31**(7), 2201–33 (1969).

Fardy, J. J.,[16] and Boyd Weaver, "Mechanisms in the Coprecipitation of Bk(IV) with Ce(IV) Iodate from Homogeneous Solution," *Anal. Chem.* **41**, 1299 (1969).

Horner, D. E., *A Mathematical Model and a Computer Program for Estimating Distribution Coefficients for Plutonium, Uranium, and Nitric Acid in Extractions with Tri-n-Butyl Phosphate,* ORNL-TM-2711 (February 1970).

McDowell, W. J., *Computer Methods of Calculating Sulfuric Acid Activity, Sulfate Ion Concentration, and Ionic Strength of Sodium Sulfate-Sulfuric Acid Solutions,* ORNL-4407 (August 1969).

Roddy, J. W., Sumio Arai,[17] and C. F. Coleman, "Mechanism of the Slow Extraction of Iron and Beryllium by Di(2-ethylhexyl)Phosphoric Acid," presented at the XII International Congress of Pure and Applied Chemistry, Sydney, Australia, Aug. 20–27, 1969.

Roddy, J. W., and C. F. Coleman, "The Extraction of Water by Tri-*n*-Octylamine and Several of its Salts in Benzene and Phenylcyclohexane," *J. Inorg. Nucl. Chem.* **31**(11), 3599–3611 (1969).

Weaver, Boyd, "Heavy Element Partitioning by Extraction (HEPEX)," presented at the 15th Annual Meeting of the American Nuclear Society, Seattle, Wash., June 15–19, 1969.

SOL-GEL PROCESSES

1. General

Bond, W. D., S. R. Buxton, and K. J. Notz, "Preparation of Carbide Microspheres by the Sol-Gel Process," presented at the 15th Annual Meeting of the American Nuclear Society, Seattle, Wash., June 15–19, 1969.

Buxton, S. R., "Sol-Gel Processes for Preparing Lanthanide and Actinide Oxide Microspheres," presented at a seminar at Arizona State University, Apr. 14, 1970.

Buxton, S. R., M. H. Lloyd, and T. E. Willmarth,[18] "Properties of Lanthanide Oxide Microspheres Prepared by Sol-Gel Methods," presented at the 8th Rare Earth Research Conference, Reno, Nev., Apr. 19–22, 1970; to be published in the *Proceedings.*

---

[15] Present address: Laboratorio di Chimica Industriale del C.N.E.N., C.S.N. Casaccia via Anguillarese, Rome, Italy.

[16] Australian Atomic Energy Commission, Lucas Heights, Sydney, Australia.

[17] Industrial Science Research Lab., Kao Soap Co., Ltd., Wakayama-shin, Japan.

[18] Analytical Chemistry Division.

Haas, P. A., *Sol-Gel Preparation of Spheres: Design and Operation of Fluidized Bed Columns,* ORNL-4398 (September 1969).

Haas, P. A., "Preparation of Sol-Gel Spheres Smaller than 200 Microns Without Fluidization," presented at the 1969 Winter Meeting of the American Nuclear Society, San Francisco, Calif., Nov. 30–Dec. 4, 1969.

Notz, K. J., R. G. Haire, W. D. Bond, and L. G. Farrar,[18] "Carbothermic Conversion of Sol-Gel Uranium and Plutonium Oxides to Carbonitrides," presented at the Sol-Gel Processes and Reactor Fuel Cycles Symposium, Gatlinburg, Tenn., May 4–7, 1970; published in the *Proceedings.*

Thomas, I. L., "Sol-Gel Processes at ORNL," presented at the Instituto Technologico y De Estudios Superiores De Monterrey, Monterrey, N.L., Mexico, Apr. 2–3, 1970.

Thomas, I. L., "Adsorption of Carbon Dioxide by Thoria Sols," *J. Colloid Interface Sci.* 32, 177 (1970).

Wymer, R. G., "Colloid Chemistry and the Nuclear Industry," presented to combined sections of the American Chemical Society and the American Institute of Chemical Engineers at Savannah River Operations, Aiken, S.C., Sept. 19, 1969.

Wymer, R. G., "Colloid Chemistry and the Nuclear Industry," presented on an American Chemistry Society Local Section Tour (including sections in the "Central South Circuit") for the first half of November 1970.

2. Development of the Thorium Fuel Cycle

Bond, W. D., B. C. Finney, P. A. Haas, C. C. Haws, and J. R. Parrott, "Sol-Gel Processes for Urania-Thoria Fuels," presented at the Sol-Gel Processes and Reactor Fuel Cycles Symposium, Gatlinburg, Tenn., May 4–7, 1970; published in the *Proceedings.*

Finney, B. C., P. A. Haas, C. C. Haws, and A. D. Ryon, "Engineering-Scale Demonstration of Thoria-Urania Microsphere Production by the Sol-Gel Process," presented at the 15th Annual Meeting of the American Nuclear Society, Seattle, Wash., June 15–19, 1969.

Notz, K. J., and A. B. Meservey, *Microsphere Forming Conditions for ThO_2-UO_3 Sols: A Factorial Experiment,* ORNL-TM-2516 (August 1969).

Parrott, J. R., F. L. Daley, F. J. Furman,[19] and J. W. Snider, "Demonstration of $^{233}UO_2$-ThO_2 Microsphere Production by the Sol-Gel Process," presented at the 1969 Annual Meeting of the American Nuclear Society, Seattle, Wash., June 15–19, 1969.

3. Uranium-Plutonium Fuel Cycle Sol-Gel Processes

Lloyd, M. H., O. K. Tallent, W. T. McDuffee, L. E. Morse, and R. G. Haire, "Sol-Gel Processes for PuO_2 and UO_2-PuO_2," presented at the Sol-Gel Processes and Reactor Fuel Cycles Symposium, Gatlinburg, Tenn., May 4–7, 1970; published in the *Proceedings.*

McBride, J. P., K. H. McCorkle, W. L. Pattison, and B. C. Finney, "The Preparation of Concentrated, Crystalline Urania Sols by Solvent Extraction," presented at the 15th Annual Meeting of the American Nuclear Society, Seattle, Wash., June 15–19, 1969.

McBride, J. P., W. L. Pattison, B. C. Finney, and K. H. McCorkle, "Process Control in Urania Preparation by the Sol-Gel Process," presented at the Sol-Gel Processes and Reactor Fuel Cycles Symposium, Gatlinburg, Tenn., May 4–7, 1970; published in the *Proceedings.*

McDuffee, W. T., M. H. Lloyd, W. D. Bond, and O. K. Tallent, "Sol-Gel Process: Plutonia and Plutonia-Urania for Special and Nuclear Applications," presented at the 15th Annual Meeting of the American Nuclear Society, Seattle, Wash., June 15–19, 1969.

---

[19] Metals and Ceramics Division.

THESIS

Pitt, W. W., Jr., *Gradient Elution Chromatography of Urinary Constituents. Mathematical Analysis of the Kinetics of Gradient Elution Chromatography,* Ph.D. dissertation, University of Tennessee, Knoxville; also published as ORNL-TM-2870 (April 1970).

TRANSURANIUM ELEMENT PROCESSING

Burch, W. D., "Organization of the Interventions on Hot Facilities: Mishaps, Maintenance, Dismantling," presented at the IAEA Symposium on Radiation Safety Problems in the Designed Operation of "Hot" Facilities, Saclay, France, Oct. 13–17, 1969; to be published in the *Proceedings.*

Burch, W. D., "Specific Safety Problems Connected with Work on Transplutonium Elements and Some Practical Solutions," IAEA Symposium on Radiation Safety Problems in the Designed Operation of "Hot" Facilities, Saclay, France, Oct. 13–17, 1969; to be published in the *Proceedings.*

Burch, W. D., "High Specific Alpha Activity – No New Contamination Problems," presented at the 17th Conference on Remote Systems Technology, San Francisco, Calif., Nov. 30–Dec. 4, 1969; to be published in the *Proceedings.*

Burch, W. D., "Recent Operating Experience in the Transuranium Processing Plant," presented at the 17th Conference on Remote Systems Technology, San Francisco, Calif., Nov. 30–Dec. 4, 1969; to be published in the *Proceedings.*

Burch, W. D., and A. J. Hill, Jr.,[20] "Organization of the Interventions on Hot Facilities: Mishaps, Maintenance, Dismantling," IAEA Symposium on Radiation Safety Problems in the Designed Operation of "Hot" Facilities, Saclay, France, Oct. 13–17, 1969; to be published in the *Proceedings.*

Campbell, D. O., "Rapid Ion Exchange Separations. Chromatographic Separation of Transplutonium Elements Using High Pressure Ion Exchange," *Ind. Eng. Chem., Process Design Develop.* **9**(1), 95–99 (1970).

Campbell, D. O., and S. R. Buxton, "Rapid Ion Exchange Separations. Chromatographic Lanthanide Separations Using a High-Pressure Ion Exchange Method," *Ind. Eng. Chem., Process Design Develop.* **9**(1), 89–94 (1970).

Campbell, D. O., and B. H. Ketelle,[21] "Rapid Chromatographic Elution of a Tracer Lanthanide Using High Pressure Ion Exchange," *Inorg. Chem. Letters* **5**, 533 (1969).

Chilton, J. M., and J. J. Fardy,[21] "Isolation of Plutonium in Chloride Media. III. Effects of Nitrate and Mono(2-ethylhexyl)phosphoric Acid on Extraction with Di(2-ethylhexyl)phosphoric Acid," *J. Inorg. Nucl. Chem.* **31**, 3871 (1969).

Fardy, J. J.,[21] and J. M. Chilton, "Isolation of Plutonium in Chloride Media II. Solvent Extraction with Di(2-ethylhexyl)phosphoric Acid," *J. Inorg. Nucl. Chem.* **31**(10), 3247–54 (1969).

Ferguson, D. E., "Recent Advances in the Separation of the Transuranium Elements," presented at the Transplutonium Research Meeting, Liege, Belgium, Apr. 21–22, 1969; to be published in the *Proceedings.*

Haire, R. G., "Thermal Analysis of Lanthanide Hydroxide Preparations," presented at the 8th Rare Earth Conference, Reno, Nev., Apr. 19–22, 1970; to be published in the *Proceedings.*

Haire, R. G., M. H. Lloyd, T. E. Willmarth,[18] and W. O. Milligan,[22] "Comparative Studies on the Lanthanides and Actinides," presented at the Sol-Gel Processes and Reactor Fuel Cycles Symposium, Gatlinburg, Tenn., May 4–7, 1970; published in the *Proceedings.*

Kappelmann, F. A., and R. D. Baybarz, "Molecular Deposition of the Transplutonium Elements from an Organic Extractant," presented at the Winter Meeting of the American Nuclear Society, Nov. 30–Dec. 4, 1969, San Francisco, Calif.; to be published in the *Proceedings.*

---

[20] Savannah River Laboratory, Aiken, S.C.

[21] Australian Atomic Energy Commission, Lucas Heights, Sydney, Australia.

[22] Baylor University, Waco, Tex.

King, L. J., and E. D. Collins, *Summary of the Campaign During July 1968 to Process Fourteen Irradiated HFIR Targets in the Transuranium Processing Plant,* ORNL-TM-2434 (December 1969).

King, L. J., and O. O. Yarbro, "Containment of Radioiodine in the Transuranium Processing Plant," presented at the 17th Conference on Remote Systems Technology, San Francisco, Calif., Nov. 30–Dec. 4, 1969; to be published in the *Proceedings.*

Leuze, R. E., and M. H. Lloyd, "Processing Methods for the Recovery of Transplutonium Elements," pp. 549–630 in Vol. 4 of *Process in Nuclear Energy,* Series III, ed. by C. E. Stevenson, A. T. Gresky, and E. A. Mason, Pergamon, Oxford, 1970.

McDuffee, W. T., V. C. A. Vaughen, F. A. Kappelmann, and W. R. Whitson, *Recovery of Multigram Quantities of Curium-242 and Curium-244 in the Curium Recovery Facility,* ORNL-4241 (December 1969).

Peterson, J. R.,[23] R. D. Baybarz, and J. B. Knauer, "A New Encapsulation Technique for Californium-252 Sources," presented at the 15th Annual Meeting of the American Nuclear Society, Seattle, Wash., June 15–19, 1969.

Peterson, J. R.,[23] J. A. Fahey,[24] and R. D. Baybarz, "Preparation and Properties of Berkelium Metal," presented at the Southeastern Regional American Chemical Society Meeting, Richmond, Va., Nov. 5–8, 1969.

Vaughen, V. C. A., J. D. Hoeschele,[25] and M. H. Lloyd, "Preparation of ^{244}Cm-^{243}Am Oxide Microspheres by a Sol-Gel Method," presented at the 15th Annual Meeting of the American Nuclear Society, Seattle, Wash., June 15–19, 1969.

Vaughen, V. C. A., W. T. McDuffee, E. Lamb,[26] and R. A. Robinson,[26] "The Preparation of Multigram Quantities of Curium-242 for SNAP-II," *Nucl. Appl.* **6**(6), 549–58 (1969).

WASTE TREATMENT AND DISPOSAL

Blanco, R. E., Eighteen lectures on waste treatment and disposal and fuel reprocessing, presented as a 3-hr lecture course at the Institute de Energia Atomica, Nuclear Engineering Division, in association with the Cidade Universitaria, Sao Paulo, Brazil, October–December 1969.

Blanco, R. E., H. W. Godbee, and E. J. Frederick, "Incorporation of Urban and Industrial Waste Residues in Asphalt or Plastics for Subsequent Burial in Sanitary Landfills," presented at the 67th Annual Meeting of the American Institute of Chemical Engineers, Symposium on Pollution Control in the Atomic Energy Program, Portland, Ore., Aug. 24–27, 1969; published in *Chem. Eng. Progr.* **66**(2), 51–56 (1970).

Blomeke, J. O., and J. J. Perona,[23] *Management of Noble-Gas Fission-Product Wastes from Reprocessing Spent Fuels,* ORNL-TM-2677 (November 1969).

Clark, W. E., and R. E. Blanco, *Encapsulation of Noble Fission Product Gases in Solid Media Prior to Transportation and Storage,* ORNL-4473 (February 1970).

Fitzgerald, C. L., H. W. Godbee, R. E. Blanco, and W. Davis, Jr., "The Feasibility of Incorporating Radioactive Wastes in Asphalt or Polyethylene," presented at the 15th Annual Meeting of the American Nuclear Society, Seattle, Wash., June 15–19, 1969.

Godbee, H. W., C. L. Fitzgerald, J. O. Blomeke, and R. E. Blanco, "Diffusion of Radioisotopes Through Waste Solids," *Trans. Am. Nucl. Soc.* **12**(2), 450–51 (1969).

Nichols, J. P., "Fuel Reprocessing Plant Containment," presented at the Winter Meeting of the American Nuclear Society, San Francisco, Calif., Nov. 30–Dec. 4, 1969; published in *Trans. Am. Nucl. Soc.* **12**(2), 455–56 (1969).

Perona, J. J.,[23] J. O. Blomeke, and W. C. T. Stoddart,[27] "Management of Noble Gas Fission-Product Wastes from Reprocessing Spent Fuels," presented at the 1969 Winter Meeting of the American Nuclear Society, San Francisco, Calif., Nov. 30–Dec. 4, 1969; published in *Trans. Am. Nucl. Soc.* **12**(2), 449–50 (1969).

[23] Consultant, University of Tennessee.

[24] Graduate student, University of Tennessee.

[25] Present address: Department of Biophysics, Michigan State University, East Lansing.

[26] Isotopes Division.

[27] General Engineering Division.

SEMINARS

1969

November 6	Protonic Structure of Molecules	I. L. Thomas
November 12	Sol-Gel Demonstration Runs for 10 kg/day ThO_2-UO_3:	
	Solvent Extraction Preparation of Sol	B. C. Finney
	Preparation of Spheres	C. D. Haws
November 19	Fuel Processing Studies at Juelich, Germany	H. O. Witte[28]
December 3	Hot Cell Tests with Short-Cooled LMFBR Fuel Specimens	V. C. A. Vaughen J. H. Goode
December 9	Uranium and Thorium Carbides by Sol-Gel	K. J. Notz T. B. Lindemer[29]

1970

January 14	Status of TRU	W. D. Burch
	Sol-Gel Preparation of Curium Oxide	E. D. Collins
	The TURF-Californium Facility	F. L. Peishel
January 21	Fundamental Concepts of Gradient-Elution Chromatography	W. W. Pitt
January 28	Studies of Radioiodine Containment in Fuel Reprocessing Plants	G. I. Cathers O. O. Yarbro
February 4	CANE Studies	W. D. Arnold
February 11	Large Scale Separations of tRNAs by Reversed Phase Chromatography	H. O. Weeren
	Desalting and Concentration of Bio-Macromolecular Solutions	C. W. Hancher
February 20	Lanthanide Spectra	J. T. Bell C. C. Thompson[30]
February 25	Isotopic Enrichment of Neutron Capture Product	D. O. Campbell
March 4	Properties of Lanthanide Oxide Sol-Gel Microspheres	S. R. Buxton
	Thermal Analysis of Lanthanide Hydroxides	R. G. Haire
March 12	Plutonium and Plutonium-Uranium Carbides	R. G. Haire L. G. Farrar[31]
March 18	Removal of Rare Earths from MSBR Fuel	F. J. Smith
	Chemical Studies in Support of the Reduction Extractant Processes for MSBR Fuels	L. M. Ferris
March 25	Preparation of PuO_2-UO_2 Fuel for EBR-II Irradiation Assembly	W. T. McDuffee
	Preparation of Sol-Gel Spheres Smaller than 200 μ Without Fluidization	P. A. Haas

[28] KFA-heisse Zellen, Juelich, Germany.
[29] Metals and Ceramics Division.
[30] Memphis State University, Memphis, Tenn.
[31] Analytical Chemistry Division.

April 1	Isolation of Isoaccepting tRNAs Using Benzoylated DEAE and Reversed-Phase Columns	R. L. Pearson D. W. Holladay
April 8	Analysis of Flowsheets for Processing Single-Fluid MSBRs	L. E. McNeese
April 15	LMFBR Solvent Extraction Flowsheet Development	R. H. Rainey D. E. Horner
April 22	Sol-Gel Preparation of UO_2 Sols and Spheres Solvent Extraction Preparation of Sol Preparation of Thoria-Urania and Urania Microspheres	 B. C. Finney A. B. Meservey
April 29	Mixed Plutonia-Urania Sols Plutonia Sols by Apex Extraction	O. K. Tallent L. E. Morse
May 6	Electrolytic Cell Development for MSBR Processing Operation of a Semicontinuous Reductive Extraction Facility for MSBR Processing	J. R. Hightower B. A. Hannaford
May 13	LMFBR Fuel Shipping Studies	A. R. Irvine J. P. Nichols J. D. Rollins R. L. Cox
May 20	LMFBR Fuel Receiving and Head-End Processing	C. D. Watson R. S. Lowrie

CHEMICAL TECHNOLOGY DIVISION

MAY 31, 1970

D. E. FERGUSON, DIRECTOR
K. B. BROWN, ASSISTANT DIRECTOR
ALICE McWILLIAMS, SECRETARY
JUNE REDMOND, SECRETARY
F. N. BROWDER, RADIATION AND SAFETY CONTROL OFFICER
A. T. GRESKY, SPECIAL ASSIGNMENT
MARTHA STEWART, REPORTS EDITOR

H. B. GRAHAM, ADMINISTRATIVE ASSISTANT
DONNA FITZGERALD, SECRETARY
W. O. GREEVER,[1] PROCUREMENT
LUCILLE KUYKENDALL, SECRETARY

LONG RANGE PLANNING COMMITTEE

J. P. NICHOLS, CHAIRMAN
E. D. ARNOLD
M. J. BELL
O. L. CULBERSON[2]
S. C. JACOBS
D. S. JOY
J. T. ROBERTS[2]
F. SALMON
H. F. SOARD
J. J. WELFARE[4]
IMOGENE LOOFF, SECRETARY
LINDA KNAUER, PROGRAMMER
TECHNICIAN: P. P. HAYDON[5]

CHEMICAL DEVELOPMENT SECTION A

R. G. WYMER, SECTION CHIEF
R. L. LEUZE, ASSISTANT SECTION CHIEF
C. F. COLEMAN,[6] ASSISTANT SECTION CHIEF
JANE WEBB, SECRETARY
CAROLYN UHLEN, SECRETARY
TECHNICIAN: C. P. KECK

SOL-GEL STUDIES

J. P. McBRIDE, GROUP LEADER
L. E. MORSE
W. L. PATTISON
TECHNICIAN: J. F. TALLEY

FUEL CYCLE STUDIES

W. D. BOND, GROUP LEADER
A. B. MESERVEY
K. J. NOTZ[7]
K. S. WARREN[8]
TECHNICIANS: C. W. GREENE
A. S. LYLE[9]

HEAVY ELEMENT SEPARATIONS AND ANALYSES

D. O. CAMPBELL, PROJECT LEADER

SEPARATIONS CHEMISTRY RESEARCH

C. F. COLEMAN,[6] GROUP LEADER
W. J. McDOWELL
J. W. RODDY
TECHNICIANS: G. N. CASE
J. E. THOMPSON

HEAVY ELEMENT SEPARATIONS

M. H. LLOYD,[6] COORDINATOR
J. R. FLANARY, FLOWSHEET IMPROVEMENT
R. WEAVER, GROUP LEADER, SEPARATIONS AND CHEMISTRY OF ACTINIDES AND LANTHANIDES
TECHNICIAN: R. R. SHOUN

R. D. BAYBARZ, GROUP LEADER, TRU FINAL SEPARATIONS AND RESEARCH
F. A. KAPPELMANN
J. B. KNAUER, JR.
F. B. ORR
TECHNICIANS: L. A. BYRD[7]
E. C. HENDREN[8]
H. L. HICKLY
A. S. LYLE[9]
J. T. WIGGINS

M. H. LLOYD,[6] GROUP LEADER, THU PROCESS RESEARCH AND DEVELOPMENT
S. R. BUXTON
J. M. CHILTON
L. G. FARRAR[6]
R. G. HAIRE
D. K. TALLENT
TECHNICIANS: S. A. McDISH
C. H. JONES
D. H. NEWMAN[6]

ACTINIDE ELEMENT OXIDES AND RADIATION EFFECTS

N. A. KROHN,[6] GROUP LEADER
K. H. McDOWELL
F. L. THOMAS
TECHNICIAN: D. H. NEWMAN[6]

ACTINIDE ELEMENT SPECTROPHOTOMETRY

N. A. KROHN,[6] GROUP LEADER
J. I. BELL
TECHNICIAN: D. M. HELTON

BIOCHEMICAL SEPARATIONS

A. D. KELMERS, GROUP LEADER
B. Z. EGAN
R. L. PEARSON
J. F. WEISS
TECHNICIANS: W. F. BAYLESS[6]
J. Y. BUBANKS
D. F. HEATHERLY
J. B. OVERTON

BODY FLUIDS ANALYSES

C. D. SCOTT, GROUP LEADER
M. R. BENNETT
W. C. BUTTS[6]
D. D. CHILCOTE
G. F. JOHNSON[6]
R. L. JOLLEY
S. KATZ
J. E. MROCHEK
W. W. PITT
E. SCHONFELD[3]
T. D. TIFFANY[6]
K. S. WARREN[8]
TECHNICIANS: S. R. DINSMORE[9]
M. L. FREEMAN
G. JONES, JR.
N. F. LEE

CHEMICAL DEVELOPMENT SECTION B

R. E. BLANCO, SECTION CHIEF
U. J. CROUSE,[7] ASSISTANT SECTION CHIEF
L. M. FERRIS,[6] ASSISTANT SECTION CHIEF
SUE DANEWOOD, SECRETARY
REA GARBER, SECRETARY
GERALDINE ODDY, SECRETARY
J. E. FARMER, DRAFTSMAN

FISSION PRODUCT SOLUBILITY AND FORMATION AND REACTIONS OF SOLVENT DEGRADATION PRODUCTS IN LMFBR FUEL PROCESSING

W. DAVIS, JR., GROUP LEADER
A. H. KIBBY
J. E. MROCHEK[10]

RADIOACTIVE WASTE STUDIES

H. W. GOODBEE, GROUP LEADER, SOLIDIFICATION OF LIQUID WASTES
C. L. FITZGERALD
W. D. YEE[12]
TECHNICIAN: N. F. SHOCKLEY

W. E. CLARK, GROUP LEADER, ENCAPSULATION OF GASEOUS WASTES

POWER REACTOR FUEL PROCESSING

V. C. A. VAUGHEN, GROUP LEADER, FLOWSHEET DEMONSTRATION ON RADIOACTIVE LMFBR, HTGR, AND LWR FUEL PROCESSING
J. H. GOODE
TECHNICIANS: L. A. BYRD
G. D. DAVIS
D. I. KIRKLAND

L. M. FERRIS,[6] GROUP LEADER, MOLTEN SALT REACTOR FUEL PROCESSING
J. C. MAILEN
C. F. SCHILLING
M. B. SEARS[11]
F. J. SMITH
TECHNICIANS: J. F. LAND
C. T. THOMPSON

R. H. RAINEY, GROUP LEADER, SOLVENT EXTRACTION IN LMFBR FUEL PROCESSING, NOBLE GAS REMOVAL, AND REPURIFICATION OF ^{233}U
D. E. HORNER
TECHNICIANS: J. R. COLLINS
R. C. LOVELACE

G. I. CATHERS, GROUP LEADER, IODINE RETENTION IN LMFBR FUEL PROCESSING
M. R. BENNETT
TECHNICIAN: C. J. SHIPMAN

SEPARATIONS PROCESSES RESEARCH

D. J. CROUSE,[6] GROUP LEADER
F. J. HURST
F. G. SELLEY
TECHNICIAN: W. B. HOWERTON

RADIOIODINE CHEMISTRY, RADIATION STABILITY OF SOLVENTS IN LMFBR FUEL PROCESSING

D. J. CROUSE,[6] GROUP LEADER
J. M. SCHMITT
J. G. MOORE

FLOWSHARE PROGRAM

D. J. CROUSE[6]
W. D. ARNOLD
TECHNICIAN: D. E. SPANGLER

UNIT OPERATIONS SECTION

M. E. WHATLEY, SECTION CHIEF
A. D. RYON,[7] ASSISTANT SECTION CHIEF
JANICE SHANNON, SECRETARY
LINDA LOVRDAY, SECRETARY

FUEL CYCLE STUDIES AND THORIUM UTILIZATION

P. A. HAAS, GROUP LEADER
B. C. FINNEY
C. C. HAWS, JR.
J. T. LONG
A. P. LUNA[13]
TECHNICIANS: R. D. ARTHUR
E. R. JOHNS[13]
K. LADD
D. A. McBRAYER
C. H. TIPTON

MOLTEN SALT PROCESSING

L. E. McNEESE, GROUP LEADER
B. A. HANNAFORD
J. R. HIGHTOWER
S. H. JURY[7]
C. W. KEE
M. S. LIN
R. B. LINDAUER
J. S. WATSON
E. L. YOUNGBLOOD
TECHNICIANS: J. BEAMS
V. L. FOWLER
R. D. PAYNE
J. S. TAYLOR

BIOCHEMICAL SEPARATIONS

A. D. RYON,[7] GROUP LEADER
C. W. HANCHER
D. W. HOLLADAY
H. O. WEEREN
TECHNICIANS: G. B. DINSMORE
F. G. KILPATRICK
W. G. SISSON[14]

POWER REACTOR FUEL PROCESSING

C. D. WATSON, GROUP LEADER
S. D. CLINTON
R. L. COX
W. S. GROENIER
H. F. JOHNSON[7]
R. S. LOWRIE
G. A. WEST
W. M. WOODS
TECHNICIANS: F. L. ROGERS
J. C. RUSE
D. E. WILLIS

PROCESS DESIGN SECTION

H. E. GOELLER,[6] SECTION CHIEF
W. E. UNGER,[6] ASSISTANT SECTION CHIEF
F. N. BROWDER,[6] DIVISION RADIATION AND SAFETY CONTROL OFFICER
H. E. GOELLER,[6] AGRO INDUSTRIAL STUDY
F. E. HARRINGTON,[6] PLUTONIUM SOL-GEL STUDIES
J. M. HOLMES, AGRO-INDUSTRIAL STUDY
F. L. FEISHEL, TRANSURANIUM ASSISTANCE
L. R. SHAPPERT, DIVISION QUALITY ASSURANCE PROGRAM
W. G. STOCKDALE,[6] SECTION EDITOR FOR N.S.I.C. AND ENVIRONMENTAL QUALITY STUDY PROJECT ASSISTANCE
W. E. UNGER,[6] RUROCHEMIC ASSISTANCE
RUBY A. MILLER,[6] CORRESPONDENT
MAY E. PEPPER, SECRETARY
MARY S. BROWN, SECRETARY
RUBY A. MILLER,[6] SECRETARY
K. F. STOCKSBURY, CLERK

DRAFTSMEN

O. E. DUNNING,[15] DRAFTING SUPERVISOR

R. L. BLAIR[16]	BARBARA A. HISE[16]
B. G. DeVALL	L. C. HUBBARD[15]
A. J. FARMER	J. W. KIDD[16]
C. K. FORD[15]	J. L. LUCKETT[16]
A. H. GREGORY[16]	R. P. OLIVER[16]
B. F. HENRY[15]	J. D. PHILLIPS[15]
J. H. FREELS[16]	F. J. UNDERWOOD[16]

WASTE STUDIES – SITING STUDIES

J. O. KLOMFKE, GROUP LEADER
B. P. BOTTENFIELD,[6] SALT MINE REPOSITORY
F. N. BROWDER,[6] ORNL WASTE SYSTEM EVALUATION
R. S. DILLON, ENGINEERING AND ECONOMIC EVALUATION
F. J. FREDERICK, SALT MINE REPOSITORY
H. W. GOODBEE, WASTE CHARACTERIZATIONS
J. J. PERONA,[2] CONSULTANT
J. C. SUDDATH, WASTE SITING STUDY

MSR STUDIES

E. L. NICHOLSON, GROUP LEADER
W. L. CARTER, MSBR FUEL PROCESSING
W. F. SCHAFFER, JR., MSBR EQUIPMENT DESIGN
E. L. YOUNGBLOOD, EQUIPMENT DEVELOPMENT

AQUEOUS LMFBR FUEL PROCESSING

A. R. IRVINE, GROUP LEADER
B. R. DEWEY,[2] CONSULTANT
B. S. KLIMA, CASK DESIGN COMPLIANCE
S. MANN, PLUTONIUM STUDIES
J. D. ROLLINS, FUEL TRANSPORT STUDIES
A. M. ROM,[6] DISSOLVER STUDIES
L. M. SHUBE,[2] CONSULTANT
O. O. YARBRO, IODINE RETENTION

Y-12 ENGINEERING ASSISTANCE

G. B. BERRY[15]
B. F. BOTTENFIELD[6]
R. V. FOLTZ[15]
J. W. LANDRY
R. P. MILFORD
A. M. ROM[6]
J. B. RUCH
W. G. STOCKDALE[6]

SOL GEL CONVERSION

J. W. SNIDER,[6] GROUP LEADER
R. J. BRAATZ[17] EQUIPMENT DESIGN

BETTIS LWBR SUPPORT PROGRAM

F. E. HARRINGTON[6]
J. W. SNIDER[6]

PILOT PLANT SECTION

R. E. BROOKSBANK, SECTION CHIEF
W. D. BURCH, ASSISTANT SECTION CHIEF
BOBBIE HOYLE, SECRETARY
SANDRA HINZ, SECRETARY
WILMA BALDRY, SECRETARY
E. C. BRANTLEY, CLERK
R. B. WATERS, DRAFTSMAN

TRANSURANIUM PROCESSING PLANT

W. D. BURCH, GROUP LEADER
L. J. KING, TECHNICAL GROUP
J. L. MATHERNE, ENGINEERING, PLANT SAFETY
F. R. CHAMTEL, OPERATIONS
F. L. FEISHEL[15]
J. E. IRGELOW
E. D. COLLINS
W. W. EVANS
J. E. VAN CLEVE[18]
L. C. WILLIAMS[18]
C. L. SHEPHERD

PROCESS SUPERVISORS

D. B. OWSLEY
C. E. WADDELL
B. J. STRADER[18]
R. C. SHIPWASH

TECHNICIANS

W. G. BARRETT	M. C. HILL
K. P. BAYNE[18]	R. R. LAXSON
W. J. BRYAN	R. E. POTTER[18]
J. H. BROCK	J. R. SLAVEN[18]
C. W. BROWN	W. M. SPROULE
H. S. CALDWELL	H. C. THOMPSON
T. L. DOUGLASS[19]	A. V. WILDER
J. E. EVE[18]	G. E. WOODALL
J. H. GROOVER	C. M. WILSON[18]
J. C. HILL[18]	

RADIOCHEMICAL OPERATIONS

J. H. PARROTT, GROUP LEADER, PLANT SAFETY
R. G. NIDDL, ^{233}U DISPENSING OPERATIONS
F. L. DALEY, SOL GEL OPERATIONS
W. T. McDUFFEE, SOL-GEL PREPARATIONS
W. R. WHITSON, IN PLANT ENGINEERING

PROCESS SUPERVISORS

W. A. SHANNON
R. J. SHANNON

TECHNICIANS

C. W. BOATMAN	S. L. SHELL
W. A. LINDSEY	D. R. TAYLOR
C. W. MARTIN	J. H. WALKER
R. E. PURKEY	

HOT CELL FACILITY

V. C. A. VAUGHEN, GROUP LEADER, PLANT SAFETY

TURF FACILITY

J. M. CHANDLER,[20] GROUP LEADER
TECHNICIAN: W. T. BOSTIC

SPECIAL PROJECTS

W. H. CARR, REPORTS, MSRE FUEL PREPARATION
F. G. KITTS, SOL-GEL FLOWSHEET AND COMPONENT DEVELOPMENT
R. W. HORTON, COMPUTER PROGRAMS, LMFBR CONVERSION SHIPPING STUDIES
F. W. MILES, TECHNICAL IMPROVEMENT PROGRAM, OPERATOR LICENSING

[1] ON LOAN FROM PLANT AND EQUIPMENT DIVISION.
[2] CONSULTANT, UNIVERSITY OF TENNESSEE
[3] ON LEAVE OF ABSENCE.
[4] ON LOAN FROM REACTOR DIVISION
[5] ON LOAN TO Y-12
[6] DUAL CAPACITY
[7] ON LOAN FROM CHEMICAL DEVELOPMENT SECTION B.
[8] ASSIGNED TO THIS PROBLEM BY THE ANALYTICAL CHEMISTRY DIVISION.
[9] GUEST SCIENTIST FROM UNIVERSITY OF NEW YORK AT BUFFALO.
[10] ON LOAN TO AGRO INDUSTRIAL SURVEY.
[11] PART-TIME EMPLOYEE.
[12] GUEST SCIENTIST FROM SPAIN
[13] ON LOAN FROM CHEMICAL DEVELOPMENT SECTION A.
[14] ON LOAN TO CHEMISTRY DIVISION
[15] ON LOAN FROM GENERAL ENGINEERING DIVISION.
[16] PART-TIME ON LOAN FROM NUCLEAR DATA PROJECT.
[17] ON LOAN FROM PROCESS DESIGN SECTION
[18] ON LOAN FROM METALS AND CERAMICS DIVISION
[19] ON EDUCATIONAL LEAVE
[20] ON LOAN TO METALS AND CERAMICS DIVISION

ORNL-4572
UC-10 — Chemical Separations Processes
for Plutonium and Uranium

INTERNAL DISTRIBUTION

1. Biology Library
2–4. Central Research Library
5. Laboratory Shift Supervisor
6–7. ORNL – Y-12 Technical Library
Document Reference Section
8. MIT Practice School
9–28. Laboratory Records Department
29. Laboratory Records, ORNL R.C.
30. H. I. Adler
31. R. D. Baybarz
32. S. E. Beall
33. Arnold Berman
34. D. S. Billington
35. C. A. Blake
36. R. E. Blanco
37. J. O. Blomeke
38. W. D. Bond
39. C. J. Borkowski
40. G. E. Boyd
41. R. E. Brooksbank
42. J. C. Bresee
43. R. B. Briggs
44. F. N. Browder
45. K. B. Brown
46. F. R. Bruce
47. W. D. Burch
48. D. O. Campbell
49. G. I. Cathers
50. J. M. Chandler
51. W. E. Clark
52. C. F. Coleman
53. W. C. Colwell
54. J. A. Cox
55. D. J. Crouse
56. F. L. Culler
57. J. E. Cunningham
58. W. Davis, Jr.
59–233. D. E. Ferguson
234. L. M. Ferris
235. J. R. Flanary
236. J. L. Fowler
237. J. H. Frye, Jr.
238. R. C. Fuller
239. J. H. Gillette
240. H. W. Godbee
241. H. E. Goeller
242. H. B. Graham
243. A. T. Gresky
244. W. R. Grimes
245. P. A. Haas
246. J. P. Hammond
247. C. S. Harrill
248. R. F. Hibbs
249. R. W. Horton
250. A. R. Irvine
251. R. L. Jolley
252. W. H. Jordan
253–258. P. R. Kasten
259. M. A. Kastenbaum
260. M. T. Kelley
261. A. D. Kelmers
262. F. Kertesz
263. N. A. Krohn
264. E. Lamb
265. J. A. Lane
266. R. E. Leuze
267. R. B. Lindauer
268. J. L. Liverman
269. R. S. Livingston
270. M. H. Lloyd
271. H. G. MacPherson
272. F. C. Maienschein
273. J. P. McBride
274. W. J. McDowell
275. L. E. McNeese
276. R. A. McNees
277. A. B. Meservey
278. E. C. Miller
279. K. Z. Morgan
280. J. P. Nichols
281. E. L. Nicholson
282. G. D. Novelli
283–284. R. B. Parker
285. J. R. Parrott
286. Helen Raaen
287. R. H. Rainey
288. M. E. Ramsey
289. J. T. Roberts
290. A. F. Rupp
291. A. D. Ryon
292. C. D. Scott
293. H. E. Seagren
294. L. B. Shappert
295. M. J. Skinner
296. A. H. Snell
297. M. G. Stewart
298. D. A. Sundberg
299. E. H. Taylor
300. D. B. Trauger
301. W. E. Unger
302. V. C. A. Vaughen
303. C. D. Watson
304. B. S. Weaver
305. A. M. Weinberg
306. M. E. Whatley
307. J. C. White
308. R. G. Wymer
309. B. J. Young
310. Gale Young
311. E. L. Youngblood
312. P. H. Emmett (consultant)
313. J. J. Katz (consultant)
314. E. A. Mason (consultant)
315. J. L. Margrave (consultant)
316. R. B. Richards (consultant)

EXTERNAL DISTRIBUTION

317. D. F. Cope, RDT Site Office (ORNL)
318. Richard Hamburger, AEC, Washington
319. J. A. Swartout, 270 Park Avenue, New York 17, New York
320. Dr. Barendregt, c/o COMPRIMO, Europahuis, James Wattstraat 79, Amsterdam, Holland
321. Giacomo Calleri, Comitato Nazionale per l'Energia Nucleare, Programma EUREX, Saluggia (Vc), Italy
322. D. J. Carswell, Radiochemical Laboratory, The New South Wales University of Technology, P.O. Box 1, Kensington, Sydney, N.S.W., Australia
323. E. Cerrai, Laboratori CISE, Casella Postale N. 3986, Milano, Italy
324. David Dryssen, The Royal Institute of Technology, Department of Inorganic Chemistry, Kemisträgen 37, Stockholm 70, Sweden
325. Syed Fareeduddin, Indian Rare Earths Ltd., Army and Navy Building, 148 Mahatma Gandhi Road, Bombay 1, India
326. T. Ishihara, Division of Fuel Research and Development, Tokai Research Establishment, JAERI, Tokai-mura, Ibaraki-ken, Japan
327. A. S. Kertes, Hebrew University, Jerusalem
328. Jorgen Klitgaard, Atomic Energy Commission Res. Estab. Risö, Roskilde, Denmark
329. Y. Marcus, Israel Atomic Energy Commission, Tel Aviv, Israel
330. E. Glueckauf, Atomic Energy Research Establishment, Harwell, Berks, England
331. P. Regnaut, C.E.N. Fontenay-aux-Roses, Boite Postale No. 6, Fontenay-aux-Roses, Seine, France
332. R. Rometsch, Eurochemic, Mol, Belgium
333. A. J. A. Roux, Director of Atomic Energy Research, South African Council for Scientific and Industrial Research, Box 395, Pretoria, South Africa
334. Jan Rydberg, Department of Nuclear Chemistry, Chalmers Tekniska Hogskola, Gibraltargatan 5 H. Goteborg, Sweden
335. M. Shaw, AEC, Washington
336. Erik Svenke, Director, Department of Chemistry, Atomic Energy Company, Stockholm 9, Sweden
337. D. G. Tuck, Associate Professor, Department of Chemistry, Simon Fraser University, Burnaby 2, British Columbia, Canada
338. B. F. Warner, United Kingdom Atomic Energy Authority, Production Group, Windscale and Calder Works, Sellafield, Seascale, Cumberland, England
339. M. Zifferero, Comitato Nazionale per l'Energia Nucleare, Laboratorio Trattamento Elementi Combustibili, c/o Istituto di Chemica Farmaceutica e Tossicologica dell 'Universita, Piazzale delle Scienze, 5, Rome, Italy
340. M. Claude Jean Jouannaud, Department Head, Plutonium Extraction Plant, Marcoule (Gard), France
341. Prof. Louis Gutierrez-Jadra, Director de Planta Pilotos e Industriales, Junta de Energia Nuclear, Ciudad Universitaris, Madrid (3), Spain
342. W. G. Belter, AEC, Washington
343. J. A. Lieberman, AEC, Washington
344. W. H. Regan, AEC, Washington
345. H. Bernard, AEC, Washington
346. P. Schmid, Federal Institute for Reactor Research, Wurenlingen, AG, Switzerland
347. Atou Shimozato, Nuclear Reactor Design Section, Nuclear Power Plant Department, Hitachi Ltd., Hitachi Works, Hitachi-Shi, Ibaraki-Ken, Japan
348. R. S. Brodsky, Division of Naval Reactors, Atomic Energy Commission, Washington, D.C.
349. R. W. Barber, AEC, Washington
350. Theodore Rockwell III, Chairman AIF Safety Task Force, MPR Associates, Inc., 815 Connecticut Avenue, N.W., Washington, D.C.
351. Guenther Wirths, NUKEM, Hanau, Germany
352. Riki Kobayashi, Professor, Rice University
353. W. Pollard, Oak Ridge Associated Universities

354. Librarian, Department of Chemical Engineering and Chemical Technology, Imperial College, Prince Consort Road, London, S.W.7, England
355. Giuseppe Orsenigo, CNEN, Via Belisario 15, Rome, Italy
356. Werner Muller, European Transuranium Institute, Euratom, Postfach 2266, 75 Karlsruhe, West Germany
357. F. Baumgartner, Heidelberg University, Karlsruhe, Postfach 947, West Germany
358. Hugo Schumacher, Swiss Federal Institute for Reactor Research, Ch-5303 Wurenlingen, Switzerland
359. B. L. Vondra, NUMEC, Apollo, Pa.
360. W. H. McVey, AEC, Washington
361. E. E. Sinclair, AEC, Washington
362. A. R. Van Dyken, AEC, Washington
363. C. L. Sumrall, Gilbert Associates, Reading, Pa.
364. Dr. Narayanan Srinivasan, Head of Fuel Reprocessing Division, Bhabha Atomic Research Center, Bombay 74, India
365. D. M. Rafi, Pakistan Institute of Nuclear Science and Technology, P.O. Box Nilore, Rawal Pindi, Pakistan
366. D. E. Bloomfield, Battelle Northwest, Richland, Washington
367. P. A. DeJonghe, Centre d'Etude de l'Energie Nucleaire, Mol, Belgium
368. T. W. McIntosh, Division of Reactor Development and Technology, USAEC, Washington, D.C.
369. R. E. Pahler, AEC, Washington
370. D. R. Miller, AEC, Washington
371. J. J. Fardy, Australian Atomic Energy Commission, Lucas Heights, Sydney, Australia
372. R. E. Norman, Gulf General Atomic, P.O. Box 608, San Diego, California
373. H. O. G. Witte, Julich Nuclear Research Center, Julich, Germany
374. Alfred Richard Boettcher, Director, Julich Nuclear Research Center, Julich, Germany
375. Julich Nuclear Research Center Library, Julich, Germany
376. Hans W. Levi, Deputy Director, Hahn – Meitner – Institut fur Kernforschung Berlin, Sektor Kernchemie, Glienicker Strasse 100, 1 Berlin 39, Germany
377. William J. Lacy, Chief, Industrial Pollution Control Branch, Division of Applied Science and Technology, Federal Water Pollution Control Administration, Department of the Interior, Washington, D.C.
378. G. Rajan, Scientific Officer, Waste Treatment Division, Bhabha Atomic Research Centre, Bombay – 85 AS., India
379. C. Djordjevic, Chemistry Department, College of William and Mary, Williamsburg, Virginia
380. G. Spaepen, Head, Chemical Technology, SCK-CEN, Mol, Belgium
381. D. W. Schüller, Managing Director, Gesellschaft zur Wiederaufarbeitung von Kernbrennstoffen MbH (GWK), Kernforschungszentrum, 7501 Leopoldshafen, Germany
382. Laboratory and University Division, AEC, ORO
383. Patent Office, AEC, ORO

384–512. Given distribution as shown in TID-4500 under Chemical Separations Processes for Plutonium and Uranium category (25 copies – CFSTI)